ORNL-4948

DATE ISSUED MAR 19 1974

ORNL
MASTER COPY

MECHANICAL PROPERTIES TEST DATA for STRUCTURAL MATERIALS

QUARTERLY PROGRESS REPORT for PERIOD ENDING JANUARY 31, 1974

[redacted]

OAK RIDGE NATIONAL LABORATORY
OPERATED BY UNION CARBIDE CORPORATION • FOR THE U.S. ATOMIC ENERGY COMMISSION

Printed in the United States of America. Available from
the U.S. Atomic Energy Commission, Technical Information Center
P.O. Box 62, Oak Ridge, Tennessee 37830
Price: Printed Copy $10.60 ; Microfiche $1.45

This report was prepared as an account of work sponsored by the United States Government. Neither the United States nor the United States Atomic Energy Commission, nor any of their employees, nor any of their contractors, subcontractors, or their employees, makes any warranty, express or implied, or assumes any legal liability or responsibility for the accuracy, completeness or usefulness of any information, apparatus, product or process disclosed, or represents that its use would not infringe privately owned rights.

ORNL-4948
UC-79b, -h, -k
(Liquid Metal Fast
Breeder Reactors)

Contract No. W-7405-eng-26

METALS AND CERAMICS DIVISION

MECHANICAL PROPERTIES TEST DATA FOR STRUCTURAL MATERIALS QUARTERLY PROGRESS REPORT FOR PERIOD ENDING JANUARY 31, 1974

Aerojet Nuclear Company

Argonne National Laboratory

Hanford Engineering Development Laboratory

Naval Research Laboratory

Oak Ridge National Laboratory

Westinghouse Advanced Reactors Division

University of Cincinnati

Compiled by M. R. Hill

MARCH 1974

OAK RIDGE NATIONAL LABORATORY
Oak Ridge, Tennessee 37830
operated by
UNION CARBIDE CORPORATION
for the
U.S. ATOMIC ENERGY COMMISSION

Reports previously issued in this series are as follows:

ORNL-4936	Period Ending October 31, 1973

CONTENTS

SUMMARY ix

1. AEROJET NUCLEAR COMPANY 1

1.1 INTRODUCTION 1

1.2 LOW CYCLE FATIGUE BEHAVIOR OF SMA TYPE 304/308 STAINLESS STEEL WELDMENTS 2

1.2.1 Materials 2

1.2.2 Results of 756K Tests 3

1.3 INCONEL 718 CODE CASE AND RELATED INVESTIGATIONS 5

1.3.1 Development of a Modified Heat Treatment for Inconel 718 5

2. ARGONNE NATIONAL LABORATORY 15

2.1 INTRODUCTION 15

2.2 FRACTURE AND FATIGUE STUDIES ON STAINLESS STEELS 15

2.2.1 Elevated-temperature True Stress-True Strain Tensile Behavior of Type 304 Stainless Steel . . . 15

2.2.2 Crack-propagation of SMA Type 304/308 Stainless Steel Weldments 22

3. HANFORD ENGINEERING DEVELOPMENT LABORATORY 33

3.1 INTRODUCTION 33

3.2 IRRADIATION DAMAGE TO REACTOR METALS 33

3.2.1 Evaluation of Microwave Extensometer 33

3.2.1.1 Objective 33

3.2.1.2 Accomplishments and Status 33

3.2.1.2.1 Scope of Work 33

3.2.1.2.2 Results 34

3.2.1.2.3 Evaluation of Results 51

3.2.1.2.4 Conclusions and/or Recommendations 55

3.2.2 Correlation of Transient Test Results with Conventional Mechanical Properties Data 55

3.2.2.1 Introduction 55

3.2.2.2 Accomplishments and Status 56

3.2.2.2.1 Life Fraction Rule and Larson-Miller Parameter 56

3.2.2.2.2 Evaluation of LMP Values . . . 59

3.2.2.2.3 Results and Discussion 63

3.2.2.2.4 Prediction of Thermal Transient Tests 70

3.2.2.3 Conclusions 72

3.2.2.4 Appendix 72

3.2.3 Stress-Rupture of 20% Cold Worked Type 316 Stainless Steel Under Variable Stress Histories 74

3.2.3.1 Objective 74

3.2.3.2 Accomplishments and Status 74

3.2.3.2.1 Scope of Work 74

3.2.3.2.2 Results 75

3.2.3.2.3 Evaluation of Results 75

3.2.3.2.4 Conclusions and/or Recommendations 86

3.2.3.2.5 Applications 86

3.2.3.3 Expected Achievements 87

3.2.4 Elastic Analysis for a Slit Tube 87

3.2.4.1 Objective 87

3.2.4.2 Accomplishments and Status 87

3.2.4.2.1 Stress Analysis 88

3.2.4.2.2 Strains and Compliance 99

3.2.4.2.3 Conclusions and/or Recommendations 104

3.3 MATERIALS PERFORMANCE AND SURVEILLANCE 104

3.3.1 FTR Component Materials Irradiation Experiment . . 104

3.3.1.1 Objective 104

3.3.1.2 Accomplishments and Status 106

3.3.2 High Strain Rate Effects 112

3.3.2.1 Objective 112

3.3.2.2 Accomplishments and Status 112

3.3.2.2.1 Test Materials 113

3.3.2.3 Results 113

3.3.2.3.1 Cladding Properties 113

3.3.2.3.2 Comparison to Previous Results 118

3.3.2.4 Discussion 123

3.3.2.4.1 Strength 123

3.3.2.4.2 Ductility 126

3.3.3 FTR Component Materials Evaluation 127

3.3.3.1 Objective 127
3.3.3.2 Accomplishment and Status 129
3.3.3.2.1 Test Material 129
3.3.3.3 Results 129
3.3.3.3.1 Tensile Behavior 131
3.3.3.3.2 Heat-To-Heat Variations 131
3.3.3.3.3 Strain Rate Effects 137
3.3.3.4 Discussion 137
3.3.4 Weldment Materials Evaluation 141
3.3.4.1 Objective 141
3.3.4.2 Accomplishments and Status 143
3.3.4.2.1 Scope of Work 143
3.3.4.2.2 Results 143
3.4 REFERENCES 154
4. NAVAL RESEARCH LABORATORY 157
4.1 INTRODUCTION 157
4.2 FATIGUE CRACK GROWTH IN TYPE 316 STAINLESS STEEL 157
4.2.1 Background 157
4.2.2 Materials and Test Procedures 157
4.2.3 Results 158
4.3 FRACTURE RESISTANCE OF TYPE 304 STAINLESS STEEL AND TYPE 308 WELD DEPOSIT 166
4.3.1 Background 166
4.3.2 Materials and Specimen Types 166
4.3.3 Test Results 166
4.3.4 Conclusions 170
4.4 NOTCH DUCTILITY OF ASTM TYPE A508 FORGINGS 171
4.5 REFERENCES 175
5. OAK RIDGE NATIONAL LABORATORY 177
5.1 INTRODUCTION 177
5.2 MECHANICAL PROPERTIES AND BEHAVIOR FOR STRUCTURAL MATERIALS 177
5.2.1 Base-Line Mechanical Property Testing of Reference Heat of Type 304 Stainless Steel 177
5.2.1.1 Creep Properties of the 2-in. (51-mm) Plate of Reference Heat 177

5.2.1.2 Strain Rate Effect on the Tensile Properties of 2-in. (51-mm) Plate 183

5.2.1.3 Measurement of Elastic Constants of Type 304 Stainless Steel 187

5.2.2 Heat-to-Heat Variation Study of Type 304 Stainless Steel 194

5.2.2.1 Tensile and Short-Term Creep Tests 198

5.2.2.2 Long-Term Creep Tests in Heat-to-Heat Variation Study 201

5.2.2.3 Effects of Aging on the Tensile Properties 204

5.2.3 Exploratory Studies on Type 304 Stainless Steel in Support of Structural Design Methods 210

5.2.3.1 Tensile Testing of Reference Heat 9T2796 1-in. (25-mm) Plate 210

5.2.3.2 Creep Testing of Reference Heat 9T2796 1-in. (25-mm) Plate 212

5.2.3.3 Creep Plasticity Interaction of Reference Heat 9T2796 1-in. (25-mm) Plate 216

5.2.3.4 Strain-Cycling of Reference Heat 9T2796 1-in. (25-mm) Plate 218

5.2.4 Mechanical Properties of Type 316 Stainless Steel 218

5.2.4.1 Procurement of Type 316 Stainless Steel Reference Heat 218

5.2.4.2 Heat-to-Heat Variation Studies of Type 316 Stainless Steel 220

5.2.5 Failure Criteria—Strain Limits 221

5.2.6 Computer Data Storage, Retrieval, and Storage Information Center 226

5.3 MECHANICAL AND METALLURGICAL BEHAVIOR OF WELDMENTS FOR LMFBR 230

5.3.1 Properties and Structure of 16-8-2 Stainless Steel Weld Metal 230

5.3.1.1 Introduction 230

5.3.1.2 Experimental Procedures and Results . . . 231

5.3.1.2.1 Test Weld Fabrication 231

5.3.1.2.2 Mechanical Properties Specimen Preparation and Testing 231

5.3.1.3 Discussion 238

5.3.1.3.1 Tensile and Creep Properties of Type 16-8-2 Weld Metal . . . 243

5.3.1.3.2 Heterogeneity and Anisotropy . 251

5.3.2 Creep-Rupture Properties of Type 308 Stainless Steel Welds Made With and Without Controlled Residual Elements 253

5.4 MECHANICAL PROPERTIES OF STEAM GENERATOR MATERIALS 255

5.4.1 Mechanical Properties of 2 1/4 Cr-1 Mo Steel for Design 255

5.4.1.1 Tensile Properties 257

5.4.1.2 Creep Properties 260

5.4.1.3 Elastic Properties 262

5.4.1.4 Subcritical Crack Growth in 2 1/4 Cr-1 Mo Steel 262

5.4.2 Evaluation of Property Listings for LMFBR Handbook for 2 1/4 Cr-1 Mo Steel 268

5.4.3 Correlation of Properties of 9 Cr-1 Mo Steel for Service Above 700°F (371°C) 268

5.4.3.1 Tensile Properties 272

5.4.3.2 Creep and Stress-Rupture 274

5.4.4 Mechanical Properties of Weld Overlaid Stainless Steel Forgings 275

5.5 HIGH-TEMPERATURE DESIGN 278

5.5.1 Exploratory Testing to Identify Behavioral Features 278

5.5.1.1 Development of Laboratory Facilities . . . 278

5.5.1.2 Stress-Strain Testing 279

5.6 INVESTIGATIONS OF CREEP FAILURE UNDER UNIAXIAL AND MULTI-AXIAL CONDITIONS 285

5.7 REFERENCES 316

6. WESTINGHOUSE ADVANCED REACTORS DIVISION 321

6.1 INTRODUCTION 321

6.2 BASIC SPECIMEN TESTING 321

6.2.1 Uniaxially Loaded Specimen Models with Uniform Gage Section (304 SS, Heat 9T2796) 321

6.2.1.1 Test Piece Description 321

6.2.1.2 Current Results 321

6.2.2 Uniaxially Loaded Specimen Models with Non-Uniform Gage Section 325

6.2.2.1 Test Piece Description 325
6.2.2.2 Current Results 325
6.2.3 Specimens with Welds (304 SS, Heat 9T2796) 325
6.3 TUBULAR SPECIMEN TESTING 330
6.3.1 Test Piece Description 330
6.3.2 Uniaxial Creep Testing (304 SS, Heat 9T2796 ORNL Reference Heat) 333
6.3.3 Multiaxial Creep Testing (304 SS, Heat 9T2796 ORNL Reference Heat) 333
6.4 REFERENCES 333
7. UNIVERSITY OF CINCINNATI 337
7.1 INTRODUCTION 337
7.2 EXPERIMENTAL PROGRAM 338
7.2.1 AISI 316 Stainless Steel 338
7.2.1.1 Effect of Stress Changes on Creep Behavior 338
7.2.1.2 Creep, Tensile and Fatigue Deformation Substructure 343
7.2.1.3 Recovery and Recrystallization Behavior of Cold Worked Rod and Sheet 350
7.2.2 AISI 304 Stainless Steel 351
7.2.2.1 Hot-hardness Correlation with the Tensile Strength at Temperatures Up to 1250°C . . 352
7.2.2.2 Creep, Tensile and Fatigue Deformation Substructure 354
7.2.2.3 Grain Boundary Sliding in 304 Stainless Steel 357
7.2.3 High Nickel Content Alloys 359
7.2.3.1 Tensile and Fatigue Deformation Substructure for Incoloy 800 359
7.3 REFERENCES 365
INDEX 367

SUMMARY

1. AEROJET NUCLEAR COMPANY

Test results are reported for strain fatigue of Type 304/308 stainless steel weldment material tested at 756°K. Weld metal is equivalent or inferior to the base metal depending on orientation with respect to the weld seam. The addition of hold times at 756°K has no effect on the cyclic life of the base metal.

Test results are reported from efforts to improve the mechanical properties of Alloy 718 through modifications of conventional thermal treatments. The data include tensile properties at both ambient and elevated (811°K to 1144°K) temperatures, stress-rupture properties from 1008°K to 1033°K, and room temperature Charpy impact results.

Data are summarized for various conditions resulting from (1) solution annealing at 1311°K or 1367°K, followed by either slow or fast cooling to below 811°K, and (2) subsequent duplex aging at 1033/922°K.

2. ARGONNE NATIONAL LABORATORY

True stress-true strain tensile data have been obtained for AISI Type 304 stainless steel at true axial strain rates of 4×10^{-3}, 4×10^{-4}, and 4×10^{-6} sec^{-1} and temperatures of 482, 538, 593, 649, and 704°C. These data indicate that the true stress at a given strain tends to decrease with an increase in temperature and with a decrease in strain rate. These effects are observed to be more pronounced at the higher temperatures. The engineering tensile strength shows the same trends with temperature and strain rate. The true axial strain to failure and the percent reduction of area are found to be significantly less for all temperatures at the slowest strain rate. The true stress-true strain data could be fit reasonably well over most of the strain range using a modified form of an empirical equation suggested by Stowell. The Hollomon equation was found to be applicable to a smaller strain range, and values for the strength coefficient and strain-hardening exponent in this strain range were obtained.

Crack-propagation studies of SMA Type 304/308 stainless steel weldment indicate the slope of crack-growth rate (da/dN) versus stress-intensity factor range (ΔK) is similar for both as-welded weld metal (Type 308) and as-annealed or subsequently aged (1000 hr at 1100°F) base metal (Type 304). However, at a given ΔK, the da/dN is slightly greater for the weld metal than the base metal. The tests were conducted with single-edge-notch (SEN) specimens under uniaxial tension loading in sawtooth stress wave form at 1100°F temperature, 0.05 stress ratio, and 30 cpm frequency.

3. HANFORD ENGINEERING DEVELOPMENT LABORATORY

A modified microwave extensometer was designed and constructed, and its performance was evaluated in a room temperature tension test and a short creep test at 992°F. Results of the tension test demonstrated that the extensometer has accuracy and sensitivity equivalent to electrical resistance strain gages. With good dimensional stability of the microwave sensor and a room temperature calibration, the error in elevated temperature strain measurement with the extensometer should not exceed about 1%, while the measurement sensitivity is ± 1 microinch per inch. The present work demonstrates that the microwave extensometer has excellent accuracy and sensitivity for the generation of design creep data.

Thermal transient test failure data for prototypic FTR cladding were correlated with failure data from conventional mechanical properties tests. The correlation was developed by the application of a life fraction rule to stress rupture, tensile and tube burst as well as transient test data and constructing a Larson-Miller plot which encompasses the stress and temperature range for all four types of tests. The high degree of correlation between the different types of test data indicates that this approach will be useful in the prediction of failures under hypothetical transient conditions.

Experimental results at 1200°F show that loading to a high stress at beginning of life and immediately unloading to a baseline creep stress (37,500 psi) has no effect on stress-rupture life. High stress loadings without hold times in the baseline mid-life range likewise do not alter stress-rupture life, but the initial baseline creep significantly lowers burst strength during rapid loading. Stress-rupture behavior after loading to a high stress at beginning of life and holding for a creep period before returning to the baseline stress correlates with a life fraction of unity. If high stress creep loadings are imposed in the mid-life range, stress-rupture results correlate with a life fraction of unity for high stress loadings to 50,000 psi. However, high stress creep loadings to 60,000 psi result in life fraction values significantly lower than unity.

The exact stress distribution for a slit tube is determined using the stress-function method for a loading configuration which is convenient for in-reactor testing. The corresponding strain distribution and displacement at the point of loading are derived from the stress-distribution. Simple approximate forms for the stress distribution and displacement are developed for the case of thin-walled tubing. It is found that for the reasonable length of the Type 316 stainless steel cladding which is under consideration, the displacements and loading forces are of readily measurable magnitudes for the desired stress levels of testing. It is therefore concluded that the slit tube configuration is feasible for in-reactor testing.

In support of FTR design confirmation, performance prediction and safety analysis, an FTR in-vessel materials irradiation experiment is

being performed to provide information on the effects of irradiation on structural material mechanical properties. A broad variety of structural and cladding base and weld materials are represented by over 1250 specimens of different types. FFTF prototypic materials included are 304L/308 base and weld metal (core basket), Inconel 600 (reflector), 304/308 base and weld metal (instrument tree and core support structure), 304/308 CRE base and weld metal (reactor vessel), CF-8 (lower core support ring), 316 autogenous weld (absorber pin weld), and 20% cold worked 316 (cladding and ducts). FFTF representative materials included are A286 (bolting material), Inconel 718 base and weld metal (control rod driveline, core basket liners, core restraint, etc.), tungsten and TZM (CLIRA meltdown cup), 20% cold worked 316 wire (fuel pin wrap), and candidate hard-facing materials (duct load pads, CLIRA seals, etc.).

The effect of deformation rate and temperature on the tensile properties of 20% cold worked Type 316 stainless steel cladding has been determined on N-3 lot cladding at strain rates from $\sim 2 \times 10^{-5}$ to 10 in/in/sec and temperatures from 800 to 1600°F. For temperatures to 1000°F tensile strength and ductility are insensitive to strain rate and for temperatures of 1200°F and above ultimate strength and uniform elongation significantly increase with strain rate. The influence of strain rate on the elevated temperature tensile properties of cladding material is very similar to that previously reported for solid specimens.

Tensile and high strain rate testing on three heats of FFTF 28-inch diameter 316H stainless steel primary piping material has been completed. Tests have been performed at temperatures from 72 to 1400°F and strain rates from 3×10^{-5} to 10 in/in/sec. Results of these tests indicate the piping material has excellent strength and ductility and that properties are not greatly influenced by strain rate over the range of this study.

An experimental characterization of the thermal and fast-neutron-irradiation effects on the elevated temperature tensile and creep-rupture properties of a GTA-deposited Type 316 stainless steel has been completed. Irradiation-induced property changes observed in the weld metal are broadly consistent with the trends established for wrought Type 316. However, the extent of irradiation effects clearly depends upon material conditions resulting from welding and heat treating as well as fluence, irradiation temperature and test temperature.

4. NAVAL RESEARCH LABORATORY

The fatigue crack growth behavior of annealed Type 316 stainless steel was investigated at several temperatures from 75 to 1100 F (24 to 593 C) as a function of the stress intensity factor range. It was found that the crack growth rates increased and the fatigue lives decreased with increasing temperature. The temperature dependence of the fatigue crack growth rate could be represented over the entire temperature range investigated by normalizing the ΔK values by the square of the elastic modulus.

The fracture toughness of austenitic stainless steel plate and weld metal is being characterized by means of J-Integral tests. The energy obtained from the load versus deflection record of a J specimen statically tested to failure permits energy-based comparisons to be made in a manner analogous to using the total energy from a Dynamic Tear or Charpy V-notch specimen. On the basis of total energy absorption of J specimens, the toughness of the weld metal was found less than one half of the plate toughness at temperatures up to 1000 F (538 C). This is consistent with previous Dynamic Tear and Charpy-V results. The difference in toughness between weld metal and plate is even greater when the comparison is based on energy to maximum load. Qualitative J-Integral comparisons of plate and weld at the point of crack initiation resulted in a rating similar to that obtained on the basis of total energy absorption.

The notch ductility of four ASTM Type A508 Class 2 forgings has been determined by Drop Weight and Charpy-V test methods. Data comparisons indicate that an arbitrary Charpy-V "energy fix" cannot be used to predict nil-ductility transition temperatures for this type material.

5. OAK RIDGE NATIONAL LABORATORY

The measurement of base-line creep data on the 2-in. (51-mm) plate of type 304 stainless steel reference Heat 9T2796 is continuing. The effect of strain rate on the tensile properties of the reference heat was completed. We varied strain rate over four orders of magnitude and temperature from 25 to 704°C (77 to 1300°F). Yield stress, ultimate engineering tensile stress, and true tensile stress data at maximum load were each fitted by regression analysis to a polynomial equation relating stress and temperature for a given strain rate. The dynamic elastic modulus, dynamic shear modulus, and Poisson's ratio were determined for Heat 346544. By regression analysis each elastic property was fitted to a quadratic equation relating the property to temperature. Above 300°C, the new shear and Young's modulus values agree favorably with the 1971 ASME Code values. Deviations of Poisson's ratio from those values given by the LMFBR Materials Handbook are large but within the standard error of the equation fit.

Additional tests have been completed in the heat-to-heat-variation study of type 304 stainless steel. The short-term tensile properties were determined for a high-nitrogen (0.14%) heat from a 28-in.-OD × 3/8-in.-wall (710 × 9.5 mm) pipe. The yield stress for this heat was higher than normal, but the ultimate tensile test was somewhat lower. For short-term tests at 593°C (1100°F), the stress-rupture and creep behavior of this heat was within the heat-to-heat variation expected from heats without the high nitrogen. The long-term creep tests have run about 14,000 hr. For a stress of 17 ksi (117 MPa) the minimum creep rates of the eight heats vary by two orders of magnitude. The total creep strains at 14,000 hr vary from 0.6 to 2.4%. Each of the

long-term creep tests has been fit with an eight-term polynomial equation. We compared the polynomial constants determined last year for each test at the end of 11,000 hr with those now after 16,000 hr. The constants remained about the same for some heats and changed drastically for others. The difficulties of extrapolation of short-term data are evident. Aging of several of the heats is in progress. Some short-term tensile tests have been completed. Changes in yield stress, ultimate stress, and ductility due to aging depended upon the particular heat.

From our exploratory tests on type 304 stainless steel, we are processing our tensile data to provide the constants associated with several tensile curve representations (i.e., the bilinear, Holloman, Ludwik, Ludwigson, Reed-Hill, and Voce equations). From our preliminary evaluation, the Voce equation is of special interest when representing the entire plastic strain region of the stress-strain curve.

Creep data of type 304 stainless steel have been analyzed on the basis of instantaneous plastic, transient creep, and linear creep components. The instantaneous plastic strain observed during loading of creep tests of the reannealed reference heat of type 304 stainless steel fall well below those given by ASME Code Case 1331. Strain cyclic hardening of the reference heat to yield stress of 17,000 psi (117 MPa) at 593°C (1100°F) result in a large reduction in instantaneous plastic strain on loading of a creep test and in values that compare reasonably with those given in the code case. Minimum creep rate data from the reference heat compare favorably with the average heat represented by the code case except at 649°C (1200°F), where the reference heat is weaker. For the primary creep strain component, we observed a discontinuity in the relationship of the strain with decreasing stress, except for the tests at 538°C (1000°F).

We are continuing our expanding study into failure criteria and strain limits. Several methods for selecting criteria and evaluating strain limits are being evaluated.

A computer-based data storage and retrieval system (DSRS) has been established for creep, tensile, fatigue, stress relaxation, and impact data. The system is operational.

Creep-rupture and tensile data have been obtained for shielded metal-arc and gas tungsten-arc as-deposited 16-8-2 weld metal. The tensile strength properties of longitudinal all-weld-metal specimens compare favorably with type 316 stainless steel base metal except at 649°C (1200°F), where the weld metal is weaker. The creep-rupture strength of all-weld-metal specimens varied greatly but within the range expected for type 316 stainless steel base metal. The time to onset of tertiary creep was short, frequently between one-tenth and one-half the rupture time. The total elongation varied to a lower limit slightly below 10% in the short-term tests. The strain at the onset of tertiary creep was about 2%, a low value, about half of which was associated with primary creep.

Babcock & Wilcox are investigating creep failure under uniaxial and multiaxial conditions. The constant-load uniaxial rupture data are now complete to over 9000 hr. Six step-loaded tests ruptured during this period. Tubular specimens have been fabricated and annealed. Multiaxial tests are in progress.

6. WESTINGHOUSE ADVANCED REACTORS DIVISION

Creep testing of the reference ORNL Type 304 stainless steel heat (9T2796) was continued with a variety of test specimen designs and conditions. Tests were performed on a variety of plate specimens with different loading conditions and testing of welded plate specimens was initiated. Two multiaxial tests of tubular specimens were completed and another two tests of this type were initiated.

7. UNIVERSITY OF CINCINNATI

We are studying the creep properties of Incoloy 800 and types 316 and 304 stainless steel with respect to the substructure as determined by TEM and SEM. Six step-loaded creep tests have been completed on type 316 stainless steel. Three were run with type 304.

The cell or subgrain intercept for tensile, creep, and fatigue has been correlated with the modulus-compensated stress. Substructures from all tests on stainless steels and Incoloy 800 are being studied.

The recovery and recrystallization of cold-worked type 316 stainless steel are under investigation. Hardness measurements at room temperature have been made after 1-hr anneals at 200, 250, 300, 350, 400, 500, 550, 600, 700, 800, 900, and 1050°C (392 to 1922°F).

Hot hardness has been correlated with the tensile strength of type 304L stainless steel.

1. AEROJET NUCLEAR COMPANY

W. C. Francis

1.1 INTRODUCTION

Aerojet Nuclear Company is conducting mechanical properties investigations under two programs sponsored by the AEC Division of Reactor Research and Development. Program 06031, Fatigue Tests on Cladding and Structural Materials, involves experimental fatigue tests on stainless steel Types 304 and 316 as well as Type 304 weldments. These tests are intended to determine the influence of irradiation, cold work, heat treatment, heat-to-heat property variations, and temperature on fatigue behavior. Irradiated, thermal control, as-received, and annealed specimens are being tested at temperatures of 900 to 1300°F (755-977°K). Recent investigations of the creep-fatigue interaction, relaxation, irradiation effects and cumulative damage behavior of Type 304[1,2,3,4], Type 316[4,5,6] and Type 304/308 weldments[2,7] have been previously reported.

Program 06084, Inconel Alloy 718 Code Case Project has as its objective the planning and testing activities deemed necessary to provide data and information on base metal and welded metal properties to safisfy requirements for Code Case approval from the ASME Boiler and Pressure Vessel Committee. The service temperature ranges: ambient to 800°F (700°K) and 800 to 1200°F (700-922°K), are covered in two separate phases of the experimental work, and a separate code case application will be submitted for each temperature range. Data from the literature are used wherever they appear sufficient. Otherwise, experimental programs were initiated to acquire the necessary data. Both base material and weldments are to be covered by the applications.

For Phase I (800°F [700°K] maximum service temperature), the mechanical property tests, apart from material characterization, are related to strain fatigue behavior of the base metal, and weldability and weld qualification studies.

Phase II tests include strain fatigue, strain rate effects, and creep/fatigue interaction, both tensile and compressive, all on base metal.

Creep-rupture sutdies were initiated for weldment material. This program is currently being rescoped; which may change the Phase I and II work described above.

1.2 LOW CYCLE FATIGUE BEHAVIOR OF SMA TYPE 304/308 STAINLESS STEEL WELDMENTS - G. E. Korth and M. D. Harper

1.2.1 Materials

Uniform gage specimens were cut from weldment blocks fabricated from 6.03 cm (2 3/8") thick plate with a double-U weld joint. The base metal was Type 304 stainless steel (Ht. 600414) and the weld metal was Type 308 stainless steel with controlled residual elements. Further documentation of the details of the weldments can be found elsewhere[8]. Since the mechanical properties are different with different orientations and levels within the weldment, specimens were taken from three orientations: transverse, parallel, and transverse fusionline; and two levels: center and surface sections. Figure 1.1 illustrates the relative position of the

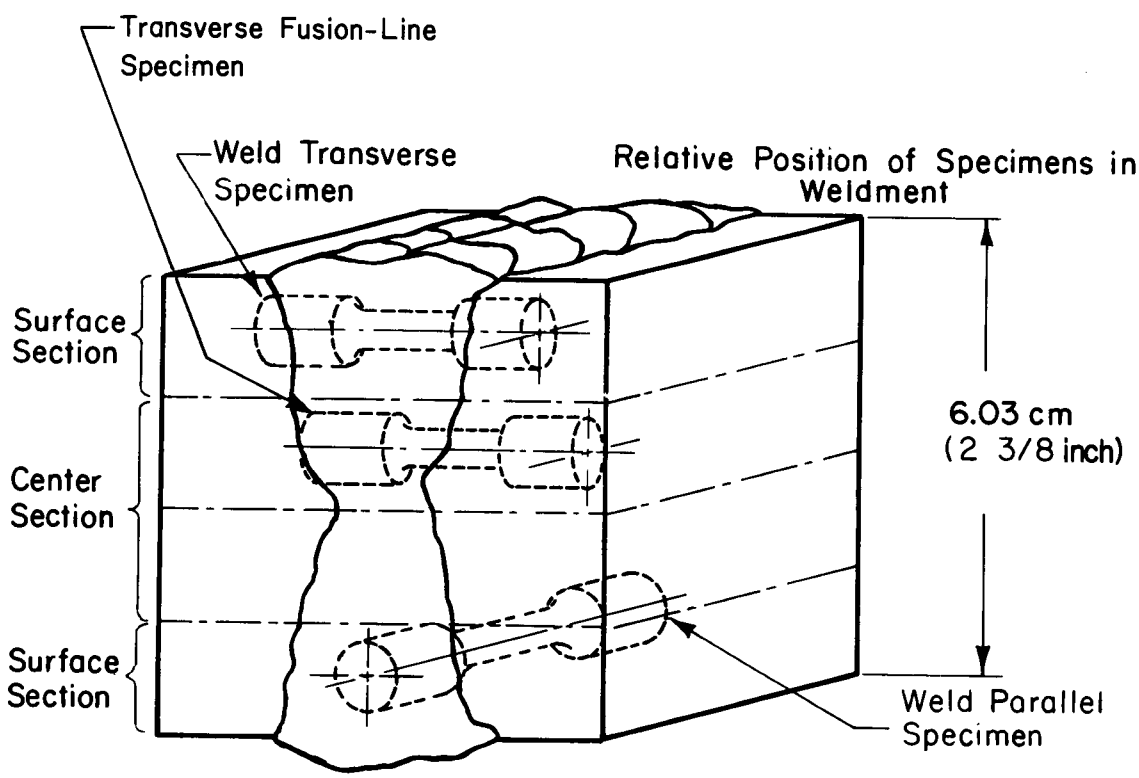

Figure 1.1. Schematic diagram illustrating relative positions of specimens with respect to weldment block.

specimens with respect to the weld seam. The fusion line specimen was fabricated such that the base-weld fusion line was in the center of the gage length. The specimens were tested in the as-welded condition.

1.2.2 Results of 756K Tests

Strain controlled low cycle fatigue tests were conducted on base metal and various orientations of weld metal. Results are shown in Figure 1.2 and Table 1.1. The weld metal is inferior to the base metal except for the parallel orientation which appears about equivalent according to tests run to date. The low strain range weld metal data is somewhat uncertain at this point due to some failures outside the gage length (see Table 1.1). Also previous data[3] showed this same weld metal to be equivalent or superior at room temperature and 867K in the high cycle region (>10^5 cycles) where a crossover was evident.

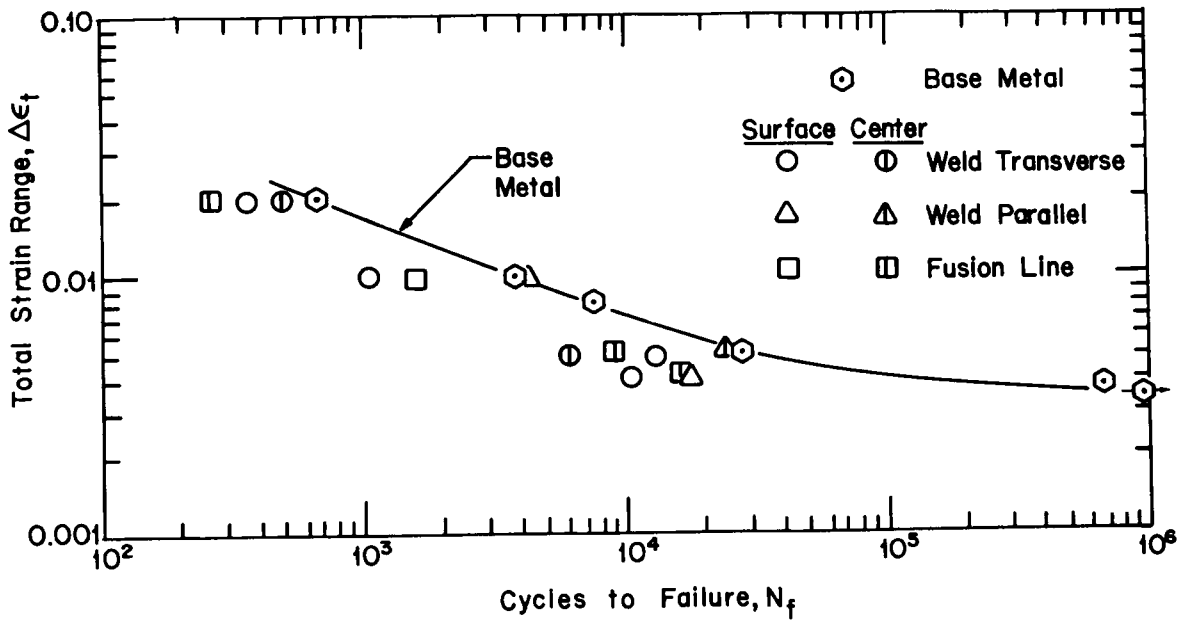

Figure 1.2. Strain fatigue behavior of Type 304/308 weldment material tested at 756K at a strain rate of $4x10^{-3}s^{-1}$

Subsequent test will hopefully resolve this uncertainty. The orientation of the weld metal with respect to the weld seam did have a definite effect on the cyclic life of the material. The transverse and transverse fusion line again showed to be inferior to the parallel

Table 1.1. Strain Fatigue Behavior of Type 304/308 Stainless Steel Weldments Tested[a] at 756 K

Specimen No.	Condition[b]	$\Delta\varepsilon_t$,%	$\Delta\varepsilon_p$,%	$\Delta\sigma$,MPa at 1st Cycle	$\Delta\sigma$,max MPa	Cycle of $\Delta\sigma$ max	$\Delta\sigma$,MPa at $N_f/2$	σ_t,MPa at $N_f/2$	$\Delta\sigma$,MPa ~3/4 N_f	N_f	t_f,h
BT-100	Base, 2a	2.02	1.53	356.5	833.6	137	799.8	384.7	789.4	685	1.85
BT-23	Base, 2a	0.99	0.59	393.0	605.4	370	555.0	281.3	533.0	3,809	5.20
BT-24	Base, 2a	0.79	0.44	398.5	520.6	440	482.6	239.9	464.0	7,662	8.50
BT-25	Base, 2a	0.50	0.21	322.7	-----	---	413.7	208.2	-----	28,176	19.60
BT-28	Base, 2a	0.37	0.03	289.6	582.6	61,500	544.7	251.0	570.9	692,520	381.30
BT-22	Base, 2a	0.33	0.01	-----	-----	---	359.2	164.8	-----	984,324[f]	467.10
WF-42	Weld, 2a,FL-C	1.98	1.46	696.4	833.6	80	830.1	399.2	821.2	262	0.70
WT-58	Weld, 2a,T-S	2.02	1.50	621.9	732.2	42	723.3	367.5	717.0	364	0.98
WT-26	Weld, 2a,T-C	1.98	1.35	639.1	654.3	6	608.1	295.1	601.2	588	1.31
WT-60	Weld, 2a,T-S	1.01	0.57	-----	619.2	160	599.2	293.7	585.4	1,042	1.43
WP-59	Weld, 2a,P-S	0.98	0.50	497.8	538.5	93	482.6	232.3	470.9	4,094	5.60
WF-57	Weld, 2a,FL-S	0.98	0.55	599.8	644.0	50	612.9	313.7	590.9	1,583	2.21
WT-22	Weld, 2a,T-C	0.50	0.12	809.4	809.4	1	522.3	257.2	544.7	6,053	4.14
WT-59	Weld, 2a,T-S	0.49	0.12	500.6	506.1	235	485.4	252.3	480.6	13,195	9.76
WP-79[g]	Weld, 2a,P-C	0.50	0.09	-----	-----	---	508.1	257.2	-----	24,833	16.92
WF-38	Weld, 2a,FL-C	0.51	0.16	601.2	601.2	1	482.6	255.1	499.9	9,020	6.10
WT-56	Weld, 2a,T-S	0.40	0.09	496.4	501.2	167	477.1	243.4	465.4	10,058	5.50
WP-56[g]	Weld, 2a,P-S	0.40	0.07	444.0	460.6	300	446.1	233.7	439.9	17,772	9.71
WF-35[g]	Weld, 2a,FL-C	0.40	0.07	584.0	584.0	1	535.7	239.9	522.6	17,732	9.52
BT-26[c]	Base, 2a	0.98	0.62	-----	-----	---	553.6	273.7/268.9[e]	-----	3,818	43.4
BT-27[d]	Base, 2a	0.98	0.60	-----	-----	---	602.6	297.8/288.9[e]	-----	3,563	353.8

[a] Triangular waveform with strain rate of $4\times10^{-3}\,s^{-1}$

[b] 2=Base metal heat 600414
a=As welded condition
T = Specimen taken transverse to weld seam
P=Specimen taken parallel to weld seam
FL=Transverse specimen across fusion line
S=Taken from section near surface of weldment
C=Taken from section near center of weldment

[c] Tensile hold time of 0.01 hr. on each cycle

[d] Tensile hold time of 0.1 hr. on each cycle

[e] First number is tensile stress at beginning of hold period and second number is tensile stress at end of hold

[f] Did not fail

[g] Failed outside gage length

orientation as has been shown previously at other temperatures[3]. The transverse and fusion line specimens did require higher stress than the parallel specimens for equivalent strains. Even though other investigations[8] have shown that material from the center section of the weldment was harder and the stress values of these tests confirm that, no significant trend of cyclic life is apparent yet between surface and center specimens. At higher temperatures (867K) when tensile hold periods are included in each cycle thereby adding a creep component, then a trend does become apparent with the center section specimens showing longer lives[9].

Since the base material showed the most significant reduction in life at 867K[9] when hold periods were added, two base metal specimens were tested at 756K with 0.01 and 0.1 hour tensile hold periods at 1.0% total strain range. Since no reduction in cyclic life was seen (see Table 1.1) and the stress relaxation during the hold period was very small, it appears that very little, if any, creep damage occurs at this temperature during fatigue cycling.

1.3 INCONEL 718 CODE CASE AND RELATED INVESTIGATIONS - D. D. Keiser W. G. Reuter, G. R. Smolik, and H. L. Brown

1.3.1 Development of a Modified Heat Treatment for Inconel 718

Problems of low and variable weld metal ductility in Inconel 718, coupled with the need for accurate characterization of the susceptibility of this material to strain-age cracking, have led to a program to develop a modified heat treatment which will give the needed improvement in mechanical properties. Concurrently, elevated-temperature stress-rupture data, now inadequate, are being taken. Both base metal and weldment response will be examined.

Specimen nomenclature and thermal treatment details for heat 83C 2E K3 are shown in Table 1.2. The effects of varying cooling rates from two different solution annealing temperatures, combined with a constant duplex aging cycle, were studied. Room temperature tensile test data for this material are reported in Table 1.3. Room temperature impact data appear in Table 1.4. Table 1.5 contains the results of tensile tests at 1033K, and stress-rupture test data at temperatures from 1008K to 1033K are summarized in Table 1.6.

Table 1.2. Specimen Nomenclature and Thermal Treatment Details for Inconel 718 Heat 83C 2E K3

Cycle 1	Sections A, B, C, D, E, F, G, H and *
	Stress relieve at 1255°K
Cycle 2	Sections E, F, G, H, and *
	Solution anneal at 1367°K
Cycle 3	Sections E, F, G, H and *
	Duplex age at 1033 - 922°K
Cycle 4	Sections E, F, G, H and *
	Stress relieve at 1228°K
Cycle 5	Sections A, E, and *
	Solution anneal at 1367°K and cool at 267°K per minute to 811°K
Cycle 6	Sections B, F, and *
	Solution anneal at 1367°K and cool at 311°K per hour to 811°K
Cycle 7	Sections C, G, and *
	Solution anneal at 1311°K and cool at 267°K per min to 811°K
Cycle 8	Sections D, H and *
	Solution anneal at 1311°K and cool at 311°K per hr to 811°K
Cycle 9	Sections AA, BB, CC, DD, EE, FF, GG, and HH
	Duplex age at 1033-922°K

*Includes related double lettered specimens ie. AA, BB, CC, etc.

Table 1.3. Room Temperature Tensile Test Data, Heat 83C 2E K3

Specimen	Treatment Cycles (from Table 1.2)	0.2% Yield Strength MPa	Ultimate Tensile Strength MPa	% Elongation	% Red. In Area
AA-1	1, 5,	1027	1324	20	26
-2	and	1048	1331	20	26
-3	9	1041	1338	19	25
EE-1	1-5	1034	1324	20	23
-2	and	1020	1317	18	24
-3	9	1034	1331	17	23
BB-1	1, 5	883	1289	17	19
-2	and	876	1282	15	20
-3	9	883	1303	17	21
B-4 (not aged)		848	1269	17	22
FF-1	1-4, 6	876	1289	18	22
-2	and	889	1289	17	22
-3	9	910	1303	17	21
CC-1	1,7	1076	1331	15	19
-2	and	1076	1345	15	19
-3	9	1076	1345	16	19
GG-1	1-4, 7	1083	1338	17	19
-2	and	1069	1338	15	20
-3	9	1089	1338	16	20
DD-1	1, 8	862	1248	11	13
-2	and	862	1269	13	17
-3	9	862	1269	16	20
HH-1	1-4, 8	883	1276	14	16
-2	and	896	1276	12	15
-3	9	889	1262	13	15

Table 1.4. Room Temperature Charpy V-Notch Impact Test Data, Heat 83C 2E K3

Specimen	Treatment Cycles (from Table 1.2)	Energy Absorbed Joules	Lateral Deformation Meters x 10^{-2}
AA-20	1, 5	35.3	.038
-21	and	35.3	.038
-22	9	34.6	.036
EE-20	1 - 5	36.6	.041
-21	and	35.3	.041
-22	9	35.3	.041
BB-20	1, 6	31.1	.033
-21	and	30.5	.033
-22	9	30.5	.033
FF-20	1-4, 6	35.3	.043
-21	and	35.3	.041
-22	9	35.9	.038
CC-20	1, 7	23.7	.025
-21	and	23.7	.023
-22	9	24.4	.023
GG-20	1-4, 7	27.1	.028
-21	and	27.1	.036
-22	9	26.4	.033
DD-20	1, 8	23.0	.025
-21	and	27.1	.036
-22	9	22.4	.025
HH-20	1-4, 8	23.0	.025
-21	and	24.4	.025
-22	9	24.4	.025

Table 1.5. 1033°K Tensile Test Data
Heat 83C 2E K3

Specimen	Treatment Cycles (from Table 1.2)	0.2% Yield Strength MPa	Ultimate Tensile Strength MPa	% Elongation	% Reduction in Area
A-4	1,5	638	765	5	7
A-4*	1,5	655	786	8	10
B-4	1,6	640	772	15	14
C-4	1,7	572	637	7	8
D-4	1,8	638	717	23	25
E-4	1-5	696	772	5	11
E-4*	1-5	676	800	7	9
F-4	1-4, 6	648	724	14	13
G-4	1-4, 7	504	554	8	9
H-4	1-4, 8	640	731	11	15

*Duplicate

Table 1.6. 1033°K Stress Rupture Test
Data, Heat 83C 2E K3

Specimen	Treatment Cycles Table 1.2	Stress Level MPa	Temp. Specimen Inserted K	Time; hrs to 1033°K Total		Temp. at Failure °K	Elong. %	Reduction Area %
A-5	1,5	690		0.6 to failure		1017	3	
A-6		621	739	0.5	0.8	1033	4	17
A-7		545	689	0.6	1.9	1033	4	12
A-8		545	728	0.9	2.5	1033	4	12
A-9		483	683	1.2	6.4	1033	5	7
A-10		483	728	1.0	5.5	1033	3	15
A-11		414	644	1.0	24.1	1033	12	20
A-12		414	700	1.4	25.5	1033	10	19
A-13		414	672	1.2	24.9	1033	13	
B-5		610	672	1.1	1.3	1033	19	25
B-6	1,6	545	617	0.6	2.4	1033	20	29
B-7		545	756	0.8	2.4	1033	19	34
B-8		483	700	0.6	8.4	1033	21	30
B-9		483	700	0.7	9.3	1033	14	27
B-10		414	667	1.5	46.9	1033	15	24
B-11		414	589	1.3	14.3	1033	18	25
B-12		414	644	1.1	13.2	1033	18	29
B-13		414	628	1.0	17.4	1033	20	28
B-14		379	617	1.3	39.1	1033	15	27

Table 1.6 Continued

Specimen	Treatment Cycles Table 1.2	Stress Level MPa	Temp. Specimen Inserted K	Time; hrs to 1033°K Total		Temp. at Failure °K	Elong. %	Reduction Area %
C-5	1,7	545	644	0.9	1.7	1033	6	17
C-6		483	756	1.0	9.1	1033	25	29
C-7		483	711	1.2	7.8	1033	17	20
C-8		414	739	0.9	34.1	1033	21	30
C-9		414	689	1.3	20.2	1033	27	36
C-10		414	683	1.2	19.9	1033	16	34
C-11		414	728	1.0	18.7	1033	17	36
C-12		545	672	0.8	1.3	1033	8	12
D-5	1, 8	610	678	0.7	1.1	1033	34	38
D-6		545	633	1.0	2.2	1033	35	41
D-7		545	644	1.1	1.8	1033	30	38
D-8		483	700	2.0	5.2	1033	25	43
D-9		483	756	1.0	4.1	1033	25	43
D-10		414	644	0.9	13.3	1033	24	39
D-11		414	689	1.0	14.4	1033	25	40
D-12		414	617	0.6	16.2	1033	22	40
E-5	1-5	724	575	0.6	0.6	1011	8	14
E-6		545	644	0.9	2.1	1033	3	7
E-7		483	656	0.7	12.4	1033	8	12
E-8		483	617	1.1	10.0	1033	5	9
E-9		414	684	0.4	40.8	1033	10	20
E-10		414	733	0.9	23.6	1033	13	15
E-11		414	767	1.3	14.3	1033	18	17
E-12		414	633	0.7	26.8	1033	13	12
E-13		545	644	0.8	2.4	1033	5	11
F-5	1-4, 6	610	700	1.2	1.4	1033	18	22
F-6		545	672	0.9	2.0	1033	22	27
F-7		545	672	1.1	1.8	1033	17	20
F-8		483	700	0.6	9.3	1033	20	22
F-9		483	617	1.0	5.7	1033	25	27
F-10		414	672	1.0	22.4	1033	14	26
F-11		414	672	1.1	19.9	1033	17	22
F-12		414	672	1.0	22.2	1033	17	27

Table 1.6 Continued

Specimen	Treatment Cycles Table 1.2	Stress Level MPa	Temp. Specimen Inserted °K	Time; hrs to 1033°K Total	Temp. at Failure °K	Elong. %	Reduction Area %
G-5	1-4, 7	610	672	0.9 to fail	1008	9	22
G-6		545	728	0.9 0.9	1033	6	17
G-7		545	644	1.2 to fail	1028	6	18
G-8		483	661	0.6 to fail	1028	1	--
G-9		483	644	0.9 2.7	1033	4	12
G-10		414	739	0.7 23.7	1033	18	27
G-11		414	728	0.7 19.7	1033	17	17
G-13		414	606	1.1 24.5	1033	18	22
G-14		545	717	0.8 to fail	1017	3	--
G-15		483	700	0.9 1.8	1033	2	13
H-5	1-4, 8	610	700	1.0 1.2	1033	18	25
H-6		545	700	0.9 2.7	1033	24	27
H-7		545	728	0.9 2.7	1033	29	27
H-8		483	700	0.6 8.4	1033	25	33
H-9		483	756	0.9 8.1	1033	17	32
H-10		414	617	1.2 16.1	1033	21	29
H-11		414	644	1.0 17.1	1033	18	34
H-12		414	661	0.7 17.9	1033	19	33

Table 1.3 indicates that the fast cooling rate from 1367°K and 1311°K resulted in the better room temperature tensile properties for the particular aging cycle used. The best room temperature tensile properties were obtained by fast cooling from the 1367°K solution treat temperature but there appears to be a slight decrease in values due to the double solution heat treat cycle.

The room temperature Charpy V-notch impact test results in Table 1.4 are not as consistent as the tensile results. For the single solution treated material the fast cool from 1367°K gave higher values, whereas from 1311°K both cooling rates gave similar values. The double solution treated material showed the reverse trend in that the Charpy V-notch results were similar regardless of cooling rate from 1367°K, but the base cool from 1311°K gave the higher values. Little difference exists in the resulting impact properties between the fast cool from 1367°K for a single solution heat treat cycle and the fast cool and slow cool from 1367°K for a double solution heat treat cycle.

Based on Tables 1.3 and 1.4, the best room temperature properties would be obtained by fast cooling from a 1367°K solution heat treat.

The 1033°K tensile test results in Table 1.5 show that the single and double-solution-heat-treated material behaved in a similar manner. The best 1033°K tensile properties resulted from either a 1367°K or 1311°K single solution treat and slow cooling. Enhanced ductility from slow cooling would help reduce failures during fabrication.

The 1033°K rupture life data in Table 1.6 show that slow cooling from 1311°K or 1367°K gave a factor of approximately four greater elongation than did fast cooling from these temperatures.

These data point out that Inconel 718 can be heat treated for the critical condition; e.g., room temperature properties or improved fabricability.

REFERENCES

1. C. R. Brinkman, G. E. Korth, and R. R. Hobbins, *Nucl. Technol.* 16:297-307 (1972).

2. C. R. Brinkman, G. E. Korth, *J. Nucl. Mats.* 48:293-306 (1973).

3. C. R. Brinkman and G. E. Korth, *Heat-to-Heat Variations in the Fatigue and Creep-Fatigue Behavior of AISI Type 304 Stainless Steel, and the Fatigue Behavior of Type 308 Stainless Steel Weld Material*, Aerojet Nuclear Co., ANCR-1097, 1973.

4. C. R. Brinkman, G. E. Korth, and J. M. Beeston, *Comparisons of the Fatigue and Creep-Fatigue Properties of Unirradiated and Irradiated Type 304 and 316 Stainless Steel at 593°C (1100°F)*, Aerojet Nuclear Co., ANCR-1078, 1972.

5. C. R. Brinkman, G. E. Korth, and J. M. Beeston, *ASTM STP-529* (1973) 473-490.

6. C. R. Brinkman and G. E. Korth, "Low Cycle Fatigue and Hold Time Comparisons of Irradiated and Unirradiated Type 316 Stainless Steel," Accepted Nov..1973 for publication in *Met. Trans.*

7. C. R. Brinkman, G. E. Korth, and J. M. Beeston, *Comparison of the Strain-Controlled Low Cycle Fatigue Behavior of Stainless Type 304/308 Weld and Base Material*, International Conference on Creep and Fatigue in Elevated Temperature Applications, ASTM, ASME,Instn. Mech. Engrs, Philadelphia, Pa., Sept. 23-27, 1973 and Sheffield UK April, 1974.

8. R. T. King et. al., *Mechanical Properties Test Data for Structural Materials Quarterly Progress Report for Period Ending Oct. 31, 1973*, ORNL 4936, p 138-152.

9. G. E. Korth and M. D. Harper, *Aerojet Nuclear Co. contribution to the Irradiation Effects on Reactor Structural Materials Semi-Annual Progress Report for Period Ending Jan. 31, 1974*, to be published by HEDL.

2. ARGONNE NATIONAL LABORATORY

R. W. Weeks

2.1 INTRODUCTION

Argonne National Laboratory (ANL) is conducting an extensive program to provide low-cycle, high-temperature fatigue data on Types 304 and 316 stainless steel in support of LMFBR component design, as outlined in the previous report.[1] The present report describes the tensile studies on Type 304 stainless steel conducted in connection with the low-cycle fatigue program and the crack-propagation work on Type 304/308 stainless steel weldments.

2.2 FRACTURE AND FATIGUE STUDIES ON STAINLESS STEELS -- D. R. Diercks, C. F. Cheng, and P. S. Maiya

2.2.1 Elevated-temperature True Stress-True Strain Tensile Behavior of Type 304 Stainless Steel -- D. R. Diercks

A series of true stress-true strain tensile tests on Type 304 stainless steel (U. S. Steel heat 9T2796) has been completed as a part of the previously outlined fatigue program.[2] The tests were conducted at temperatures of 482 (900°F), 538 (1000°F), 593 (1100°F), 649 (1200°F), and 704°C (1300°F) and constant true axial strain rates of 4×10^{-3}, 4×10^{-4}, and 4×10^{-6} sec^{-1}. The tests supplement those of Conway *et al.*[3] on a different heat (Allegheny Ludlum heat 55697) of the same material at temperatures of 21 (70°F), 430 (806°F), 650 (1202°F), and 816°C (1500°F) and strain rates of 4×10^{-3} and 4×10^{-5} sec^{-1}. The hourglass fatigue specimens were tested after solution annealing and aging for 1000 hr at 593°C (1100°F). The tests were conducted on hydraulically actuated, closed-loop fatigue machines modified for tensile testing at a constant true axial strain rate. Equipment modifications and experimental procedures are described in detail elsewhere.[4]

Test results for five test temperatures and true axial strain rates of 4×10^{-3}, 4×10^{-4}, and 4×10^{-6} sec^{-1} are presented in Fig. 2.1. It is immediately apparent that the flow stress at a given strain tends to

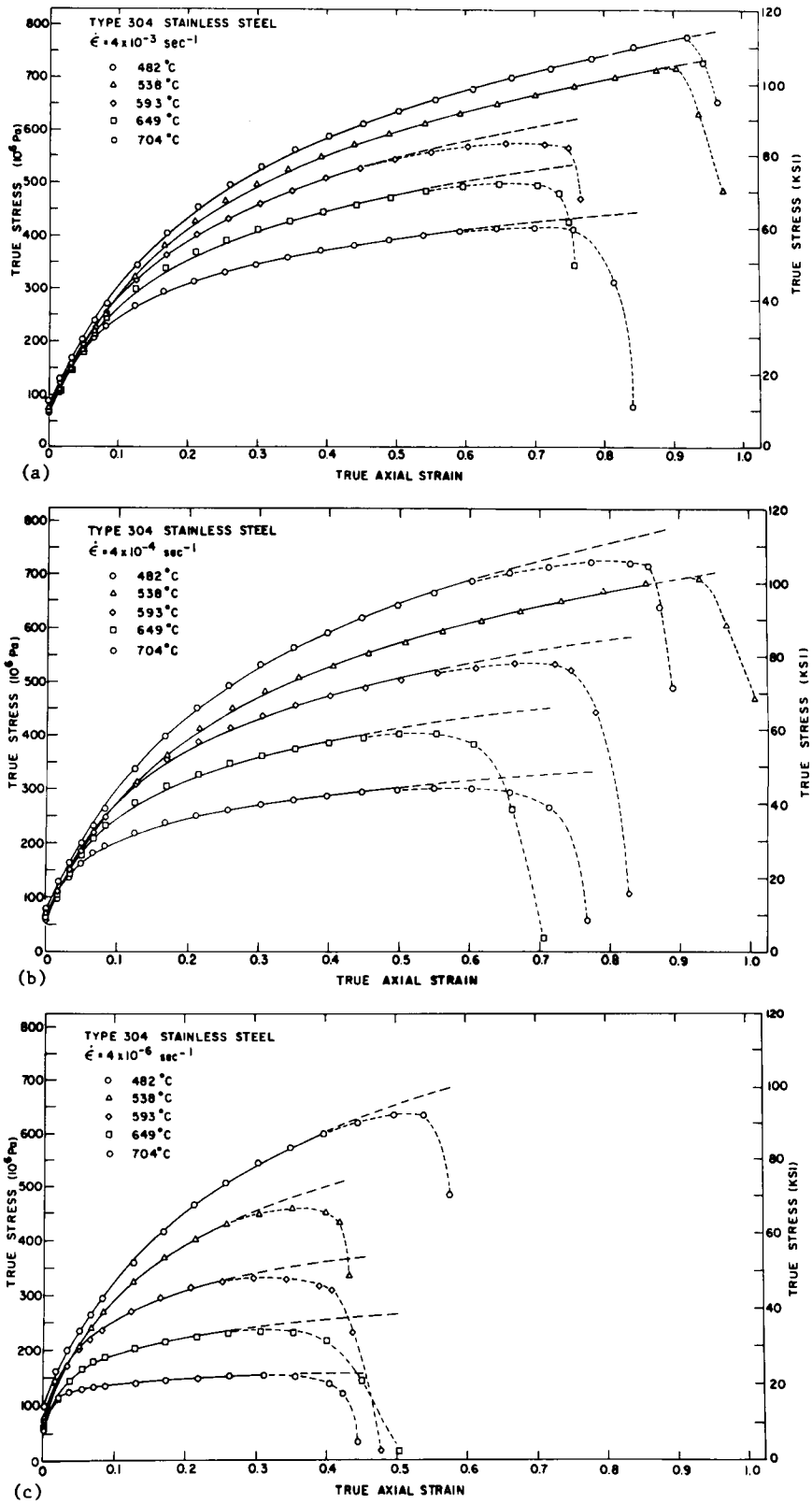

Fig. 2.1. Plots of True Stress vs True Total Axial Strain for Five Test Temperatures and True Total Axial Strain Rates of (a) 4 x 10^{-3} sec^{-1}, (b) 4 x 10^{-4} sec^{-1}, and (c) 4 x 10^{-6} sec^{-1}.

decrease with an increase in temperature and a decrease in strain rate. An exception occurs at 482°C (900°F), for which the 4×10^{-4} sec^{-1} strain-rate curve lies slightly above the 4×10^{-3} sec^{-1} curve. Also, the true axial strain to failure is found to be much less at all temperatures for a strain rate of 4×10^{-6} sec^{-1} than for the higher strain rates. These results are in qualitative agreement with those of Conway et al., who found that the flow stress decreased as the temperature increased and decreased as the strain rate decreased at 650 (1202°F) and 816°C (1500°F). At 430°C (806°F), they found that the tensile curve for a strain rate of 4×10^{-5} sec^{-1} lay above that for a strain rate of 4×10^{-3} sec^{-1}, thus tending to corroborate the behavior observed in the present series of tests at 900°F. However, Conway et al. observed considerably lower values of true axial strain to failure than were seen in the present work. The corresponding values at 649°C (1200°F) and a strain rate of 4×10^{-3} sec^{-1} are 0.56 from Conway et al. and 0.76 from the present work.

The tendency for the true stress to drop off near the end of the test, as seen in Fig. 2.1, was also observed by Conway et al. They suggested that this effect was, at least in part, due to the opening up of internal voids, thus reducing the effective load-carrying cross section at the minimum diameter. Posttest metallography and fractography in the present series of tests tended to verify this hypothesis, and indicated an increasing tendency toward intergranular fracture with increasing temperature and decreasing strain rate.[4]

Attempts were made to fit data from the present series of tests to several phenomenological stress-strain relationships, including the Holloman[5] equation, the Ludwik[6] equation, the Voce[7] equation, and a hyperbolic sine function originally suggested by Stowell[8] and modified by Conway et al. This modified Stowell equation was found to give the best fit, in general, and may be written as

$$\varepsilon = \varepsilon_o + b \sinh (\sigma/\sigma_c), \tag{1}$$

where ε is the true total axial strain, σ is the true stress, and ε_o, b, and σ_c are constants. Since the stress is more commonly expressed as a function of strain, Eq. (1) was solved for the stress to yield

$$\sigma = \sigma_c \log_e \left[\left(\frac{\varepsilon - \varepsilon_o}{b} \right) + \sqrt{\left(\frac{\varepsilon - \varepsilon_o}{b} \right)^2 + 1} \right] . \tag{2}$$

The fit of Eq. (2) to the present data is shown as the solid curves of Fig. 2.1. (The curves are extended as dashed lines beyond the data to which they are fit.) Table 2.1 lists the values of the constants of Eq. (2) used in fitting the tensile curves. These values are found to be consistent with those used by Conway et al. in fitting their data to Eq. (1). The quantity $\overline{\Delta\sigma}$ listed in the table is defined as

$$\overline{\Delta\sigma} = \left[\frac{1}{m} \sum_m (\sigma_{calc} - \sigma_{exp})^2 \right]^{1/2} , \tag{3}$$

where σ_{calc} is the stress calculated from Eq. (2) for a given strain, σ_{exp} is the experimental stress at that strain, and m is the number of data points to which the curve has been fit. The quantity is thus a measure of the departure of the experimental points from the fitted curve and is analogous to the standard deviation for a set of data displaying random scatter.

The Holloman, or power-function, equation relating true stress σ and true axial plastic strain ε_p was also considered because of its relative simplicity and popularity. This equation may be written as

$$\sigma = K\varepsilon_p^n , \tag{4}$$

where K and n are constants known as the strength coefficient and strain-hardening exponent, respectively. However, the present test data, when plotted as log σ versus log ε_p, displayed a flattened S-shape, and so values for K and n that are applicable to the entire strain range cannot be defined. However, values applicable to a significant portion of the range were obtained (see Ref. 4) and are listed in Table 2.1. The strain-hardening exponent generally decreases with an increase in temperature and a decrease in strain rate, as previously noted by Conway et al. The decrease of n with a decrease in strain rate is more pronounced at the higher temperatures.

Table 2.1 Tensile Data for AISI Type 304 Stainless Steel

Temperature, °C	ε_o	b	σ_c,[a] 10^6 Pa	$\overline{\Delta\sigma}$,[a] 10^6 Pa	K,[a,b] 10^6 Pa	n[b]	UTS,[a] 10^6 Pa	% Reduction in Area Extens	% Reduction in Area RT
				$\dot{\varepsilon} = 4 \times 10^{-3}$ sec^{-1}					
482	-0.02583	0.07985	245.9 (35,660)	3.94 (571)	821.9 (119,210)	0.380	394 (57,200)	61.9	62.0
538	-0.01972	0.06989	220.9 (32,040)	4.87 (706)	761.4 (110,430)	0.355	372 (53,900)	62.2	62.3
593	-0.02388	0.06109	192.8 (27,960)	2.35 (341)	705.2 (102,280)	0.362	341 (49,500)	53.4	(c)
649	-0.01565	0.03917	146.2 (21,210)	5.86 (850)	586.5 (85,060)	0.301	304 (44,100)	53.0	(c)
704	-0.01191	0.02030	100.6 (14,590)	3.43 (498)	471.9 (68,440)	0.264	257 (37,300)	56.8	59.4
				$\dot{\varepsilon} = 4 \times 10^{-4}$ sec^{-1}					
482	-0.02668	0.08698	258.9 (37,520)	3.81 (553)	838.1 (121,660)	0.382	400 (58,000)	58.9	60.1
538	-0.02206	0.07369	216.2 (31,360)	4.03 (585)	728.3 (105,630)	0.348	359 (52,100)	63.5	59.6
593	-0.01410	0.04028	157.1 (22,790)	4.99 (724)	630.5 (91,450)	0.310	324 (47,000)	56.3	58.2
649	-0.01319	0.02590	113.1 (16,410)	5.59 (811)	496.8 (72,050)	0.272	270 (39,200)	50.7	48.5
704	-0.009223	0.009984	66.1 (9,580)	4.27 (619)	351.1 (50,930)	0.216	205 (29,800)	53.6	51.6

Table 2.1 Tensile Data for AISI Type 304 Stainless Steel (Contd.)

Temperature, °C	ε_o	b	σ_c,[a] 10^6 Pa	$\overline{\Delta\sigma}$,[a] 10^6 Pa	K,[a,b] 10^6 Pa	n[b]	UTS,[a] 10^6 Pa	% Reduction in Area Extens	% Reduction in Area RT
				$\dot{\varepsilon} = 4 \times 10^{-6}$ sec^{-1}					
482	-0.03462	0.07678	248.3 (36,020)	4.96 (719)	829.6 (120,330)	0.353	407 (59,000)	43.7	43.6
538	-0.02240	0.04471	177.8 (25,790)	3.40 (507)	625.1 (90,670)	0.278	334 (48,500)	35.0	33.6
593	-0.006098	0.008031	78.8 (11,430)	3.99 (578)	352.9 (51,180)	0.212	256 (37,200)	37.9	34.1
649	-0.005237	0.003929	48.3 (7,000)	4.48 (650)	295.4 (42,840)	0.184	183 (26,600)	39.5	34.6
704	-0.0004454	0.00001003	14.1 (2,040)	0.69 (100)	171.2 (24,830)	0.082	126 (18,300)	35.8	(c)

[a]Stress values in psi are given within parentheses.

[b]Note that these values apply only to a limited range of strains (see Ref. 4).

[c]Reliable room-temperature values could not be obtained for these specimens.

Finally, values of engineering ultimate tensile strength (UTS) and percent reduction of area (% RA) are included in Table 2.1. A noteworthy aspect of the UTS values is that they actually tend to increase slightly with a decrease in strain rate at 482°C (900°F), which is in contrast to the behavior at the higher temperatures. However, this increase is probably within the experimental scatter for these data. The reduction of area values given were calculated in two ways. For the extensometer (extens) values, the initial specimen diameters were taken to be those calculated at test temperature, and the final diameters were those indicated by the extensometer at failure. The room-temperature (RT) reductions of area were obtained using room-temperature micrometer measurements of the initial and final average diameters. For a few specimens, reliable room-temperature values of reduction of area could not be obtained because the two pieces of the fractured specimen could not be refit satisfactorily.

Although no experimental values for yield strength are given in the table, it may be seen from Fig. 2.1 that the values lie in the range from about 60 to 90 x 10^6 Pa (9,000 to 13,000 psi) for essentially all of the tests. These values for yield strength are significantly lower than those given by Smith[9] (90-115 x 10^6 Pa or 13,000-16,500 psi) for the same temperature range, whereas the tensile strengths and reductions of area for a strain rate of 4 x 10^{-3} sec^{-1} given in Table 2.1 are in reasonable agreement with those quoted by Smith[9] and Simmons and Van Echo.[10]

The values of UTS and % RA reported in Table 2.1 may be compared with those obtained by McCoy[11] for the same heat of material (2-in. plate) in a series of conventional engineering stress-strain tensile tests at constant engineering axial strain rate. If one compares the present 4 x 10^{-3}, 4 x 10^{-4}, and 4 x 10^{-6} sec^{-1} data to the McCoy 0.4, 0.04, and 0.0004 min^{-1} data, respectively, one finds, in general, good agreement between UTS values. The % RA values reported by McCoy tend to be somewhat greater than those found in the present work at the lower temperatures and somewhat lower at the higher temperatures. It is interesting to note that McCoy's values for the yield strength of the material are in the same range as were observed in the present work and are thus also somewhat lower than the values quoted by Smith[9] and Simmons and Van Echo.[10]

2.2.2 Crack-propagation of SMA Type 304/308 Stainless Steel Weldments -- C. F. Cheng

ANL is studying the crack growth of SMA Type 304/308 stainless steel welded plates with controlled residual elements made by Combustion Engineering to simulate the seam and girth welds of the FFTF vessel. The details of the fabrication and mechanical properties of the welded plates have been reported by ORNL.[12] Weld-metal and base-metal specimens in single-edge-notch (SEN) configuration were machined from the welded plates as shown in Fig. 2.2. The specimen was cycled under uniaxial tension loading in saw-tooth wave form at a constant stress ratio $R(\sigma_{min}/\sigma_{max})$. The crack growth was viewed through a microscope, and the number of cycles was recorded as the crack traversed a series of parallel scribed marks at 50-mil increments from the side-notch. The test was stopped when the crack length attained 500 mils. The actual crack length was subsequently obtained from the crack-front contours at the fracture surface corresponding to the scribed marks. The cross-sectional area of the cracked surface up to the crack front of the fracture surface divided by the thickness of the specimen gives the average crack length. The measurement was made from a Polaroid micrograph (∿10X). Several exploratory experiments were made to sharpen the crack-front contour at the scribed marks, and they are described in Table 2.2.

Table 2.2. Test Conditions

Frequency: 30 cpm Stress Ratio R: 0.05 Temperature: 1100°F

Weld Plates: CE 32, 33, and CE 41 (ORNL Designation)[12]

Test Number	Specimen Number	Specimen Description	Cycling at Scribed Marks	Remarks
2C	CE 32 B1	Base Metal (annealed)	30 cpm	Fig. 2.3, open circles
1C	CE 32 B3		30 cpm	Fig. 2.3, cross circles
4C	CE 32 B5		Stop and restart	Fig. 2.3, slant circles
6C	CE 33 B5	Base Metal 10^3 hr Aged at 1100°F)	1-min tension hold	Fig. 2.4, open circles
7C	CE 33 B1		1 cycle at 0.3 cpm	Fig. 2.4, cross circles
8C	CE 41 W1	Weld Metal (As-welded)	0.1-min tension hold	Fig. 2.5, open circles

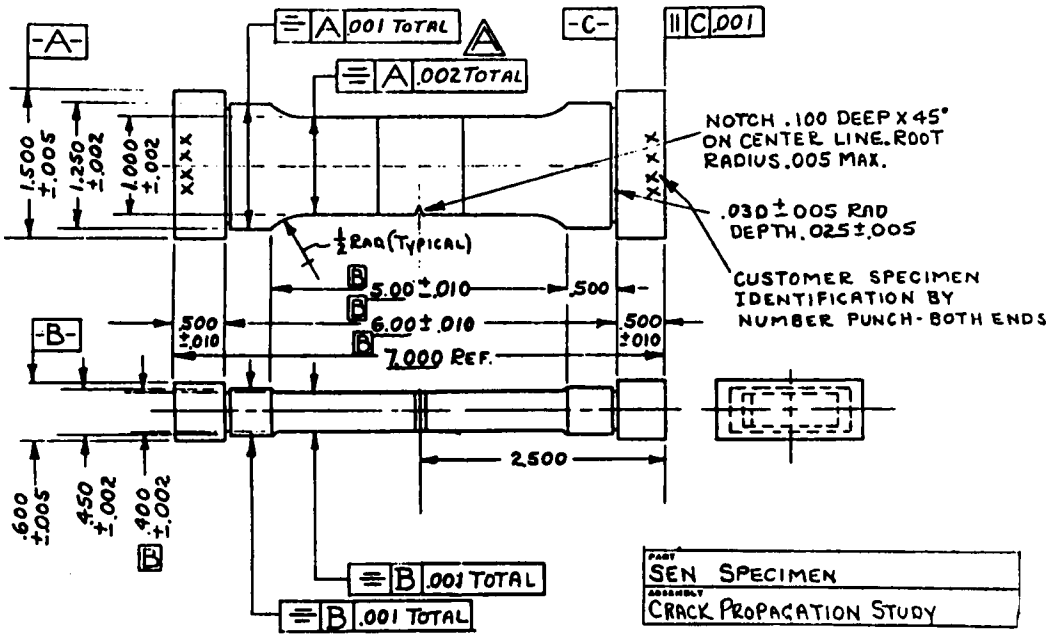

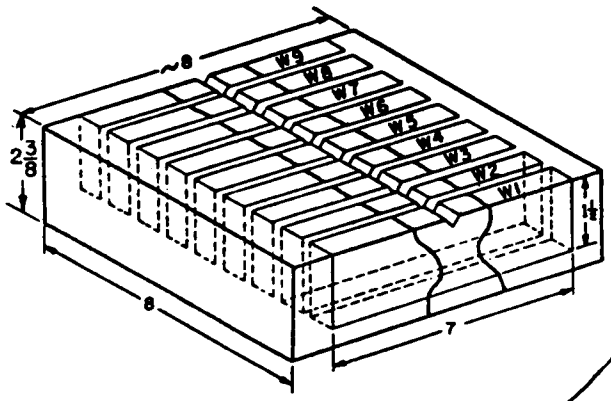

SEN Weld-metal Specimen.

All dimensions in inches.

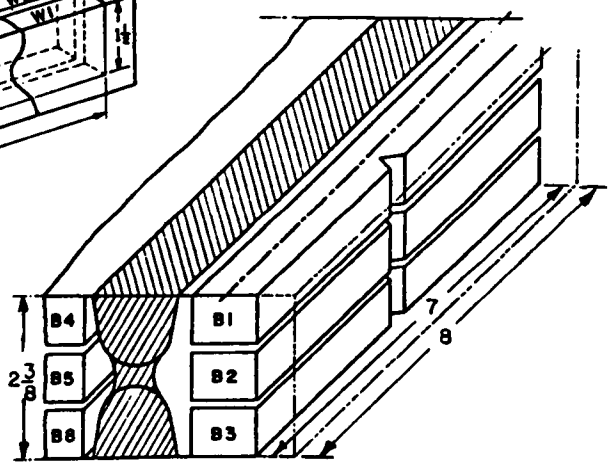

SEN Base-metal Specimen.

Fig. 2.2. Single-edge-notch Specimen.

The crack-growth rate da/dN was calculated for each increment of crack extension, and the stress-intensity factor range ΔK was based on the average crack length for that increment from the expression

$$\Delta K = (\Delta P/BW) \cdot f\ (a/W),$$

where

ΔP = cycling load range,

B = specimen thickness (0.400 in.),

W = specimen width (1.00 in.),

$f(a/W)$ = shape function as given in ASTM STP-410 (1969),

$= [1.99 - 0.41\ (W/a) + 18.70\ (W/a)^2 - 38.48\ (W/a)^3 + 53.85\ (W/a)^4]$.

Analysis of the fatigue crack-growth data was made on the basis of the power law relating da/dN to ΔK, which is expressed as

$$da/dN = C\ (\Delta K)^m,$$

where C and m are constants.

Figs. 2.3, 2.4, and 2.5 are the plots of da/dN versus ΔK for annealed base metal, aged base metal, and as-welded weld metal, respectively. The solid line in Fig. 2.3 represents NRL data[13] for the SEN specimen (2-1/2 in. wide by 1/2 in. thick) cycled at 10 cpm in cantilever bending under zero-to-tension loading. This line agrees with our data for Type 304 annealed base metal. The slope of the aged base metal in Fig. 2.4, is not significantly different from the annealed base metal (dashed line). Similarly, test 6C (Fig. 2.4, open circles) with a 1-min tension hold at each scribed mark behaves the same as the other tests in Figs. 2.3 and 2.4. Test 6C gives a distinctive crack-front contour, as shown in Fig. 2.6. At a given ΔK in Fig. 2.5, the crack-growth rate of as-welded weld metal (Type 308) is slightly greater than the annealed base metal, but slope m is similar. However, in the NRL case,[13] the weld-metal data were rather scattered, and, at a given ΔK, the crack-growth rate is slightly less than the annealed base metal. The discrepancy may be attributed to the different techniques used to measure crack length.

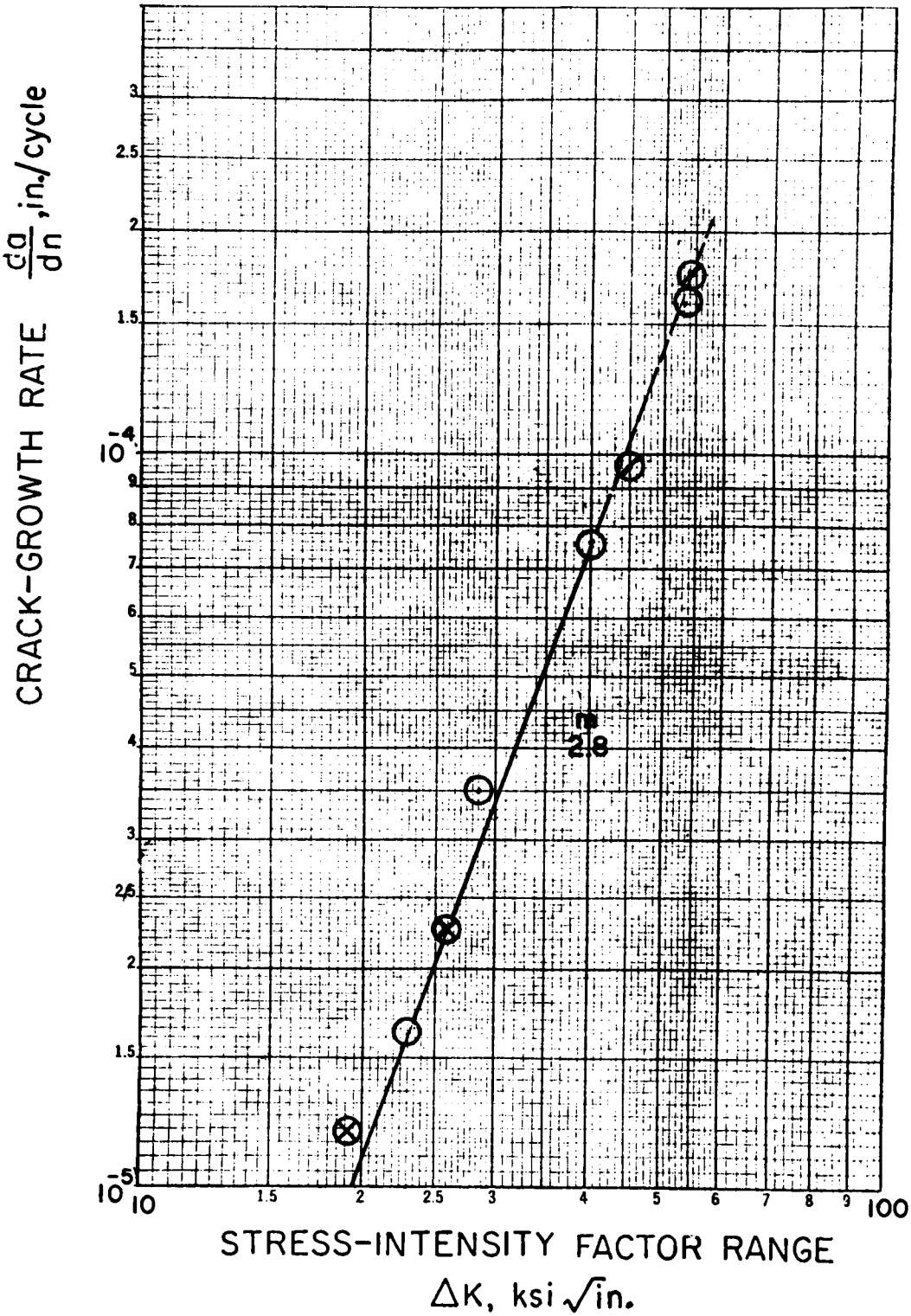

Fig. 2.3. Crack-growth Rate vs Stress-intensity Factor Range at 1100°F in Type 304 Base Metal (annealed). Different symbols represent separate tests. Solid line is NRL data.[13]

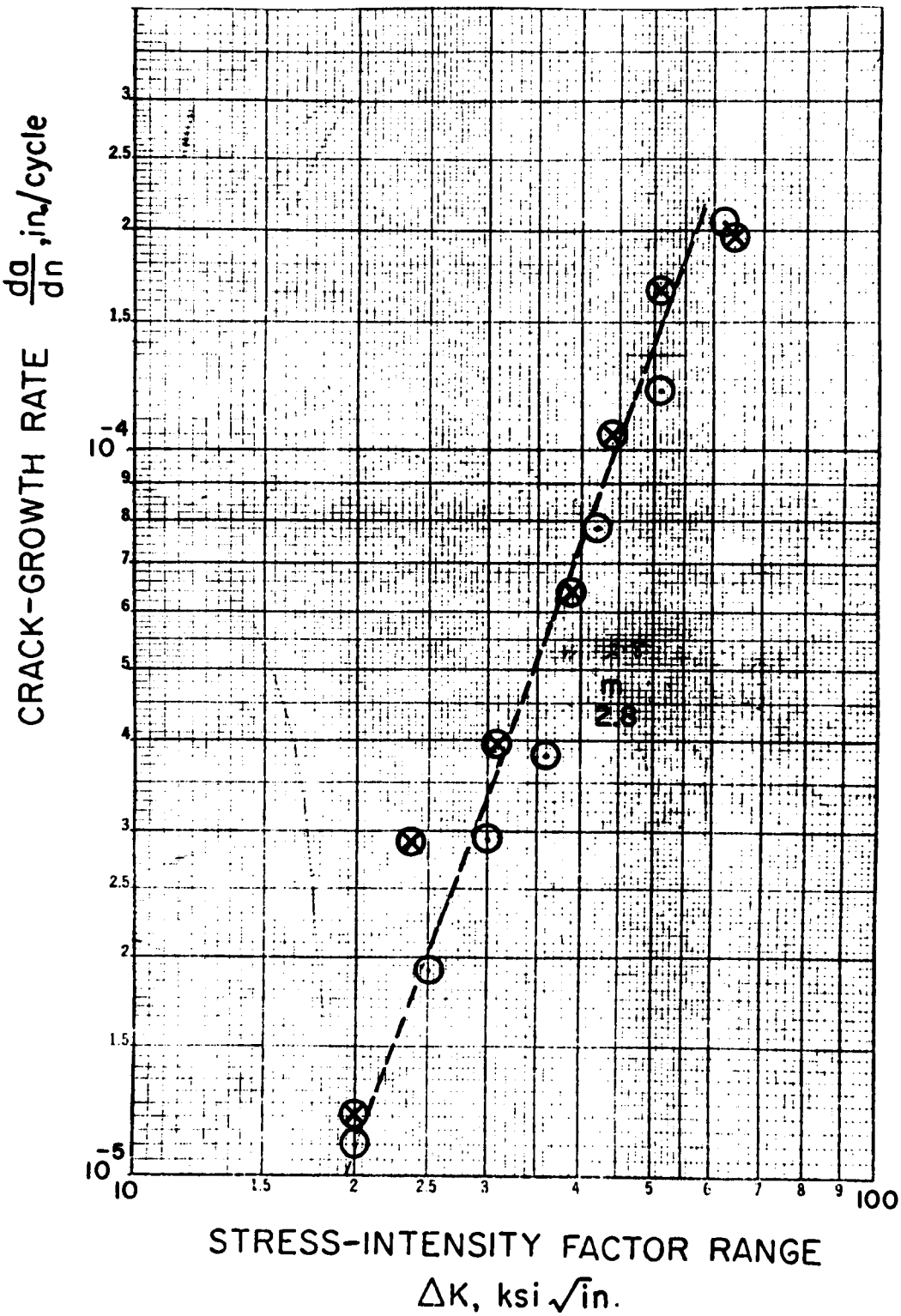

Fig. 2.4. Crack-growth Rate vs Stress-intensity Factor Range at 1100°F in Aged Type 304 Base Metal. Different symbols represent separate tests. Dashed line is annealed data.

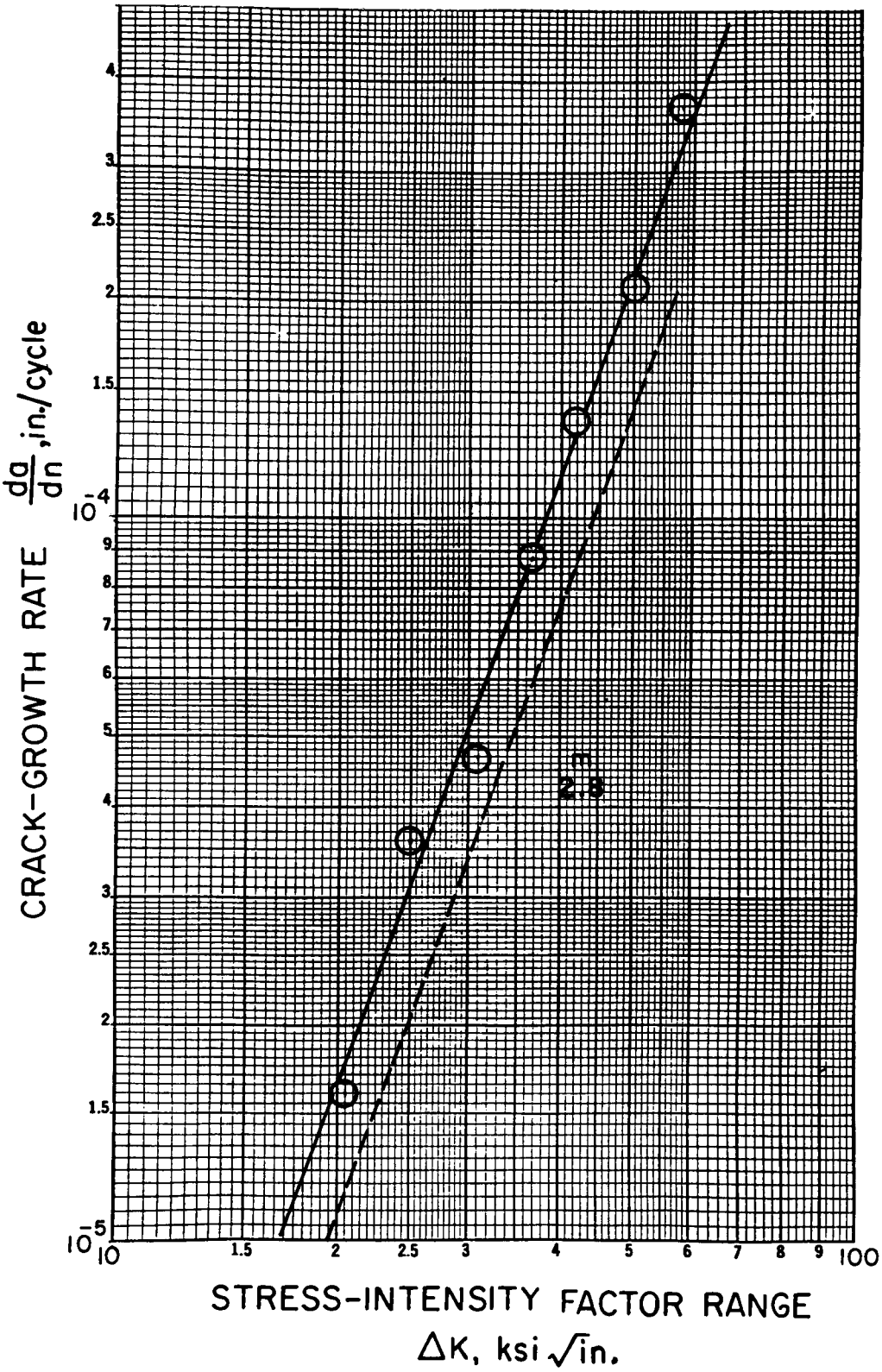

Fig. 2.5. Crack-growth Rate vs Stress-intensity Factor Range at 1100°F in As-welded Type 308 Weld Metal. Dashed line is base metal (annealed).

Typical micrographs of crack-front contours at the fracture surface are shown in Fig. 2.6. The crack-front contour for base metal runs uniformly across the fracture surface; therefore, the crack-length measurement is not expected to be significantly different between the fracture-surface technique used at ANL and the side-edge viewing used at NRL. However, in the case of a nonuniform crack front for the weld metal, the difference in crack-length measurements can be significant. Likewise, Bathias and Pelloux[14] observed a difference in the growth rate between striation-spacing measurement with SEM and macroscopic measurement at the side-edge.

Preliminary observations from the crack-propagation study of SMA Type 304/308 stainless steel weldments indicate that the slope of the growth rate (da/dN) versus stress-intensity factor range (ΔK) at 1100°F is similar for the as-welded weld metal (Type 308) and the as-annealed or subsequently aged base metal (Type 304). At a given ΔK, the weld metal has a slightly higher da/dN than the base metal, whereas da/dN is the same for both the as-annealed and the aged conditions.

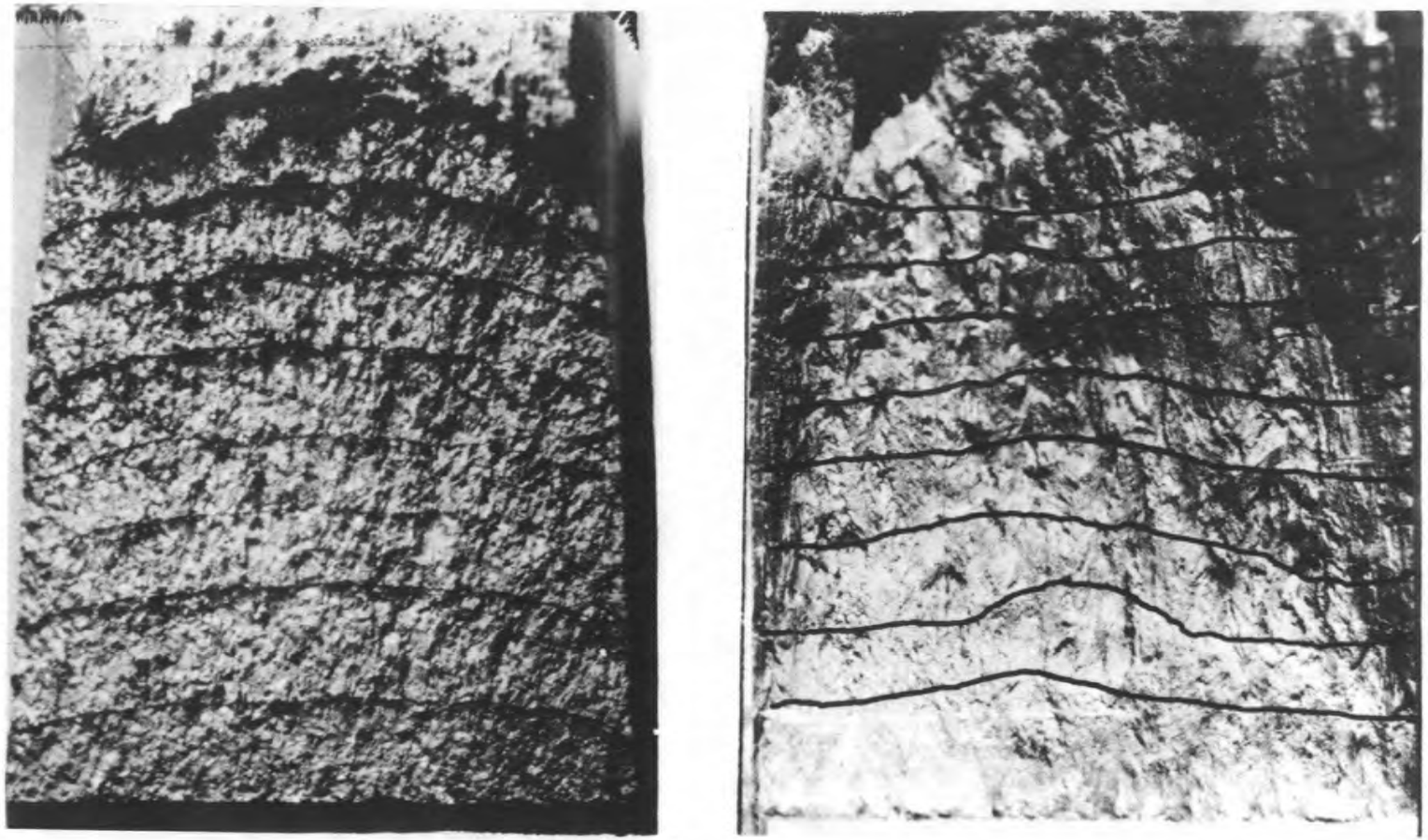

(a) (b)

Fig. 2.6. Crack-front Contour at Fracture Surface. (a) Aged base metal: 1-min tension hold at each 50-mil scribed mark. (b) Weld metal: 0.1-min tension hold at each 50-mil scribed mark. (Contour lines have been darkened by inking.) Mag. 10X. Neg. Nos. MSD-5958(a) and 59597(b).

REFERENCES

1. Mechanical Properties Test Data for Structural Materials Quarterly Progress Report for Period October 31, 1973, ORNL-4936, pp. 15-33.

2. R. W. Weeks, D. R. Diercks, and C. F. Cheng, "ANL Low-cycle Fatigue Studies -- Program, Results, and Analysis," ANL-8009 (Nov 1973).

3. J. B. Conway, J. T. Berling, R. H. Stentz, and D. G. Salyards, "Stress-Strain Behavior of Several Stainless Steels at Elevated Temperatures," General Electric Company Nuclear Systems Programs Report, GEMP 686, 1969.

4. D. R. Diercks and W. F. Burke, "Elevated-Temperature True Stress-True Strain Tensile Behavior of AISI Type 304 Stainless Steel," submitted to 1974 Spring Meeting of the Pressure Vessel and Piping Division of ASME, Miami, Fla., June 24-28, 1974.

5. J. H. Hollomon, "The Effect of Heat Treatment and Carbon Content on the Work Hardening Characteristics of Several Steels," Trans. ASM 32, 123-133 (1944).

6. P. Ludwik, Elemente der Technologischen Mechanik, Springer, Berlin (1909).

7. E. Voce, "A Practical Strain Hardening Function," Metallurgia 51, 219-226 (1955).

8. E. Z. Stowell, "A Study of the Energy Criterion for Fatigue," Nucl. Eng. and Design 3, 32-40 (1966).

9. G. V. Smith, "An Evaluation of the Yield, Tensile, Creep, and Rupture Strengths of Wrought 304, 316, and 347 Stainless Steels at Elevated Temperatures," American Society for Testing and Materials, ASTM DS-5S2 (1969).

10. W. F. Simmons and J. A. Van Echo, "Report on the Elevated-Temperature Properties of Stainless Steels," American Society for Testing and Materials, ASTM DS-5S1 (1965).

11. Mechanical Properties Test Data for Structural Materials Quarterly Progress Report for Period Ending October 31, 1973, ORNL-4936, pp. 88-94.

12. Mechanical Properties Test Data for Structural Materials Quarterly Progress Report for Period Ending October 31, 1973, ORNL-4936, pp. 138-151.

REFERENCES (Contd.)

13. P. Shahinian, H. H. Smith, and J. R. Hawthorne, "Fatigue Crack Propagation in Stainless Steel Weldments at High Temperature," Welding J., Research Supplement, 51, 527S-532S (Nov 1972).

14. C. Bathias and R. M. Pelloux, "Fatigue Crack Propagation in Martensitic and Austenitic Steels," Met. Trans. 4, 1265, (May 1973).

3. HANFORD ENGINEERING DEVELOPMENT LABORATORY

T. T. Claudson

3.1 INTRODUCTION

The objectives of the structural materials investigation conducted at the Hanford Engineering Development Laboratory are to provide control data for the in-reactor and postirradiation tests and to provide direct and timely assistance to FFTF and Demonstration plant structural design and analysis programs. The HEDL efforts involve evaluation of mechanical properties at high strain rates, creep testing and analysis, fatigue crack growth, and tensile tests of such materials as FFTF weldments, vessel and piping, core support structures, reflectors as well as duct and cladding. Those test results and analyses appropriate to the "Structural Materials Quarterly Report" will be reported herein; however those investigations associated with irradiation effects per se will continue to be reported in the "Irradiation Damage to Reactor Structural Materials" Quarterly Report published at HEDL.

3.2 IRRADIATION DAMAGE TO REACTOR METALS - T. T. Claudson and J. J. Holmes

3.2.1 Evaluation of Microwave Extensometer

3.2.1.1 Objective

The objective of this work is the development of a multiple-specimen test machine (MTM) utilizing microwave extensometers for conducting precision, long-term creep tests on stainless steels. Material creep data obtained from such equipment will support the structural design and performance analysis of reactor system components.

3.2.1.2 Accomplishments and Status

3.2.1.2.1 Scope of Work. A new design for the test specimen and microwave extensometer was completed, components were fabricated, and performance was evaluated in a room temperature tension test and an elevated temperature creep test on Type 304 stainless steel. In the tension test, strain

measurements from the microwave extensometer were compared with simultaneous measurements from four electrical resistance strain gages located at the specimen mid-length and equally spaced around the circumference. The purpose of this test was to: (1) demonstrate satisfactory mechanical design of the specimen and extensometer attachment; (2) demonstrate the performance of a dual-sensor microwave extensometer in minimizing effects of specimen bending on strain readings; (3) determine any difference between nominal gage length and actual effective gage length resulting from the method of extensometer attachment; and (4) demonstrate overall extensometer accuracy. The purpose of the creep test was to obtain a basic confirmation of elevated temperature performance.

The tension test was conducted in an Instron machine with manual operation to set and control load. A lever arm creep machine with dead weight loading was used for the creep test. Reading and recording of data from the extensometer and strain gages was done manually. The manufacturer's specifications for the gage factor of the strain gages was ± 1%. Resonant frequency of the microwave sensors was measured to an accuracy of ± 2 parts in 10^7. Direct measurements of specimen gage lengths before and after both tests were made on an optical measuring device to an accuracy of about ± 50 microinches.

3.2.1.2.2 Results. A single gage length specimen was used in these evaluation tests. Small ridges were machined on the reduced section to define the gage length and provide for attachment of the extensometer. Details of specimen design are shown in Figure 3.1. Split extensometer attachment arms, as shown in Figure 3.2, were made with machined grooves to mate with specimen ridges for fixing the extensometer to the specimen. The microwave sensor consists basically of a copper-lined stainless steel cylinder and a stainless steel piston which form a hollow cavity absorbing energy at microwave frequencies. Details of the sensor are shown in Figure 3.3. Two cylinders and two pistons are press fit into the top and bottom extensometer attachment arms, respectively, to form a dual-sensor extensometer.

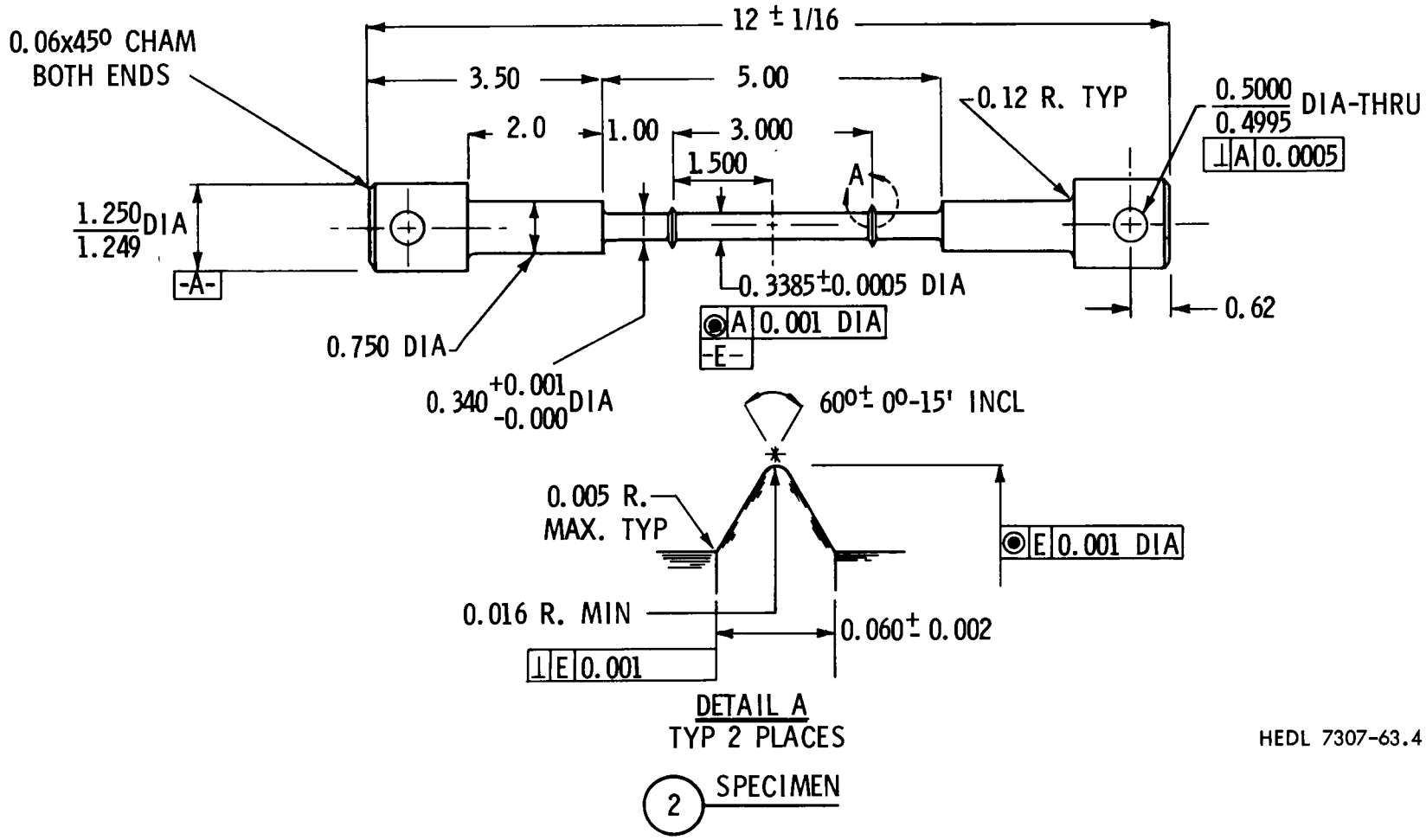

Figure 3.1 Details of Test Specimen.

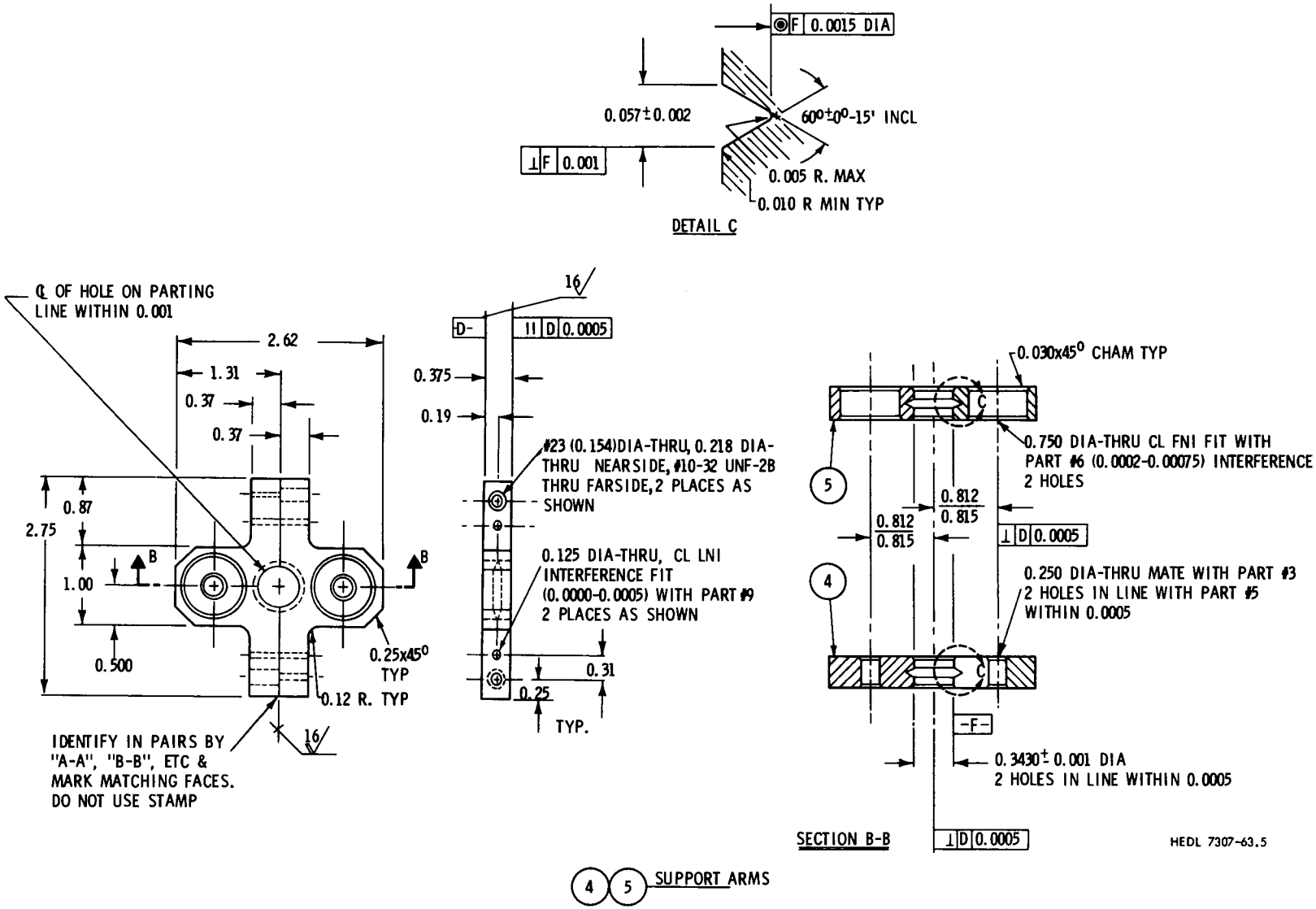

Figure 3.2. Details of Extensometer Attachment Arms.

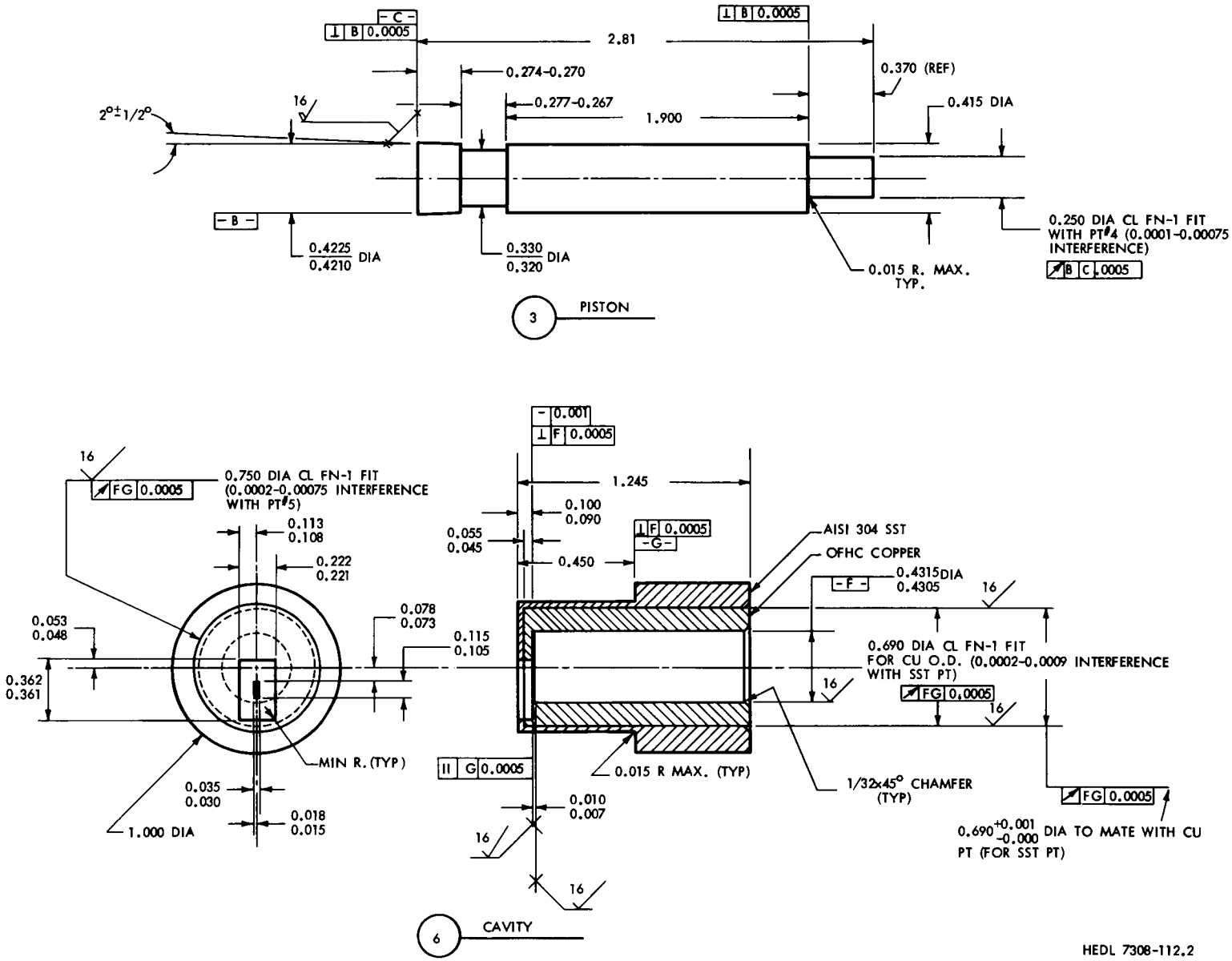

Figure 3.3. Details of Microwave Sensor.

In this application, the hollow cavity (sensor) absorbs incident microwave energy at a multiplicity of frequencies, the values of which depend on cavity size and the mode of excitation. The theoretical relation between resonant frequency, cavity dimensions and mode of excitation is:

$$f = \frac{c}{2} \left[\left(\frac{n}{L}\right)^2 + \left(\frac{U_{l,m}}{\pi R}\right)^2 \right]^{1/2} \tag{3.1}$$

where f is the resonant frequency

c is the speed of light in the medium interior to the cavity

L is the cavity length

R is the cavity radius

l, m, n are mode designators, and

$U_{l,m}$ is the argument for which the Bessel function (or its spatial derivative) equals zero for the chosen mode.

The modes used in this work are TM110 and TE113, yielding the following relations between frequency and dimensions:

$$f_{TM110} = \frac{(5899)(3.832)}{\pi R}, \text{ MHz} \tag{3.2}$$

$$f_{TE113} = 5899 \left[\left(\frac{3}{L}\right)^2 + \left(\frac{1.8411}{\pi R}\right)^2 \right]^{1/2}, \text{ MHz} \tag{3.3}$$

where L and R are in inches. Thus, measurement of f_{TM110} yields the value of R, and then measurement of f_{TE113} yields the value of L, which is the measure of specimen strain. Experimental calibration for the TE113 mode of both sensors used in the extensometer was conducted at room temperature. The accuracy of input piston displacements (i.e., change in sensor length) in these calibrations was about ± 10 microinches. These experimental calibrations showed that the theoretical calibration given by Equation (3.3) was approximately 3% low for displacements up to 0.02 inches. At greater displacements (0.035 to 0.1 inches), the theoretical calibration was about 1.5% low.

Experimental sensor calibrations at elevated temperatures are more difficult to conduct with the same degree of accuracy obtained at ambient temperature. Precise temperature control is required to minimize thermal expansion

length changes over the relatively long linkage connecting the input micrometer outside the furnace to the microwave sensor inside the furnace. Although an elevated temperature calibration was not attempted in the present work, earlier experiments with a third microwave sensor indicated that the theoretical calibration from Equations (3.2) and (3.3) was about 1 to 2% low relative to 1000°F experimental calibration data over a displacement of about 0.007 inches. If theoretical calibrations at 75°F and 994°F are compared for the sensors employed in the present work, using the radius thermal expansion results described later, it is found that length change based on the 994°F theoretical calibration is about 0.65% low relative to the 75°F results. It seems reasonable to expect that this relation would also apply to experimental calibrations, in which case the error introduced by applying room temperature calibration to elevated temperature measurements should not exceed about 1%.

The relations in Equations (3.2) and (3.3) show that the resonant frequency depends on sensor dimensions; and therefore, if microwave sensors are to accurately measure specimen strain, the sensors themselves must exhibit good dimensional stability. During the creep test at 992°F, frequency measurements for the TM110 mode showed a significant decrease in sensor radius, as summarized in Table 3.1. This instability was attributed to a reaction of the copper lining with the gas environment in the test chamber. The creep test was conducted in an argon/8% hydrogen gas mixture to prevent oxidation of the copper lining in the sensor. The copper lining was specified to be OFHC copper, but subsequent inquiry revealed that the vendor actually supplied electrolytic tough pitch copper, a material with high oxygen content. The reaction of hydrogen with the dissolved oxygen to form water vapor within the copper is probably responsible for the dimensional changes in the material. Density measurements on this same copper showed a 2.7% decrease in density after a short exposure to the argon/hydrogen environment at 1000°F, supporting the explanation of the dimensional changes. This problem does not occur with OFHC copper linings. Earlier tests with sensors of OFHC copper showed no significant change in sensor radius after exposure at 1000°F for several hundred hours.

The changes in sensor radius during the creep test force the use of a theoretical calibration (Equation (3.3) for converting TE113 frequencies to

Table 3.1. Change in Radius of Microwave Sensors During Creep Test

Temperature, °F	Time, Hours	Sensor 2 TM110 Frequency, MHz	Sensor 2 Radius, in.	Sensor 4 TM110 Frequency, MHz	Sensor 4 Radius, in.
75	-----	33420	0.215301	33462	0.215031
992	3.37	33164.63	0.216959	33228.88	0.216540
993	44.62	33195	0.216761	33273	0.216252
992	68.70	33219.7	0.216599	33303.8	0.216052
992	92.45	33232.5	0.216516	33323.0	0.215928
993	95.48	33233.8	0.216508	33325.25	0.215913
994	95.78	33233.58	0.216509	33325.78	0.215910
995	98.53	33234.6	0.216502	33327.48	0.215899
996	99.50	33235.05	0.216499	33327.92	0.215896
993	164.62	33263.04	0.216317	33366.99	0.215643
75	-----	33573.3	0.214318	33679	0.213646

length changes. Values of sensor radius required in the calculations were determined from a smooth curve constructed through the data in Table 3.1 plotted as radius against time. As discussed above, the use of a theoretical, rather than experimental, calibration may introduce somewhat larger errors in the strain measurement. In addition, some dimensional changes of the copper lining at the closed end of the cavity may contribute to sensor length changes and introduce a further error in the measured specimen strain.

Thermal expansion behavior of the microwave sensors was measured over the temperature range from 75 to 994°F with the extensometer attached to the creep specimen. Results are summarized in Table 3.2. The calculated mean expansion coefficients for cooling are in good agreement with values for stainless steel[1] and copper[2]. The calculated coefficients on heating are somewhat higher than those on cooling for the length measurements, but are substantially lower than those on cooling for the radius measurements. It is possible that permanent radius decreases of the type observed at 992°F occurred during the relatively long heating period (i.e., approximately 24 hours) and offset some of the thermal expansion. For a volumetric change, as indicated by the density measurements described earlier, it is expected that some permanent increase in thickness of the closed-end copper lining (decrease in apparent length of cavity) should occur, again offsetting part of the length thermal expansion. In fact, the measurements indicate that some other effect which adds to thermal expansion has occurred. Later discussion will show that this additional length increase appears to a real specimen strain, rather than purely a sensor effect.

The results in Table 3.2 also illustrate one attractive feature of the microwave extensometer. For the three-inch specimen gage length, the variation in length measurement with temperature is about 5.5 μ-in/°F. A rod-in-tube extensometer over this same gage length would have a variation of about 30 μ-in/°F. In addition, the microwave extensometer is not subject to thermal expansion errors in extension rods leading from the extensometer to a cold sensor located outside the furnace.

Turning now to the performance of the extensometer system as a unit, the results of the room temperature tensile test, in which strain measured by the extensometer is compared with strain measured by strain gages, are presented

Table 3.2. Thermal Expansion of Microwave Sensors

Sensor	Length or Radius	Heating: Dimension at 75°F, in.	Heating: Dimension at 994°F, in.	Heating: Mean Expansion Coefficient, α, μ-in/in/°F	Cooling: Dimension at 75°F, in.	Cooling: Dimension at 994°F, in.	Cooling: Mean Expansion Coefficient, α, μ-in/in/°F
2	Length	0.541480	0.546929	10.9	0.542988	0.548047	10.1
	Radius	0.215301	0.216964	8.4	0.214318	0.216317	10.1
4	Length	0.534208	0.539384	10.6	0.535054	0.540176	10.4
	Radius	0.215031	0.216552	7.6	0.213646	0.215643	10.2

$$\alpha = \frac{D(994) - D(75)}{D(75)\ [994-75]}$$

in Table 3.3. Graphical comparisons are shown in Figures 3.4 and 3.5. In Table 3.3, the measured frequencies were converted to length change using the experimental calibration data for each sensor. Strain values were computed by dividing average length change by the 3.000-inch gage length. Agreement between strain values measured by strain gages and by the extensometer is generally excellent. At the high loads, the very rapid time-dependent deformation made it difficult to obtain manual readings from either the extensometer or the strain gages rapidly enough for good accuracy. All four strain gages failed in the strain range above 2% (20,000 μ-in/in), so a comparison of strain measurements in the unloaded condition at the end of the test was not possible. When the extensometer was originally mounted on the specimen there was no tendency for attachment arms to rotate or tilt on specimen ridges. After the test, it was observed that the extensometer attachment arms could be rotated or tilted slightly with ease. However, there was no indication that the two halves of an attachment arm would tilt relative to one another thereby leading to gross errors in the averaging capability of the extensometer.

As a further evaluation of extensometer performance, a creep test was conducted at 992°F under a stress of 20,000 psi. No attempt was made to include strain gages or other independent strain measuring instruments in this test. However, preliminary elastic loadings were performed at room temperature to obtain an elastic modulus value based on the microwave extensometer measurements. Results of these loading tests are presented in Table 3.4. Using the experimental calibration data to convert frequency to length changes, these data give an elastic modulus of 28.7×10^6 psi. This value is higher than measured in the tensile test (27.6×10^6 psi), but is in good agreement with the data of Garofalo, et al[3].

Data obtained during loading, constant-load creep, unloading, and zero load recovery at 992°F are presented in Table 3.5. An elastic modulus value can be computed from the strain determined on the basis of either the experimental calibration at room temperature or the theoretical calibration at 992°F, since the change in sensor radius is insignificant during the time of elastic loading. The modulus value based on experimental calibration was 23.2×10^6 psi. This value should be subject to smaller calibration error

Table 3.3. Results of Room Temperature Tension Test on Type 304 Stainless Steel

Load, Pounds	Hold Time, min.	Sensor 4 TE113 Frequency, MHz	Sensor 4 Length Change, μ-in.	Sensor 2 TE113 Frequency, MHz	Sensor 2 Length Change, μ-in.	Strain, μ-in/in Extensometer	Strain, μ-in/in Strain Gages
0	--	36561.23		36260.79			
200	--	36544.63	313	36252.84	154	78	79
400	--	36530.55	578	36241.41	376	159	159
600	--	36517.35	827	36228.89	619	241	240
800	--	36503.45	1088	36217.03	849	323	322
1000	--	36488.95	1361	36205.18	1059	403	403
1100	--	36481.70	1497	36199.48	1169	444	445
1200	--	36473.84	1645	36193.51	1285	488	489
1305	--	36464.69	1818	36187.44	1403	537	536
1500	--	36445.20	2188	36174.63	1651	640	638
1700	--	36424.47	2582	36161.20	1912	749	746
1693	--	36423.28	2605	36159.78	1939	757	755
2000	--	36394.51	3153	36137.12	2375	921	918
2000	6	36391.34	3214	36132.51	2464	946	944
2000	11	36389.32	3252	36130.97	2493	958	955
2300	--	36363.43	3746	36105.70	2979	1121	1113
2300	8	36358.28	3845	36101.47	3061	1151	1149
2300	15	36357.58	3858	36100.11	3088	1158	1157
2700	--	36320.78	4560	36065.68	3753	1386	1386
2700	5	36316.03	4651	36058.65	3889	1423	1423
2700	10	36314.19	4686	36057.23	3916	1434	1432
3200	--	36262.83	5670	36003.45	5000	1778	1772
3200	6	36253.51	5848	35996.61	5133	1830	1820
3600	--	36208.65	6708	35947.86	6083	2132	2126
3600	4	36200.44	6865	35941.70	6203	2178	2172
3200	--	36226.21	6371	35964.24	5764	2023	2011
3200	3	36226.87	6359	35964.97	5750	2018	2011
2700		36259.26	5738	35994.30	5178	1819	1809
2300		36287.51	5197	36018.22	4676	1646	1644
2000		36308.10	4803	36036.12	4327	1522	1518

Table 3.3. (continued)

Load, Pounds	Hold Time, min.	Sensor 4 TE113 Frequency, MHz	Sensor 4 Length Change, μ-in.	Sensor 2 TE113 Frequency, MHz	Sensor 2 Length Change, μ-in.	Strain, μ-in/in Extensometer	Strain, μ-in/in Strain Gages
1700	--	36330.78	4370	36054.69	3965	1389	1389
1300	--	36361.18	3789	36079.50	3486	1213	1211
1000	--	36385.55	3324	36097.80	3132	1076	1076
700	--	36409.44	2868	36117.33	2756	937	936
400	--	36432.74	2425	36139.45	2330	793	793
200	--	36447.61	2142	36155.21	2027	695	695
0	--	36465.98	1793	36171.18	1718	585	587
	16 hr.						
0	--	36470.01	1717	36173.32	1677	566	563
400	--	36443.05	2229	36150.87	2111	723	723
700	--	36419.28	2681	36135.92	2398	847	846
1000	--	36396.83	3109	36119.69	2710	970	971
1300	--	36375.17	3522	36101.33	3064	1098	1097
1700	--	36347.58	4049	36075.77	3558	1268	1268
2000	--	36325.82	4464	36054.80	3963	1405	1403
2700	--	36276.75	5403	36003.38	4965	1728	1726
3600	--	36207.84	6723	35931.10	6374	2183	2183
4000	--	36164.35	7560	35880.12	7373	2489	2491
4500	--	36076.76	9256	35797.02	9015	3045	3047
4500	5	36061.25	9560	35773.23	9488	3175	3169
5000	--	35971.32	11324	35687.06	11203	3755	3759
5000	9	35945.42	11831	35647.61	11995	3971	3962
5500	--	35847.08	13773	35548.03	14036	4635	4643
5500	5	35811.31	14485	35489.09	15260	4958	4935
6000	--	35563.16	19470	35286.60	19392	6477	6814
6000	3	35474.79	21277	35094.00	23832	7518	7444
6000	9	35360.61	23669	35027.17	25325	8166	8175
6300	--						11047
6300	4						15821
6400	3						18815
6400	6						21832
6400	10						23025
0		33704.22	59465	33418.17	60121	19931	-----

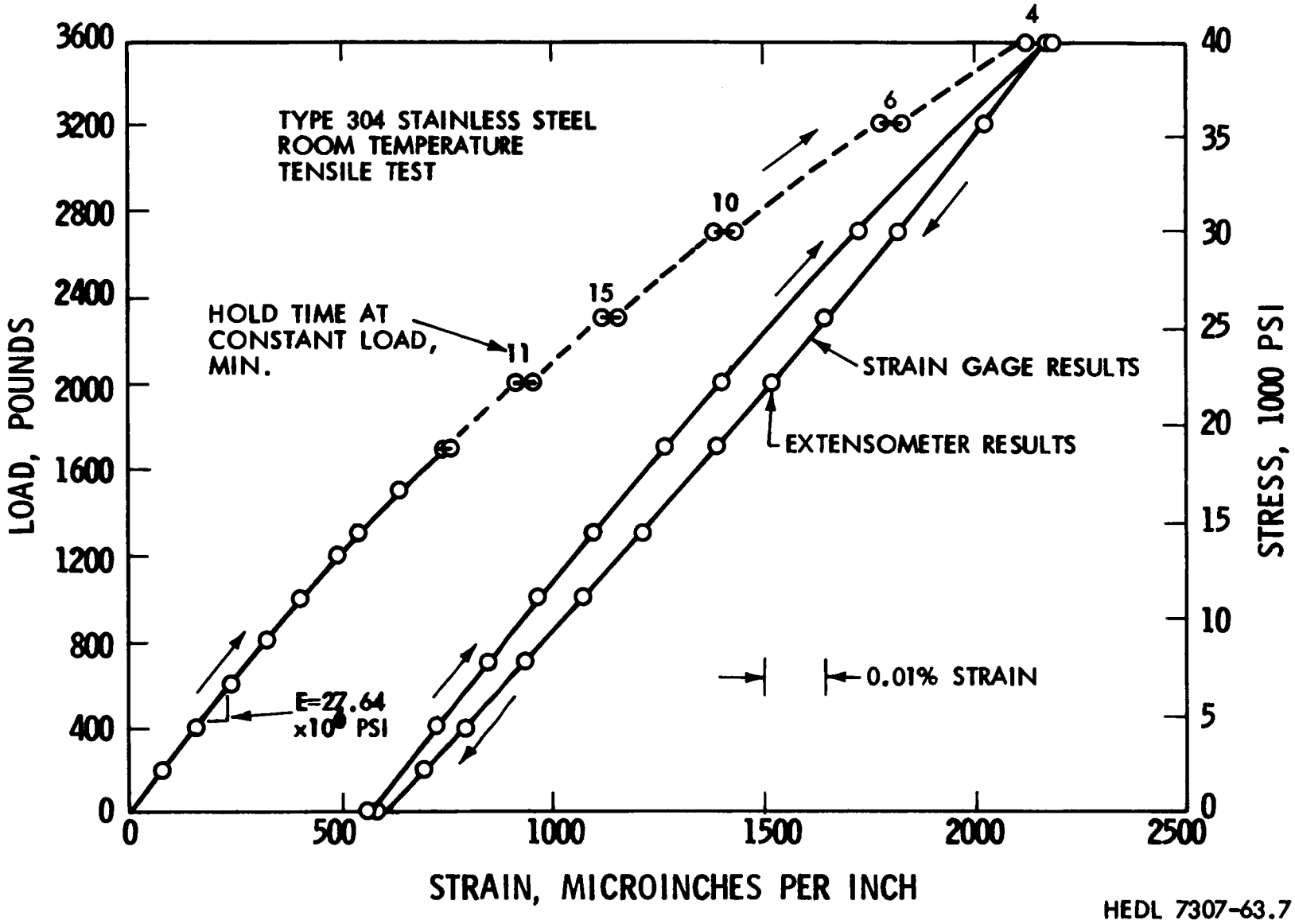

Figure 3.4. Comparison of Extensometer and Strain Gage Measurements in Tension Test.

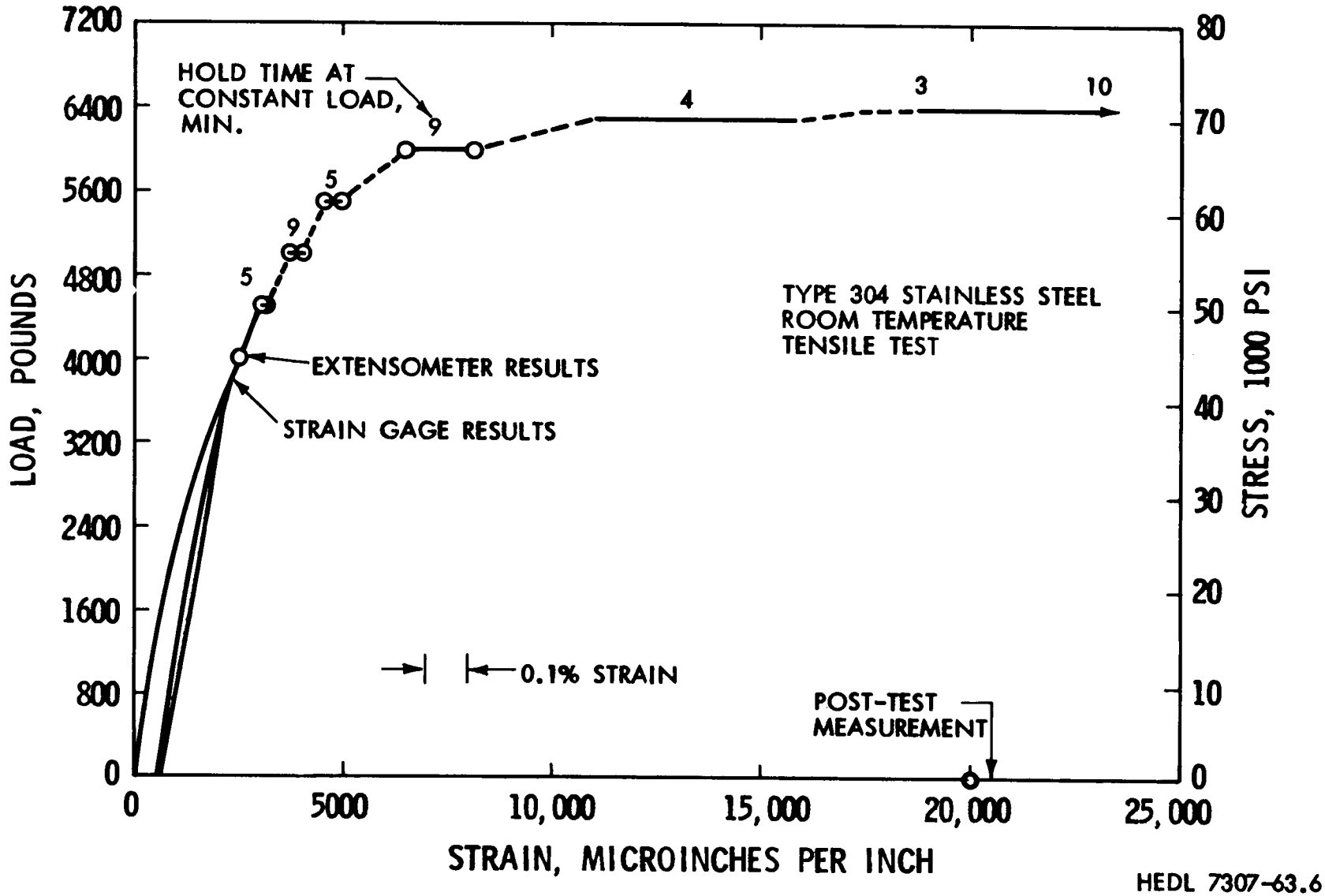

Figure 3.5. Comparison of Extensometer and Strain Gage Measurements in Tension Test.

Table 3.4. Results of Room Temperature Elastic Loading of Creep Test Specimen

Load, Pounds	Sensor 2 TE113 Frequency, MHz	Sensor 2 Length[a] Change, μ-in.	Sensor 4 TE113 Frequency, MHz	Sensor 4 Length[b] Change, μ-in.	Strain, μ-in/in
0	36413.09	0	36823.95	0	0
100	36412.50	11	36813.20	198	35
200	36413.86	-14	36799.43	451	73
0	36414.86	-33	36822.30	30	-1
0	36414.45	0	36822.45	0	0
100	36412.60	35	36813.47	165	34
200	36412.08	45	36801.70	381	71
300	36409.50	94	36791.50	569	111
400	36396.32	341	36791.26	573	153
300	36399.73	277	36799.88	414	116
200	36405.18	175	36807.62	272	75
100	36409.77	88	36815.23	132	37
0	36415.57	-21	36822.31	2	-3
0	36415.57	0	36822.31	0	0
100	36413.75	35	36812.55	180	36
200	36410.96	87	36802.76	360	75
300	36407.44	153	36794.74	507	110
400	36401.21	271	36787.85	634	151
500	36393.66	413	36783.20	719	189
600	36386.57	546	36776.40	844	232
500	36390.40	474	36784.06	703	196
400	36396.70	355	36791.22	572	155
300	36400.90	276	36798.68	435	119
200	36405.07	198	36807.77	269	78
100	36408.80	128	36816.00	116	41
0	36413.96	31	36822.57	- 5	5

[a] Based on sensitivity of 0.05313 MHz/μ-in.

[b] Based on sensitivity of 0.0544 MHz/μ-in.

Table 3.5. Results of Creep Test (992°F; 20,000 psi) on Type 304 Stainless Steel

			Sensor 2			Sensor 4				
Load, Pounds	Time, Hours	Temp., °F	Radius, inches	TE113 Frequency, MHz	Length[a] Change, μ-in.	Radius, inches	TE113 Frequency, MHz	Length[a] Change, μ-in.	Strain,[a] μ-in/in	Strain[b] μ-in/in
0	0.42	994	0.216964	36067.58	0	0.216552	36486.63	0	0	0
100	0.42	994	0.216964	36057.08	198	0.216552	36481.77	89	48	49
200	0.42	994	0.216964	36048.62	357	0.216552	36475.70	200	93	96
300	0.42	994	0.216964	36039.31	533	0.216552	36469.97	305	140	144
400	0.42	994	0.216964	36031.78	675	0.216552	36462.62	440	186	192
500	0.42	993	0.216964	36024.84	806	0.216552	36454.68	585	232	239
400	0.42	993	0.216964	36031.64	678	0.216552	36462.83	436	186	191
300	0.42	993	0.216964	36038.22	553	0.216552	36471.05	285	140	144
200	0.42	993	0.216964	36046.00	407	0.216552	36478.67	146	92	95
100	0.42	992	0.216964	36054.69	242	0.216552	36484.55	38	47	48
0	0.42	992	0.216964	36067.56	0	0.216552	36486.79	-3	0	0
0	0.13	992	0.216964	36067.45	0	0.216552	36487.32	0	0	0
100	0.13	992	0.216964	36057.67	184	0.216552	36482.53	87	45	47
200	0.13	992	0.216964	36048.68	354	0.216552	36476.47	198	92	95
300	0.13	992	0.216964	36040.79	503	0.216552	36469.50	326	138	142
400	0.13	992	0.216964	36033.39	643	0.216552	36461.73	468	185	191
500	0.13	992	0.216964	36026.40	775	0.216552	36453.91	611	231	239
600	0.13	992	0.216964	36018.68	921	0.216552	36446.08	755	279	288
1000	0.13	993	0.216964	35990.49	1454	0.216552	36412.97	1363	470	485
1400	0.13	992	0.216964	35961.41	2006	0.216552	36379.80	1973	663	685
1800	0.00	992	0.216964	35932.00	2565	0.216552	36345.05	2615	863	891
1800	0.05	992	0.216964	35928.75	2627	0.216552	36344.33	2628	876	
1800	0.13	992	0.216964	35927.90	2643	0.216552	36342.77	2657	883	
1800	0.22	992	0.216964	35926.91	2662	0.216551	36341.90	2673	889	
1800	0.30	991	0.216964	35926.29	2674	0.216551	36340.95	2691	894	
1800	0.38	991	0.216964	35926.02	2679	0.216551	36340.48	2700	896	
1800	0.97	990	0.216963	35921.47	2766	0.216499	36335.20	2828	932	
1800	1.38	994	0.216963	35919.12	2811	0.216498	36332.99	2870	947	
1800	1.68	994	0.216962	35918.08	2832	0.216497	36331.74	2894	954	
1800	2.28	994	0.216961	35916.03	2871	0.216494	36330.93	2910	964	
1800	2.87	992	0.216960	35914.91	2893	0.216493	36329.66	2935	971	
1800	3.37	992	0.216959	35913.40	2923	0.216491	36328.12	2964	981	
1800	4.27	992	0.216958	35911.81	2954	0.216487	36326.52	2996	992	

Table 3.5 (continued)

Load, Pounds	Time, Hours	Temp., °F	Sensor 2 Radius, inches	Sensor 2 TE113 Frequency, MHz	Sensor 2 Length Change, μ-in.	Sensor 4 Radius, inches	Sensor 4 TE113 Frequency, MHz	Sensor 4 Length Change, μ-in.	Strain, μ-in/in
1800	20.43	993	0.216919	35892.78	3341	0.216458	36310.18	3316	1110
1800	22.43	993	0.216912	35891.62	3367	0.216446	36309.02	3345	1119
1800	24.28	993	0.216905	35891.03	3383	0.216434	36308.11	3369	1125
1800	26.45	993	0.216896	35890.10	3406	0.216420	36306.11	3415	1137
1800	28.28	994	0.216887	35888.66	3440	0.216406	36305.12	3441	1147
1800	44.60	993	0.216761	35881.43	3656	0.216252	36296.81	3688	1224
1800	48.37	993	0.216713	35879.90	3716	0.216210	36259.30	3742	1243
1800	52.87	994	0.216677	35878.18	3771	0.216167	36293.88	3794	1261
1800	68.62	992	0.216600	35874.37	3892	0.216052	36292.21	3895	1298
1800	72.12	993	0.216586	35873.10	3925	0.216033	36292.10	3909	1306
1800	72.43	993	0.216585	35872.97	3929	0.216030	36291.60	3920	1308
1800	92.23	991	0.216518	35869.81	4031	0.215928	36289.50	4021	1342
1800	95.57	994	0.216508	35868.88	4055	0.215913	36289.34	4033	1348
0	95.67	994	0.216507	36000.10	1555	0.215912	36432.62	1383	490
0	96.15	994	0.216505	36002.08	1518	0.215910	36438.33	1280	466
0	97.18	995	0.216502	36003.98	1484	0.215905	36441.85	1218	450
0	98.45	995	0.216499	36005.54	1456	0.215899	36444.27	1177	439
0	99.53	996	0.216496	36006.92	1432	0.215896	36445.95	1148	430
0	164.55	993	0.216317	36029.35	1118	0.215643	36473.56	792	318
0	Before Creep	75	0.215301	36413.96	0	0.215031	36822.57	0	0
0	After Creep	75	0.214318	36365.10	1508	0.213646	36821.17	846	392

(a) Based on theoretical calibration at 992°F.

(b) Based on experimental calibration at 75°F.

and is in good agreement with the results of Garofalo, et al[3]. The modulus based on theoretical calibration is 24.0 x 10^6 psi, reflecting the observation that theoretical calibration tends to underestimate strain. A graphical presentation of the data for creep, unloading, and recovery (all based on theoretical calibration) is shown in Figure 3.6. The extensometer exhibits excellent resolution in the creep and recovery stages, and the contraction on unloading agrees with the loading extension to within 5 μ-in/in. Extensometer readings at room temperature before and after the creep test show a greater specimen strain than the measurements made at 992°F. Direct length measurements discussed below confirm the room temperature extensometer results, so the additional strain is not attributable to extensometer error. Apparently a small permanent strain occurred during heating to the test temperature under an applied load of only 100 pounds (1111 psi). This strain would account for the larger apparent thermal expansion on heating discussed earlier.

As a further check on the strain measurements obtained with the extensometer, direct length measurements were made on the tension specimen and creep specimen before and after each test. Measurements were made of: (1) the length between fiducial marks scribed on the reduced section inside the ridges, (2) the length between ridges from inside-to-inside, and (3) the length between ridges from outside-to-outside. The average of the latter two measurements is the length between ridges center-to-center, which can be compared to extensometer results. A summary of the results obtained from these direct length measurements is presented in Table 3.6. Strain values determined from direct measurements of the tension test specimen agree with extensometer results to within 2%. In addition, the direct measurements show a dependence of strain on gage length, indicating that constraint around the specimen ridge may be reducing the effective gage length slightly at a strain level of 20,000 μ-in/in (2%). Direct measurements of the creep test specimen also show good agreement with extensometer results, but the measurements are not precise enough to conclude that there is a real reduction in effective gage length at this low strain level.

3.2.1.2.3 Evaluation of Results. The comparison between strain gage and microwave extensometer results in the tension test shows excellent agreement

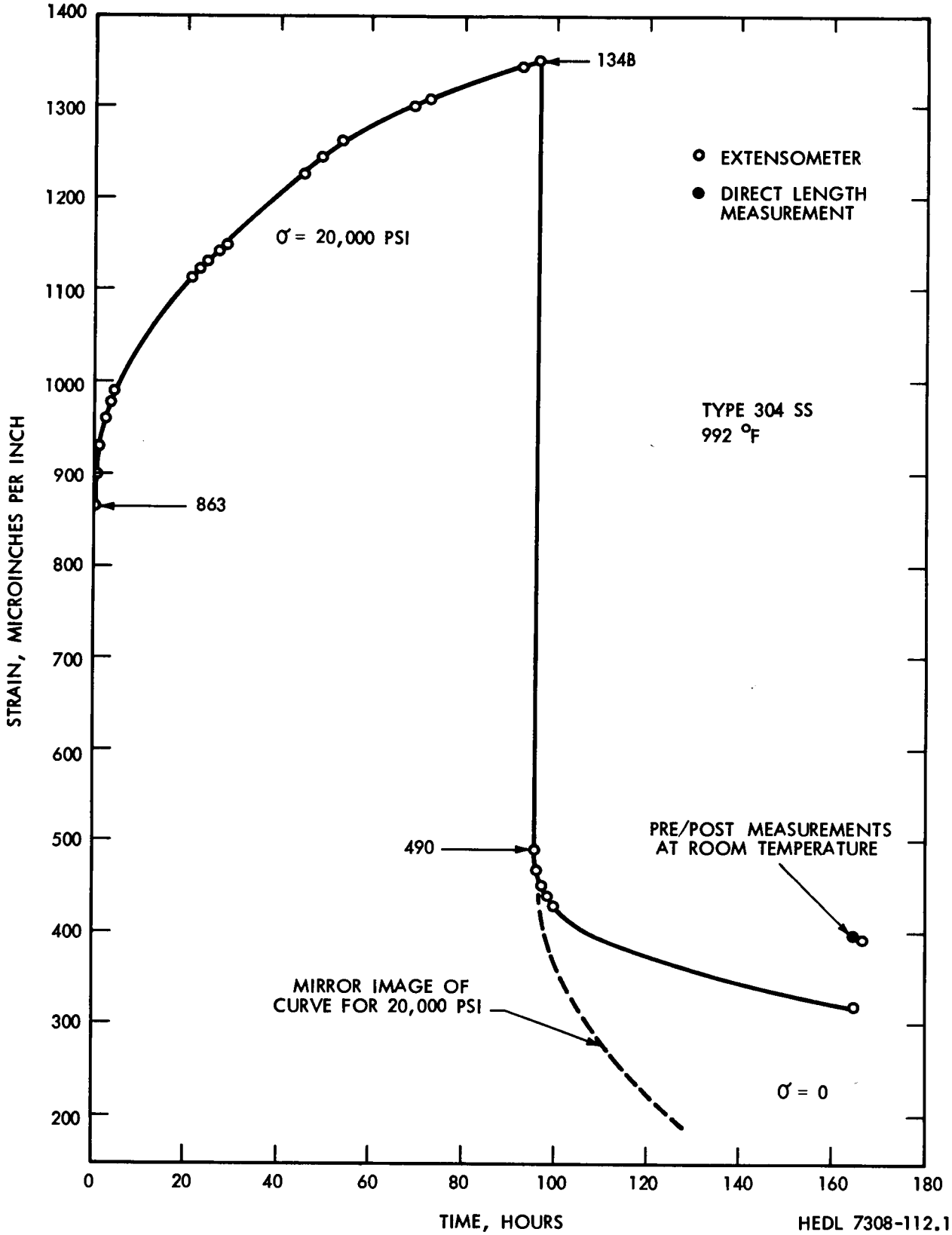

Figure 3.6. Creep Strain Measurements Using Microwave Extensometer.

Table 3.6. Results of Pre/Post Length Measurements of Tension and Creep Test Specimens

	Between Fiducial Marks	Dimension Measurements, inches Between Ridges		
		Inside to Inside	Center to Center*	Outside to Outside
Tension Test:				
Before	2.84595 (2)	2.94508 (2)	3.00452	3.06395 (2)
After	2.90538 (4)	3.00546 (7)	3.0656	3.12574 (7)
ΔL	0.05943	0.06038	0.06108	0.06179
Strain, μ-in/in	20880	20500	20330	20170
Creep Test:				
Before	2.75315 (2)	2.9400 (2)	2.99965	3.0593 (2)
After	2.75465 (2)	2.94125 (2)	3.00085	3.06045 (2)
ΔL	0.0015	0.00125	0.0012	0.00115
Strain, μ- in/in	545	425	400	376

( ) Number of measurements to yield average values shown.

* Computed as average of columns 2 and 4.

between the two methods of strain measurement. The major discrepancy between the two measurements occurs at the 6000 pound load, and may be largely due to difficulty in taking manual readings rapidly enough during the rapid straining. Results from the tension test demonstrate that the calibrated extensometer has accuracy and sensitivity equivalent to resistance strain gages. The test illustrates that the extensometer properly measures strain produced by load increases and constant-load creep, and can detect narrow hysteresis loops during unloading and reloading.

Up to strains of at least 5000 μ-in/in (0.5%), the specimen ridges have no measurable influence on the deformation, as evidenced by the agreement between strain gages and extensometer. However, the post-test measurements indicate that at a strain level of 20,000 μ-in/in (2%) there may be some constraint near the ridges leading to an effective gage length which is slightly smaller (i.e., by about 2%) than the nominal gage length. This difference is not judged to be a significant deficiency in the present specimen and extensometer design.

The sensitivity and resolution of the microwave extensometer in the creep test were excellent. Absolute accuracy is more difficult to assess. The elastic modulus at 992°F based on experimental sensor calibration at room temperature is about 3% lower than the modulus based on the theoretical calibration at 992°F. This difference is similar to that between experimental and theoretical room temperature calibrations. Also, the lower elastic modulus value is in better agreement with published data. These considerations suggest the theoretical calibration may yield strains which are too low by a small amount. The dimensional instability in sensor radius observed during the creep test may also be present to a smaller extent in the length measurements, leading to errors in strain measurement on the low side. However, pre/post measurements at room temperature made with the extensometer are only about 2% lower than direct length measurements. Thus it appears that combined errors from theoretical calibration and dimensional instability are around 2-3%. With good dimensional stability of the sensors and a room temperature calibration, the errors in elevated temperature strain measurement should not exceed 1%.

A study of the data tables shows the averaging of the dual-sensor extensometer is imperative for good accuracy. Errors resulting from the use of a single microwave sensor would be much larger than those reported here.

3.2.1.2.4 Conclusions and/or Recommendations. The present work demonstrates that the microwave extensometer with ridge-and-groove attachment to the test specimen has excellent accuracy and sensitivity for application to the generation of design creep data, especially at low stresses and/or temperatures.

3.2.2 Correlation of Transient Test Results With Conventional Mechanical Properties Data

3.2.2.1 Introduction

Recent studies at HEDL have been concerned with the response of internally pressurized tubes (prototypic FTR cladding) to rapid thermal transients which cover the range of transient conditions being considered for the FTR. In tests performed so far, the internal pressure is maintained constant while the temperature is increased at a constant rate until failure. The heating rates (10°F/sec and 200°F/sec) and other test conditions (constant pressure, constant heating rate) approximate the expected loading conditions of cladding during transients. However, we cannot expect these tests to provide precise simulation of the multitude of conditions and variations that may occur during hypothetical transients that analysts may wish to consider. For example, the temperature may vary in a nonlinear manner and some variation in stress may also be anticipated. It is therefore desirable to develop correlation schemes which allow a limited number of transient test data to be applied to the multitude of transient conditions which may be expected.

High temperature designers have experienced considerable success in using the life fraction technique and Larson-Miller parameter correlations to predict failure after rather complex load-time-temperature histories.

Although this type of correlation is normally applied to structures loaded over rather long periods of time, we have found that it is applicable to the results obtained from our transient tests on unirradiated materials. This has practical significance because it suggests that the correlation may be used to predict failure under transient conditions which do not correspond precisely with our transient test conditions. This report describes the development of the correlation and its application to the prediction of failure under transient conditions.

3.2.2.2 Accomplishments and Status

3.2.2.2.1 Life Fraction Rule and Larson-Miller Parameter. The life fraction rule considered in this work predicts that failure will occur when:

$$\int_0^{t^*} \frac{dt}{t_r(\sigma,T)} = 1 \qquad (3.4)$$

where t^* is the failure time and t_r is the stress-rupture life of material subjected to the engineering stress σ at temperature T. There is, of course, no fundamental reason that such a criterion should work, but high temperature design experience indicates that reasonable correlations are often obtained. The stress-rupture life is conventionally obtained from stress-rupture or creep test data and it is often found that the temperature and stress dependence of the rupture life may be adequately represented by a plot of log σ vs. Larson-Miller parameter (LMP) given by:

$$LMP = T\,[\log t_r + C] \qquad (3.5)$$

T = absolute temperature, °Rankine

t_r = time to rupture, hours

C = constant usually on the order of 20.

Since the transient tests were conducted over a much wider stress range than the available stress-rupture data, we found it necessary to deviate from conventional correlation procedures in two ways: (1) we used results from standard tensile tests and burst tests (in addition to stress-rupture tests) in order to obtain data at higher stress ranges, and (2) the stress values

used were modified to account for the variation in elastic modulus with temperature.

The necessity of including the modulus correction may be seen by considering the schematic stress-rupture plot in Figure 3.7a and the strain rate dependence of the UTS shown in Figure 3.7b. Figure 3.7b may be divided into two regions: a region of thermally activated flow, in which the UTS varies with strain rate, and an athermal region in which the UTS is essentially independent of strain rate. In the athermal region, the UTS is not governed by thermally activated processes, but it is temperature dependent and has approximately the same temperature dependence as the elastic modulus. Since the athermal UTS is insensitive to strain rate, it represents the maximum stress that can be applied to a specimen. Consequently, the "athermal" failure stress can be represented by the horizontal line in the stress rupture plot (Figure 3.7a). Figure 3.7c is a schematic representation of a Larson-Miller plot of the stress-rupture behavior in Figure 3.7a, demonstrating how the stress-rupture data at difference temperatures has been condensed to one curve. But the "athermal" failure lines were not condensed to a single plot in Figure 3.7c, since the Larson-Miller parameter involves only the temperature and rupture time. However, a universal plot can be obtained if the temperature dependence of the "athermal" region is taken into account using σ/E (where E is the elastic modulus), as the stress variable rather than σ, as shown in Figure 3.7d. The optimum correlation for the two different stress parameters would of course require slightly different values for the constant C in the LMP, but major differences are not expected since the temperature dependence of the modulus is weak in comparison with the temperature dependence of the rupture life. In the present work, the following modified stress parameter was used:

$$\sigma_m = \sigma_T \frac{E_{1400}}{E_T} \tag{3.6}$$

where σ_T = stress at temperature T

E_{1400} = modulus at 1400°F

E_T = modulus at temperature T.

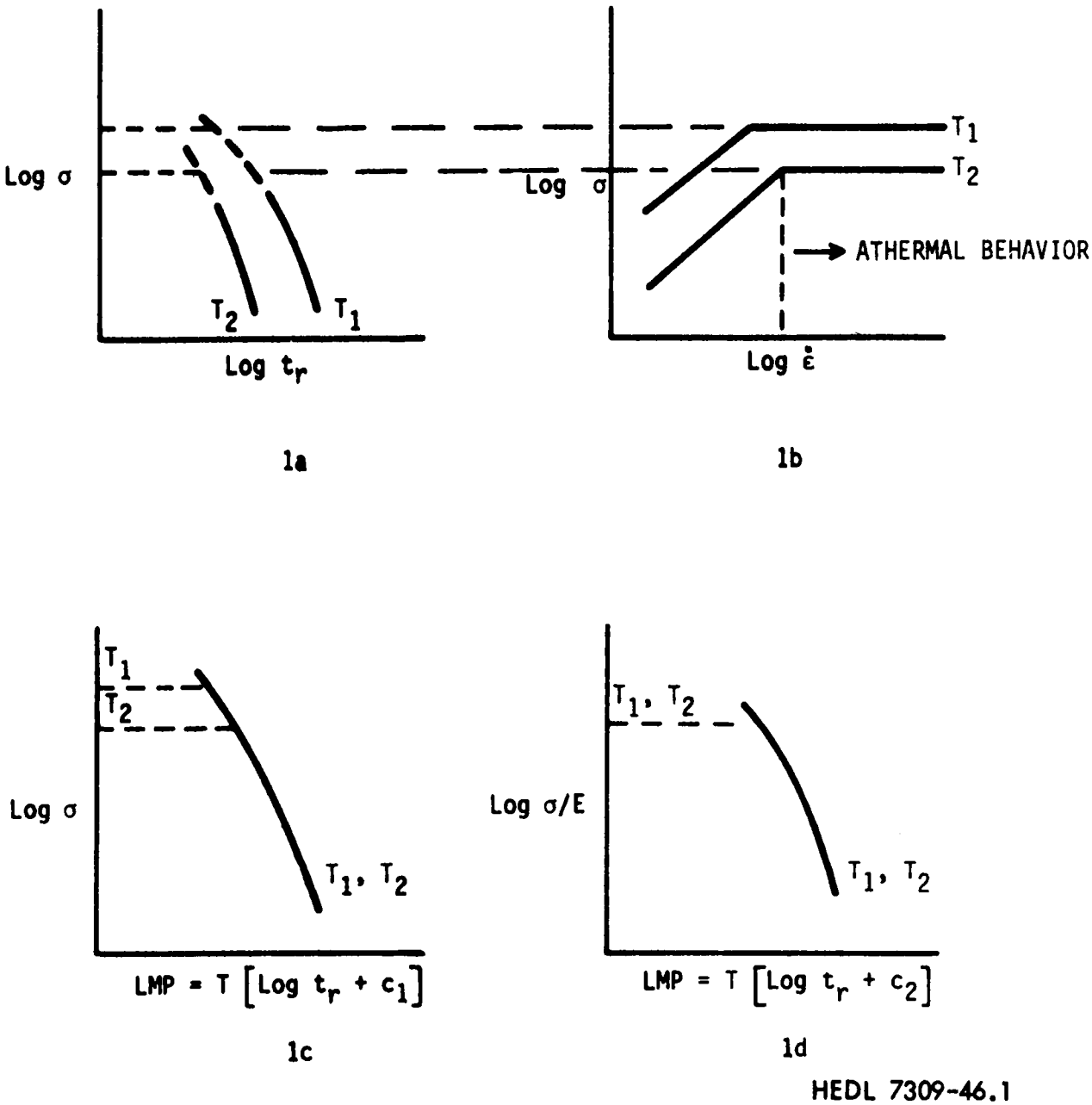

Figure 3.7. Schematic Representation of Various Ways to Represent Stress-Rupture Data.

The constant, C, in the LMP was arbitrarily taken to be equal to 20. Although it will be seen that this value provides a reasonable correlation of the test data, it is expected that the correlation can be improved by adjusting this parameter.

3.2.2.2.2 Evaluation of LMP Values. Stress-rupture[4], burst[4], tensile, and thermal transient[5] strength data have been used to determine the LMP over a wide stress range. All data were obtained from tests performed on 20% cold worked Type 316 stainless steel (N-lot) cladding. The stress-rupture tests[4] were formed by pressurizing tubular specimens to a predetermined level and maintaining a constant temperature and pressure until rupture. The stress at the inside surface of the cladding was calculated using the thick-walled formula for a pressurized tube:

$$\sigma = P\,[(b^2+a^2)\,/\,(b^2-a^2)] \tag{3.7}$$

where P = internal pressure, psi

a = inside radius

b = outside radius.

The LMP values were calculated from the rupture lives and Equation (3.5).

An estimate of LMP values from burst test data required consideration of how the tests were performed. The tubular specimens were heated to a predetermined temperature which was maintained constant throughout the test. The specimens were then pressurized with an approximately linear pressure ramp until rupture occurred. Thus, the load-time character of a burst test is not similar to that of a stress-rupture test. However, the test may be used to estimate LMP values if the time to rupture is modified to reflect an integration of the stress vs. time curve to the point of rupture. That is, we assume that failure occurs when Equation (3.4) is satisfied. For a particular temperature the stress-rupture curve may be approximated by:

$$t_r(\sigma) = a\sigma^b \tag{3.8}$$

where a and b are constants. Also, we may approximate the pressure ramp by:

$$\sigma(t) = \dot{\sigma}t \tag{3.9}$$

where $\dot{\sigma}$ = pressure ramp rate (assumed constant) and t = test time.

Substituting Equations (3.8) and (3.9) into Equation (3.4) and integrating yields:

$$\sigma^{*(1-b)} = (1-b)a\dot{\sigma} \tag{3.10}$$

where σ^* is the stress attained at failure (burst stress). The rupture time for that stress is:

$$t_r(\sigma^*) = a\sigma^{*b} \tag{3.11}$$

Equations (3.10) and (3.11) may be combined to obtain:

$$t_r(\sigma^*) = \frac{\sigma^*}{\dot{\sigma}\ (1-b)} = \frac{t^*}{(1-b)} \tag{3.12}$$

where t^* is the test time to rupture.

The LMP value for a particular burst stress, σ^* was therefore obtained by using the rupture life calculated from Equation (3.12). The slope, b, used in modifying the actual test time to rupture was determined by using the stress-rupture data trend line at the corresponding burst stress level. At the lower LMP levels ($< 3.2 \times 10^4$, Figure 3.8) the slope of the log σ vs. log t_r trend line was considered negligible; therefore, no modification was applied to the test time to rupture below that LMP level. The burst stress level is calculated using Equation (3.7) and the modulus correction was applied, Equation (3.6), for correlation purposes.

The tensile test results used in this correlation study were generated by heating the tubular specimen to a predetermined temperature and applying a constant strain rate in a uniaxial mode until failure occurs. The load on the specimen increases relatively fast and for most of the test maintains a relatively high level, thus duplicating in an approximate manner the load-temperature-time character of the stress-rupture test. The total elongation for each test was divided by the strain rate to provide a value for time to rupture in calculating the LMP. The ultimate tensile strength was used as the stress level against which to correlate the LMP.

Plastic stability considerations, as explained in the Appendix, were used to make stress state corrections on UTS data obtained in the high strain rate (athermal) region. The correction applied is given by:

$$BS/UTS = \frac{2}{(\sqrt{3})^{(\varepsilon+1)}}$$

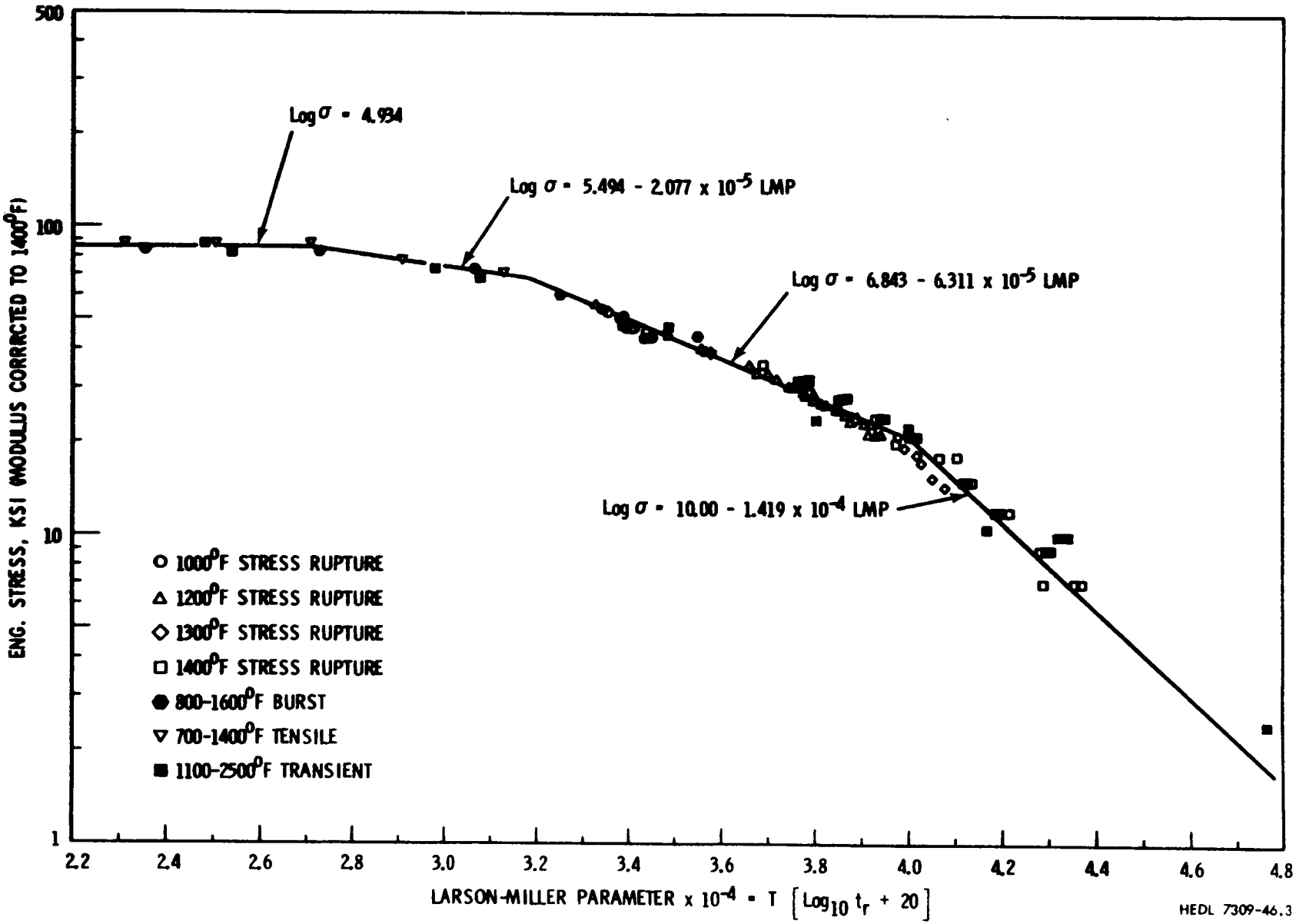

Figure 3.8. Correlation of Stress-Rupture, Burst, Tensile and Transient Strength Data With Larson-Miller Parameter for 20% C.W. Type 316 Stainless Steel Cladding.

where UTS = ultimate tensile strength

BS = ultimate burst strength that would be obtained under biaxial loading

ε = uniform elongation in the tensile test.

The uniform elongation in the tests of interest were about 7%, so the correction factor amounts to BS/UTS = 1.11. No simple basis exists for making stress state corrections in the strain-rate sensitive region. In this region of behavior, the maximum principle stress was used as it was found to provide good correlation. At temperatures above 1400°F, the load-time character of the tensile test is not sufficiently similar to the stress-rupture test to allow correlation with the LMP.

The thermal transient tests[5] were performed by pressurizing the tubular specimen to a predetermined load and increasing the temperature from a start temperature of 700°F at a constant rate until rupture occurs. The stress for this type of test is again calculated using Equation (3.7) and the modulus correction applied using Equation (3.6).

The Larson-Miller parameters for the thermal transient tests were estimated by integrating on a life fraction basis the temperature-time path during the test to the point of failure. For a constant stress, we may use the LMP to express the rupture life as a function of temperature:

$$t_r = 10^{-20}\, e^{2.3P/T}$$

where P = Larson-Miller Parameter

T = temperature, °R

For a linear temperature ramp:

$$T = T_1 + \dot{T}t$$

where T_1 = initial temperature

$\dot{T}$ = ramp rate.

Substituting these relationships into Equation (3.4) yields:

$$\frac{10^{20}}{\dot{T}} \int_{T_1}^{T^*} e^{-2.3P/T}\, dT = 1.$$

This equation may be written as:

$$\int_{T_1}^{T^*} e^{2.3P\,(T-T^*)/TT^*}\, dT = \dot{T}\,[10^{(P/T^*)-20}]\ .$$

For a linear temperature ramp, the integrand becomes significant only when T approaches T*. In this temperature range TT* varies slowly in comparison with T-T* and TT* may be approximated by T^{*2}. Integration then yields:

$$\frac{T^{*2}}{2.3P}\,[1-e^{2.3P(T_1-T^*)/T^{*2}}] = \dot{T}\,10^{(P/T^*)-20}\ .$$

Since P is typically on the order of 20T* and T_1 is $\sim$ 0.5T*, the exponent in the square brackets is of the order of e^{-20} and is therefore negligible compared to 1. Making this approximation yields:

$$P/T^* + \log P/T^* = 19.64 - \log \dot{T}/T^*.$$

Since the test was performed with a thermal ramp in °F/sec, the equation is altered to reflect time in hours and temperature in °R.

$$P/T^* + \log P/T^* = 16.08 - \log \dot{T}/T^*.$$

The Larson-Miller parameters estimated by this expression were used in conjunction with the hoop stress, as modified by the modulus correction factor, Equation (3.6).

3.2.2.2.3 Results and Discussion. The engineering hoop stress, modulus modified stress, rupture life, and corresponding Larson-Miller parameters for all of the stress-rupture tests at test temperatures of 1000, 1200, 1300 and 1400°F are presented in Table 3.7.

The tubular burst hoop stress, modulus modified stress, estimated rupture life and corresponding LMP's for burst tests at 800, 1000, 1200, 1400 and 1600°F are presented in Table 3.8.

Table 3.9 presents the critical tensile test parameters and results required to determine the corrected stress and LMP values. Included in the table are test temperature, UTS, equivalent hoop stress, modulus modified stress, strain rate, total elongation, test time, and Larson-Miller parameter.

Table 3.10 presents the hoop stress, modulus modified stress, thermal ramp rate, failure temperature, and Larson-Miller parameter for the thermal transient tests.

Table 3.7. Biaxial Stress-Rupture Data

Test Temp., (°F)	Hoop Stress, (ksi)	Modulus Modified Hoop Stress, (ksi)	Rupture Life, (Hours)	LMP x 10^{-4}
1000	65.2	55.1	744.3	3.339
1000	63.8	53.9	904.5	3.352
1000	63.0	53.2	1107.0	3.364
1000	60.0	50.7	1458.8	3.382
1000	56.0	47.3	2051.1	3.404
1000	52.0	43.9	4017.1	3.446
1000	65.2	55.1	785.6	3.343
1000	63.8	53.9	816.6	3.345
1000	62.0	52.4	1107.0	3.364
1000	60.0	50.7	1570.0	3.387
1000	56.0	47.3	2101.3	3.405
1000	52.0	43.9	3355.8	3.435
1000	65.2	55.1	821.0	3.345
1000	63.0	53.2	1091.0	3.364
1000	62.0	52.4	1013.0	3.359
1000	56.0	47.3	2296.5	3.411
1000	52.0	43.9	4377.5	3.452

Table 3.7 (continued)

Test Temp., (°F)	Hoop Stress, (ksi)	Modulus Modified Hoop Stress, (ksi)	Rupture Life, (Hours)	LMP x 10^{-4}
1200	61.6	56.6	1.2	3.333
1200	49.0	45.0	9.5	3.482
1200	43.5	39.9	32.8	3.572
1200	36.3	33.3	193.6	3.700
1200	33.0	30.3	404.3	3.753
1200	32.5	29.8	559.5	3.776
1200	31.5	28.9	669.7	3.789
1200	29.0	26.6	1042.3	3.821
1200	28.0	25.7	1697.0	3.856
1200	27.0	24.8	2503.0	3.884
1200	25.0	23.0	2209.4	3.875
1200	23.0	21.1	3975.1	3.917
1200	56.0	51.4	2.7	3.392
1200	49.0	45.0	10.6	3.490
1200	44.0	40.4	28.1	3.560
1200	39.0	35.8	114.9	3.662
1200	35.0	32.1	270.1	3.724
1200	33.0	30.3	497.7	3.768
1200	31.5	28.9	754.2	3.798
1200	30.0	27.5	739.6	3.796
1200	28.0	25.7	1543.0	3.849
1200	27.0	24.8	1910.0	3.865
1200	25.0	23.0	3393.0	3.906
1200	23.0	21.1	4905.8	3.933
1200	50.0	45.9	5.4	3.442
1200	43.5	39.9	37.9	3.582
1200	36.5	33.5	141.4	3.677
1200	33.0	30.3	358.1	3.744
1200	32.0	29.4	687.5	3.791
1200	31.0	28.5	787.0	3.801
1200	29.0	26.6	989.3	3.817
1200	28.0	25.7	1668.3	3.855
1200	27.0	24.8	2729.0	3.890
1200	26.0	23.9	2681.0	3.889
1200	25.0	23.0	4096.0	3.920
1200	23.0	21.1	5473.0	3.941

Table 3.7 (continued)

Test Temp., (°F)	Hoop Stress, (ksi)	Modulus Modified Hoop Stress, (ksi)	Rupture Life, (Hours)	LMP x 10^{-4}
1300	16.0	15.36	1109.6	4.056
1300	26.0	24.95	125.3	3.889
1300	22.0	21.10	403.4	3.979
1300	19.0	18.24	685.4	4.019
1300	15.0	14.40	1477.6	4.078
1300	16.0	15.36	LEAKER	-----
1300	18.0	17.28	743.0	4.025
1300	20.0	19.20	481.5	3.992
1400	36.0	-----	0.7	3.691
1400	32.0	-----	1.9	3.772
1400	28.0	-----	5.1	3.852
1400	24.0	-----	14.0	3.933
1400	21.0	-----	37.3	4.012
1400	15.0	-----	142.0	4.120
1400	12.0	-----	357.6	4.195
1400	9.0	-----	997.8	4.278
1400	7.0	-----	2590.0	4.355
1400	32.0	-----	2.1	3.780
1400	28.0	-----	6.0	3.865
1400	24.0	-----	17.4	3.951
1400	21.0	-----	37.3	4.012
1400	20.0	-----	23.0	3.973
1400	18.0	-----	70.0	4.063
1400	15.0	-----	169.0	4.134
1400	12.0	-----	473.6	4.218
1400	9.0	-----	1246.4	4.296
1400	7.0	-----	3006.4	4.367
1400	32.0	-----	1.8	3.767
1400	28.0	-----	6.1	3.866
1400	24.0	-----	17.2	3.950
1400	21.0	-----	33.3	4.003
1400	18.0	-----	111.3	4.101
1400	15.0	-----	156.2	4.128
1400	12.0	-----	331.7	4.189
1400	9.0	-----	1344.1	4.302
1400	7.0	-----	1121.3	4.287

Table 3.8. Tube Burst Test Data

Temp., (°F)	Hoop Stress, (ksi)	Modulus Modified Hoop Stress, (ksi)	Test Time (hr)	LMP x 10^{-4}
800	106.56	84.5	0.05056	2.357
1000	97.92	82.8	0.05083	2.731
1200	79.2	72.7	0.03028	3.068
1400	60.48	60.5	3.13×10^{-3}	3.254
1600	41.76	45.1	1.71×10^{-3}	3.550

Table 3.9. Tensile Test Data

Test Temp. (°F)	Uniaxial Ultimate Tensile Strength (ksi)	Equiv. Hoop Stress (ksi)	Modulus Modified Hoop Stress (ksi)	Strain Rate (1/min)	Total Elongation (%)	Test Time (hr)	LMP x 10^{-4}
700	103.0	114.3	88.3	1.82×10^{-3}	9.7	0.888	2.314
800	101.0	112.1	88.8	1.82×10^{-3}	8.6	0.788	2.507
900	99.0	109.9	89.3	1.82×10^{-3}	9.3	0.852	2.711
1000	92.6	-----	78.2	1.82×10^{-3}	8.6	0.788	2.905
1100	80.2	-----	70.5	1.82×10^{-3}	9.8	0.897	3.126
1200	58.6	-----	53.8	1.82×10^{-3}	16.6	1.520	3.350
1300	41.3	-----	39.7	1.82×10^{-3}	22.4	2.051	3.575
1400	32.9	-----	32.9	1.82×10^{-3}	24.1	2.207	3.784

Table 3.10. Thermal Transient Test Data

Internal Pressure (psi)	Hoop Stress (psi)	Modulus Modified Stress (ksi)	Thermal Ramp Rate (°F/sec)	Fail Temp. (°F)	Larson-Miller Parameter
1000	7200.0	9.9	10	2050	4.33×10^4
1000	7200.0	9.9	10	2055	4.34×10^4
2500	18000.0	22.3	10	1860	3.99×10^4
6000	43200.0	46.5	10	1570	3.48×10^4
10000	72000.0	70.2	10	1340	3.08×10^4
13500	97200.0	84.1	10	1030	2.54×10^4
180	1296.0	2.4	200	2510	4.77×10^4
1000	7200.0	10.5	200	2150	4.17×10^4
2500	18000.0	23.2	200	1935	3.82×10^4
6000	43200.0	49.0	200	1680	3.40×10^4
10000	72000.0	72.6	200	1420	2.98×10^4
13500	97200.0	86.8	200	1115	2.49×10^4

The stress-LMP data from all four of these tables are plotted on the semi-log chart shown in Figure 3.8. The Larson-Miller plot may be adequately described by four linear segments of the form $\log \sigma = A + B$ LMP, where B is the slope of the trend line and A is the $\log \sigma$ axis intercept. The trend lines were constructed on an engineering judgement basis for a best fit of the data points.

The region of behavior characterized by a constant stress (86,000 psi, LMP $< 2.7 \times 10^4$) is thought to be associated with shear deformation processes leading to a transgranular failure mode. The deformation is athermal in nature and is therefore independent of Larson-Miller parameter. At LMP values above about 3.18×10^4, the dominate failure mode is thought to be that of intergranular fracture. The deformation processes are diffusion controlled and behavior is therefore dependent on time and temperature. The region between LMP's of about 2.7 and 3.18×10^4 is a transition region where both types of deformation and failure processes may be affecting the material behavior. The change in behavior for LMP values above 4.0×10^4 is thought to be due to recrystallization.

The stress-rupture test data represent only two regions of behavior on this Larson-Miller parameter plot. Both the tensile and burst test data represent only two major regions of behavior (athermal and thermal). However, the thermal transient test data span the entire range of LMP's. The good correlation between the transient test results and the other tests demonstrates that the Larson-Miller parameter is satisfactory for defining failure behavior over a wide range of temperature and loading conditions.

3.2.2.2.4 <u>Prediction of Thermal Transient Tests</u>. Once the Larson-Miller parameter correlation has been established for this material and the mathematical expressions for the material behavior have been determined, then prediction of failure for any one of the mechanical tests becomes possible. This is illustrated for the thermal transient tests in Figure 3.9. The failure temperatures are plotted as a function of hoop stress. Although tests were performed at ramp rates of 10 and 200°F/sec only, predictions for 1°F/sec and 1000°F/sec are illustrated in this figure also. These predictions were made on the basis of given stress levels and thermal ramp rates.

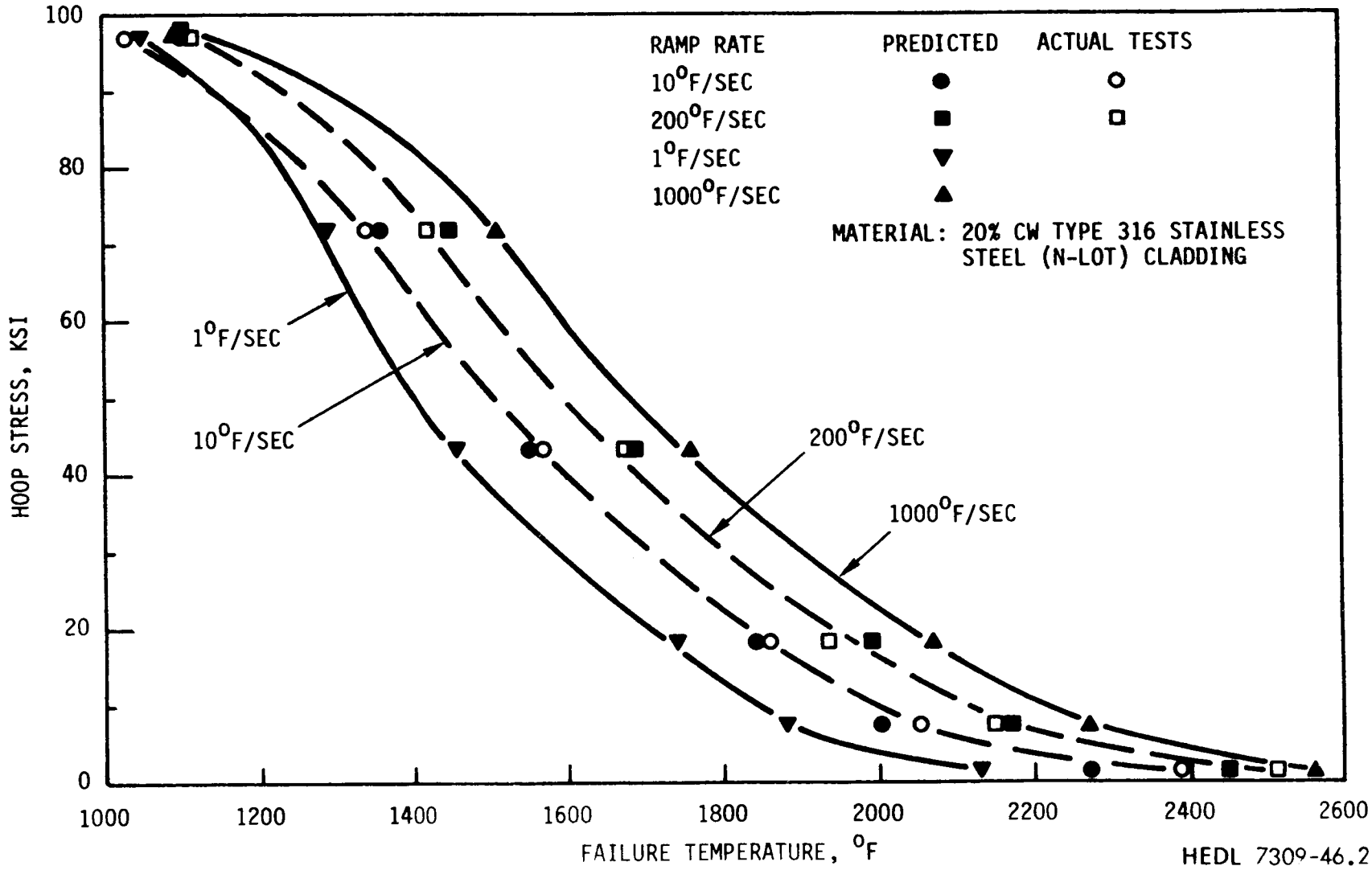

Figure 3.9. Prediction of Failure Temperature During Thermal Transient Test.

Life fractions were calculated and summed every 10°F for each temperature-time interval (based on the respective LMP) until the sum of life fractions exceeded the value of 1.0.

3.2.2.3 Conclusions

The Larson-Miller parameter has proved satisfactory for the correlation of unirradiated 20% C.W. Type 316 stainless steel cladding (N-lot) mechanical property stress-failure data from four completely different types of tests. Correlation of the Larson-Miller parameter with the stress required to cause failure, for stress-rupture tests, burst tests, tensile tests, and thermal transient tests has resulted in the following mathematical expressions:

$\log \sigma = 4.934$ $\quad$ $LMP < 2.7 \times 10^4$

$\log \sigma = 5.494 - 2.077 \times 10^{-5}\ LMP$ $\quad$ $2.7 < LMP < 3.18 \times 10^4$

$\log \sigma = 6.843 - 6.311 \times 10^{-5}\ LMP$ $\quad$ $3.18 < LMP < 4.0 \times 10^4$

$\log \sigma = 10.000 - 1.419 \times 10^{-4}\ LMP$ $\quad$ $LMP > 4.0 \times 10^4$

Prediction of failure results for any one of the above mentioned mechanical property tests is possible given the standard test parameters for the respective test. These correlations should prove particularly valuable in the prediction of failures under conditions hypothesized to exist during reactor transients.

3.2.2.4 Appendix

The following describes the development of general expressions for the ultimate tensile strength in a uniaxial tensile test and the burst strength in a biaxial burst test to be used for stress state correction.

The basic material stress-strain behavior was assumed to follow the relationship $\sigma = K\,\varepsilon^n$, where σ is the true stress, ε is the true strain and K and n are material parameters.

For a tensile test the stability criterion may be expressed as $dL = 0$ where L is the load on the material. For the stress-strain relationship assumed, this criteria yields $d\sigma/d\varepsilon = \sigma$, and therefore:

$$\varepsilon^* = n$$

$$\sigma^* = Kn^n \quad \text{where } \varepsilon^* = \text{true strain at max. load}$$

$$\sigma^* = \text{true stress at max. load.}$$

The engineering ultimate tensile strength is:

$$UTS = L^*/A_o = \sigma^* A^*/A_o = \sigma^* e^{-\varepsilon^*} = \sigma^* e^{-n}.$$

Substituting for σ^* yields:

$$UTS = Kn^n e^{-n}.$$

For a tube burst test the stability criterion can be given as $dP = 0$. Lankford and Saibel have shown that for this criterion, the following describes the true hoop strain at peak pressure:

$$\varepsilon^*_\theta = n/2.$$

Assuming that effective true stress and strain are given by:

$$\bar{\sigma} = \{1/2[\sigma_\theta-\sigma_r)^2 + (\sigma_r-\sigma_z)^2 + (\sigma_z-\sigma_\theta)^2]\}^{1/2}$$

and

$$\bar{\varepsilon} = 2/3\ [\varepsilon^2_\theta + \varepsilon_r^{\ 2} + \varepsilon_z^{\ 2}]\}^{1/2}$$

where $\sigma_r = 0$, $\sigma_z = \sigma_\theta/2$, $\varepsilon_r = -\varepsilon_\theta$, and $\varepsilon_z = 0$, then $\bar{\sigma} = (\sqrt{3}/2)\sigma_\theta$ and $\bar{\varepsilon} = (2/\sqrt{3})\varepsilon_\theta$. The strain hardening assumption in terms of σ_θ and ε_θ would therefore become:

$$(\sqrt{3}/2)\sigma_\theta = (2/\sqrt{3})^n\ K\ \varepsilon_\theta^{\ n} \quad \text{or} \quad \sigma_\theta = (2/\sqrt{3})^{n+1}\ K\ \varepsilon_\theta^{\ n}.$$

The true stress at maximum pressure is then given by the following expression:

$$\sigma_\theta^* = [2/3^{((n+1)/2)}]\ Kn^n.$$

Converting this true stress burst strength to an engineering burst stress, BS: $BS = P\ r_o/t_o$ where r_o = radius
t_o = thickness
P = pressure.

$$BS = Pr/t\ (t/t_o)(r_o/r) = \sigma_\theta^*\ e^{\varepsilon_r}\ e^{-\varepsilon_\theta} = \sigma_\theta^* e^{-2\varepsilon^*_\theta} = \sigma_\theta^* e^{-n}.$$

Substituting for σ_θ^* yields:

$$BS = \frac{2}{(3)^{(n+1)/2}}\ Kn^n\ e^{-n}.$$

Examining the ratio of engineering burst stress to engineering ultimate tensile strength, the following factor results:

$$BS/UTS = 2/(\sqrt{3})^{n+1}.$$

3.2.3 Stress-Rupture of 20% Cold Worked Type 316 Stainless Steel Under Variable Stress Histories

3.2.3.1 Objective

The purpose of this work is to define the salient features of stress-rupture of 20% cold worked Type 316 stainless steel under variable stress histories. This information supports the design and performance of reactor components operating under other than steady loading conditions.

3.2.3.2 Accomplishments and Status

3.2.3.2.1 Scope of Work. A series of tests was conducted to evaluate the stress-rupture behavior of 20% cold worked Type 316 stainless steel under variable stress-history conditions. The baseline creep stress for this study was selected to produce rupture in approximately 100 hours under steady loading conditions. The basic procedure was to interrupt stress-rupture tests at the baseline stress by applying stepwise increases in stress. In some cases, the high stress loading was sufficient to fail the specimen; in other cases, failure on loading did not occur and the high stress was maintained to rupture; in still other tests, the high stress was maintained for times from 0 to 4 hours before returning to the baseline stress. These high stress loadings were imposed at the beginning of life and at various fractions of the baseline life.

All tests were conducted on tubular samples. The tubing, designated as N-3 lot prototypic cladding, has been described previously.[6] Three-inch long samples of 0.230-inch O.D., 0.200-inch I.D., closed-end tubing were loaded by internal pressurization at 1200°F. Specimens were heated to 1200°F in about two hours and then held at temperature for about two hours prior to initial pressurization. Pressure increased approximately linearly with time during loading.

The data from these speciments are interpreted in terms of the life fraction approach to variable-stress rupture behavior.

3.2.3.2.2 Results. Experimental results are tabulated in Table 3.11 in the first eight columns. The life fraction calculations summarized in columns 8-16 of Table 3.11 are discussed in the next section. Examples of reading the table for stress-history tests are illustrated as follows: Test 30--age for 40.8 hours at 1200°F, pressurize to 8332 psi in 30 seconds and maintain pressure to rupture in 0.8 hours; Test 10--pressurize to 5207 psi in 18 seconds, hold pressure for 40 hours, increase pressure until burst occurs at 9020 psi, 9 seconds after initiation of pressure increase; Test 9--pressurize to 10,000 psi in 45 seconds, immediately decrease pressure to 5207 psi in 10 seconds, maintain pressure until rupture occurs in 198.3 hours.

All hoop stresses in Table 3.11 are calculated at the tube I.D. using the thick wall formula:

$$\sigma_h = p \frac{b^2 + a^2}{b^2 - a^2}$$

where σ_h is hoop stress,
p is internal pressure,
b is external tube radius, and
a is internal tube radius.

One experiment was conducted to measure the plastic deformation after loading to a hoop stress of 72,000 psi at 1200°F. Diameter measurements were made at two positions 90° apart for each of five axial locations on an as-fabricated specimen at room temperature. The specimen was heated to 1200°F, prssurized to 10,000 psi, unloaded, and cooled to room temperature where diameter measurements were repeated. Results presented in Table 3.12 show a plastic hoop strain at the tube O.D. of 0.0074.

3.2.3.2.3 Evaluation of Results. The constant-pressure stress-rupture results in Table 3.11 are consistent with Paxton's data[7] on the same tubing. In order to obtain best values of mean rupture life, t_r, at various stress levels, the present results and those of Paxton in the stress rang 25,000 to 60,000 psi were fit to the following equation:

$$\log_{10} t_r = \sum_{i=0}^{n} A_i \, [\log_{10} \sigma]^i . \qquad (3.13)$$

Table 3.11. Experimental Results and Life Fraction Calculations for Stress Rupture and Burst Tests

Test No.	Loading/Unloading Pressure, psi	Loading/Unloading Time, sec	Hoop Stress, 1000 psi	Time at Stress, hours	Time to Rupture, hours	Burst Test Pressure, psi	Burst Test Time, sec	Basis for t_r: Experimental t/t_r	Experimental $\Sigma\, t/t_r$	n = 1 t/t_r	n = 1 $\Sigma\, t/t_r$	n = 2 t/t_r	n = 2 $\Sigma\, t/t_r$	n = 3 t/t_r	n = 3 $\Sigma\, t/t_r$
5	10,000	30	72	0.047	0.047	----	--	1.0	1.0	-----	-----	-----	-----	-----	-----
4	9,720	35	70	0.13	0.13	----	--	1.0	1.0	-----	-----	-----	-----	-----	-----
X	9,025	60	65	0.3	0.3	----	--	1.0	1.0	-----	-----	-----	-----	-----	-----
3	8,332	90	60	1.6	1.6	----	--	1.0	1.0	1.013	1.013	1.185	1.185	1.081	1.081
2	6,943	55	50	6.6	6.6	----	--	1.0	1.0	0.791	0.791	0.790	0.790	0.858	0.858
1A	5,207	60	37.5	123.5	123.5	----	--	1.0	1.0	1.068	1.068	0.978	0.978	0.980	0.980
30	0	0	0	40.8	---	----	--	0	---	0	0	0	0	0	-----
	8,332	30	60	0.8	0.8	----	--	0.5	0.5	0.506	0.506	0.593	0.593	0.541	0.541
7	0	0	0	80	---	9480	9								
10	5,207	18	37.5	40	---	9020	19								
12	5,207	18	37.5	40	---	9360	14								
13	5,207	19	37.5	40	---	8900	18								
14	5,207	8	37.5	40	---	9200	17								
15	5,207	15	37.5	40	---	8960	15								
6	5,207	35	37.5	80	---	9150	1								
8	6,943	36	50	4	---	9280	5								
9	10,000	45	72	0	---	----	--	0		0		0		0	
	5,207	10	37.5	198.3±0.5	198.3±0.5	----	--	1.606	1.606	1.715	1.715	1.570	1.570	1.574	1.574
25	9,720	21	70	0	---	----	--	0		0		0		0	
	5,207	26	37.5	134.6±7.5	134.6±7.5	----	--	1.090	1.090	1.164	1.164	1.066	1.066	1.068	1.068
26B	9,026	20	65	0	0	----	--	0		0		0		0	
	5,207	30	37.5	161.5	161.5	----	--	1.308	1.308	1.397	1.397	1.279	1.279	1.282	1.282
27	8,332	34	60	0	0	----	--	0		0		0		0	
	5,207	24	37.5	109.5±7.3	~109.5±7.3	----	--	0.887	0.887	0.947	0.947	0.867	0.867	0.869	0.869

Table 3.11 (continued)

Test No.	Loading/Unloading Pressure, psi	Loading/Unloading Time, sec	Hoop Stress, 1000 psi	Time at Stress, hours	Time to Rupture, hours	Burst Test Pressure, psi	Burst Test Time, sec	Basis for t_r: Experimental t/t_r	Experimental $\Sigma\ t/t_r$	n = 1 t/t_r	n = 1 $\Sigma\ t/t_r$	n = 2 t/t_r	n = 2 $\Sigma\ t/t_r$	n = 3 t/t_r	n = 3 $\Sigma\ t/t_r$
28	6,943	50	50	0	-----	----	--	0		0		0		0	
	5,207	50	37.5	151.3	151.3	----	--	1.225	1.225	1.309	1.309	1.198	1.198	1.201	1.201
16	5,207	30	37.5	40	-----	----	--	0.324		0.346		0.317		0.317	
	8,332	20	60	0	-----	----	--	0		0		0		0	
	5,207	20	37.5	108.5	148.5	----	--	0.879	1.203	0.939	1.285	0.859	1.176	0.861	1.179
20	5,207	24	37.5	40	-----	----	--	0.324		0.346		0.317		0.317	
	6,943	10	50	0	-----	----	--	0		0		0		0	
	5,207	10	37.5	129.6	169.6	----	--	1.049	1.373	1.121	1.467	1.026	1.343	1.029	1.346
11	10,000	49	72	0.0167	-----	----	--	0.355		0.355*		0.355*		0.355*	
	5,207	22	37.5	112±5.3	112±5.3	----	--	0.907	1.262	0.969	1.324	0.887	1.242	0.889	1.244
22	6,943	45	50	4	-----	----	--	0.606		0.480		0.479		0.520	
	5,207	31	37.5	57.6	61.6	----	--	0.466	1.072	0.498	0.978	0.456	0.935	0.457	0.977
17	5,207	37	37.5	40	-----	----	--	0.324		0.346		0.317		0.317	
	8,332	55	60	0.33	40.33	----	--	0.206	0.530	0.209	0.555	0.244	0.561	0.223	0.540
								(0.413)**	(0.747)**	(0.413)**	(0.759)**	(0.413)**	(0.730)**	(0.413)**	(0.730)**
18	5,207	45	37.5	40	-----	----	--	0.324		0.346		0.317		0.317	
	8,332	22	60	0.1	40.1	----	--	0.063	0.387	0.063	0.409	0.074	0.391	0.068	0.385
								(0.125)**	(0.449)**	(0.125)**	(0.471)**	(0.125)**	(0.442)**	(0.125)**	(0.442)**
19	5,207	15	37.5	40	-----	----	--	0.324		0.346		0.317		0.317	
	6,943	16	50	4.7	44.7	----	--	0.712	1.036	0.564	0.901	0.563	0.880	0.611	0.928
21	5,207	18	37.5	40	-----	----	--	0.324		0.346		0.317		0.317	
	6,943	14	50	3	-----	----	--	0.455		0.360		0.359		0.390	
	5,207	15	37.5	48.5	91.5	----	--	0.393	1.172	0.420	1.126	0.384	1.060	0.385	1.092

Table 3.11 (continued)

Test No.	Loading/Unloading Pressure, psi	Loading/Unloading Time, sec	Hoop Stress, 1000 psi	Time at Stress, hours	Time to Rupture, hours	Burst Test Pressure, psi	Burst Test Time, sec	Basis for t_r: Experimental t/t_r	Experimental $\Sigma\, t/t_r$	n = 1 t/t_r	n = 1 $\Sigma\, t/t_r$	n = 2 t/t_r	n = 2 $\Sigma\, t/t_r$	n = 3 t/t_r	n = 3 $\Sigma\, t/t_r$
23	5,207	32	37.5	20	----	---	--	0.162		0.173		0.158		0.159	
	6,943	14	50	2	----	---	--	0.303		0.240		0.240		0.260	
	5,207	14	37.5	20	----	---	--	0.162		0.173		0.158		0.159	
	6,943	13	50	2	----	---	--	0.303		0.240		0.240		0.260	
	5,207	13	37.5	11.7	55.7	---	--	0.095	1.025	0.101	0.927	0.093	0.889	0.093	0.931
24	6,943	55	50	1	----	---	--	0.152		0.120		0.120		0.130	
	5,207	33	37.5	20	----	---	--	0.162		0.173		0.158		0.159	
	6,943	22	50	1	----	---	--	0.152		0.120		0.120		0.130	
	5,207	22	37.5	20	----	---	--	0.162		0.173		0.158		0.159	
	6,943	14	50	1	----	---	--	0.152		0.120		0.120		0.130	
	5,207	18	37.5	20	----	---	--	0.162		0.173		0.158		0.159	
	6,943	20	50	0.5	63.5	---	--	0.076	1.018	0.060	0.939	0.060	0.894	0.065	0.932

*t_r based on experimental result for Test 5

**t_r based on experimental result for Test 30

Table 3.12. Experimental Measurement of Plastic Strain in Deformed Tube Specimen

Axial Distance From Tube End, inches	Before Loading		After Loading*	
	d_o, inches	d_{90}, inches	d_0, inches	d_{90}, inches
0.5	0.2302	0.2304	0.2320	0.2321
1.0	0.2303	0.2304	0.2320	0.2319
1.5	0.2302	0.2305	0.2320	0.2320
2.0	0.2302	0.2304	0.2322	0.2320
2.5	0.2302	0.2304	0.2320	0.2320
Average	0.2303		0.2320	

*Specimen pressurized to 10,000 psi at 1200°F in 15 seconds; depressurized in 1 second.

Results of the least squares analysis are summarized in Tables 3.13 and 3.14. The standard error of the estimate of log t_r decreases slightly in going from n=1 to n=3, indicating a slightly better fit with the higher order terms. Figure 3.10 illustrates the fit of the second order equation to the experimental data. These descriptions of the experimental data form the basis for mean rupture life values used in life fraction calculations discussed below.

The actual stress values which can be achieved during an incremental stress increase are limited by the burst pressure of the tube. The present results and the data of Paxton[8] show that even after a relatively small fraction of life is expended at the baseline creep stress, the subsequent burst pressure is reduced significantly, Figure 3.11. This lower burst stress is apparently independent of baseline creep stress (in the range 29,000 to 50,000 psi hoop stress) or fraction of rupture life expended. The single test on unstressed, aged tubing indicates that this lowering of burst pressure is primarily a thermal effect.

Turning now to the stress-rupture results, we first consider the effect of a high stress with zero hold time applied at the beginning of life. Experimental results are easily evaluated in terms of the life fraction for these loadings. Four slightly different life fraction calculations are presented in Table 3.11, differing only in the basis for establishing mean rupture life, t_r. All four calculations lead to the same basic conclusions and are included in Table 3.11 for completeness. For the zero-hold-time stress increase tests at beginning of life (Tests 9, 25, 26B, 27, 28), only one (Test 27) of the five experiments shows a life fraction less than unity. Four of these tests exhibit a rupture life within the expected range for the baseline stress of 37,500 psi (see Table 3.14), with only Test 9 showing a rupture life slightly higher than the predicted maximum. We therefore conclude that high stresses without hold time applied at beginning of life are not damaging.

In these tests, no damage would be expected if the high stress loading is purely elastic, but some damage might be envisaged if plastic deformation during the high stress loading exhausts some of the ductility normally available during baseline creep. The test results in Table 3.12 confirm that

Table 3.13. Constants, A_i, for $\text{Log}_{10}\, t_r\ (\text{hr}) = \sum_{i=0}^{n} A_i\, [\log_{10} \sigma\ (\text{ksi})]^i$

And Standard Error of Estimate of $\text{Log}_{10}\, t_r$, S

n	A_0	A_1	A_2	A_3	A_4	S
1	16.4512	-9.14093	- - - -	- - - -	- - - -	0.09361
2	9.42823	-0.220648	-2.81708	- - - -	- - - -	0.08867
3	-74.8063	160.122	-104.23	21.3105	- - - -	0.08522
4	419.148	-1091.71	1082.59	-477.55	78.4411	0.08602

Table 3.14. Values of Mean Rupture Life, t_r, and Minimum and Maximum Rupture Life Determined From $\text{Log}_{10}\, t_r = \sum_{i=0}^{n} A_i\, [\log \sigma]^i \pm 2S$

Stress, 1000 psi	n	t_r, hr	t_{min}, hr	t_{max}, hr
60	1	1.58	1.02	2.43
	2	1.35	0.90	2.03
	3	1.48	1.00	2.19
50	1	8.34	5.42	12.84
	2	8.35	5.55	12.56
	3	7.69	5.19	11.39
37.5	1	115.6	75.1	177.9
	2	126.3	84.0	190.0
	3	126.0	85.1	186.6

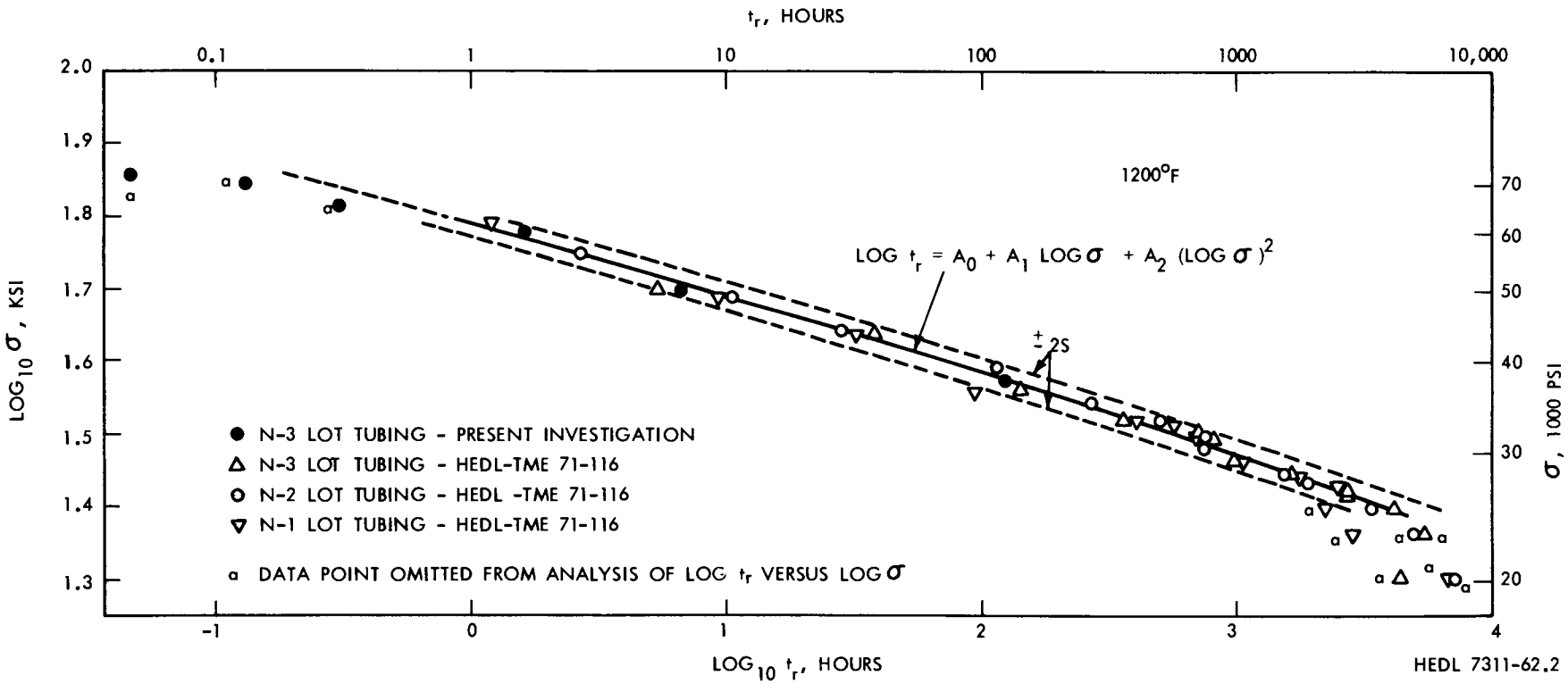

Figure 3.10. Results of Second Order Polynomial Fit to Stress-Rupture Data on 20% C.W. 316 Stainless Steel Tubing.

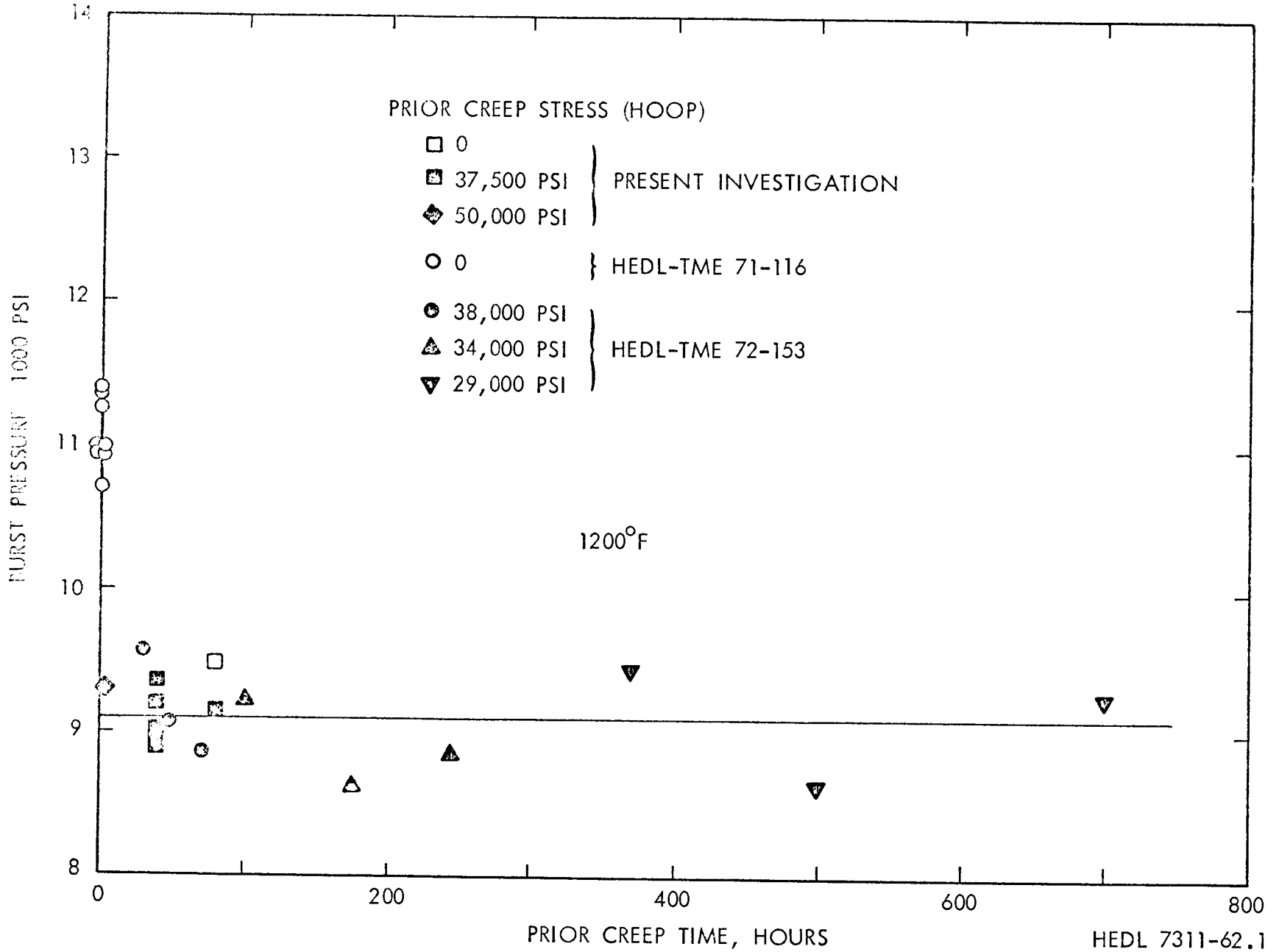

Figure 3.11. Effect of Prior Creep on Burst Pressure of 20% C.W. 316 Stainless Steel Cladding.

plastic deformation occurs on loading to 72,000 psi hoop stress, but this deformation is not damaging to rupture life. Further analysis of this test leads to estimates of 2×10^{-4} sec^{-1} and 3×10^{-3} sec^{-1} for the elastic and average plastic strain rates, and calculations of average effective stress and average effective strain yield values of 62,400 psi and 0.0099, respectively. This value is in reasonable agreement with the results of other HEDL tests. Accounting for the thermal recovery effect, we can make the following rough estimates of average effective plastic strain for other hoop stresses in this test series: 0.008 at 70,000 psi; 0.0045 at 65,000 psi; 0.0025 at 60,000 psi; and < 0.001 at 50,000 psi.

When high stresses without a hold time are applied in the baseline mid-life range, the life fraction is again greater than unity, as shown for Tests 16 and 20. The residual uniaxial tensile properties after the initial 40-hours at baseline creep stress are available from the work of Paxton.[8] From these results, we estimate the effective plastic strain for a 60,000 psi hoop stress (Test 16) to be about 0.0025, while the effective plastic strain for a 50,000 psi hoop stress (Test 20) should be very small.

The next group of experiments explores the effect of high stress application with hold times. When high-stress creep is imposed at the beginning of baseline life, there is no damaging effect and the life fraction remains near unity (Tests 11 and 22). However, when a creep stress of 60,000 psi is imposed in the mid-life range, the life fraction drops significantly (Tests 17 and 18). The result from Test 30 indicates that only a portion of this effect can be attributed to thermal aging in the absence of stress. We conclude that rupture strength at 60,000 psi is reduced significantly following prior thermal exposure under an applied stress.

When the high creep stress level is reduced from 60,000 psi to 50,000 psi, the life fraction returns to near unity (Tests 19 and 21). The

introduction of the high stress creep in a periodic fashion interspersed with baseline creep does not affect the life fraction (Tests 23 and 24). Life fraction values for these tests tend to be slightly less than unity (unless the experimental value from Test 2 is used as the basis of t_r at 50,000 psi), while life fraction values for all other tests are predominantly greater than unity. Nevertheless these variations do not exceed the range to be expected from the scatter of constant-loading stress-rupture tests. We therefore conclude that creep at 50,000 psi is not detrimental to baseline stress-rupture strength, and vice versa.

3.2.3.2.4 Conclusions and/or Recommendations. Results of the present investigation lead us to the following conclusions:

1. Hoop stresses up to 72,000 psi (plastic hoop strains < 0.01) without a hold time applied at beginning of life do not significantly affect subsequent baseline stress-rupture life at 37,500 psi hoop stress.
2. Hoop stresses to 60,000 psi without hold times can be imposed in the mid-life range without affecting stress-rupture life at 37,500 psi. Hoop stresses higher than about 65,000 psi produce burst failure after prior baseline creep into the mid-life range. This loss of burst strength from the starting value of about 80,000 psi is attributed primarily to a thermal aging effect.
3. For high-stress creep at stresses to 72,000 psi introduced at the beginning of life, stress-rupture behavior correlates with a life fraction of unity. Creep at 60,000 psi imposed in the mid-life range produces life fraction values significantly lower than unity. This damage is attributable to a combination of the thermal exposure and the applied stress during initial baseline creep. High-stress creep at 50,000 psi imposed in the mid-life range correlates with a life fraction of unity.

3.2.3.2.5 Applications. The results of this investigation provide a preliminary confirmation of the validity of the life fraction approach for 20% cold worked Type 316 stainless steel. This life fraction approach may be

useful in the design and performance prediction of reactor components operating under variable stress histories.

3.2.3.3 Expected Achievements

Further experimental work of this type will await more detailed analysis of its application to specific components and conditions.

3.2.4 Elastic Analysis for a Slit Tube

3.2.4.1 Objective

Present plans call for the use of "slit tube" specimens* in an irradiation experiment to determine the effects of history on irradiation creep. The objective of the present effort is to evaluate the state of stress in the specimen and to assure that data obtained from study of the specimen can be related to creep phenomena in an unambiguous fashion.

3.2.4.2 Accomplishments and Status

This report will detail elastic analysis done for a slit tube. This analysis is motivated by the goal of doing in-reactor mechanical testing on previously irradiated specimens of Type 316 stainless steel tubing as part of a general program to investigate the effects of irradiation history on mechanical properties. Because of the constraints of space and difficulty in carrying out instrumented tests in the reactor, the technique of stress relaxation appears to be an attractive possibility for this program. As a first step in establishing the feasibility of this technique, it is necessary to determine the stress and strain distribution resulting from the planned loading method.

The elastic response of the slit tube for the loading configurations under consideration at HEDL has been independently calculated in order to evaluate the utility of the slit tube for such testing.

---

*The concept of using a slit tube for in-reactor measurements was first suggested by J. E. Flynn.

3.2.4.2.1 Stress Analysis. The stress-strain and stress-displacement relationships for a slit tube are derived in this section for the loading sketched in Figure 3.12. This form of loading is intended to be used in stress-relaxation experiments and consists of a uniform stress on both of the open faces of the slit. Although solutions for similar loading arrangements are available in textbooks, this particular case was not found so the solution is derived below.

The symmetry of the loading arrangement makes it possible to consider only a loaded half cylinder as shown in Figure 3.13 facing end on. The half cylinder of inner and outer radius a and b, respectively, is considered to be rigidly fastened at $\theta = \pi$ and loaded with a uniformily distributed normal force p per unit length at $\theta = 0$. The stress distribution resulting from this loading will be of a simple two-dimensional nature as long as the tube is either very short (plane stress) or very long (plane strain) compared to its wall thickness, which is the case to be considered here. When body forces are negligible as they are here, the stress distribution (in the r-θ plane) will be the same in both plane stress and plane strain so that no distinction need be made between the cases until displacements are calculated.[9]

The method used for derivation of the stress distribution follows closely a similar problem detailed by Timoshenko and Goodier.[9] The stress distribution can be conveniently obtained from the stress function ϕ which in polar coordinates is defined by:

$$\left(\frac{\partial^2}{\partial r^2} + \frac{1}{r}\frac{\partial}{\partial r} + \frac{1}{r^2}\frac{\partial^2}{\partial \theta^2}\right)\left(\frac{\partial^2 \phi}{\partial r^2} + \frac{1}{r}\frac{\partial \phi}{\partial r} + \frac{1}{r^2}\frac{\partial^2 \phi}{\partial \theta^2}\right) = 0 \qquad (3.14)$$

The stresses are obtained from ϕ by the relationships:

$$\sigma_r = \frac{1}{r}\frac{\partial \phi}{\partial r} + \frac{1}{r^2}\frac{\partial^2 \phi}{\partial \theta^2} \qquad (3.15a)$$

$$\sigma_\theta = \frac{\partial^2 \phi}{\partial r^2} \qquad (3.15b)$$

$$\tau_{r\theta} = \frac{1}{r^2}\frac{\partial \phi}{\partial \theta} - \frac{1}{r}\frac{\partial^2 \phi}{\partial r \partial \theta} \qquad (3.15c)$$

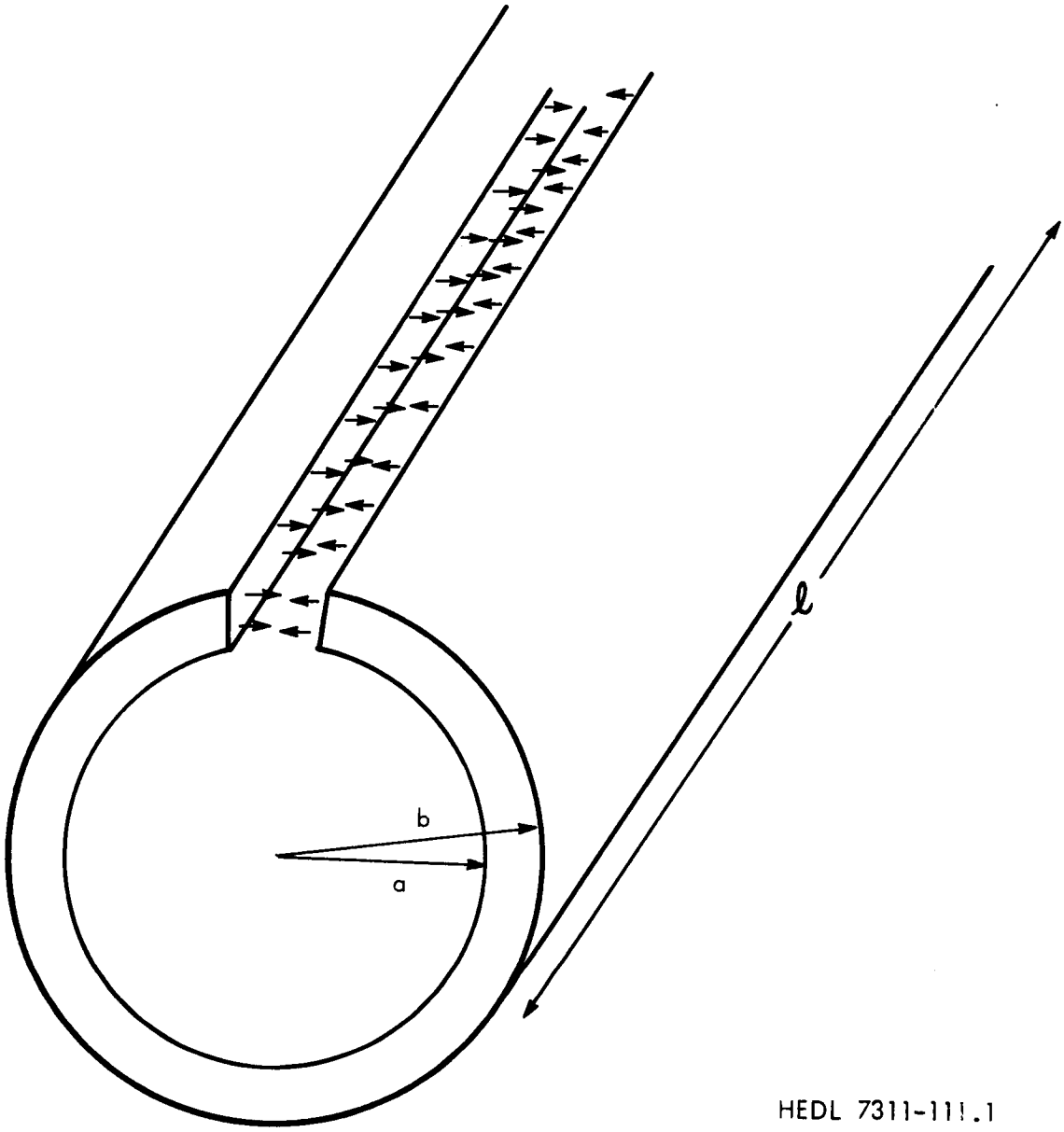

Figure 3.12. Loaded Slit Tube.

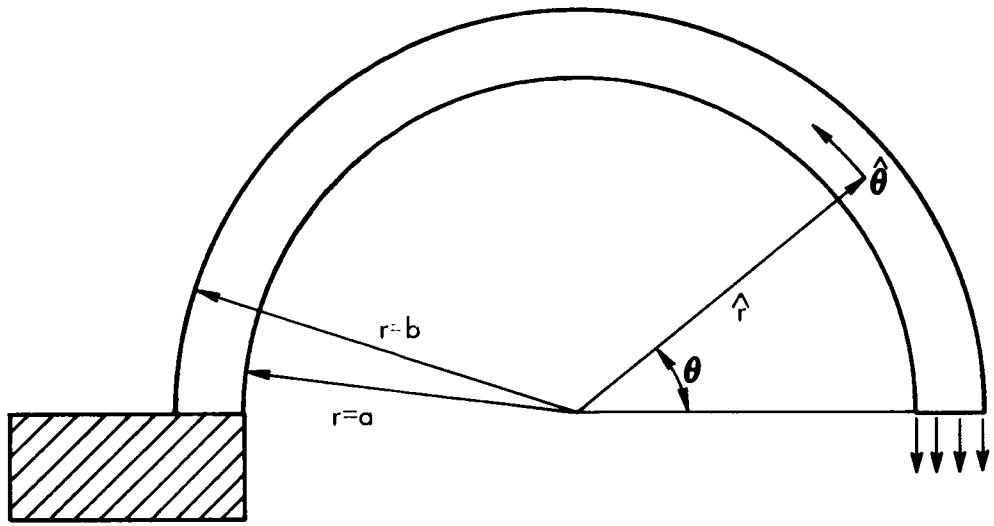

HEDL 7311-111.5

Figure 3.13. Elastically Equivalent Configuration to the Loaded Slit Tube in Figure 3.12.

As an aid in obtaining the stress function ϕ, it is known in bending of thin curved bars[10] that the bending moment produced by the applied load will be proportional to the normal stress, in this case σ_θ. The bending moment produced by the applied load is proportional to $(1-\cos\theta)$ so that the angular dependence of σ_θ as well as ϕ is expected to be something like $(1-\cos\theta)$. With this hint, the trial function:

$$\phi = f(r)\cos\theta \tag{3.16}$$

inserted into Equation (3.14) leads to the equation:

$$\left(\frac{d^2}{dr^2} + \frac{1}{r}\frac{d}{dr} - \frac{1}{r^2}\right)\left(\frac{d^2 f}{dr^2} + \frac{1}{r}\frac{df}{dr} - \frac{f}{r^2}\right) = 0 \ . \tag{3.17}$$

The general solution of Equation (3.17) is:

$$f(r) = Ar^3 + B/r + Cr + D\log(r). \tag{3.18}$$

The function f(r) leads to the stresses:

$$\sigma_{r1} = \left(2Ar - \frac{2B}{r^3} + \frac{D}{r}\right)\cos\theta \tag{3.19a}$$

$$\sigma_{\theta 1} = \left(2Ar + \frac{2B}{r^3} + \frac{D}{r}\right)\cos\theta \tag{3.19b}$$

$$\tau_{r\theta 1} = \left(2AR - \frac{2B}{r^3} + \frac{D}{r}\right)\sin\theta \tag{3.19c}$$

where the subscripts "1" have been introduced for convenience later.

The constants A, B, and D must be chosen so that the inner and outer surfaces of the cylinder are free of forces; so that σ_{r1} and $\tau_{r\theta 1} = 0$ at r=a and r=b. This boundary condition leads to the relations:

$$2Aa - \frac{2B}{a^3} + \frac{D}{a} = 0 \tag{3.20a}$$

$$2Ab - \frac{2B}{b^3} + \frac{D}{b} = 0 \ . \tag{3.20b}$$

The third boundary condition is that:

$$\int \sigma_{\theta 1}\, dr = P \tag{3.21}$$

at $\theta = 0$, which leads to the relation

$$3A\,(b^2-a^2) + B\left(\frac{b^2-a^2}{a^2b^2}\right) + D\log b/a = 0 \tag{3.22}$$

combining the three relationships in Equations (3.20) and (3.22) leads to:

$$A = -P/2N \tag{3.23a}$$

$$B = \frac{a^2b^2P}{2N} \tag{3.23b}$$

$$D = \frac{(b^2+a^2)\ P}{N} \tag{3.23c}$$

where N is given by

$$N = a^2 - b^2 + (a^2 + b^2) \log (b/a). \tag{3.24}$$

The stress distribution described by Equations (3.19) and (3.23) constitutes a satisfactory solution to the problem except that radial dependence of the applied stress (σ_θ at $\theta = 0$) is very strong. A plot of σ_θ vs. r for the parameters of interest reveals that σ_θ varies nearly linearly over the tube thickness, reaching a maximum value at r = a and a minimum value $\sigma_\theta \sim - \sigma_{max}$ at 4 = b. Another way of stating this is that the applied stress corresponding to Equation (3.19) has a non-zero moment about the center of the tube wall which is:

$$M_z = \int_a^b \sigma_\theta\Big|_{\theta=0} \left(r - \frac{a+b}{2}\right) dr = - \frac{P(a+b)}{2} . \tag{3.25}$$

Hence, this applied force would tend to twist the tube in contrast to the desired loading of a uniform stress σ_θ.

This problem can be overcome by adding to the above solution another component corresponding the pure bending of the tube. The magnitude of the bending moment will be chosen to cancel out that given in Equation (3.25), so that the resulting stress distribution $\sigma_\theta|_{\theta=0}$ has no moment about the midpoint of the tube wall. The solution for pure bending of cylinder is given in detail in Reference 14 (p. 63) so that it is sufficient to quote the results here. The stress distribution for pure bending is:

$$\sigma_{r2} = \alpha \left(\frac{a^2b^2}{r^2} \log b/a + b^2 \log r/b + a^2 \log a/r\right) \tag{3.26a}$$

$$\sigma_{\theta 2} = \alpha \left(\frac{-a^2b^2}{r^2} \log b/a + b^2 \log r/b + a^2 \log a/r + b^2-a^2\right) \tag{3.26b}$$

$$\tau_{r\theta 2} = 0 \tag{3.26c}$$

where α is proportional to the bending moment applied.

The solution for pure bending (Equation (3.26) obeys the first boundary condition that σ_r and $\tau_{r\theta} = 0$ at r=a and r=b. Further, it can be seen by integrating Equation (3.26b) that there is no resultant force due to σ_θ at $\theta = 0$, that is $\int_a^b \sigma_{\theta 2}\, dr = 0$ for pure bending. Hence, the solution desired is the sum of Equation (3.19) and (3.26) where α is determined by requiring that the bending moment balance out that due to the stress distribution in Equation (3.19a) i.e.,

$$\int_a^b \sigma_{\theta\partial} \left(r - \frac{a+b}{2}\right) dr = \frac{P(a+b)}{2} . \tag{3.27}$$

Carrying out this integration leads to:

$$\alpha = \frac{2P(a+b)}{N'} \quad \text{where } N' = (b^2-a^2)^2 - 4a^2b^2 (\log b/a)^2 . \tag{3.28}$$

The complete solution is then given by:

$$\begin{aligned} \sigma_r = {} & \frac{P}{N} \left(-r - \frac{a^2b^2}{r^3} + \frac{a^2+b^2}{r}\right) \cos\theta \\ & + 2\frac{P}{N'}(a+b)\left(\frac{a^2b^2}{r^2} \log b/a + b^2 \log r/b + a^2 \log a/r\right) \end{aligned} \tag{3.29a}$$

$$\begin{aligned} \sigma_\theta = {} & \frac{P}{N} \left(-3r + \frac{a^2b^2}{r^3} + \frac{a^2+b^2}{r^2}\right) \cos\theta \\ & + 2P\frac{(a+b)}{N'}\left(\frac{-a^2b^2}{r^2} \log b/a + b^2 \log r/b + a^2 \log a/r + b^2-a^2\right) \end{aligned} \tag{3.29b}$$

$$\tau_{r\theta} = \frac{P}{N} \left(-r - \frac{a^2b^2}{r^3} + \frac{a^2+b^2}{r}\right) \sin\theta . \tag{3.29c}$$

The stress distributions in Equation (3.29) appear somewhat complicated in form, and in order to see better the relationship among the various components plots of the function are made in Figures 3.14-3.17 for the parameters a=0.1 and b=0.115 which are of experimental interest. First it can be seen in Figure 3.14 that the stress σ_θ at the boundary $\theta = 0$ now is almost constant over the thickness of the tube as desired for the idealized conditions of loading. Secondly, it is seen that σ_θ is the most predominant stress over most of the region of the slit cylinder. The next largest component is the

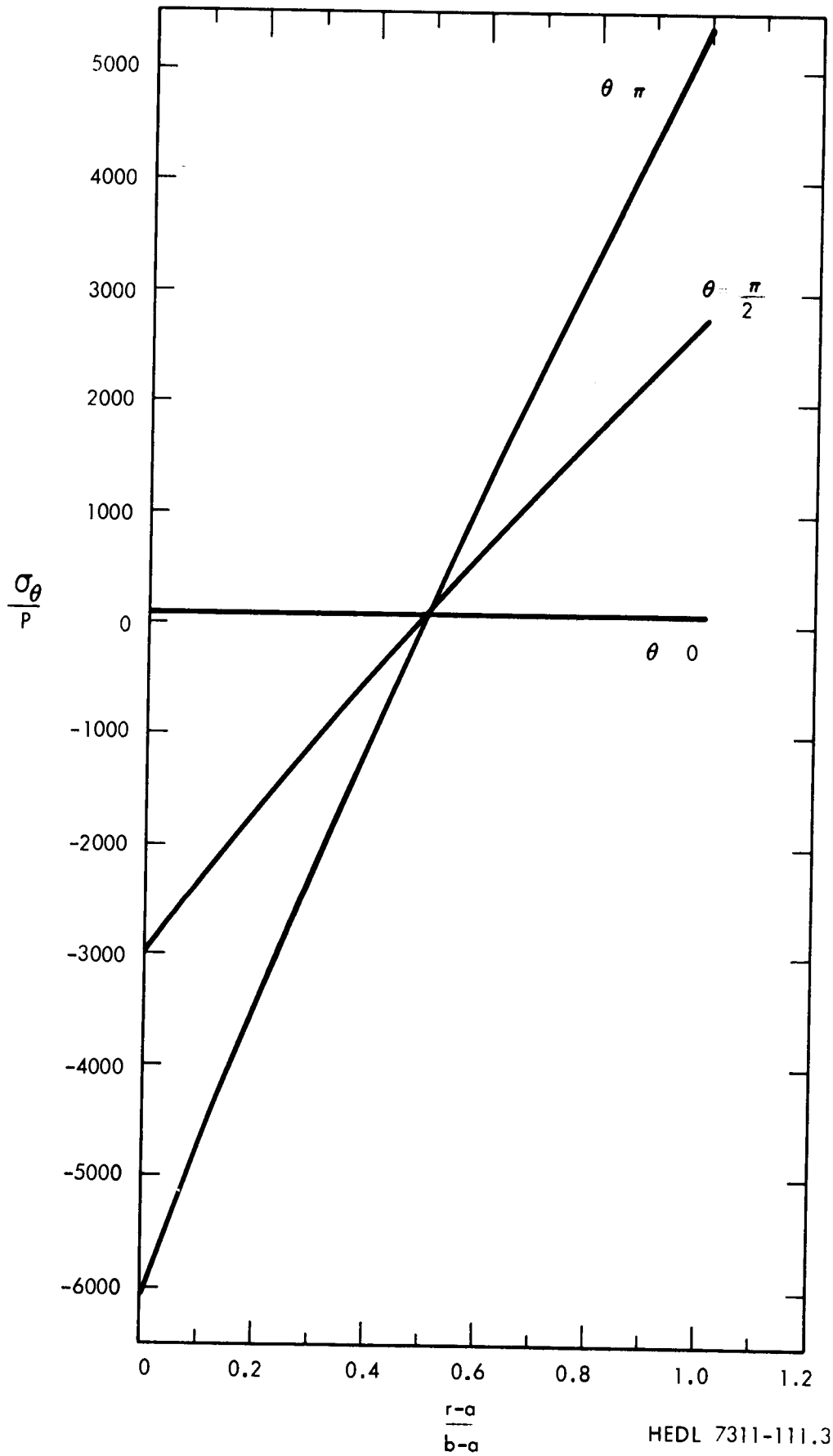

Figure 3.14. Radial Dependence of the Normal Stress Distribution in a Loaded Slit Tube.

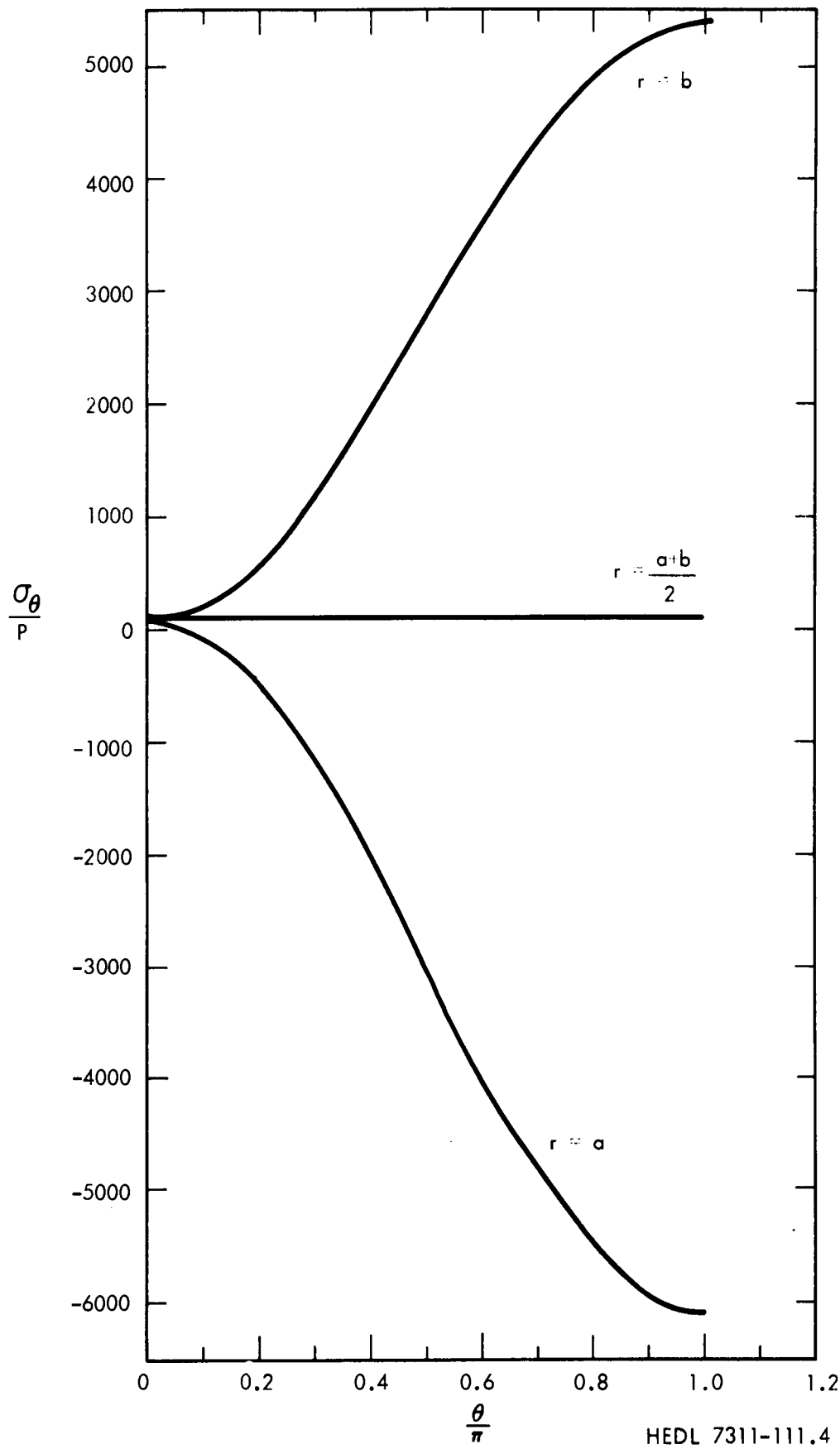

Figure 3.15. Angular Dependence of the Normal Stress Distribution in a Loaded Slit Tube.

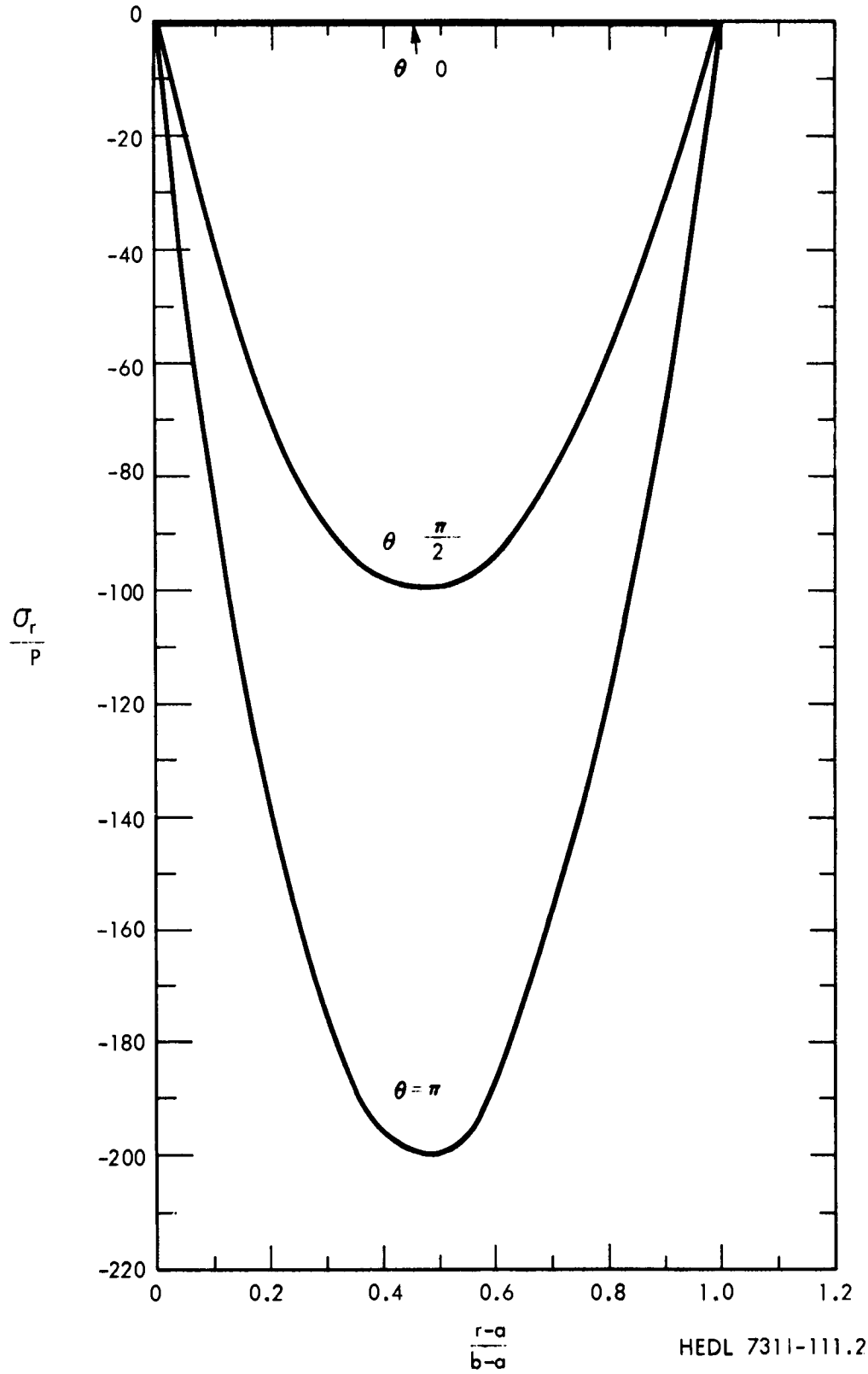

Figure 3.16. Radial Dependence of the Radial Stress Distribution in a Loaded Slit Tube.

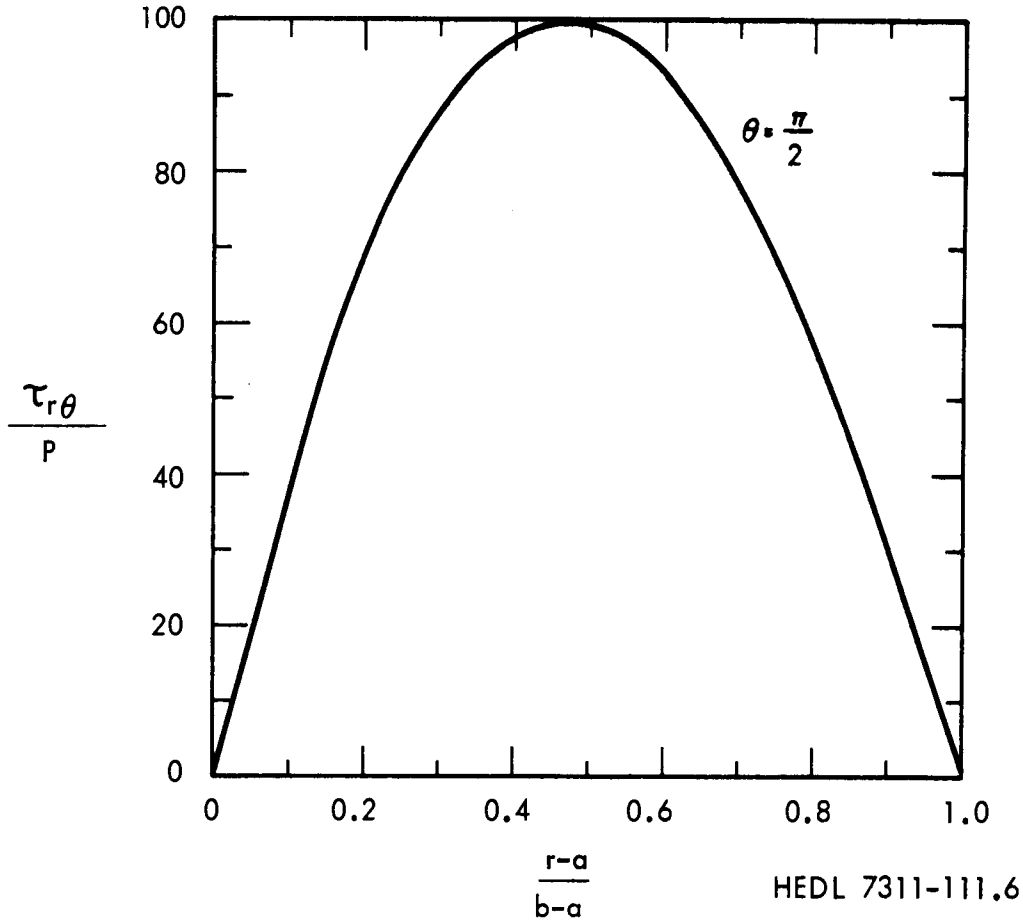

Figure 3.17. Radial Dependence of the Shear Stress Distribution in a Loaded Slit Tube.

radial stress and its maximum value is less than 4% of the maximum normal stress. The largest magnitude of the normal stress σ_θ occurs at $\theta = \pi$ and $r = a$ where the bending moment of the applied force is largest, and it is seen that the applied stress has in effect been amplified by a factor of about 88 due to the geometry of the loading. The dependence of the normal stress σ_θ stress on θ has to a fair approximation the form that predicted earlier from the simple bending moment argument, i.e., $\sigma_\theta \alpha (1-\cos\theta)$ as will be shown below.

The radial dependence of σ_θ is qualitatively the same as that obtained for a thin curved beam using elementary bent beam analysis,[10] that is σ_θ is nearly linear in r obtaining a value of zero at a radius slightly less than the midpoint of the beam.

The apparently simple dependence of σ_r, σ_θ and $\tau_{r\theta}$ on r and θ for the present parameters of interest suggests that a simpler form of Equation (3.29) is obtainable in this case. Such a form can be obtained by expanding the stress functions in a Taylor series about the points r=a dnd b-a. The expansion is tedious but straightforward, as long as one is careful to remember that these functions must be expanded in terms of two independent variables r and b. The Taylor series in two variables is:

$$f(r,b) = f(r_o,b_o) + \frac{\partial f}{\partial r}\Big|_{r_o,b_o}(r-r_o) + \frac{\partial f}{\partial b}\Big|_{r_o,b_o}(b-b_o)$$

$$+ \frac{1}{2}\left(\frac{\partial^2 f}{\partial_r{}^2}\right)\Big|_{r_o,b_o}(r-r_o)^2 + 2\frac{\partial^2 f}{\partial r^{2b}}\Big|_{r_o,b_o}(r-r_o)(b-b_o) \tag{3.30}$$

$$+ \frac{\partial^2 f}{\partial_b{}^2}\Big|_{r_o,b_o}(b-b_o)^2 + \ldots$$

using as an abbreviation $\Delta=b-a$, $\eta=r-a$ the stress dependence on r and θ can be written:

$$\sigma_r = \frac{6P(\eta)(\Delta-\eta)}{\Delta^3}\left[\left(1 + \frac{\Delta-2\eta}{a}\right)(\cos\theta-1) + \frac{\Delta-2\eta}{6a}\right] \tag{3.31a}$$

$$\sigma_\theta = \frac{6Pa(\Delta-2\eta)}{\Delta^3}\left(1 + \frac{\Delta-\eta}{a}\right)(\cos\theta-1) + P/\Delta \tag{3.31b}$$

$$\tau_{r\theta} = \frac{6P\eta(\Delta-\eta)}{\Delta^3}\left(1 + \frac{\Delta-2\eta}{a}\right) \sin\theta \tag{3.31c}$$

This simplified form is in error by at most 2% at $\theta = 0$ and over most of the range it is accurate to better than 1%.

3.2.4.2.2 Strains and Compliance. Before going on to derive the compliance for the slit cylinder, it is necessary to consider the difference between the two extremes of plane stress and plane strain in the present problem. Hooke's law for an isotropic material in polar coordinates is:

$$\varepsilon_r = \frac{\sigma_r - \nu(\sigma_\theta\ \sigma_z)}{E} \tag{3.32a}$$

$$\varepsilon_\theta = \frac{\sigma_\theta - \nu(\sigma_r+\sigma_z)}{E} \tag{3.32b}$$

$$\varepsilon_z = \frac{\sigma_z - \nu(\sigma_r+\sigma_\theta)}{E} \tag{3.32c}$$

$$\gamma_{r\theta} = \frac{2(1+\nu)}{E}\tau_{r\theta} \tag{3.32d}$$

where E is Young's Modulus and ν is Poisson's ratio. In the case of plane stress (very short cylinder) $\sigma_z = 0$ and Equation (3.32) becomes:

$$\varepsilon_r = \frac{\sigma_r-\nu\sigma_\theta}{E}$$

$$\varepsilon_\theta = \frac{\sigma_\theta-\nu\sigma_r}{E} \tag{3.33}$$

$$\gamma_{r\theta} = \frac{2(1+\nu)}{E}\tau_{r\theta}$$

In the case of plane strain (very long cylinder) $\varepsilon_z = 0$. From Equation (3.32c) it is seen that:

$$\sigma_z = \nu(\sigma_r + \sigma_\theta). \tag{3.34}$$

Hence, in the case of plane strain there is a stress component σ_z which is now important in magnitude compared to σ_θ. Using Equation (3.33), Hooke's law for plane strain can be written in terms of σ_r, σ_θ, and $\gamma_{r\theta}$ yielding:

$$\varepsilon_r = \frac{\sigma_r - \nu'_\theta}{E'} \tag{3.35a}$$

$$\varepsilon_\theta = \frac{\sigma_\theta - \nu'\sigma_r}{E'} \tag{3.35b}$$

$$\gamma_{r\theta} = \frac{2(1+\nu')}{E'}\,\tau_{t\theta} \tag{3.35c}$$

where $E' = E/(1-\nu^2)$ and $\nu' = \nu/(1-\nu)$.

For relatively thin-walled tubing (b-a<<tube length) such as is of interest here (O.D. = 0.230", wall thickness = 0.015") the plane strain case is obtained for all practical situations. To illustrate this, it is only necessary to recognize that plane stress would correspond to the a length ℓ of the tube much less than the wall thickness (0.015") which is the minimum dimension of the specimen in the plane of loading. A length ℓ of 1" is planned for the actual experimental program so that the plane strain case is clearly obtained.

It is worthwhile to note that in an actual experimental situation it is probably more convenient not to constrain the specimen along its length. In this case, there will be end effects as the stress σ_z must be zero on the free ends. By an application of St. Venant's principle, however, the stress distribution should become the same as that predicted for the plane strain case within a distance of a few times the tubing wall thickness. Hence, specimens of a length of about 1 inch should have truly negligible end effects for a=0.1 and b=0.115.

The remaining part of the elastic analysis is a calculation of the displacements produced by the loading shown in Figure 3.12. The displacement is defined in terms of the strains in Equation (3.34) and the following relationships:

$$\varepsilon_r = \frac{\partial u}{\partial r} \tag{3.36a}$$

$$\varepsilon_\theta = \frac{u}{r} + \frac{\partial v}{r\partial\theta} \tag{3.36b}$$

$$\gamma_{r\theta} = \frac{1}{r}\frac{\partial u}{\partial r} + \frac{\partial v}{\partial r} - \frac{v}{r} \tag{3.36c}$$

where u is the radial displacement and v is the displacement in the θ direction. The calculation of displacements for the pure bending component is

done in Reference 14 (p. 66-69) so it will only be necessary to calculate the displacements for the stress distribution specified by Equation (3.19).

The calculation will be done for the plane stress case and at the end use will be made of the correspondence $\nu \rightarrow \nu'$ and $E \rightarrow E'$ to obtain the plane strain results. By using Hooke's law to eliminate the strains, Equations (3.36a), (3.33), (3.19a) and (3.19b) can be combined to yield:

$$\frac{\partial u1}{\partial r} = \frac{\cos\theta}{E}\left[2Ar(1-3\nu) - \frac{2B}{r^3}(1+\nu) + \frac{D}{r}(1-\nu)\right] \tag{3.37}$$

so that upon integrating the radial displacement is found to be:

$$u_1 = \frac{\cos\theta}{E}\left(Ar^2(1-3\nu) + \frac{B(1+\nu)}{r^2} + D\log r\,(1-\nu)\right] + f(\theta) \tag{3.38}$$

where $f(\theta)$ is a function of θ only.

Now using Equations (3.36b) and (3.38) for u an equation for v can be obtained in the same way as Equation (3.37) to yield:

$$\frac{\partial v_1}{\partial r} = \frac{\cos\theta}{E}\left[Ar^2(5+\nu) + \frac{B}{r^2}(1+\nu) + D(1-\nu)\,(1-\log r)\right] - f(\theta) \tag{3.39}$$

Integrating Equation (3.39) yields:

$$v_1 = \frac{\sin\theta}{E}\left[Ar^2(5+\nu) + \frac{B}{r^2}(1+\nu) + D(1-\nu)(1-\log r) - \int f(\theta)d\theta + F(r)\right. \tag{3.40}$$

where $F(r)$ is a function of r only. Finally, using Equation (3.36c), and the expressions for u, v and the strain $\gamma_{r\theta}$ in terms of $\tau_{r\theta}$ one obtains:

$$\frac{4D\sin\theta}{E} = \frac{df(\theta)}{d\theta} + \int f(\theta)\,d\theta - F(r) + \frac{rdF}{dr}\ . \tag{3.41}$$

This equation is satisfied by taking

$$f(\theta) = \frac{2D}{E}\,\theta\sin\theta + K\sin\theta + L\cos\theta \text{ and } F(r) = Hr \tag{3.42}$$

where H is a constant. Substituting Equation (3.42) into Equations (3.38) and (3.40) yields:

$$u_1 = \frac{\cos\theta}{E}\left[Ar^2(1-3\nu) + \frac{B(1+\nu)}{r^2} + D\log r\,(1-\nu)\right] \tag{3.43a}$$

$$+ \frac{2D}{E}\quad \sin\theta + K\sin\theta + L\cos\theta$$

$$v_1 = \frac{\sin\theta}{E}\left[Ar^2(5+\nu) + \frac{B}{r^2}(1+\nu) + D(1-\nu)(1-\log r)\right] + \frac{2D}{E}(\theta\cos\theta - \sin\theta) - L\sin\theta + K\cos\theta + Hr \tag{3.43b}$$

The constants H and K are determined by the constraints that the cylinder not life off its fixture; i.e., v and $\partial v/\partial r = 0$ at $\theta = \pi$ so that from Equation (3.43b) it is seen

$$H = 0,\ K = \frac{2\pi D}{E}\ . \tag{3.44}$$

The constant L can be determined by requiring u = 0 at the center of the tube wall at the fixture, i.e.,

$$L = -\left[Ar_o^{\,2}(1-3\nu) + \frac{B(1+\nu)}{r_o^{\,2}} + D\log r_o\,(1-\nu)\right] / E \tag{3.45}$$

where $r_o = \frac{a+b}{2}$. Finally, the displacements due to the loading are (at $\theta = 0,\ r = r_o$)

$$u_1 = 0 \tag{3.46a}$$

$$v_1 = \frac{-2\pi}{E}\,\frac{(b^2+a^2)P}{N} \quad \left(\begin{matrix}\text{Plane Stress}\\ \text{Half-Circle}\end{matrix}\right) \tag{3.46b}$$

The displacements due to the bending component (based on data by J. E. Flynn) are as follows:

$$u_2 = \frac{4P(a+b)}{N'E}\left\{\frac{-2(1+\nu)a^2b^2\log b/a}{a+b} + \frac{(b^2-a^2)}{2}(a+b)\left[(1-\nu)\log r_o - \frac{(1+\nu)}{2}\right] + \frac{(a+b)(1-\nu)}{2}\left[a^2\log a - b^2\log b - \frac{(b^2-a^2)}{2}\right]\right\} \tag{3.47a}$$

$$v_2 = \frac{-2P\pi(a+b)^2\,(b^2-a^2)}{N'E} \quad \text{(Plane Stress, Half Circle)} \tag{3.47b}$$

The net displacement for the slit cylinder loaded as in Figure 3.12 is then obtained by summing the results in Equations (3.46) and (3.47). For plane-strain the same formula is used except that it must be remembered to use $E \to \frac{E}{1-\nu^2}$ and $\nu \to \frac{\nu}{1-\nu}$. It is interesting to note that the displacement v depends only on E as shown in Equations (3.46) and (3.47) so that the displacement in the θ direction in plane strain is reduced only to 0.91 of that for plane strain with $\nu = 0.3$. Further, for thin tubes, in plane stress, the radial displacement u_2 is a nearly independent of ν, so that in this case

the same reduction in the plane strain displacement holds for the radial displacement. As an example, the displacements for a=0.100, b=0.115 are:

$$v_1 = -4.2214\ P\ \frac{(1-\nu^2)}{(1-.3^2)}\ \frac{(30 \times 10^6)}{E} \times 10^{-4} \tag{3.48a}$$

$$v_2 = -8.4239\ P\ \frac{(1-\nu^2)}{(1-.3^2)}\ \frac{(30 \times 10^6)}{E} \times 10^{-4} \tag{3.48b}$$

$$v = -1.2645\ P\ \frac{(1-\nu^2)}{(1-.3^2)}\ \frac{(30 \times 10^6)}{E} \times 10^{-4} \tag{3.48c}$$

$$u = +5.3502\ P\ \frac{(1-\nu^2)}{(1-.3^2)}\ \frac{(30 \times 10^6)}{E} \times 10^{-4} \tag{3.48d}$$

(Plane-Strain Full Circle)

Another useful way of expressing the results is to express the maximum absolute value of stress in terms of the slit width change, the quantity which is likely to be most easily measurable. For the same constants used in Equation (3.48) it is found from Equations (3.29) and (3.48):

$$\sigma_{max} = 4.8098\ v\left(\frac{1-.3^2}{1-\nu^2}\right)\left(\frac{E}{30 \times 10^6\ \text{psi}}\right) \times 10^6\ \text{psi} \tag{3.49}$$

From Equations (3.48) and (3.49) it is seen that for a cladding specimen of length one inch a load P of 8 lb/in gives rise to a maximum stress of 48,600 psi and a slit width change of 10.1 mills. The accuracy required for a nominal error of 500 psi in σ_{max} is 0.1 mill in displacement change or 0.08 lb in load change for this slit tube arrangement. Either of these measurement techniques should be obtainable without use of elaborate techniques, so that it may be concluded that the slit tube is feasible for stress relaxation experiments.

Finally, an alternate method of calculating the displacement v, which serves as a check on Equation (3.49) is presented. The theorem of Castligiano (described in most standard elasticity texts) allows the calculation of the displacement from the elastic energy associated with the displacement. In the present situation the theorem reduces to:

$$v = \frac{\partial E}{\partial (P\ell)} \tag{3.50}$$

where E is the elastic energy, ℓ is the tube length and v and P are as defined above. Using the approximate stress distribution (Equation (3.31)) to obtain the elastic energy density and integrating over the volume of the tube one obtains:

$$v_{Cast} \simeq \frac{36\pi Pa^3}{E'\Delta^3}\left(1 + \frac{3\Delta}{2a}\right) \text{ (Plane Strain, Full Circle)} \qquad (3.51)$$

which becomes

$$v_{Cast} \simeq 1.245\ P\ \frac{(1-v^2)}{(1-.3^2)}\ \frac{(30 \times 10^6)}{E} \times 10^{-3} \qquad (3.52)$$

for a=0.1 and b=0.115. This is in very good agreement with the exact result derived earlier.

3.2.4.2.3 Conclusions and/or Recommendations. There are three main conclusions resulting from this analysis:

(1) The stress distribution in a slit section of Type 316 stainless steel cladding is of a relatively simple nature for the case of loading at the slit.

(2) The displacements and loading forces are of conveniently measurable magnitude for the desired maximum stress levels.

(3) In-reactor mechanical testing of stainless steel cladding is feasible using the slit-tube configuration.

3.3 MATERIALS PERFORMANCE AND SURVEILLANCE - T. T. Claudson and J. J. Holmes

3.3.1 FTR Component Materials Irradiation Experiment

3.3.1.1 Objective

The purpose of this activity was to prepare a structural materials irradiation experiment for insertion into EBR-II. The objective of this experiment is to define and evaluate the effects of fast reactor irradiation and environment on the mechanical properties, microstructure, and dimensional stability of various materials representing FTR in-vessel components. Basically, the experiment is restricted to those properties most needed for

confirming design, performance prediction and safety analyses for FFTF. Specifically, included are the following:

1. Determine the degradation of tensile properties, particularly ductility, in tungsten and TZM in support of FTR CLIRA meltdown cups.

2. Describe fast reactor environmental effects on tensile, creep and swelling properties of Inc-600 in support of FTR reflectors.

3. Evaluate effects of irradiation on the tensile and creep properties of Inc-718 and welds in support of FTR core basket, control rod driveline and absorber shaft and other components.

4. Describe effects of irradiation on the tensile ductility of Type 304L and welds for predicting FTR core basket performance.

5. Obtain postirradiation tensile and microstructural data for CF-8 in support of the FTR core support structure.

6. Study the effects of neutron irradiation on the ductility of alloy A286 bolting material.

7. Determine effects of irradiation and fast reactor environments on structure and on tensile and creep properties of weld deposited Type 308 prototypic of the FTR vessel, core basket and instrument tree.

8. Describe effects of fast reactor irradiation and environment on duct base materials and carbide coatings in terms of tensile creep, bond strength and stability properties in support of FTR ducts and wear pads.

9. Add needed experimental data for the fluence-temperature matrix for cold worked Type 316 and consider combined effects of irradiation, fast reactor environments, variable cold work levels and thermal aging in support of FTR cladding and ducts and general LMFBR base technology considerations.

3.3.1.2 Accomplishments and Status

An overall summary of the experiment content is given in Figure 3.18, and additional detailed information is given in Tables 3.15 through 3.18. FFTF prototypic materials included are 304L/308 base and weld metal (instrument tree and core support structure), 304/308 CRE base and weld metal (reactor vessel), CF-8 (lower core support ring), 316 autogenous weld (absorber pin weld), and 20% cold worked 316 (cladding and ducts). FFTF representative materials included are A286 (bolting material), Inconel 718 base and weld metal (control rod driveline, core basket liners, core restraint, etc.), tungsten and TZM (CLIRA meltdown cup), 20% cold worked 316 wire (fuel pin wrap), and candidate hardfacing materials (duct load pads, CLIRA seals, etc.).

Over 1250 specimens of various configurations are contained in thirteen EBR-II Mark B-7A capsules (pins) identified as B-95 through B-107. These capsules are divided into four groups so as to provide four distinct peak fluence values. The maximum peak fluence of 1×10^{23} n/cm^2 (E > 0.11 MeV) will be achieved in pin-group A (Pins B-95, 96, 97 and 98) in 20 EBR-II runs. During the initial 2 runs the subassembly will be made up of pin-group A and pin-group B (Pins B-99, 100 and 101) thus providing a peak fluence of 1×10^{22} n/cm^2 (E > 0.11 MeV) in pin-group B. Peak fluences of 3×10^{22} and 6×10^{22} n/cm^2 will be achieved in pin-groups C (Pins B-102, 103 and 104) and D (Pins B-105, 106 and 107), respectively, by means of pin-group interchanges after 2 and 8 runs.

Irradiation temperatures will be maintained primarily by having the specimens encapsulated in sodium-filled subcapsules which utilize a combination of gamma heating and thermal insulation (gas-gap) to regulate heat flow. Design temperatures were calculated on the basis of subcapsule density, gamma heating, and heat flow across the gas-gap between the subcapsule wall and the

S U M M A R Y

OBJECTIVES

- PROVIDE POSTIRRADIATION DATA KEYED TO FTR COMPONENT MATERIALS AND SERVICE CONDITIONS
- COMPLETE BASE-TECHNOLOGY DATA MATRICES FOR FFTF/LMFBR APPLICATIONS

COMPONENTS REPRESENTED

- FTR VESSEL
- CORE SUPPORT STRUCTURE
- RADIAL AND AXIAL REFLECTORS
- DUCTS--CLOSED LOOP, CONTROL ROD, DRIVER FUEL
- ABSORBER PIN CLOSURE WELD
- CONTROL ROD DRIVE MECHANISM
- INSTRUMENT TREE
- IVHM
- CLIRA
- CORE BASKET
- MELTDOWN CUP (CLIRA)
- FUEL CLADDING

MATERIALS

- TUNGSTEN AND TZM
- INCONEL-718 (BASE AND WELD)
- TYPE 316 (ANNEALED AND COLD WORKED)
- HARDFACING - CARBIDE AND INCONEL-718
- INCONEL-600
- TYPE 304L, 304
- TYPE 308 WELDS
- A-286
- CF-8
- 16-8-2

EXPERIMENT IRRADIATION CONDITIONS

- 4 PINS -- 10×10^{22} n/cm^2, 700 - 1300°F (PIN GROUP A)
- 3 PINS -- 6×10^{22} n/cm^2, 700 - 1200°F (PIN GROUP D)
- 3 PINS -- 3×10^{22} n/cm^2, 700 - 1200°F (PIN GROUP C)
- 3 PINS -- 1×10^{22} n/cm^2, 700 - 1200°F (PIN GROUP B)

POSTIRRADIATION EXAMINATION

- TENSILE
- SWELLING
- OPTICAL METALLOGRAPHY
- BEND TEST
- BOND TEST
- CREEP-RUPTURE
- TEM

Figure 3.18. FTR Components Materials Irradiation Experiment

Table 3.15. Pin Group "A" (20 Runs), B-95, B-06, B-97, B-98

Pin No.	Level	Material	No. Of Spec.	Spec. Type	Calculated Irrad. Temp., °F	Est. Fluence (10^{22} n/cm^2) E>.11 MeV	Est. Fluence (10^{22} n/cm^2) Total	Approx. A (in.)
B-95 (w)	1	316	7	Clad.	700	2.1	4.4	-14
B-95 (w)	2	316	7	Clad.	700	2.9	5.4	-11.5
B-95 (w)	3	316	7	Clad.	700	4.4	6.8	- 9.3
B-95 (w)	4	316	7	Clad.	700	7.3	9.2	- 6.5
B-95 (w)	5	316	7	Clad.	710	8.9	10.8	- 4.2
B-95 (w)	6	316	1	Abs. Pin.	725	9.7-10.0	12.0-12.4	-3, +3
B-95 (w)	6a	316	3	Clad.	725	10.0	12.4	∿0
B-95 (w)	7	316	7	Clad.	740	8.9	10.8	4.2
B-95 (w)	8	316	7	Clad.	750	6.8	9.0	6.5
B-95 (w)	9	Inc-600/16/8/2	8/2	Ten.	760	4.6	6.8	8.8
B-95 (w)	10	Inc-600/16/8/2	8/2	Ten.	765	3.5	5.4	10.7
B-95 (w)	11	Inc-600/16/8/2	8/2	Ten.	775	2.5	4.7	12.7
B-95 (w)	12	316	1	Abs. Pin.	785	1.3	2.9	16.7
B-95 (w)	13	Inc-718	7	Ten.	805	.62	1.7	20.7
B-95 (w)	14	Inc-718	7	Ten.	810	.39	1.2	22.5
B-96	1	316	16	Fl. Ten.	750	.26-2.1	.92-4.4	-24, -14
B-96	2	316	8	Clad.	1000	2.1-5.0	4.4-7.4	-14, -8
B-96	3	316	8	Wire	1000	5.0-9.3	7.4-11.6	- 8, -3.5
B-96	4	316	4 8	Fl. Ten. Wire	1200	9.7-10.0	12.0-12.4	-3, +3
B-96	5	Inc-600/16/8/2	14/8	Ten.	1100	2.9-9.3	5.0-11.6	3.5, 12
B-96	6	316	12	Clad.	900	.70-2.9	1.9-5.0	12, 20
B-97	1	Hard-Fac.	6/25	Disc/Coup.	900	.79-1.5	2.1-3.6	-19, -15.5
B-97	2	Hard-Fac.	6/25	Disc/Coup.	1000	1.7-2.8	4.0-5.2	-15, -12
B-97	3	316	1	Abs. Pin.	830	2.9-8.7	5.4-10.6	-11.5, -4.5
B-97	4	316	14	Clad.	1200	9.1-10.0	11.2-12.4	-4, +4
B-97	5	316	15	Clad.	1100	2.6-9.1	4.8-11.2	4, 12.5
B-97	6	316	12	Clad.	900	.58-2.6	1.6-4.8	12.5, 21
B-98	1	316	8	Fl. Ten.	750	.26-.79	.92-2.1	-24, -19
B-98	2	316	8	Clad.	800	.79-2.4	2.1-4.8	-19, -13
B-98	3	Inc-600/16/8/2	14/8	Ten.	1000	2.4-8.7	4.8-10.6	-13, -4.5
B-98	4	316	12	Clad.		9.1-10.0	11.2-12.4	-4, +4
B-98	5	Inc-600/16/8/2	14/8	Ten.	1060	2.6-9.1	4.8-11.2	4, 12.5
B-98	6	Inc-718	19	Ten.	900	.58-2.4	1.6-4.4	13, 21

Table 3.16. Pin Group "B" (2 Runs), B-99, B-100, B-101

Pin No.	Level	Material	No. Of Spec.	Spec. Type	Calculated Irrad. Temp., °F	Est. Fluence (10^{22} n/cm^2) E>.11 MeV	Est. Fluence (10^{22} n/cm^2) Total	Approx. Z (in.)
B-99	1	CF-8	19	Ten.	800	.036-.17	.11-.40	-23, -15
B-99	2	304	19	Ten.	830	.17-.75	.40-.94	-15, -6
B-99	3	Hard Fac.	12/12/34	Ten/Disc/Coup.	1000	.75-1.0	.94-1.2	-6, +6
B-99	4	316	12	Clad.	1050	.21-.75	.40-.94	6, 14
B-100	1	308	12	Ten.	800	.02-.17	.064-.40	-25, -15
B-100	1	A286	12	Ten.	800	.02-.17	.046-.40	-25, -15
B-100	2	316	12	Clad.	1000	.17-.75	.40-.94	-15, -6
B-100	3	Inc-718	27	Ten.	1100	.75-1.0	.94-1.2	-6, +6
B-100	4	316	12	Clad.	1050	.18-.75	.37-.94	6, 14.5
B-100	5	304	14	Ten.	900	.06-.17	.35-.16	15, 21
B-101(w)	1	Inc-600/16/8/2	8/2	Ten.	700	.13	.34	-16
B-101(w)	2	Inc-600/16/8/2	8/2	Ten.	700	.21	.44	-14
B-101(w)	3	Inc-600/16/8/2	8/2	Ten.	700	.25	.50	-12.5
B-101(w)	4	TZM	7	Ten.	700	.37	.60	-10.5
B-101(w)	5	W	7	Ten.	700	.48	.72	- 8.6
B-101(w)	6	304L	7	Ten.	700	.70	.88	- 6.7
B-101(w)	7	308	7	Ten.	710	.86	1.04	- 4.7
B-101(w)	8	304L	7	Ten.	715	.97	1.2	- 3
B-101(w)	9	W	7	Ten.	720	1.0	1.24	- 1
B-101(w)	10	TZM	7	Ten.	730	1.0	1.24	1
B-101(w)	11	Inc-718	7	Ten.	735	.97	1.2	3
B-101(w)	12	Inc-718	7	Ten.	745	.86	1.04	4.7
B-101(w)	13	Inc-718	7	Ten.	750	.70	.88	6.7
B-101(w)	14	Inc-718	7	Ten.	760	.50	.70	8.6
B-101(w)	15	304L/308	7	Ten.	765	.36	.56	10.5
B-101(w)	16	304L	7	Ten.	775	.26	.48	12.5
B-101(w)	17	304L	7	Ten.	780	.18	.37	14.4
B-101(w)	18	304L	7	Ten.	785	.14	.31	16.0

Table 3.17. Pin Group "C" (6 Runs), B-102, B-103, B-104

Pin No.	Level	Material	No. Of Spec.	Spec. Type	Calculated Irrad. Temp., °F	Est. Fluence (10^{22} n/cm^2) E>.11 MeV	Est. Fluence (10^{22} n/cm^2) Total	Approx. Z (in.)
B-102	1	316	12	Clad.	1000	.72-2.4	1.4-2.9	-13, -5.5
B-102	2	Inc-718	24	Ten.	1200	2.6-3.0	3.1-3.7	-5, +5
B-102	3	Inc-718	19	Ten.	1100	.66-2.6	1.2-3.1	5, 13.5
B-102	4	304/308	14	Ten.	900	.21-.62	.57-1.2	14, 20
B-103	1	304L/308	14	Ten.	800	.20-.62	.56-1.3	-20, -14
B-103	2	304/Hardfac.	9/6/34	Ten/Disc/Coup.	950	.62-2.2	1.3-2.8	-14, -6.5
B-103	3	316	8	Fl. Ten.	1000	2.2-3.0	2.8-3.7	- 6.5, 0
B-103	4	316	8	Fl. Ten.	1160	2.5-3.0	3.1-3.7	0, 5
B-103	5	Hard Fac.	8/6	Ten/Disc	1100	.92-2.3	1.5-2.9	5.5, 11.5
B-103	6	316	15	Clad.	950	.21-.92	.60-1.5	11.5, 20
B-104(w)	1	316	7	Clad.	700	.76	1.5	-12.5
B-104(w)	2	316	7	Clad.	700	1.2	2.0	-10
B-104(w)	3	316	7	Clad.	700	1.7	2.5	- 7.5
B-104(w)	4	316	7	Clad.	705	2.6	3.1	- 5
B-104(w)	5	316	7	Clad.	715	3.0	3.6	- 2.5
B-104(w)	6	316	7	Clad.	725	3.0	3.7	0
B-104(w)	7	316	7	Clad.	735	3.0	3.7	2.5
B-104(w)	8	316	7	Clad.	745	2.5	3.1	5
B-104(w)	9	316	7	Clad.	755	1.7	2.5	7.5
B-104(w)	10	316	7	Clad.	765	1.2	1.8	10
B-104(w)	11	316	7	Clad.	775	.80	1.4	12.5
B-104(w)	12	316	7	Clad.	785	.51	1.1	15
B-104(w)	13	316	7	Clad.	790	.34	.79	17.5
B-104(w)	14	316	7	Clad.	800	.21	.57	20
B-104(w)	15	316	7	Clad.	810	.12	.37	22.5
B-104(w)	16	316	7	Clad.	820	.067	.18	25

Table 3.18. Pin Group "D" (12 Runs), B-105, B-106, B-107

Pin No.	Level	Material	No. Of Spec.	Spec. Type	Calculated Irrad. Temp., °F	Est. Fluence (10^{22} n/cm^2) E>.11 MeV	Est. Fluence (10^{22} n/cm^2) Total	Approx. Z (in.)
B-105(w)	1	316	7	Clad.	700	1.5	3.0	-12.5
B-105(w)	2	316	7	Clad.	700	2.3	3.9	-10
B-105(w)	3	316	7	Clad.	700	3.5	4.9	- 7.5
B-105(w)	4	316	7	Clad.	710	5.1	6.2	- 5
B-105(w)	5	316	7	Clad.	715	6.0	7.4	- 2.5
B-105(w)	6	316	7	Clad.	725	6.0	7.5	0
B-105(w)	7	316	7	Clad.	735	6.0	7.5	2.5
B-105(w)	8	316	7	Clad.	745	5.0	6.2	5
B-105(w)	9	316	7	Clad.	755	3.5	4.9	7.5
B-105(w)	10	316	7	Clad.	765	2.3	3.6	10
B-105(w)	11	316	7	Clad.	775	1.6	2.9	12.5
B-105(w)	12	316	7	Clad.	785	1.0	2.1	15
B-105(w)	13	316	7	Clad.	790	.67	1.6	17.5
B-105(w)	14	316	7	Clad.	800	.43	1.2	20
B-105(w)	15	316	7	Clad.	810	.23	.75	22.5
B-105(w)	16	316	7	Clad.	820	.13	.36	25
B-106	1	Hard Fac.	6/25	Disc/Coup.	850	.39-.80	1.1-2.0	-20, -16
B-106	2	Inc-600/16/8/2	21/8	Ten.	900	.80-4.7	2.0-5.8	-16, -5.5
B-106	3	316	19	Clad.	1200	5.1-6.0	6.2-7.5	-5, +5
B-106	4	Inc-718	24	Ten.	1000	.84-4.6	1.9-5.8	5.5, 16
B-106	5	316	8	Fl. Ten.	880	.35-.84	.96-1.9	16, 21
B-107	1	Hard Fac.	6/25	Disc/Coup.	850	.39-.80	1.1-2.0	-20, -16
B-107	2	Hard Fac.	8/6	Ten/Disc	900	.80-2.3	2.0-3.9	-16, -10
B-107	3	Hard Fac.	8/6	Ten/Disc	1160	2.3-5.4	3.9-6.7	-10, -4
B-107	4	Inc-718	14	Ten.	1200	5.5-6.0	6.9-7.5	- 3.5, +3.5
B-107	5	Inc-718	19	Ten.	1150	1.7-5.5	3.0-6.0	3.5, 12
B-107	6	304	19	Ten.	900	.43-1.7	1.2-3.0	12, 20

B7A pin wall. B7A Pins B-95, 101, 104 and 105 are exceptions to the temperature-maintenance practice described above. These pins are "weepers" which allow free ingress of EBR-II coolant sodium thereby permitting the lowest possible irradiation temperatures in EBR-II.

Fluences will be confirmed by postirradiation analysis of dosimeters contained in the subassembly and temperatures will be verified by postirradiation examination of melt-wire sentinels.

3.3.2 High Strain Rate Effects

3.3.2.1 Objective

The objective of this study is to describe the effects of high tensile strain rates on the mechanical properties of FFTF and LMFBR structural and cladding materials. Information from this study is being used to perform safety analyses of hypothetical reactor incidents and also for fuel clad failure analyses.

3.3.2.2 Accomplishments and Status

High strain rate tensile testing of 20% cold worked Type 316 stainless steel prototypic FTR cladding has been completed at strain rates from $\sim 2 \times 10^{-5}$ to 10 in/in/sec and temperatures from 800 to 1600°F. Data obtained from these tests included the ultimate and 0.2% yield strength and total and uniform elongation. The extensive results of these tests have been condensed for presentation in this report. Detailed results including data tables and additional figures are presently being compiled in a topical report.[12]

3.3.2.2.1 Test Materials. The 20% cold worked Type 316 stainless steel cladding material used for this study was obtained from the FFTF Cladding Evaluation Program and was representative of fuel cladding to be used in the FFTF. All specimens were obtained from lot N-3 cladding. Detailed fabrication history, chemical analyses, and mechanical properties for the subject material have been reported previously.[13]

Two specimen geometries were employed in this evaluation. Both were obtained from 0.230 inch O.D. by 0.200 inch I.D. tubing with the first having a 1.37 inch and the second a 2.37 inch gage length. Data were obtained for both gauge lengths because (1) most unirradiated test results available have been obtained on 2.37 inch gauge length specimens, (2) most specimens presently being irradiated in EBR-II contain a 1.37 inch gauge length, and (3) data from both gauge lengths could be used to establish correlations between tensile properties and specimen geometry.

All testing was performed in air within recommended ASTM practice. Detailed test procedures have been described previously.[14,15]

3.3.2.3 Results

3.3.2.3.1 Cladding Properties. The effect of strain rate and temperature on the uniaxial tensile properties of cladding material is presented in Figures 3.19-3.22. In Figure 3.19 the strain rate and temperature dependence of the ultimate strength of both 1.37 and 2.37 inch gauge length specimens is presented. At temperatures to 1000°F the ultimate strength is completely insensitive to strain rate since it remains constant over the entire range of rates. At the higher temperature range (1200 to 1600°F) the ultimate strength first increases rapidly with strain rate to a characteristic temperature dependent strain rate and then only increases gradually at higher rates. Similar behavior is observed for the 0.2% yield strength as shown in Figure 3.20.

The total elongation of 20% C.W. Type 316 stainless steel cladding behaves in a complex manner over the strain rate and temperature range of this study as illustrated in Figure 3.21. For temperatures to 1200°F total

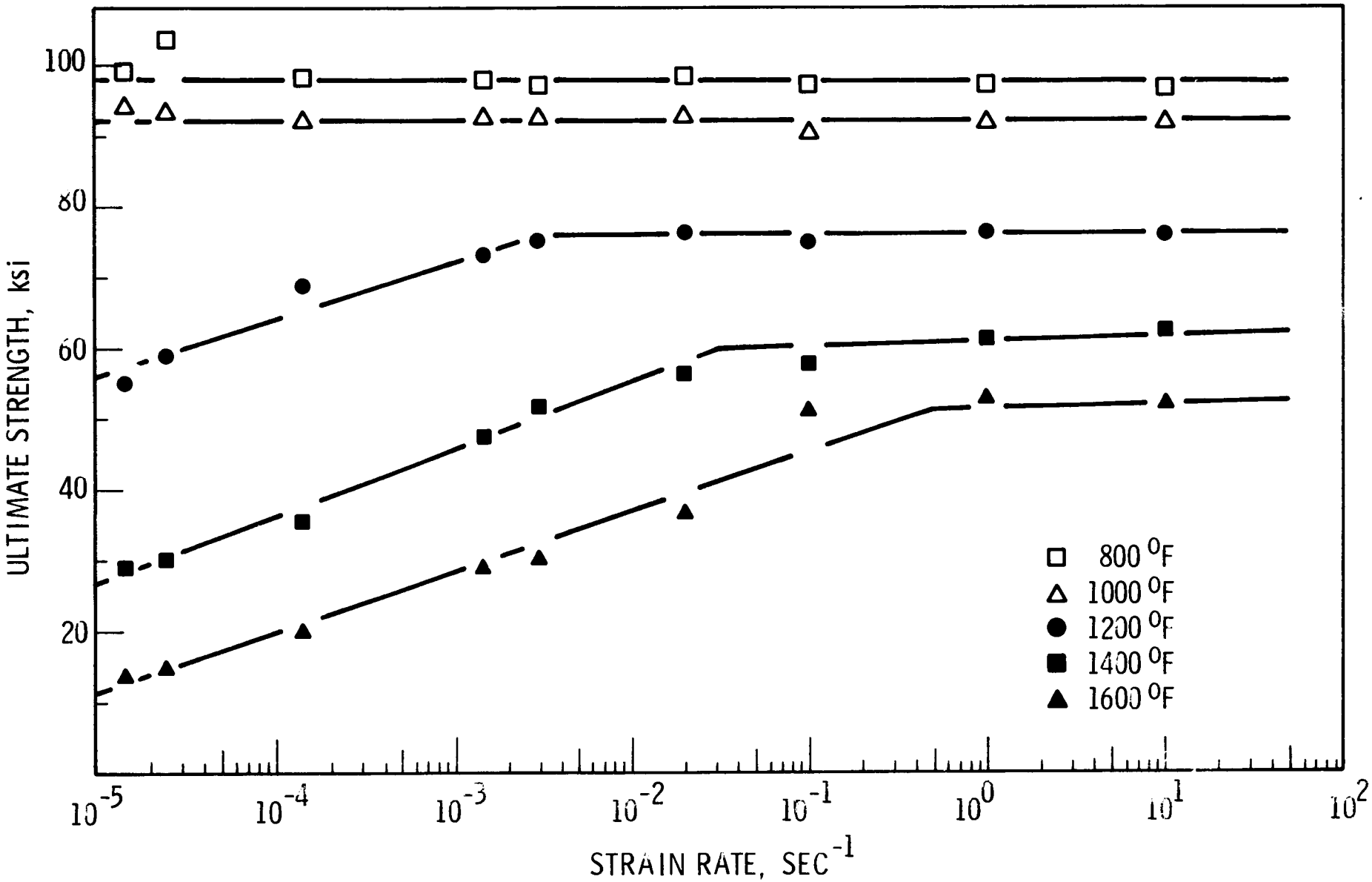

Figure 3.19. Effect of Strain Rate and Temperature on the Ultimate Strength of 20% C.W. Type 316 Stainless Steel N-3 Lot Cladding.

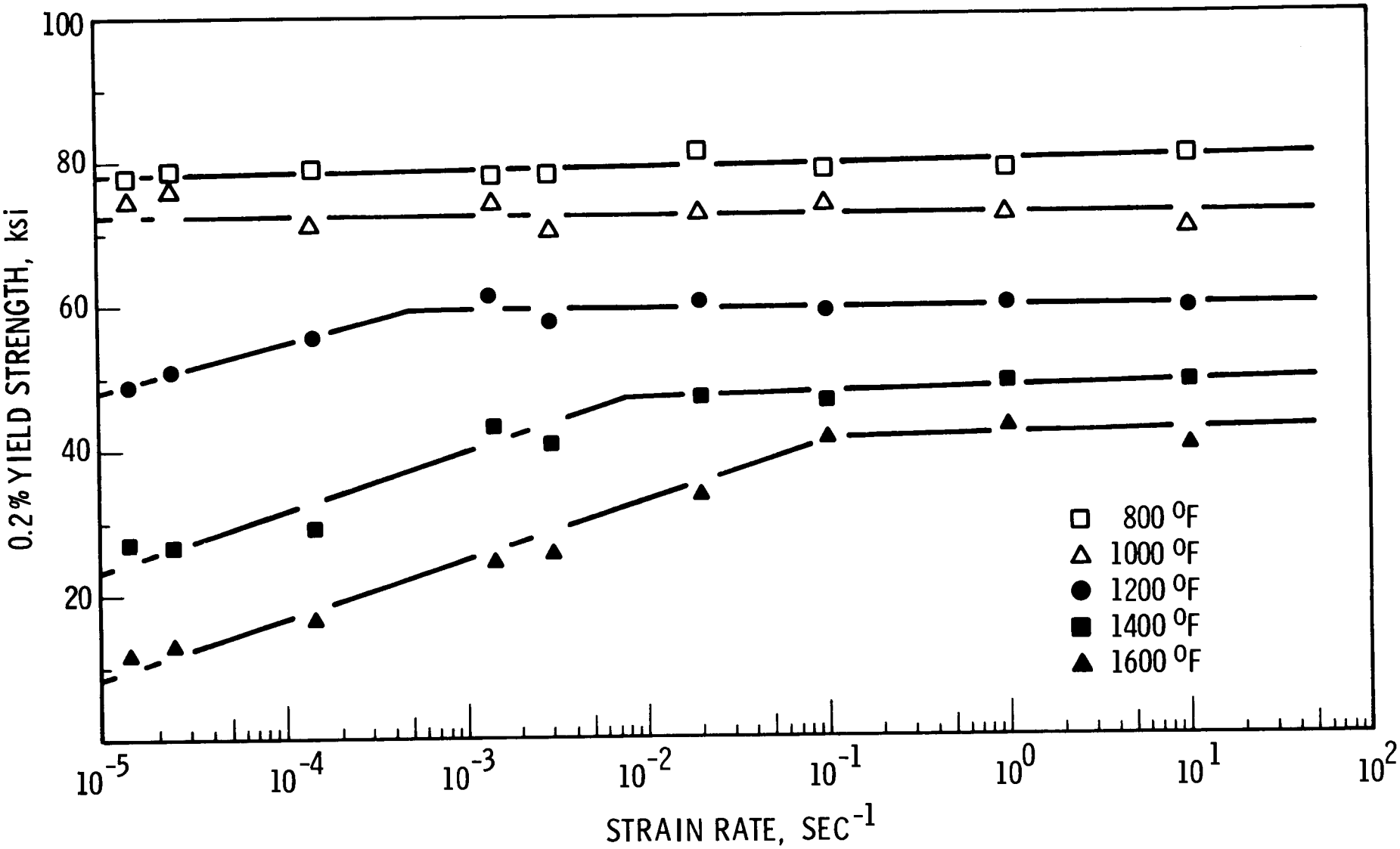

Figure 3.20. Effect of Strain Rate and Temperature on the 0.2% Yield Strength of 20% C.W. Type 316 Stainless Steel N-3 Lot Cladding.

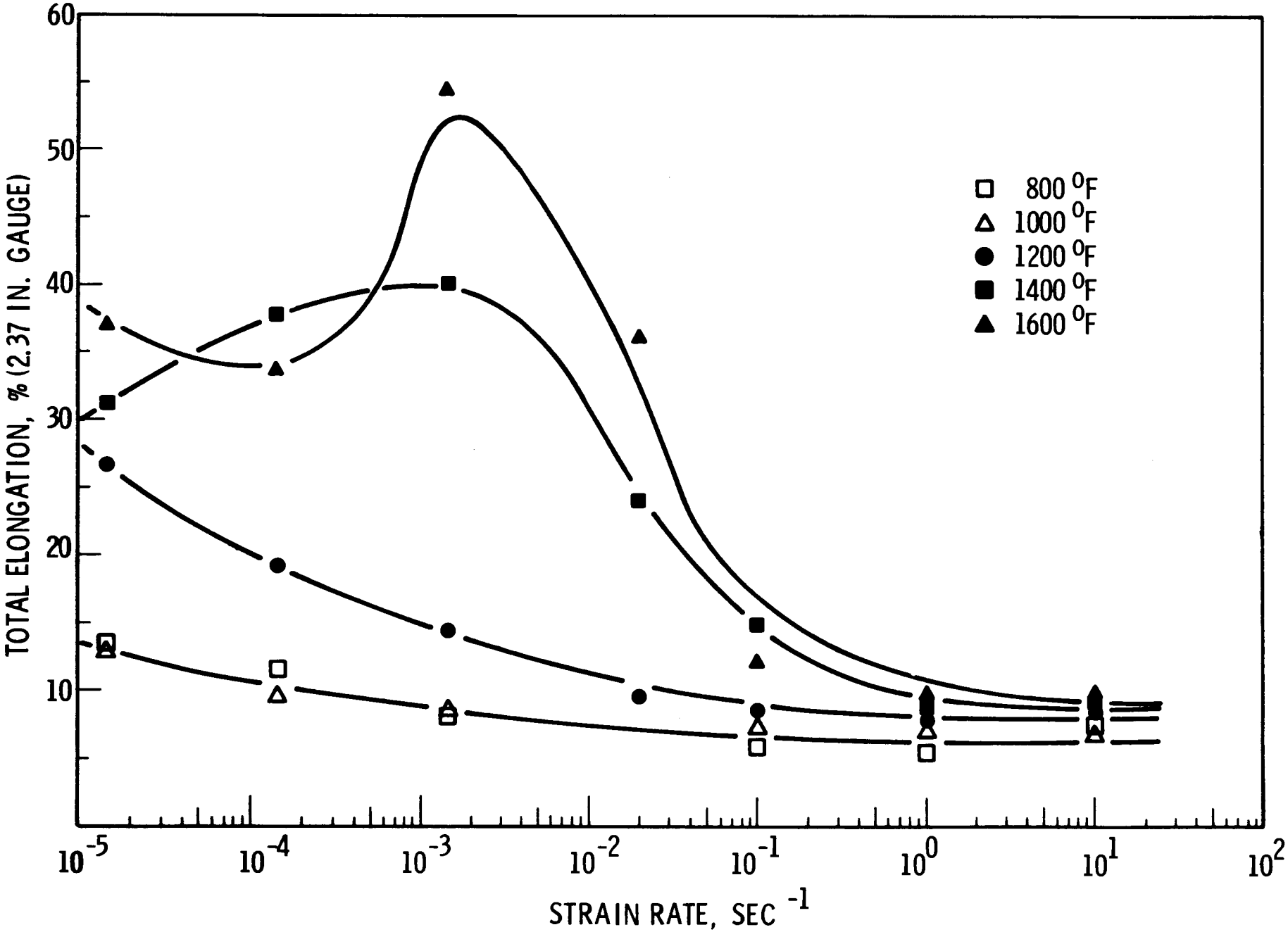

Figure 3.21. Effect of Strain Rate and Temperature on the Total Elongation of 20% C.W. Type 316 Stainless Steel N-3 Lot Cladding.

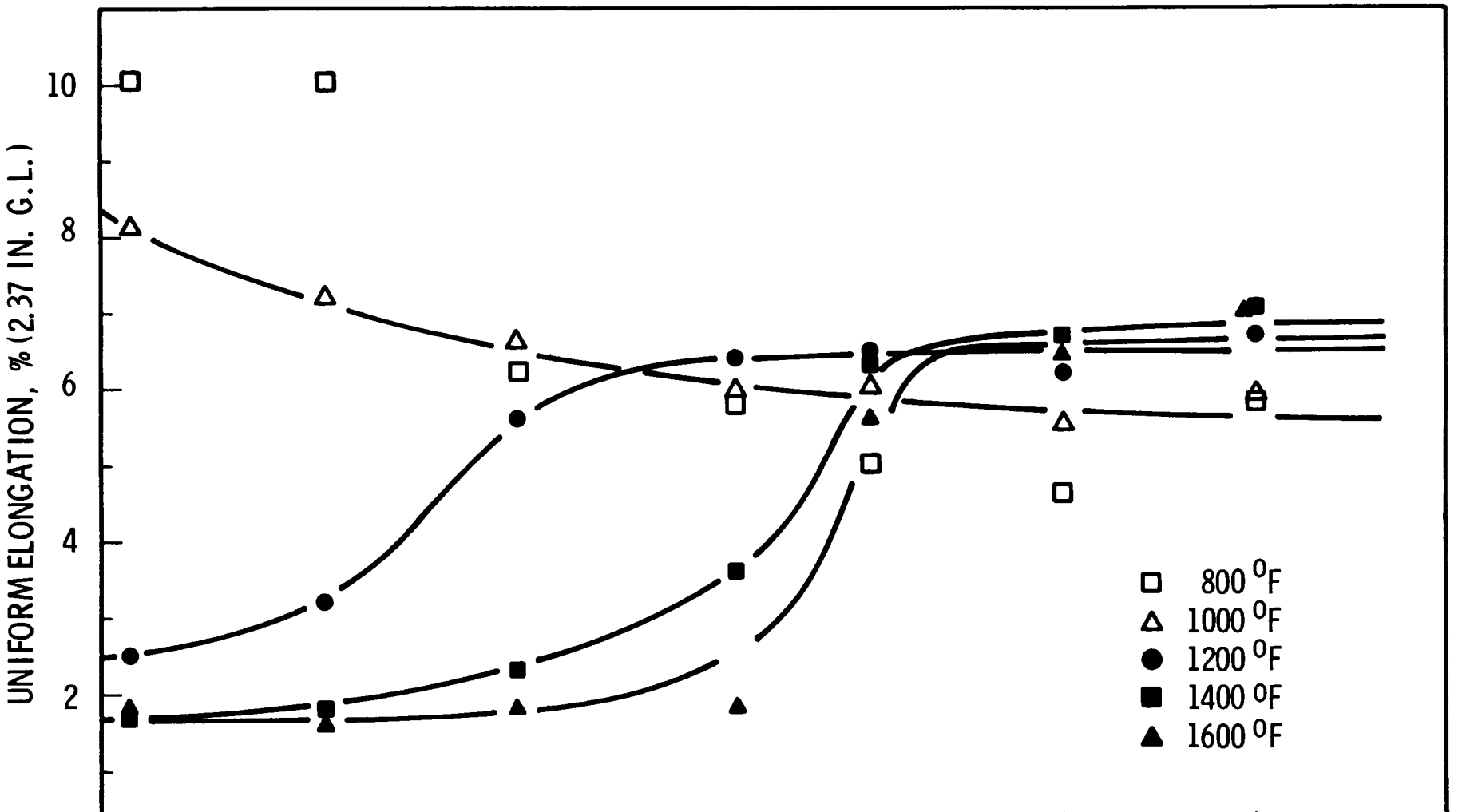

Figure 3.22. Effect of Strain Rate and Temperature on the Uniform Elongation of 20% C.W. Type 316 Stainless Steel N-3 Lot Cladding.

elongation decreases with strain rate while at 1400 and 1600°F it increases with strain rate to a maximum and then rapidly decreases with increasing strain rate. Although minor variations were observed, the trends in ductility for specimens with 1.37 inch gauge lengths were similar to trends for 2.37 inch gauge length specimens.

Figure 3.22 presents the strain rate and temperature dependence of the uniform elongation (elongation at maximum load). For 800 and 1000°F the uniform elongation decreases with strain rate. At the higher test temperatures uniform elongation rapidly increases with strain rate to a maximum level and then remains essentially constant with strain rate.

3.3.2.3.2 Comparison to Previous Results. Extensive elevated temperature high strain rate test results on 20% C.W. Type 316 stainless rod specimens have been reported previously.[16] These results were obtained on the same heat of material that was used to make the N-3 lot of cladding and from specimens at a comparable level of cold work. The recent completion of testing on cladding provides additional data to confirm previous trends and provides a means to correlate tensile properties between the different geometry forms.

The ultimate and 0.2% yield strengths of both solid and cladding specimens of the same heat of 20% C.W. Type 316 stainless steel vs. temperature for three strain rates are presented in Figures 3.23 and 3.24, respectively. At temperatures to 1200°F the cladding (open symbols) exhibits slightly greater ultimate strength than the rod specimens. At 1400 and 1600°F the ultimate strength is essentially equal for both product forms. The strain rate sensitivity at the various temperatures is nearly identical between the two specimen types.

The 0.2% yield strength of cladding is slightly lower than that of the solid specimens for all test temperatures (Figure 3.24). As with the ultimate strength, the strain rate sensitivity of the yield strength is essentially identical between produce forms.

The influence of specimen geometry on the elevated temperature total and uniform elongation of 20% C.W. Type 316 stainless steel at a strain rate of $\sim 2 \times 10^{-5}$ in/in/sec is shown in Figures 3.25 and 3.26. Total elongation

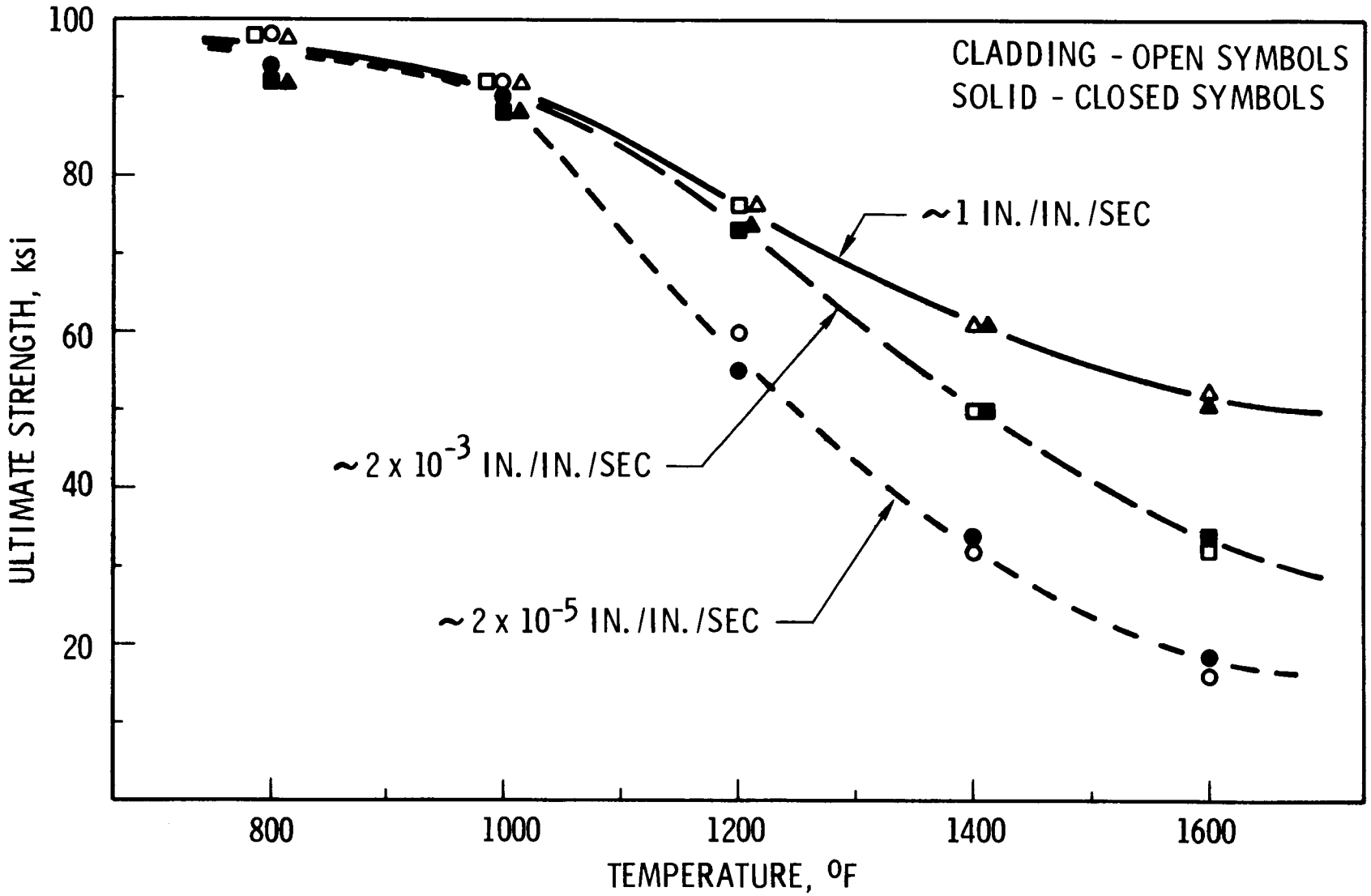

Figure 3.23. Influence of Specimen Geometry on the Elevated Temperature Ultimate Strength of 20% C.W. Type 316 Stainless Steel for Three Strain Rates.

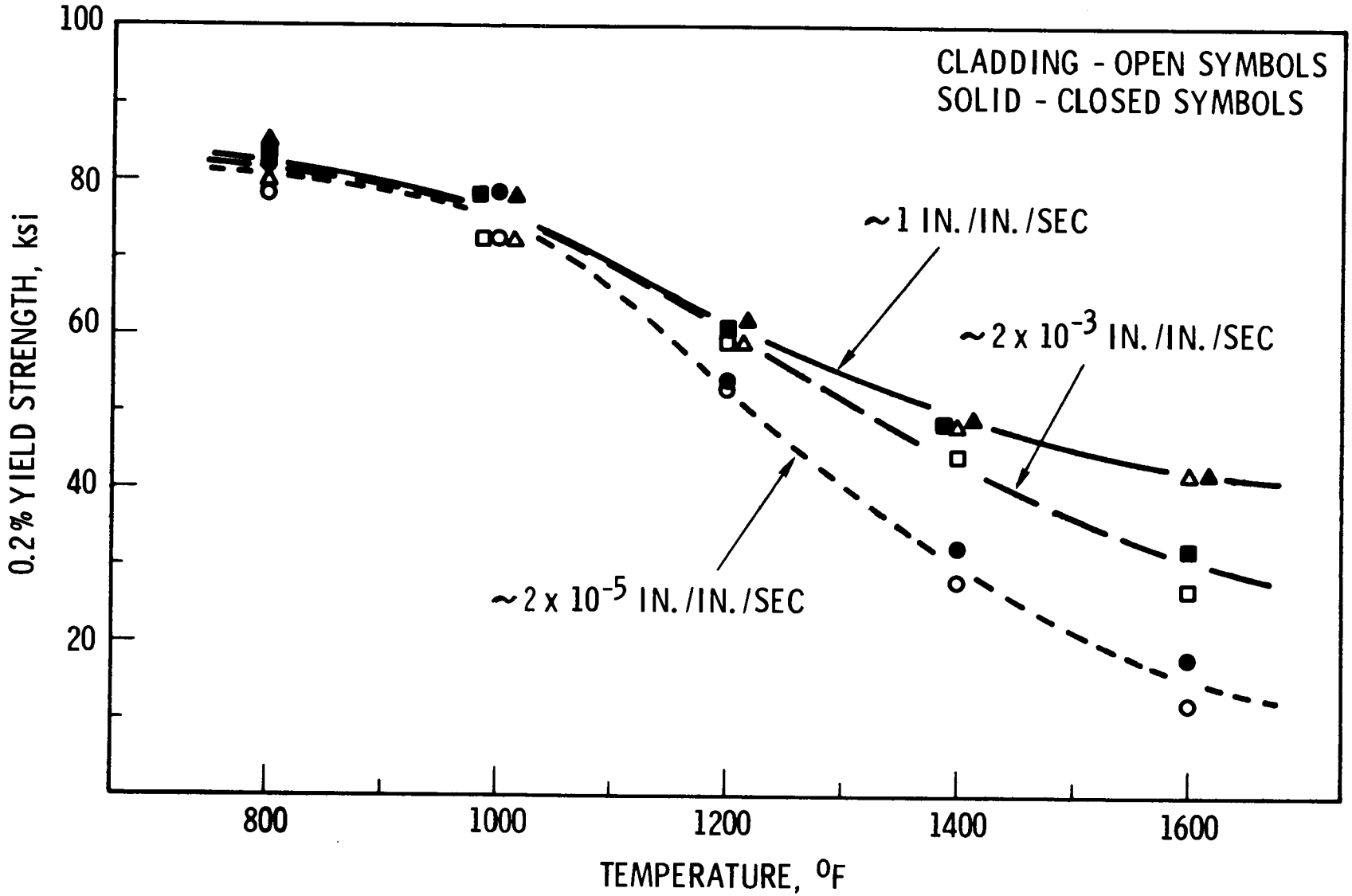

Figure 3.24. Influence of Specimen Geometry on the Elevated Temperature 0.2% Yield Strength of 20% C.W. Type 316 Stainless Steel for Three Strain Rates.

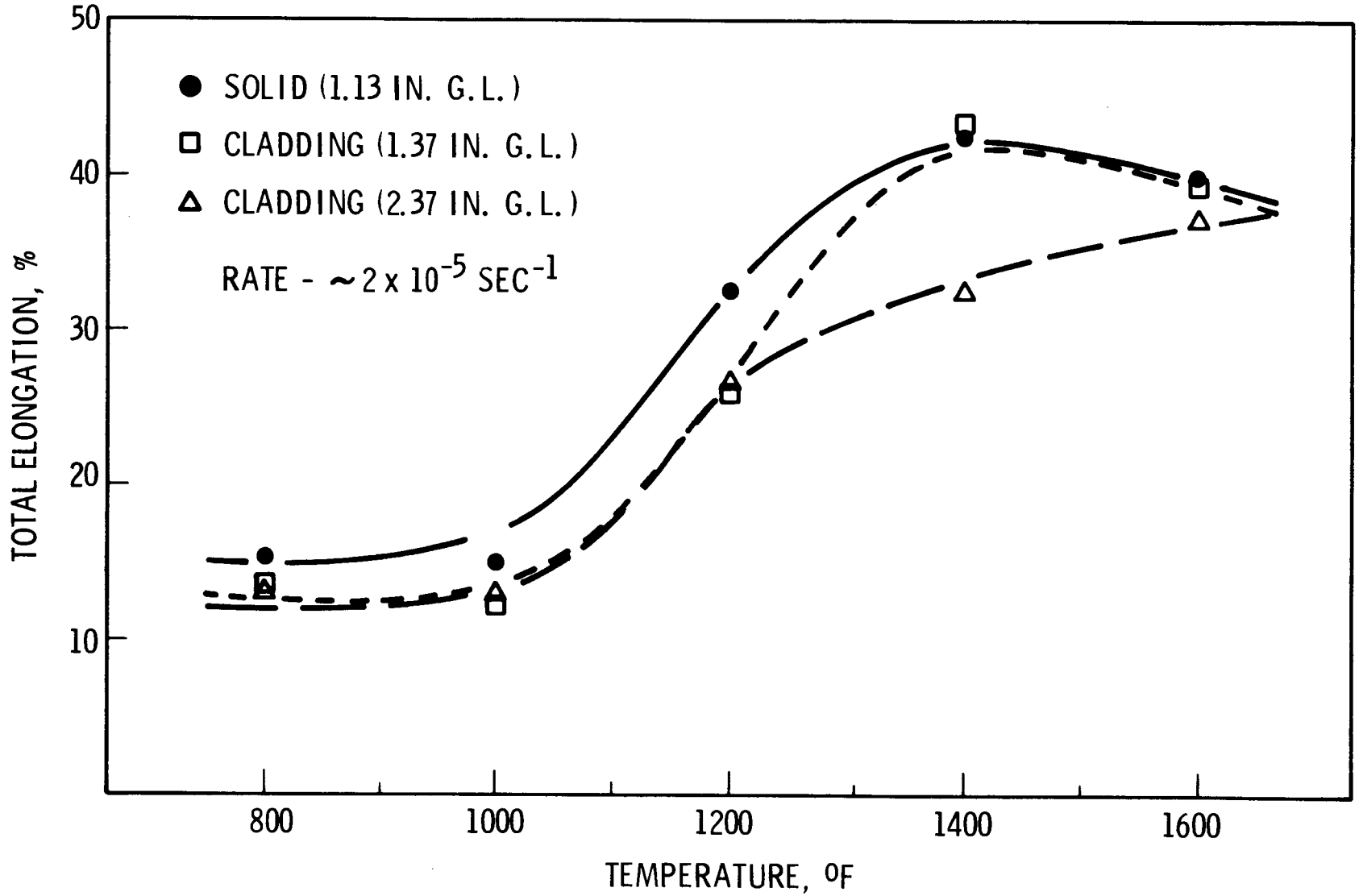

Figure 3.25. Influence of Specimen Geometry on the Elevated Temperature Total Elongation of 20% C.W. Type 316 Stainless Steel for a Strain Rate of 2×10^{-5} sec^{-1}.

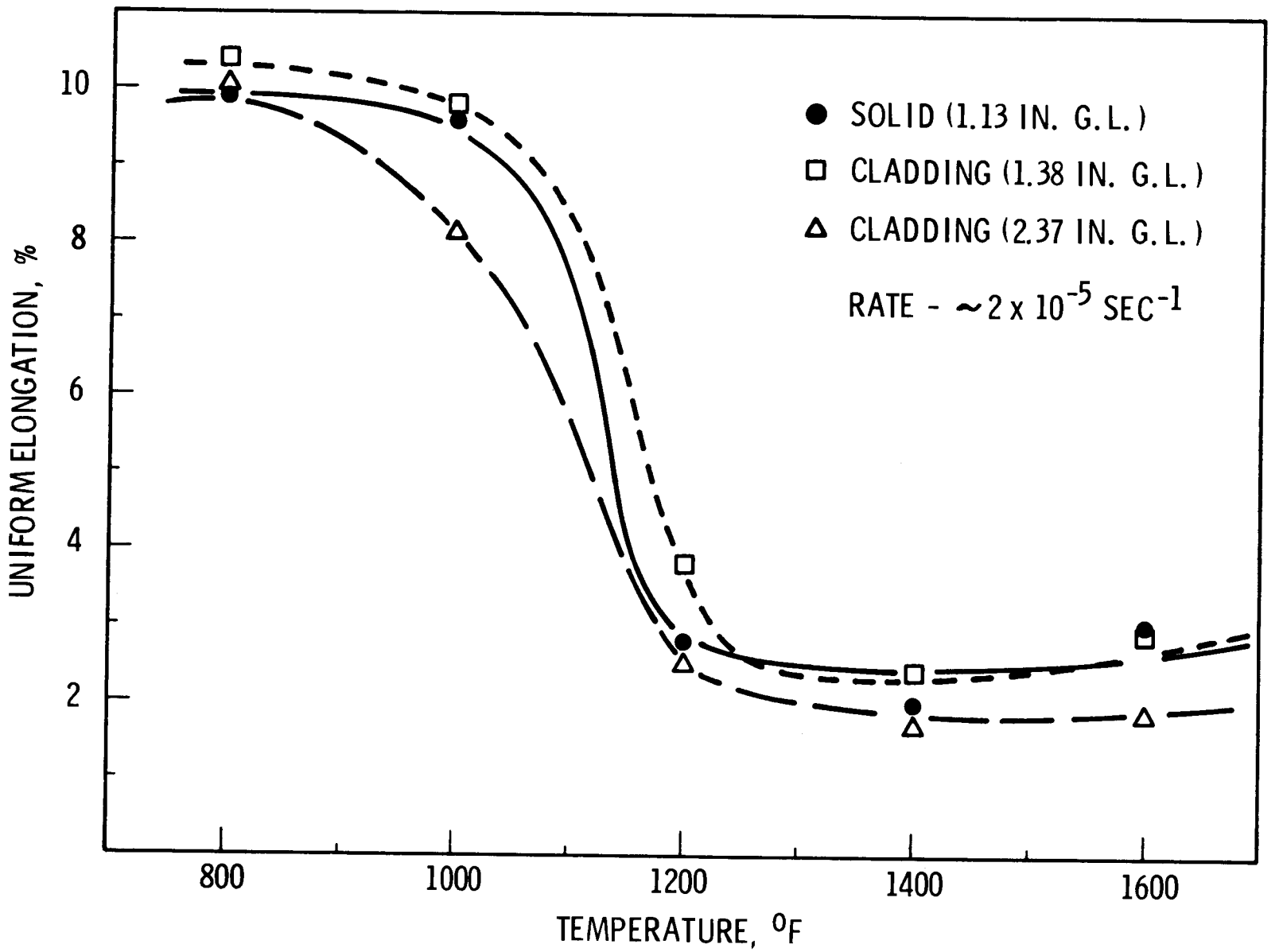

Figure 3.26. Influence of Specimen Geometry on the Elevated Temperature Uniform Elongation of 20% C.W. Type 316 Stainless Steel for a Strain Rate of 2×10^{-5} sec^{-1}.

(Figure 3.25) increases with temperature for all three specimen geometries. The solid specimens exhibited the greatest total elongation with the short gauge length cladding being very similar and the long gauge length cladding having the lowest ductility. At the same strain rate ($\sim 2 \times 10^{-5}$ in/in/sec) uniform elongation decreased with temperature (Figure 3.26) and was very similar between product forms.

Increasing strain rate significantly altered the influence of specimen geometry on observed ductility as illustrated for a strain rate of 1 in/in/sec (Figures 3.27 and 3.28). In Figure 3.27 total elongation increases with temperature for each specimen type, however, large differences in ductility between the specimen types are observed. As with the lowest test rate, the solid specimens have the greatest ductility, the short gauge length cladding intermediate ductility, and the long gauge length cladding the least ductility. Results of Barraclough, et al.[17] indicate similar behavior for elevated temperature torsion tests at a strain rate of 1 in/in/sec on annealed Types 304 and 321 stainless steel solid and tubing specimens.

Uniform elongation increases with temperature at a strain rate of 1 in/in/sec as shown in Figure 3.28. For temperatures of 1000°F uniform elongation is essentially the same between the specimen types. At higher temperatures the solid specimens and 1.37 inch gauge length cladding exhibit greater uniform elongation than the 2.37 inch gauge length cladding.

3.3.2.4 Discussion

3.3.2.4.1 Strength. The strain rate dependence of the ultimate strength of 20% C.W. Type 316 stainless steel indicates that different deformation mechanisms control behavior over the temperature and strain rate range of this study. At test temperatures of 800 and 1000°F athermal deformation controls behavior resulting in tensile properties which are insensitive to strain rate or test temperature. Similarly, athermal deformation controls behavior at high strain rates at temperatures of 1200, 1400 and 1600°F.

Deformation at high temperatures (1200-1600°F) and low strain rates results in large increases in strength with increasing strain rate. In this region thermally activated mechanisms control deformation; therefore,

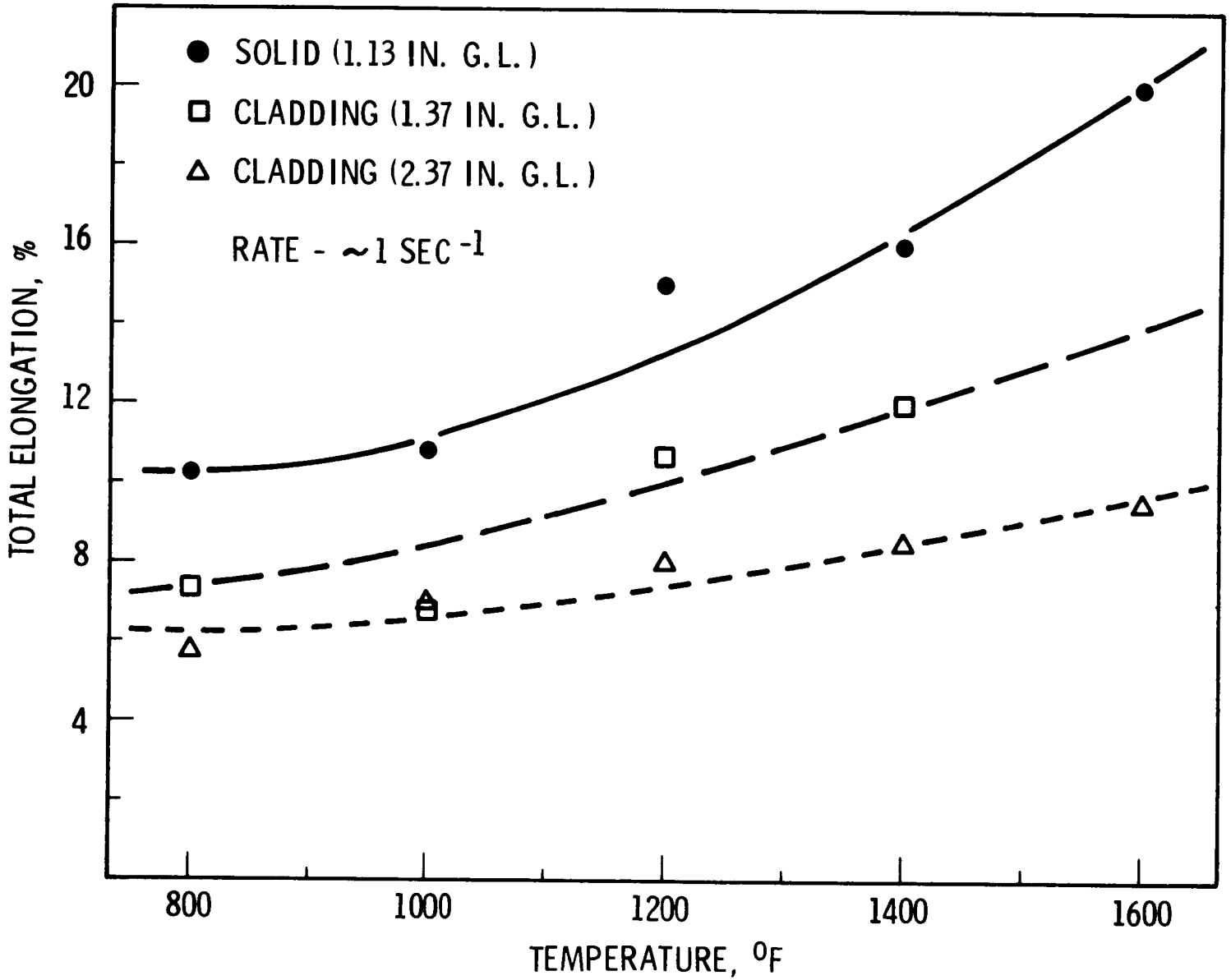

Figure 3.27. Influence of Specimen Geometry on the Elevated Temperature Total Elongation of 20% C.W. Type 316 Stainless Steel for a Strain RAte of 1.0 sec^{-1}.

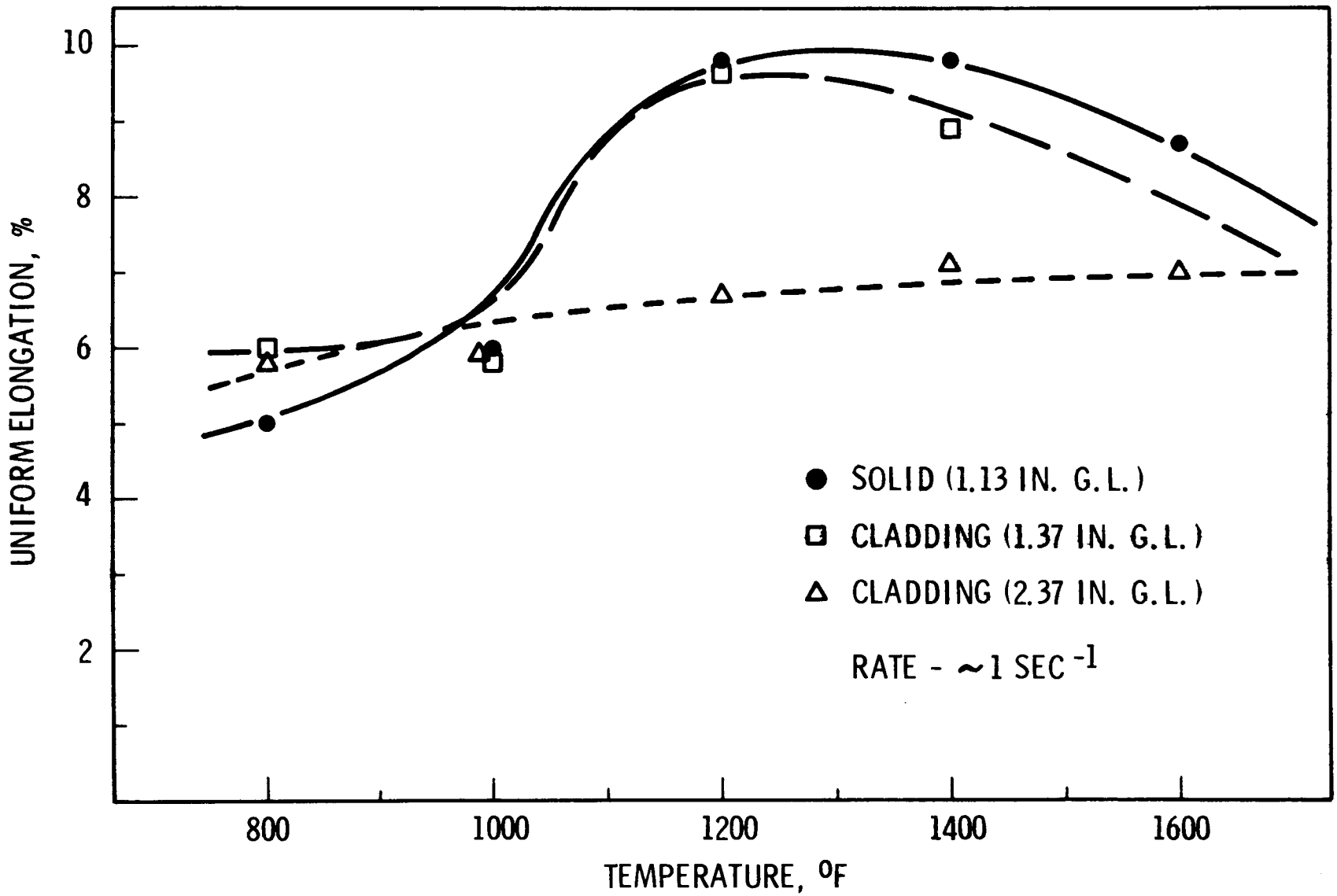

Figure 3.28. Influence of Specimen Geometry on the Elevated Temperature Uniform Elongation of 20% C.W. Type 316 Stainless Steel for a Strain Rate of 1.0 sec^{-1}.

mechanical properties are strongly dependent on test temperature and strain rate. A detailed description of the elevated temperature deformation of austenitic stainless steels has recently been completed by Holmes and Lovell.[18]

3.3.2.4.2 Ductility. The ductility of the subject material behaves in a complex manner over the strain rate and temperature range of this study. At the lower test temperatures ($\leq$ 1000°F) both total and uniform elongation are not greatly rate sensitive although both decrease with increasing strain rate. Similar behavior has been observed in annealed Type 304 stainless steel[19] and results from the decreased strain hardening ability of the material with increasing strain rate.

At the higher temperatures ($\geq$ 1200°F) total elongation appears to increase to a maximum at low strain rates and then decrease with increasing rate. At these same temperatures uniform elongation increases with strain rate. These trends were observed for both cladding and solid specimens; however, the solid specimens exhibited consistently higher ductility than the cladding. The ductility of the test material in this temperature region is influenced by at least two mechanisms. First, temperatures are high enough and test times long enough for recovery to be initiated in the cold worked material[20] and secondly, a transition in fracture mode (intergranular to transgranular) occurs at these temperatures and strain rate ranges.[19] The combination of these two mechanisms is likely responsible for the observed complex behavior in ductility at low strain rates.

Trends in ductility were very similar for both solid and cladding specimens although the solid specimens had greater ductility. At the lowest test rate ($\sim 2 \times 10^{-5}$ in/in/sec) total and uniform elongations were very similar between the three specimen types, however, at a high test rate (1 in/in/sec) significant differences in ductility were observed between the specimen types. As previously stated, trends in ductility obtained at the high rate are in agreement with torsion results of Barraclough, et al.[17] on Type 304 stainless steel heavy walled tubing and solid specimens. In this study they showed that (1) increasing the gauge length to diameter ratio reduced both elongation at maximum load and elongation at fracture; (2) increasing strain rate at elevated

temperature increased elongation to maximum load for any gauge length to diameter ratio and (3) the elevated temperature ductility of solid specimens was greater than that of tubes. The reduced ductility of the tubes at high temperatures resulted since the time to propagate an intergranular crack across the tube wall would be much less than the time required to fracture a solid specimen of the same diameter. This observation appears to be in conflict with observed elevated temperature ductility obtained at the lowest strain rate in the present study (Figure 3.25).

In order to explain the ductility of the cladding at the lowest strain rate, an additional factor must be considered. The tubing used in this study had a wall thickness of only 0.015 inch; therefore, it could be expected to collapse during uniaxial tensile testing resulting in increased ductility. To determine the extent of tubing collapse, final diameter measurements were made on several tested cladding specimens. The results are summarized in Table 3.19.

Measurements presented in the table show that for low strain rates and temperatures of 1200°F and above the long gauge length cladding collapses more than does the short gauge length cladding. Also, the amount of tubing collapse is strain rate dependent with final diameters being much smaller at the lowest rate. At the high strain rate the specimen diameter is essentially the same for both specimen lengths (athermal deformation). At the low test rates (thermal deformation region) ductility is likely enhanced by the collapse of the tubing even though intergranular fracture occurs. The net result is ductility values for the tubular specimens which approach those of solid specimens.

3.3.3 FTR Component Materials Evaluation

3.3.3.1 Objective

The objective of this study is to determine the mechanical properties of FTR component materials for anticipated service conditions for use in performance prediction and safety analyses. Included as an integral part of the program is the influence of both thermal history and fast neutron irradiation

Table 3.19. Tubing Diameter Measurements

Test Temperature (°F)	Strain Rate, sec^{-1}	Distance From Fracture, in.	Specimen Diameter (in.) 1.37 in. G.L.	Specimen Diameter (in.) 2.37 in. G.L.
1200	2×10^{-5}	Fracture	.176	.170
		1/4	.198	.190
		1/2	.210	.202
1200	1.0	Fracture	.211	.208
		1/4	.222	.219
		1/2	.224	.222
1600	2×10^{-5}	Fracture	.186	.178
		1/4	.192	.186
		1/2	.198	.191
1600	1.0	Fracture	.204	.202
		1/4	.221	.220
		1/2	.223	.222

on observed behavior. Results of this study will optimize materials selection and application for future LMFBRs.

3.3.3.2 Accomplishment and Status

The influence of test temperature and strain rate on the tensile properties of actual FTR primary piping (28-inch diameter--316H) material have been determined. Tensile results were obtained at a rate of $\sim 3 \times 10^{-5}$ in/in/sec at temperatures from room temperature to 1400°F. High strain rate testing was performed at temperatures of 900, 1050, and 1200°F to a rate of 10 in/in/sec. Three heats of piping material were used for this evaluation. Results of each test included the proportional elastic limit (PEL), 0.2% yield and ultimate strengths, total and uniform elongation, and reduction of area. The preliminary results of the completed tests are presented in this report.

3.3.3.2.1 Test Material. The 316H stainless steel used for this study was obtained from actual FFTF 28-inch diameter primary piping material. Three heats of piping material were evaluated in this study. Chemical analyses for these heats are presented in Table 3.20.

Specimens were machined from the longitudinal forming direction of the 0.375 inch wall pipe samples. The specimens were miniature buttonhead type with gauge sections 1.125 inch long and 0.125 inch diameter.

All testing was performed in air within recommended ASTM practice. Detailed test procedures have been described previously.[22]

3.3.3.3 Results

Tensile and high strain rate testing on FFTF primary piping material has been completed at several temperatures and strain rates. The majority of testing has been performed on one heat of piping material (Heat 55320) to provide a complete characterization and limited testing has been performed on the other two heats (Heats 55318 and 55319) to identify heat-to-heat variations. Results of the completed tests are tabulated in Tables 3.21 and

Table 3.20. Chemical Analyses of 28-Inch Diameter 316H FFTF Primary Piping Material* (Wt. %)

Element	Heat Number 55318	55319	55320
C	0.046	0.051	0.050
Mn	1.87	1.86	1.78
Ni	13.60	12.15	11.92
Cr	16.70	16.50	17.40
Mo	2.38	2.27	2.33
N	0.0882	0.1028	0.1124

*Check analyses on pipe samples used for testing.

3.22 and discussed in the subsequent sections entitled tensile behavior, heat-to-heat variations and strain rate effects.

3.3.3.3.1 Tensile Behavior. The effect of test temperature on the ultimate strength of FFTF primary piping material for a conventional test rate is illustrated in Figure 3.29. Included in the figure are curves from G. V. Smith[28] which indicate the minimum and mean ultimate strength to be expected for the subject material at the various test temperatures. Data obtained from tests on the three heats of piping material are represented by symbols. These data show that for temperatures to 1100°F the strength exceeds the mean behavior of 316-316H stainless steel. At higher test temperatures convergence with minimum behavior is noted. Only minor heat-to-heat variations on ultimate strength are observed.

The 0.2% yield strength of the subject materials is influenced by strain rate as illustrated in Figure 3.30. For all test temperatures the strength of the piping material is essentially equal to the mean behavior described by G. V. Smith. As with the ultimate strength, only minor heat-to-heat variations of the 0.2% yield strength are observed.

Figure 3.31 shows the influence of temperature on the ductility (total and uniform elongation and reduction of area) of one heat of piping material (Heat 55320). Both total elongation and reduction of area slightly decrease with temperature to a temperature of 1050°F and then rapidly increase with increasing test temperature; uniform elongation (elongation at maximum load) slightly decreases with temperature to 1050°F and then rapidly decreases with increasing temperature. Similar trends were observed for the other two heats of piping. Ductility values for the piping material are in agreement with those presented by G. V. Smith[24] for 316-316H stainless steel. (At 1050°F the total elongation of the piping material was ∿ 44% and the mean value from G. V. Smith was ∿ 45%).

3.3.3.3.2 Heat-To-Heat Variations. A comparison between the tensile properties of the three heats of piping material is presented in Table 3.21. For the test temperature and strain rates presented only minor variations in tensile strength or ductility are observed for the three heats. The maximum

Table 3.21. Heat-To-Heat Variations in Tensile Properties of 316H FTR Primary Piping

Strain Rate, sec^{-1}	Heat No.	Temp., °F	Strength, ksi			Elongation, %		Reduction of Area, %
			PEL	0.2% Yield	Ultimate	Total	Uniform	
3×10^{-5}	55318	72	32.5	38.9	88.4	47.5	41.3	81.4
			32.5	37.9	87.6	50.0	42.0	79.6
	55319		32.0	39.7	89.8	55.9	48.7	82.1
			32.8	39.2	89.0	56.1	49.1	78.8
	55320		34.0	39.8	91.7	56.2	44.2	85.4
			32.0	39.7	90.9	56.1	47.3	81.3
3×10^{-5}	55318	1050	16.4	21.1	69.4	43.4	37.6	72.3
			16.8	22.0	69.0	43.5	37.7	73.7
	55319		13.4	19.5	69.0	44.5	38.8	69.9
			14.6	19.1	68.9	44.1	37.2	72.4
	55320		12.2	19.8	68.5	44.4	37.6	72.4
			14.3	19.5	69.8	45.2	38.8	73.8
6×10^{-2}	55318	1050	14.2	19.9	65.7	36.9	31.9	83.8
			17.2	22.5	66.1	35.7	31.0	80.3
	55319		15.8	21.0	65.6	37.0	32.4	74.0
			15.6	20.3	65.9	37.5	32.7	77.9
	55320		17.6	23.8	68.0	37.0	32.4	72.1
			18.0	24.1	68.5	39.5	34.9	73.2
1.0	55318	1050	17.5	23.9	65.0	37.2	31.3	77.2
			17.6	23.6	64.3	38.2	32.5	79.5
	55319		17.2	22.5	64.4	37.5	31.9	76.2
			17.6	24.1	62.5	37.5	32.3	77.9
	55320		17.5	23.6	65.4	41.1	33.6	80.5
			17.2	22.3	66.0	39.1	33.2	77.0
10.0	55318	1050	17.6	23.0	64.4	36.1	29.9	73.8
			18.0	24.2	64.3	38.0	32.1	77.0
	55319		18.4	23.4	64.5	37.2	31.4	73.0
			18.4	23.6	64.5	36.9	31.0	77.9
	55320		20.5	26.2	65.8	37.8	32.6	74.6
			19.5	23.9	65.7	36.8	31.8	78.0

Table 3.22. Tensile Properties of FTR Primary Piping
316H Stainless Steel, Heat 55320

Strain Rate, sec^{-1}	Temp. °F	Strength, ksi			Elongation, %		Reduction of Area, %
		PEL	0.2% Yield	Ultimate	Total	Uniform	
3×10^{-5}	72	34.0	39.8	91.7	56.2	44.2	85.4
	72	32.0	39.7	90.9	56.1	47.3	81.3
	700	16.3	23.4	79.7	44.6	40.6	70.7
	700	14.2	23.3	78.5	44.3	40.5	69.1
	900	13.4	21.5	77.2	46.0	40.3	63.4
	900	12.2	22.1	76.8	46.6	39.5	65.0
	1050	12.2	19.8	68.5	44.4	37.6	72.4
	1050	14.3	19.5	69.8	45.2	38.8	73.8
	1100	15.0	20.2	63.7	44.3	34.4	72.4
	1100	14.1	19.3	62.8	44.4	35.0	71.5
	1200	12.2	20.6	49.3	48.4	30.2	73.2
	1200	14.2	19.9	51.2	48.5	30.6	71.5
	1400	13.9	18.9	26.5	73.1	8.2	95.9
	1400	13.8	18.1	27.1	74.5	9.6	95.1
3×10^{-3}	900	17.6	22.3	72.6	41.2	36.7	73.8
	900	16.0	23.2	72.9	38.9	34.5	71.3
	1050	17.1	22.9	69.4	47.6	34.6	75.4
	1050	16.3	21.5	68.8	47.8	34.7	71.5
	1200	13.0	18.5	61.3	41.0	33.1	78.0
	1200	13.0	19.3	61.5	40.1	32.3	76.4
6×10^{-2}	900	17.7	24.7	72.1	39.7	35.3	75.4
	900	18.4	24.1	71.1	40.5	35.8	74.6
	1050	17.6	23.8	68.0	37.0	32.4	72.1
	1050	18.0	24.1	68.5	39.5	24.9	73.2
	1200	15.0	20.6	61.4	33.3	28.5	73.2
	1200	14.9	19.7	62.4	35.1	29.0	73.6
1.0	900	20.0	25.8	69.7	37.8	32.5	76.4
	900	19.3	25.9	69.7	38.1	32.4	75.4
	1050	17.5	23.6	65.4	41.1	33.6	80.5
	1050	17.2	22.3	66.0	39.1	33.2	77.0
	1200	16.8	22.9	60.1	35.8	39.2	83.6
	1200	15.4	21.3	59.6	35.0	29.7	78.0
10.0	900	20.7	26.2	67.9	39.0	33.3	77.2
	900	21.5	27.9	68.9	39.2	33.4	78.0
	900	20.7	24.8	68.7	37.9	32.2	77.2
	1050	20.5	26.2	65.8	37.8	32.6	74.6
	1050	----	----	66.5	38.8	32.2	74.6
	1050	19.5	23.9	65.7	36.8	31.8	78.0
	1200	20.9	24.2	61.3	36.4	30.2	75.4
	1200	18.0	23.8	60.7	38.2	31.0	77.0
	1200	17.1	21.7	60.3	38.3	32.9	76.4

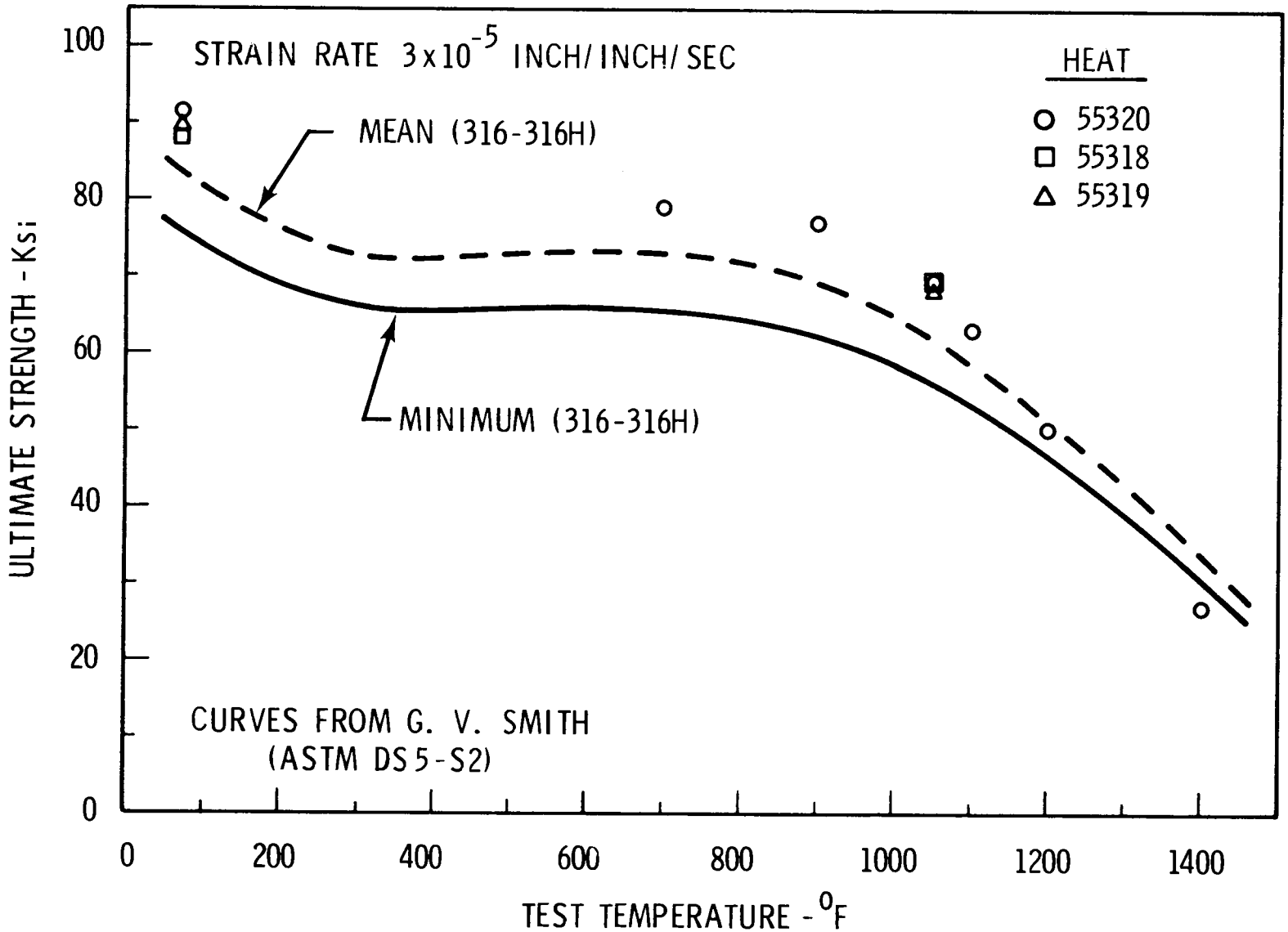

Figure 3.29. Effect of Test Temperature on the Ultimate Strength of 316H FTR Primary Piping Material.

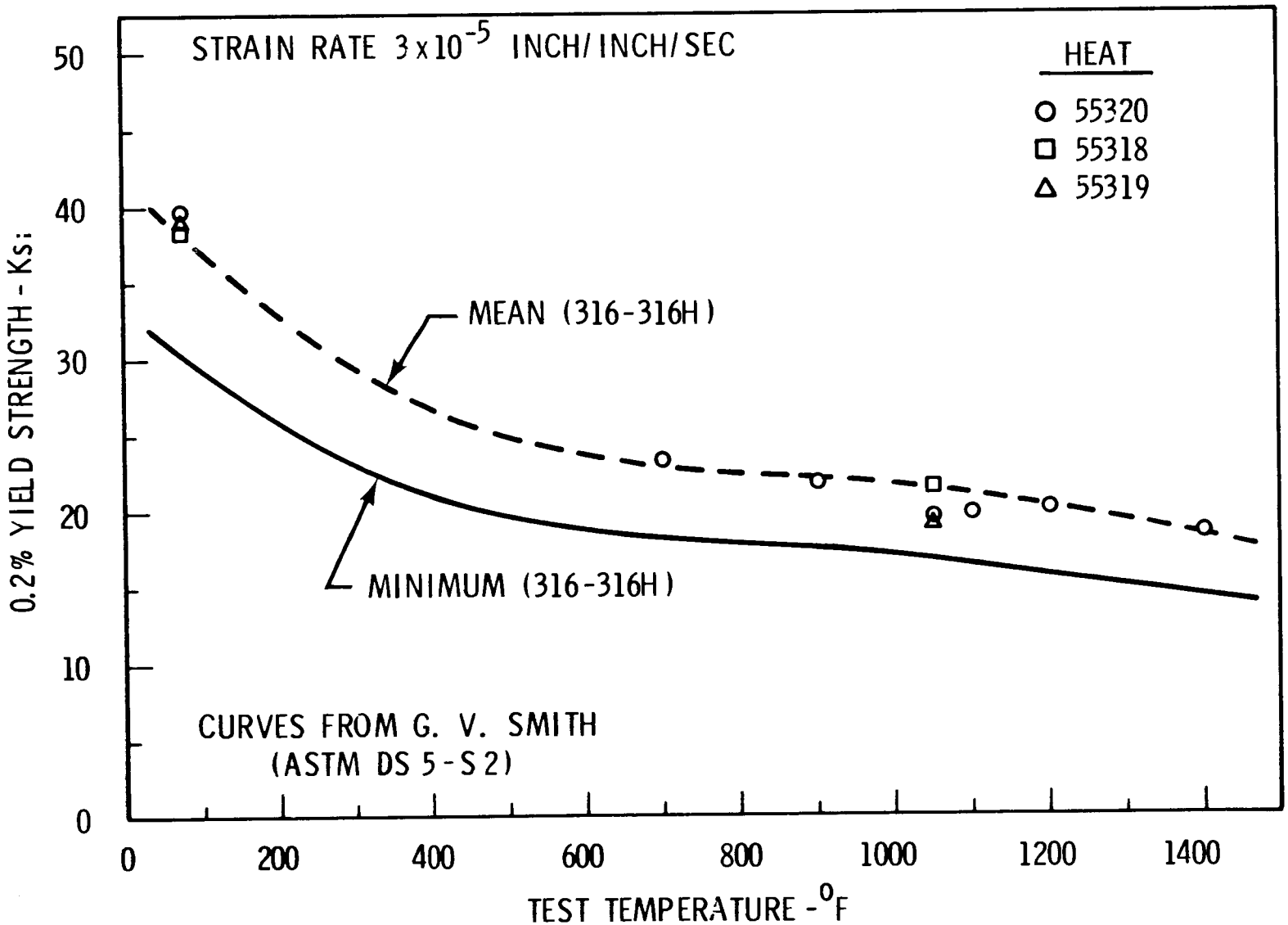

Figure 3.30. Effect of Test Temperature on the 0.2% Yield Strength of 316H FTR Primary Piping Material.

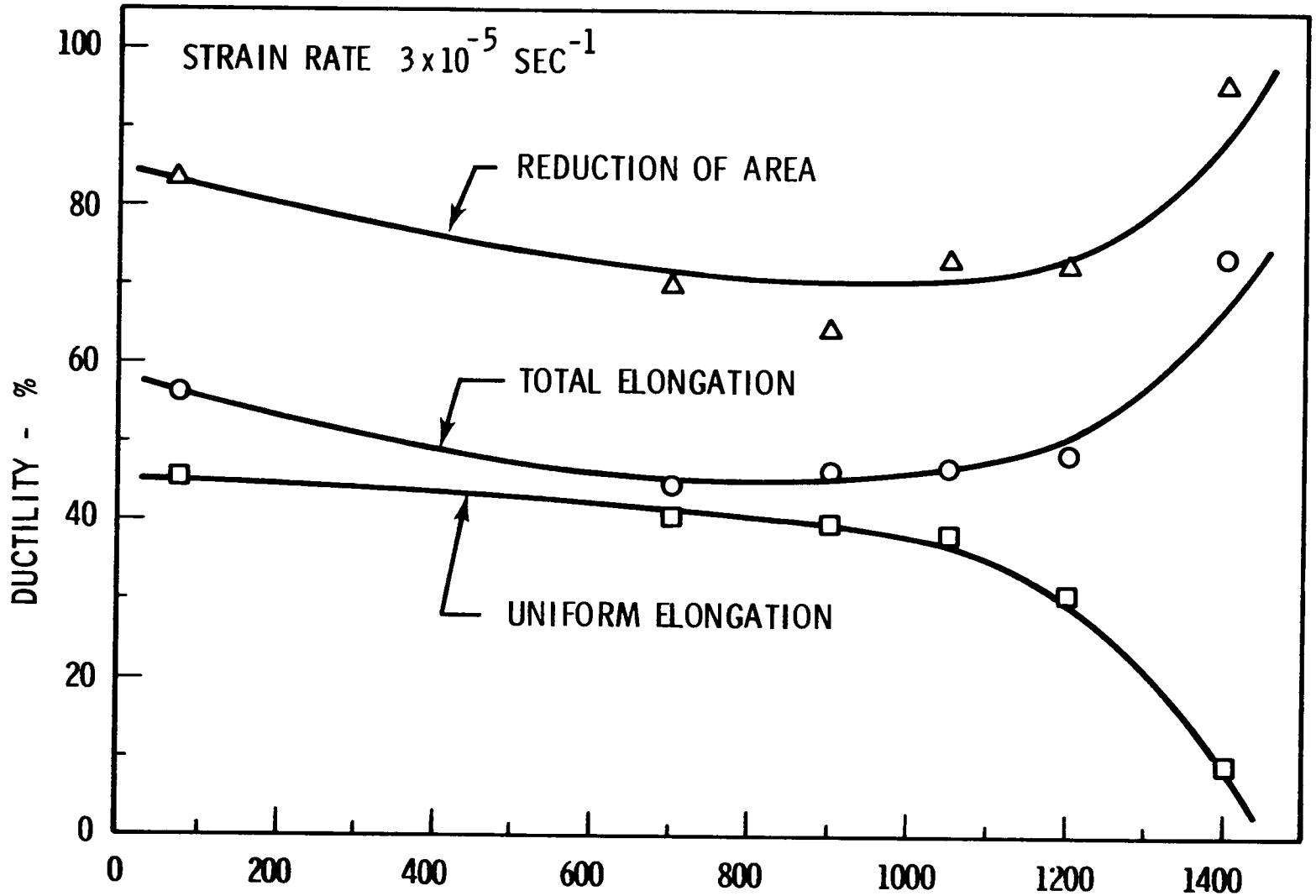

Figure 3.31. Effect of Test Temperature on the Ductility of 316H FTR Primary Piping Material.

variation in strength (PEL, 0.2% yield or ultimate) for any strain rate and test temperature is ∿ ±1.5 ksi and in ductility (total and uniform elongation and reduction of area) is ∿ ±3.5%. Heat 55320 appears to have slightly greater strength and ductility than the other two heats of material.

3.3.3.3.3 Strain Rate Effects. The effect of strain rate on the strength of 316H piping material for temperatures of 900, 1050 and 1200°F is presented in Figure 3.32. For temperatures to 1050°F the ultimate strength slightly decreases with increasing strain rate for all rates. At 1200°F the strength initially rapidly increases with strain rate to a rate of ∿ 3×10^{-3} in/in/sec and then remains constant with increasing rate. The 0.2% yield strength slightly increases with strain rate for all test temperatures (Figure 3.32). Although data presented in this figure only represent results from Heat 55320; the other heats of material exhibit similar trends as indicated in Table 3.21.

The total and uniform elongation of 316H piping material is affected by strain rate for temperatures of 900, 1050 and 1200°F as shown in Figure 3.33. At all three temperatures total elongation decreases with increasing strain rate (from ∿ 47% to 38%). Uniform elongation also decreases with increasing strain rate for temperatures of 900 and 1050°F. At 1200°F uniform elongation remains essentially constant over the strain rate range of this study. As with the strength properties, data presented in this figure was obtained on Heat 55320; the other heats of material exhibited similar trends as indicated in Table 3.21.

3.3.3.4 Discussion

The strain rate dependence of the ultimate strength of the 316H stainless steels used in this study indicates that different deformation mechanisms control behavior over the temperature and strain rate range of this study. At temperatures of 900 and 1050°F the material exhibits a substantial ability to work harden, and tensile properties are not greatly influenced by strain rate or test temperature. In this temperature region (athermal deformation) the ultimate strength slightly decreased with increasing strain rate. Previous work on Type 304 stainless steel indicated that this decrease likely resulted

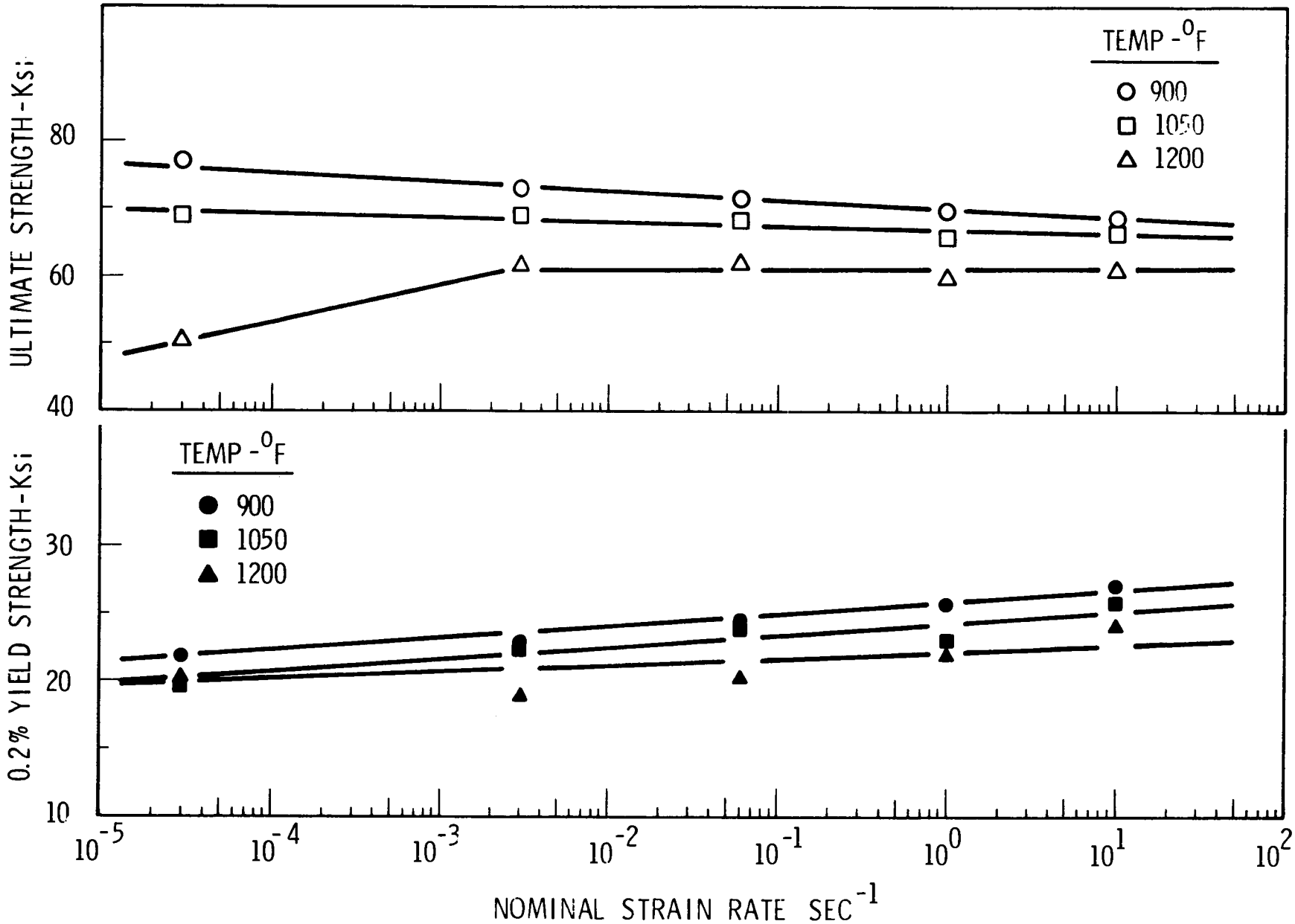

Figure 3.32. Effect of Strain Rate and Temperature on the Strength of 316H FTR Primary Piping Material (Heat 55320).

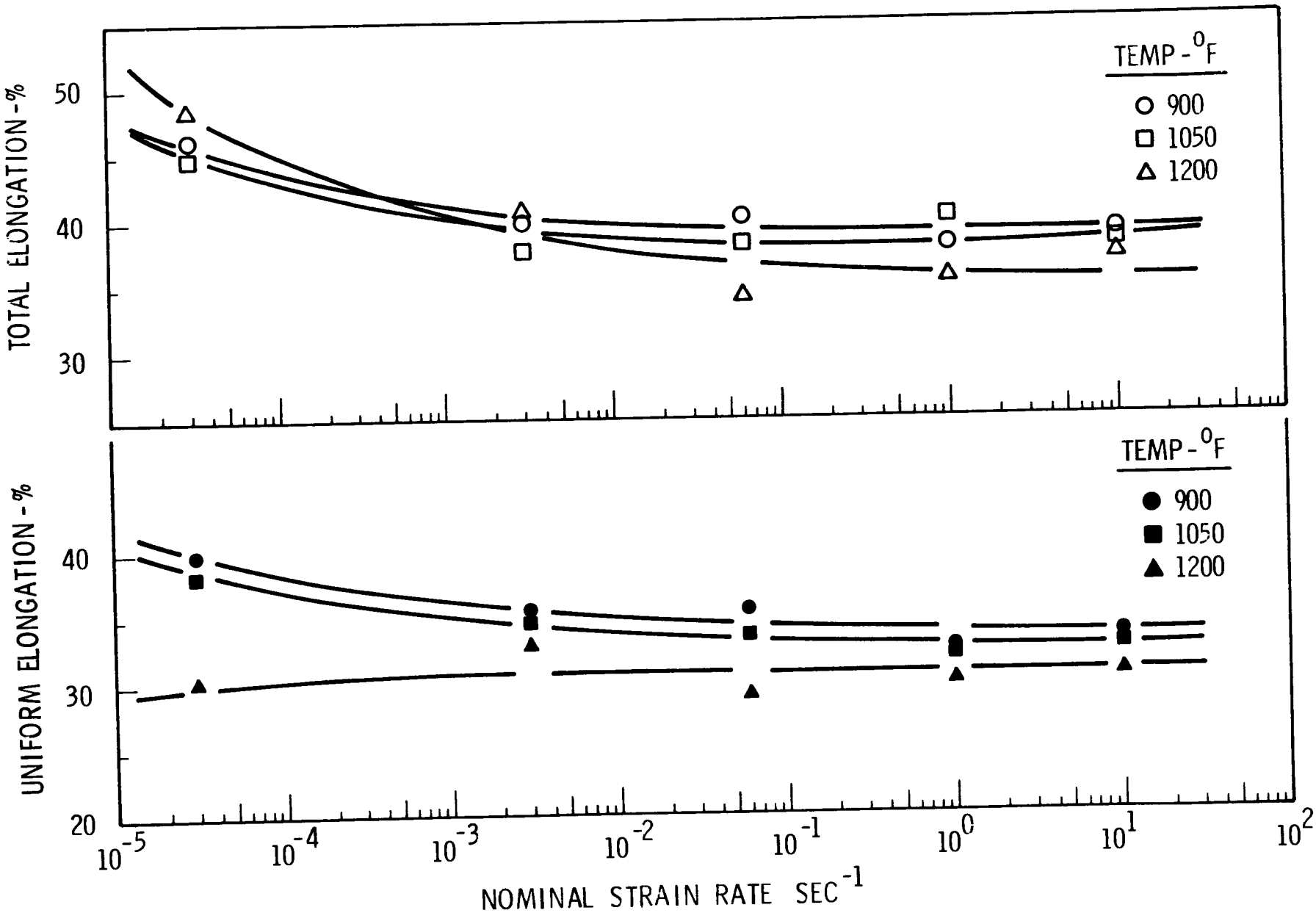

Figure 3.33. Effect of Strain Rate and Temperature on the Ductility of 316H FTR Primary Piping Material (Heat 55320).

from adiabatic heating and/or the time and temperature-dependent effects of dynamic strain aging.[25]

Its influence on tensile behavior is to enhance the strain hardening ability of the material resulting in increased strength and ductility. Since the materials used in this study had a high nitrogen content (see Table 3.20), dynamic strain aging would be expected to exhibit a pronounced influence on tensile behavior. Increasing strain rate would be expected to retard dynamic strain aging resulting in decreased strength and ductility. Test results presented in Figures 3.32 and 3.33 confirm the predicted behavior.

Deformation at 1200°F and low strain rates results in large increases in ultimate strength with increasing strain rate. In this region thermally activated mechanisms (bulk diffusion) control deformation and mechanical properties are more dependent on test rate. At the lowest test rate (3×10^{-5} in/in/sec) dynamic strain aging does not greatly influence properties as previously illustrated by ORNL. This minimum influence results because the temperature is high enough and rate low enough to allow the carbon and nitrogen atoms to migrate along with the dislocations. As rate increases the carbon and nitrogen atoms retard dislocation movement resulting in increased strain hardening. Thus, at high temperatures ($\gtrsim$ 1200°F) bulk diffusion is retarded and dynamic strain aging enhanced by increasing strain rate resulting in the observed behavior.

As previously mentioned, ductility at temperatures of 900 and 1050°F is strongly influenced by dynamic strain aging resulting in the observed behavior. At 1200°F ductility has been shown to be influenced by dynamic strain aging and by intergranular failure. Work on Type 304 stainless steel at this temperature (1200°F) showed that a transition in fracture mode from intergranular to transgranular occurs with increasing strain rate.[25] Also, reduction of area measurements provides a good indication of fracture mode with low measurements (< 50%) resulting from intergranular fractures. In the present study reduction of area values at 1200°F ($\sim$ 73%) did not change with increasing strain rate (see Table 3.21), consequently, intergranular failures would not

be expected and were not observed in the tested specimens. Apparently the fracture behavior of the 316H stainless steel used in this study is slightly different than that observed previously for Type 304 stainless steel. Failed specimens presently being creep tested will provide additional information on the fracture behavior of the subject materials.

In the application of the tensile data on the subject material to safety analyses of the FFTF primary piping, it is desirable to develop equations to describe flow behavior as a function of temperature and/or strain rate. Such a description has been completed in the past for Type 304 stainless steel[27] and has been incorporated to describe the 1050°F stress-strain behavior of the primary piping material. The description uses the expression developed by Ludwigson[28] which is:

$$\sigma = K_1 \varepsilon^{n_1} + e^{(K_2 + n_2 \varepsilon)}$$

where σ is true stress, ε is true plastic strain and n_1, K_1, n_2 and K_2 are constants.

To obtain the desired description, the constants were determined for each test and were fitted to a linear relationship ($n = A + B \log \dot{\varepsilon}$) by a least squares data analyses. The resulting description for each of the constants is presented in Table 3.23. These equations allow reconstruction of true stress-strain curves at 1050°F for any strain rate within the range of this study.

3.3.4 Weldment Materials Evaluation

3.3.4.1 Objective

The objective of this program is to describe the effects of elevated temperatures and fast reactor environments on the mechanical properties and microstructures of austenitic stainless steel weldments and weld-deposited materials. The extent of property change due to neutron irradiation and thermal instability in these materials is largely undefined.

One of the weldments studied under this program is an automated gas tungsten-arc (GTA) butt weld in one-half inch Type 316 plate using Type 316 filler metal. Pre- and postirradiation characterization of this weld

Table 3.23. Mathematical Description of the Effect of Strain Rate On n_1, K_1, n_2 And K_2 for 316H FTR Primary Piping Material at 1050°F

$$n_1 = 0.457 - 0.010 \log \dot{\varepsilon}$$

$$K_1 = 162{,}000 - 3{,}470 \log \dot{\varepsilon}$$

$$n_2 = -51.15 + 0.05 \log \dot{\varepsilon}$$

$$K_2 = 9.582 + 0.010 \log \dot{\varepsilon}$$

material is now complete and the results are summarized here.

3.3.4.2 Accomplishments and Status

Pre- and postirradiation characterization of the tensile and creep-rupture properties of a Type 316 GTA weldment has been completed. A complete report is presently being prepared for open literature publication. Reported here is the final summary of the subject characterization.

3.3.4.2.1 Scope of Work. This characterization includes comparison of weld-deposited and wrought base (or parent) material properties of the Type 316 GTA weldments, the effects of heat treatments on the structure and properties of the weld-deposits, and the effects of fast reactor (EBR-II) neutron irradiation on the tensile and creep-rupture behavior of the weld and base metals. Experimental irradiations and test temperatures were selected to span much of the range between inlet and outlet coolant operating temperatures anticipated for the Fast Flux Test Facility (FFTF) and, therefore, they are expected to be applicable to many conditions in advanced Liquid Metal Fast Breeder Reactor (LMFBR) systems.

The irradiation effects portion of this study was based upon data from specimens irradiated in EBR-II structural materials subassembly X-137 (Row 4). The subject materials represent total fluences ranging from 0.9×10^{21} to 8.2×10^{21} n/cm^2 (0.8×10^{21} to 7.2×10^{21} n/cm^2, $E_n > 0.1$ MeV) and irradiation temperatures of 870 ± 30°F and 1000 ± 40°F.

3.3.4.2.2 Results. The as-welded metal has high yield strengths, reduced strain hardening rates and low ductility compared to the wrought parent metal. Solution annealing (1950°F/1 hour) results in recovery to base metal property values as a result of matrix recrystallization and delta-ferrite spheroidization. Stress relief at 1472°F for 10 hours produced reductions in yield

strength, increases in tensile strength and no significant changes in ductility.[29]

High yield strength and relatively low strain hardening rates[29] are apparently attributable to the prestrain introduced during welding and the presence of the ferrite phase acting as barriers to deformation. The 1472°F treatment lowered the yield stress by stress relief in the austenite matrix but raised the UTS as a result of the long-range deformation barriers being stiffened by a ferrite-to-sigma transformation. The result is a lower yield stress and a greater ability to strain harden but no real improvement in the total energy absorbtion capacity. The behavior following the anneal at 1950°F is straightforward since the small amount of residual ferrite phase present is distributed in isolated pools in a recrystallized matrix.

Results of creep rupture tests on the Type 316 weld metal show that, the short-term tensile behavior does not carry through to the low strain-rate creep properties[29] (Figures 3.34 - 3.36). At 1000 and 1100°F the stress dependence of the rupture life (Figure 3.34) is similar to that of the wrought alloy with the data falling generally between the average and minimum trend curves for annealed wrought Type 316 stainless steel. The rupture strength is apparently lowered by solution annealing although the data are limited and definite conclusions are precluded by the data scatter. Heat treating at 1472°F for 10 hours had no discernable effect on the rupture life. In terms of average behavior, the tendency toward shorter rupture life in the annealed metal is attributable to somewhat higher minimum creep rates (Figure 3.35). At high stresses (short times) the weld metal compares favorably with the minimum rupture ductility values for wrought Type 316 (Figure 3.36) and as the stresses decrease the trend is toward lower ductility in the weld metal with no clear distinction among test temperatures or among material conditions.

The pre- and postirradiation tensile data for the subject Type 316 weld-deposited materials are illustrated in Table 3.24. Irradiation induced tensile property changes observed in the weld metal are broadly consistent with the trends established in wrought austenitic stainless steels. However, the extent of irradiation hardening clearly depends upon material conditions as well as fluence, irradiation temperature and test temperature. The as-deposited material showed little or no yield strength increase as a result

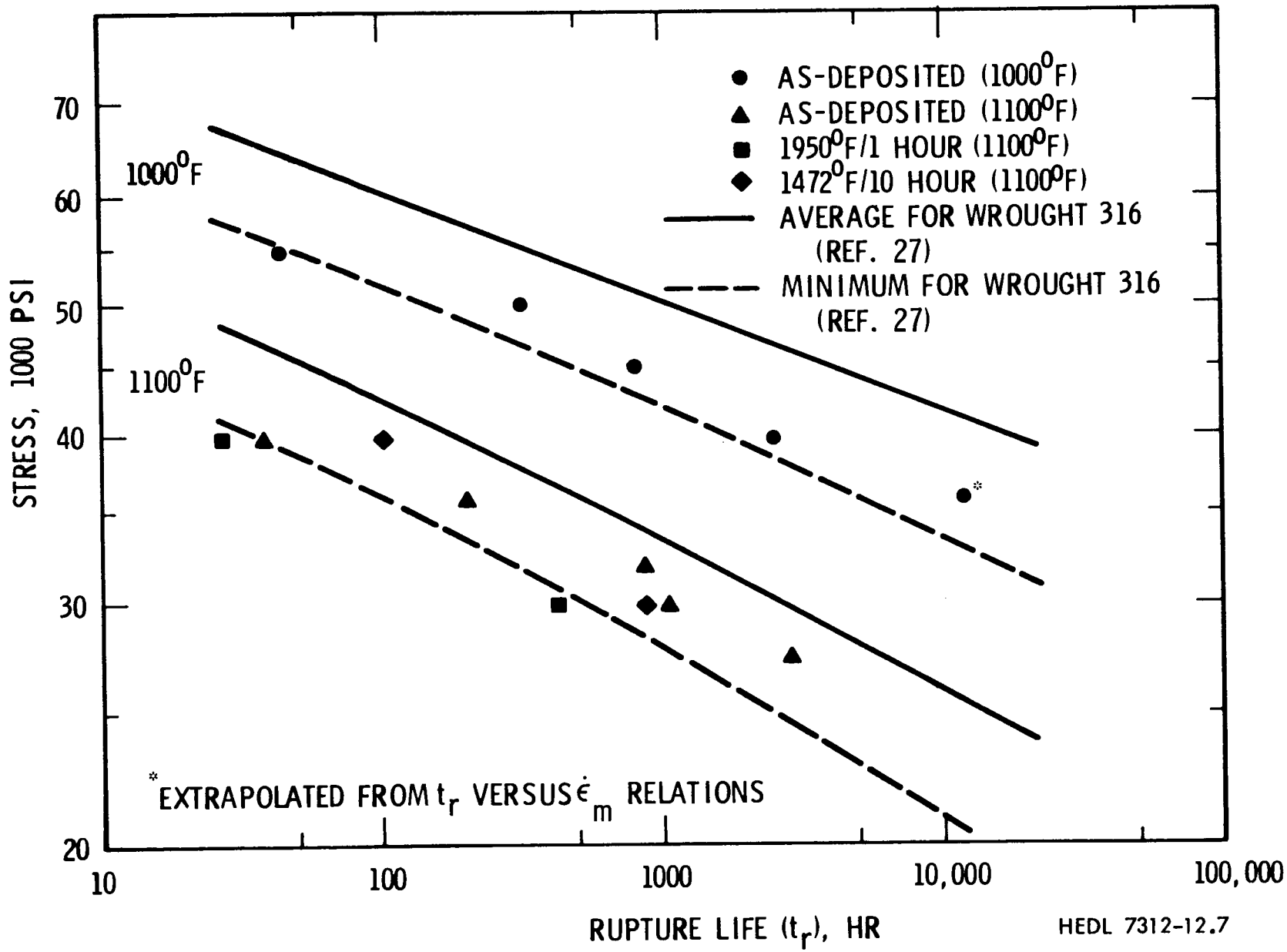

Figure 3.34. Stress Dependence of Rupture Life for Wrought and Weld-Deposited Type 316.

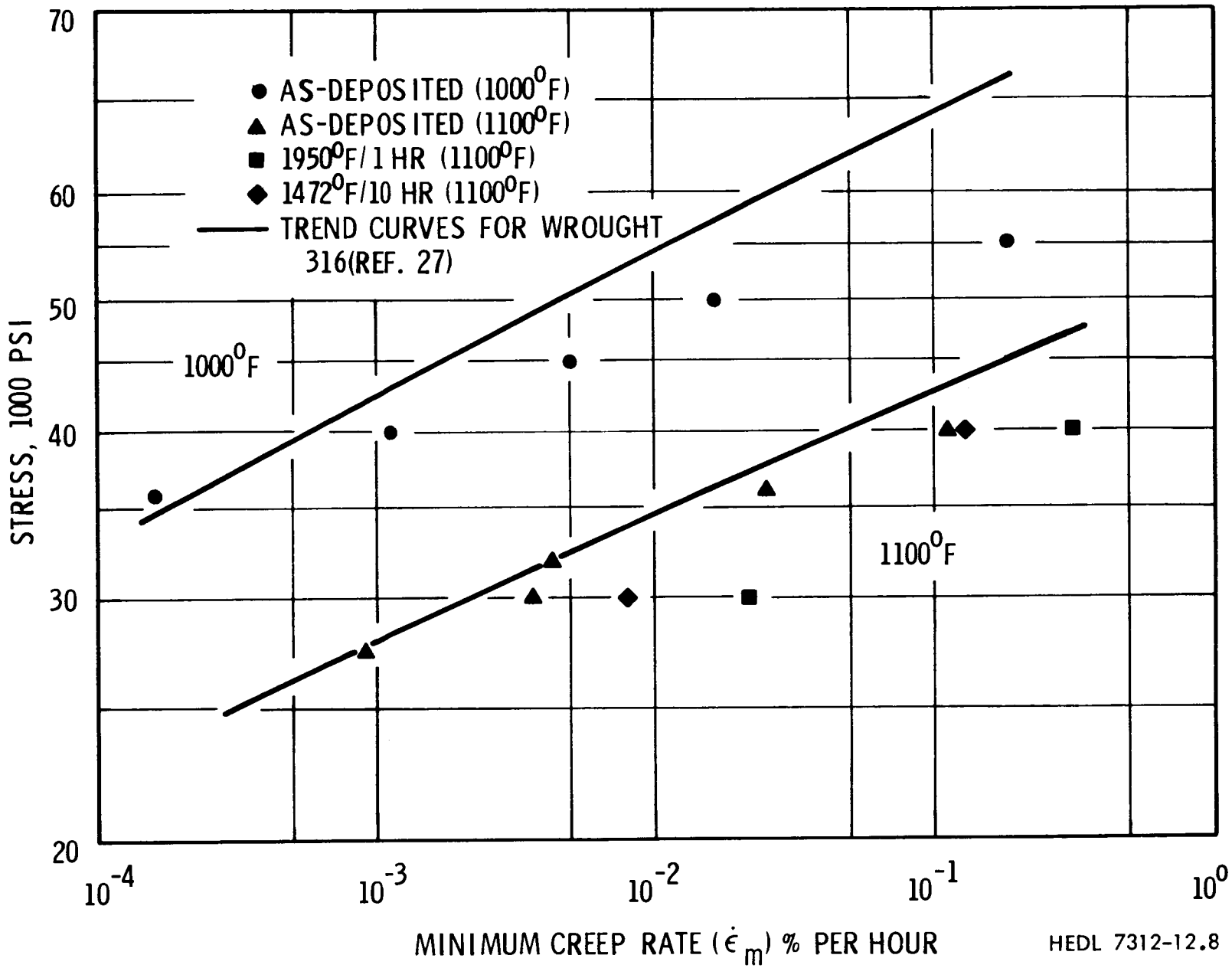

Figure 3.35. Stress Dependence of Minimum Creep Rate of Wrought and Weld-Deposited Type 316.

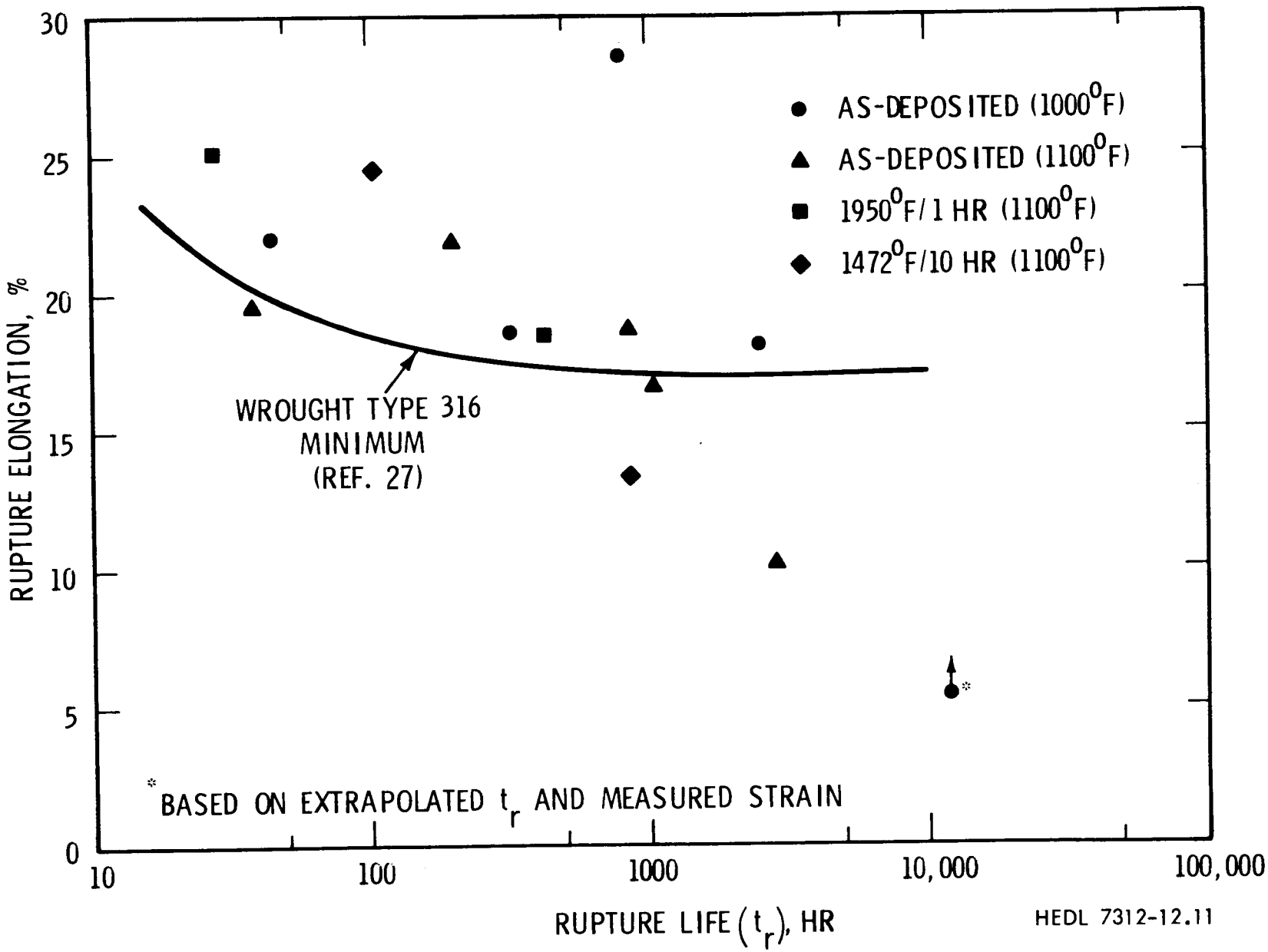

Figure 3.36. Creep-Rupture Ductility of Wrought and Weld-Deposited Type 316.

Table 3.24. Fractional Irradiation-Induced Property Changes in GTA-Deposited Type 316. Values Listed Are: Postirradiation Property ÷ Preirradiation Property.

Material Condition	Test Temp. (°F)	8.2×10^{21} n/cm^2 - 1000°F					7.8×10^{21} n/cm^2 - 850°F					0.8×10^{21} n/cm^2 - 850°F				
		YS	UTS	UE	TE	RA	YS	UTS	UE	TE	RA	YS	UTS	UE	TE	RA
As-Deposited	800	.90	1.08	.89	.73	.88	1.24	1.26	.54	.51	.65	.97	1.16	.89	.79	.93
	900	----	----	---	---	---	----	----	---	---	---	.94	1.05	.69	.73	.84
	1000	----	----	---	---	---	1.23	1.17	.40	.48	.78	1.01	1.05	.65	.65	1.09
	1100	1.01	1.08	.44	.54	.59	----	----	---	---	---	1.01	.97	.45	.71	.96
	1200	1.01	.98	.34	.48	.58	1.14	1.04	.20	.44	.62	.94	.89	.32	.67	.75
1472°F 10 hours	800	1.19	1.01	.71	.69	.68	1.75	1.23	.48	.51	.55	----	----	---	---	---
	1000	1.19	.93	.80	.74	.64	----	----	---	---	---	----	----	---	---	---
	1200	1.18	.93	.37	.33	.36	1.41	1.00	.21	.30	.26	----	----	---	---	---
1950°F 1 hour	800	2.11	1.09	.54	.54	.82	----	----	---	---	---	1.04	1.02	.74	.72	.95
	1000	----	----	---	---	---	----	----	---	---	---	1.28	1.04	.72	.68	.94
	1200	2.63	1.02	.17	.16	.26	----	----	---	---	---	1.29	.89	.45	.50	.69

of irradiation to 8.2×10^{21} n/cm^2 at ∿ 1000°F even though substantial decreases in total elongation were observed. At an approximately equivalent fluence (7.8×10^{21} n/cm^2) but a lower temperature (∿ 870°F), both higher strength and lower ductility were noted. For an irradiation temperature of ∿ 870°F and a much lower fluence of 0.9×10^{21} n/cm^2, substantially lower ductility was again observed without any real increase in strength.

In specimens given a post-weld stress relief treatment at 1472°F for 10 hours, moderate but consistent strength increases did occur along with strong ductility losses for a fluence of 8.2×10^{21} n/cm^2 at 1000°F. At the lower irradiation temperature (870°F) yield strengths were 41 to 75% higher and total elongation values 49 to 70% lower than the unirradiated material (Table 3.24).

The largest proportional property changes were observed in the solution annealed (1950°F for 1 hour) weld metal. A fluence of 8.2×10^{21} n/cm^2 at ∿ 1000°F produced strength increments of 111 and 163% and total elongation decrements of 46 and 84%. The lowest fluence (0.9×10^{21} n/cm^2) which resulted in no change in the yield strength of the as-deposited metal produced increases up to 29% in the solution annealed material accompanied by moderate (28-50%) decreases in total elongation.

The fractional property changes reported above are given as ranges largely because of the effects of test temperature. For each material and irradiation condition represented the lowest ductility invariably occurs at the highest test temperature. This is consistent with the helium embrittlement mechanism which is thought to operate at temperatures above about Tm/2 (∿ 1050°F). The tendency toward greater damage accumulation rates at lower irradiation temperatures established in wrought Type 316 also holds for the weld deposits. This is illustrated by the larger increments in strength and decrements in ductility following irradiation at 870°F as compared to 1000°F for essentially equivalent fluence values. In general, the as-deposited metal shows the least effect of irradiation and the solution annealed metal the most severe effect. It should be noted, however, that in absolute terms the lowest strengths and highest ductilities after similar irradiation still occur in the solution annealed metal.

The postirradiation creep-rupture data are summarized in Figures 3.37 - 3.39 along with the unirradiated control data. Specimens included in this portion of the study represent fluences of 7.8 to 8.2 x 10^{21} n/cm^2 (total), an irradiation temperature of $\sim$ 1000°F and a test temperature of 1100°F.

Little or no irradiation effect is detectable in the rupture life or minimum creep rate behavior of the as-deposited weld metal (Figures 3.37 and 3.38). The same may be true for the stress relieved (1472°F/10 hour) material although the postirradiation creep rates appear to be somewhat lower than the control data. In the solution annealed weld metal there is a noticeable increase in rupture life and a decrease in the creep rate. A strong irradiation-induced ductility loss, as measured by total elongation, is common to all weld metal conditions (Figure 3.39).

Annealed wrought Type 316 stainless steel, for similar irradiation conditions, has exhibited large reductions in rupture life and ductility with little or no change in minimum creep rate thus indicating that losses in ductility are reflected in rupture life decreases. Irradiation-induced ductility losses in the weld metal apparently did not impose a significant penalty on the available rupture life. Comparison of the pre- and postirradiation secondary and tertiary creep strains indicate that, in general, the large reductions in total creep elongation are attributable to reductions in tertiary creep strain. This is particularly true at the higher stresses and in the as-deposited weld metal. The behavior of the heat-treated weld metal is not as well-defined in terms of creep strain distribution; for example the second-stage creep strain exceeds the tertiary strain in the solution annealed case. Somewhat lower postirradiation creep rates apparently compensate for the ductility loss in the stress relieved material, to result in essentially unchanged rupture life. In the solution annealed metal, irradiation produced a sufficient decrease in creep rate that the rupture life was actually increased despite severe reductions in total creep elongation.

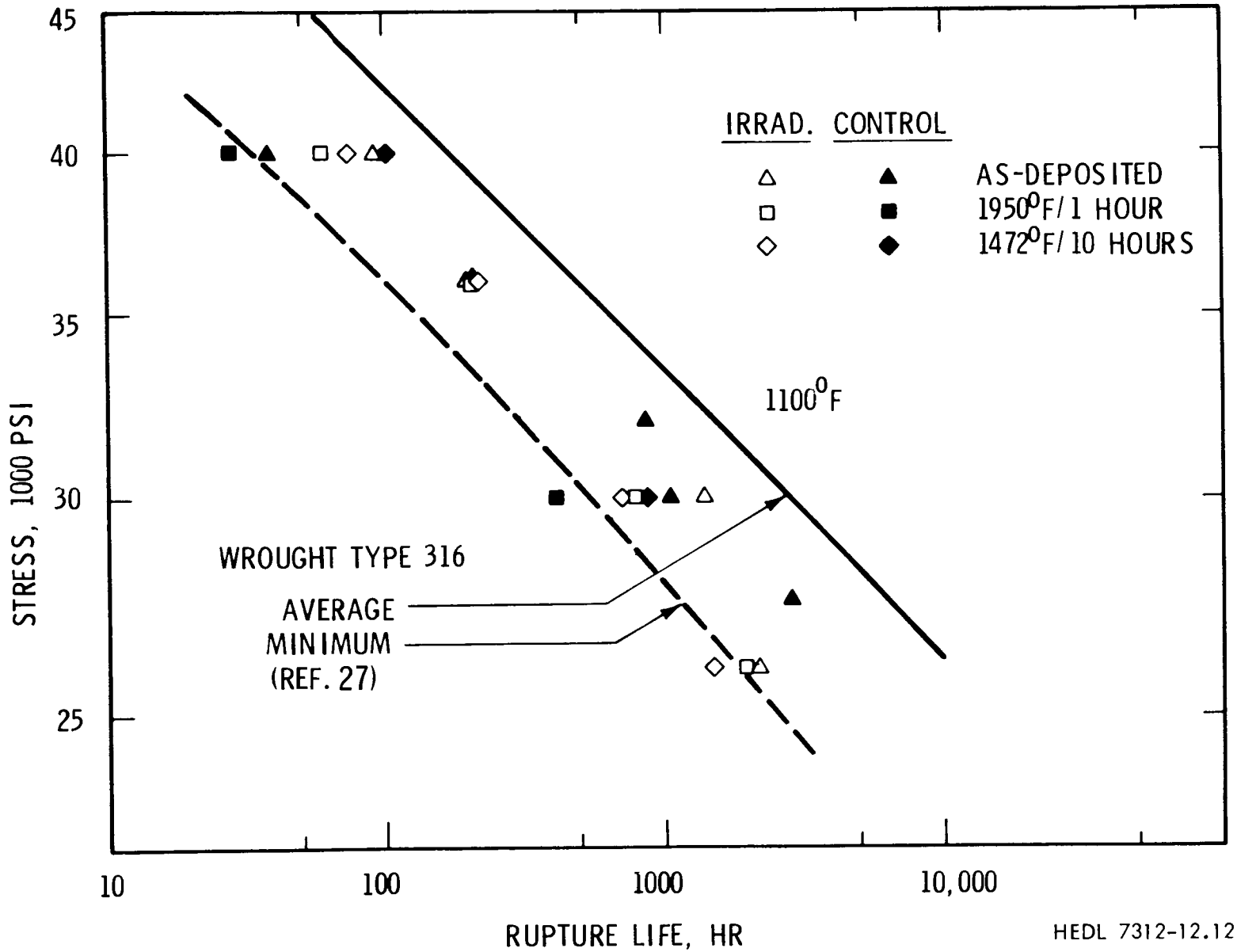

Figure 3.37. Effects of Irradiation (7.8-8.2 x 10^{21} n/cm^2 at ∿ 1000°F) on the Stress Versus Rupture Life Relation for Weld-Deposited Type 316.

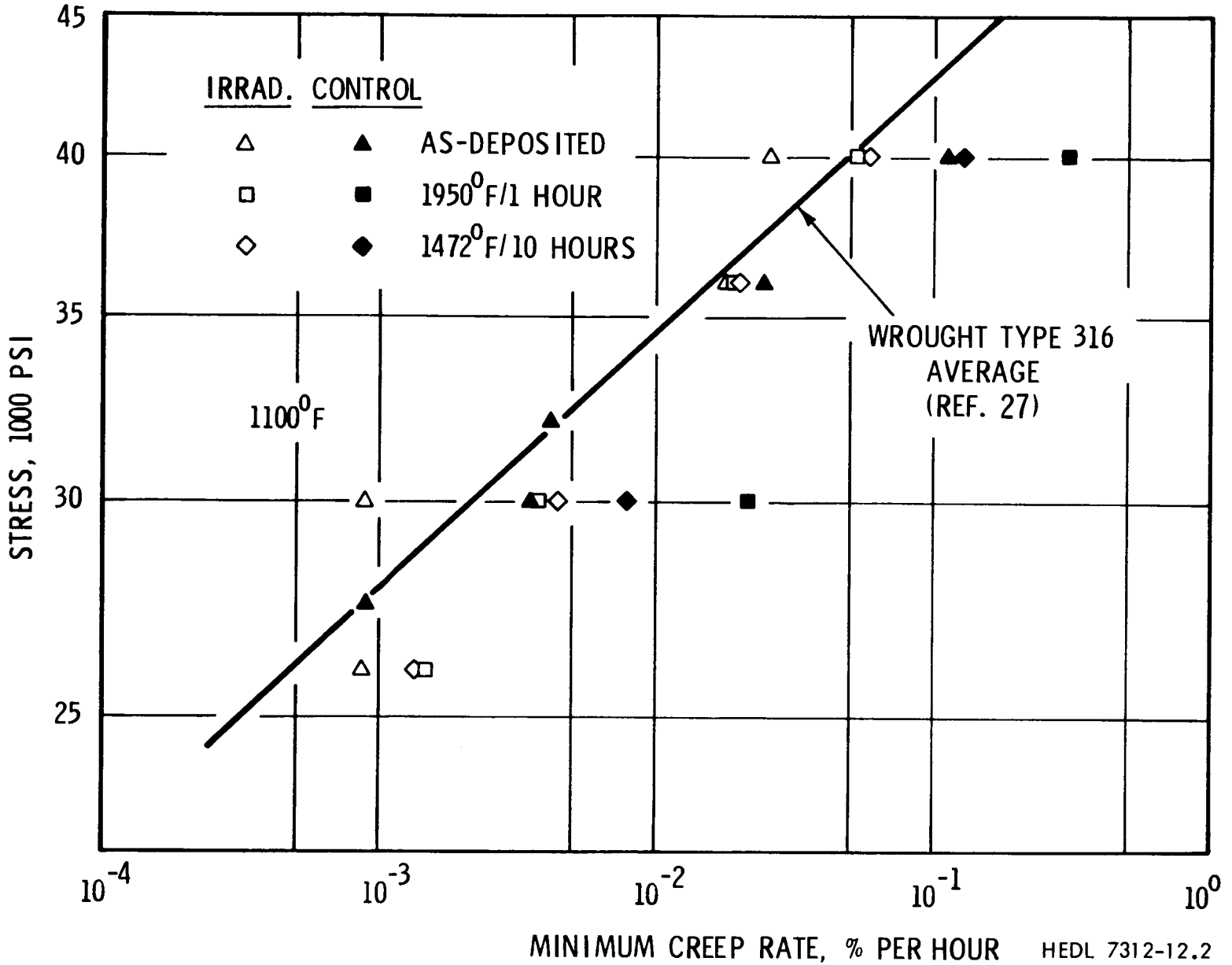

Figure 3.38. Effects of Irradiation ($7.8-8.2 \times 10^{21}$ n/cm^2 at ∿ 1000°F) on the Stress Versus Minimum Creep Rate Relation for Weld-Deposited Type 316.

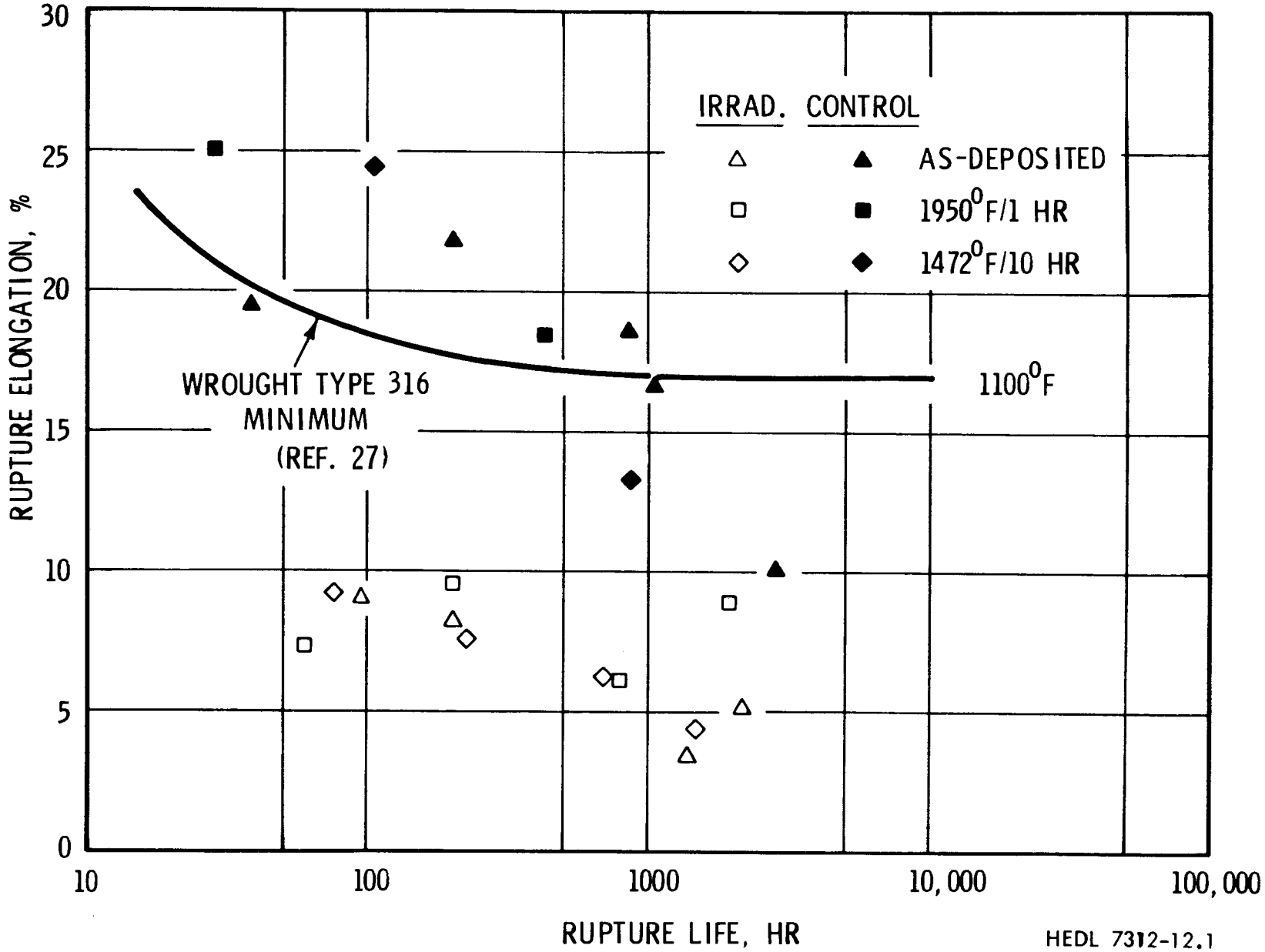

Figure 3.39. Pre- and Postirradiation (7.8-8.2 x 10^{21} n/cm^2 at ∿ 1000°F) Creep-Rupture Ductility of Weld-Deposited Type 316.

3.4 REFERENCES

1. Metals Handbook, Eighth Edition, Vol. 1, "Properties and Selection of Metals," American Society for Metals, Metals Park, Novelty, Ohio, 1961, p. 422.
2. Ibid, p. 1203.
3. F. Garofalo, P. R. Malenock, and G. V. Smith, *The Influence of Temperature on the Elastic Constants of Some Commercial Steels,* ASTM STP 129, American Society for Testing and Materials, Philadelphia, Pennsylvania, 1952, p. 10.
4. M. M. Paxton, *Mechanical Properties of Prototypic FTR Cladding--20% C.W. Type 316 Stainless Steel Tubing,* Hanford Engineering Development Laboratory, HEDL-TME 71-59, April 1971.
5. C. W. Hunter and R. L. Fish, *Behavior of Irradiated 20% C.W. Type 316 Stainless Steel Cladding Specimens During Temperature Transients,* IERSM Quarterly, May-June-July 1973.
6. M. M. Paxton, *Mechanical Properties of Prototypic FTR Cladding--20% C.W. Type 316 Stainless Steel Tubing,* Hanford Engineering Development Laboratory, HEDL-TME 71-59, April 1971.
7. M. M. Paxton, R. L. Knecht and T. T. Claudson, *Irradiation Effects on Reactor Structural Materials Quart. Progr. Rep.*, Hanford Engineering Development Laboratory, HEDL-TME 71-116, September 1971, p. HEDL-6.
8. M. M. Paxton, *Effect of Prior Creep Strain on Residual Mechanical Properties of 20% Cold Worked Type 316 Stainless Steel (RM-30),* Hanford Engineering Development Laboratory, HEDL-TME 72-153, January 1973.
9. S. Timoshenko and J. M. Goodier, "Theory of Elasticity," 2nd Edition, McGraw-Hill, 1951, p. 25.
10. S. Timoshenko, "Strength of Materials II," 2nd Edition, D. Van Nostrand Inc., 1941, p. 67.
11. S. Timoshenko, "Strength of Materials I," D. Van Nostrand Company, Inc., 1941, Art. 69.
12. J. M. Steichen, *High Strain Rate Tensile Properties of Prototypic FFTF Cladding,* to be completed.

13. M. M. Paxton, *Mechanical Properties of Prototypic FTR Cladding--20% C.W. Type 316 Stainless Steel Tubing,* Hanford Engineering Development Laboratory, HEDL-TME 71-59, April 1971.

14. M. M. Paxton, *Elevated Temperature Tensile Grips for Tubing,* ASTM STP-488, 1971, p. 95-99.

15. J. M. Steichen and M. M. Paxton, *The Effect of Strain Rate on the Mechanical Properties of Austenitic Stainless Steels,* Hanford Engineering Development Laboratory, HEDL-TME 71-56, May 1971.

16. J. M. Steichen, *High Strain Rate Mechanical Properties of Types 304 and 316 Stainless Steel,* Hanford Engineering Development Laboratory, HEDL-TME 71-164, November 1971.

17. A. R. Barraclough, H. J. Whittaker, K. A. Nair and C. M. Sellars, "Effect of Specimen Geometry on Hot Torsion Test Results for Solid and Tubular Specimens," *Jnl. of Testing and Evaluation,* 1(3): 220-226 (May 1973).

18. J. J. Holmes and A. J. Lovell, "Application of Deformation Mechanism Maps to Reactor Component Performance Prediction," *ANS Transactions,* 17: 210 (November 1973).

19. J. M. Steichen, "High Strain Rate Tensile Properties of AISI Type 304 Stainless Steel," *Jnl. of Engineering Matls. and Technol.* 95(3): 182-185, (July 1973).

20. M. M. Paxton, *Recovery and Recrystallization of Prototypic FTR Fuel Cladding--20% C.W. Type 316 Stainless Steel Tubing,* Hanford Engineering Development Laboratory, HEDL-TME 71-126, September 1971.

21. J. M. Steichen, *FFTF Primary Piping Fabrication Comparison,* Hanford Engineering Development Laboratory, HEDL-TME 72-133, October 1972.

22. J. M. Steichen and M. M. Paxton, *The Effect of Strain Rate on the Mechanical Properties of Austenitic Stainless Steels,* Hanford Engineering Development Laboratory, HEDL-TME 71-56, May 1971.

23. G. V. Smith, *An Evaluation of the Yield, Tensile, Creep and Rupture Strengths of Wrought 304, 316, 321 and 347 Stainless Steels at Elevated Temperatures,* ASTM Data Series DS5-S2, 1969.

24. G. V. Smith, *The Elevated-Temperature Properties of Stainless Steel,* ASTM Data Series DS5-81, 1965

25. J. M. Steichen, "High Strain Rate Tensile Properties of AISI Type 304 Stainless Steel," *Jnl. of Engr. Matls. and Technol.* 95(3): 182-185 (July 1973).

26. D. Fahr, *Analysis of Stress-Strain Behavior of Type 316 Stainless Steel,* Oak Ridge National Laboratory, ORNL-TM-4292, November 1973.

27. J. M. Steichen, "A Mathematical Description of the Elevated Temperature Flow Behavior of Type 304 Stainless Steel," *Jnl. of Testing and Evaluation,* 1(6): 520 (November 1973).

28. D. C. Ludwigson, "Modified Stress-Strain Relation for FCC Metals and Alloys," *Metal. Trans.* 2: 2825 (1971).

29. *Monthly Technical Progress Report,* Hanford Engineering Development Laboratory, HEDL-TME 71-11, November 1971.

30. *Monthly Technical Progress Report,* Hanford Engineering Development Laboratory, HEDL-TME 72-2, February 1972.

4. NAVAL RESEARCH LABORATORY

L. E. Steele

4.1 INTRODUCTION - L. E. Steele

The research program of the NRL, Metallurgy Division, Reactor Materials Branch, includes the study of the behavior of structural materials useful in reactor construction. Within the scope of the title above much unirradiated data are developed. This report is developed using such data to support the USAEC objective of compiling structural materials properties data for use in national reactor development programs. The NRL program is sponsored by the Office of Naval Research, the U. S. Atomic Energy Commission, and the U. S. Army Engineer Power Group. The unirradiated materials properties data contributed here include that developed in the course of research in the areas of high temperature materials, radiation damage, and fracture mechanics.

4.2 FATIGUE CRACK GROWTH IN TYPE 316 STAINLESS STEEL - D. J. Michel and H. H. Smith

4.2.1 Background

The resistance to fatigue crack growth in alloys and weldments intended for fast breeder reactor applications is being investigated. The effects of composition and microstructure are among the variables being considered at temperatures of primary liquid-metal fast-breeder reactor (LMFBR) interest. This report reviews and summarizes results of prior NRL studies by Shahinian, Smith, and Watson on fatigue crack growth in Type 316 stainless steel (SS) plate[1-4] as background for the discussion of new data in forthcoming reports.

4.2.2 Materials and Test Procedures

The chemical composition and tensile properties of the Type 316 SS used in this work are given in Table 4.1. Fatigue crack growth rates

for annealed material were determined at several temperatures. Single-edge-notched specimens containing side grooves and oriented in the RW direction were cycled at 10 cpm in cantilever bending under zero-to-tension loading to a constant maximum load. Induction heating was used for the elevated temperature tests. All data were analyzed to determine crack growth rate as a function of stress intensity at the crack tip. This procedure allows the direct comparison of the fatigue crack growth resistance of materials and provides useful design data.

4.2.3 Results

The fatigue crack growth behavior of 316 SS at 75 F (24 C) is shown in Fig. 4.1 for the annealed condition.[1,2] A common sigmoidal curve shape is seen for the data in Fig. 4.1. It is also seen that the data points for all three loads can be represented by a single curve despite the result that the calculated crack surface fiber stress was in excess of the yield strength of the annealed material in some instances. It is probable, however, that strain hardening significantly increased the yield strength of the material at the crack tip to a value above that of the crack surface fiber stress. Surface deformation ahead of the crack tip was observed to approximately coincide with the upper inflection in Fig. 4.1.

Figure 4.2 illustrates the fatigue crack growth behavior of 316 annealed SS at elevated temperatures.[1,2] It is seen that the fatigue crack growth rate increased with increasing temperature for a given ΔK value. The general form of the crack growth rate curves are not uniform and no consistent trend is evident when comparing the inflections and the change in test temperature. Between 75 and 1100 F (24 and 593 C), the crack growth rate was found to increase by approximately a factor of six. Correspondingly, smaller increases in crack growth rate occur for smaller temperature changes though the changes cannot be catalogued by a single relationship as changes depend importantly upon the contribution of ΔK value and temperature. Comparison of the crack growth data[3] at 77, 800, and 1100 F (25, 427, and 593 C), Fig. 4.3, also illustrates the increase in crack growth rate with increasing temperature for annealed Type 316 SS. At very low crack growth rates, it is seen that the

Table 4.1. Chemical Analysis and Mechanical Properties of Type 316 Stainless Steel

Chemical Composition - (Heat 65808)					
C	0.60	Ni	13.30	Sn	0.013
Mn	1.72	Mo	2.33	Co	0.030
P	0.012	Cu	0.065	B	0.0005
S	0.007	Al	0.012	N_2	0.048
Si	0.40	Ti	0.003	Ce	0.0006
Cr	17.30	Pb	0.0014		
		Total Rare Earths	0.0010		

Mechanical Properties					
0.2% Yield Strength	Ultimate Tensile Strength	Elongation	Reduction of Area	BHN	Grain Size
44,100 psi	82,100 psi	68%	63.4%	163	4

Table 4.2. Effect of Temperature on Fatigue Life

Temperature (F)	Temperature (C)	Load (lb)	Life (10^3 Cycles)
75	24	1100	50.3
500	260	1000	42.6
700	370	1000	22.3
900	480	1100	10.8
900	480	700	49.5
1100	590	700	23.0

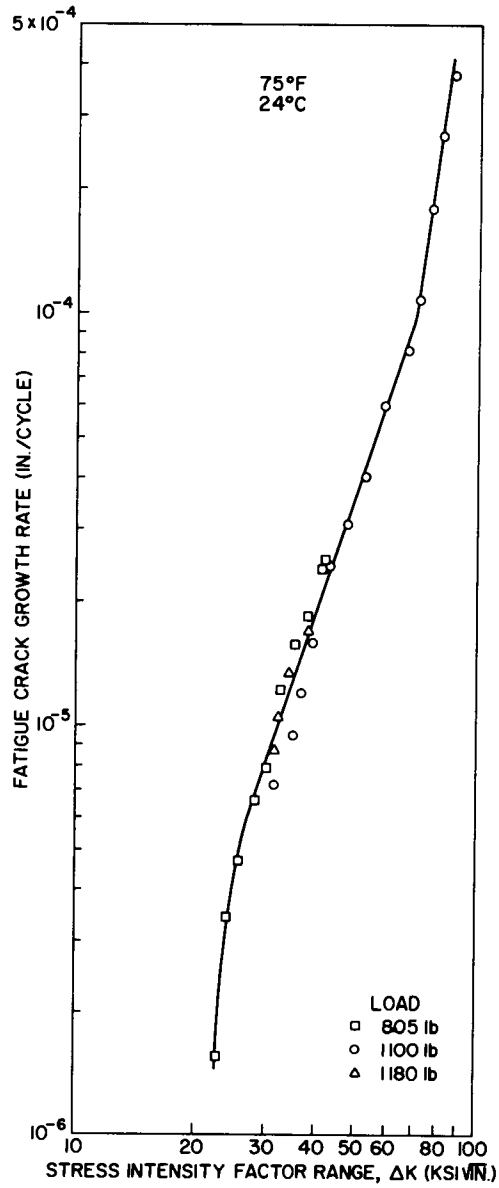

Fig. 4.1. Fatigue Crack Growth Rate as a Function of Stress Intensity Factor Range for Annealed Type 316 Stainless Steel at Room Temperature.

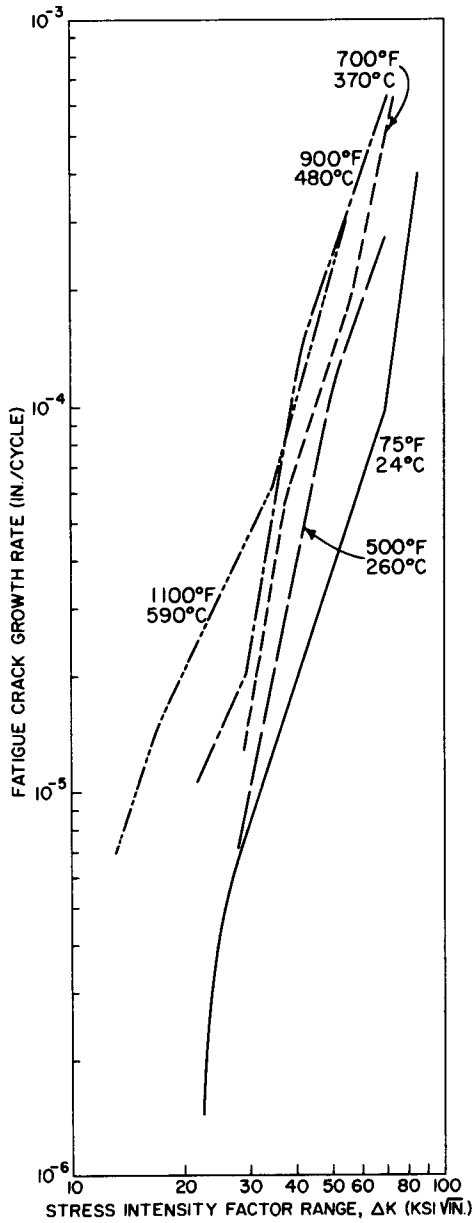

Fig. 4.2. Fatigue Crack Growth Behavior of Annealed Type 316 Stainless Steel at Several Temperatures.

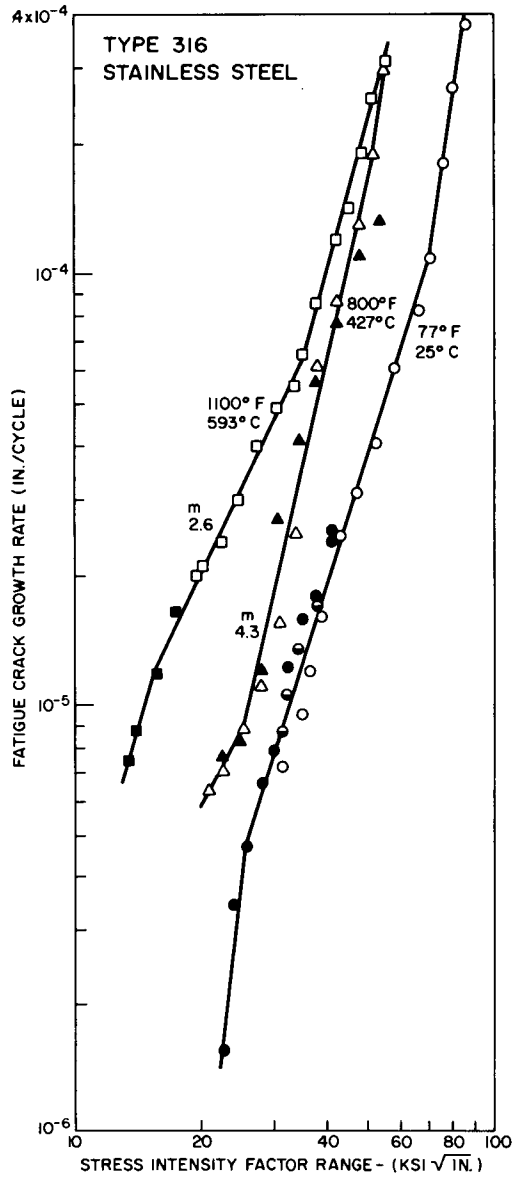

Fig. 4.3. Fatigue Crack Growth Behavior of Annealed Type 316 Stainless Steel at 77, 800, and 1100 F (25, 427, and 593 C).

curves are displaced toward lower ΔK values, suggesting lower stress intensity threshold values for crack propagation, with increasing temperature.

The effect of temperature on fatigue life is given in Table 4.2. The results[1,2] show the expected decrease in fatigue life with increased test temperature. The variation in fatigue life with load is also apparent at 900 F (370 C).

The dependence of fatigue crack growth rate on temperature for annealed Type 316 SS is shown in Fig. 4.4 for several ΔK levels. However, the results[2] do not give clear evidence for Arrhenius-type behavior which would permit the general identification of those thermally activated processes which control the fatigue crack growth. This illustrates the complex microstructural nature of the fatigue process which must be understood to develop the necessary predictive capability. However, on a broad scale, it appears possible to unify the fatigue crack growth rate dependence on temperature for annealed Type 316 SS by normalizing the ΔK values by the square of the elastic modulus, E, at each test temperature. As shown in Fig. 4.5, this approach[1,4] provides a reasonable representation of the experimental results by a single parameter which may be useful in predicting general crack growth behavior.

In summary, the fatigue crack growth results for annealed Type 316 SS indicate that crack growth rate is related to the stress intensity factor range for the temperature range investigated. The crack growth rates were found to increase with increasing temperature for given ΔK values. Correspondingly, the increased crack growth rate decreased the fatigue life. It was found, however, that crack growth rate is not controlled by one thermally activated process over the entire range of test temperatures even though it is possible to represent the data by normalizing ΔK values by the square of the elastic modulus. Further information concerning these important areas is being sought during other phases of the present fatigue crack growth investigations.

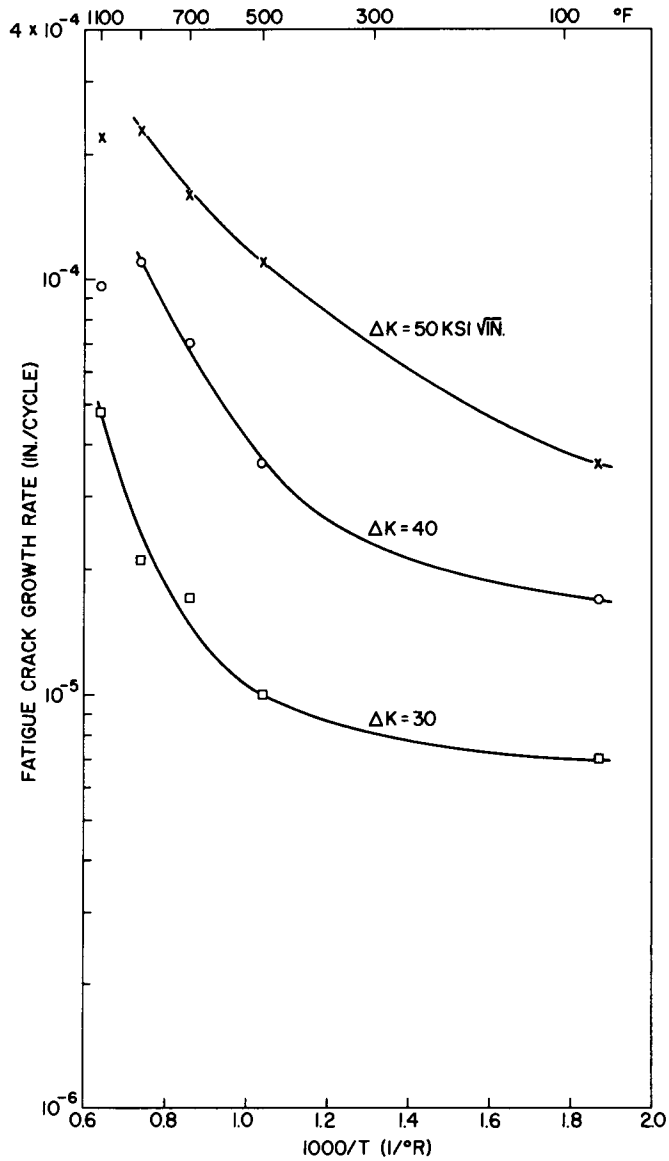

Fig. 4.4. Temperature Dependence of Fatigue Crack Growth Rate for Annealed Type 316 Stainless Steel for Several ΔK Ranges.

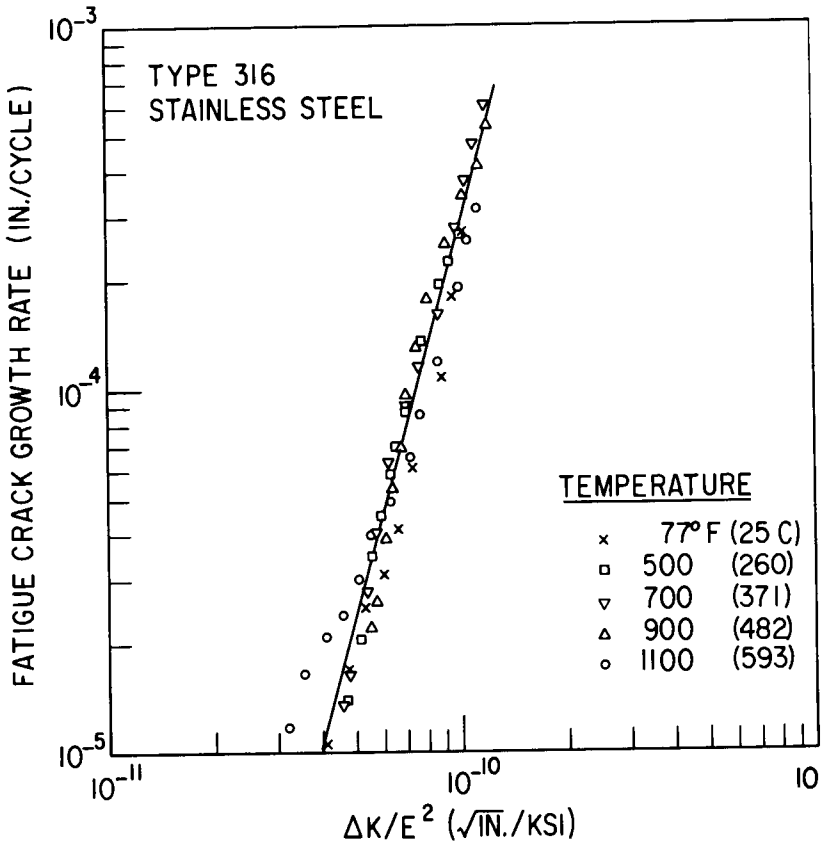

Fig. 4.5. Fatigue Crack Growth Rate as a Function of the Ratio of Stress Intensity Factor Range to Square of Elastic Modulus for Annealed Type 316 Stainless Steel.

4.3 FRACTURE RESISTANCE OF TYPE 304 STAINLESS STEEL AND TYPE 308 WELD DEPOSIT - F. J. Loss and R. A. Gray,Jr.

4.3.1 Background

The fracture toughness of austenitic SS is being characterized with the following experimental procedures: J-Integral, Dynamic Tear (DT), and Charpy V-Notch (C_v) tests. Emphasis is being placed on the J-Integral tests as a means to express flaw instability in quantitative terms that are related to structural design parameters when the material exhibits elastic-plastic behavior. The DT and C_v trends developed for Type 304 SS plate and Type 308 SS weld deposit[5] have shown the latter to exhibit a lower energy absorption than the plate at temperatures from 75 F (24 C) to 900 F (482 C). These trends are being further investigated by means of J-Integral tests.

4.3.2 Materials and Specimen Types

J-Integral specimens were cut from a Type 304 SS plate and a Type 308 SS submerged arc weld deposit. The tensile properties and chemical analyses for the materials are listed in Table 4.3 of Ref. 6. The tests were conducted statically using three-point, notched bend specimens having the dimensions: width (W) = 0.394 in., thickness (B) = 0.197 in., and length (L) = 2.165 in. The specimens described here contained a 1/16-in. wide machined notch of depth equal to 0.3 W. The notch tip consisted of a 60 degree Vee that was sharpened by means of a knife edge pressed to a depth of approximately 0.003 in. All specimens were cut with the plane of the notch perpendicular to the plate surface and the direction of crack propagation either parallel (WR) or perpendicular (RW) to the primary rolling direction. The direction of crack propagation in the weld metal specimens was parallel to the welding direction and the plane of the notch was perpendicular to the weldment surface.

4.3.3 Test Results

Figure 4.6 illustrates load versus midspan deflection records for specimens cut from the Type 304 SS plate and Type 308 SS weld deposit.

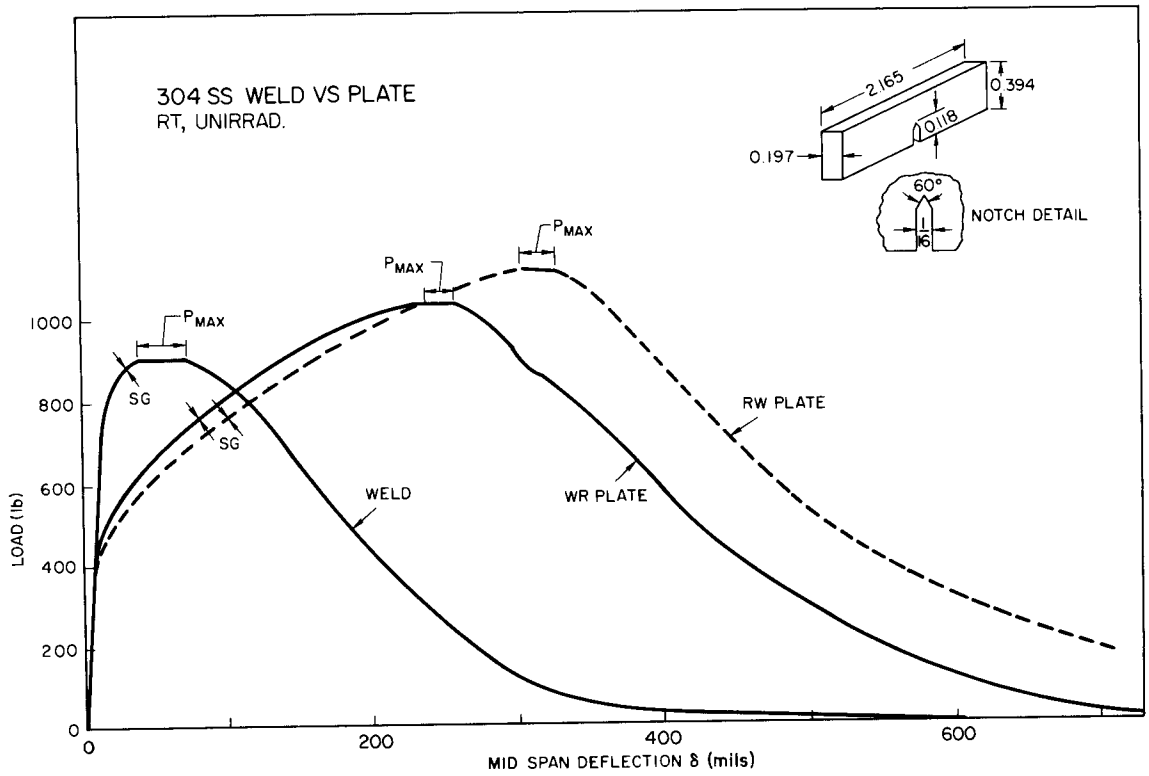

Fig. 4.6. Comparison of Load vs Midspan Deflection Records for a Type 304 SS plate and a Type 308 SS Weld Metal. The Plate Specimens were Tested in the Weak (WR) and Strong (RW) Orientations. Crack Initiation (labeled SG) was Visually Observed During the Test at the Tip of the Machined Notch. Indications of Crack Extension on the Surface of the Specimens are not Observed Below the Maximum Load (P_{MAX}).

A comparison of the area under the curves (i.e., energy) shows the weld metal to absorb less energy than the plate at 75 F (24 C). This fact is consistent with the observation of Hawthorne[5] showing the C_v and DT energy absorption of the submerged arc weld to be significantly less (~1/2) that that of the plate. The comparison of total energy absorption for plate and weld metal specimens is presented in Table 4.3. These results show the total energy of the weld metal specimens to be between 38 and 69% of the total energy absorbed by plate specimens at temperatures of 75 and 1000 F (24 and 538 C). Also, a comparison of plate material has been made at 75 and 1000 F which shows a considerable reduction in plate energy absorption at the higher temperature.

An alternative comparison of the plate and weld metal performance can be made on the basis of energy to maximum load rather than total energy absorption. For example, certain structural elements are considered failed after having attained maximum load when the load is not relieved as a result of deformation as in the case with thermal stresses. For example, a cantilever beam with dead weight loading or a pressure vessel that is pneumatically loaded will continue to deform without limit once maximum load has been achieved. For these cases it would appear that a toughness characterization on the basis of energy to maximum load is more rational than a criterion based on total specimen energy absorption.

Table 4.3 comparisons on the basis of energy to maximum load suggest that the toughness of the weld metal is even <u>lower</u> than that defined on the basis of total energy, such as might be obtained with a DT or C_v test. A similar conclusion can be drawn for the comparison of plate specimens at 75 and 1000 F.

As described in Reference 6, the area under the load versus deflection trace is proportional to the toughness in terms of the J Integral. However, current mathematical approaches are insufficient to define J in the presence of considerable slow crack extension that characteristically occurs near maximum load.

In a strict interpretation, J can be defined only up to the point of initiation of slow growth (labeled SG in Fig. 4.6). If initiation of slow crack extension is taken as a design criterion, it can be

Table 4.3. Energy Absorption Ratios of Plate and Weld Metal

Temp.	Plate Spec. Orien.	Total Energy Basis: Weld / Plate	Total Energy Basis: 1000F Plate* / 75 F Plate	Maximum Load Energy Basis: Weld / Plate	Maximum Load Energy Basis: 1000F Plate / 75 F Plate
75	RW	.38		.15	
1000	WR	.47		.20	
1000	RW	.51		.36	
	WR	.69		.53	
(Ratio*)	RW		.45		.30
	WR		.41		.27

concluded qualitatively, from the area under the curves up to the SG position, that the toughness of the weld still will be less than that of the plate. However, the weld toughness will be a greater fraction of the plate toughness than would be the case for the comparisons based on maximum load. This conclusion follows from the different location of the SG position with respect to maximum load for the plate and weld metal in Fig. 4.6. In fact, a comparison on the basis of crack initiation would rate the materials similar to that obtained on the basis of total energy.

4.3.4 Conclusions

Preliminary investigation of Type 304 SS plate under static loading suggests a sharp decrease in toughness at 1000 F in comparison to 75 F tests. Type 308 SS submerged arc weld metal also exhibits this decrease in toughness with elevated temperature. In addition, the toughness of the weld metal at both 75 and 1000 F is significantly below that of the plate. Overall, however, the toughness of the weld does not appear to be sufficiently low so that brittle behavior will be exhibited in thin sections (~1 in.).

A qualitative J-Integral comparison of weld and plate on the basis of crack initiation, projects a smaller difference in toughness between the two materials than was defined using energy to maximum load. It is clear that further studies in this area are needed.

4.4 NOTCH DUCTILITY OF ASTM TYPE A508 FORGINGS - J. R. Hawthorne

Notch ductility performance of four ASTM Type A508 Class 2 forgings produced commercially have been determined by Drop Weight (DW) and C_v test methods. The determinations were made in support of irradiation effects investigations. The chemical composition and strength of each forging are indicated in Table 4.4. Forging heat treatments are indicated in Table 4.5. Notch ductility properties are compared in Table 4.6.

Figures 4.7 and 4.8 show the C_v versus DW performance of two of the forgings. Although both forgings depict comparable nil-ductility transition (NDT) temperatures (40 F, 4 C versus 50 F, 10C), a major difference is evident in their average C_v energy level at NDT (100 versus 44 ft-lb). The forgings thus demonstrate that an arbitrary C_v "energy fix" cannot be used to predict NDT temperatures for this type material. From Tables 4.4 and 4.6 differences in strength or C_v upper shelf level which could account for the wide variance in the C_v energy versus NDT correlation were not evident. DT test assessments of selected forgings are planned.

Table 4.4. Chemical Composition and Strength of the A508 Forgings

Forging	Thickness (in.)	Yield Strength (ksi)	Tensile Strength (ksi)	Chemical Composition (Wt-%)								
				C	Mn	P	S	Si	Ni	Cr	Mo	Cu
1	9.5	69.8 69.7[a]	91.9 92.3[a]	.21	.68	.005	.008	.27	.71	.39	.59	.09
2	12.0	80.5 80.0[a]	100.5 98.6[a]	.19	.69	.007	.009	.31	.82	.38	.62	.13
3[b]	6.6	68.3	88.0	.16	.57	.011	.010	.28	.69	.36	.62	.11
4[b]	6.6	66.0	92.5	.20	.60	.010	.008	.27	.68	.36	.62	.11

[a] Transverse orientation.
[b] Courtesy supplier.

Table 4.5. Heat Treatment of A508 Forgings

Forging	Heat Treatment
1 (9.5 in.)	Austenitized 1550 F (843 C)-9 hr, WQ; Tempered 1210 F (654 C)-12 hr, AC; Stress Relieved 1125 F (607 C)-20 hr, FC 40 F (22 C)/hr max to 600 F (316 C)
2 (12.0 in.)	Austenitized 1688 F (920 C)-3½ hr, WQ; Tempered 1220 F (660 C)-7 hr, FC; Stress Relieved 1140 F (616 C)-18 hr, FC to 600 F (316 C)
3,4 (6.6 in.)	Austenitized 1575 F (857 C)-5 hr, WQ; Tempered 1200 F (649 C)-6¼ hr, FC Stress Relieved 1150 F (621 C)-30 hr, FC 60 F (33 C)/hr max to 600 F (316 C)

Table 4.6. Notch Ductility of A508 Forgings

Forging	Drop Weight-NDT[a]		Charpy-V Energy (ft-lb)	
	(F)	(C)	@NDT	@Upper Shelf
1 (9.5 in.)	40	4	100	161
2 (12.0 in.)	50	10	44	137
3 (6.6 in.)	10	-12	122	154
4 (6.6 in.)	-10	-23	120	155

[a] ASTM Type P-3 Drop Weight Test Specimens.

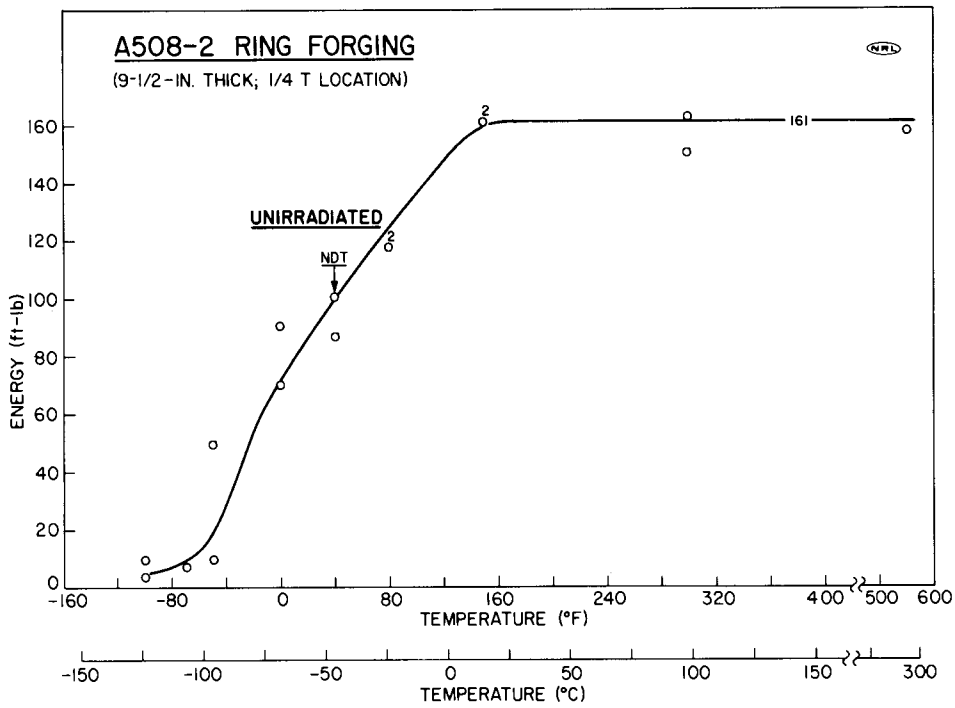

Fig. 4.7. Notch Ductility of Forging 1 Determined by Drop Weight and Charpy-V Test Methods.

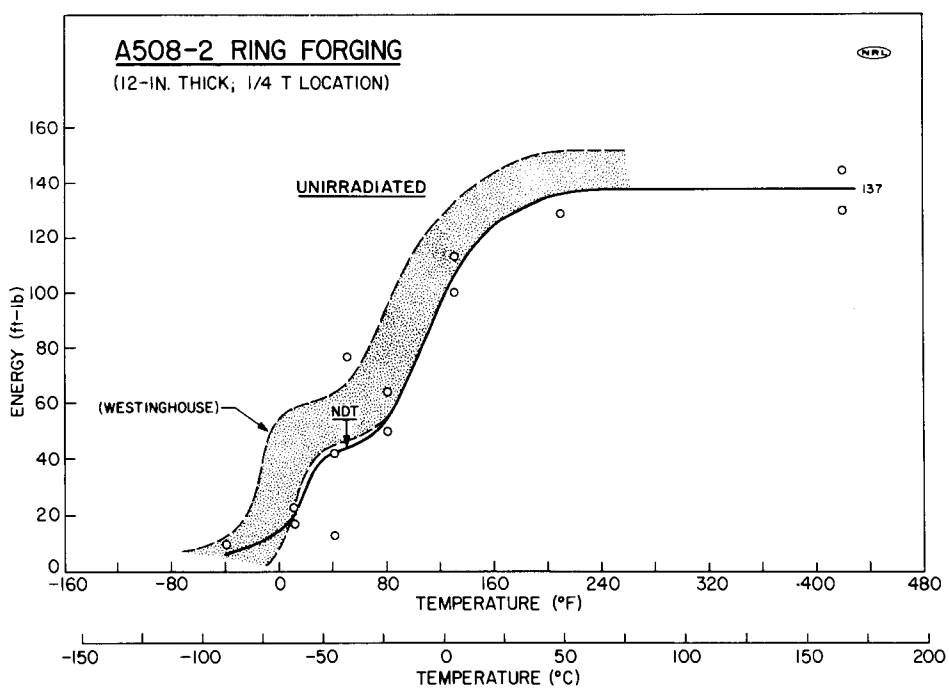

Fig. 4.8. Notch Ductility of Forging 2 Determined by Drop Weight and Charpy-V Test Methods. Charpy-V Performance Observed by Westinghouse is also Indicated (shaded band).

4.5 REFERENCES

1. P. Shahinian, H. H.Smith, and H. E. Watson in Irradiation Effects on Reactor Structural Materials Quart. Progr. Rep. 1 Feb-30 April 1971, Naval Research Laboratory, NRL Memorandum Report 2259, pp. 13-20; also Hanford Engineering Development Laboratory, HEDL-TME-71-66,
2. P. Shahinian, H. H. Smith, and H. E. Watson, Trans. ASME, J. Engrg. for Ind. 93:976 (1971).
3. P. Shahinian, H. H. Smith, and H. E. Watson, in Fatigue at Elevated Temperatures, ASTM STP 520, 1973, p. 387.
4. P.Shahinian, H. E. Watson, J. Materials 7:527 (1972).
5. Mechanical Properties Test Data for Structural Materials Quart. Progr. Rep. for Period Ending Oct. 31, 1973, Oak Ridge National Laboratory, ORNL-4936, Jan. 1974, pp. 51-61.
6. IBID, pp. 46-51.

5. OAK RIDGE NATIONAL LABORATORY

5.1 INTRODUCTION

5.2 MECHANICAL PROPERTIES AND BEHAVIOR FOR STRUCTURAL MATERIALS — W. R. Martin

The objective of this program is to collect mechanical property data and material behavior for LMFBR structural and component materials. Included in the scope of this effort are the following: (1) basic tensile, creep, creep-rupture, and relaxation base-line data that are directly applicable to design criteria and methods for types 304 and 316 stainless steel reference heats and cyclic stress-strain tests performed with emphasis on loading and history effects, (2) find the variations in properties for several heats of types 304 and 316 stainless steel to allow establishment of minimum and average values of specific properties and the equation parameters required for design purposes. This work will include determination of property variation of samples from different mill products within a given heat of stainless steel.

5.2.1 Base-Line Mechanical Property Testing of Reference Heat of Type 304 Stainless Steel

5.2.1.1 Creep Properties of the 2-in. (51-mm) Plate of Referenct Heat — H. E. McCoy

The need for comprehensive mechanical property data on a single heat of type 304 stainless steel for use in developing constitutive equations for design purposes was recognized during the last few years. A large heat of type 304 stainless steel (designated Heat 9T2796) was purchased in several product forms, and the testing began in 1972. The test program included creep tests to accurately define the strain-time response. The details of the averaging extensometer and associated electronics for creep testing were described previously.[1] We now have 19 lever-arm creep machines and six deadload machines equipped to do this caliber of testing.

Some of the test information was summarized in the last two quarterlies[2,3] and will be updated in the current report. The tests that have been completed and those that are in progress are given in Table 5.1. The tests have all been run on the 2-in.-thick plate, and samples were

Table 5.1. Creep Tests on Type 304 Stainless Steel Reference Heat 9T2796 2-in.-thick (51-mm) Plate[a]

Test	Temperature (°C)	Temperature (°F)	Stress (ksi)	Stress (MPa)	Time in Test (hr)	Loading Strain (%)	Ratio of Creep Stress to Yield Stress[b]	Comments[c]
11595	427	800	20.0	138	5,200	2.67	1.57	
12368	427	800	18.0	124	2,171	1.91	1.42	
12472	427	800	16.0	110	1,306	1.17	1.26	
12570	427	800	14.0	97	978	0.83	1.10	
11569	482	900	20.0	138	5,319	3.27	1.70	
12375	482	900	18.0	124	2,111	2.40	1.53	
11675	482	900	16.0	110	2,451	1.48	1.36	Discontinued
11693	482	900	14.0	97	2,690	0.92	1.19	Discontinued
11830	482	900	12.0	83	1,682	0.35	1.02	Discontinued
10489	538	1000	20.0	138	10,217	3.80	1.80	
12250	538	1000	18.0	124	2,680	2.62	1.62	
11625	538	1000	16.0	110	5,081	1.79	1.44	
10491	538	1000	14.0	97	10,237	1.16	1.26	
12444	538	1000	14.0	97	1,650	1.18	1.26	
12445	538	1000	14.0	97	1,675	1.17	1.26	
11568	538	1000	12.0	83	5,326	0.53	1.08	
11626	538	1000	10.0	69	5,081	0.071	0.90	
11641	538	1000	8.0	55	3,170	0.040	0.72	Discontinued
10853	593	1100	18.0	124	4,545	2.84	1.65	Ruptured
10852	593	1100	16.0	110	8,508	2.29	1.47	
10554	593	1100	14.0	97	8,710	1.40	1.28	Discontinued
11596	593	1100	12.0	83	4,895	0.52	1.10	
10490	593	1100	10.0	69	10,212	0.22	0.92	
11227	593	1100	8.0	55	6,103	0.041	0.73	Discontinued
12459	593	1100	5.0	34	1,388	0.024	0.46	
10855	649	1200	16.0	110	304	2.41	1.57	Ruptured
10854	649	1200	14.0	97	761	1.60	1.37	Ruptured
11563	649	1200	12.0	83	2,674	0.59	1.18	Ruptured
11226	649	1200	10.0	69	7,205	0.18	0.98	
10851	649	1200	8.0	55	8,395	0.044	0.78	
12255	649	1200	5.0	34	992	0.030	0.49	Discontinued
12443	649	1200	5.0	34	1,345	0.024	0.49	
12460	649	1200	3.0	21	1,361	0.020	0.29	
10856	704	1300	10.0	69	568	0.067	0.90	Ruptured
10562	704	1300	10.0	69	653	0.12	0.90	Ruptured
11222	704	1300	8.0	55	2,760	0.031	0.72	Ruptured
12254	704	1300	5.0	34	2,565	0.030	0.45	
12461	704	1300	3.0	21	1,386	0.018	0.27	
12462	704	1300	2.0	14	1,360	0.010	0.18	

[a]Annealed 0.5 hr at 1093°C before testing. All tests loaded at a strain rate of 0.005/min.

[b]Yield stresses used in this ratio were 12,700 psi (88 MPa) at 427°C (800°F), 11,800 psi (81 MPa) at 482°C (900°F), 11,100 psi (77 MPa) at 538°C (1000°F), 10,900 psi (75 MPa) at 593°C (1100°F), 10,200 psi (70 MPa) at 649°C (1200°F), 11,100 psi (77 MPa) at 704°C (1300°F).

[c]Unless otherwise noted, tests in progress.

taken from the center line in the primary working direction. Test samples have a gage section 0.25 in. in diam × 2.25 in. long (6.35 × 57.2 mm) and were reannealed 0.5 hr at 1093°C (2000°F) in argon. The test environment was air. The test matrix for long-term tests is given in Table 5.2. The numbers in parentheses are the test numbers and can be used to refer to Table 5.1. All the A priority tests are completed or in progress, and only one creep test having a C priority in Table 5.2 remains to be started.

Some creep tests of about 1000 hr duration are needed to determine the primary creep behavior. The tests of A-1 priority are shown in Table 5.3, and five remain to be started. Four of these tests are in the loading rate series and will be started as soon as a new loading device is completed. There is some duplication of tests between Tables 5.2 and 5.3, so only a total of five tests remain to be started. These should all be started within the next few months.

Previously we had analyzed the strains that occurred when the tests in Table 5.1 were loaded. The additional data obtained during this report period have been added to Figs. 5.1 and 5.2, and the previous correlations still hold. Five tests loaded below the proportional limit strained amounts about equal to those predicted by elastic behavior.

Plots are currently being updated on all tests in progress. A computer program is being written for more efficiently fitting the test data. Further analyses will be performed in the near future.

Temperature control has received a large amount of attention during this report period. Tests 10554 with 8710 hr and 11227 with 6103 hr were discontinued because controller malfunctions allowed too high a temperature. A few other tests cooled below the desired control temperature, but these tests were reheated with no obvious effect on the creep rate. These malfunctions lead us to the conclusion that 6000 to 8000 hr is likely the maximum time that these controllers can operate continuously without major maintenance. Although electronic improvements have been made in control instruments, the servo action is still mechanical. Thus, mechanical wear and hardening of lubricants pose a major problem. We have performed major maintenance on each instrument that has operated over 4000 hr, and we plan to repeat this every six months (about 4400 hr).

Table 5.2. Test Matrix for Uniaxial Creep of Type 304 Stainless Steel

Stress		Priority and Test Number[a] for Each Temperature, °F (°C)					
(MPa)	(psi)	800 (427)	900 (482)	1000 (538)	1100 (593)	1200 (649)	1300 (704)
14	2,000						C (12462)
21	3,000					C (12460)	B (12461)
34	5,000				C (12459)	C(12255, 12443)	A-1 (12254)
55	8,000			C (11641)	A-1 (11227)	A-1 (10851)	A-1 (11222)
69	10,000		C	C (11626)	A-1 (10490)	A-2 (11226)	A-1 (10856, 11562)
83	12,000		C (11830)	A-2 (11568)	B (11596)	B (11563)	
97	14,000	C (12570)	C (11693)	A-1 (10491)	A-1 (10554)	A-1 (10854)	
110	16,000	C (12472)	C (11675)	B (11625)	A-1 (10852)	A-1 (10855)	
124	18,000	C (12368)	C (12375)	B (12250)	A-1 (10853)		
138	20,000	A-2 (11595)	A-2 (11569)	A-1 (10489)			

[a]Test number refers to Table 3.1.

Table 5.3. Short-Time A-1 Priority Uniaxial Creep Tests of Type 304 Stainless Steel[a]

Stress (ksi)	Stress (MPa)	Loading Strain Rate (min^{-1})	Tests at Each Temperature, °F (°C) 800 (427)	900 (482)	1000(538)	1100 (593)	1200 (649)	1300 (704)
3	21	0.005						12461
5	34	0.005				12459	12255, 12443	12254
8	55	0.005			11641	11227	10851	11222
10	69	0.005		b	11626	10490	11226	10856, 11562
		0.0005				b		
		0.25				b		
12	83	0.005		11830	11568	11596	11563	
14	97	0.005	12570	11693	10491, 12444, 12445	10554	10854	
16	110	0.005	12472	11675	11625	10852		
		0.0005				b		
		0.25				b		
20	138	0.005	11595	11569	10489			

[a]Numbers listed refer to test numbers in Table 3.1. Some of the same tests are also part of the long-term test matrix shown in Table 3.2.

[b]Test called for but not yet started.

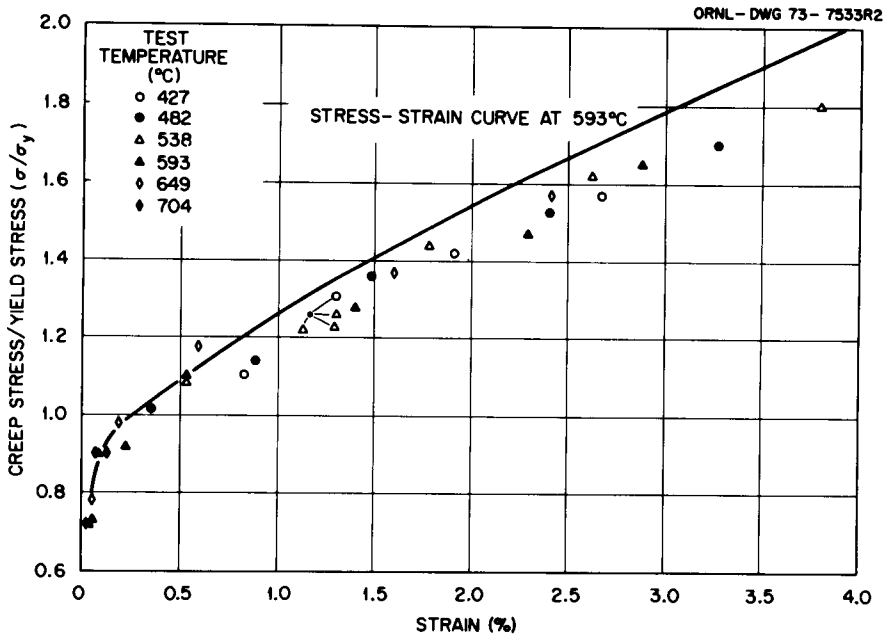

Fig. 5.1. Comparison of Strain on Loading With Stress Ratio for Type 304 Stainless Steel (Heat 9T2796) Annealed 0.5 hr at 1093°C (2000°F).

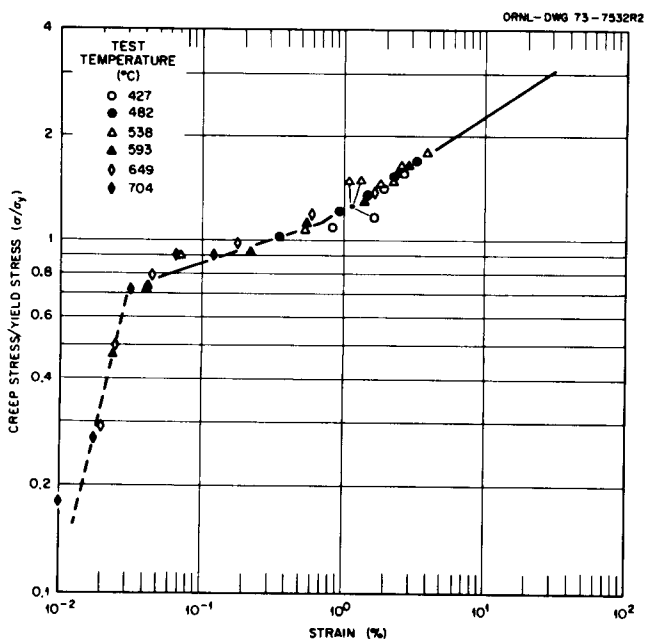

Fig. 5.2. Comparison of Strain on Loading With Stress Ratio in Type 304 Stainless Steel (Heat 9T2796) Annealed 0.5 hr at 1093°C (2000°F).

A second control problem involves the width of the control band. Control is normally maintained to within a ±1°C cycle. Adjustment of our L & N proportioning controllers to obtain tighter control resulted in instability. Control is based on a percentage of the total instrument span, so we decreased the width of the control cycle by reducing the instrument span. Most of our instruments had ranges from 0 to 2000°F, and we have procured special ranges that are only 100°F wide. For example, the span used for a 1000°F (538°C) test is 950 to 1050°F. This had decreased the control cycle to less than ±0.1°C, although some infrequent cycles up to ±0.3°C occur over long time periods. This change has brought about a basic improvement in our control accuracy and further refines our precision testing.

5.2.1.2 Strain Rate Effect on the Tensile Properties of 2-in. (51-mm) Plate — H. E. McCoy and C. W. Nestor*

The type 304 stainless steel reference heat has been tensile tested in air over the range 25 to 704°C (77 to 1300°F) and at initial strain rates from 0.40 to 0.0004/min. The samples were all taken from the 2-in.-thick (51-mm) plate, and the gage section was parallel to the primary working direction. All samples were reannealed 0.5 hr in argon at 1093°C (2000°F) before testing. The gage section of the sample was 1.25 in. long × 0.250 in. in diameter (31.8 × 6.35 mm). An averaging extensometer was joined to the center line of the specimen gage section and was used to measure the first few percent strain.

The updated test results are summarized in Table 5.4. The results at each strain rate were fit by regression analysis to a polynomial of the form:

$$P = A + BT + CT^2 + DT^3 + ET^4 \quad ,$$

where P = property in ksi (yield stress, ultimate tensile stress, true tensile stress), T = temperature in °C, and A, B, C, D, and E are constants. The results at all four strain rates were also combined and analyzed as a

*Mathematics Division.

Table 5.4. Tensile Properties of Type 304 Stainless Steel (Heat 9T2796), 2-in.-Thick (51-mm) A 240 Plate Reannealed 0.5 hr at 1093°C (2000°F)

Temperature		Strain Rate	Stress, ksi(MPa)		Strain, %		Reduction of area
(°C)	(F°)	(min^{-1})	Yield	Ultimate	Uniform	Total	(%)
25	77	0.4	28.4(196)	75.3(519)	65.6	76.5	81.5
		0.040	25.8(178)	78.1(538)	85.6	91.4	83.0
			27.7(191)	78.6(542)	76.3	89.0	83.3
		0.004	26.7(184)	80.0(532)	85.2	102.0	85.1
			26.5(183)	82.1(566)	82.5	98.0	85.2
		0.0004	23.4(161)	78.0(538)	96.0	106.0	83.8
100	212	0.044	19.6(135)	64.0(441)	60.0	66.0	83.2
200	392	0.044	15.7(108)	57.7(398)	46.7	62.0	79.2
260	500	0.4	14.9(103)	56.3(388)	45.6	50.8	75.1
		0.04	14.7(101)	57.2(394)	47.2	51.2	73.3
		0.004	15.7(108)	55.9(385)	44.0	48.3	72.6
			15.8(109)	59.3(409)	47.7	49.9	63.7
		0.0004	13.2(91)	59.1(407)	52.3	53.4	71.6
350	662	0.04	12.4(85)	56.6(390)	43.6	43.9	68.7
427	800	0.4	12.3(85)	55.8(385)	45.6	47.3	66.9
		0.04	12.4(85)	57.2(394)	45.6	44.6	59.8
		0.004	12.5(86)	60.2(415)	45.9	52.2	63.8
			12.9(89)	61.1(421)	45.3	50.4	71.5
		0.0004	11.7(81)	60.7(419)	50.9	56.2	65.8
482	900	0.4	11.5(79)	54.0(372)	45.6	49.9	70.0
		0.04	12.2(84)	55.8(385)	46.4	51.5	71.4
		0.004	11.6(80)	58.0(400)	43.2	50.3	64.8
			12.0(83)	57.0(393)	47.5	54.7	58.9
		0.0004	11.1(77)	56.6(390)	51.8	56.8	63.7
538	1000	0.4	12.0(83)	51.8(357)	40.0	45.9	71.1
		0.04	10.9(75)	47.4(327)	48.0	51.9	71.1
		0.004	11.0(76)	53.2(367)	43.3	52.1	64.1
			11.2(77)	54.1(373)	39.4	52.5	67.3
		0.0004	10.2(70)	47.7(329)	46.3	46.2	41.1
593	1100	0.4	9.94(69)	46.9(323)	41.6	47.2	70.6
		0.04	10.1(70)	46.7(322)	48.0	49.6	63.3
		0.004	10.7(74)	45.4(313)	34.6	38.0	32.4
			11.0(76)	45.7(315)	32.8	45.4	43.2
		0.0004	10.2(70)	36.8(254)	28.8	31.8	32.3
649	1200	0.4	9.87(68)	42.5(293)	40.0	49.2	63.4
		0.04	10.4(72)	40.2(277)	36.0	48.3	49.2
		0.004	10.2(70)	35.8(247)	25.5	33.1	31.9
			10.2(70)	41.0(283)	28.0	37.0	33.4
		0.0004	9.80(68)	26.4(182)	20.2	30.9	26.2
704	1300	0.4	9.33(64)	35.9(248)	31.7	44.7	43.5
		0.04	9.60(66)	31.2(215)	28.8	42.8	41.9
		0.004	11.0(76)	26.9(185)	19.0	39.0	32.4
			11.1(77)	26.8(185)	19.4	40.0	33.8
		0.0004	10.1(70)	18.9(130)	10.1	29.2	24.4

single set of data. The values of the constants for each data set are tabulated in Table 5.5. In all cases, the model accounted for greater than 99% of the variability of the property.

Table 5.5. Coefficients of Polynomial Equation Relating Tensile Properties and Temperature for Type 304 Stainless Steel, Heat 9T2796

Strain Rate (min^{-1})	Number of Data Points	Value of Coefficients[a]				
		A, ksi	B, ksi/°C	C, ksi/°C^2	D, ksi/°C^3	E, ksi/°C^4
				Yield Stress		
0.4	8	31.38	−0.1277	3.521×10^{-4}	-4.643×10^{-7}	2.250×10^{-10}
0.04	12	29.77	−0.1343	4.286	−6.389	3.461
0.004	16	28.93	−0.1001	2.902	−4.574	2.782
0.0004	8	26.00	−0.1133	3.791	−5.990	3.461
all	44	29.23	−0.1238	3.943	−6.086	3.466
				Ultimate Tensile Stress		
0.4	8	81.32	−0.2646	0.9866×10^{-3}	-1.482×10^{-6}	6.879×10^{-10}
0.04	12	85.47	−0.3171	1.237	−1.930	9.370
0.004	16	90.46	−0.4194	1.767	−2.815	13.78
0.0004	8	90.40	−0.5653	2.917	−5.486	32.34
all	44	87.09	−0.3717	1.579	−2.591	13.18
				True Tensile Stress		
0.4	8	137.5	−0.5595	2.007×10^{-3}	-2.948×10^{-6}	1.376×10^{-9}
0.04	12	160.0	−0.8175	2.997	−4.417	2.084
0.004	16	173.2	−1.073	4.408	−7.116	3.716
0.0004	8	184.1	−1.406	6.693	−12.18	7.165
all	44	164.6	−0.9500	3.880	−6.297	3.309

[a]Coefficients of the equation $P = A + BT + CT^2 + DT^3 + ET^4$, where P is the yield stress, ultimate tensile stress, or true tensile stress in ksi and T is the temperature in °C. For P in MPa, all coefficients should be multiplied by 6.895.

The combined set of data for the yield stress as a function of temperature is shown in Fig. 5.3. The yield stress does not appear to be a function of strain rate. The largest spread in yield stress was noted at 25°C (77°F). The largest deviation between calculated and experimental values was about ±10%, although generally the agreement was better. The slight upturn of the yield stress predicted by the model

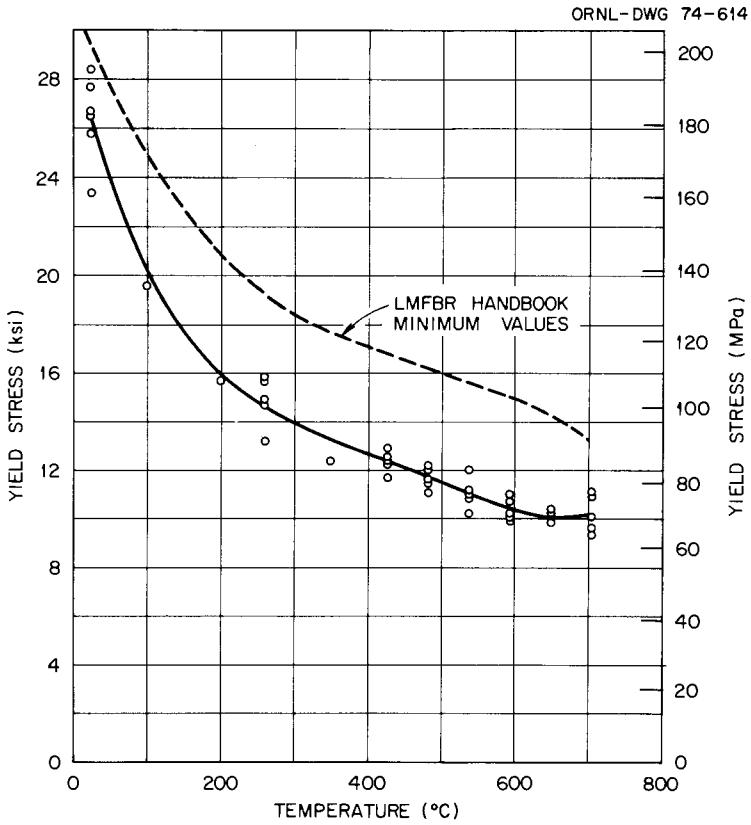

Fig. 5.3. Variation of Yield Stress with Temperature for Type 304 Stainless Steel (Heat 972796) Reannealed 0.5 hr at 1093°C (2000°F). Tests run at strain rates from 0.4 to 0.0004/min.

above 650°C (1200°F) is likely not real. The values for this heat are all below the minimum values appearing in the LMFBR Handbook and in ASME Pressure Vessel Code Case 1331-8.

The combined set of data for the engineering tensile stress is shown in Fig. 5.4. Strain rate was obviously an important variable at 593°C (1100°F) and above, and the tensile stress decreased with decreasing strain rate at a given temperature. The coefficients in Table 5.5 all reflect systematic variations with strain rate, and further analyses will be made to develop expressions for the dependence of these coefficients on strain rate. The best-fit line in Fig. 5.4 agrees quite closely with the line for the minimum values reported in the LMFBR Handbook and ASME Pressure Vessel Code Case 1331-8. The disagreement between the two correlations would be even less if the data at the low strain rate of 0.0004/min were dropped from the correlation.

The best fit for true tensile stress as a function of temperature for the combined sets of data is shown in Fig. 5.5. The correlation is quite good at temperatures below 538°C, but the results are obviously dependent upon strain rate at higher temperatures.

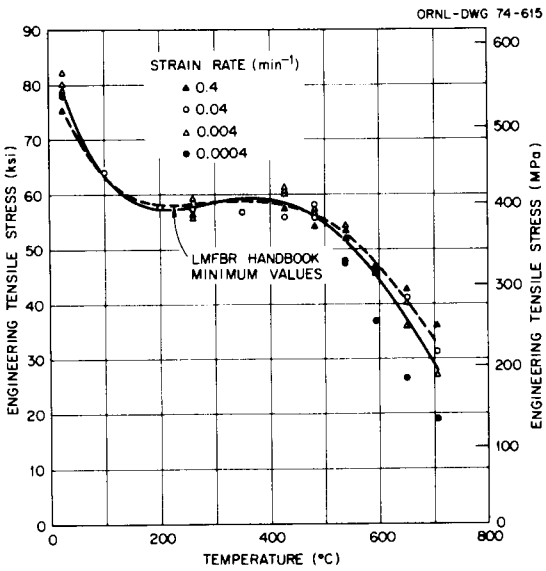

Fig. 5.4. Variation of Engineering Tensile Stress with Temperature for Type 304 Stainless Steel (Heat 9T2796) Reannealed 0.5 hr at 1093°C (2000°F).

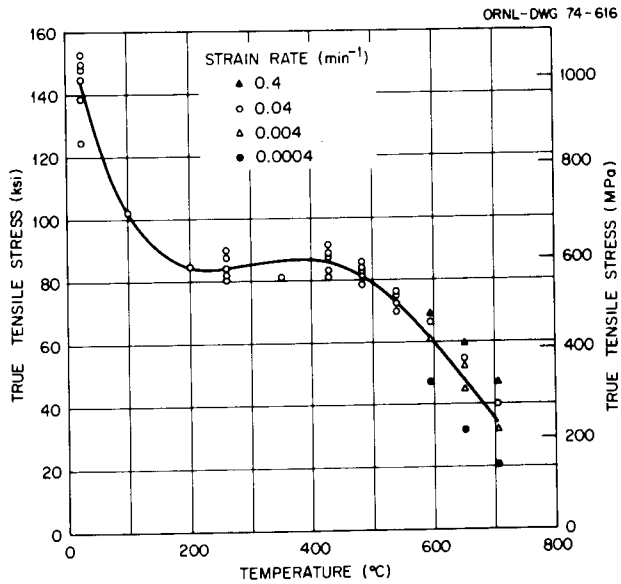

Fig. 5.5. Variation of True Tensile Stress With Temperature for Type 304 Stainless Steel (Heat 9T2796) Reannealed 0.5 hr at 1093°C (2000°F).

5.2.1.3 Measurement of Elastic Constants of Type 304 Stainless Steel — H. E. McCoy, M. W. Moyer,* and T. W. Dews*

The sonic velocities and moduli of type 304 stainless steel (Heat 346544) at temperatures ranging from 24°C (75°F) to at least 650°C (1200°F) were determined. Measurements were made by two methods: (1) a double-pulse contact pulse-echo technique, which gives better resolution at room temperature with bulk samples, and (2) a magnetorestrictive method for generating ultrasound in thin wires. The bulk samples were plates 1 in. square × 1/4 and 1/2 in. thick (25.4 × 6.4 and 12.7 mm), and the wire specimen was 1/16 in. in diameter × about 6 ft (1.6 mm × 1.8 m).

The double-pulse technique consists of an oscillator and gating circuitry that allows two successive oscillations to trigger the transducer.

---

*Laboratory Development, Y-12.

The frequency of the oscillator was adjusted to obtain superposition of the of the multiple reflections in the samples caused by the two excitation pulses. A counter enabled the oscillator period and, thus, the transit time between two successive multiple reflections in the sample to be measured. From these data, the velocity was calculated by $V = 2d/t$, where d represents thickness and t represents two-way transit time.

When the longitudinal and shear velocities are measured, the moduli and Poisson's ratio can be calculated from the following relationships:[1]

$$\sigma = \frac{1 - 2(V_S/V_L)^2}{2 - 2(V_S/V_L)^2} , \tag{1}$$

$$Y = V_L{}^2\rho \frac{(1 + \sigma)(1 - 2\sigma)}{(1 - \sigma)} , \tag{2}$$

$$S = V_S{}^2\rho , \tag{3}$$

$$K = \frac{Y}{3(1 - 2\sigma)} , \tag{4}$$

$$V_E = V_L \frac{(1 + \sigma)(1 - 2\sigma)}{(1 - \sigma)} , \tag{5}$$

where:

σ = Poisson's ratio,
ρ = density,
Y = Young's modulus,
S = shear modulus,
K = bulk modulus,
V_E = extensional velocity,
V_L = longitudinal velocity, and
V_S = shear velocity.

Table 5.6 summarizes the velocities and moduli obtained on bulk samples of type 304 stainless steel at 24°C (75°F).

Table 5.6. Ultrasonic Measurements on Type 304 Stainless Steel at 24°C (75°F)

Property	Value
Velocity, m/sec	
V_L	5766
V_S	3145
V_E	4419
Poisson's ratio (σ)	0.2883
Moduli, GPa	
Young's (Y)	201.5
Shear (S)	78.2
Bulk (K)	158.7
Moduli, psi	
Young's	29.23×10^6
Shear	11.35×10^6
Bulk	23.01×10^6
Density, kg/m^3	7909

The magnetostrictive method of generating ultrasound in thin wires enabled a wire to be inserted into a furnace without causing damage to the transducer by the heat. In a thin wire in which the diameter is less than one-tenth the wavelength of sound, extensional and torsional waves can be generated. Extensional waves are longitudinal waves with a radial component and have a lower velocity than longitudinal waves in bulk material. The stiffness term is Young's modulus, Y. Torsional waves are shear waves with a circumferential particle motion. The stiffness term is the shear modulus S. The relation between the velocities and moduli is given by $Y = V_E{}^2\rho$ for extensional waves, where V_E = extensional velocity, and by $S = V_T{}^2\rho$ for torsional waves, where V_T = torsional (shear) velocity.

Measurements made at temperatures higher than 24°C were normalized to data taken at 24°C. The coefficient of thermal expansion was used to

correct the length and density before we calculated the normalized velocities and moduli:

$$d' = d(1 + \alpha\Delta T) \text{ and}$$

$$\rho' = \rho/(1 + 3\alpha\Delta T) \ ,$$

where:

d' = corrected length,

ρ' = corrected density,

α = coefficient of thermal expansion, and

ΔT = change in temperature.

This correction accounted for a 1.4% change in velocity and a 1.3% change in modulus for type 304 stainless steel at 760°C (1400°F).

To determine the sonic moduli of type 304 stainless steel as a function of temperature, the transit time in a short section of wire inserted in a furnace was measured. A weld bead was placed on the wire 10 cm (4 in.) from the end to provide a reflecting interface to define the length of the sample being heated. The weld bead provided an impedance mismatch, which gave the boundary conditions needed to reflect both extensional and torsional waves. The temperature was determined with a thermocouple attached to the midpoint of the sample. The test section of the wire sample was placed in a furnace in air and heated at 10°C/min (18°F/min) to 760°C (1400°F). The reflected signal from the heated sensor was displayed on an oscilloscope. Transit times between the weld bead and end of the wire were measured with a time-interval meter. Gates were set up on the appropriate reflections so trigger pulses could be obtained. A block diagram of the ultrasonic system is shown in Fig. 5.6.

The normalized velocities and moduli were calculated and the transit time obtained from the time-interval meter. Measurements were made during both the heating and cooling cycles for each material. Lower velocities and moduli were obtained on some tests during cooling below 200°C, because the sample was removed from the furnace, causing the wire surface to cool off faster than the interior of the sample.

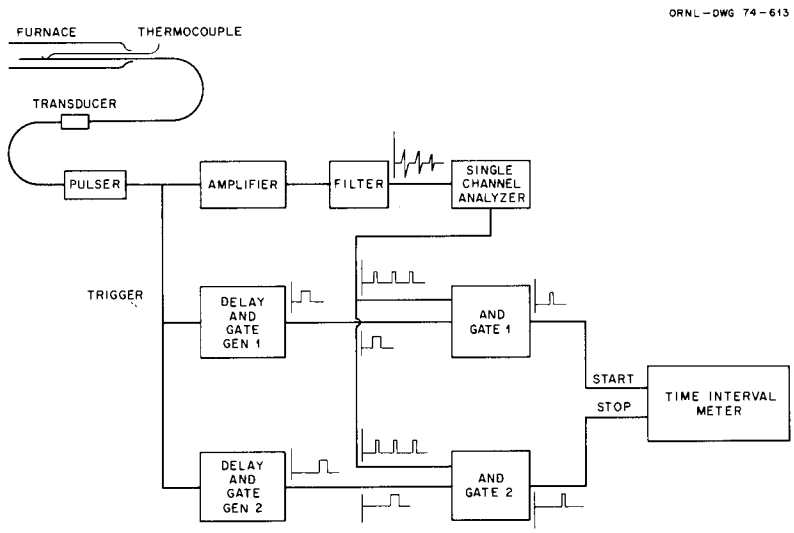

Fig. 5.6. Block Diagram of Ultrasonic Velocity Test System.

The results of a typical run are shown graphically in Fig. 5.7. Data were taken over two complete cycles of heating and cooling. The data appear anomalous about 700°C, and the results above this temperature were not used in analyzing the data. The results obtained below 200°C during cooling were likewise suspect because of the uneven temperature through the sample.

The data from all four runs (two cycles of heating and cooling) were fit separately by a quadratic equation by regression analysis, and these were combined into a single set. The combined results for the four sets are shown in Fig. 5.8. The results from this study are represented by the following equation:

$$Y = (29.64 \pm 0.09) \times 10^6 - (1.474 \pm 0.052) \times 10^4\, T$$

$$+ (2.615 \pm 0.662) T^2 \ ,$$

where Y is Young's Modulus in psi, and T is temperature in °C. The calculated values generally agreed with the experimental values within ±0.3%, and the maximum difference noted was 1.4%.

The dynamic modulus results from this study are compared in Fig. 5.8 with the static modulus values currently in the LMFBR Handbook and the

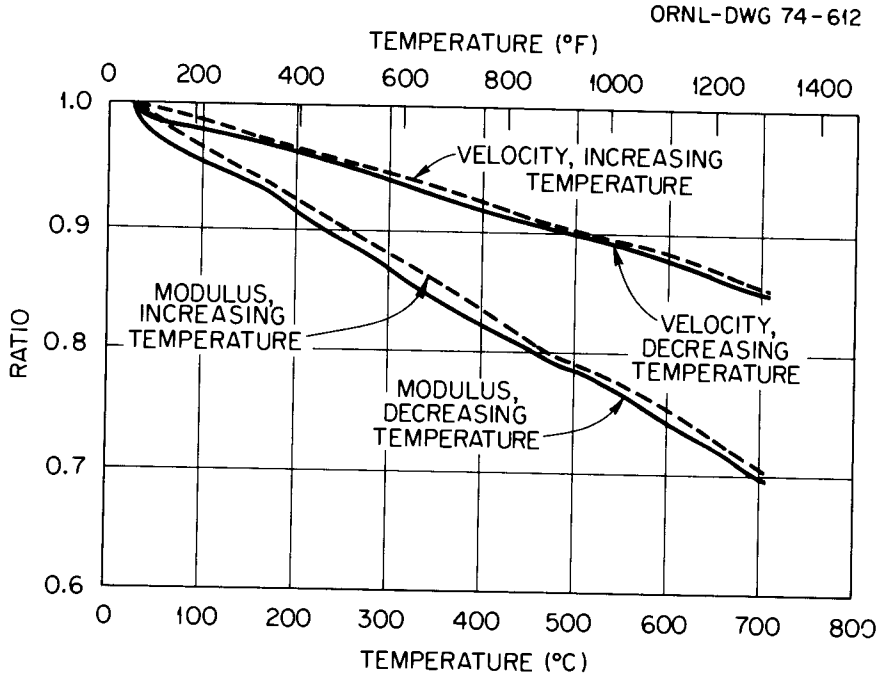

Fig. 5.7. Normalized Velocity and Young's Modulus of Type 304 Stainless Steel Thin Rod, Run 1.

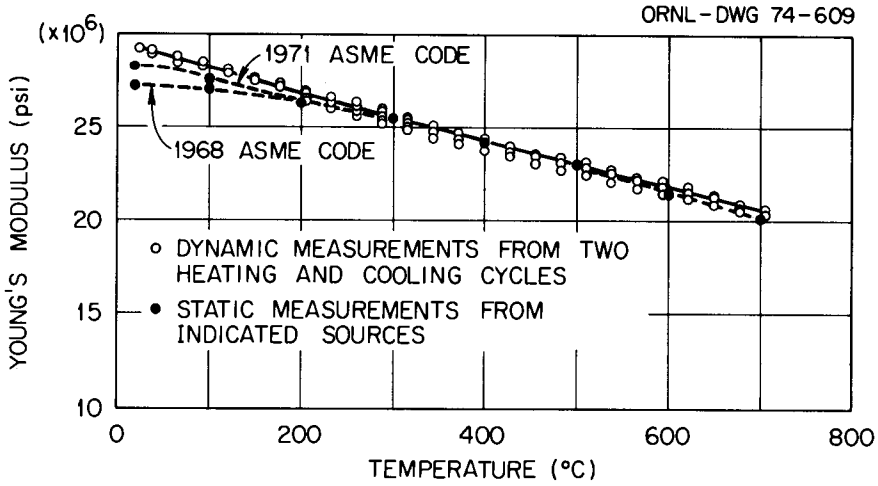

Fig. 5.8. Young's Modulus as a Function of Temperature for Type 304 Stainless Steel.

ASME Pressure Vessel Codes. There is some disagreement (<7%) between the various techniques at room temperature, but excellent agreement was obtained over the range 300 to 700°C (570 to 1290°F).

The experimental data for the shear modulus were also analyzed for each run, and then all data were combined for regression analysis. The computed values are shown in Fig. 3.9, and the data are described by the equation

$$S = (11.41 \pm 0.042) \times 10^6 - (4.76 \pm 0.240) \times 10^3\, T$$

$$- (0.993 \pm 0.306) T^2 \ ,$$

where S = shear modulus in psi, and T = temperature in °C. The data generally agree with the computed values to within ±0.9%, and the maximum deviation is ±2.5%. The results from this study are compared in Fig. 5.9 with the static modulus values currently appearing in the LMFBR Handbook. The Handbook values are about 5% lower at 24°C than those obtained in this study, but the results agree at temperatures between 200 and 700°C.

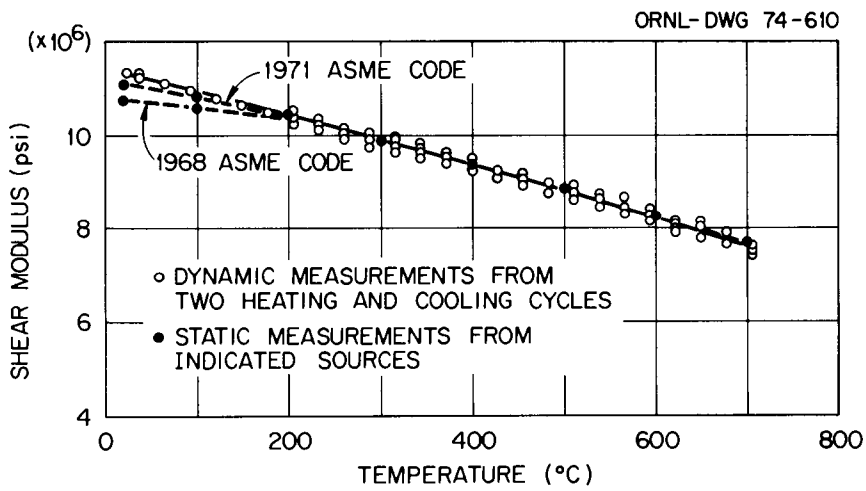

Fig. 5.9. Shear Modulus as a Function of Temperature for Type 304 Stainless Steel.

Poisson's ratio, σ, was calculated for temperatures where values had been determined for Young's and shear moduli from the relationship $\sigma = Y/2S - 1$. Data were available to calculate 90 values of Poisson's ratio as a function of temperature. These data were fit by regression analysis to the following cubic equation:

$$\sigma = 0.293 \pm 0.013 - (0.211 \pm 1.38) \times 10^{-4}\, T - (0.122 \pm 0.424) \times 10^{-6}\, T^2 + (0.411 \pm 0.377) \times 10^{-9}\, T^3 \ .$$

The standard errors for the coefficients are quite large except for the first term. The errors are so large for the coefficients for the linear and squared terms that they have little meaning. As shown in Fig. 5.10, the individual data points deviate from the best fit line by ±20%. The results from this study agree reasonably well with those in the LMFBR Materials Handbook.

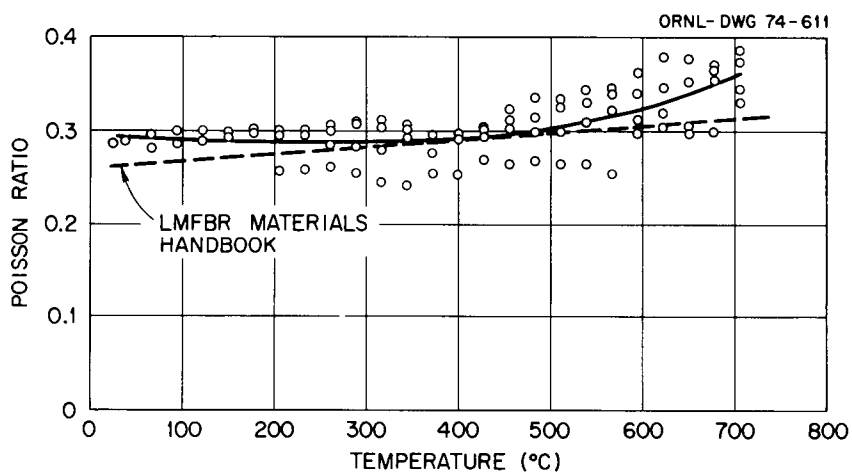

Fig. 5.10. Poisson's Ratio as a Function of Temperature for Type 304 Stainless Steel.

5.2.2. Heat-to-Heat Variation Study of Type 304 Stainless Steel

The test plan being followed in this program is outlined in Fig. 5.11. We are studying 20 heats of type 304 stainless steel, and some of their

ORNL-DWG 74-1601

Select 20 Heats

(A)
As-Received
Tensile Tests
(Strain Rate 0.04/min)
(RT–800 1100–1200°F)

(B)
Annealed (1 hr at 1950°F)
Tensile Tests
(Strain Rate 0.04/min)
(RT–800–1100–1200°F)

20 Heats

9 Selected Heats

(D)
Creep and Rupture Study (1100°F)
(10- to 500-hr tests)

As-Received	Annealed
35,000 psi	35,000 psi
30,000 psi	30,000 psi

(C)
Aging Program

X-22807
600414
300380
9T2796K
R22926
346845
8043813
346544
3121

Time (hr)	Temperature (°F)
1,000	900
2,000	1100
4,000	1200
10,000	

(1) Microstructure
(2) Tensile Properties, RT, 1100°F
(3) Creep Behavior at
1100°F – 30 ksi (100 to 2000 hr)
1100°F – 17 ksi (Disc. 2000 hr)
1200°F – 14 ksi (Disc. 2000 hr)
900°F – 20 ksi (Disc. 2000 hr)

(E)
Tests on selected heats to determine stress and temperature dependence

9 heats	8 heats	2 heats	13 heats
1000°F	1100°F	1100°F	1200°F
46 ksi	17 ksi	25 ksi	25 ksi
100–1000 hr	30,000 hr	20,000 hr	10–1000 hr

Select 4 heats for detailed study in the reannealed condition* X-22807 (weakest), 346544 (medium), 346845 (strongest), 9T2796K (reference heat)

(F)
Tensile Tests in Addition to Above**

Temperature (°F)	Strain Rate (min^{-1})
1000	0.004
1100	0.004
1200	0.004
1100	0.0004

(G)
Creep Tests in Addition to Above**

Temperature (°F)	Stress (ksi)	Loading Strain Rate (min^{-1})	Duration (hr)
1000	14	0.005	50,000
1100	10	0.0005	1,000
1100	10	0.005	50,000
1100	10	0.25	1,000
1100	14	0.005	35,000
1100	16	0.0005	1,000
1100	16	0.005	10,000
1100	16	0.25	1,000
1200	14	0.005	10,000

*Reannealed 0.5 hr at 1093°C for heat 9T2796K, 0.5 hr at 1065°C for all other heats.
**These tests are currently in progress or completed for reference heat 9T2796K.

Fig. 5.11. Heat-to-Heat Variation Program, Type 304 Stainless Steel.

important characteristics are given in Table 5.7. These heats have come from many souces and are believed to represent a fair sample of products.

Parts A and B involve tensile tests at a strain rate of 0.04/min at 25, 427, 593, and 650°C (77, 800, 1100, and 1200°F) on all 20 heats in the as-received and annealed conditions. These tests have been completed, and the results are being analyzed in an effort to correlate properties with grain size and chemical composition.

The aging program described in Part C is in progress and the results will be discussed in more detail. Samples of all nine heats have been aged at least 2000 hr at all three temperatures. Some material has been aged about 8000 hr. Some tensile tests have been run, and some creep tests are in progress.

All the short-term creep tests in Part D have been completed or are in progress. The results are being analyzed in an effort to relate properties with composition and microstructure.

All the tests in Part E have been completed or are in progress. The purpose of these tests is to give results at test temperatures other than 593°C (1100°F), so that some parametric correlations can be made involving temperature, stress, and time. The tests at 593°C and 17,000 and 25,000 psi (117 and 172 MPa) have run about 2 years (17,000 hr), and the results will be discussed in more detail.

Parts F and G involve large amounts of test time, and the number of heats must be reduced. Several factors were considered in reducing the number of heats. We wanted to include heats that represented the extreme and mean strength properties, but also had to consider the quantity of material available for further testing. Heat X22807 had the lowest creep strength at 593°C, low carbon and nitrogen contents, and a 1620-lb (735-kg) inventory. Heat 346544 had about average creep strength at 593°C, intermediate carbon and nitrogen levels, and a 10,242-lb (4646-kg) inventory. Heat 346845 had near maximum creep strength and a 7320-lb (3320-kg) inventory. Some heats were slightly stronger, but we had insufficient material for further testing. The reference heat, 9T2796, was also chosen for further study. The 2-in.-thick (51 mm) plate was chosen, and this material is already being studied extensively. For

Table 5.7. Type 304 Stainless Steel Heats Being Investigated In the Heat-to-Heat Variation Program

Heat	Sample	Content, wt %																					Product[a] Size		Grain Size
		C	N	P	B	O	H	Ni	Mn	Cr	Si	Mo	S	Ti	Cu	Co	Pb	Sn	Ta	Ta + Nb	Nb	V	(in.)	(mm)	
544086	086-14	0.050	0.045	0.025		0.0091	0.0005	9.46	1.23	18.4	0.53	0.2	0.016	0.01	0.10	0.05	0.01	0.02		0.08			1	25	2-3
337187	187-7	0.058	0.034	0.021		0.0034	0.0006	9.27	0.97	18.1	0.42	0.03	0.010	0.01	0.07	0.05	0.01	0.02		0.08			1 1/2	38	1-2
337330	330-8	0.068	0.031	0.018		0.0042	0.0005	9.43	0.83	18.2	0.59	0.07	0.008	0.03	0.15	0.05	0.01	0.02		0.08			1 1/8	29	5-6
300380	380-24	0.063	0.068	0.018		0.0260	0.0009	8.30	0.97	18.4	0.55	0.07	0.010	0.03	0.10	0.05	0.01	0.02		0.08			2 3/8	60	2-4
600414	414-23	0.073	0.058	0.016		0.0190	0.0004	9.52	0.94	18.7	0.69	0.1	0.015	0.03	0.10	0.05	0.01	0.02		0.08			2 3/8	60	2-3
55697	697-7	0.057	0.034	0.016		0.0150	0.0005	9.38	0.91	18.5	0.50	0.05	0.037	0.01	0.10	0.05	0.01	0.02		0.08			5/8 bar	16	1-2
9T2796R	796	0.047	0.031	0.029		0.0110	0.0006	9.58	1.22	18.5	0.47	0.1	0.012	0.01	0.10	0.05	0.01	0.02		0.08			5/8 bar	16	1-3
R22926	926-6	0.053	0.041	0.020		0.0084	0.0007	9.79	1.16	19.0	0.68	0.1	0.025	0.01	0.07	0.05	0.01	0.02		0.08			2	51	3-4
X23283	283-1	0.043	0.025	0.018	0.0003	0.0140	0.0009	9.12	1.32	18.2	0.45	0.3	0.020	0.027	0.14	0.05	0.01	0.01		0.02			3/4	19	2-3
346845	845-1	0.057	0.024	0.023	0.0002	0.0092	0.0013	9.28	0.92	18.4	0.53	0.1	0.006	0.033	0.11	0.07	0.01	0.01		0.03			2 3/4	70	2-3
346544	544-7	0.063	0.019	0.023	0.0002	0.0081	0.0006	9.12	0.99	18.4	0.47	0.2	0.006	0.036	0.12	0.05	0.01	0.01		0.02			2	51	2-4
60551	551-1	0.043	0.027	0.022	0.0010	0.0220	0.0013	9.40	1.20	18.5	0.59	0.3	0.018	0.037	0.25	0.08	0.01	0.01		0.02			5 × 7 bar	13 × 18	3-4
345866	866-8	0.044	0.022	0.023	0.0002	0.0096	0.0010	8.98	1.51	18.5	0.47	0.2	0.007	0.031	0.13	0.04	0.01	0.01		0.02			3	76	3-4
X22807	807-1	0.029	0.021	0.024	0.0005	0.0100	0.0012	9.67	1.26	18.8	0.50	0.2	0.023	0.025	0.11	0.03	0.01	0.01		0.02			2 1/2	64	2-3
346779	779-1	0.065	0.023	0.024	0.0002	0.0056	0.0009	9.46	0.94	18.1	0.47	0.2	0.005	0.035	0.16	0.02	0.01	0.01		0.02			2 1/2	64	3-4
8043813	813	0.062	0.033	0.040	0.0003			8.95	1.87	17.8	0.48	0.32	0.004										1	25	3-4
9T2797	797	0.059	0.055	0.028	0.0020	0.0075	0.0007	9.78	1.49	18.3	0.60	0.3	0.011	0.010	0.3	0.07	0.0020	0.0050	0.0030		0.0050	0.1	1	25	
616737	070	0.064	0.075	0.026	0.00005	0.0072	<0.0001	9.01	1.71	18.3	0.50	0.3	0.012	0.0020	0.3	0.07	<0.0003	0.0050	0.0010		0.0050	0.1	2 5/8	67	
310390	111	0.066	0.086	0.018	0.0020	0.0052	<0.0001	8.75	1.57	18.6	0.60	0.3	0.006	0.0070	0.2	0.07	0.0007	0.0020	0.03		0.0020	0.07	2	51	
3121	121	0.065	0.14	0.019	0.00005	0.0026	0.0011	9.19	1.92	18.1	0.30	0.14	0.010	0.001	0.07	0.07	<0.0003	0.002	<0.001		<0.002		b	b	

[a]Product form is plate unless specified otherwise.

[b]28-in.-OD × 3/8-in.-wall (710 × 9.5 mm) pipe.

comparison, the rupture lives at 593°C (1100°F) and 30,000 psi (207 MPa) in the reannealed conditions were 45, 96, 170, 356, 1275, and 2000 hr, respectively, for the 1331-8 minimum, Heat X22807, Heat 9T2796, Heat 346544, Heat 346845, and the strongest heat studied.

The tensile tests in Part F have been completed. The long-term creep tests in Part G are already in progress for Heat 9T2796. Several of the tests at 10,000 psi (69 MPa) will be initiated in about two months when additional machines become available.

5.2.2.1 Tensile and Short-Term Creep Tests — H. E. McCoy

The results of tensile tests on 16 heats were reported previously,[4] and the results for the remaining four heats are given in Table 5.8. These results have been added to the composite plots in Figs. 5.12 and 5.13. In the as-received condition the yield stresses are above the minimum values from Code Case 1331-8 except for Heat 797, which is weaker at 427, 593, and 649°C (800, 1100, and 1200°F). After reannealing 0.5 hr at 1065°C (1950°F) the yield stress of Heat 797 at 25°C (77°F) is above the minimum value, yield stresses of the other three heats at 25°C are below the minimum value, and the yield stresses of all four heats at 427, 593, and 649°C are below the minimum values.

Heat 121 is quite unique in that it has a very large grain size and an exceptionally high nitrogen content of 0.14%. This material was fabricated in 28-in.-OD × 3/8-in.-wall pipes. The yield strength of this material was about the same as that of Heats 737 and 390, but the ultimate tensile stress was consistently lower.

Some short-term stress-rupture tests have also been completed on the four additional heats, and these results are summarized in Table 5.9. Heat 737 seems unusually strong in the as-received condition, and this test will be repeated. The range of rupture lives observed for the other 16 heats in the reannealed condition at 593°C and 35,000 psi was 18 to 721 hr. Although the four new heats have very different rupture lives, they are not outside the range observed previously.

The test matrix in Part F of Fig. 5.11 is intended to determine the effects of strain rate on the tensile properties of the heats chosen for

Table 5.8. Summary of Tensile Properties on Several Heats of Type 304 Stainless Steel

Heat[a]	Condition[b]	Yield or Tensile Stress, ksi(MPa), at Each Temperature			
		25°C 77°F	427°C 800°F	593°C 1100°F	649°C 1200°F
		Yield Stress			
797	A 240	31.3(216)	16.7(115)	14.0(97)	12.9(89)
	1065°C	27.0(186)	13.2(91)	11.7(81)	10.3(71)
737	A 240	33.8(233)	20.8(143)	16.0(110)	15.8(109)
	1065°C	30.5(210)	15.3(105)	12.3(85)	13.1(90)
390	A 240	37.3(257)	20.0(138)	16.4(113)	16.9(117)
	1065°C	32.4(223)	15.4(106)	12.6(87)	12.4(85)
121	A 312	36.7(253)	20.3(140)	16.5(114)	16.3(112)
	1065°C	31.2(215)	15.3(105)	12.4(85)	12.2(84)
		Tensile Stress			
797	A 240	82.2(567)	61.5(424)	50.0(345)	43.1(297)
	1065°C	80.9(558)	61.1(421)	50.3(347)	43.1(297)
737	A 240	84.7(584)	64.9(447)	52.8(364)	46.6(321)
	1065°C	83.5(576)	63.6(439)	52.6(363)	46.8(323)
390	A 240	88.2(608)	64.5(445)	53.8(371)	46.4(320)
	1065°C	87.2(601)	64.0(441)	52.5(362)	46.5(321)
121	A 312	74.3(512)	55.7(384)	46.2(319)	40.3(278)
	1065°C	72.3(498)	55.1(380)	45.4(313)	39.3(271)

[a]Last three digits of number in Table 5.7.

[b]As received per indicated specification or reannealed 0.5 hr at 1065°C (1950°F).

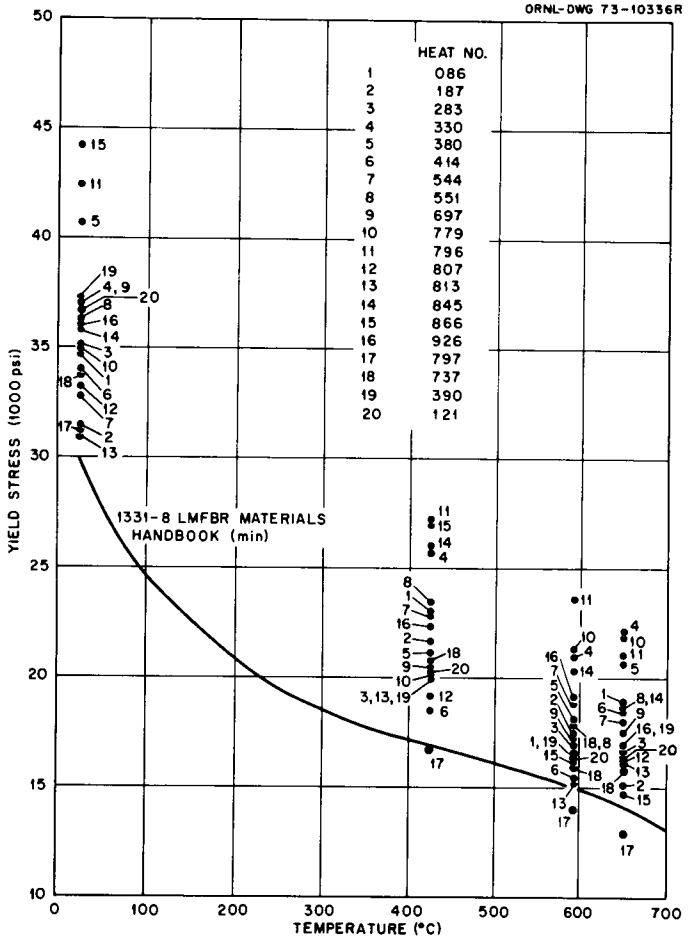

Fig. 5.12. Comparison of the Observed Yield Stress of As-Received Type 304 Stainless Steel with the 1331-8 Minimum.

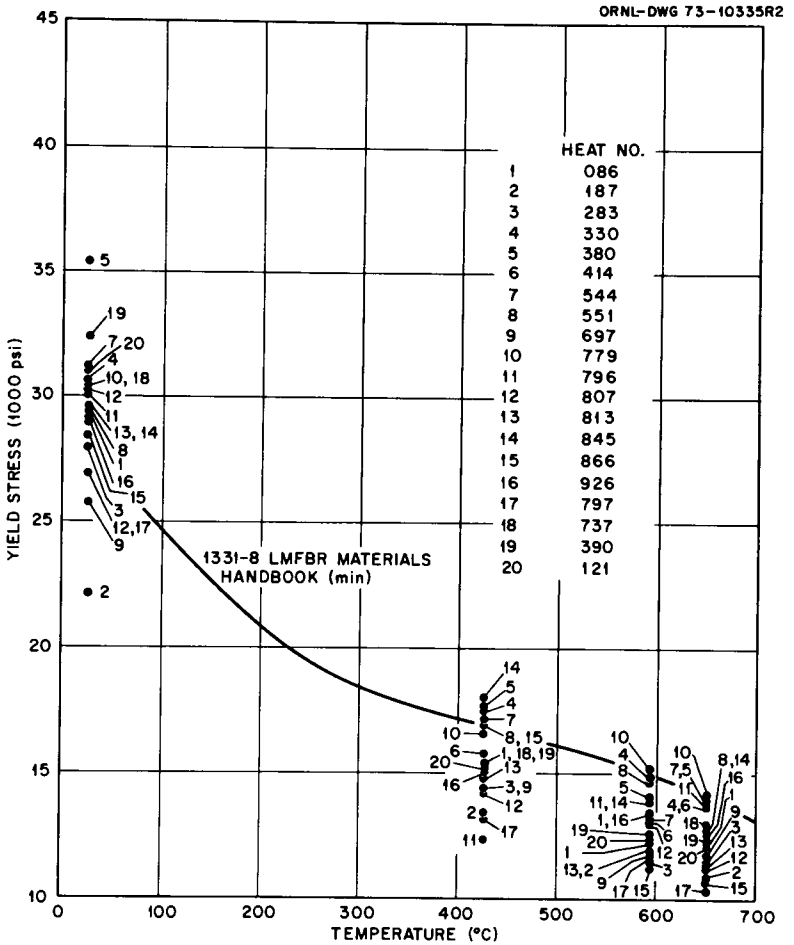

Fig. 5.13. Comparison of the Observed Yield Stress of Reannealed (0.5 hr at 1065°C, 1950°F) Type 304 Stainless Steel with the 1331-8 Minimum.

Table 5.9. Stress-Rupture Results at 593°C (1100°F) for Various Heats of Type 304 Stainless Steel

Heat	Stress		Rupture Life, hr		Minimum Creep Rate, %/hr	
	(ksi)	(MPa)	As Received[a]	Reannealed[b]	As Received[a]	Reannealed[b]
797	30	207	352.6	138.9	0.017	0.039
797	35	241	39.8	27.9	0.24	0.22
737	35	241	1174.5	864.6	0.0047	0.0065
390	35	241	287.0	295.7	0.013	0.013
121	35	241	165.9	149.9	0.047	0.048

[a]Specification A 240 or A 312.

[b]0.5 hr at 1065°C (1950°F).

further study. These tests have been run, and the results are summarized in Table 5.10 for Heats X22807, 346544, and 346845.

The general influences of decreasing the strain rate at a given temperature are no change in the yield stress, a decrease in the ultimate tensile stress, and a decrease in all ductility measures. Although Heat X22807 is weaker than the other two, the percent changes in tensile strength with temperature are almost equivalent. However, the effects on ductility are quite different for the three heats. The total strain at 593°C changes very little over the range of strain rates studied for Heat X22807. The fracture strain of Heat 346845 varies from 50.5 to 45.2% and that for Heat 346544 varies from 47.8 to 27.8%. The reduction of area was reduced from 74.9 to 43.1% for Heat X22807, underwent a similar change from 73.6 to 40.2% for Heat 346845, and changed from 65.9 to 28.5% for Heat 346544.

5.2.2.2 Long-Term Creep Tests in Heat-to-Heat Variation Study — H. E. McCoy

Ten long-term creep tests are in progress on several heats of type 304 stainless steel at 593°C (1100°F). The test conditions and status of each test are described in Table 5.11. The heats of material are described

Table 5.10. Tensile Properties of Three Heats of Type 304 Stainless Steel at Several Test Conditions[a]

Temperature (°C)	Temperature (°F)	Strain Rate (min^{-1})	Stress, ksi (MPa) Yield	Stress, ksi (MPa) Ultimate	Strain, % Uniform	Strain, % Total	Reduction of Area (%)
			Heat X22807				
538	1000	0.004	13.3(92)	52.0(359)	39.2	49.2	60.1
593	1100	0.04	13.0(90)	47.9(330)	36.0	45.7	74.9
593	1100	0.004	12.9(89)	42.2(291)	35.2	48.4	50.8
593	1100	0.0004	12.5(86)	36.0(248)	33.6	45.4	43.1
649	1200	0.04	11.3(78)	39.3(271)	30.9	53.0	53.5
649	1200	0.004	11.7(81)	33.1(228)	27.2	52.5	45.4
			Heat 346544				
538	1000	0.004	15.1(104)	59.5(410)	44.1	51.2	63.5
593	1100	0.04	13.3(92)	52.0(359)	40.0	47.8	65.9
593	1100	0.004	14.2(98)	48.6(335)	34.4	43.9	47.8
593	1100	0.0004	13.6(94)	41.7(288)	23.2	27.8	28.5
649	1200	0.04	14.0(97)	42.6(294)	33.6	52.4	55.1
649	1200	0.004	14.5(100)	37.1(256)	28.8	36.4	37.2
			Heat 346845				
538	1000	0.004	14.0(97)	57.4(396)	44.0	51.4	69.3
593	1100	0.04	13.8(95)	52.2(360)	36.8	50.5	73.6
593	1100	0.004	13.6(94)	48.6(335)	36.8	51.7	62.5
593	1100	0.0004	13.4(92)	42.6(294)	33.8	45.2	40.2
649	1200	0.04	12.7(88)	41.1(283)	34.4	47.0	68.0
649	1200	0.004	13.1(90)	37.8(261)	28.8	57.0	52.3

[a]All material reannealed 0.5 hr at 1065°C (1950°F).

Table 5.11. Status of Several Long-Term Creep Tests of Type 304 Stainless Steel at 593°C (1100°F)

Test	Heat	Condition[a]	Stress, (ksi)	Stress, (MPa)	Test Time (hr)	Strain, % Loading	Strain, % Creep	Minimum Creep Rate (%/hr)
10396	60551	A 479	25.0	172	9474	1.81	3.09	1.9×10^{-4}
10395	346845	A 240	25.0	172	9626	1.37	3.47	1.6×10^{-4}
9499	300380	Reannealed	17.0	117	15905	0.72	1.17	
9483	600414	Reannealed	17.0	117	15962	1.49	0.89	
9464	337330	A 240	17.0	117	16269	−0.20	0.91	3.8×10^{-6}
9446	9T2796	A 479	17.0	117	16268	0.13	0.93	2.1×10^{-5}
9443	337187	A 240	17.0	117	16290	0.47	2.76	9.6×10^{-5}
9371	55697	A 479	17.0	117	16436	0.62	2.45	1.4×10^{-4}
9221	600414	A 240	17.0	117	18065	0.18	0.67	
9508	346544	A 240	17.0	117	15788	0.22	1.77	3.5×10^{-5}

[a]As received per indicated specification or reannealed 0.5 hr at 1065°C (1950°F).

in Table 5.7. Two specimens of different heats are being stressed at 25,000 psi (172 MPa) at 593°C (1100°F). The total strains and the minimum creep rates of these two tests agree rather well. The individual creep curves of the eight tests at 17,000 psi (117 MPa) differ widely, with the minimum creep rates varying by two orders of magnitude. The creep strains in 14,000 hr vary from 0.6% for Heat 414 to 2.4% for Heat 187. The almost linear creep curve for Heat 697 is unusual and a deviation from the behavior of the other heats. The HEDL one- and two-exponential equations were compared with the experimental curves; neither adequately describes the wide range of creep behavior.

The curves were fit with an eight-term polynomial equation. The equation and the constants are given in Table 5.12. These curves had been fit about 5000 hr previously[5] with the same equation. The constants remained about the same for some heats and changed drastically for others. The constants changed very little for tests 10395, 9499, 9443, 9371, and 9221. The estimates of the standard error varied from 100 to 460 μin./in. The range observed previously was 90 to 478 μin./in., so the error band has changed very little. The extensometer on test 9508 is the averaging type. All other tests have nonaveraging extensometers because these tests were started before enough of our new averaging extensometers were available.

5.2.2.3 Effects of Aging on The Tensile Properties — H. E. McCoy

The mechanical properties of type 304 stainless steel are known to be influenced by aging. The aim of the present program is to determine how the property changes vary from heat to heat. The scope of the program was described in Fig. 5.11, and the compositions of the particular heats were given in Table 5.7. The status of the program is illustrated in Fig. 5.14. A block of material large enough to make six test samples is being aged at each condition.

Several of the aged samples have been tested. The results for Heat 3121 are given in Table 5.13. This heat was aged only in the as-received (A-312) condition. Aging for 2000 hr at 482°C (900°F) had

Table 5.12. Values of Constants in Polynomial Creep Equation for Heat-to-Heat Variation Tests[a]

Test	Value of Constants								Estimate of Standard Error (μin./in.)
	A_0	A_1	A_2	A_3	A_4	A_5	A_6	A_7	
	$\times 10^{-4}$	$\times 10^{-1}$	$\times 10^{-1}$	$\times 10^{-1}$	$\times 10^{-1}$	$\times 10^{-1}$	$\times 10^{-2}$	$\times 10^{-3}$	
10396	−0.220	0.146	−0.376	0.341	−0.128	−0.0165	0.0254	−0.0437	171
10395	−0.648	1.36	−4.29	5.44	−3.74	1.42	−2.14	1.37	267
9499	0.150	0.0373	0.0235	−0.0758	0.0636	−0.0254	0.0390	−0.0255	305
9483	0.0342	0.0353	−0.133	0.164	−0.0980	0.0317	−0.0371	0.0172	159
9464	1.19	−0.396	1.07	−1.11	0.617	−0.193	0.228	−0.115	305
9446	0.998	−0.512	1.37	−1.44	0.828	0.268	0.333	−0.176	460
9443	−0.208	0.429	−1.33	1.65	−1.10	0.407	−0.591	0.367	223
9371	−0.328	0.387	−1.18	1.42	−0.920	0.334	−0.474	0.289	383
9221	−0.528	0.108	−0.262	0.241	−0.109	0.0246	−0.0116	−0.00631	275
9508	−0.176	0.286	−0.890	1.12	−0.766	0.289	−0.427	0.269	100

[a]Equation of the form: $\varepsilon = A_0 + A_1 t^{0.14} + A_2 t^{0.28} + A_3 t^{0.43} + A_4 t^{0.58} + A_5 t^{0.71} + A_6 t^{0.86} + A_7 t^{1.01}$, where ε = strain, and t = time in hours.

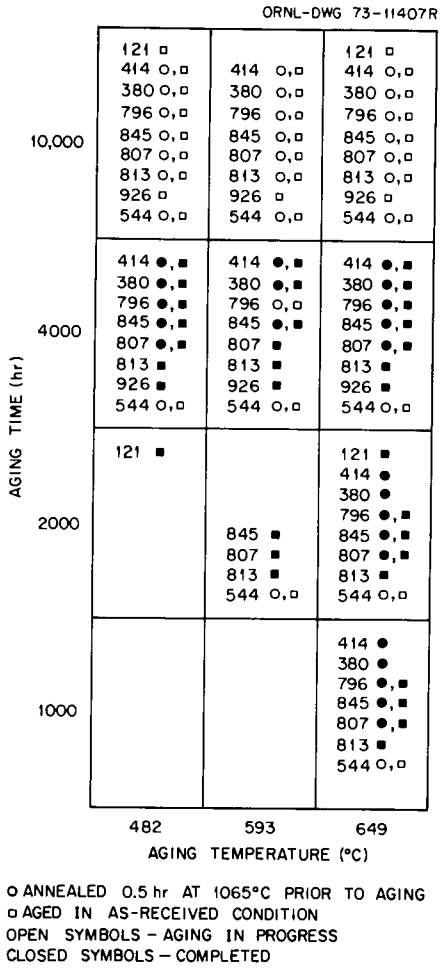

Fig. 5.14. Aging Program for Type 304 Stainless Steel.

no detectable effect on the tensile properties at 25 and 593°C (77 and 1100°F). Aging 2000 hr at 649°C (1200°F) increased the strength slightly and decreased the ductility slightly.

The results of tensile tests on Heat R22926 are shown in Table 5.14. Aging had very little effect on the strength of this material. However, aging for 4000 hr at 593 and 649°C (1100 and 1200°F) did cause slight reductions in the ductility.

The tensile test results in Table 5.15 for Heat X22807 indicate slight decrease in strength and ductility due to aging the as-received material, and no systematic change in strength and a decrease in ductility due to aging the reannealed material. This heat has relatively low carbon and nitrogen contents of 0.029 and 0.021%, respectively, so

Table 5.13. Tensile Properties of Type 304 Stainless Steel Heat 3121 at a Strain Rate of 0.044/min

Condition	Treatment			Stress, ksi(MPa)		Strain, %		Reduction of Area (%)
	Time (hr)	Temperature (°C)	Temperature (°F)	Yield	Ultimate Tensile	Uniform	Total	
				Tested at 25°C (77°F)				
Reannealed	0.5	1065	1900	31.2(215)	72.3(498)	48.9	60.3	88.1
A 312				36.7(253)	74.3(512)	44.4	58.4	85.9
A 312, aged	2000	482	900	35.9(248)	74.1(511)	46.2	58.7	84.5
A 312, aged	2000	649	1200	37.4(258)	81.7(563)	37.8	44.5	59.6
				Tested at 593°C (1100°F)				
Reannealed	0.5	1065	1900	12.4(85)	45.4(313)	34.2	37.6	87.2
A 312				16.5(114)	46.2(319)	31.1	37.2	82.6
A 312, aged	2000	482	900	16.4(113)	46.5(321)	31.1	38.3	81.3
A 312, aged	2000	649	1200	18.7(129)	46.0(317)	24.0	29.4	70.9

Table 5.14. Tensile Properties of Type 304 Stainless Steel Heat R22926 at a Strain Rate of 0.040/min

Condition	Treatment			Stress, ksi(MPa)		Strain, %		Reduction of Area (%)
	Time (hr)	Temperature (°C)	Temperature (°F)	Yield	Ultimate Tensile	Uniform	Total	
				Tested at 25°C (77°F)				
Reannealed	0.5	1065	1950	29.0(200)	87.4(603)	72.8	84.2	82.0
A 240				36.1(249)	88.9(613)	68.4	82.7	
A 240, aged	4000	482	900	38.8(268)	85.7(591)	72.0	85.0	81.3
A 240, aged	4000	593	1100	36.8(254)	87.3(602)	68.0	76.7	72.1
A 240, aged	4000	649	1200	36.9(254)	88.2(608)	63.2	72.0	62.0
				Tested at 593°C (1100°F)				
Reannealed	0.5	1065	1950	13.4(92)	50.5(348)	42.3	49.0	59.0
A 240				19.1(132)	52.0(359)	39.0	45.1	71.0
A 240, aged	4000	482	900	17.1(118)	52.6(363)	40.0	52.6	71.1
A 240, aged	4000	593	1100	18.5(128)	50.9(351)	36.0	42.8	62.7
A 240, aged	4000	649	1200	20.3(140)	49.3(340)	28.8	40.6	62.9

Table 5.15. Tensile Properties of Type 304 Stainless Steel Heat X22807 at a Strain Rate of 0.040/min

Condition	Treatment			Stress, ksi(MPa)		Strain, %		Reduction of Area (%)
	Time (hr)	Temperature (°C)	Temperature (°F)	Yield	Ultimate Tensile	Uniform	Total	
Tested at 25°C (77°F)								
A 240				33.2(229)	83.4(575)	67.2	82.0	75.7
A 240, aged	2000	593	1100	32.1(221)	78.9(544)	66.4	74.1	68.9
A 240, aged	1000	649	1200	30.7(212)	79.5(548)	65.6	73.5	62.8
A 240, aged	2000	649	1200	29.3(202)	79.6(549)	64.0	72.2	63.8
Reannealed	0.5	1065	1900	27.0(186)	81.1(559)	72.8	83.0	78.3
Reannealed, aged	1000	649	1200	28.0(193)	79.2(546)	68.8	74.0	60.7
Reannealed, aged	2000	649	1200	27.9(192)	80.0(552)	64.0	70.4	56.5
Tested at 593°C (1100°F)								
A 240				17.9(123)	45.2(312)	33.6	45.3	68.0
A 240, aged	2000	593	1100	16.7(115)	42.7(294)	30.4	38.4	53.8
A 240, aged	1000	649	1200	16.8(116)	43.5(300)	32.8	39.6	57.3
A 240, aged	2000	649	1200	15.5(107)	43.3(249)	33.6	40.1	49.7
Reannealed	0.5	1065	1900	13.0(90)	47.9(330)	36.0	45.7	74.9
Reannealed, aged	1000	649	1200	13.4(92)	43.3(299)	32.0	41.3	51.7
Reannealed, aged	2000	649	1200	14.0(97)	44.0(303)	32.0	36.5	44.3

only a small aging response due to carbide and nitride precipitation would be anticipated.

The tensile results in Table 5.16 for Heat 346845 indicate that the as-received material underwent the following changes when aged 4000 hr at 482°C (900°F): the yield stress was decreased, the tensile stress was unchanged, and all ductility measures were increased. Aging at 593°C (1100°F) seemed to increase the strength and decrease the ductility. Aging for 1000 hr at 649°C (1200°F) increased the strength and decreased the ductility. However, further aging time at 649°C brought about very little further change in properties. Aging the reannealed material at 649°C increased the yield stress, had very little effect in the tensile stress, and decreased all ductility measures.

The most general effect of aging seems to be a reduction in the ductility. The only exception seems to be Heat 346845, which increased in ductility after aging at 482°C (900°F). However, the ductility is still very high, with fracture strains 40% at 593°C (1100°F) and 70% at 25°C (77°F) prevailing after aging. Generally, aging seems to increase the yield stress, but the fragmentary results to date challenge this general statement. Detailed metallographic studies will be performed to determine the structural changes that occurred in these materials.

5.2.3 Exploratory Studies on Type 304 Stainless Steel in Support of Structural Design Methods — R. W. Swindeman

5.2.3.1 Tensile Testing of Reference Heat 9T2796 1-in. (25-mm) Plate

We have completed better than 90% of our tensile test matrix. These data are being processed to provide the constants associated with the several tensile curve representations. These include the bilinear,[6] Holloman,[7] Ludwik,[8] Ludwigson,[9] Reed-Hill,[10] and Voce[11] equations. We are especially interested in the Voce equation, and to examine its potential we selected our data at 593°C (1100°F) and performed preliminary graphical fits to the equation. The estimated equation constants are presented in Table 5.17, and data calculated from the Voce equation

Table 5.16. Tensile Properties of Type 304 Stainless Steel Heat 346845 at a Strain Rate of 0.04/min

Condition	Treatment			Stress, ksi(MPa)		Strain, %		Reduction of Area (%)
	Time (hr)	Temperature (°C)	Temperature (°F)	Yield	Ultimate Tensile	Uniform	Total	
Tested at 25°C (77°F)								
A 240				35.9(248)	88.7(612)	69.7	79.0	76.0
A 240, aged	4000	482	900	32.7(225)	86.7(598)	78.4	86.8	83.0
				34.4(237)	89.0(614)	76.0	86.4	81.4
A 240, aged	2000	593	1100	34.6(239)	87.6(604)	72.0	78.0	62.2
A 240, aged	4000	593	1100	40.4(279)	93.3(643)	68.0	75.4	71.4
A 240, aged	1000	649	1200	36.2(250)	91.6(632)	66.4	74.0	68.5
A 240, aged	2000	649	1200	34.3(236)	91.3(629)	64.8	70.8	68.3
A 240, aged	4000	649	1200	34.9(241)	91.4(630)	62.4	69.8	68.4
Reannealed	0.5	1065	1900	29.7(205)	87.1(601)	76.7	89.0	84.5
Reannealed, aged	1000	649	1200	33.5(231)	90.0(621)	68.8	77.4	72.8
Reannealed, aged	2000	649	1200	31.0(214)	90.6(625)	67.2	72.1	68.3
Tested at 593°C (1100°F)								
A 240				20.3(140)	51.8(357)	39.2	48.8	68.1
A 240, aged	4000	482	900	15.5(107)	51.2(353)	40.0	52.6	71.6
				17.1(118)	51.5(355)	40.0	50.9	72.4
A 240, aged	2000	593	1100	21.5(148)	51.0(352)	36.0	45.8	70.9
A 240, aged	4000	593	1100	23.0(159)	50.5(348)	32.0	34.5	69.4
A 240, aged	1000	649	1200	21.5(148)	50.2(346)	31.2	38.0	66.6
A 240, aged	2000	649	1200	20.4(141)	48.4(334)	28.8	39.9	64.3
A 240, aged	4000	649	1200	20.0(138)	48.3(333)	28.0	40.1	68.2
Reannealed	0.5	1065	1900	13.8(95)	52.2(360)	36.8	50.5	73.6
Reannealed, aged	1000	649	1200	16.5(114)	50.5(348)	34.4	45.1	67.4
Reannealed, aged	2000	649	1200	17.2(119)	48.8(336)	31.2	40.4	59.7

Table 5.17. Values for the Constants in the Voce Equation for Type 304 Stainless Steel (Heat 9T2796) at 593°C (1100°F)

Specimen	Strain Rate (min^{-1})	σ_∞ (ksi)	σ_∞ (MPa)	k	σ_0 (ksi)	σ_0 (MPa)
RP 165	0.00009	45	310	12.78	10	69
RP 195	0.0004	56	386	8.86	10	69
RP 192	0.004	69	476	6.38	10	69
RP 193	0.04	83	572	5.06	10	69
RP 182	0.4	86	593	4.77	10	69

using these constants are compared with the smooth experimental curves in Fig. 5.15.

Sufficient tensile data now exist over a broad range of temperatures and strain rates to allow us to investigate the contribution of creep to the high-temperature tensile curve. Tensile ultimate strengths, when plotted against strain rates, appear to blend into data representing the stress dependence of the minimum creep rate. This trend is shown in Fig. 5.16 for temperatures ranging from 482 to 760°C (900 to 1400°F).

5.2.3.2 Creep Testing of Reference Heat 9T2796 1-in. (25-mm) Plate

Creep data have been analyzed on the basis of instantaneous plastic, transient creep, and linear creep components. These components have been compared to the trends expected for an "average" heat of type 304 stainless steel according to the equations[12] used to develop the ASME Boiler and Pressure Vessel Code Case 1331-8. Figure 5.17 shows the variation with stress and temperature of the instantaneous plastic strain component observed during the loading of creep tests. These strains, on the average, fall below the band covering tensile data for the same material and are about 35% greater than would be expected from the tensile tests. The code case curves fall well above the data for reannealed material but are reasonably close to data obtained after precycling specimens to raise the yield to near 17,000 psi (117 MPa).

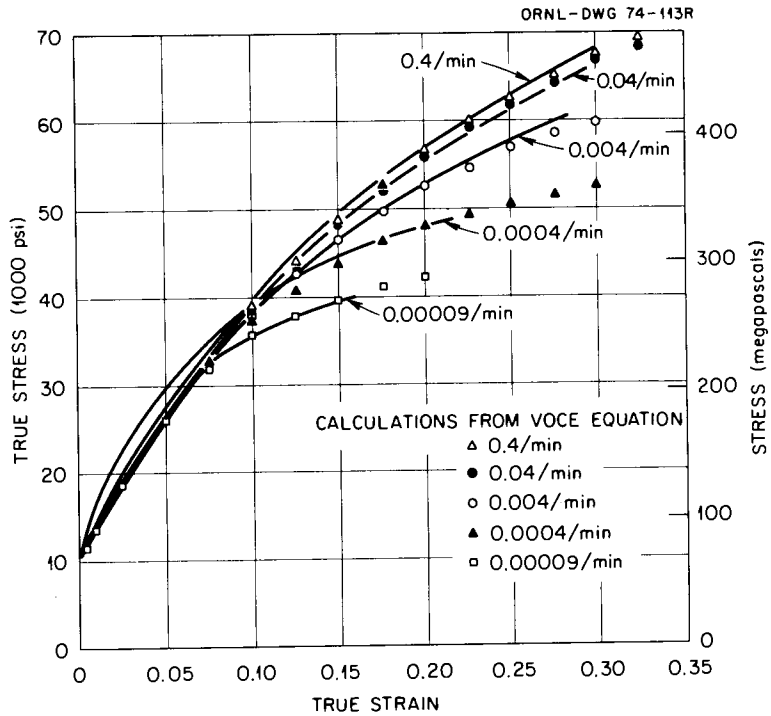

Fig. 5.15. Comparison of Data Calculated From the Voce Equation with Tensile Curves for Type 304 Stainless Steel at 593°C (1100°F). Heat 9T2796 1-in. (25-mm) plate reannealed at 1093°C (2000°F).

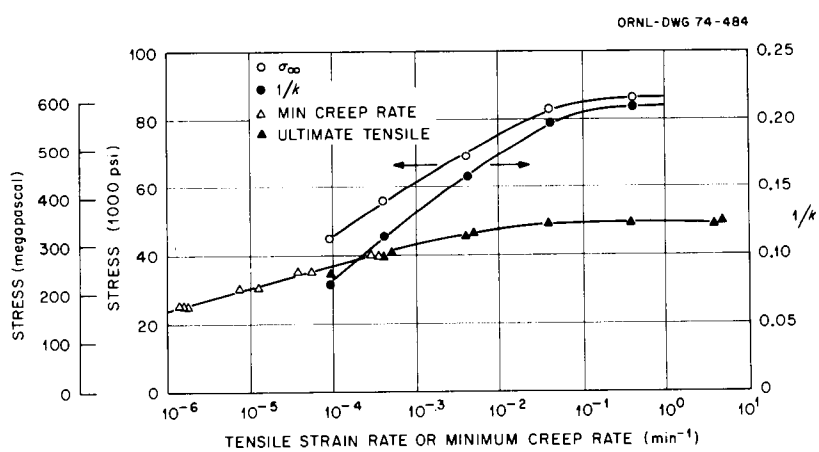

Fig. 5.16. Comparison of Ultimate Tensile Strength Data with Minimum Creep Rate Data for Type 304 Stainless Steel Heat 9T2796 1-in. (25-mm) Plate Reannealed at 1093°C (2000°F).

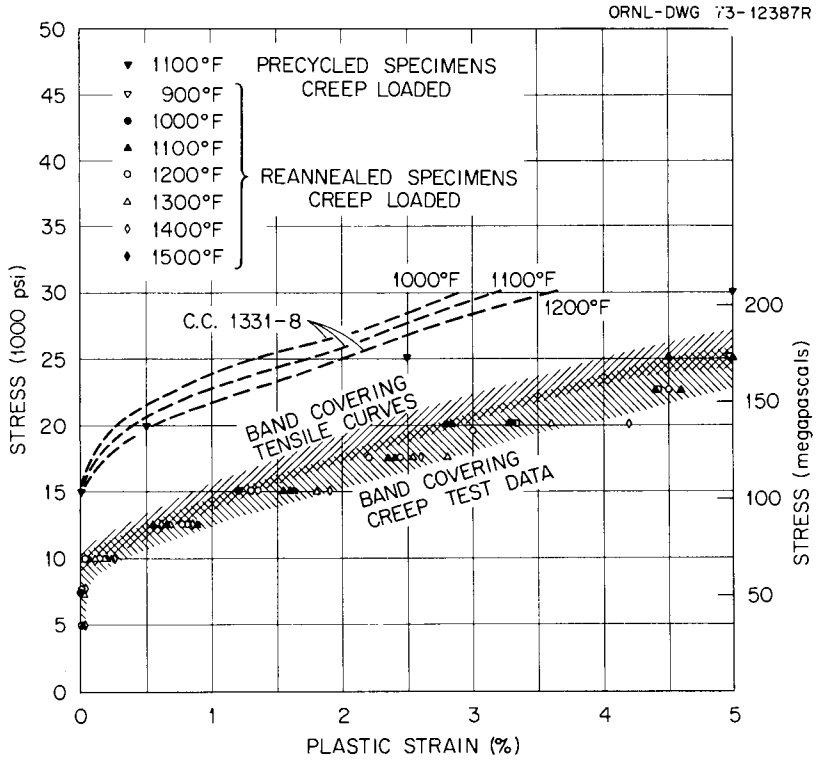

Fig. 5.17. Stress vs Plastic Strain Data Obtained From Tensile and Creep Tests for Type 304 Stainless Steel Heat 9T2796 1-in. (25-mm) Plate.

Figure 5.18 shows a replot of the instantaneous plastic strains assuming a relation:

$$\sigma = a\varepsilon_p^{3/4} + \sigma_0 ,$$

where σ is the creep stress, ε_p is the instantaneous plastic strain, and a and σ_0 are constants.

Figure 5.19 compares the minimum creep rate data we have collected with the expected trend curves for an average heat of type 304 stainless steel according to the equations used to develop Code Case 1331-8. Data show fair agreement except at 649°C (1200°F), where our heat is weaker.

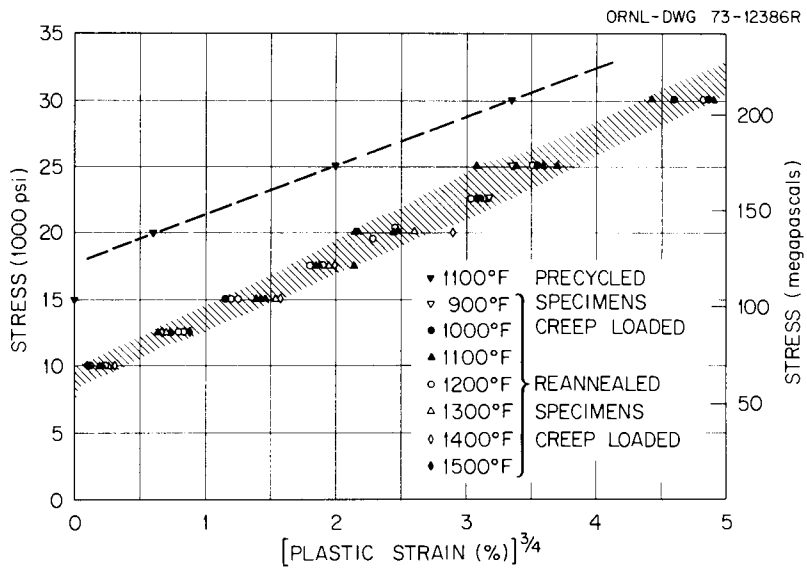

Fig. 5.18. Stress vs Reduced Plastic Strain Assuming the Ludwik Strain Hardening Coefficient to be 3/4. Type 304 stainless steel Heat 9T2796 1-in. (25-mm) plate.

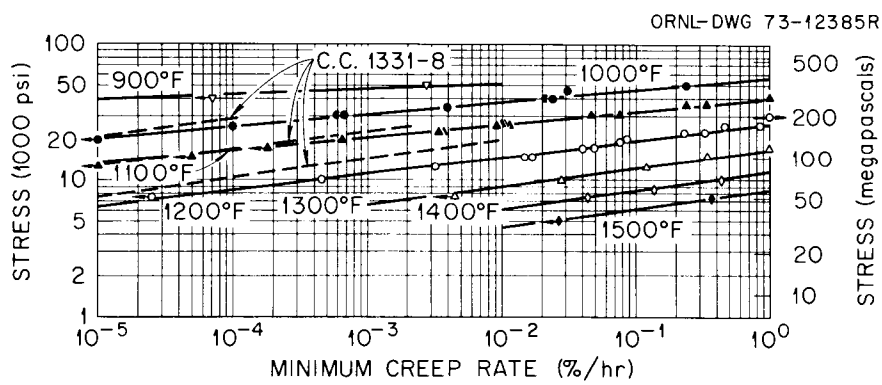

Fig. 5.19. Stress vs Minimum Creep Rate for Type 304 Stainless Steel Heat 9T2796 1-in. (25-mm) Plate.

Figure 5.20 shows a fit of a hyperbolic sine type of stress dependence to temperature-compensated minimum creep rate data assuming the validity of the Dorn parameter. This plot is useful for interpolation but should not be used for extrapolation since the data for temperatures below 649°C (1200°F) appear to diverge from the master curve with decreasing stresses.

Figure 5.21 shows the variation with temperature and stress of the primary creep strain component. At every temperature except 538°C (1000°F) we observed a discontinuity in the trend of the primary creep strain with decreasing stress. Above the stress where the discontinuity was observed, the primary strain was either constant or decreased with decreasing stress. Below the stress where the discontinuity was observed we were not able to define the stress dependency, except at 760 and 816°C (1400 and 1500°F) where the primary strain component appeared to increase with decreasing stress. Additional testing is under way to better define the data trend. Curves based on the equations used to develop Code Case 1331-8 are shown for 538, 593, and 649°C (1000, 1100, and 1200°F).

5.2.3.3 Creep Plasticity Interaction of Reference Heat 9T2796 1-in. (25-mm) Plate

The results of a creep-plasticity interaction test at 649°C (1200°F) are summarized by Fig. 5.22. This shows several strain-cycling hysteresis loops as they are influenced by creep at 15,000 psi (103 MPa). Loop A corresponds to the first cycle of a virgin specimen tested at 0.6% strain range. Loop B represents the tenth cycle. About 0.2% creep strain was introduced between loops B and C. This required 143 hr at 15,000 psi (103 MPa). Upon resumption of the cycling (loop C) we observed a decrease in the cyclic stress range. The 20th cycle (loop D) was similar to the tenth cycle (loop B). Another 143-hr creep period at 15,000 psi (103 MPa) was introduced, and when we resumed cycling (loop E) results were qualitatively similar to those we observed after the previous resumption. This specimen was exposed to additional interspersions of creep and strain cycling for the purpose of examining the influence of cyclic straining on creep. In general, we found that the influence of cyclic straining was not pronounced — that is, the creep rate was never below one-tenth of the rate expected from constant-load monotonic creep tests.

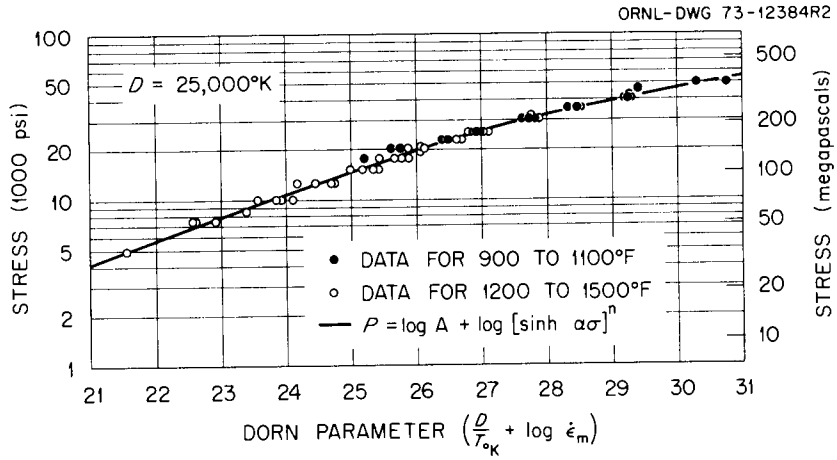

Fig. 5.20. Fit of the Hyperbolic Sine Stress Dependence to Temperature-Compensated Minimum Creep Rate Data for Type 304 Stainless Steel Heat 9T2796 1-in. (25-mm) Plate.

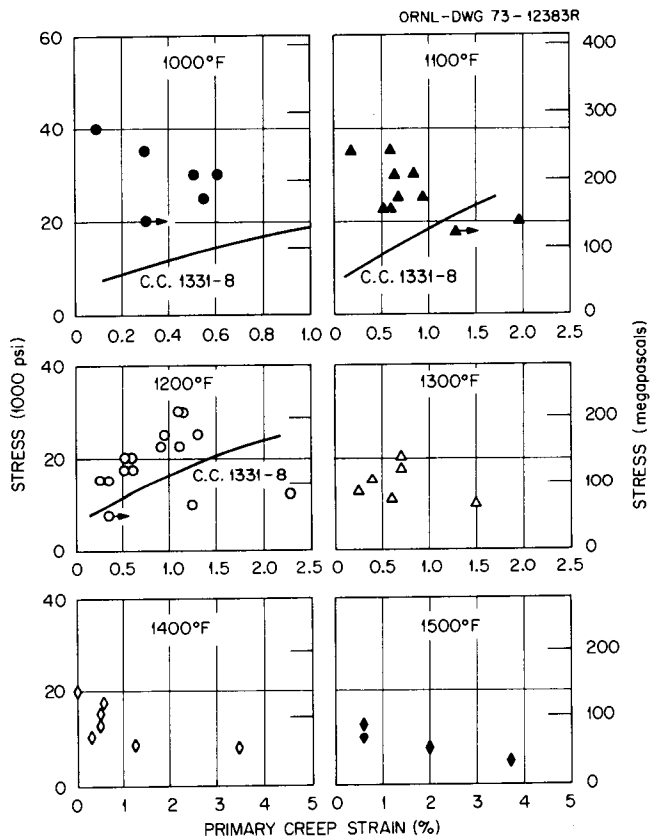

Fig. 5.21. Stress vs Primary Creep Strain for Type 304 Stainless Steel Heat 9T2796 1-in. (25-mm) Plate.

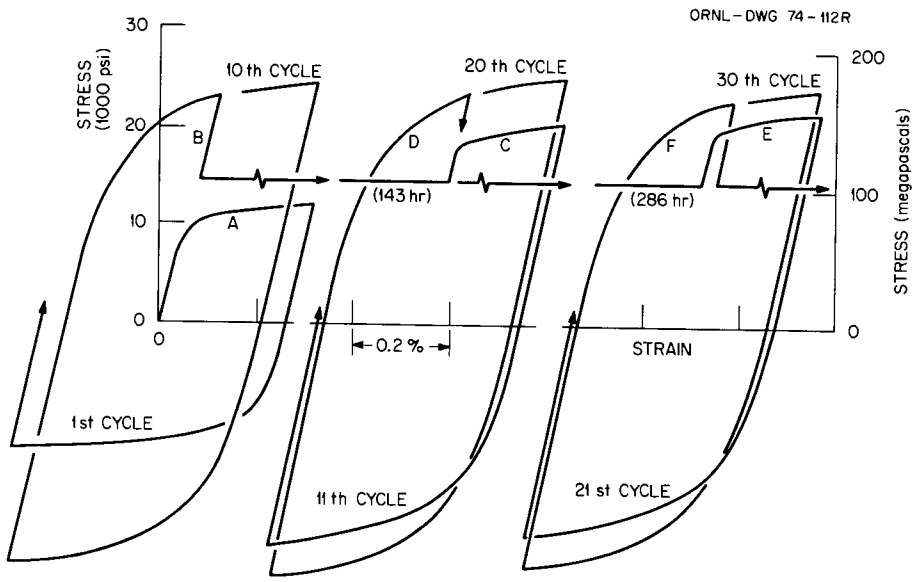

Fig. 5.22. Influence of Creep on the Strain-Cycling Hysteresis Loops at 649°C (1200°F). Type 304 stainless steel-Heat 9T2796 1-in. (25-mm) plate.

5.2.3.4 Strain-Cycling of Reference Heat 9T2796 1-in. (25-mm) Plate

Additional strain-cycling tests were performed in the creep-plasticity testing facility. The results from these and earlier tests are summarized in Table 5.18. An interesting phenomenon, which needs to be confirmed, is the rapid hardening at 649°C (1200°F), which we observed at the 0.6% strain range. The stress range, $\Delta\sigma$, at 10 cycles and 649°C (1200°F) is higher than $\Delta\sigma$ at 10 cycles for any other temperature above 427°C (800°F).

5.2.4 Mechanical Properties of Type 316 Stainless Steel

5.2.4.1 Procurement of Type 316 Stainless Steel Reference Heat — R. J. Beaver

The Republic Steel Quality Verification Program was reviewed on November 14. The vendor plans to melt the single 200-ton heat on January 29, 1974. Currently, the plans for procurement of this heat are progressing smoothly.

Table 5.18. Summary of Strain-Cycling Tests Performed in the Creep-Plasticity Testing Machine on Type 304 Stainless Steel (Heat 9T2796) 1-in. (25-mm) Plate

Specimen	Temperature		Strain Range (%)	Stress Range			
				First Cycle		Tenth Cycle	
	(°C)	(°F)		(ksi)	(MPa)	(ksi)	(MPa)
FRP 57	20	70	1.0	59.0	407	69.0	476
FRP 55	20	70	1.0	58.5	403	69.0	476
FRP 56	20	70	0.95	58.0	400	68.5	472
FRP 54	20	70	0.95	58.5	403	70.0	483
FRP 58	20	70	1.0	64.5	445	72.5	500
FRP 64	538	1000	1.0	28.3	195	59.5	410
FRP 75	649	1200	1.0	31.5	217	59.0	407
FRP 60	204	400	0.64	37.5	259	45.5	314
FRP 62	427	800	0.6	29.4	203	42.0	290
FRP 67	427	800	0.6	29.5	203		
FRP 76	482	900	0.6	27.7	191	39.4	272
FRP 63	538	1000	0.6	25.7	177		
FRP 82	538	1000	0.6	26.1	180	42.8	295
FRP 74	649	1200	0.6	24.9	172	48.5	334
FRP 61	427	800	0.4	27.4	189	33.6	232
FRP 66	482	900	0.4	26.5	183	33.0	228
FRP 65	538	1000	0.4			32.5	224

We expect a more detailed fabrication schedule from Republic after the melt is completed. We will then be able to inform all interested parties of a more precise date of material availability. Contracts are being negotiated with Rollmet for the 16- and 28-in.-diam (405 and 710 mm) pipe product form using ingots of the reference heat supplied by Republic.

5.2.4.2 Heat-to-Heat Variation Studies of Type 316 Stainless Steel — H. E. McCoy

Four heats of type 316 stainless steel are being studied in this program. Their chemical compositions and tensile properties were reported previously.[13] All these heats are being aged, and the aging matrix is shown in Fig. 5.23. Test samples are being machined from the aged blocks for testing.

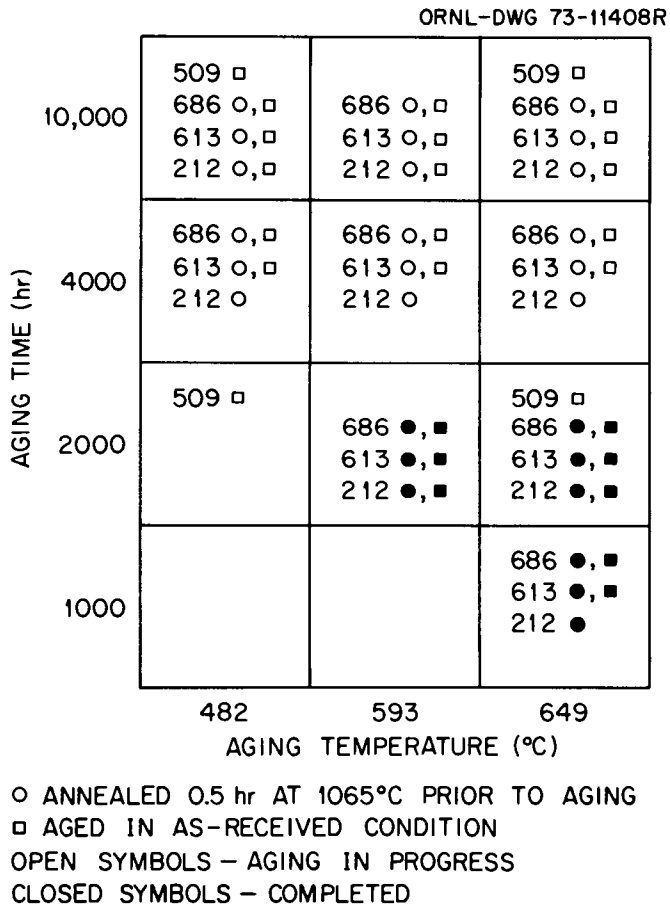

Fig. 5.23. Aging Program for Type 316 Stainless Steel.

Four additional heats were obtained from WARD and have been included in the program. Three of the heats are 2 1/16-in.-diam (52.4 mm) bar, and one heat is as cast. A horizontal section will be taken from the center of the ingot, and the properties of the cast metal tested. Samples of these four heats are being machined.

5.2.5 Failure Criteria—Strain Limits — C. R. Brinkman

The total strain at failure of a metal subjected to elevated-temperature deformation is a function of many variables, including state of stress, time at temperature, environment, composition and processing history, and strain rate. Furthermore, these variables may interact synergistically, making the prediction of inelastic deformation at failure particularly difficult for reactor components under expected operating conditions. Because of the difficulty of calculating deformation at failure and for other reasons, ASME Code Case 1331-8 places a limit on the allowable deformation that may be accrued in service. The objective of ORNL's program on strain limits is to determine how material and material processing variables influence strain at failure as a guide in establishing meaningful deformation limits.

Most of the creep and stress-rupture data that are available for the austenitic stainless steels were obtained from uniaxial tests, most of which did not exceed 20,000 hr in duration. These tests have generally shown a decrease in total elongation with increasing test time. Since many LMFBR components are expected to see elevated-temperature service for periods up to 30 years (2.63×10^5 hr), a method of estimating the total stress-rupture elongation for specimens subjected to initial stress levels that would result in failure in say 10^5 hr (11.4 years) and longer would be particularly useful. Such a method was suggested by Smith,[14,15] who noted that the initial stress in a creep or stress-rupture test was a straight line when plotted on log-log coordinates as a function of average strain rate to failure, defined as the total elongation divided by the total time to failure. The straight line suggests that an extrapoloation may be made to lower strain rates and, with the aid of an appropriate stress-rupture diagram, that rupture

ductility may be estimated for any time over which the extrapolation is valid. An example of this technique is shown in Fig. 5.24, in which the 10^5-hr stress-rupture total elongation and strain to the onset of tertiary creep are estimated for a single heat of type 316 stainless steel tested at 1000°F (538°C).

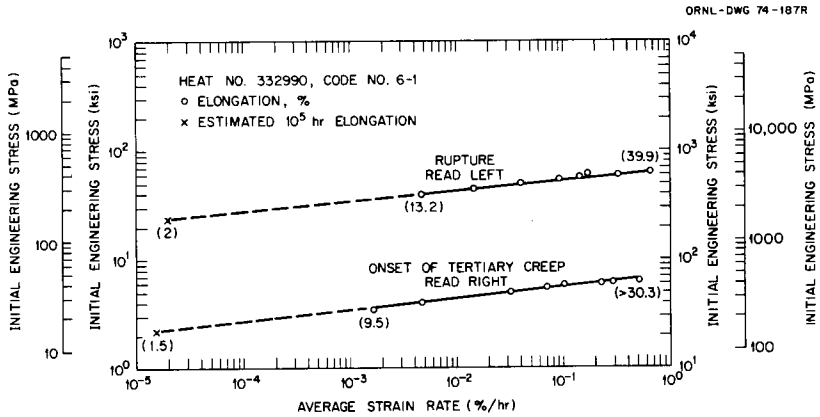

Fig. 5.24. Initial Engineering Stress as a Function of Average Strain Rate to Rupture or Onset of Tertiary Creep, Showing Estimated 10^5-hr Stress-Rupture Elongation and Strain to the Onset of Tertiary Creep for a Single Heat of Type 316 Stinless Steel at 1000°F (538°C).

Creep and stress-rupture data for type 316 stainless steel bar stock were obtained from the literature,[16,17] and the 10^5-hr elongation was estimated by the above method. All data analyzed were obtained from tests conducted on material meeting ASME code composition requirements. Heat treatments employed are given in Table 5.19.

Examples of heat-to-heat and pretest heat treatment variations at a single test temperature, 1100°F (593°C), are shown in Fig. 5.25, where the estimated 10^5-hr total elongation is seen to range from 1 to 28%. Codes 6-3 and -4, Table 5.19, are data from the identical heat of material given different pretest heat treatments. Code 6-4 material was given a carbide stabilization anneal, and over the range of the data the ductility was nearly stable or increased slightly in comparison with Code 6-3 material, which, as shown, decreases (29 to 19%) with increasing test time or decreasing average strain rate. This suggests that carbide stabilization anneals following general solution annealing are beneficial to end-

Table 5.19. Pretest Heat Treatment of Type 316 Stainless Steel Used in 10^5-hr Ductility Estimates

Code	Anneal Temperature (°C)	Anneal Temperature (°F)	Anneal Time (hr)	Postanneal Treatment[a]
6-1	1065	1950		AC
6-3	1093	2000		WQ
6-4	1093	2000		WQ and 24 hr at 816°C (1500°F)
6-5	1150	2100		AC and 2 hr at 760°C (1400°F)
6-6	1093	2000		WQ
6-7	1093	2000		WQ
6-8	1065	1950	20	AC
6-9	1093	2000		WQ and 1 hr at 955°C (1750°F), AC
6-10	955	1750	4	AC
6-11	1093	2000		WQ and 5 hr at 871°C (1600°F), FC
6-12	1093	2000		WQ and 5 hr at 955°C (1750°F), AC
6-13	1093	2000		WQ and 1 hr at 871°C (1600°F), FC
6-14	1093	2000		WQ and 5 hr at 871°C (1600°F), AC
6-15	1093	2000		WQ and 1 hr at 955°C (1750°F), AC
6-16	1093	2000		WQ
6-17	1093	2000		WQ
6-18	1150	2100		AC and 760°C (1400°F), AC
6-19	1093	2000		Q
6-20	1093	2000		WQ and 5 hr at 871°C (1600°F), FC

[a]AC = air cooled, WQ = water quenched, Q = quenched, FC = furnace cooled.

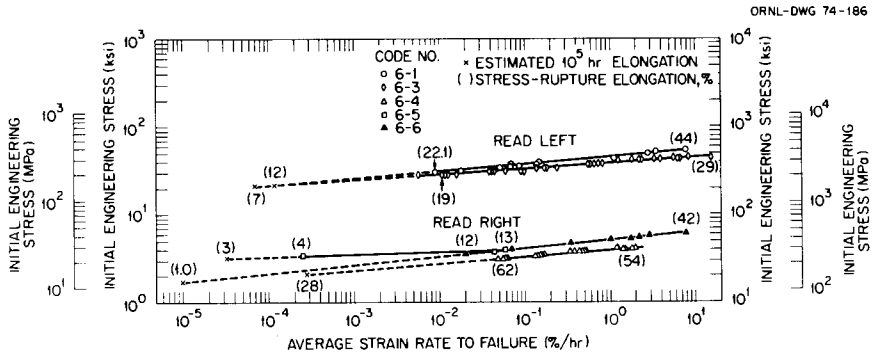

Fig. 5.25. Engineering Stress as a Function of Average Strain Rate to Failure for Type 316 Stainless Steel at 593°C (1100°F) Showing Estimated 10^5-hr Creep Rupture Elongation. Heat-to-heat variations and variations in pretest heat treatment produce variations in ductility.

of-life ductility, as recent experimental evidence suggests.[18] Indeed, in the case of a number of heats given a stabilization anneal, Codes 6-9, -11, and -14, and stress-rupture tested at 1200°F (650°C), the ductility remained nearly constant or increased with test time in comparison with material given only a solution anneal before testing at 1200°F (650°C)(i.e., Codes 6-8, -16, and -17). The results was a higher 10^5-hr estimated total elongation for the stabilized material. However, there were also also a number of apparent exceptions, in that some heats, Codes 6-5, -12, -13, and -20, which were given stabilization anneals before testing showed a continuous decrease in ductility with increasing test time. Yet some materials, Codes 6-7 and -19, which were not given any pretest carbide stabilization, showed near stable ductilities over the test times. The reasons for these seemingly conflicting results with respect to carbide stabilization heat treatment are obscure; however, they may be due to subtle differences in composition — e.g., contents of C, N, B, Ti, Nb, etc.

The estimated 10^5-hr stress-rupture ductilities obtained by this technique for type 316 stainless steel are compared over the range of 1000 to 1500°F (538 to 816°C) in Fig. 5.26. The initial stress to cause rupture in 10^5 hr for each code was obtained by linear extrapolation of that particular set of stress-rupture data. Curvature was taken into account where it was apparent. The stress to cause rupture at 10^5 hr,

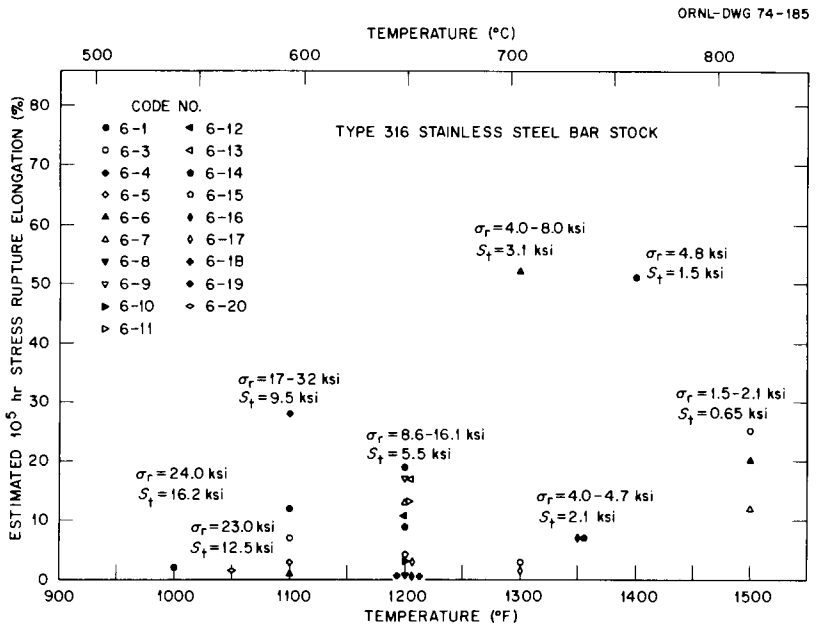

Fig. 5.26. Estimated 10^5-hr Stress-Rupture Elongation as a Function of Temperature. Estimated initial stress (σ_r) levels required for failure in 10^5-hr along with code-allowable stress (S_t) levels are also given. Multiply stresses by 6.895 to convert from ksi to MPa.

σ_r, or the range of stress values for each temperature found by this method are compared with ASME Code Case 1331-8 allowable stress levels, S_t, in Fig. 3.26 as well. Comparing the estimated 10^5-hr σ_r values required to obtain the indicated stress-rupture elongations with the S_t values, we see that, while one can obtain stress-rupture elongations in the vicinity of 1%, the allowable stress levels are low enough to prevent failure (assuming other approximations are correct) in actual reactor design.

In conclusion, log-log plots of initial stress against average strain rate to failure plotted for type 316 stainless steel bar stress-rupture tested over the range 1000 to 1500°F (538 to 816°C) showed linearity; some exceptions at low strain rates were seen at 1500°F (816°C). Smith,[15] in analyzing a considerable amount of type 304 stainless steel data from the same sources, also found linearity in the data plots. The method, therefore, holds promise for use in extrapolating available ductility data to longer times at temperature than are presently available. However, caution must be exercised as to the

extent the data are extrapolated since (1) the technique involves a double extrapolation, and (2) long time at temperature leads to structural instability, as evidenced by the variations in ductility produced by carbide stabilization anneals, and could further complicate the results. Work is continuing.

5.2.6 Computer Data Storage, Retrieval, and Storage Information Center — J. W. Woods

The type of computer program developed for the storage and retrieval of mechanical property data is illustrated by the flow diagram shown in Fig. 5.27. This shows the flow of data from the time of observation until it is used by designers and manufacturers. The total program may be broken down into three steps:

A. The observation of data, manual acquisition, and processing of the data to obtain summary characteristics.

B. The Data Storage and Retrieval System (DSRS) for summary characteristics.

C. Structural Materials Information Center (SMIC).

In step B, the raw data is processed to obtain the type of summary characteristics as shown by the data forms in Figs. 5.28 and 5.29. Three computer programs are actually involved in step B. ADSEP (Automatic Data Set Editing Program) organizes the data into a consistent format so that some other program may retrieve it. This is illustrated by the data forms. The second program involved is the TSO (Time Sharing Option). TSO stores each user's program on a disc and moves each one in turn into the computer for a few milliseconds computation. The ØRLØØK program provides for one-line retrieval of information by a user operating from a remote typewriter terminal. Calculations are not performed in this step of the program. Only retrieval of information stored is obtained.

At present, approximately 160 tensile tests have been input to the DSRS. Instructional meetings on the use of the new data forms have been held with personnel who will input the data. A thesaurus has been prepared, and instruction manuals are being updated. Trial runs of the ØRLØØK retrieval program do not indicate any problems. Input of data is now accelerating.

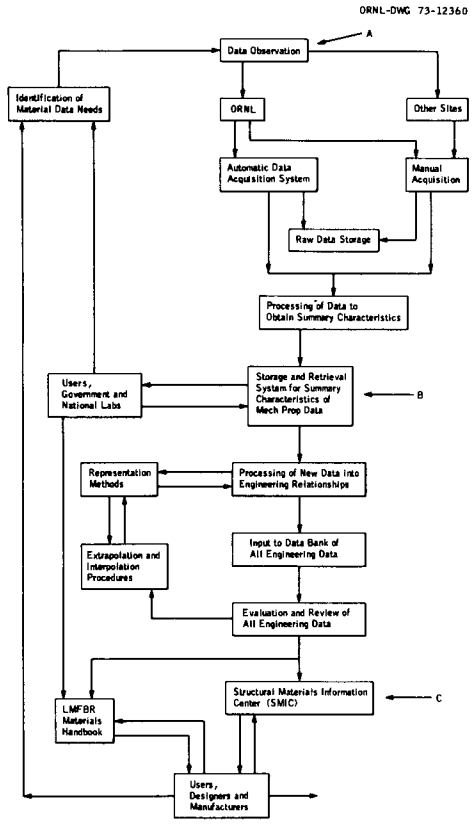

Fig. 5.27. Flow of Mechanical Property Data.

In step C information from the DSRS will be further processed to develop engineering relationships, which in turn will be input to SMIC. SMIC is to be developed in such a manner that users can not only retrieve stored information, but they may ask questions of the center, and ask for calculations to be performed.

As phase I of SMIC, the computer-based version of the LMFBR Materials Handbook has been set up. The program is designated as HANDBK and is written in FORTRAN IV for use in the timesharing environment of the PDP-10 System at ORNL. It is a fully interactive program, relying heavily on user input to direct program control and locate the desired records. The program accesses our on-line disk file containing instructions, tables of contents, and information from the LMFBR Handbook. A main program regulates the calling of several subroutines to do read operations and perform calculations.

MECHANICAL PROPERTIES DATA STORAGE FORM

TENSILE

Test Number ( )

Specimen Number <NØ>

Type of Test ⟨TY⟩ _____

Institution/Program/Date/
Engineer/Technician ⟨IP⟩ _____; _____; _____; _____; _____

Temperature ⟨TE⟩ _____;(°C)

Irradiation Data:

Experiment No. ⟨EX⟩ _____
Irradiation Temp. ⟨IT⟩ _____;(°C)
Fluence ⟨FL⟩ _____;(N/cm²)
Reactor and Position ⟨RP⟩ _____

Environment ⟨EN⟩ _____

Material ⟨MA⟩ _____

Heat Number ⟨HN⟩ _____

Alloy Base ⟨AB⟩ _____

Heat Treatment ⟨HT⟩ _____

Specimen Description ⟨SD⟩ _____

Comments ⟨CM⟩ _____

Nominal Properties ⟨NP⟩ Proportional Limit _____;(psi) .02% Offset Yield _____;(psi) Apparent Modulus _____;(psi)

Engineering Properties

.2% Offset Yield ⟨EY⟩ _____;(psi)
Ultimate Stress ⟨US⟩ _____;(psi)
Fracture Stress ⟨FS⟩ _____;(psi)
Uniform Elongation ⟨UE⟩ _____;(%)
Total Elongation ⟨ET⟩ _____;(%)
Reduction of Area ⟨RA⟩ _____;(%)
Upper/Lower Yield ⟨UL⟩ _____; _____;(psi)

Elongation in 4D ⟨ED⟩ _____;(%)
Nominal Strain Rate ⟨SR⟩ _____;(%/min)
True Properties

Ultimate Stress ⟨TU⟩ _____;(psi)
Fracture Stress ⟨TF⟩ _____;(psi)
Uniform Elongation ⟨TL⟩ _____;(%)
Total Elongation ⟨TT⟩ _____;(%)

Extensometer Results

Modulus ⟨YM⟩ _____;(psi)
Proportional Limit ⟨PL⟩ _____;(psi)
.02% Offset Yield ⟨YO⟩ _____;(psi)
.2% Offset Yield ⟨Y2⟩ _____;(psi)
Extensometer Class ⟨EC⟩ _____

Stress ⟨SE⟩	Total Strain ⟨SN⟩
_____;(psi)	_____;(%)
_____;	_____;
_____;	_____;
_____;	_____;
_____;	_____;
_____;	_____;

MECHANICAL PROPERTIES DATA STORAGE FORM

IMPACT - SLOW BEND

Test Number ( )

Specimen Number <NØ> _____

Type of Test ⟨TY⟩ _____

Institution/Program/Date
Engineer/Technician ⟨IP⟩ _____; _____; _____; _____; _____

Temperature ⟨TE⟩ _____;(°C)

Irradiation Data:

Experiment No. ⟨EX⟩ _____
Irradiation Temp. ⟨IT⟩ _____;(°C)
Fluence ⟨FL⟩ _____;(N/cm²)
Reactor and Position ⟨RP⟩ _____

Environment ⟨EN⟩ _____

Material ⟨MA⟩ _____

Heat Number ⟨HN⟩ _____

Alloy Base ⟨AB⟩ _____

Heat Treatment ⟨HT⟩ _____

Specimen Description ⟨SD⟩ _____

Comments ⟨CM⟩ _____

Specimen Orientation Code ⟨SØ⟩ _____

Specimen Location:

<DG> _____;(deg.)
⟨X⟩ _____;(in.)
⟨Y⟩ _____;(in.)
⟨Z⟩ _____;(in.)
⟨TI⟩ _____;(t)

Depth of Precrack ⟨PC⟩ _____;(in.)

Speed ⟨SP⟩ _____;(ft/sec,in/min)
Total Fracture Energy ⟨FE⟩ _____;(ft-lbs)
Lateral Expansion ⟨LE⟩ _____;(in.)
Fracture Appearance ⟨FA⟩ _____;(% Fibrous)
Fract. Toughness Param. ⟨FP⟩ _____;(kpsi-in.$^{1/2}$)

Slope Elastic Portion ⟨SL⟩ _____;(lbs/in)
Load-Time Trace <TA> _____;(yes or no)

Load at ⟨LD⟩ Start of Fast Fracture _____;(lbs) Fracture Arrest _____;(lbs) Maximum _____;(lbs) General Yield _____;(lbs)

Deflection to ⟨DD⟩ Fast Fracture _____;(in.) Max. Load _____;(in.)

Energy to ⟨EG⟩ Fast Fracture _____;(ft-lbs) Max. Load _____;(ft-lbs)

Fig. 5.28. Mechanical Properties Data Storage Forms — Tensile and Impact.

MECHANICAL PROPERTIES DATA STORAGE FORM

CREEP

Test Number ⟨ ⟩ Specimen Number <NØ> Type of Test ⟨TY⟩ _____

Institution/Program/Date Engineer/Technician ⟨IP⟩ _____; _____; _____; _____; _____

Temperature ⟨TE⟩ _____;(°C) Irradiation Data:

Environment ⟨EN⟩ _____ Experiment No. ⟨EX⟩ _____

Irradiation Temp. ⟨IT⟩ _____;(°C)

Material ⟨MA⟩ _____ Fluence ⟨FL⟩ _____;(N/cm²)

Reactor and Position ⟨RP⟩ _____

Heat Number ⟨HN⟩ _____

Alloy Base ⟨AB⟩ _____

Heat Treatment ⟨HT⟩ _____

Specimen Description ⟨SD⟩ _____

Comments ⟨CM⟩ _____

_____

Stress ⟨ST⟩ _____;(psi) Loading Data:

Minimum Creep Rate ⟨CR⟩ _____;(%/hr) Elastic Strain on load ⟨EL⟩ _____;(%)

Rupture Time ⟨RT⟩ _____;(hrs)

Time Discontinued ⟨TD⟩ _____;(hrs) Plastic Strain on load ⟨EP⟩ _____;(%)

Time to Third Stage Creep ⟨SC⟩ _____;(hrs) Loading Method ⟨LM⟩ _____

Primary Creep Strain ⟨PS⟩ _____;(%) Reduction of Area ⟨RA⟩ _____;(%)

Quality of Test ⟨QT⟩ _____

Extensometer Class ⟨EC⟩ _____

MECHANICAL PROPERTIES DATA STORAGE FORM

RELAXATION

Test Number ⟨ ⟩ Specimen Number <NØ> _____ Type of Test ⟨TY⟩ _____

Institution/Program/Date Engineer/Technician ⟨IP⟩ _____; _____; _____; _____; _____

Temperature ⟨TE⟩ _____;(°C) Irradiation Data:

Environment ⟨EN⟩ _____ Experiment No. ⟨EX⟩ _____

Irradiation Temp. ⟨IT⟩ _____;(°C)

Material ⟨MA⟩ _____ Fluence ⟨FL⟩ _____;(N/cm²)

Reactor and Position ⟨RP⟩ _____

Heat Number ⟨HN⟩ _____

Alloy Base ⟨AB⟩ _____

Heat Treatment ⟨HT⟩ _____

Specimen Description ⟨SD⟩ _____

Comments ⟨CM⟩ _____

_____

Initial Nominal Strain ⟨NS⟩ _____;_____;_____(%) Final Stress and Strain ⟨SF⟩ _____;_____;

Initial Actual Stress ⟨AS⟩ _____;_____;_____(psi) Stress ⟨SS⟩ _____;(psi) at Time ⟨TM⟩ _____;(hrs)

Loading Strain Rate ⟨SR⟩ _____;(%/min) _____; _____;

Test Time ⟨TI⟩ _____;_____;_____(hrs) _____; _____;

Modulus ⟨YM⟩ _____;(psi) _____; _____;

.02% Yield ⟨YO⟩ _____;(psi) _____; _____;

.2% Yield ⟨Y2⟩ _____;(psi)

Retest .02% Yield ⟨YA⟩ _____;_____;(psi)

Retest .2% Yield ⟨YB⟩ _____;_____;(psi)

Fig. 5.29. Mechanical Properties Data Storage Forms — Creep and Relaxation.

Preliminary work on the computer HANDBK was started in June 1973 and is not as yet in its final form. Much work needs to be done to improve the capabilities of the program by increasing the computational capabilities, instituting a graphical output, and adding flexibility with "prompts" so that a user may stop at any point in the program.

5.3 MECHANICAL AND METALLURGICAL BEHAVIOR OF WELDMENTS FOR LMFBR — P. Patriarca, G. M. Slaughter, and W. R. Martin

5.3.1 Properties and Structure of 16-8-2 Stainless Steel Weld Metal — R. T. King, N. C. Cole, R. G. Berggren, and G. M. Goodwin

5.3.1.1 Introduction

Type 16-8-2 (16% Cr—8% Ni—2% Mo) stainless steel was introduced in the mid-1950's as a suitable filler metal for elevated-temperature service that was less susceptible to hot cracking than commonly used electrodes.[19] Since then, the 16-8-2 filler metal has been selected to join types 316 and 346 stainless steel base metal in numerous applications, including the steam piping for at least one large conventional power plant.[20] However, there are relatively few high-temperature mechanical properties data in the literature for 16-8-2 weld metal. Sigma phase, formed in deposited weld metal that is orginally composed of austenite and ferrite, can cause low ductility in creep tests for welds in austenitic stainless steel.[21] Loss of room-temperature impact strength has been observed for 16-8-2 weld metal after long aging at 732°C (1350°F), and it was attributed to the formation of sigma phase.[19] The suspected formation of sigma phase is an important incentive for investigating the long-time creep ductility of 16-8-2 weld metal. A further incentive is to gain additional experience with the range of creep strength properties of a variety of these welds, so that it may be compared with the range of creep strength properties reported for type 316 stainless steel, a candidate material for use in the primary coolant piping systems of sodium-cooled power reactors.

5.3.1.2 Experimental Procedures and Results

5.3.1.2.1 Test Weld Fabrication. All the welds for this study were made in 12.7-mm-thick (0.5-in.) plates from a single heat of type 316 stainless steel. The chemical composition of the steel is given in Table 5.20. All the filler metals were deposited in V-groove butt joints having a 75° included angle, a 0.16-cm (0.062-in.) root gap, and a 0.038-cm (0.015-in.) minimum root land. The plates were restrained from flexing about the weld but were free to move in the plane of the plate.

The welding parameters are given in Table 5.21. Welds V-32 to V-35 and V-46 were made with the same heat of filler metal but different welding techniques; weld V-90 was made from a remelt of that wire to which 1.58% Ni, 0.40% Si, and 0.33% Mn had been added as starting stock. The automatically deposited welds V-66 to V-74 were made by the oscillating torch (weave) technique at about 2.2 kJ/mm (57 kJ/in.) after the first three passes had been deposited manually.

The chemical compositions of the deposited filler metal are given in Table 5.20. Radiography was used to confirm the soundness of the finished welds.

5.3.1.2.2 Mechanical Properties Specimen Preparation and Testing. Two kinds of test specimens were used in this program: for all welds except V-66 through V-74, a buttonhead specimen with a 2.86-cm-long × 0.32-cm-diam (1.125 × 0.125 in.) gage section was used, while for welds V-66 through V-74, a threaded-end specimen with a 3.17-cm-long × 0.64-cm-diam (1.25 × 0.250 in.) gage section was used. The grips on the threaded-end specimens were welded on. Both kinds of specimens had all-weld-metal gage sections, with the specimen axis parallel to the welding direction. The center lines of all specimens were located approximately 5 mm below the weld surface. Nondestructive eddy-current testing techniques verified that the gage sections of the threaded-end specimens did not contain base metal.[22]

Table 5.20. Deposit Compositions of Type 16-8-2 Welds

Weld	Deposit Composition, wt %									
	Cr	Ni	Mo	C	B	P	Ti	Si	S	Mn
V-3, V-4	16.5	8.92	1.7	0.064	0.0001	0.015	<0.02	0.039	0.015	1.36
V-32 to V-35	15.48	7.34	1.77	0.072		0.017		0.010	0.013	1.63
V-46	15.48	7.34	1.77	0.072		0.017		0.010	0.013	1.63
V-55, V-56	15.57	7.05	1.82	0.080		0.024		0.28	0.020	1.79
V-57, V-58	16.80	8.28	2.00	0.077		0.012		0.22	0.017	1.54
V-66 to V-74	15.18	7.19	1.68	0.060		0.018		0.28	0.013	1.68
V-90	15.29	8.71	1.72	0.039	0.002	0.020	0.01	0.42	0.014	1.6
Base Metal[a]	17.0	12.9	2.2	0.010		0.016		0.44	0.012	1.65

[a]Type 316 stainless steel plate.

Table 5.21. Welding Conditions for Depositing Type 16-8-2 Filler Metal

Weld	Process	Method[a]	Filler Metal Diameter (mm)	Filler Metal Diameter (in.)	Voltage[a] (V)	Current[a] (A)	Number of Passes[b]
V-03, V-04	SMA	Manual, IG	4.0	0.16	29	130	10
V-32 to V-35	GTA	Manual, IG	3.2	0.13	13	185	9
V-46	GTA	Manual, IG	3.2	0.13	15	170	10
V-55, V-56	GTA	Manual, IG	0.76[c]	0.030	19	170	18
V-57, V-58	GTA	Manual, IG	1.1[d]	0.043	19	170	19
V-66 to V-74	GTA	Automatic, IG	1.1[d]	0.043	14	190	9
V-90	GTA	Manual, IG	3.2	0.13	10	170	11

[a]Conditions for root pass differ from those given for filler passes in manual welds; conditions for root pass and first two filler passes differ from those given for filler passes in automatic welds.

[b]Interpass temperatures were less than 120°C (248°F).

[c]Nine wires braided together.

[d]Four wires braided together.

Tensile test have been performed on the threaded-end specimens from welds V-66 to V-74 on an Instron tensile testing machine at nominal strain rates of 0.016, 0.004, and 0.0004/min at room temperature, 482, 593, and 649°C (900, 1100, and 1200°F). Data are available from averaging extensometers on a 25.4-mm (1-in.) gage section and from the Instron chart. Tables 5.22 and 5.23 summarize all the tensile data, including engineering values of stresses and strains and true values (assuming constancy of volume). Plastic anisotropy was observed and characterized by maximum and minimum diametral strain measurements at the point of fracture and at an arbitrary location away from the necked region. The portion of the true stress—true strain (σ_{true},ε_{true}) curve from the yield point to the ultimate point was fitted to

$$\sigma_{true} = k\varepsilon^{n}_{true} ,$$

where k and n are material constants. These results, together with the standard deviation for each test, are reported in Table 5.23. Strain-rate effects are noted, particularly in the tests at 593 and 649°C.

A limited number of specimens from the other welds was tensile tested at 649°C (1200°F) at 0.04 or 0.004/min strain rate without extensometers. Data from the Instron charts and post-test reduction of area measurements are given in Table 5.24.

Creep tests have been conducted on the threaded-end specimens from automatic welds V-66 to V-74 at 482, 593, and 649°C (900, 1100, and 1200°F). Four specimens from these welds are still in test. The specimens were all fitted with averaging extensometers with 10-μin. (0.25 μm) sensitivity, and the load application rate was manually controlled through a pneumatic loading device to produce approximately 0.004/min strain rates during loading. Temperatures were controlled to within ±3°C of the nominal test temperature, with thermocouples made from wire having ±3/8% specified accuracy. Creep tests were also performed at 649°C (1200°F) on buttonhead specimens on which strain measurements were made from the load train. Accurate loading strains for the buttonhead specimens are not available, and creep strain accuracy was estimated to be ±1%. The same

Table 5.22. Results of Tensile Tests on Type 16-8-2 Longitudinal All-Weld-Metal Specimens From Automatic Gas Tungsten-Arc Welds V-66 to V-74

Strain Rate (min^{-1})	Instron Measurements							Reduction of Area (%)
	Strength, ksi (MPa)					Strain, %		
	Engineering			True				
	0.2% Offset Yield	Ultimate	Fracture	Ultimate	Fracture	Uniform Eng. (True)	Total Eng. (True)	
				Tests at 25°C (77°F)				
0.16	41.0 (283)	92.0 (634)	60.7 (419)	139.4 (961)	211.3 (1457)	51.6 (0.42)	61.8 (1.25)	71.3
0.004	40.2 (277)	111.8 (771)	77.6 (535)	167.5 (1155)	228.1 (1573)	49.8 (0.40)	58.4 (1.08)	66.0
0.0004	37.5 (259)	112.0 (772)	76.4 (527)	155.9 (1075)	248.0 (1710)	39.1 (0.33)	48.2 (1.18)	69.2
				Tests at 482°C (900°F)				
0.16	28.9 (199)	54.6 (376)	39.2 (270)	68.9 (475)	95.8 (661)	25.9 (0.23)	34.0 (0.89)	59.0
0.004	29.2 (201)	61.3 (423)	42.4 (292)	77.8 (536)	107.2 (739)	26.9 (0.24)	37.2 (0.93)	60.4
0.0004	28.6 (197)	58.5 (403)	54.0 (372)	75.8 (523)	128.7 (887)	29.5 (0.26)	31.1 (0.87)	58.0
				Tests at 593°C (1100°F)				
0.16	26.0 (179)	48.7 (336)	35.6 (245)	58.8 (405)	104.1 (718)	20.8 (0.19)	33.0 (1.1)	65.8
0.004	26.2 (181)	46.2 (319)	34.2 (236)	58.9 (406)	75.2 (518)	27.6 (0.24)	40.4 (0.79)	54.6
0.0004	27.1 (187)	39.1 (270)	19.4 (134)	45.7 (315)	52.2 (360)	16.7 (0.15)	57.3 (0.99)	62.8
				Tests at 649°C (1200°F)				
0.16	23.7 (163)	42.8 (295)	29.3 (202)	54.5 (376)	75.8 (523)	27.3 (0.24)	40.9 (0.95)	61.4
0.004	25.6 (177)	37.6 (259)	20.7 (143)	45.8 (316)	48.6 (335)	21.9 (0.19)	53.7 (0.85)	57.4
0.0004	24.8 (171)	30.1 (208)	16.5 (114)	32.5 (224)	47.5 (337)	8.0 (0.08)	55.4 (1.06)	65.3

Table 5.23. Additional Tensile Results on Type 16-8-2 Longitudinal All-Weld-Metal Specimens From Automatic Gas Tungsten-Arc Welds V-66 to V-74

Test Temperature (°C)	Test Temperature (°F)	Strain Rate (min^{-1})	Diametral Strain: At Fracture (%) max (min)	Diametral Strain: At Fracture Ratio	Diametral Strain: Away from Fracture (%) max (min)	Diametral Strain: Away from Fracture Ratio	Extensometer Measurements ksi (MPa): Elastic Limit	Extensometer Measurements ksi (MPa): 0.2% Offset Yield Stress	Regression Analysis $\sigma_{true}(psi) = k\varepsilon_{true}^{n}$: n	Regression Analysis: ln k	Regression Analysis: Standard Deviation (log cycles)
25	77	0.16	51.2 (42.0)	1.2	17.6 (14.8)	1.2	25.5 (176)	44.0 (303)	0.209	11.77	0.17
		0.004	44.8 (38.7)	1.2	12.9 (9.7)	1.3	24.1 (166)	45.9 (317)	0.244	11.91	0.21
		0.0004	48.0 (41.2)	1.2	12.8 (10.4)	1.2	21.4 (146)	37.7 (260)	0.256	11.91	0.22
482	900	0.16	41.2 (31.2)	1.3	9.6 (6.8)	1.4	15.9 (110)	27.3 (188)	0.176	11.27	0.08
		0.004	38.7 (35.5)	1.1	12.1 (10.5)	1.2	18.4 (127)	26.5 (183)	0.195	11.40	0.09
		0.0004	39.4 (31.3)	1.3	13.0 (8.4)	1.5	10.3 (71)–21.6 (149)[a]	28.2 (194)	0.194	11.35	0.10
593	1100	0.16	45.2 (38.0)	1.2	12.4 (9.6)	1.3	14.0 (96.5)	24.4 (168)	0.179	11.19	0.08
		0.004	35.1 (30.2)	1.2	14.9 (10.5)	1.4	14.9 (103)	26.0 (179)	0.168	11.15	0.06
		0.0004	41.9 (36.2)	1.2	25.8 (17.8)	1.4	15.7 (108)	26.4 (182)	0.120	10.91	0.03
649	1200	0.16	45.1 (31.4)	1.4	13.0 (9.8)	1.3	12.2 (84)	23.6 (163)	0.170	11.06	0.07
		0.004	38.7 (31.0)	1.2	20.2 (15.3)	1.3	<20.7 (143)[b]	26.6 (183)	0.126	10.90	0.03
		0.0004	45.7 (36.8)	1.2	18.1 (13.4)	1.3	16.1 (111)	25.0 (172)	0.077	10.58	0.006

[a]Stress-strain graph could have been interpreted to yield values in this range.

[b]Electronic difficulties experienced during early part of test.

Table 5.24. Tensile Data at 649°C (1200°F) for Type 16-8-2 Longitudinal All-Weld-Metal Specimens From Manual Gas Tungsten-Arc Welds

Weld	Strain Rate (min^{-1})	Strength, ksi (MPa)		Elongation, %		
		0.2% Offset Yield	Ultimate Tensile	Uniform	Total	Reduction of Area (%)
V-03, V-04	0.04	31.7 (219)	44.5 (307)	17.5	26.4	66.5
V-03, V-04	0.04	30.7 (212)	43.2 (298)	17.2	26.8	64.6
V-32 to V-36	0.04	36.5 (252)	46.4 (320)	12.2	20.1	58.7
V-32 to V-36	0.04	35.1 (242)	48.0 (331)	19.4	30.3	60.8
V-46	0.04	36.8 (254)	47.6 (328)	12.3	19.3	63.8
V-55, V-56	0.04	41.0 (293)	48.9 (337)	5.3	12.2	62.5
V-57, V-58	0.04	42.9 (296)	51.2 (353)	6	13.1	67.4
V-90	0.004	32.6 (225)	36.3 (250)	7.5	20.0	64.0

temperature control was maintained as for the threaded-end specimens, but loading was accomplished by one of three techniques: manual step-loading, loading with a screwjack, or using a pneumatic device.

The creep strain data are summarized in Tables 5.25 and 5.26 for the manual and automatic welds, respectively. The reported strains to the end of first-stage creep and second-stage creep were obtained manually as points of deviation of the strain-time curve from straight lines drawn through the linear (minimum creep rate) portions of the individual curves; neither they nor the strain at the onset of tertiary creep by the 0.2% offset method includes loading strains. Reduction of area and total strain to failure were derived from post-test measurements.

Tables 5.27 and 5.28 summarize the times to various events, based on creep strain. However, since the loading strains were measured accurately for threaded-end specimens from automatic welds V-66 to V-74, the times to 0.5, 1.0, and 2.0% total strain are also included for these welds. The loading strains generally tend to agree with the measured strains from tensile tests at the test temperatures and given loads.

Finally, a diamond-pyramid hardness traverse at 1 kg load was run up the center of the weld from the root pass to the top surface of the weld. The hardness data are shown in Fig. 5.30. The root pass region is somewhat harder than the top surface region, but the data exhibit a great deal of scatter. Spot checks on other automatic welds from the V-66 to V-74 series confirm these trends. Several hardnesses measurements were made in both base metal and weld metal near the fusion line; they failed to reveal any significant hardness gradient across the fusion line. A hardness traverse was run through the heat-affected zone and weld metal in the root pass at a distance of 1.5 mm from the bottom of the plate; no significant hardness gradients occurred over a distance of about 5 mm.

5.3.1.3 Discussion

The ASME Boiler and Pressure Vessel Code[23,24] presently does not give properties or allowable stresses for weld metal. However, it is generally recognized that for many applications at elevated temperatures where creep occurs, the local stresses and strains in weldments can be

Table 5.25. Creep Deformation Data for Type 16-8-2 Weld Metal, Welds V-65 to V-74

Welds	Stress (ksi)	Stress (MPa)	Strain, % First Stage	Strain, % First and Second Stage	Strain, % 0.2% Offset Third Stage	Strain, % Total at Failure	Reduction of Area (%)	Minimum Creep Rate (%/hr)
V-03, V-04	25.0	172	0.2	0.4	0.85	24.9	64.7	1.5×10^{-2}
	25.0	172	0.2	0.75	1.3	30.0	60.7	4.2×10^{-2}
	22.0	152	<0.3[a]	0.3[a]	1.2	25.6	69.7	2.1×10^{-3}
	22.0	152	0.2	1.2	1.5	36.0	56.3	1.0×10^{-2}
	20.0	138	0.2	0.7	1.0	27.0	65.6	2.6×10^{-4}
V-32 to V-35	25.0	172	0.15	0.5	0.8	27.6	60.4	1.0×10^{-2}
	22.0	152	0.1	0.65	1.2	10.5	29.0	1.4×10^{-2}
	22.0	152	0.1[a]	0.5	1.2	33.2	54.7	1.1×10^{-2}
	20.0	138	0.1[a]	0.65	1.35	9.8	21.3	6.1×10^{-3}
V-46	25.0	172	0.5	2.0	2.5	29.6	47.7	8.0×10^{-3}
	22.0	152	0.25	0.75	1.1	21.6	53.6	3.0×10^{-3}
	20.0	138	0.5	1.3	1.75	21.7	56.3	2.8×10^{-3}
V-55	28.0	193	0.25	0.55	0.95	12.5	50.6	3.3×10^{-3}
	25.0	172	0.15	0.55	0.8	11.9	55.6	1.0×10^{-3}
	22.0	152	0.45	1.05	1.25	8.25	14.6	4.8×10^{-4}
V-57, V-58	28.0	193	0.1	0.7	1.1	22.0	51.6	2.3×10^{-2}
	25.0	172	0.6	1.0	1.4	16.6	64.5	6.2×10^{-3}
	23.5	162	0.2	1.1	1.4	27.6	47.2	3.3×10^{-3}
	22.0	152	0.5	0.75	1.2	14.9	48.8	2.7×10^{-3}
	21.0	145	0.3	0.7	1.25	10.9	27.4	8.2×10^{-4}
V-90	25.0	172	0.1	0.7	1.2	25.6	67.8	4.7×10^{-2}
	20.0	138	<0.2[a]	1.2	1.9[a]	34.4	73.0	1.6×10^{-2}
	18.0	124	0.02	0.8	1.0	43.7	54.8	2.5×10^{-3}

[a]Result of uncertain accuracy.

Table 5.26. Creep Deformation Data for Type 16-8-2 Weld Metal, Welds V-66 to V-74

Stress (ksi)	Stress (MPa)	Strain, % Loading	First Stage	First and Second Stage	0.2% Offset Third Stage	Total at Failure	Reduction of Area (%)	Minimum Creep Rate (%/hr)
				Tests at 482°C (900°F)				
55.0	379	15.0	~0.12	1.7	2.86	40.7	53.1	1.8×10^{-3}
40.0[a]	345	7.8	1.3	>1.5	>1.5	>9.3		$\sim 4.4 \times 10^{-5}$
45.0[a,b]	310	5.2	>1.37	>1.37	>1.37	>6.57		1.2×10^{-4}
				Tests at 593°C (1100°F)				
35.0	241	2.78	3.0	7.8	9.1	60.5	63.9	2.1×10^{-1}
30.0	207	0.45	1.7	4.07	5.47	42.5	52.6	2.1×10^{-2}
25.0	172	0.24	1.12	1.47	1.98	10.9	8.2	2.6×10^{-4}
22.5[a]	155	>0.17	0.62	>1.17	>1.17	>1.34		1.1×10^{-4}
				Tests at 649°C (1200°F)				
25.0	172	0.35	0.6	~11	~11	62.9	54.0	2.1×10^{-1}
20.0	138	0.125	0.08	1.08	1.6	47.6	44.8	4.55×10^{-3}
18.0	124	0.085	0.23	0.68	1.14	29.8	37.1	1.25×10^{-3}
16.0[a]	110	0.066	0.13	0.25	0.61	>2.86		1.2×10^{-4}

[a]Test still in progress; total strain to date is given rather than total strain to failure.

[b]Unexplained 3.2% strain increment at about 2350 hr not included in this analysis.

Table 5.27. Creep-Time Data for Type 16-8-2 Weld Metal at 649°C (1200°F)

Welds	Stress (ksi)	Stress (MPa)	Time, hr, to Various Events: End First Stage	End Second Stage	0.2% Offset Third Stage	Fracture	0.5% Creep Strain	1% Creep Strain	2% Creep Strain
V-03, V-04	25.0	172	2	17.5	32	114.7	22	34	48
	25.0	172	2	10	16	113.2	6	12	25
	22.0	152	<50[a]	95	210	531.8	12	150	275
	22.0	152	5	100	125	256.8	25	75	140
	20.0	138	100	1400	1640	2590.6	880	1640	1900
V-32 to V-35	25.0	172	1	32	50	241.0	32	55	82
	22.0	152	3	40	70	230.5	30	60	100
	22.0	152	2	40	85	406.1	40	80	115
	20.0	138	2	90	170	432.2	65	137	220
V-46	25.0	172	5	36	45	190.4	5	20	40
	22.0	152	25	175	240	804.2	100	230	355
	20.0	138	30	320	400	1339.3	30	200	440
V-55	28.0	193	17.5	100	180	358.5	90	190	255
	25.0	172	35	385	450	791.6	375	500	600
	22.0	152	50	1500	1750	3204.9	300	1390	2300
V-57, V-58	28.0	193	1.0	25	36	126.9	18	17	52
	25.0	172	17	75	107	328.5	11	75	145
	23.5	162	15	290	340	843.9	125	265	400
	22.0	152	30	200	310	817.7	120	260	420
	21.0	145	60	500	800	1775.4	250	725	1110
V-90	25.0	172	1	10	16	97.1	7.5	14	24
	20.0	138	<2[a]	75[a]	100[a]	431.8	35	60	110
	18.0	124	0.1[a]	100[a]	150	1204.0	80	150	250

[a]Result of uncertain accuracy.

Table 5.28. Creep-Time Data for Type 16-8-2 Weld Metal, Welds V-66 to V-74

Stress (ksi)	Stress (MPa)	Time, hr, to Various Events: End First Stage	End Second Stage	0.2% Offset Third Stage	Fracture	0.5% Creep Strain	1% Creep Strain	2% Creep Strain	0.5% Total Strain	1% Total Strain	2% Total Strain
					Tests at 482°C (900°F)						
55.0	379	∿2	800	1300	2047.1	200	450	970	∿0	∿0	∿0
50.0[a]	345	2000	>6539	>6539	>6539	∿2000	>6539	>6539	∿0	∿0	∿0
45.0[a]	310	>6700	>6700	>6700	>6700	∿2100	∿6140	>6700	∿0	∿0	∿0
					Tests at 593°C(1100°F)						
35.0	241	10	33	39	91.6	0.8	2.5	6.5	∿0	∿0	∿0
30.0	207	25	138	190	563.3	0.1	7	40	6	17.5	62
25.0	172	900	2100	3400	5600.0	23	246	2830	100	580	3450
22.5[a]	155	1500	>6346	>6346	>6346	700	5040	>6346	180	3340	>6346
					Tests at 649°C (1200°F)						
25.0	172	1	∿50	∿50	104.3	0.1	1	6	0.8	2	8
20.0	138	2	190	225	765.6	50	180	263	49	65	255
18.0	124	20	300	500	1703.2	175	440	685	110	405	675
16.0[a]	110	50	1000	2320	>4016	2030	2940	3670	1830	2940	3620

[a]Test still in progress.

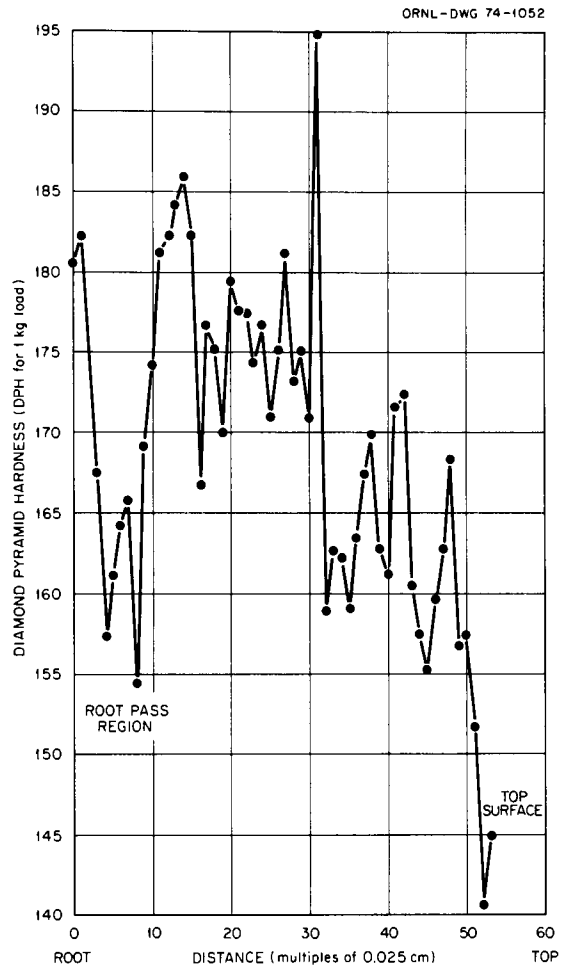

Fig. 5.30. Diamond Pyramid Hardness Traverse Through 16-8-2 Weld.

minimized by close matching of the mechanical and physical properties of the weld metal and base metal. For this reason, it is useful to make such comparisons, even though simply matching the uniaxial tensile and creep properties of all-weld-metal specimens to those of base metal does not assure satisfactory mechanical performance of a weldment in service. Other important considerations include the ductility of the weld metal, anisotropy effects, and concomitant resolution of how much of the total strain that a material can undergo in a uniaxial test should be considered as useful strain for design purposes.

5.3.1.3.1 Tensile and Creep Properties of Type 16-8-2 Weld Metal. The basic tensile data at 649°C (1200°F) for all welds (Tables 5.22 and 5.24) exhibit considerable scatter, which must be attributed to the

numerous variables of materials, welding parameters, and testing methods; without more data, comparisons of tensile properties between these welds are not advisable. The total tensile elongations all exceed 12%, and the uniform strains are all greater than 5%, while reductions of area are greater than 54%. At 649°C (1200°F) and perhaps at 593°C (1100°F), the ultimate tensile strength of automatically deposited weld metal from welds V-66 to V-74 appears to be sensitive to strain rate, and it decreases with decreasing strain rate.

The rules for deriving time-independent allowable stresses for austenitic stainless steel base metal for the design of Class 1 components of nuclear power stations are given by the ASME Boiler and Pressure Vessel Code.[23,24] The time-independant allowable stresses are fixed fractions of the minimum expected yield and ultimate strengths of base metal as a function of temperature. Although there are no rules at present for deriving allowable stresses for weld metal, the rules for base metal were applied to the data from 0.004/min-strain-rate tensile tests on type 16-8-2 filler metal (see Table 5.29). With one exception, the derived allowable stresses for weld metal exceeded those for type 316 stainless steel base metal. The exception results from the ultimate tensile strength of welds V-66 to V-74 and V-90 being less than the

Table 5.29. Derived Allowable Stresses for 16-8-2 Filler Metal Based on 0.004/min Strain Rate Tensile Tests

Temperature (°C)	Temperature (°F)	Weld	16-8-2 Derived Allowable Stress, ksi (MPa), Based on: Yield Stress	16-8-2 Derived Allowable Stress, ksi (MPa), Based on: Ultimate Stress	Allowable Stress, ksi (MPa), for Type 316 Stainless Steel
25	77	V-66 to V-74	36.3 (250)	37.3 (257)	30.0 (207)
482	900	V-66 to V-74	26.3 (181)	22.5 (155)	15.7 (108)
593	1100	V-66 to V-74	23.6 (163)	17.0 (117)	14.7 (101)
649	1200	V-66 to V-74	23.1 (159)	13.8 (95)	14.5 (100)
		V-90	29.3 (202)	13.3 (92)	

minimum expected ultimate tensile strength of type 316 stainless steel base metal at 649°C (1200°F). (Because of the observed strain-rate effect, data from 0.04/min tests on other welds were not considered.) This finding might prove to be important if allowable stresses for welds were set in the future by the same rules used for base metal.

The creep data given in Tables 5.25 through 5.28 are relatively comprehensive. They are provided to assist individuals who might attempt to set time-dependent allowable stresses for weld metal. It is not clear at this time that the rules for deriving time-dependent allowable stresses for base metal[24] are appropriate for weld metal.

A convenient means for comparing the creep-rupture properties of type 16-8-2 weld metal with those of base metal is the Larson-Miller parameter, $(T + 460) \times (20 + \log_{10} t_r)$, where $(T + 460)$ is absolute temperature (Rankine) and t_r is rupture time (hours). Average rupture times from Blackburn's analysis[25] for type 316 stainless steel are plotted against the Larson-Miller parameter in Fig. 5.31. Curves have also been drawn at ±1.645 standard deviations (σ) to estimate the range of rupture time values that might be expected for type 316 stainless steel.[25] All these curves are contained in the envelope bounded by (100,000 hr, $+1.645\sigma$) points as an upper limit, and by a combination of (100,000 and 10 hr, -1.645σ) points as a lower limit that was arbitrarily chosen as a basis for comparison in later graphs.

The rupture times for type 16-8-2 longitudinal all-weld-metal specimens from this test program are plotted versus the Larson-Miller parameter in Fig. 5.32, 5.33, and 5.34, together with the envelope described above for type 316 stainless steel. Rupture times at 649°C (1200°F) vary by about an order of magnitude from the weakest weld to the strongest weld. Although the statistical significance of these observations has not been assessed, it is of interest to note that GTA welds V-55 and V-56, which have the highest carbon and phosphorus contents (Table 5.20), consistently have the longest rupture times at 649°C (1200°F), and usually have lowest ductility of these welds. Weld V-90, which has the lowest carbon content and relatively low phosphorous content, has the shortest rupture times and relatively high ductility.

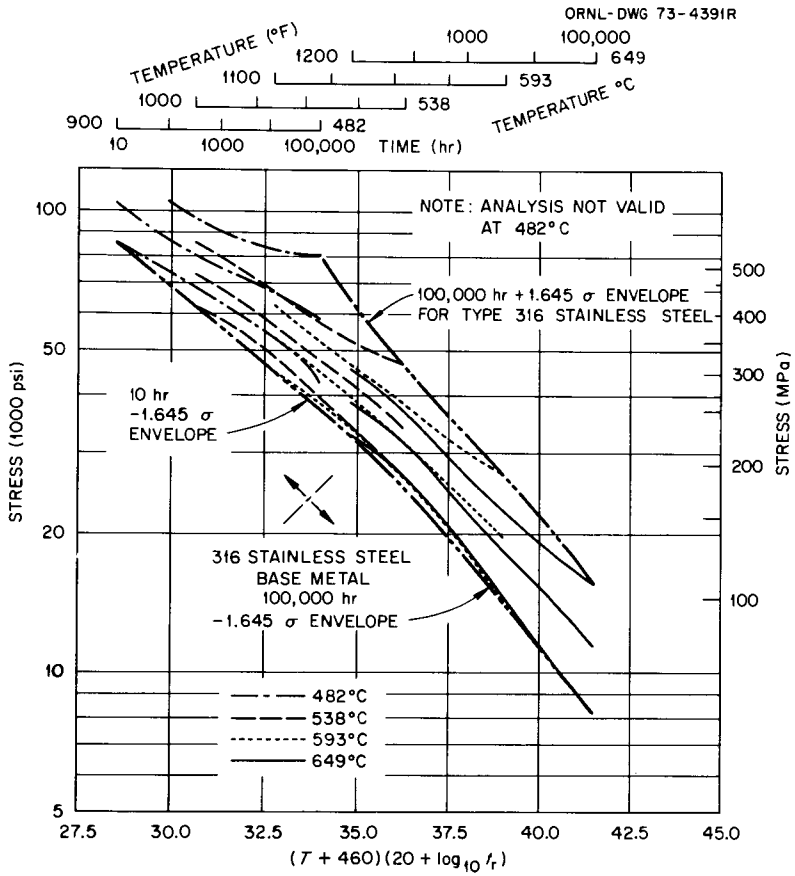

Fig. 5.31. Blackburn's Stress-Rupture Analysis of Type 316 Stainless Steel. Ref: L. D. Blackburn, "Isochronous Stress-Strain Curves for Austenitic Stainless Steels," p. 15 in *Generation of Isochronous Stress-Strain Curves*, A. O. Schafer, ed., American Society of Mechanical Engineers, New York, 1972.

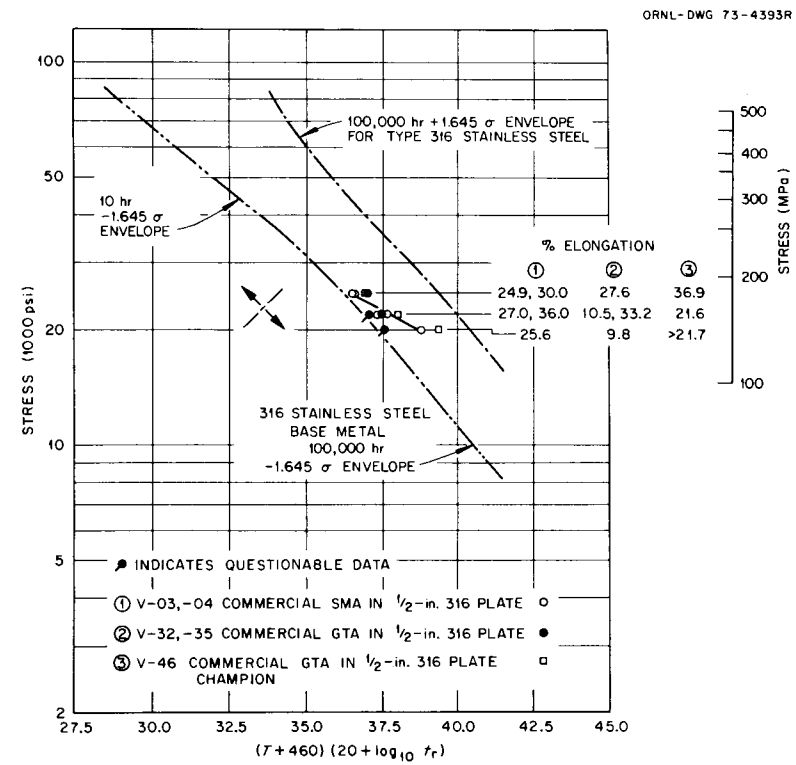

Fig. 5.32. Comparison of Creep-Rupture Properties for Various Shielded Metal-Arc and Gas Tungsten-Arc Welds of 16-8-2 Filler Metal on Type 316 Stainless Steel Base Metal.

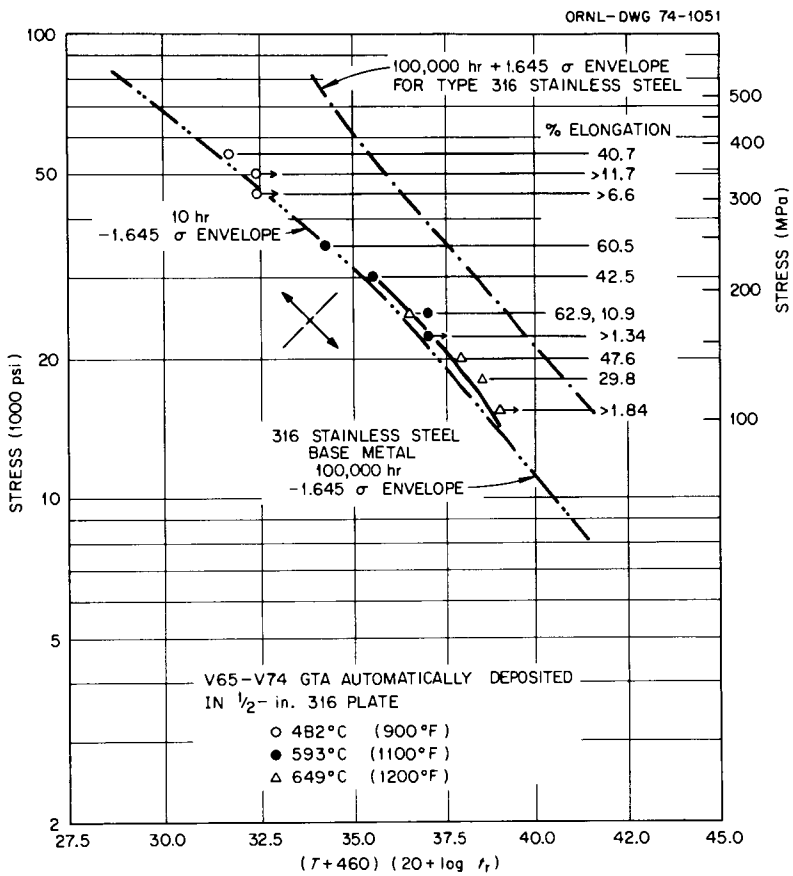

Fig. 5.33. Comparison of Creep-Rupture Data for Automatically Deposited 16-8-2 Weld Metal on Type 316 Stainless Steel Base Metal Properties.

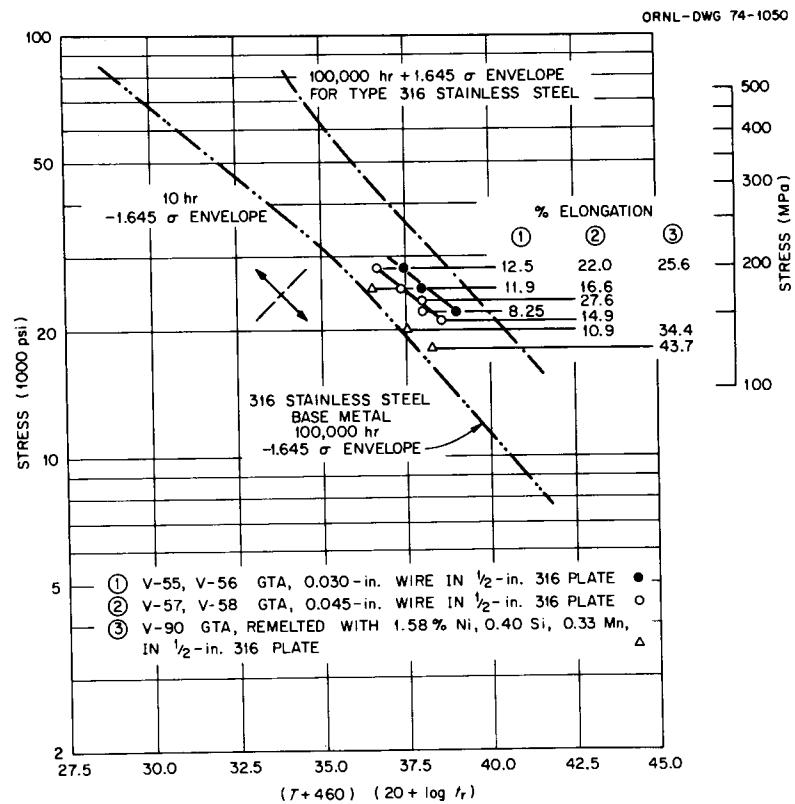

Fig. 5.34. Comparison of Creep-Rupture Properties of 16-8-2 Manual Gas Tungsten-Arc Welds on Type 316 Stainless Steel Plate.

While carbon and phosphorus are known to be potent strengthening agents in certain stainless steel base metals[26] and carbon is important in determining the strength of austenitic filler metal,[27] other factors are also important in determining the strength of these welds, such as concentration of other chemical elements, joint design, welding process, and welding parameters.

Published creep data for as-deposited type 16-8-2 weld metal have been summarized by Voorhees and Freeman[28] (see Fig. 5.35). All the data are for shielded metal-arc (SMA) welds. The data nearly span the arbitrary envelope for type 316 stainless steel base metal, and strain values as low as 2.5% are reported. (The filler metal having "ductility too low to measure" is not typical of current practice, according to the organization that originally reported the data.[29])

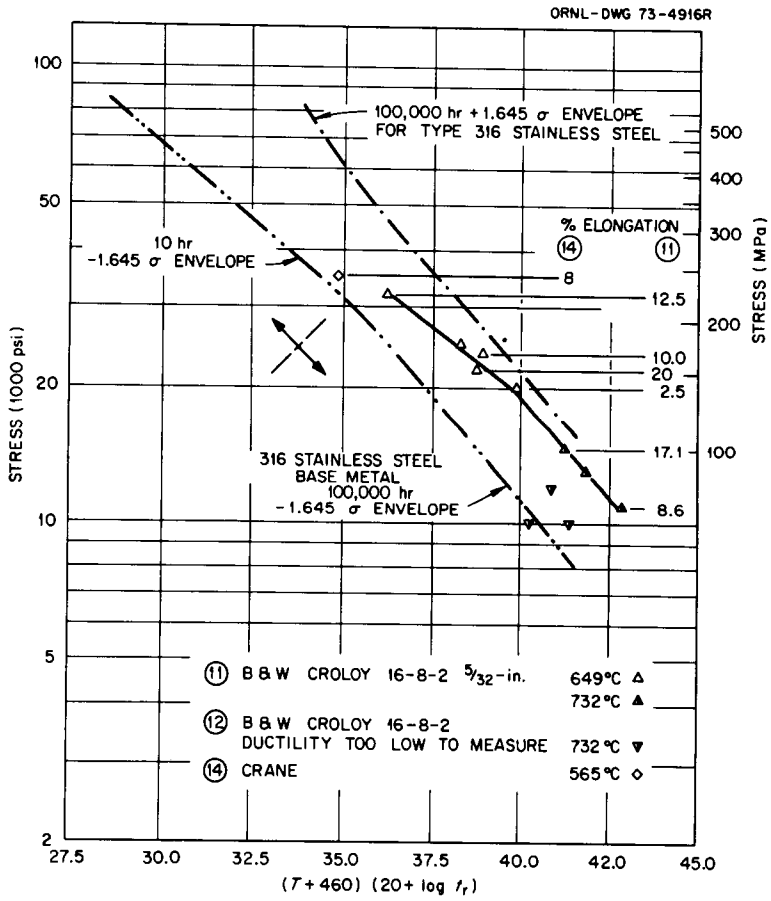

Fig. 5.35. Type 16-8-2 Stainless Steel Shielded Metal Arc-Weld Metal Creep-Rupture Data (As-Welded Condition). Ref: H. R. Voorhees and J. W. Freeman, pp. 126–27 in *The Elevated-Temperature Properties of Weld-Deposited Metal and Weldments, Spec. Tech. Publ.* 226, American Society for Testing Materials, Philadelphia, 1958.

It should be noted that the proposed maximum service temperature of these welds in nuclear power stations is about 649°C (1200°F), and creep effects are recognized[24] in austenitic steels at all temperatures above 427°C (800°F). A need exists for weld metal creep data spanning more of this temperature regime, such as those obtained for welds V-66 to V-74.

Total elongation and reduction of area are universally recognized to be important measures of creep ductility. The lowest total elongation measured in this work was 8.25% (with 14.6% reduction of area, for the "strong" V-55 weld), while the lowest reduction of area was 8.2% (with 10.9% total elongation, for the V-66 to V-74 series specimen that failed under the extensometer indentation on the gage section). However, other strain criteria such as the strain to the onset of tertiary creep by the 0.2% offset method are also important in modern design technology. The creep component of strain before tertiary creep is plotted against the time to the onset of tertiary creep in Fig. 5.36. The creep strains to

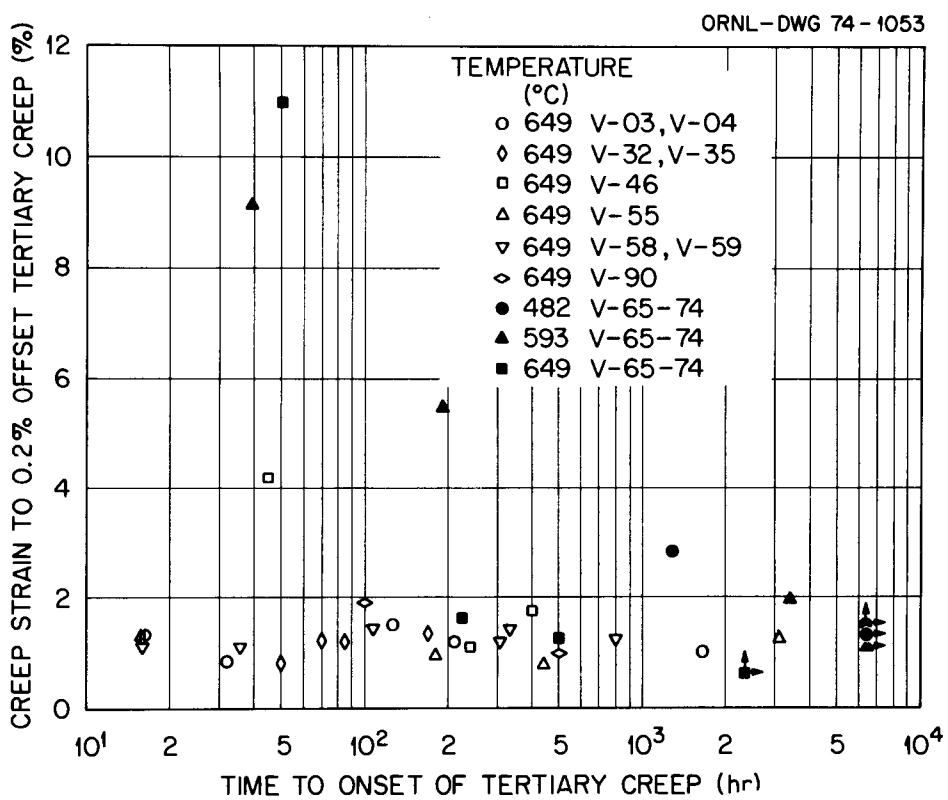

Fig. 5.36. Third-Stage Creep Strains and Times to 0.2% Third-Stage Creep for Type 16-8-2 Weld Deposits.

the onset of tertiary creep tend to be concentrated in the 0.8 to 2% range, although values up to 11% are reported, especially for relatively short-time tests. The fractior of the total test time *not* involved in tertiary creep is plotted against rupture time in Fig. 5.37; values from 0.1 to 0.63 were observed, and the data are quite scattered. While that fraction appears to tend to increase with increasing rupture time, the observation may not be statistically significant. Note that the time to first-stage creep frequently amounts to half the test time before tertiary creep.

Parametric correlations between the minimum creep rate and rupture time have been proposed for other materials; Monkman and Grant[30] suggest that the product of the two should be constant. A log minimum creep rate versus log rupture time plot (Fig. 5.38) exhibits a scatter band with a width of approximately one-third of a log cycle. This observation suggests that the Monkman-Grant hypothesis works reasonably well

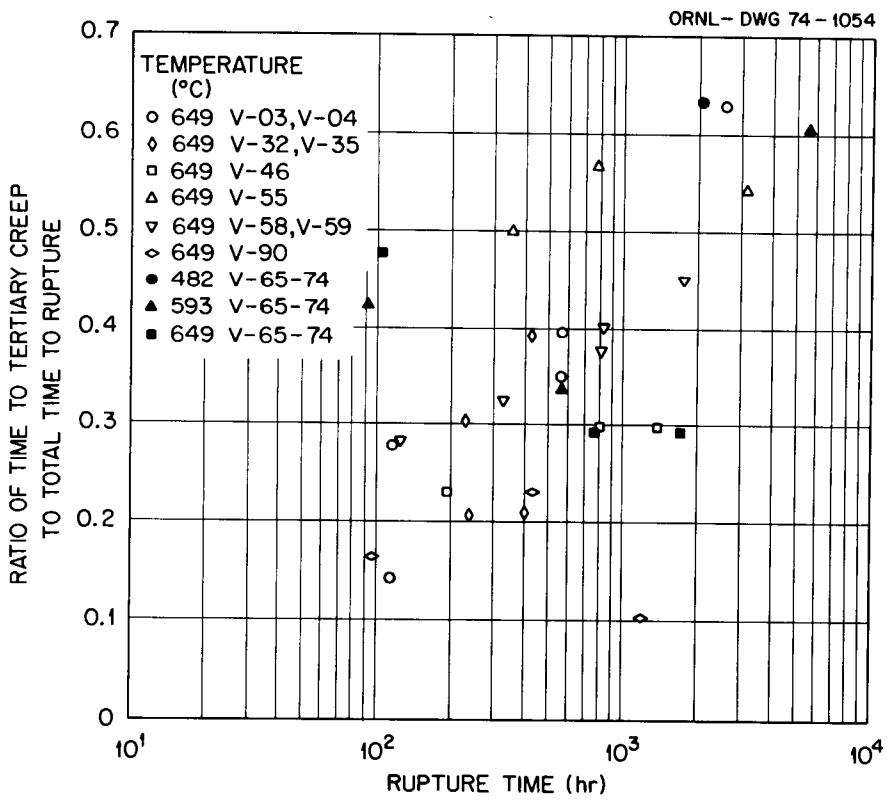

Fig. 5.37. Ratio of Time to 0.2% Offset Third-Stage Creep to Total Time to Rupture, Plotted Against Rupture Time for Type 16-8-2 Welds.

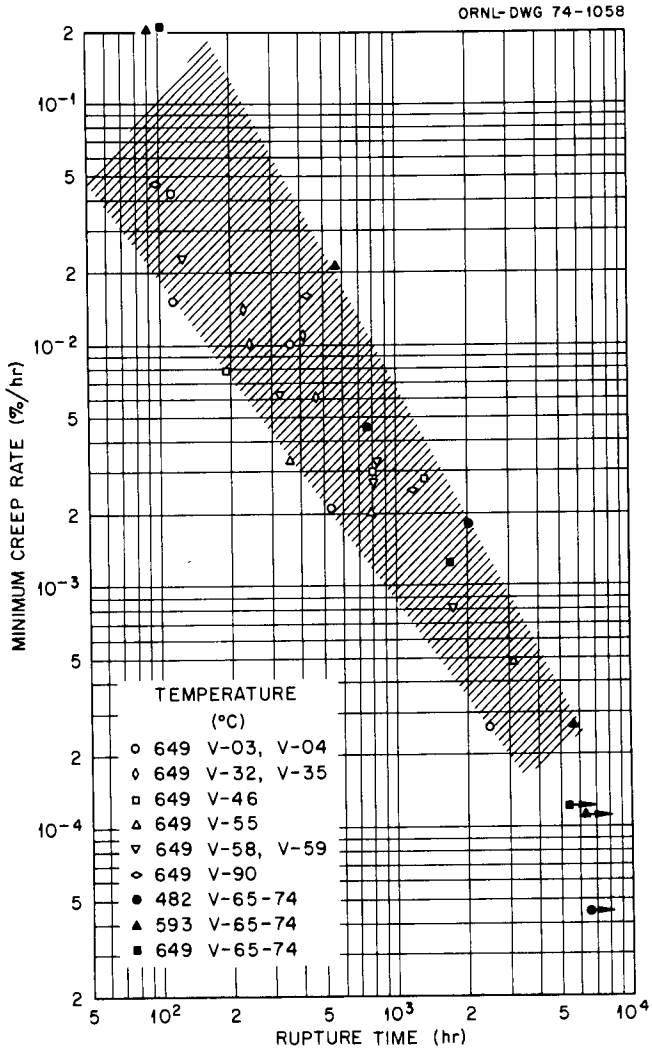

Fig. 5.38. Relation Between Rupture Time and Minimum Strain Rate for Type 16-8-2 Weld Metal.

for type 16-8-2 weld metal for the test conditions investigated. A correlation of rupture time with the average creep rate appears to be equally valid. (See Fig. 5.39).

5.3.1.3.2 Heterogeneity and Anisotropy. The heterogeneous microstructure observed in welds V-66 to V-74 is at least partly the result of the repeated thermal and mechanical cycling that occurred while successive passes of filler metal were being deposited. The first few passes are subjected to more cycles than later passes, but other

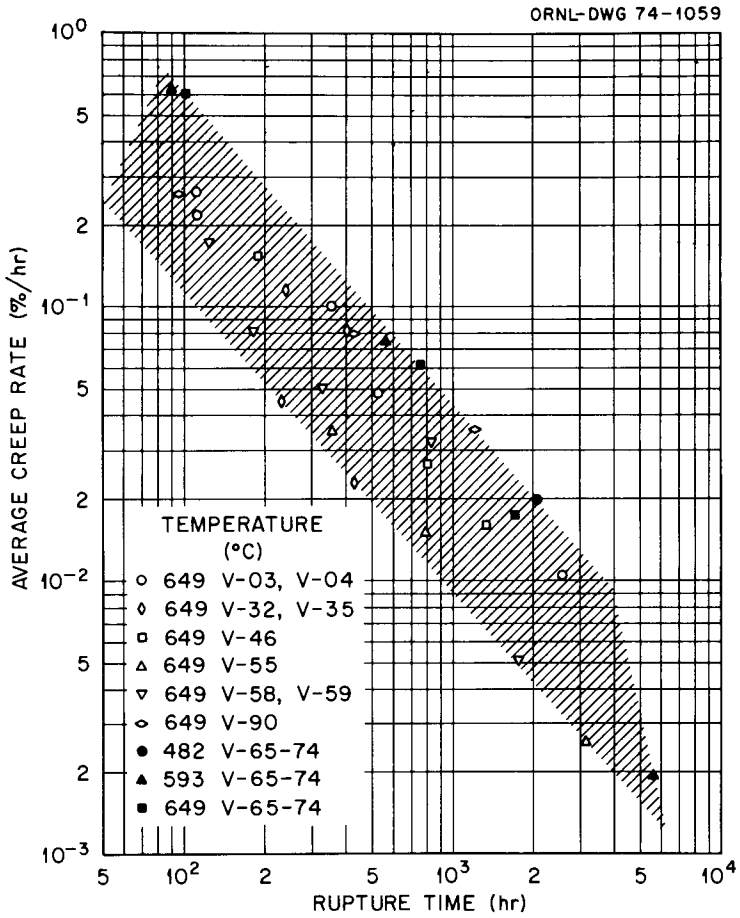

Fig. 5.39. Relation Between Rupture Time and Average Strain Rate (Rupture Time/Strain at Rupture) for Type 16-8-2 Filler Metal.

important differences between the root and surfaces passes occurred. For example, geometric effects and the use of manual welding for root passes can cause different base-metal dilution.

A simple hardness traverse revealed variations in mechanical flow properties from the bottom to the top of the weld (Fig. 5.30). Other austenitic weld metal[21] that exhibited such hardness and structure variations was shown to exhibit significant systematic creep and tensile property variations from the root to surface passes of the weld. This analogy suggests that the type 16-8-2 specimens may not have uniform properties in a specimen cross section, and perhaps that the results of the tests may be affected by the longitudinal all-weld-metal specimen design. The need for further testing to examine this problem is apparent.

Anisotropy of deformation occurred in tensile tests; generally, the greatest diametral contractions occurred in the direction parallel to the solidification growth direction. Similar effects were noted in creep specimens. Uniaxial tests performed on longitudinal, all-weld-metal specimens clearly do not provide adequate characterization for a weldment that may be stressed in other directions in service.

5.3.2 Creep-Rupture Properties of Type 308 Stainless Steel Welds Made With and Without Controlled Residual Elements — R. T. King, G. M. Goodwin, J. O. Stiegler, and E. Bolling

We are investigating the creep-rupture properties of SMA type 308 stainless steel welds made with controlled residual elements (CRE) to simulate the longitudinal seam and girth welds of the FFTF vessel. Testing is also in progress on welds made in the same heat of base metal, at the same shop, and using the same procedures, but using conventional lime-coated electrodes that do not have the CRE composition. The nomenclature of the welds and the deposit analyses have been reported previously.[31] The CRE weld for which data are reported here is a 6:2-2 type weld, while the conventional control weld is a 7:1-1 type weld.

The methods used to prepare longitudinal all-weld-metal specimens with a 6.35-mm-diam × 31.75-mm-long gage section have been described previously, as have the testing procedures.[32] We have conducted creep tests at 593 and 649°C (1100 and 1200°F) on specimens cut from the near-surface region (L1 specimens) and from an intermediate position (L2 specimens), but control specimens from the root pass (L3) region have not yet been tested.

The data are presented graphically in Fig. 5.40. At 593°C (1100°F), two L1 control specimens have been tested. Although the rupture times for these control specimens are about one-third to one-sixth those for comparable specimens of CRE weld metal, the measured total elongations cannot be considered significantly different from the CRE weld metal.

At 649°C, both L1 and L2 control specimens without CRE have been tested. The control specimens exhibit rupture times that are about one-tenth those of comparable CRE weld metal specimens. For both

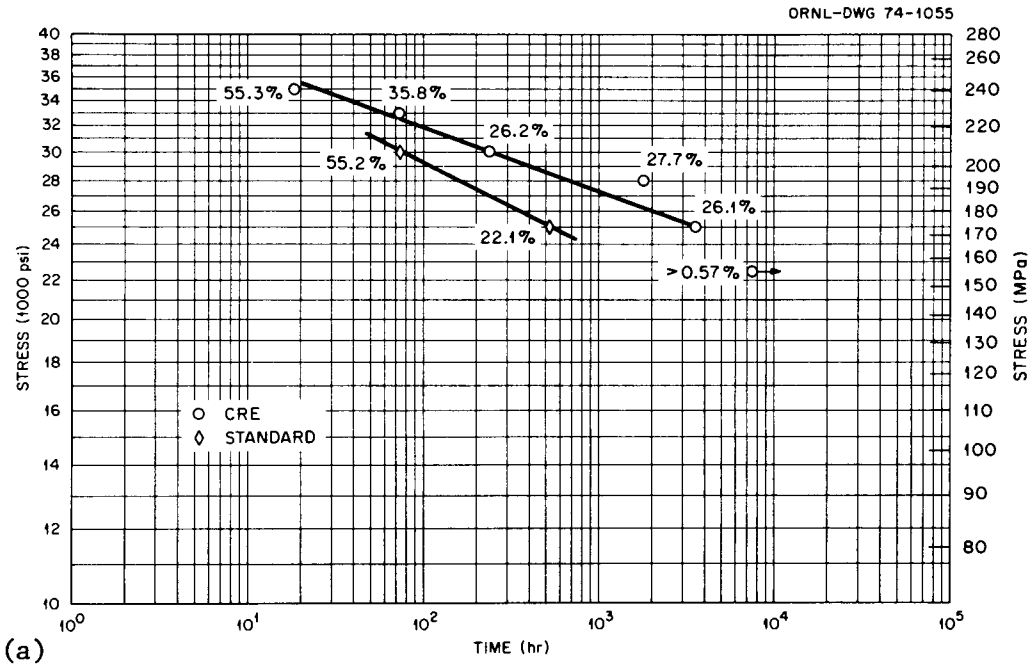

(a)

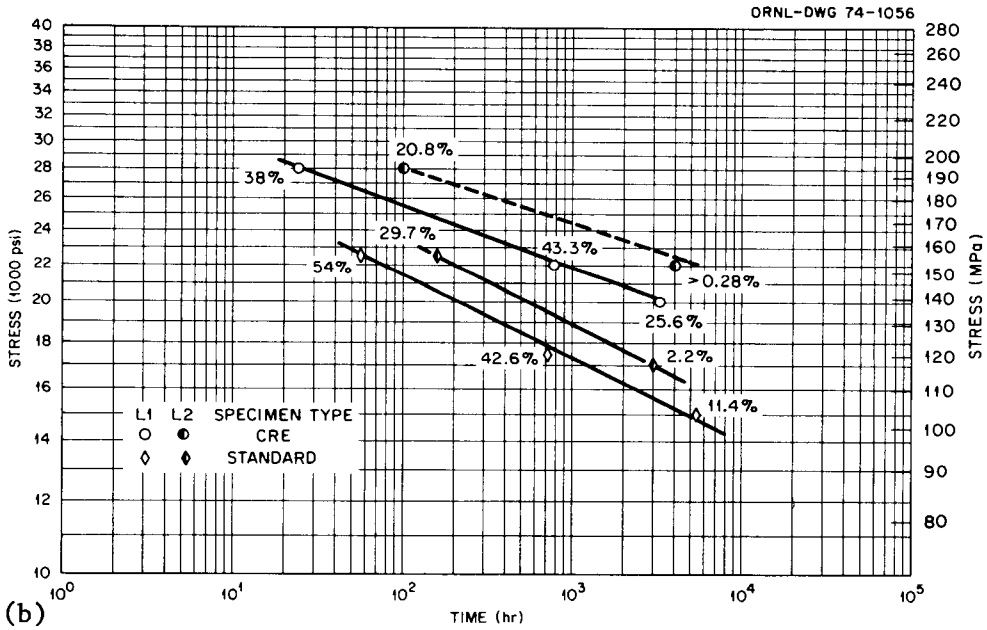

(b)

Fig. 5.40. Stress-Rupture Behavior of Standard and CRE Shielded Metal Arc Type 308 Stainless Steel Longitudinal Arc-Weld-Metal Specimens [2 3/8-in.-thick (60-mm) Plate Welds]. (a) At 593°C (1100°F). (b) At 649°C (1200°F).

L1 and L2 control specimens, the total elongation decreases with increasing rupture time. The lowest total elongation for an L2 specimen was 11.4%, while the lowest total elongation for an L1 specimen was 2.2%.

The L1 control specimen that failed at 649°C after straining 2.2% ruptured at the point on the gage section where an extensometer had been attached. The gage section had been indented and deformed sharply at that point to assure that the extensometer was firmly attached. Scanning electron microscopy showed that the fracture morphology was similar to that previously associated with interphase cracking along austenite-sigma phase boundaries and low ductility in austenitic weld metal.[33] One half of the fractured specimen was sectioned, polished, and etched to reveal the microstructure under the extensometer indentation and in other areas of the gage section. Under the indentation in the mechanically worked area, Fig. 5.41(a) shows that extensive sigma phase formation had occurred and that internal separations at austenite-sigma phase boundaries oriented transverse to the tensile axis appeared to extend and form cracks joining the sigma phase particles. The other regions away from both the final fracture surface and the extensometer indentation, less sigma phase and no internal cracking were observed. We are presently examining failed CRE weld metal specimens to determine whether extensive sigma phase formation under extensometer indentations can be found in that material.

5.4 MECHANICAL PROPERTIES OF STEAM GENERATOR MATERIALS — W. R. Martin

5.4.1 Mechanical Properties of 2 1/4 Cr-1 Mo Steel for Design — R. L. Klueh

The objective of the mechanical property tests now under way on 2 1/4 Cr-1 Mo steel is the determination of exact experimental properties that are needed for use in the elastic and inelastic analyses required to design the steam generator for the LMFBR demonstration plant. Unless otherwise specified, the tests are conducted on specimens taken from a 1-in. (25-mm) plate of 2 1/4 Cr-1 Mo steel obtained from Babcock & Wilcox (Heat 20017); the chemical composition of this heat is given in Table 5.30. Present plans call for tests on 2 1/4 Cr-1 Mo steel in the two most commonly used heat treatments: annealed, and normalized and tempered; the definitions

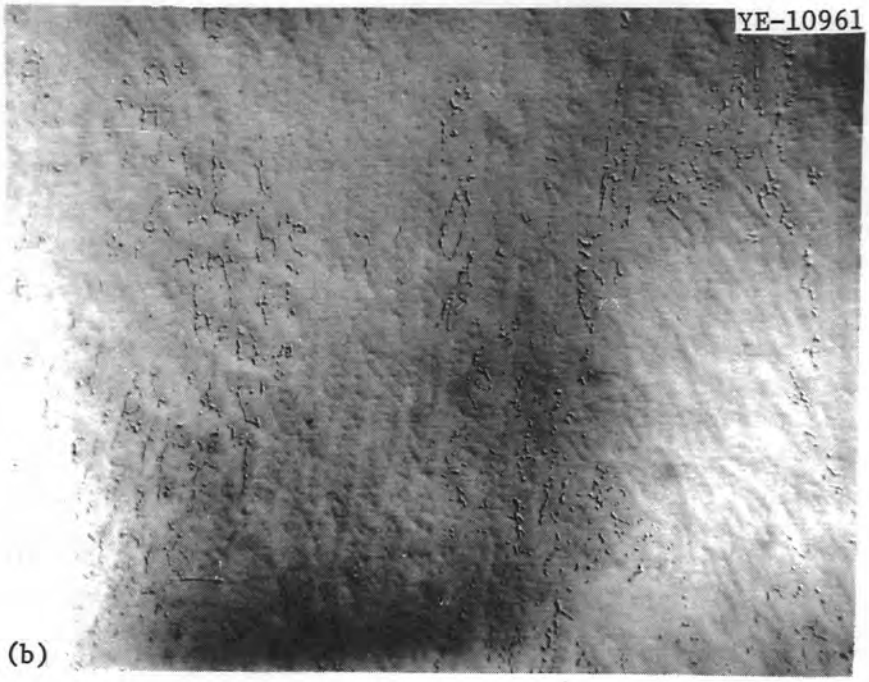

Fig. 5.41. Conventional Type 308 Stainless Steel Weld Metal, Creep Tested at 649°C and 117 MPa (17 ksi) Stress. 150×. (a) Region under extensometer indentation, showing finely dispersed sigma phase and internal separations. (b) Region away from extensometer indentation, with less sigma phase and no internal separations.

Table 5.30. Information on 1-in. (25-mm) Plate of 2 1/4 Cr-1 Mo Steel (Heat 20017) to be Used for Mechanical Property Tests

Analysis	Chemical Composition, wt %							
	C	Mn	Si	Cr	Mo	Ni	S	P
Vendor	0.11	0.55	0.29	2.13	0.90		0.014	0.011
ORNL	0.135	0.57	0.37	2.2	0.92	0.16	0.016	0.012

Heat Treating Definitions

Annealed (full anneal): 1 hr 927°C (1700°F), then furnace cooled at ∿50°C/hr (90°F/hr)

Normalized: 1 hr at 927°C (1700°F), then air cooled

Normalized and Tempered: After normalization, 1 hr at 704°C (1300°F), then air cooled

of these heat-treating terms, as used here, are also given in Table 5.30. As heat-treated, the microstructures are a proeutectoid ferrite with a fine pearlite and a tempered bainite for the annealed and normalized-and-tempered steels, respectively. It should be pointed out that the term "annealed," as commonly used, leaves a lot to be desired.[34] A vendor specification that a steel is in the "annealed" or "fully annealed" condition generally implies that the steel was slowly cooled (furnace cooled) from the austenitizing temperature. Although the cooling rate can affect the properties, it is rarely specified.

5.4.1.1 Tensile Properties

The uniaxial tensile test matrices for both the annealed and normalized-and-tempered steels are the same. For the steel in each of the heat-treated conditions, the matrix consists of 16 tests at each of the temperatures 25, 204, 371, 454, 510, 538, 565, and 593°C (77, 400, 700, 850, 950, 1000, 1050, and 1100°C). At each temperature, four tests will be run for each condition at each of the strain rates 0.0004, 0.004, 0.025, and 0.25/min.

Results to date — one set of tests at 0.04/min for each condition — are given in Table 5.31. Figure 5.42 shows the stress-strain diagrams determined from an extensometer on the gage section out to 5% strain.

Table 5.31. Tensile Properties[a] of 2 1/4 Cr-1 Mo Steel

Temperature		Estimated Static Modulus		Proportional Limit		0.2% Yield Stress		Ultimate Tensile Stress		Fracture Stress		Elongation		Reduction of Area (%)
(°C)	(°F)	(psi)	(GPa)	(ksi)	(MPa)	(ksi)	(MPa)	(ksi)	(MPa)	(ksi)	(MPa)	Uniform (%)	Total (%)	
						Annealed								
25	77	31.9×10^6	220	16.2	112	36.9	254	74.1	511	44.2	305	12.8	29.2	73.2
95	203	28.3	195	20.4	141	34.3	237	68.3	471	41.7	288	12.6	28.6	73.4
204	400	25.3	174	23.3	161	31.2	215	63.8	440	40.0	276	12.2	26.8	72.3
316	600	20.3	140	16.2	112	32.7	226	69.8	481	48.6	335	9.2	19.8	66.8
371	700	18.3	126	20.4	141	33.7	232	73.5	507	51.9	358	10.1	20.9	59.9
454	850	24.5	169	18.3	126	31.0	214	67.3	464	38.6	260	10.0	23.0	64.6
510	950	24.6	170	15.4	106	29.9	206	59.6	411	28.8	199	8.2	26.3	77.3
565	1049	22.9	158	15.8	109	28.7	198	49.5	341	16.2	112	8.3	41.8	86.2
						Normalized and Tempered								
25	77	24.8×10^6	171	71.2	491	82.0	565	99.4	685	53.1	366	7.4	21.8	75.7
95	203	32.4	223	55.8	385	78.3	540	94.0	648	52.8	364	7.2	19.8	75.4
204	400	30.1	208	64.7	446	75.1	518	91.4	630	55.5	383	6.8	18.5	72.9
316	600	29.9	206	42.0	290	71.4	492	91.9	634	55.7	384	6.5	18.9	70.2
371	700	29.0	200	40.7	281	71.3	492	90.7	625	53.4	368	6.4	18.4	71.3
454	850	28.4	196	35.6	246	68.2	470	82.4	568	42.7	294	4.8	18.9	74.1
510	950	23.2	160	34.8	240	59.1	408	71.9	496	30.3	209	4.7	21.9	79.7
565	1049	19.3	133	33.0	228	57.3	395	62.4	430	20.3	193	1.7	31.4	85.3

[a]Tested at strain rate of 0.04/min.

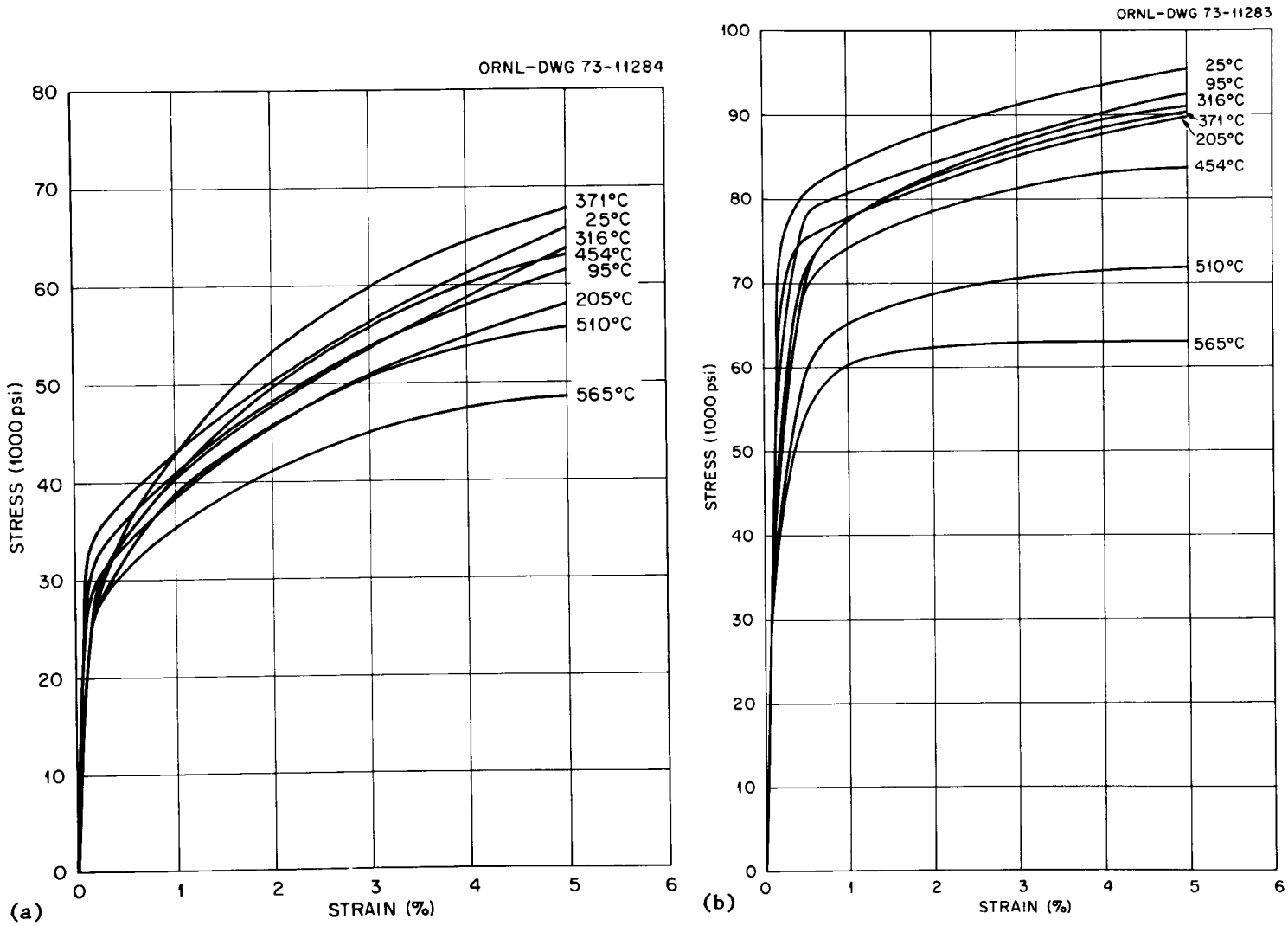

Fig. 5.42. Tensile Curves for 2 1/4 Cr-1 Mo Steel Over the Range 25 to 565°C (77 to 1050°F). (a) Annealed. (b) Normalized and tempered.

Where possible, an analytical expression best describing the material behavior will be determined.

5.4.1.2 Creep Properties

Uniaxial creep tests under varying conditions of stress and loading rate over the range 371 to 593°C in air are planned for 2 1/4 Cr-1 Mo steel as annealed and normalized and tempered. These include: (1) constant-load short-term tests (out to 1% strain or 1000 hr), (2) constant-load long-term tests (out to 50,000 hr), (3) constant-load compressive tests, and (4) constant-stress tests (both tensile and compressive). From these tests, precise base-line data are to be obtained for stresses of interest to the steam generator. These data will be used to develop the constitutive equations that define the stress-strain-time temperature behavior of the materials.

The short-term creep test matrix for the 2 1/4 Cr-1 Mo steel in the annealed condition is given in Table 5.32. The data collected to date for the annealed steel is shown in Table 5.33. In Fig. 5.43 the strain-time

Table 5.32. Short-Term[a] Tensile Creep Tests for Annealed 2 1/4 Cr-1 Mo Steel (Primary Creep Tests)

Stress		Number of Tests for Each Temperature					
(ksi)	(MPa)	371 700	454 850	510 950	538 1000	565 1050	593°C 1100°F
3	21						1
4	28				1	1	1
6	41				1	1	1
8	55			1	1	1	1
10	69			1	2[b]	1	1
12	83			1	1	1	1
14	97	1	1	1	1	1	
18	124	1	1	1	2[b]		
22	152	1	1	1			

[a]Tests out to 1% strain or 1000 hr.

[b]Two loading rates: $\dot{\varepsilon}$ = 0.0005 and 0.25/min.

Table 5.33. Creep Properties of Annealed 2 1/4 Cr-1 Mo Steel

Temperature (°C)	Temperature (°F)	Stress (psi)	Stress (MPa)	Elongation in 1000 hr (%)	Minimum Creep Rate (%/hr)	Time to 1% Strain (hr[a])
454	850	22,000[b]	152			
		30,000[b]	207			
510	950	10,000[b]	69			
		12,000[b]	83			
		14,000	97	0.072	0.000012	81,000
		18,000	124	0.17	0.000038	23,000
		22,000	152	0.43	0.00013	1,520
565	1050	10,000	69	0.25	0.000043	18,600
		12,000	83	0.27	0.000075	10,600
		14,000	97	0.50	0.00021	3,380
		18,000	124	6.2	0.0055	150

[a]Extrapolated assuming steady-state creep continues to 1% strain.

[b]Tests in progress.

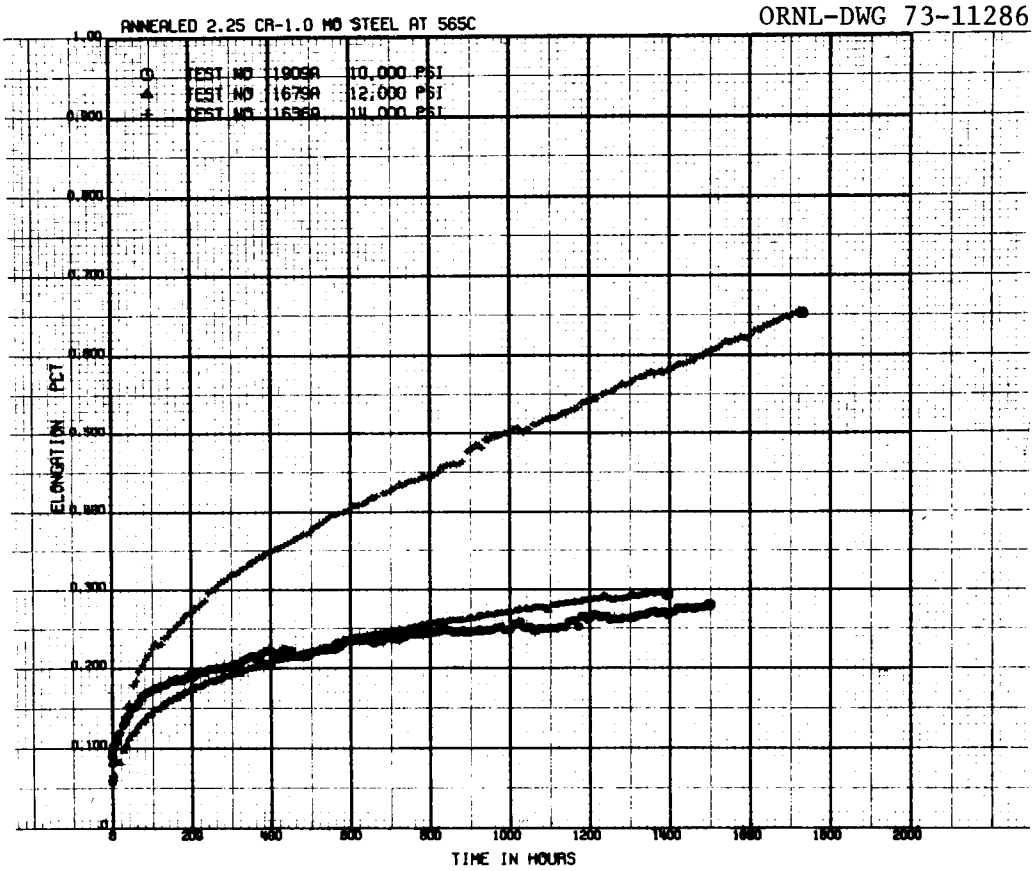

Fig. 5.43. Creep Curves for Annealed 2 1/4 Cr-1 Mo Steel Tested at 565°C to Determine Primary Creep Behavior.

curves are given for the 565°C tests. Creep-rupture tests are also being run for the annealed material, the results to be compared with those previously obtained for the normalized-and-tempered steel.[34]

Table 5.34 gives the test matrix for the normalized-and-tempered steel. The results obtained to date are given in Table 5.35 and Fig. 5.44 shows the strain-time curves for the 565°C tests.

5.4.1.3 Elastic Properties — T. W. Dews* and W. R. Martin

The sonic velocities and moduli of annealed 2 1/4 Cr-1 Mo steel were determined from room temperature to 732°C (1350°F). Measurements were made using two methods, (1) a double-pulse contact pulse-echo technique and (2) a magnetostructive method for generating ultrasound in thin wires.

At room temperature we found that Poisson's ratio was 0.2840, Young's modulus was 31.35×10^6 psi (216.2 GPa), the shear modulus was 12.21×10^6 psi (84.2 GPa), and the bulk modulus was 24.18×10^6 (166.7 GPa).

Values of ratios of moduli at temperature to the value at room temperature are given in Tables 5.36 and 5.37 for runs 1 and 2. These values are now being fitted to an equation for submission to the LMFBR Materials Handbook.

5.4.1.4 Subcritical Crack Growth in 2 1/4 Cr-1 Mo Steel — C. R. Brinkman

Subcritical crack growth studies are presently under way on a single heat of 2 1/4 Cr-1 Mo steel, the prime candidate for the LMFBR steam generator material. Test parameters of concern include temperature (room to 593°C = 1100°F), stress ratio (R), environment (air, steam, helium, vacuum, and OH^-), specimen geometry, heat treatment, and test frequency.

Material for initial investigations was obtained from a commercial heat[34] with a carbon content of 0.135. Wedge-open-loading (WOL) specimens (0.5 in. or 12.7 mm thick) were fabricated from 1-in.-thick (25 mm) plate that had been solution annealed for 1 hr at 927°C (1700°F) and furnace cooled. Center-notched specimens (1/16 in. = 1.6 mm thick) were fabricated and then annealed at 927°C (1700°F) for 1 hr and air cooled.

---

*Y-12 Development Division.

Table 5.34. Short-Term[a] Tensile Creep Tests for Normalized and-Tempered 2 1/4 Cr-1 Mo Steel

Stress		Number of Tests for Each Temperature					
(ksi)	(MPa)	371 700	454 850	510 950	538 1000	565 1050	593°C 1100°F
6	41						1
10	69				1	1	1
14	97				1	1	1
18	124		1	1	2[b]	1	1
22	152		1	1	1	1	
25	172		1	1	1		
30	207		1	1	2[b]		
35	241		1	1			
40	276	1	1				
45	310	1	1				
50	345	1	1				

[a]Tests out to 1% strain or 1000 hr.

[b]Two loading rates: $\dot{\varepsilon}$ = 0.0005 and 0.25/min.

Table 5.35. Creep Properties of Normalized-and-Tempered 2 1/4 Cr-1 Mo Steel

Temperature		Stress		Elongation in 1000 hr (%)	Minimum Creep Rate (%/hr)	Time to 1% Strain (hr[a])
(°C)	(°F)	(psi)	(MPa)			
454	850	25,000[b]	172			
		30,000[b]	207			
		35,000[b]	241			
		40,000[b]	276			
		50,000	345	0.43	0.00013	5,460
510	950	18,000	124	0.19	0.000023	36,200
		25,000	172	0.33	0.000054	13,100
		30,000	207	0.53	0.00016	2,940
565	1050	14,000	97	0.31	0.00011	7,360
		18,000	124	0.52	0.00029	2,660
		20,000	138	0.71	0.00043	1,680

[a]Extrapolated assuming that steady-state creep continues to 1% strain.

[b]Tests in progress.

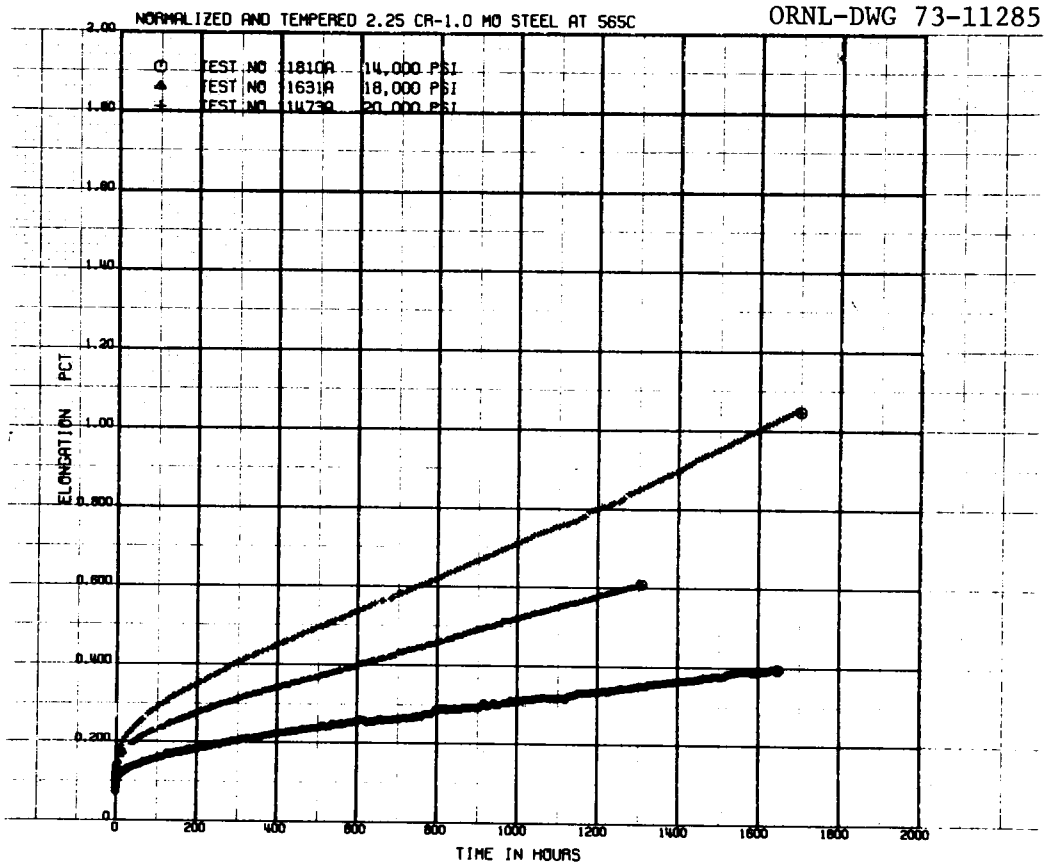

Fig. 5.44. Creep Curves for Normalized-and-Tempered 2 1/4 Cr-1 Mo Steel Tested at 565°C to Determine Primary Creep Behavior.

Table 5.36. Shear Modulus of 2 1/4 Cr-1 Mo Steel

Temperature		Ratio of Modulus at Temperature to Value at 24°C			
		Run 1		Run 2	
(°C)	(°F)	Increasing Temperature	Decreasing Temperature	Increasing Temperature	Decreasing Temperature
24	75	1.000	1.000	1.000	1.000
38	100			0.998	0.999
66	150			0.993	0.992
93	200	0.985	0.980	0.980	0.976
121	250	0.982	0.972	0.982	0.961
149	300	0.964	0.954	0.983	0.957
177	350	0.945	0.937	0.970	0.952
204	400	0.927	0.924	0.956	0.945
232	450	0.923	0.917	0.943	0.939
260	500	0.909	0.911	0.934	0.928
288	550	0.897	0.895	0.917	0.920
316	600	0.880	0.886	0.906	0.905
343	650	0.875	0.874	0.895	0.885
371	700	0.865	0.862	0.882	0.880
399	750	0.856	0.854	0.874	0.860
427	800	0.836	0.838	0.863	0.849
454	850	0.818	0.824	0.855	0.830
482	900	0.820	0.808	0.845	0.824
510	950	0.804	0.796	0.841	0.827
538	1000	0.792	0.783	0.829	0.807
566	1050	0.783	0.776	0.807	0.803
593	1100	0.771	0.759	0.792	0.777
621	1150	0.763	0.740	0.779	0.755
649	1200	0.745	0.726	0.767	0.743
677	1250	0.706	0.709	0.741	0.717
704	1300	0.693	0.697	0.711	0.705
732	1350	0.680	0.685	0.694	0.680
760	1400			0.674	0.658

Table 5.37. Young's Modulus of 2 1/4 Cr-1 Mo Steel

Temperature		Ratio of Modulus at Temperature to Value at 24°C			
		Run 1		Run 2	
(°C)	(°F)	Increasing Temperature	Decreasing Temperature	Increasing Temperature	Decreasing Temperature
24	75	1.000	1.000	1.000	1.000
38	100	0.998	0.957	0.995	0.981
66	150	0.981	0.948	0.987	0.976
93	200	0.967	0.931	0.980	0.976
121	250	0.955	0.943	0.972	0.966
149	300	0.940	0.931	0.963	0.958
177	350	0.925	0.924	0.954	0.947
204	400	0.913	0.917	0.945	0.939
232	450	0.901	0.913	0.936	0.929
260	500	0.897	0.889	0.926	0.921
288	550	0.888	0.881	0.915	0.909
316	600	0.882	0.873	0.905	0.901
343	650	0.875	0.861	0.895	0.891
371	700	0.868	0.850	0.885	0.881
399	750	0.861	0.842	0.871	0.869
427	800	0.853	0.830	0.858	0.856
454	850	0.845	0.831	0.850	0.841
482	900	0.835	0.835	0.835	0.829
510	950	0.824	0.812	0.824	0.816
538	1000	0.816	0.801	0.808	0.803
566	1050	0.800	0.790	0.796	0.789
593	1100	0.784	0.779	0.778	0.775
621	1150	0.768	0.768	0.763	0.759
649	1200	0.753	0.746	0.747	0.742
677	1250	0.731	0.730	0.728	0.723
704	1300	0.708	0.723	0.709	0.705
732	1350	0.694	0.709	0.685	0.685
760	1400	0.689		0.662	0.662
788	1450			0.649	

Crack growth measurements are being made using optical and electrical potential[35,36] measurement techniques.

Results of three room temperature tests are compared in Fig. 5.45. Specimens 1ATL and 1ALT were fabricated such that the crack would propagate in the rolling and transverse rolling directions, respectively. The results given in Fig. 5.45 indicate that within the scatter of the data crack growth rates were not a function of crack orientation with respect to the microstructure. Further, within the frequency range studied the crack growth rate was not a function of frequency. The crack growth data given

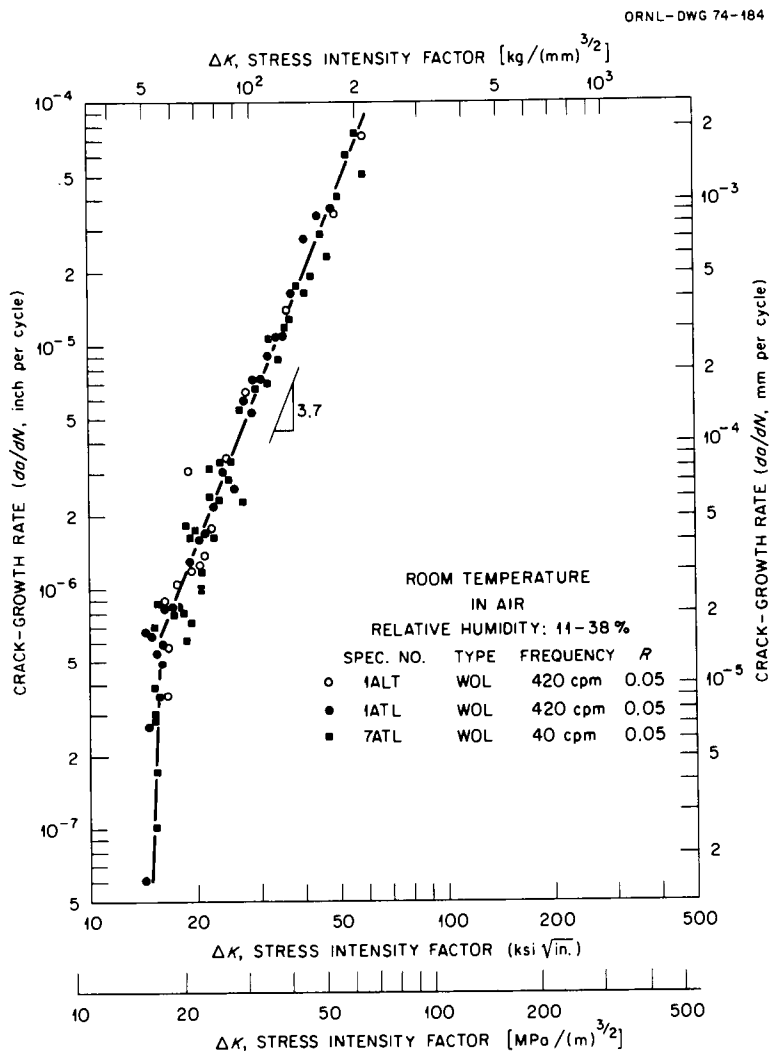

Fig. 5.45. Crack Growth Rate as a Function of the Change in Stress Intensity for 2 1/4 Cr-1 Mo Steel Tested at Room Temperature.

in Fig. 5.45 correlate well with the change in stress intensity factor, ΔK. The curve exhibits the characteristic knee above which the data may be represented by the relation:

$$\frac{da}{dN} = 2.52 \times 10^{-11} \Delta K^{3.7} ,$$

where crack length a is in inches, and ΔK is in ksi $(\text{in.})^{1/2}$. Testing at 950°F (510°C) is under way.

5.4.2 Evaluation of Property Listings for LMFBR Handbook for 2 1/4 Cr-1 Mo Steel — P. L. Rittenhouse, D. O. Hobson, and T. L. Hebble

Several of the mechanical-properties-related subjects of the Listing (Table 5.38) have been compiled in the form of pages for the LMFBR Handbook and issued for review. These include subjects 1, 2, and 3 — chemical composition, product form and applicable specifications, and minimum room-temperature mechanical properties per RDT Standards, respectively. These forms were sent to GE and HEDL for review.

In addition, work is in progress on other mechanical properties subjects for the Listing. Creep data from several different sources (listed in Table 5.39) are being analyzed to determine time to rupture, minimum creep rate, time to start of tertiary creep, total creep strain (isochronous relationship), and the creep equation. An initial total of over 2700 data sets were obtained. This was reduced for instance, by elimination of duplicates — to a little more than 1700 creep test results. Statistical evaluation has been started to obtain the equations for minimum creep rate and time to rupture as functions of stress and temperature. Work is presently under way to generate the creep equation (considered by several participants in the steam generator material program as the most needed piece of information) using information generated by the above analyses. The double exponential, the single exponential, and other models are being considered in the evaluation of the creep equation.

5.4.3 Correlation of Properties of 9 Cr-1 Mo Steel for Service Above 700°F (371°C) — P. L. Rittenhouse

In previous reports[37,38] we discussed our efforts in collecting, analyzing, correlating, and treating data on the elevated-temperature

Table 5.38. Partial Design Property Listing for 2 1/4 Cr-1 Mo Steel

Subject	Handbook Format				Comments	(Recommended) Dates
	Table	Graph	Equation	Other		
1. Chemical Composition	X				Referenced to appropriate ASTM, ASME, and RDT specifications	
2. Product Form and Applicable Specifications				Listing	All product forms will be included and referenced to appropriate ASTM, ASME, and RDT specifications	
3. Minimum Room-Temperature Mechanical Properties per RDT Standards	X				None	
4. Mechanical Properties						
(a) Ultimate tensile strength and true fracture stress	X	X			Expected values will be determined by regression analysis; max and min values will be defined by upper and lower tolerance limits. Values from room temperature to 593°C (1100°F).	2/74[a]
(b) Yield strength (0.2% offset)	X	X			As 4(a)	2/74[a]
(c) Proportional limit	X	X			As 4(a)	9/74
(d) (1) Total elongation	X	X			As 4(a) tensile data	9/74
(d) (2) Total elongation	X	X			As 4(a) creep data	9/74
(e) Uniform elongation	X	X			As 4(a)	9/74
(f) Reduction in area	X	X			As 4(a)	9/74
(g) Young's modulus (static and dynamic)	X	X			Expected value; $f(T)$, room temperature to 593°C (1100°F) in 28°C (50°F) increments	9/74
(h) Shear modulus	X	X			As 4(g)	9/74
(i) Poisson's ratio	X	X			As 4(g)	9/74
(j) Charpy impact values	X	X			Expected value; -18 to 371°C (0 to 700°F)	9/74
(k) Brittle-to-ductile transition temperature	X	X			Expected value	9/74
(l) Hardness	X	X			Expected value and confidence limits; $f(T)$ room temperature to 593°C (1100°F)	9/74
(m) Subcritical crack growth		X	X		Expected value and limits; $f(T)$, room temperature to 593°C (1100°F)	6/75
(n) K_c values	X	X			In the transition and upper-shelf temperature range of Charpy V-notch results	6/75

Table 5.38. (Continued)

Subject	Handbook Format				Comments	(Recommended) Dates
	Table	Graph	Equation	Other		
(o) Energy per unit volumes at failure in the necked region (area under stress-strain curve)	X	X			As 4(m)	6/74
(p) Stress rupture	X	X	X		Expected, minimum, and maximum values. 371 to 593°C (700 to 1100°F) as $f(T,\sigma)$	2/74[a]
(q) Minimum creep rate	X	X	X		As 4(p)	2/74[a]
(r) Time to start of tertiary creep	X	X	X		As 4(p)	9/74
(s) Total creep strain (isochronous relationship)	X	X			Expected, minimum, and maximum values. 371 to 593°C (700 to 1100°F) as $f(T,t,\sigma)$. Both conventional creep and isochronous curves will be given.	9/74
(t) Creep equation			X		For temperatures of 371 to 593°C (700 to 1100°F)	9/74
(u) (1) True-stress-true-strain relationship	X	X	X		Expected, minimum, and maximum values. ε to 5%, room temperature to 593°C (1100°F). Monotonic	6/74
(u) (2) True-stress-true-strain relationship	X	X	X		Cyclic and saturated conditions	9/74
(v) Effect of $\dot{\varepsilon}$ on σ-ε			X		Expected, minimum, and maximum values. $\dot{\varepsilon}$ to 200/sec, room temperature to 593°C (1100°F)	6/74
(w) Fatigue (low cycle)		X			Expected, minimum, and maximum cycles to failure. Effect of strain range to 5%. Room temperature to 593°C (1100°F); strain rate 10^{-5} to 10^{-3}/sec	2/74[a]
(x) Fatigue (high cycle)		X			Room temperature to 593°C (1100°F). Strain rate 10^{-5} to 10^{-3}/sec	2/74[a]
(y) Fatigue creep interactions		X			Effect of strain range, frequency, hold time, $\dot{\varepsilon}$. 371 to 593°C (700 to 1100°F)	2/74[a]
(z) Relaxation		X			Expected values. 371 to 593°C (700 to 1100°F)	2/74[a]

[a]This date is subject to readjustment later.

Table 5.39. Sources of Creep Data on 2 1/4 Cr-1 Mo Steel

1. Mechanical Properties Data Center, Traverse City, Michigan, Oct. 11, 1973 attritubed to the following:
   a. R. M. Brown, R. A. Rege, and C. E. Spaedor, Jr., "The Properties of Normalized and Tempered and of Quenched and Tempered 2 1/4 Cr-1 Mo Steel," Reprinted from *Heat-Treated Steels for Elevated Temperature Service;*
   b. L. I. Mandick, E. L. Fogleman, and J. A. Gulya, *Elevated Temperature Properties of Heavy Gauge Cr-Mo Steel Plates*, Lukens Steel Company;
   c. R. A. Swift and J. A. Gulya, "Temper Embrittlement of Pressure Vessel Steels," *Weld. J. (Miami)* 52: 57-s–68-s (1973);
   d. M. C. Murphy and G. D. Branch, "Metallurgical Changes in 2.25CrMo Steels During Creep-Rupture Test," *J. Iron Steel Inst.* 209: 546–61 (1971);
   e. The Timken Roller Bearing Company, *Resume of High Temperature Investigations Conducted During 1963–65.*
2. R. L. Klueh, *Effect of Carbon on the Mechanical Properties of 2 1/4 Cr-1 Mo Steel*, ORNL-4922 (November 1973).
3. Data Sheets on the Elevated-Temperature Properties of 2 1/4 Cr-1 Mo Steel for Boiler and Heat Exchanger Seamless Tubes (STBA24), NRIM Creep Data Sheet No. 3, National Research Institute for Metals, Tokyo, Japan (1972).
4. E. B. Norris, G. J. Schnabel, and R. D. Wylie, "Properties of Cr-Mo Piping Materials after Service at 1000°F and 1050°F," paper C227/73 in International Conference on Creep and Fatigue in Elevated-Temperature Applications, Philadelphia, September 1973.
5. G. V. Smith, *Supplemental Report on the Elevated-Temperature Properties of Chromium-Molybdenum Steels (An Evaluation of 2 1/4 Cr-1 Mo Steel), ASTM Data Ser. Publ.*, DS 6-S2, American Society for Testing and Materials, Philadelphia, March 1971.
6. A. O. Schaefer, Ed., *Current Evaluation of 2 1/4 Cr-1 Mo Steel in Pressure Vessels and Piping, Metal Properties Council, Third Annual Pressure Vessels and Piping Conference*, American Society for Testing and Materials, Philadelphia, 1972.
7. J. A. Van Echo and W. F. Simmons, *Supplemental Report on the Elevated-Temperature Properties of Cr-Mo Steels, ASTM Data Ser. Pub. Publ.*, DS 6-S1, American Society for Testing and Materials, Philadelphia.
8. The Data of Creep Rupture Properties of 2.25 Cr-1 Mo Steel, Nippon Kokan K. K., ID-47039 (Nov. 1972).
9. The Data of Short Time Tensile Properties of 2.25 Cr-1 Mo Steel at Elevated Temperature, Nippon Kokan K. K., ID-47040 (Nov. 1972).
10. W. F. Simmons and H. C. Cross, *Report on the Elevated Temperature Properties of Chromium-Molybdenum Steels, ASTM Spec. Tech. Publ.* 151 (DS 6), American Society for Testing and Materials, Philadelphia, 1953.
11. A. O. Shaefer Ed., *Symposium on 2 1/4 Chrome/Molybdenum Steel in Pressure Vessels and Piping, Metal Properties Council, Second Annual Pressure Vessels and Piping Conference, ASTM*, Denver, Sept. 1970.
12. Proprietary information from Babcock & Wilcox and Gulf General Atomic.

tensile and creep properties of 9 Cr-1 Mo steel. The purpose of these efforts was (1) to evaluate correlation techniques for ferritic steels other than 2 1/4 Cr-1 Mo and (2) to determine whether sufficient information was available to permit the preparation of a data package for ASME qualification of this material for elevated-temperature service. This data package involved no significant number of new tests. Based on review of the work we have performed to date, we have concluded that a formal request can be forwarded to the ASME to establish some referenceable code values for this alloy. The following paragraphs describe modifications to our original treatment of the data,[4,5] which we believe are necessary. This study has been valuable for many reasons, one of which is that it has given creditability to the techniques we are using for the 2 1/4 Cr-1 Mo steel correlation, which is our most important effort.

5.4.3.1 Tensile Properties

Our original suggestions for 0.2% offset yield strength (YS) and ultimate tensile strength (UTS) minima at 371°C (700°F) and above were based simply on visual estimates of minimum curves. Minima for lower temperatures were accepted as those given in Section III of the ASME Code for 5 to 9% Cr ferritic chromium-molybdenum steels. Two additional methods of treating the data to obtain minima have recently been employed for comparison and to obtain trend curves for the range between room temperature (RT) and 704°C (1300°F). In one of these methods (designated method 1), each elevated-temperature data point (YS or UTS) from a given heat of material is first divided by RT value of that property for that heat. The resultant ratios are fit using a polynomial of fifth order in temperature to obtain a ratio-temperature relationship. For RT (where the ratio is, by definition, unity) the minimum values of YS and UTS are selected as those given in Section III of the ASME Code (30 and 60 ksi, respectively). Minimum values for all other temperatures are obtained by multiplying the RT minimum values by the YS or UTS ratio given by the fifth-order polynomial fit of the data. Results obtained using this method are shown under Method 1 in Tables 5.40 and 5.41 for YS and UTS, respectively.

Table 5.40. Minimum 0.2% Offset Yield Strengths for 9 Cr-1 Mo Steel

Temperature		Minimum 0.2% Offset Yield Strength, ksi, MPa			
(°C)	(°F)	Method 1	Method 2	ASME[a]	Visual[b]
24	75	30.0, 207	30.0, 207	30.0, 207	
93	200	27.5, 190	27.0, 186	28.0, 193	
149	300	26.2, 181	25.5, 176	26.9, 185	
204	400	25.3, 174	24.4, 168	26.2, 181	
260	500	24.4, 168	23.5, 162	25.7, 177	
316	600	23.3, 161	22.6, 156	25.0, 172	
371	700	21.9, 151	21.6, 149	23.4, 161	22.0, 152
427	800	20.0, 138	20.2, 139	22.4, 154	21.3, 147
482	900	17.7, 122	18.4, 127	21.1, 145	20.0, 138
538	1000	15.0, 103	16.3, 112	19.6, 135	18.3, 126
593	1100	12.1, 83	13.8, 95		15.4, 106
649	1200	9.0, 62	10.9, 75		11.1, 77
704	1300	6.2, 43	7.8, 54		8.0, 55

[a]From Section III of ASME Code. Values given are for 5 to 9% Cr ferritic Cr-Mo steels.

[b]Visual fit through minimum of all data points.

In the second method used, the raw data points are fit with a fifth-order polynomial to obtain a relationship between temperature and the expected value of the property. The expected value for each elevated temperature is then multiplied by the RT ratio of ASME minimum to expected value [e.g., 30 ksi/(RT expected value of YS)] to arrive at a minimum value. Results obtained using this technique (Method 2) are shown in Tables 5.40 and 5.41 along with those of Method 1, our earlier predictions, and minimum values from Section III of the ASME Code. Comparison of YS values given by all of the above shows no large discrepancies in predicted minimum values. Slightly larger but still not extreme differences are seen in comparison of UTS values.

Table 5.41. Minimum Ultimate Tensile Strengths For 9 Cr-1 Mo Steel

Temperature		Minimum Ultimate Tensile Strength, ksi, MPa			
(°C)	(°F)	Method 1	Method 2	ASME[a]	Visual[b]
24	75	60.0, 414	60.0, 414	60.0, 414	
93	200	54.0, 372	53.4, 368		
149	300	52.3, 361	51.5, 355		
204	400	51.7, 356	51.0, 352		
260	500	51.3, 354	50.9, 351		
316	600	50.3, 347	50.2, 346		
371	700	48.1, 332	48.2, 332		53.8, 371
427	800	44.4, 306	44.8, 309		51.3, 354
482	900	39.2, 270	39.8, 274		47.0, 324
538	1000	32.7, 225	33.4, 270		41.4, 285
593	1100	25.5, 176	26.1, 180		30.9, 213
649	1200	18.2, 125	18.9, 130		22.2, 153
704	1300	11.9, 82	12.6, 87		15.9, 110

[a]From Section III of ASME Code. Values given are for 5 to 9% Cr ferritic Cr-Mo steels.

[b]Visual fit through minimum of all data points.

We plan to modify our previously determined values of S_m (the ASME time-independent stress intensity limit defined as the lesser of (2/3) × minimum YS and (1.1/3) × minimum UTS) based on the results derived using Method 2. Although the determination of minima by this technique does not have a statistical basis (nor do the others used), we judge this method to provide the most reasonable approach now available.

5.4.3.2 Creep and Stress-Rupture

The stress-rupture correlation previously obtained for 9 Cr-1 Mo using the Larson-Miller parameter approach is being revised by adding approximately 50 data points obtained since the original analysis was performed. Further,

all the stress-rupture data have been reexamined by use of 20 additional parametric treatments of time, temperature, and stress. The Larson-Miller approach still seems to give the most satisfying and consistent results for the 9 Cr-1 Mo data set. Values of S_t (the ASME time-dependent stress intensity limit defined as the least of 2/3 of the minimum stress to cause rupture, 80% of the minimum stress to initiate third-stage creep, and minimum stress to cause 1% total strain) will be revised, if necessary, based on the new Larson-Miller stress-rupture correlation

The final items requiring modification before submittal of the 9 Cr-1 Mo data package to the ASME are the isochronous stress-strain curves. These were originally developed as average curves (i.e., based on expected values) from the Larson-Miller correlation of creep strain-time data. The curves to be included in the ASME data package will be based on the minimum values (i.e., the lower tolerance limits) predicted by the analysis.

5.4.4 Mechanical Properties of Weld Overlaid Stainless Steel Forgings — R. L. Klueh

Last quarter[39] we reported on the tensile properties of the forging region that was unaffected by the overlay process. This quarter we completed tensile tests on the type 308 stainless steel weld metal over the range 25 to 649°C (77 to 1200°F). Tests were made on two different orientations and three different strain rates.

In Table 5.42, the tensile properties for the radial and tangential specimens are given. We tried to get specimens from two levels of the overlay, and the first value at each temperature and 0.04/min were from the upper level, the other two from the lower level. However, as a result of the limited thickness of the overlay and the specimen size, the distance between specimens was not large enough to call them different; thus they are all combined in Table 5.42.

Figure 5.46 shows the yield and tensile strengths as functions of temperature; in Fig. 5.47 the elongation and reduction of area are given. It is seen that properties differ little for the radial and tangential orientations.

Since no difference could be detected with orientation, only radial specimens were tested at the low strain rates. Figure 5.46 shows that, as

Table 5.42. Tensile Properties of Type 308 Stainless Steel Filler Metal on Overlaid Forging

Temperature (°C)	Temperature (°F)	Nominal Strain Rate (min^{-1})	0.2% Offset Yield Stress (ksi)	0.2% Offset Yield Stress (MPa)	Ultimate Tensile Stress (ksi)	Ultimate Tensile Stress (MPa)	Total Elongation (%)	Reduction of Area (%)
			Radial Orientation					
25	77	0.04	63.8	440	89.4	616	34.2	51.5
			63.3	436	90.6	625	39.3	43.3
427	800	0.04	43.0	296	63.0	434	26.7	46.9
			43.4	299	64.7	446	33.0	46.5
482	900	0.04	45.0	310	63.5	438	26.1	45.0
			44.9	310	61.8	426	21.4	45.7
538	1000	0.04	40.9	282	57.6	397	26.8	37.8
			43.6	301	56.6	390	20.8	43.7
593	1100	0.04	37.9	261	51.5	355	28.2	43.8
			37.9	261	50.3	347	24.6	53.2
649	1200	0.04	33.8	233	41.9	289	31.1	42.7
			35.6	246	44.6	308	27.3	43.1
482	900	0.004	47.6	328	67.0	462	22.2	49.5
593	1100	0.004	39.0	269	49.8	343	26.9	40.6
649	1200	0.004	35.3	243	39.5	272	25.3	45.7
482	900	0.0004	45.0	310	64.4	444	22.0	43.2
593	1100	0.0004	47.8	330	43.7	301	25.5	32.3
649	1200	0.0004	32.2	222	34.7	239	21.5	35.4
			Tangential Orientation					
25	77	0.04	64.6	445	90.5	624	42.7	47.1
			65.8	454	93.0	641	41.1	44.4
427	800	0.04	40.6	280	63.9	441	31.4	41.0
482	900	0.04	37.2	257	61.9	429	32.3	39.2
538	1000	0.04	41.1	283	57.7	398	26.3	47.8
			38.0	262	56.9	392	26.9	44.8
593	1100	0.04	32.4	223	50.5	348	33.9	44.5
			37.0	255	52.3	361	23.0	35.8
649	1200	0.04	32.0	221	43.2	298	34.4	41.4

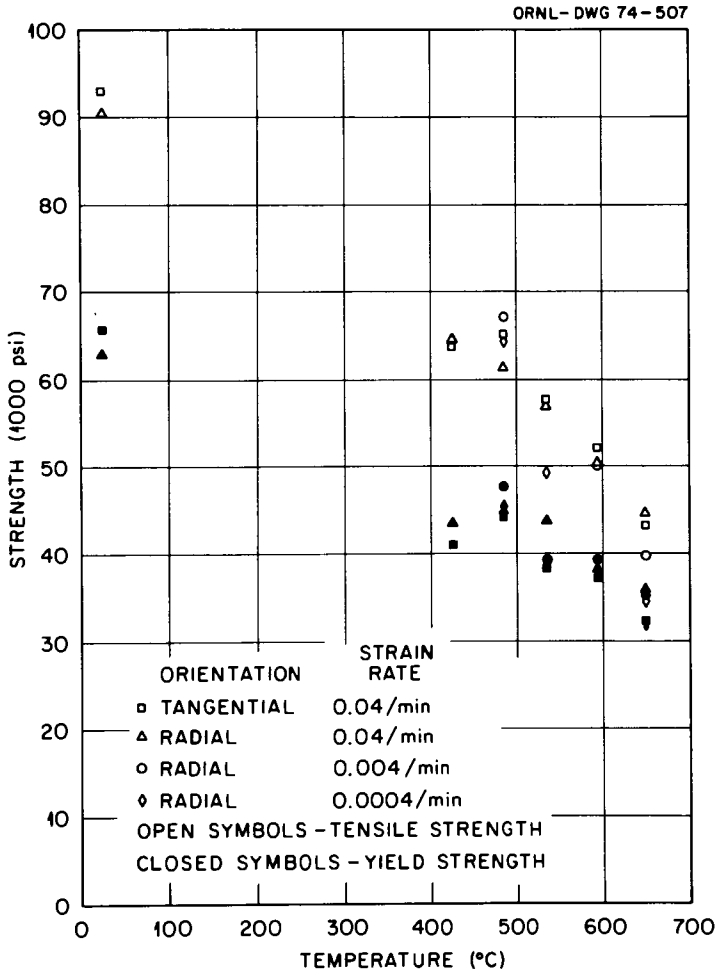

Fig. 5.46. Yield and Ultimate Tensile Strengths for Type 308 Stainless Steel Weld Metal for Two Orientations and Three Strain Rates as Functions of Temperature.

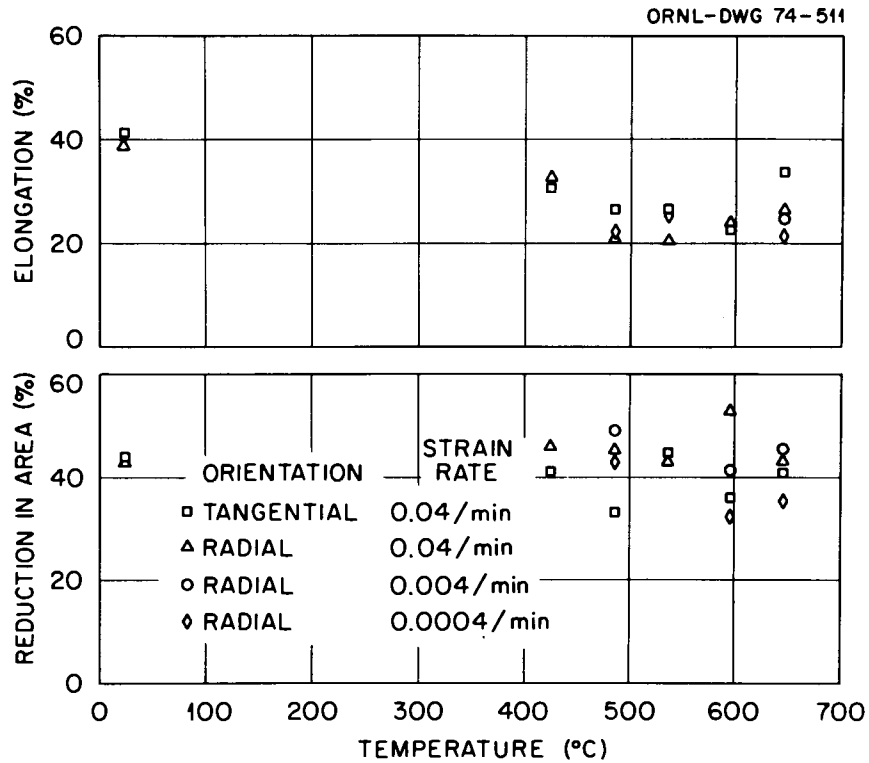

Fig. 5.47. Elongation and Reduction of Area of Type 308 Stainless Steel Weld Metal for Two Orientations and Three Strain Rates as a Function of Temperature.

was the case for the forging, there was little effect of strain rate on yield stress, but there was an effect on tensile stress; namely, a decrease in ultimate tensile stress with increasing temperature and decreasing strain rate. As with all ductility measurements, there was considerable data scatter. However, all indications are that the only effect of strain rate appears to occur at 649°C and 0.0004/min, where a decreased elongation and reduction of area were noted.

Visual and metallographic observations showed results similar to those of the forging. All specimens tested at 0.04 and 0.004/min, and those tested at 482°C (900°F) and 0.0004/min showed transgranular failures. Only the specimens at 0.0004/min at 593 and 649°C (1100 and 1200°C) showed any indication of intergranular fracture, and only a slight amount at 593°C. Although the specimens maintained a circular cross section during deformation, anisotropic behavior was noted for the radial specimens in that they had a "knobby" appearance. That is, usually one or more points on the specimen gage section, in addition to the region that necked to failure, appeared to be in the process of neck formation. "Knobby" deformation was not evident for the tangential specimens.

5.5 HIGH-TEMPERATURE DESIGN — W. L. Greenstreet, J. M. Corum, and C. E. Pugh

5.5.1 Exploratory Testing to Identify Behavioral Features — R. W. Swindeman

5.5.1.1 Development of laboratory facilities

The eight creep machines currently being used for exploratory studies have been instrumented with high-precision extensometers[40] compatible with the data acquisition system being installed in the Materials Property Complex Testing Laboratory.

The two cyclic creep machines currently in use are being modified to assure reliability in regard to maintaining alignment and load. An inelastic analysis was performed on the specimen design used in the machines, and the results of the analysis suggested that the specimen gage lengtn

should be extended and extensometer relocated away from the shoulders. We are doing this now.

We have received a conceptual design and a proposal regarding a long-time relaxation testing facility. We will probably procure this machine subject to the approval of funds.

Efforts are still under way to make the new 50,000-lb strain-cycling machine operational for high-temperature testing. Currently we are examining the heating system in regard to its capability of producing a flat temperature profile in a 1-in.-long 1/2-in.-diam testing section.

5.5.1.2 Stress-strain testing

The series of tensile tests on 1-in. plate of type 304 stainless steel (heat 9T2796) described in Table 5.43 represent the planned tensile test matrix for this product form (excluding history effect studies). Emphasis is placed on the nominal 0.005/min strain rate, since this represents the maximum rate expected for transients in fast breeder reactors. Tests at higher strain rates are included so that monotonic data will be available at rates which overlap those used in strain cycling and fatigue testing programs. High rate data are also helpful in separating time-dependent and time-independent inelastic deformation. Similarly, low rates are of interest because they provide data on conditions where creep can occur during testing which can be used to verify methods of separating strain components.

One group of tests (Table 5.43) were performed under servocontrolled conditions and were discontinued at about 0.5% strain. These data were collected for use in a detailed analysis of yielding around the knee of the flow curve.[41] The other group of tests, for which only yield stresses are reported, were discontinued at 5% total strain. More detailed information about these test results will be forthcoming along with bilinearization of the data according to recommended procedures.[6] In addition to obtaining bilinear constants, we are examining the fit of true stress—true strain data to several equations that have been proposed in the literature to represent the full tensile curve. These include proposals by Holloman,[7] Ludwik,[8] Ludwigson,[9] Reed-Hill et al.,[10] and Voce.[11] We are especially

Table 5.43. Tensile data for type 304 stainless steel (heat 9T2796) 1-in. plate

Specimen No.	Temperature (°C)	Strain rate (min^{-1})	Stress (ksi)		Uniform strain (%)	Elongation in 4 × diameter (%)	Reduction of area (%)
			0.2% yield	Ultimate			
RP 175	25	0.0004	23.9	81.5	79.9	95.0[a]	84.5
RP 176		0.004	25.7	83.4	80.3	95.0	84.4
RP 65		0.0045	24.8	*b*			
RP 66		0.005	24.8	*b*			
RP 10		0.005	26.4	84.7	76.7	85.0[a]	85.5
RP 177		0.04	27.3	83.4	70.6	88.0	83.8
RP 231		0.40	29.7	77.6	57.3	70.8	79.4
RP 186		5.0		73.4	54.7	70.0	77.2
RP 181	93	0.004	21.0	67.7	60.0	78.0	85.4
RP 204		0.004	19.7	66.7	60.7	77.0	82.2
RP 222		0.40	*c*				
RP 246	203	0.00009	*c*				
RP 183		0.004	16.5	61.5	39.8	52.0	75.0
RP 207		0.004	15.2	60.6	41.6	52.5	75.6
RP 235		0.40	*c*				
RP 244	316	0.00009	*c*				
RP 185		0.004	15.9	62.6	42.3	52.0	72.1
RP 11		0.005	14.2	63.0	39.5	47.0	73.5
RP 236		0.40	*c*				

[a]Elongation in 8 × diameter.

[b]Test discontinued at 5% strain.

[c]Test not yet performed.

Table 5.43. (continued)

Specimen No.	Temperature (°C)	Strain rate (min^{-1})	Stress (ksi)		Uniform strain (%)	Elongation in 4 × diameter (%)	Reduction of area (%)
			0.2% yield	Ultimate			
RP 253	427	0.00009	11.5	61.6	44.3	47.5[a]	69.6
RP 174		0.0004	12.1	62.9	41.2	50.0	72.0
RP 224		0.0004	12.4	61.3	40.8	45.0	62.8
RP 187		0.004	12.9	61.8	39.7	50.0	63.3
RP 88		0.0045	12.1	*b*			
RP 12		0.005	13.0	62.1	37.9	45.0[a]	70.5
RP 132		0.005	12.8	*d*			
RP 178		0.04	14.6	60.5	38.1	49.0	74.5
RP 225		0.04	12.8	59.7	39.2	46.2	73.9
RP 226		0.40	13.8	57.5	38.1	43.9	67.4
RP 188		5.0		56.5	35.3	46.5	64.8
RP 252	482	0.00009	11.3	57.6	43.0	46.3[a]	53[d]
RP 189		0.004	11.8	59.5	39.6	48.0	67.1
RP 13		0.005	12.2	59.4	40.4	48.0[a]	70.0
RP 128		0.005	11.3	*e*			
RP 254	538	0.00009	10.9	45.0	24.0	21.0[a]	32.0[d]
RP 227		0.0004	11.6	49.0	28.0	27.0	31.0[d]
RP 20		0.0005	11.1	52.8	35.7	42.5	41.0
RP 190		0.004	10.5	54.5	39.6	45.0	54.0[d]
RP 203		0.004	10.3	53.7	40.2	48.0	66.8
RP 14		0.005	11.6	55.8	39.9	50.5[a]	68.0
RP 127		0.005	11.7	*e*			

[d]Ruptured at extensometer contact point.

[e]Servocontrolled test discontinued at 0.5% strain.

Table 5.43. (continued)

Specimen No.	Temperature (°C)	Strain rate (min^{-1})	Stress (ksi)		Uniform strain (%)	Elongation in 4 × diameter (%)	Reduction of area (%)
			0.2% yield	Ultimate			
RP 228	538	0.04	12.0	54.5	38.7	47.8	70.4
RP 18		0.05	11.7	55.2	33.5	41.0[a]	70.0
RP 229		0.40	12.2	53.2	37.3	43.1	64.3
RP 201		5.0		52.5	35.8	49.2	66.2
RP 165	593	0.00009	10.7	34.2	17.0	20.6[a]	23.4[d]
RP 256		0.00009	10.2	34.4	17.4	20.5[a]	23.2[d]
RP 113		0.00009	10.2	*b*			
RP 114		0.00009	11.2	*b*			
RP 195		0.0004	12.1	39.4		27.0	30.0[d]
RP 115		0.00045	11.2	*b*			
RP 116		0.00045	10.0	*b*			
RP 192		0.004	10.5	45.2	28.8	38.0	41.2[d]
RP 91		0.0045	10.2	*b*			
RP 15		0.005	11.1	46.5	35.7	37.5[a]	51.5[d]
RP 131		0.005	10.0	*e*			
RP 193		0.04	11.2	49.3	34.0	46.0	66.4
RP 92		0.045	10.1	*b*			
RP 96		0.045	10.2	*b*			
RP 182		0.40	11.2	49.9	31.8	46.0	74.1
RP 93		0.45	11.6	*b*			
RP 95		0.45	10.6	*b*			
RP 194		4.0		48.8	32.2	40.7	75.5
RP 202		5.0		49.9	32.7	47.0	70.7
RP 94		5.0	10.8	*b*			

Table 5.43. (continued)

Specimen No.	Temperature (°C)	Strain rate (min^{-1})	Stress (ksi)		Uniform strain (%)	Elongation in 4 × diameter (%)	Reduction of area (%)
			0.2% yield	Ultimate			
RP 257	649	0.00009	9.9	23.9	20.4	40.0[a]	23.2
RP 209		0.0004	10.9	29.1	16.6	32.2	35.7[d]
RP 21		0.0005	10.8	30.6	44.0	57.5[a]	34.5[d]
RP 179		0.004	11.6	36.3	24.4	42.0	38.5
RP 16		0.005	10.5	37.1	23.6	34.0	26.0[d]
RP 217		0.04	9.8	40.9	29.3	47.7	46.1
RP 19		0.05	10.4	42.1	30.6	43.5[a]	29.0
RP 199		0.40	10.4	44.3	33.2	45.0	68.6
RP 230		0.40	11.0	44.1	31.6	45.7	70.8
RP 206		5.0		46.5	29.3	44.4	71.4
RP 197	704	0.0004	11.1	20.3	9.8	49.0	33.5
RP 232		0.0004	10.4	20.3	7.2	33.0	24.7[d]
RP 180		0.004		26.2	18.6	50.0	40.0
RP 17		0.005	10.9	27.8	16.0	41.0[a]	40.5[d]
RP 184		0.04	10.0	32.9	21.4	48.0	40.3
RP 233		0.04	10.5	33.3	23.8	50.4	48.0
RP 200		0.40	9.8	37.6	26.8	39.0	34.9
RP 223		0.40	9.0	38.3	28.9	41.9	37.3
RP 208		5.0		43.0	28.1	43.2	77.1
RP 221	760	0.0004	11.0	13.8	7.8	23.1	32.3[d]
RP 161		0.004	10.0	18.7	11.1	54.0	37.8[d]
RP 218		0.004	9.7	18.6	14.0	36.2	37.0[d]
RP 242		0.04	10.5	25.3	16.3	47.6	39.2
RP 240		0.40	10.2	31.5	22.7	49.1	36.8
RP 196		5.0		39.7	26.0	51.6	66.0

interested in the Voce equation, and to examine its potential we have obtained preliminary fits to our 1100°F data using graphic methods.

The Voce equation may be written in the form

$$\bar{\sigma} = (\sigma_0 - \sigma_\infty)\, e^{-k\bar{\varepsilon}_p} + \sigma_\infty \,, \tag{1.1}$$

where $\bar{\sigma}$ is the true stress, $\bar{\varepsilon}_p$ is the true plastic strain, and σ_0, σ_∞, and k are material constants. Differentiating Eq. (1.1) with respect to strain and eliminating the exponential term results in the following expression for the strain-hardening behavior:

$$\left(\frac{d\bar{\sigma}}{d\bar{\varepsilon}_p}\right) = k(\sigma_\infty - \bar{\sigma}) \,. \tag{1.2}$$

Inspection of Eqs. (1.1) and (1.2) reveals a deformation model consisting of general yielding at a critical stress σ_0 and a finite strain-hardening rate given by $k(\sigma_\infty - \bar{\sigma}_0)$. With progressive straining, the hardening rate diminishes linearly with stress and approaches zero as $\bar{\sigma}$ approaches σ_∞.

The engineering stress-strain curves at 1100°F were converted to true stress—true plastic strain curves in the usual way. We then evaluated the slopes of the curves $(\Delta\bar{\sigma}/\Delta\bar{\varepsilon}_p)$ at several stress levels, plotted them against stress, and solved Eq. (1.2) for k and σ_∞. Values for these constants are given in Table 5.17. Data calculated from the Voce equation, assuming σ_0 to be 10,000 psi, are compared with smooth experimental curves in Fig. 5.15. The experimental curves were discontinued at the engineering ultimate strength, whereas the data derived from the Voce equation were plotted to values near σ_∞.

The Voce equation seems to be a fairly good model for representing laboratory reannealed material, and the fit will probably improve when we develop a numerical method for curve fitting. After this we will examine the strain rate and temperature dependency of the constants. The data in Table 5.17 can be used for preliminary examination of the strain rate dependency. For example, Fig. 5.16 shows, along with tensile and creep strengths, σ_∞ values as a function of strain rate. These values were converted to true stresses. This plot indicates that the σ_∞ values are

merging into the creep rate data at low rates and are more or less rate independent at high rates. Implied is the possibility that σ_∞ is controlled by thermal recovery at low rates and dynamic recovery at high rates.

5.6 INVESTIGATIONS OF CREEP FAILURE UNDER UNIAXIAL AND MULTIAXIAL CONDITIONS — C. C. Schultz (Babcock and Wilcox)

The status of the constant-load, step-load, and interrupted uniaxial tests at the end of this report period is given in Tables 5.44 through 5.46 respectively.

Test BWC-5B (20 ksi), now completed, extends the constant load uniaxial rupture data to over 9000 hr. As previously indicated, the strain-time data, which appear in Fig. 5.48, are considerably different than the data from the higher stress tests. Specifically, since secondary creep was never well established, the initiation of tertiary creep was delayed.

Six of the step-loaded uniaxial specimens ruptured during this reporting period. Four of these tests (BWR-10, BWR-12, BWC-7, and BWC-8) were transferred to this test series after elimination from the interrupted test series. Test BWLF-5 was initiated prior to revising the stress levels for this test series, and test BWLF-5B represents the first test in this series since revision of the selected stress levels. The life fractions indicated in Table 5.45 are based on the time-to-rupture values of Table 5.47 and should be considered tentative at this time. The results of these step-load tests reflect the large variation in rupture times seen in the constant-load tests and are possibly the result of the grain size variations subsequently discussed. The exceptionally low usage value for test BWLF-5B is not understood. Two additional step-load tests were initiated this reporting period, BWLF-7 and BWLF-9. Test BWLF-7 is to continue at 21 ksi until rupture; test BWLF-9 is to remain at 21 ksi for 1000 hr, at which time the stress will be increased to 25 ksi for 135 hr then reduced to 21 ksi until rupture. The strain-time data for the step-load tests, with the exception of BWLF-9, is shown in Figs. 5.49 through 5.57.

Figure 5.58 is a comparison, previously reported, of the strain-time data for four constant-load tests (28 ksi). In an effort to determine the reason for the wide variability in rupture times, 227 to 415 hr, the microstructure of each was examined. Figures 5.59 and 5.60 offer a

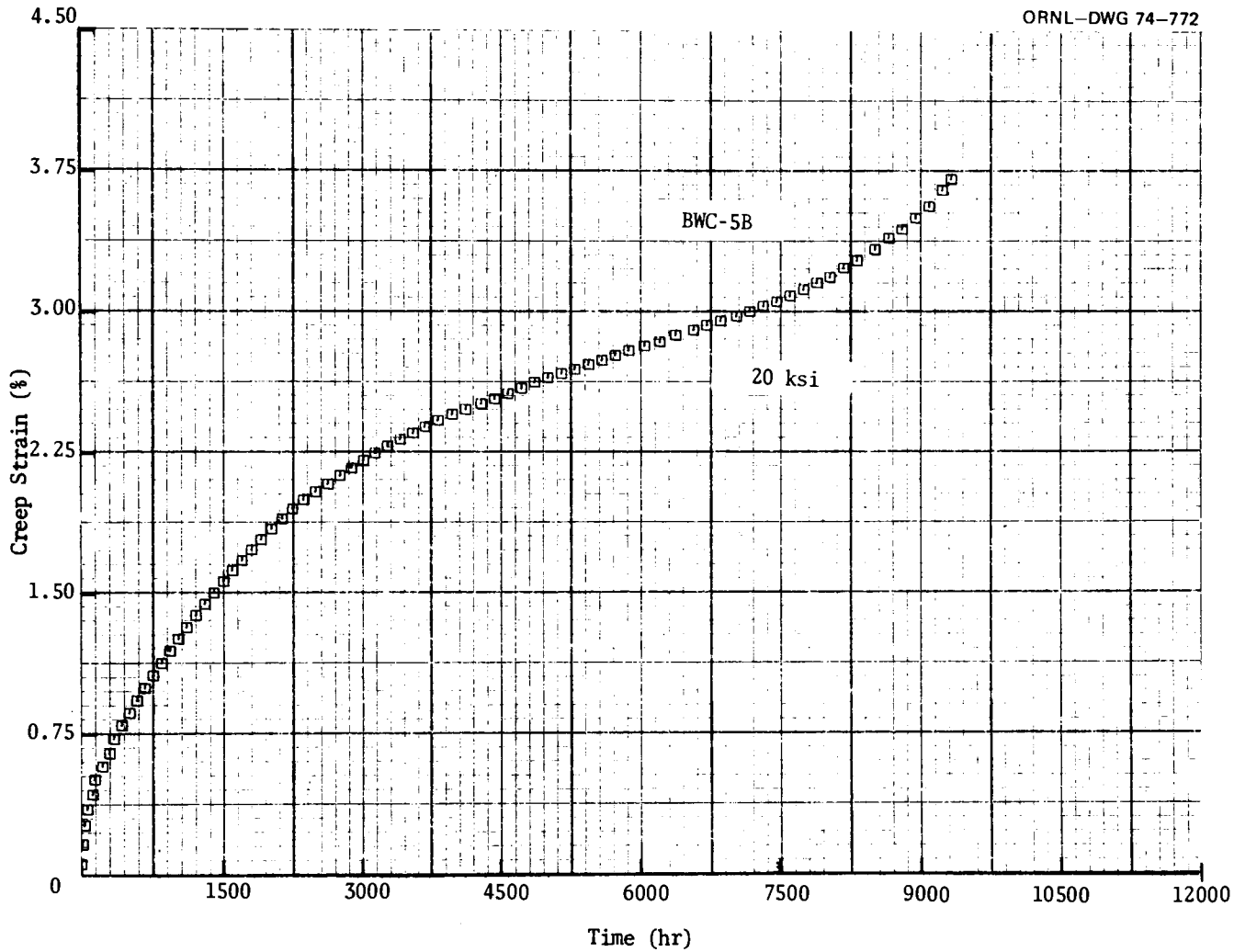

Fig. 5.48. Constant-load uniaxial rupture test for 304 stainless steel (heat 9T2796) 5/8-in. rod. Loaded at 20 ksi at 593°C.

Table 5.44. Status of uniaxial constant-load rupture tests — type 304 stainless steel (heat 9T2796), 593°C (1100°F)

Test No.	Specimen No.	Stress (ksi)	Total strain on loading[a] (%)	Time to secondary creep (hr)	Minimum creep rate (%/hr)	Time to tertiary creep[b] (hr)	Intercept creep strain[c] (%)	Test time[d] (hr)	Fracture elongation[e] (%)	Reduction in area (%)
BWC-1	7-15	30	4.7					187 R	19.0	30.5
BWR-1	7-1	30						138 R	21.5	32.9
BWC-2	2-22	28	5.8	40	0.016	195	0.50	227 R	13.0	20.4
BWR-2	2-1	28		40	0.022	230	0.65	368 R	16.5	29.0
BWR-13	7-13	28		60	0.023	215	0.88	276 R	16.5	18.9
BWC-9	7-25	28	3.8	85	0.021	330	1.16	415 R	18.3	25.2
BWC-3[f]	7-28	25	3.8	80	0.0065	500	0.45	667 R	12.7	12.0
BWR-3	7-8	25		100	0.0079	585	0.71	948 R	17.0	23.2
BWC-4	2-28	22	3.7	175	0.0014	1400	0.60	2,130 R	10.7	13.7
BWR-4	7-7	22		160	0.0030	1170	0.72	2,026 R	12.5	16.6
BWC-5[g]	2-15	20						D		
BWC-5B	2-16	20	1.8	5000	0.000165	8700	1.84	9,584 R	10.5	12.0
BWR-5[h]	2-14	20						4,842 D		
BWR-6	7-14	19						12,460 I		
BWR-9	7-11	18						11,470 I		
BWR-11[i]	2-12	17						94 D		
BWR-11	2-10	17						11,640 I		
BWR-7	2-4	16						12,140 I		
BWR-14	2-9	20	2.02					4,900 I		
BWC-10	7-18	20	1.52					580 I		

Table 5.44. (continued)

[a]All specimens were step loaded at 1.87-ksi increments, except test BWC-5B, which was step-loaded at 1.49-ksi increments. Loading curves on BWR series include load train displacements; thus not reported.

[b]Time to tertiary creep based on the 0.2% offset from the minimum rate line.

[c]Intercept creep strain does not include the elastic and initial plastic components.

[d]R = rupture; D = discontinued; I = in test.

[e]Elongation over 3 in. in BWC series; over 2 in. in BWR series.

[f]Failure occurred near end of gage length.

[g]Temperature excursion to 704°C (1300°F) prior to loading; replaced by test BWC-5B.

[h]Temperature excursion to 749°C (1380°F) at 4842 hr; terminated.

[i]Temperature excursion at 704°C (1300°F) at 94 hr; replaced by test BWR-11B.

Table 5.45. Status of uniaxial step-load rupture tests — type 304 stainless steel (heat 9T2796), 593°C (1100°F)

Test No.	Specimen No.	Stress (ksi)	Total strain on loading (%)	Time to secondary creep (hr)	Minimum creep rate (%/hr)	Time to tertiary creep[a] (hr)	Intercept creep strain[b] (%)	Time at load[c] (hr)	Life fraction (%)	Fracture elongation[d] (%)	Reduction in area (%)
BWC-6	2-17	16	0.42					3,871	6		
		25						136	17		
		20						8,130 I	108		
BWR-10	2-11	16						3,871	6		
		25						136	17		
		20						5,703	76		
								9,710 R	99	11.5	17.8
BWC-7	2-18	17	0.76					3,699	11		
		25						136	17		
		20						5,066	68		
								8,901 R	96	12.0	20.6
BWR-8	2-5	17						3,703	11		
		25						136	17		
		20						8,140 I	108		
BWLF-5	2-25	20	2.06					503	7		
		25						198	25		
		20						5,246	70		
								5,947 R	102	12.5	17.0
BWC-8	7-16	18	1.78					5,071	25		
		25						136	17		
		20						5,420	72		
								10,627 R	114	8.0	15.5
BWR-12	7-12	18						5,071	25		
		25						136	17		
		20						3,840	51		
								9,047 R	93	11.5	17.2
BWLF-5B	2-21	21	2.62					500	10		
		25						200	25		
		21						1,236	25		
								1,936 R	60	10.3	15.9

Table 5.45. (continued)

BWLF-7	2-26	21		750	15
		25		136	17
		21		2,100 I	42
BWLF-9	7-24	21	2.21	400 I	
		25			
		21			

[a]Time to tertiary creep based on the 0.2% offset from the minimum rate line.

[b]Intercept creep strain does not include the elastic and initial plastic components.

[c]R = rupture; I = in test.

[d]Elongation over 3 in. in BWC series; over 2 in. in BWR series.

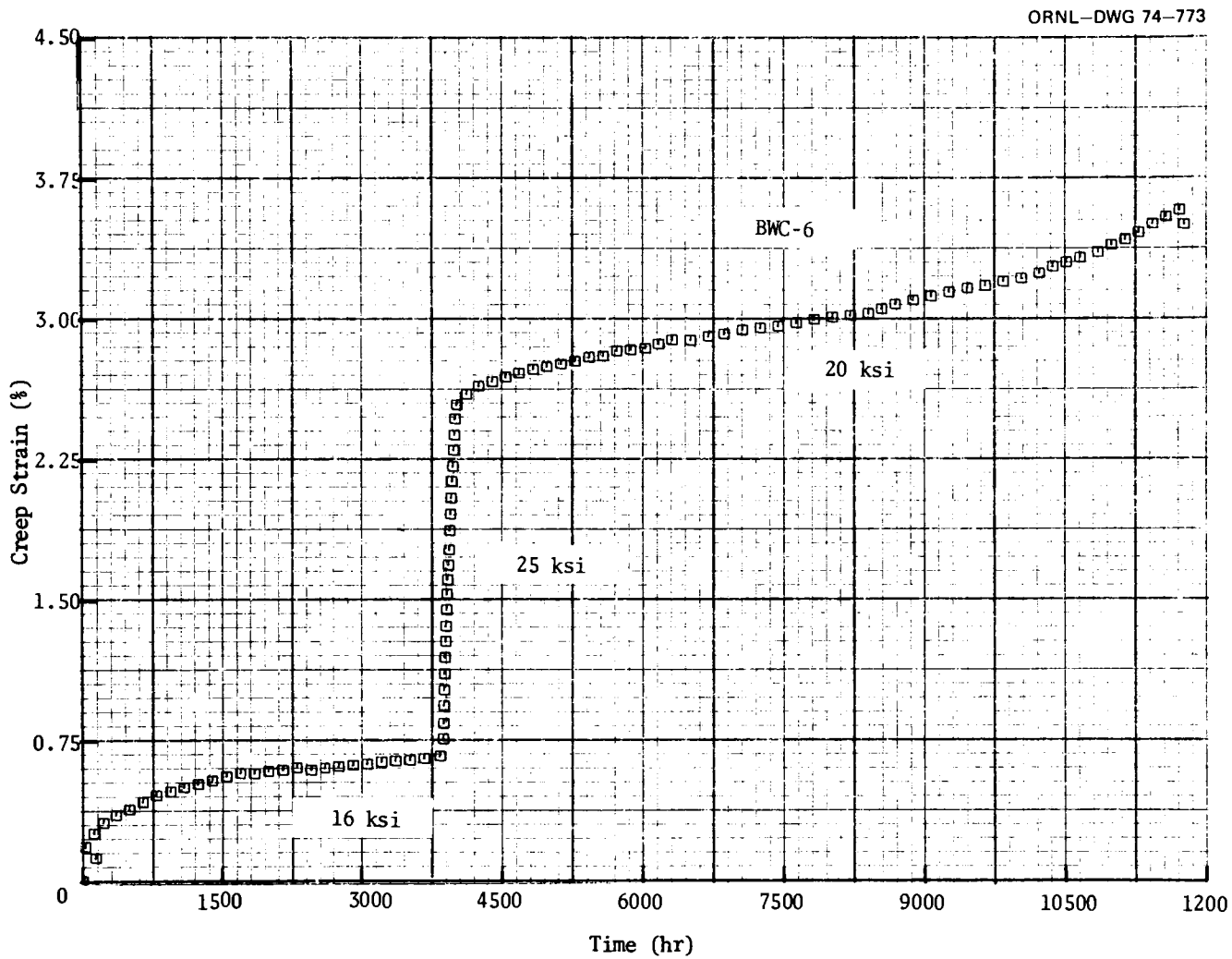

Fig. 5.49. Step-loaded uniaxial rupture test at 593°C. Type 304 stainless steel (heat 9T2796) 5/8-in. rod.

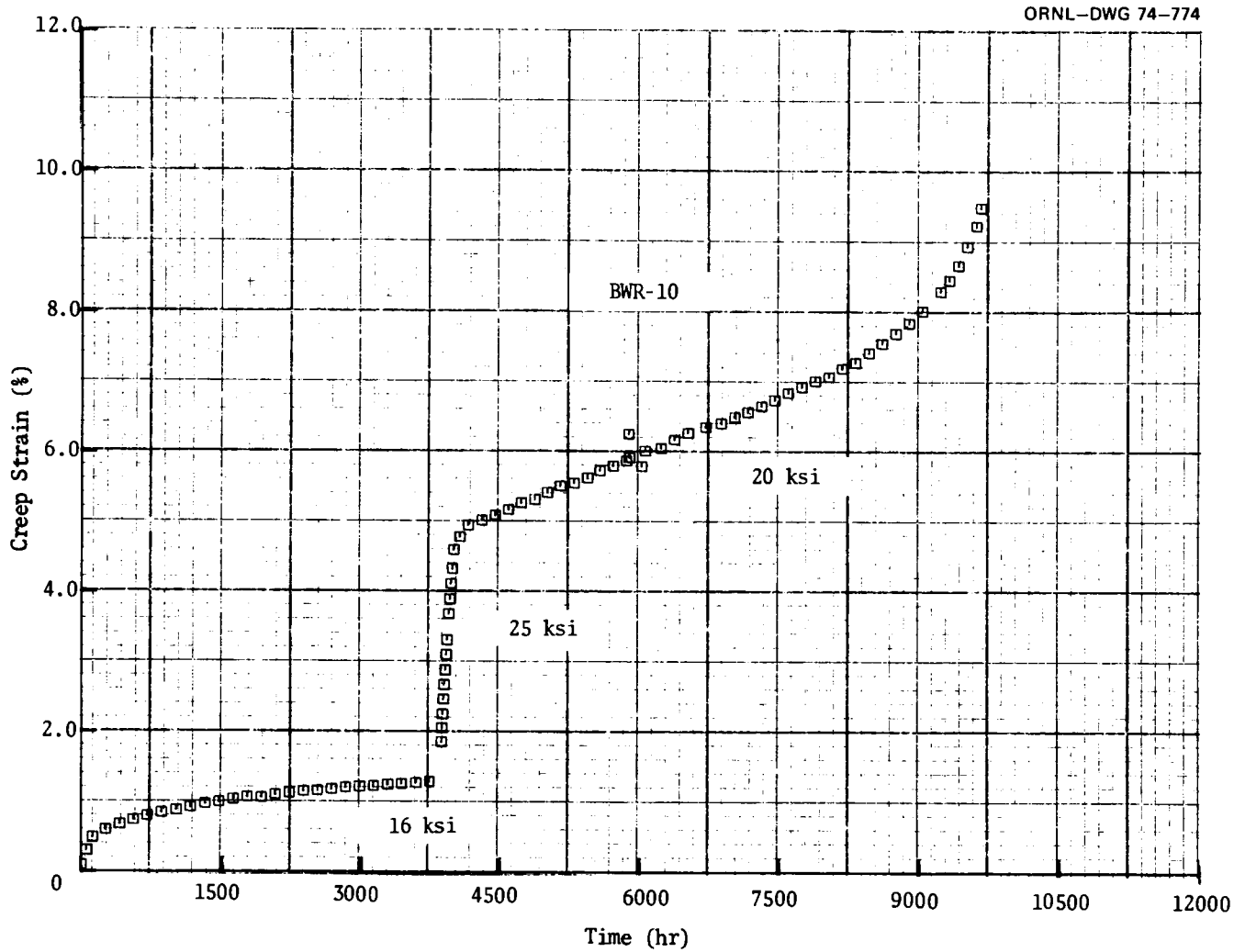

Fig. 5.50. Step-loaded uniaxial rupture test at 593°C. Type 304 stainless steel (heat 9T2796) 5/8-in. rod.

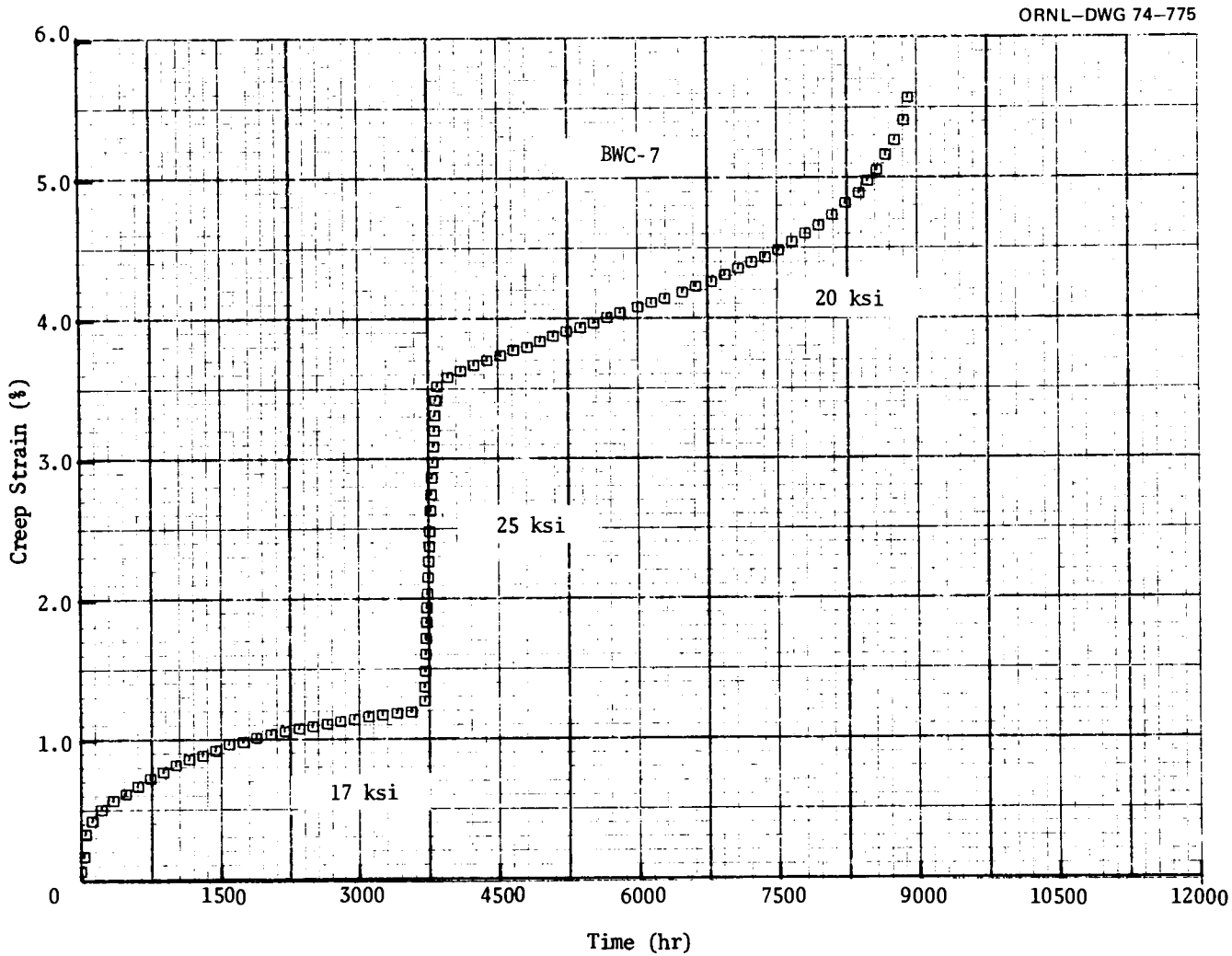

Fig. 5.51. Step-loaded uniaxial rupture test at 593°C. Type 304 stainless steel (heat 9T2796) 5/8-in. rod.

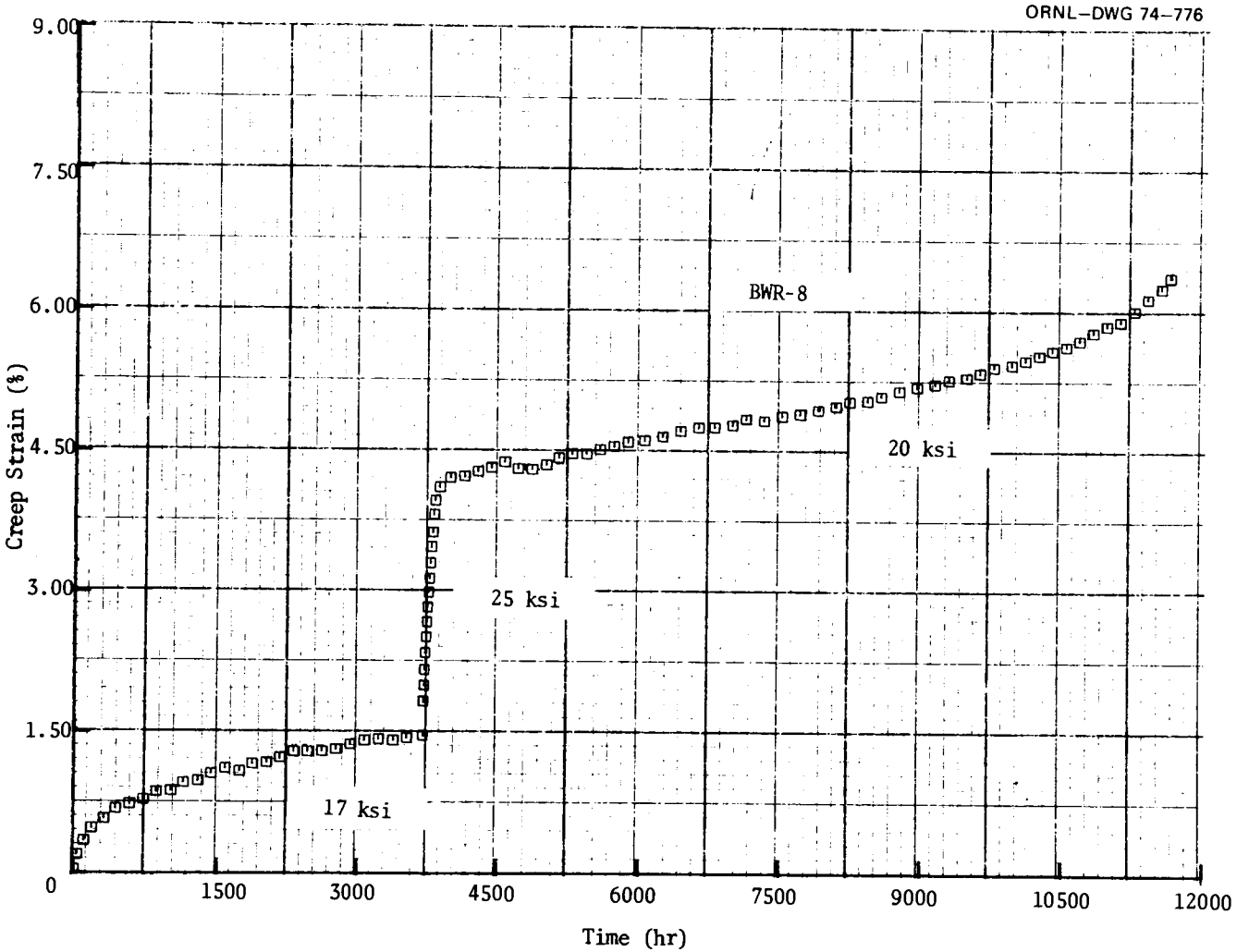

Fig. 5.52. Step-loaded uniaxial rupture test at 593°C. Type 304 stainless steel (heat 9T2796) 5/8-in. rod.

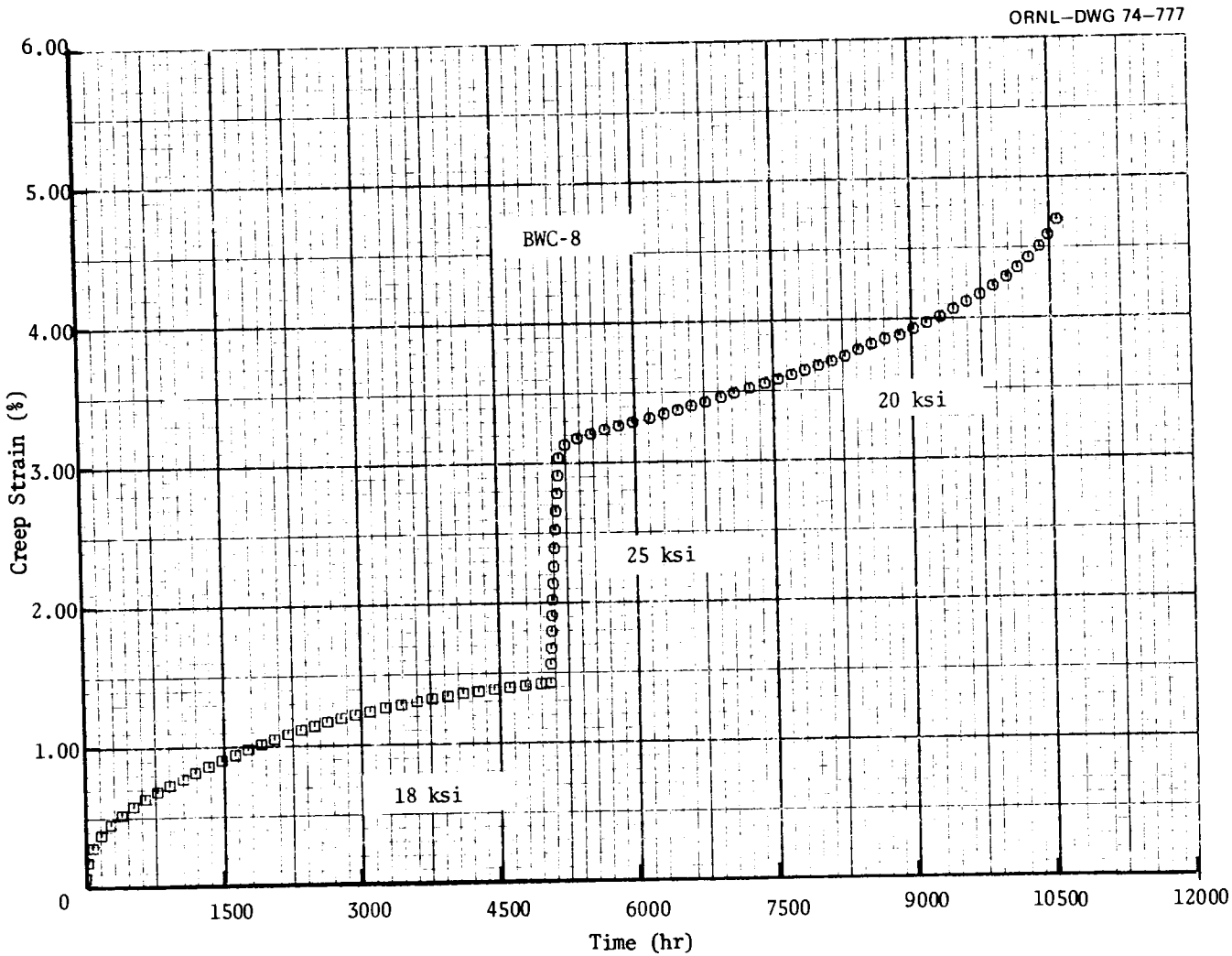

Fig. 5.53. Step-loaded uniaxial rupture test at 593°C. Type 304 stainless steel (heat 9T2796) 5/8-in. rod.

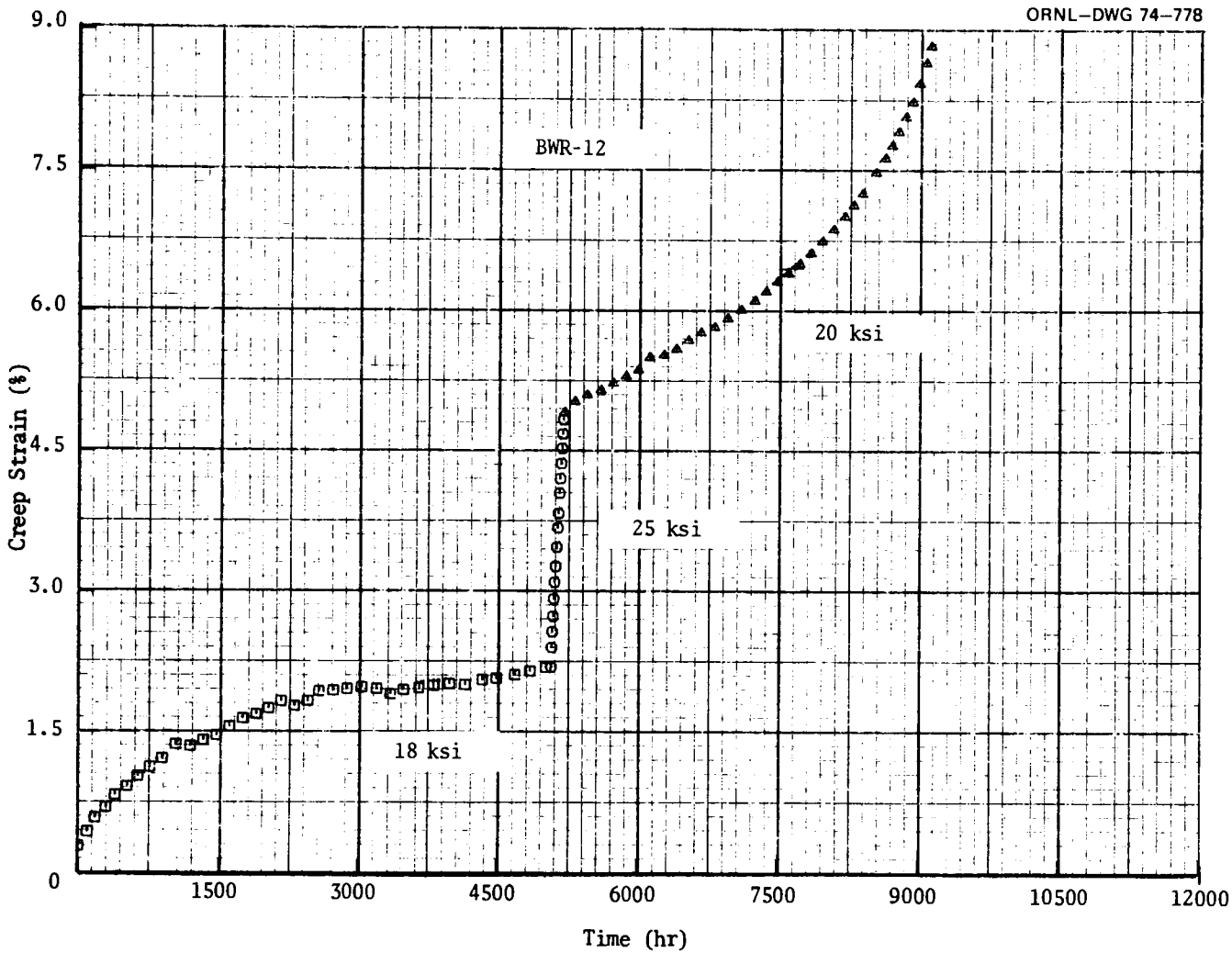

Fig. 5.54. Step-loaded uniaxial rupture test at 593°C. Type 304 stainless steel (heat 9T2796) 5/8-in. rod.

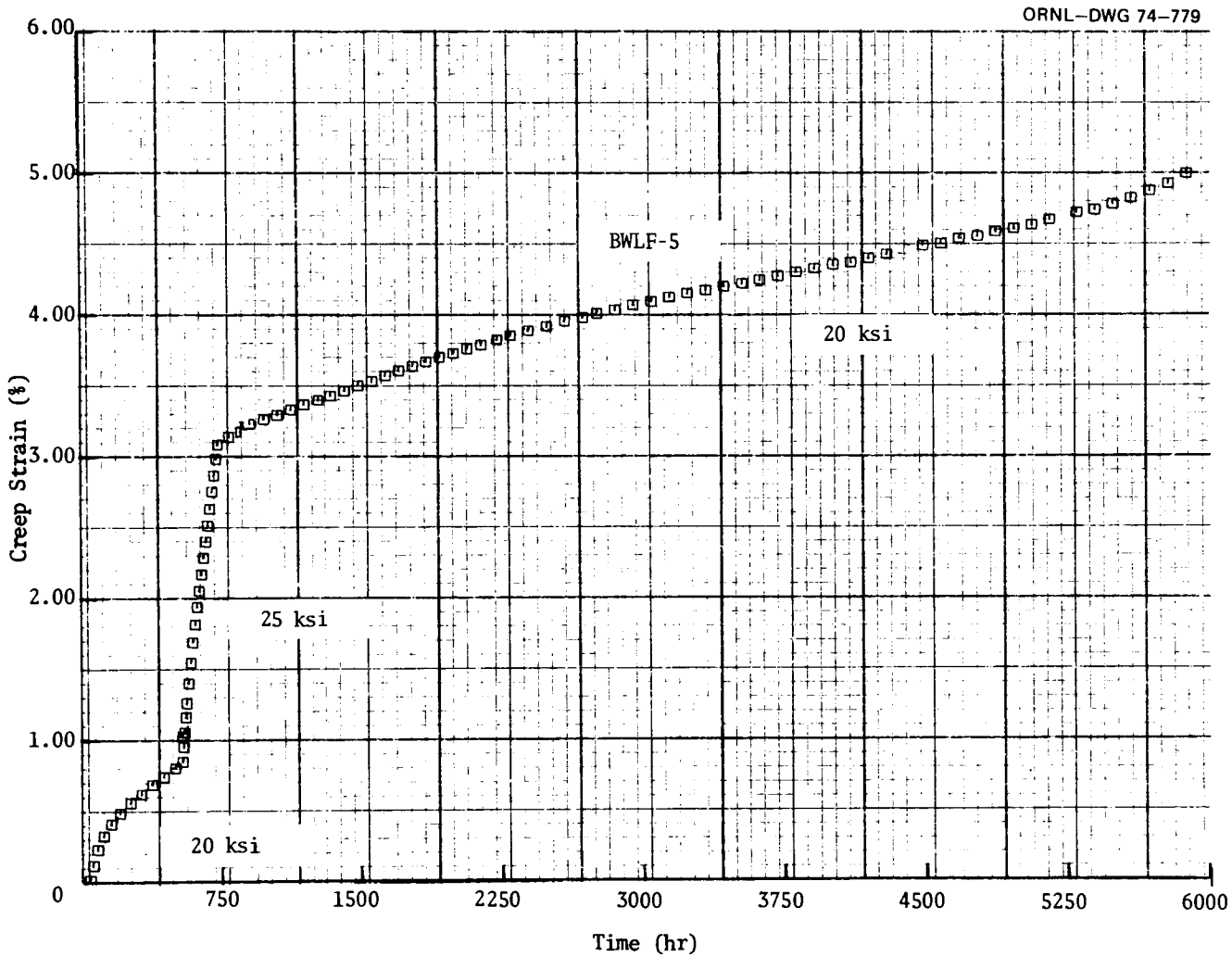

Fig. 5.55. Step-loaded uniaxial rupture test at 593°C. Type 304 stainless steel (heat 9T2796) 5/8-in. rod.

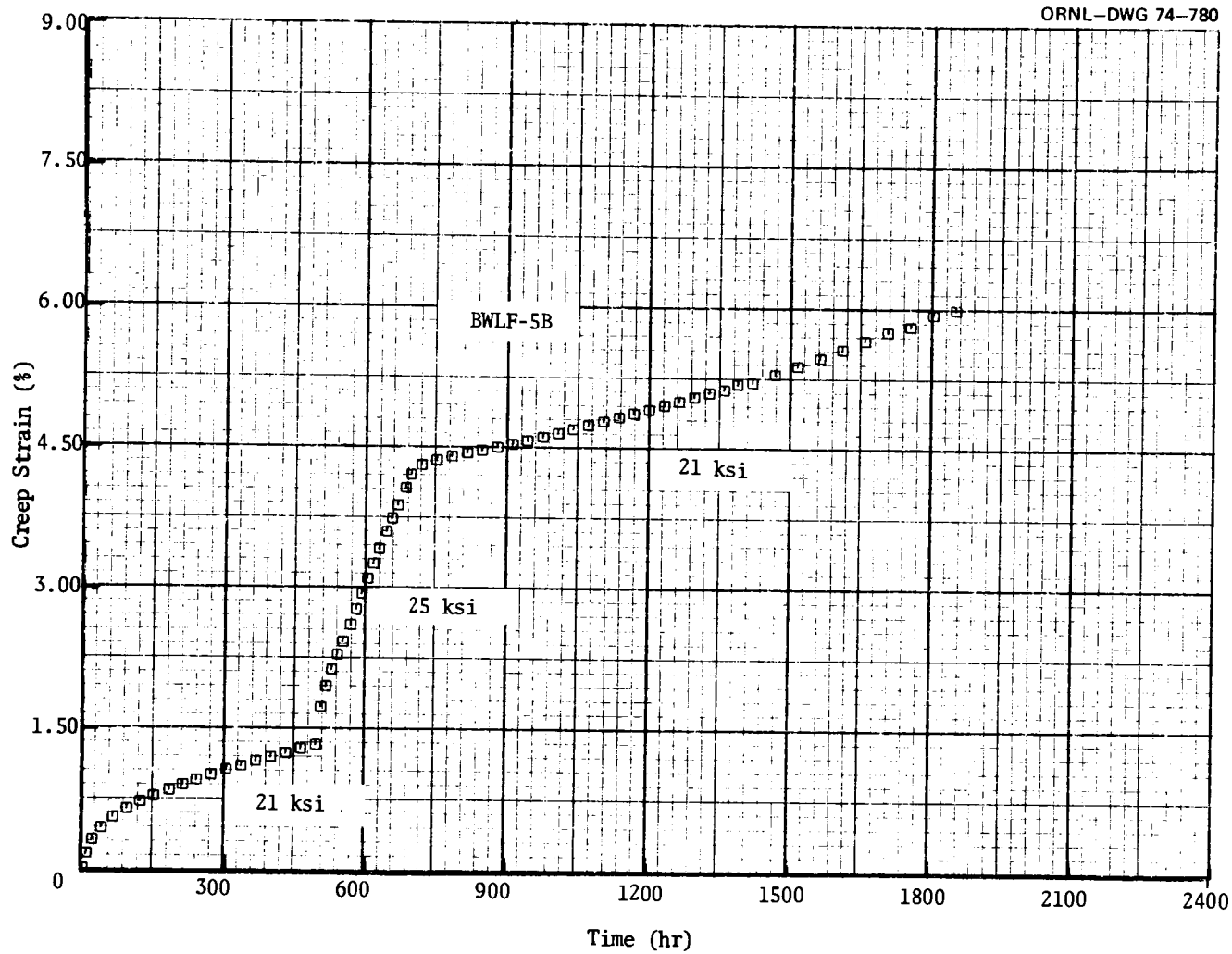

Fig. 5.56. Step-loaded uniaxial rupture test at 593°C. Type 304 stainless steel (heat 9T2796) 5/8-in. rod.

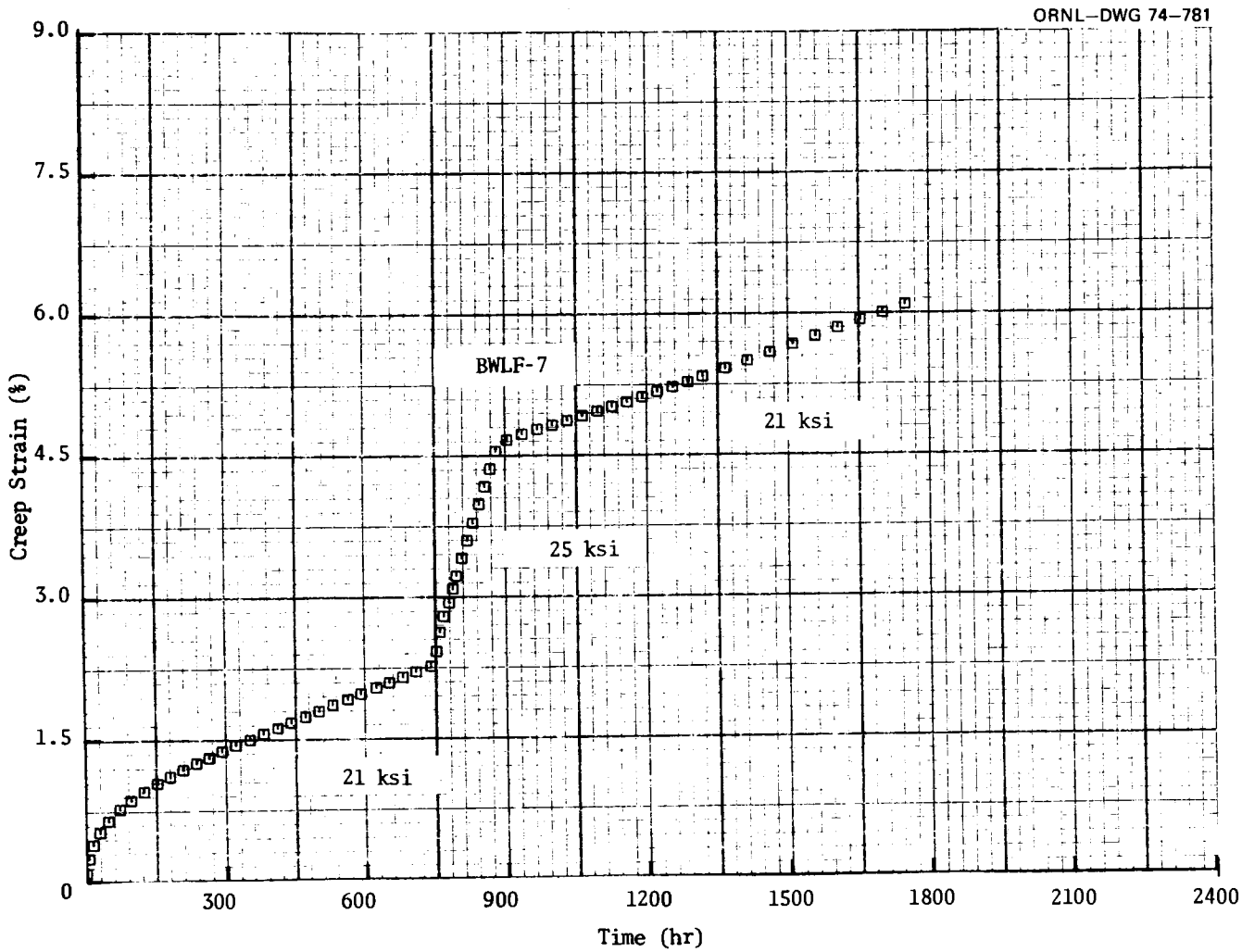

Fig. 5.57. Step-loaded uniaxial rupture test at 593°C. Type 304 stainless steel (heat 9T2796) 5/8-in. rod.

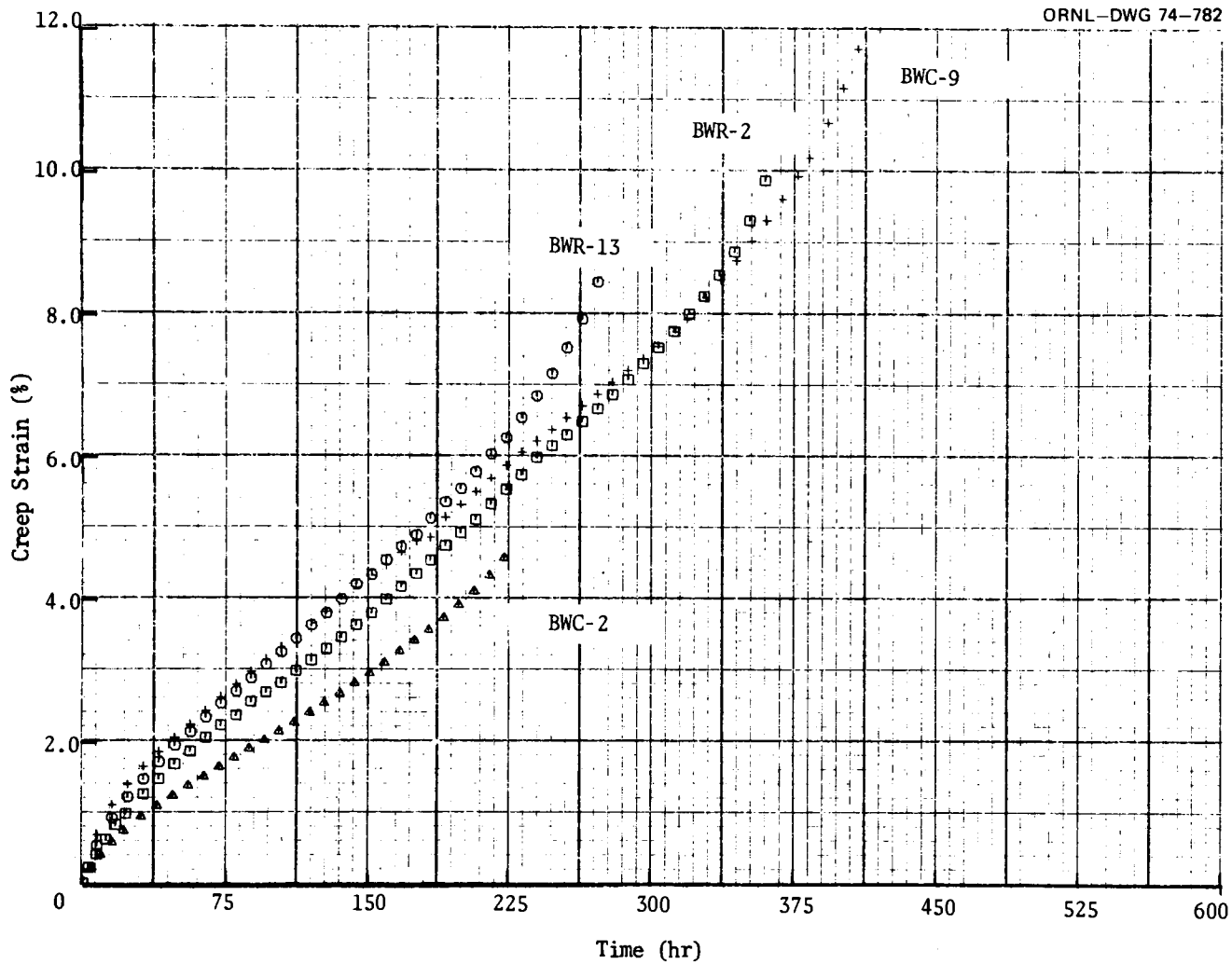

Fig. 5.58. Constant-load uniaxial rupture tests. Loaded at 28 ksi at 593°C. Type 304 stainless steel (heat 9T2796) 5/8-in. rod.

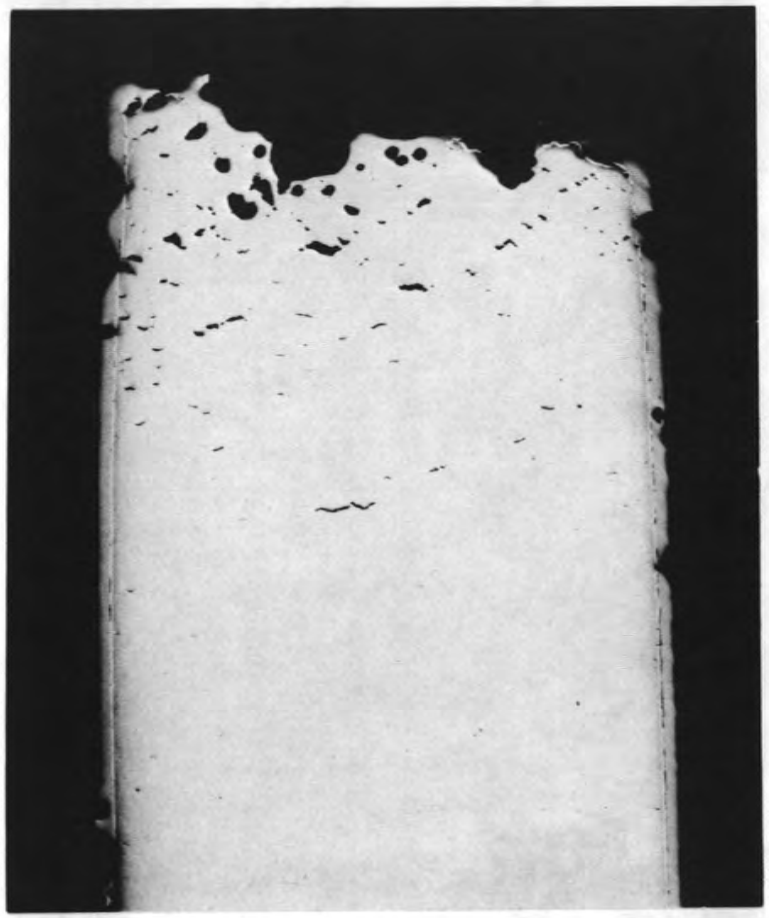

TEST BWC-2
RUPTURE LIFE 227 HOURS

10X

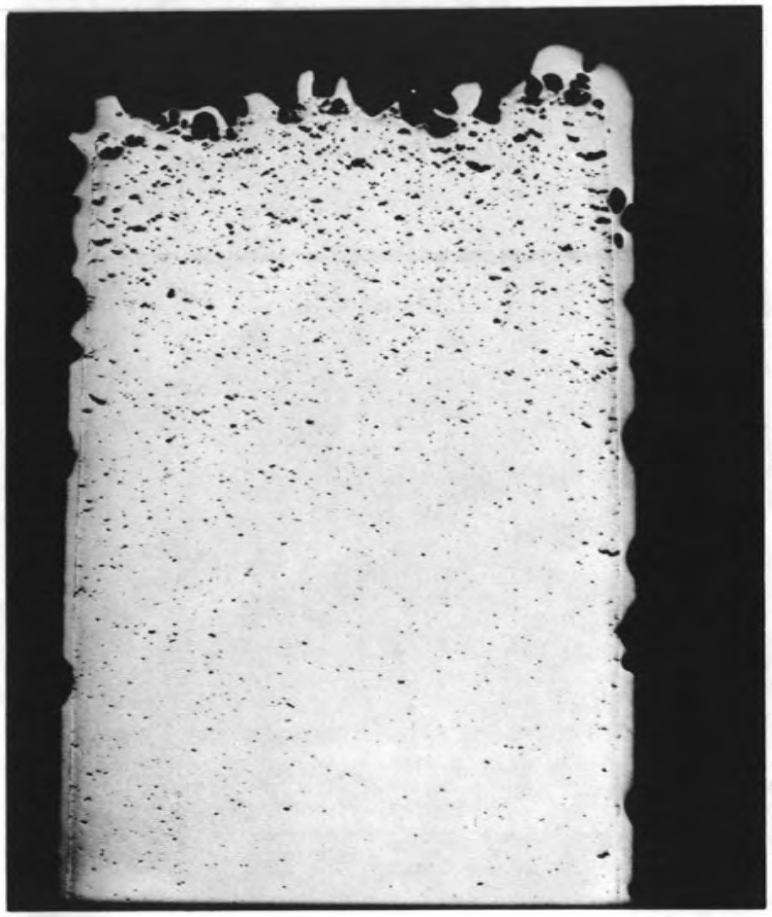

TEST BWC-9
RUPTURE LIFE 415 HOURS

10X

Fig. 5.59. Longitudinal sections (as polished) of uniaxial specimens ruptured at 28 ksi at 593°C. Type 304 stainless steel (heat 9T2796) 5/8-in. rod. Pretest diameter nominally 0.320 in.

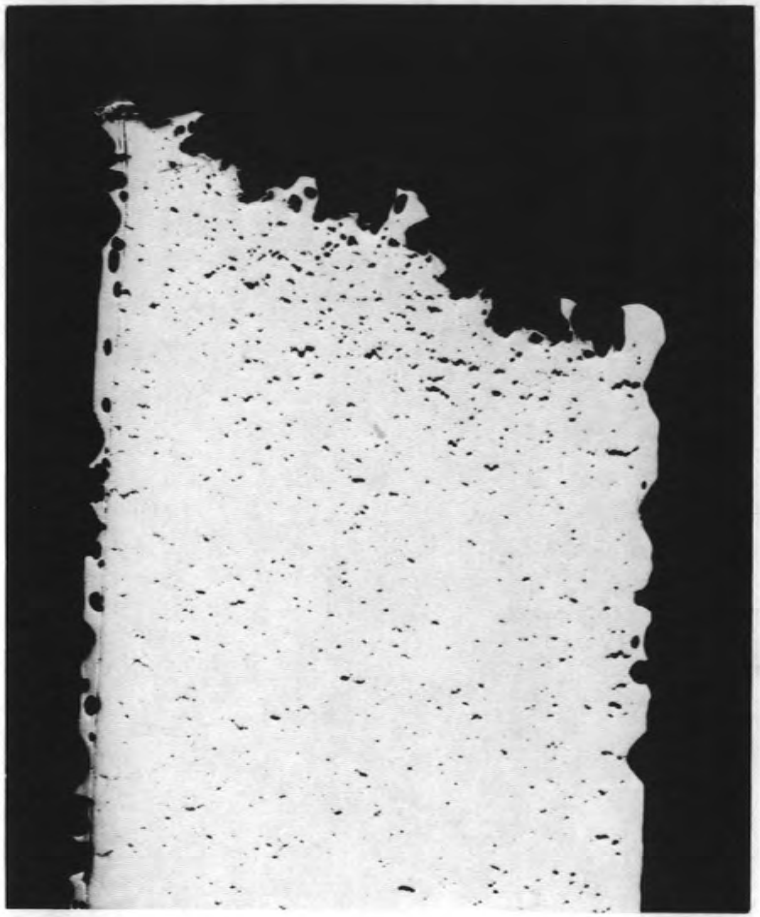

TEST BWR-2 10X
RUPTURE LIFE 368 HOURS

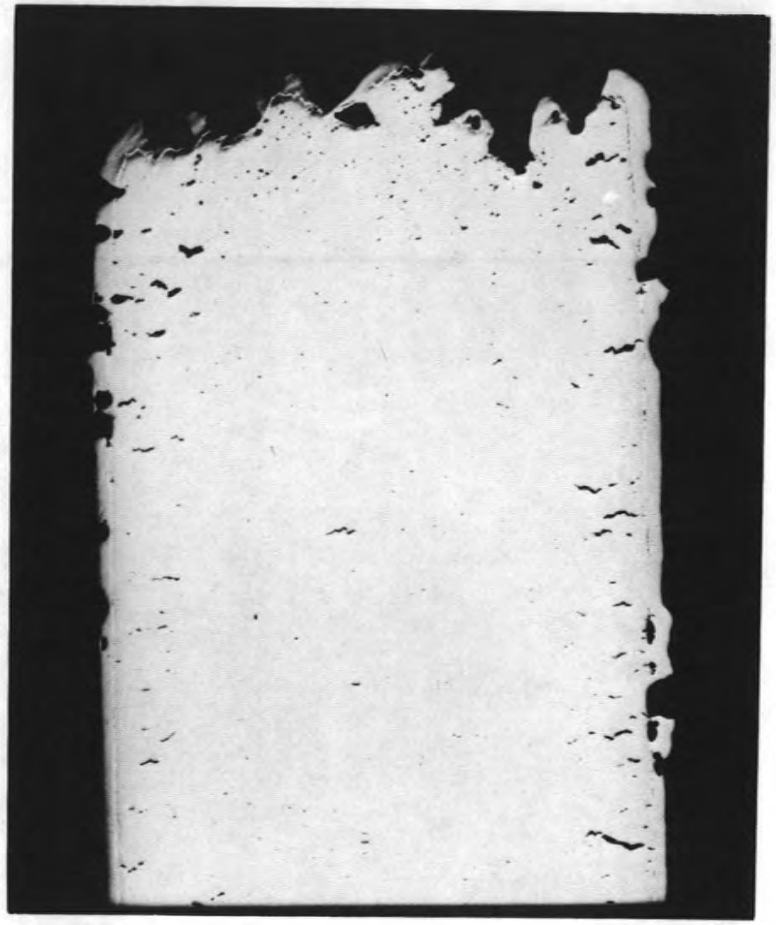

TEST BWR-13 10X
RUPTURE LIFE 276 HOURS

Fig. 5.60. Longitudinal sections (as polished) of uniaxial specimens ruptured at 28 ksi at 593°C. Type 304 stainless steel (heat 9T2796) 5/8-in. rod. Pretest diameter nominally 0.320 in.

Table 5.46. Status of uniaxial interrupted tests — type 304 stainless steel (heat 9T2796), 593°C (1100°F)

Test No.	Specimen No.	Stress (ksi)	Time at load (hr)
BWI-1	4-6	19.5	5930
BWI-2	5-6	19.5	5930
BWI-3	6-6	19.5	5930

Table 5.47. Time to rupture used in estimating life fractions

Stress (ksi)	Rupture time (hr)
16	60,000
17	35,000
18	20,000
20	7,500
25	800

comparison of the damage which occurred in each specimen near the failure. These photographs are of longitudinal sections, as polished, at 10×. Figures 5.61 and 5.62 show the same sections after oxalic etching to reveal the grain structure. The specimens with the longer rupture times showed more voids, although they were, in general, smaller and more blunt than those in the specimens with shorter rupture times. That is, the damage seen in the longer life specimens is more typical of creep damage than that seen in the shorter life specimens. The relationship with grain size is opposed to what one would expect for creep; that is, the

TEST BWC-2
RUPTURE LIFE 227 HOURS

10X

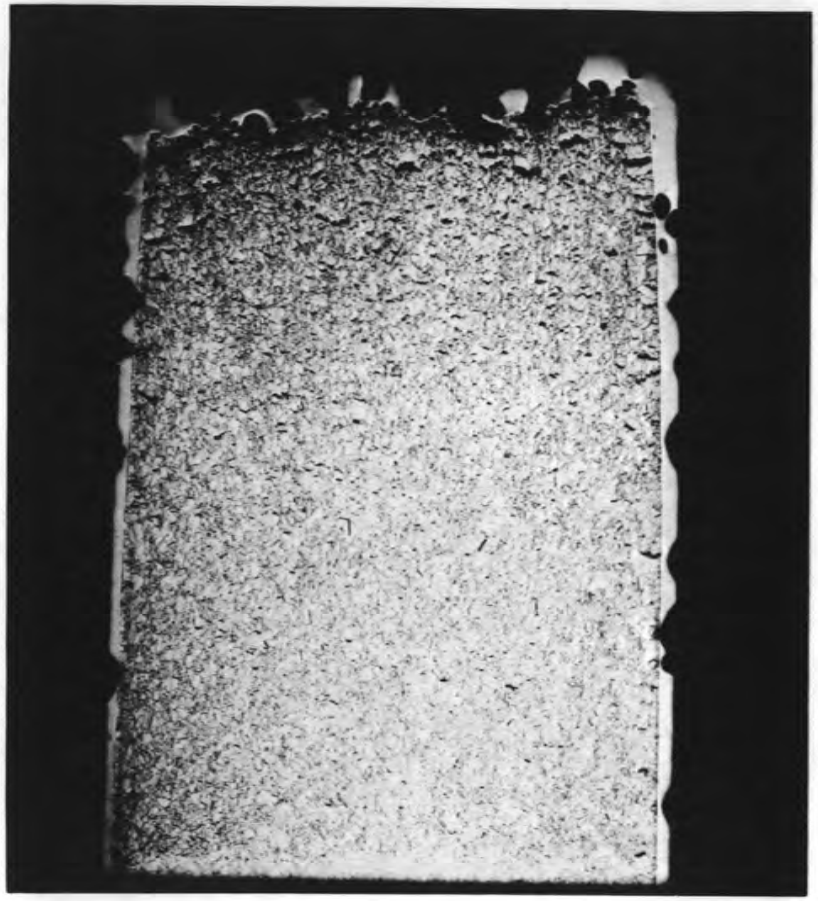

TEST BWC-9
RUPTURE LIFE 415 HOURS

10X

Fig. 5.61. Longitudinal sections (oxalic etch) of uniaxial specimens ruptured at 28 ksi at 593°C. Type 304 stainless steel (heat 9T2796) 5/8-in. rod. Pretest diameter nominally 0.320 in.

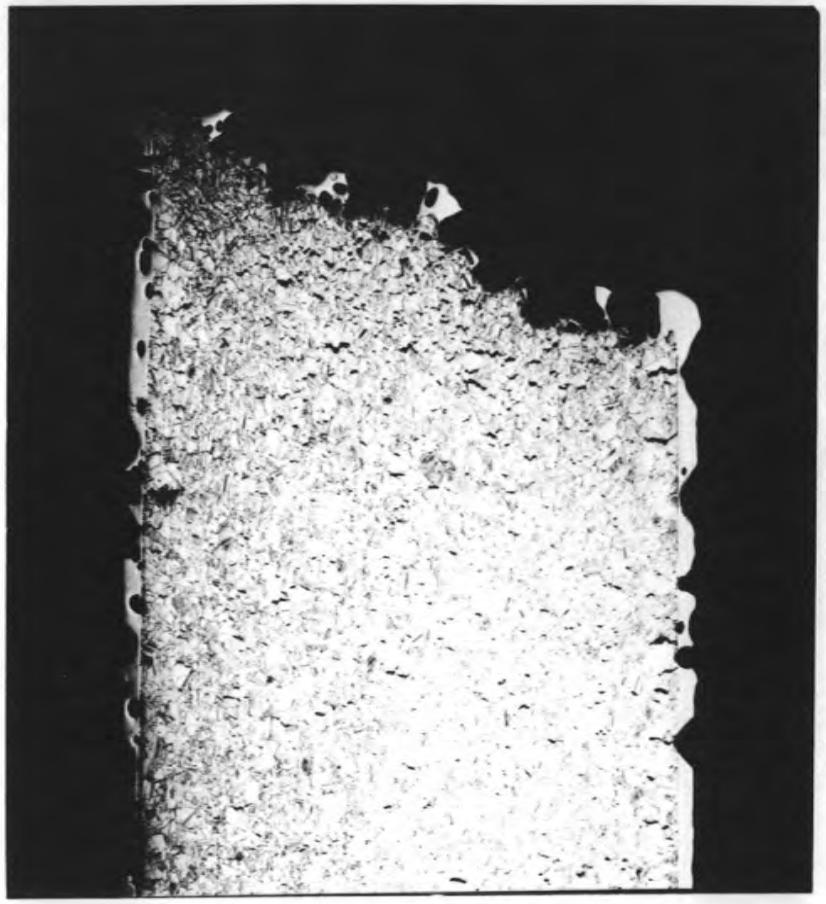

TEST BWR-2
RUPTURE LIFE 368 HOURS

10X

TEST BWR-13
RUPTURE LIFE 276 HOURS

10X

Fig. 5.62. Longitudinal sections (oxalic etch) of uniaxial specimens ruptured at 28 ksi at 593°C. Type 304 stainless steel (heat 9T2796) 5/8-in. rod. Pretest diameter nominally 0.320 in.

smaller grain structure yielded longer life than the larger grain specimens. This is probably due to the fact that the tests were all relatively short-time tests and should not be considered as typical creep tests. Specifically, the short-time damage occurring in the large-grain specimens more than offsets any advantage these specimens might have under normal creep conditions. The stress-strain behavior during loading for tests BWC-2 (227-hr life) and BWC-9 (415-hr life) is shown in Fig. 5.63. It is seen that the short-life specimen (BWC-2) was subjected to considerably more strain on loading than specimen BWC-9. Specimens BWR-2 and BWR-13 were tested on rupture machines; thus the corresponding loading data are not available. There is nothing within the records of the laboratory annealing procedure to indicate a reason for the variation of grain size.

Nine tubular specimens have been fabricated and annealed. The center test section of a tenth specimen has been machined and annealed and will have reference marks applied prior to final assembly. The first attempt at applying reference marks to this specimen, by sputtering platinum, was unsuccessful in that the masking procedure failed and permitted platinum to be deposited over a considerable part of the surface. No explanation of the failure was available, so that method has been abandoned. Presently, we are attempting to deposit gold by a plating process, but no evaluation of this method is yet available. The first tubular specimen (BWTR-1) which was loaded in pure tension at 21,850 psi ruptured at 1997 hr. As previously reported, an oil seal in the axial loading system failed during the loading process, so the specimen was transferred to a different machine. After 886 hr under load, a power shutdown occurred for 34 hr. The specimen remained under load during this period, but with no heat input to the furnace. The strain-time data for this test appear in Fig. 5.64. Two additional tubular tests (BWTR-2 and BWTR-4) have been loaded. Test BWTR-2 was loaded by internal pressure only with a circumferential stress of 21,850 psi (based on the mean diameter formula); test BWTR-4 was loaded with internal pressure and additional axial load, such that the axial stress was twice the circumferential stress (again based on the mean diameter) — axial stress, 21,850 psi; circumferential stress, 10,925 psi. The axial strain-time results are shown in Fig. 5.65. This test also experienced a leak in the axial load system and was moved to another

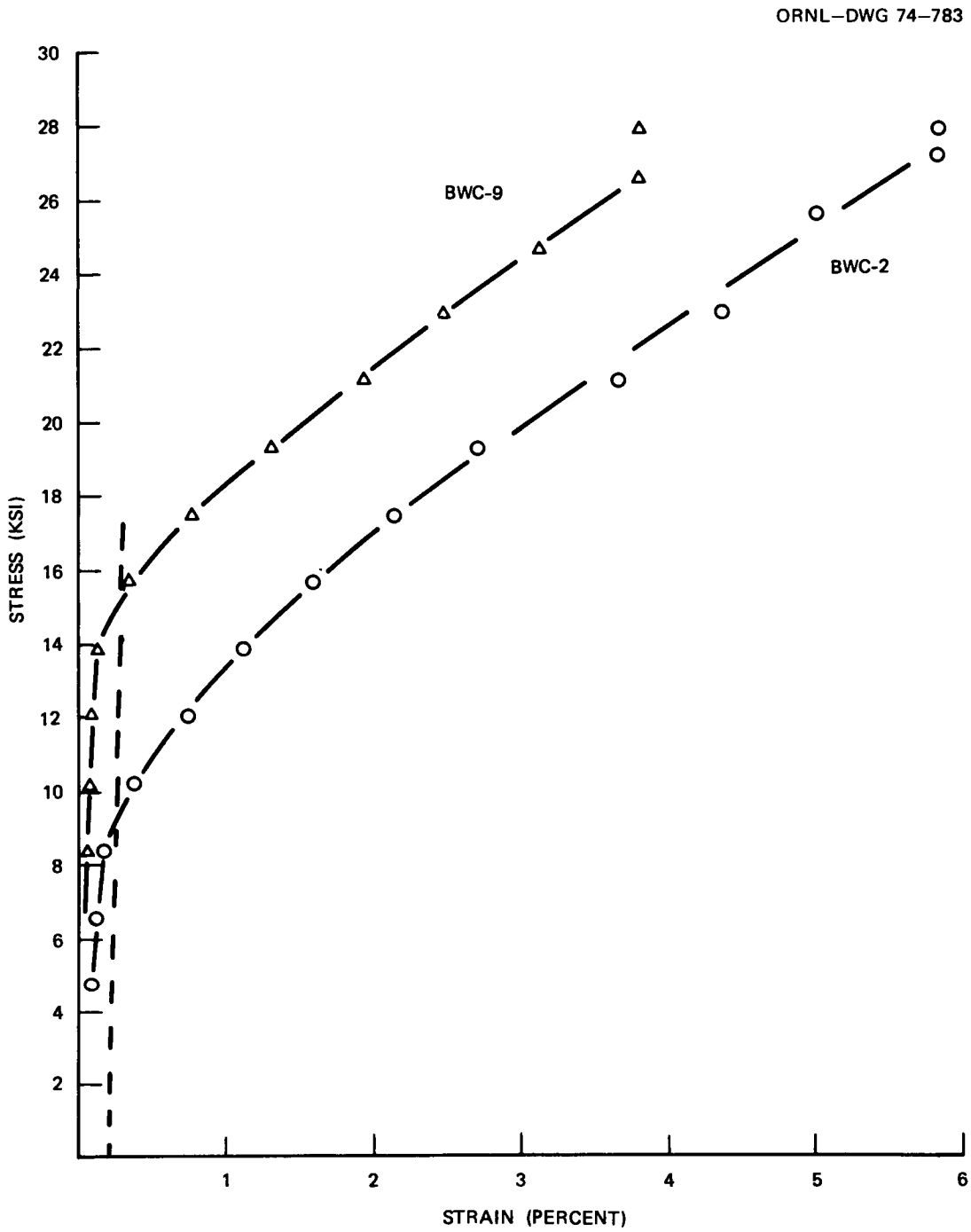

Fig. 5.63. Stress-strain behavior, on loading, for constant-load uniaxial rupture tests at 593°C. Type 304 stainless steel (heat 9T2796) 5/8-in. rod.

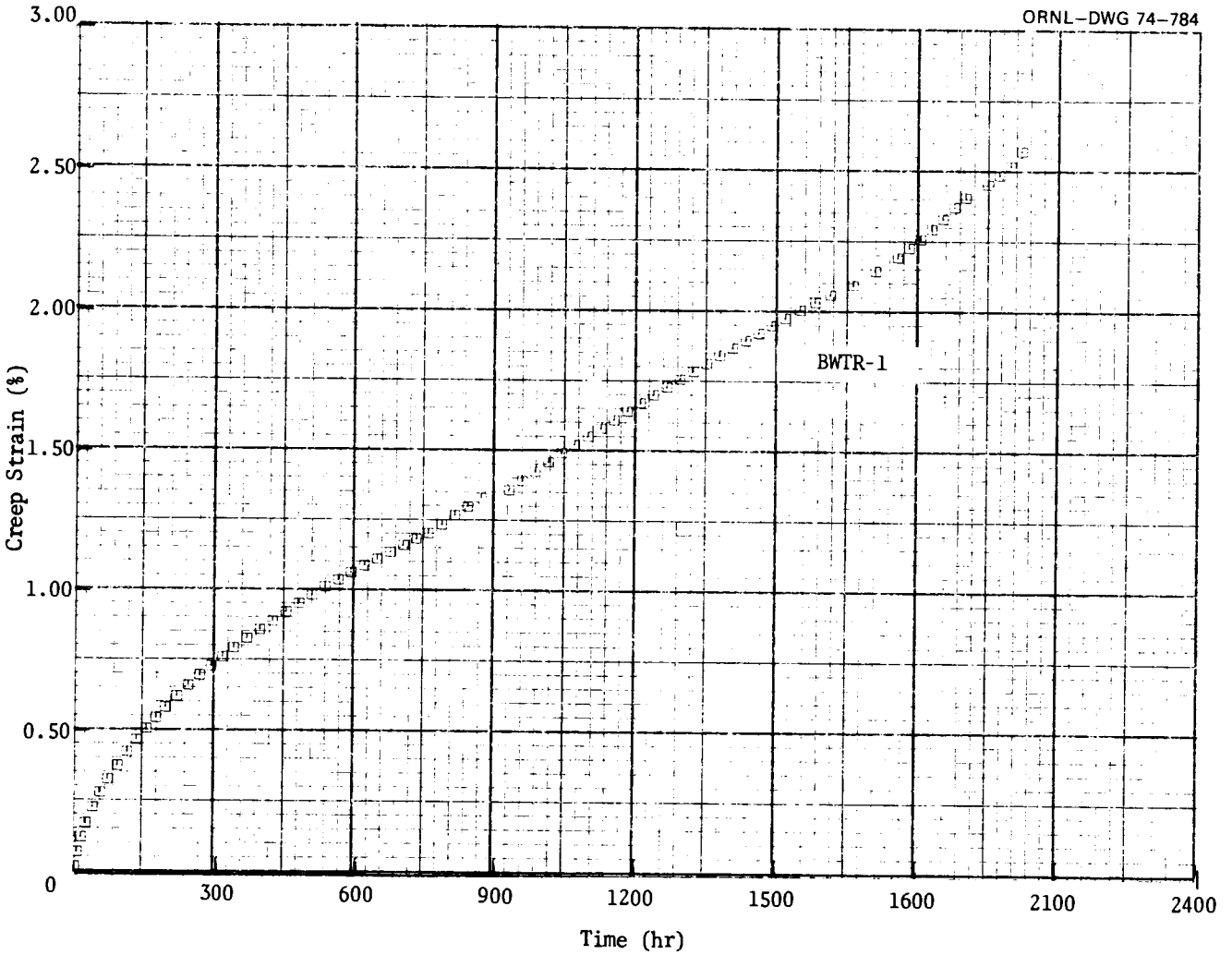

Fig. 5.64. Constant-load uniaxial rupture test. Tubular specimen loaded at 21,850 psi axial stress at 593°C (1.50-in. outside diameter, 0.075-in. wall thickness). Type 304 stainless steel (heat 9T2796) 1.927-in. rod.

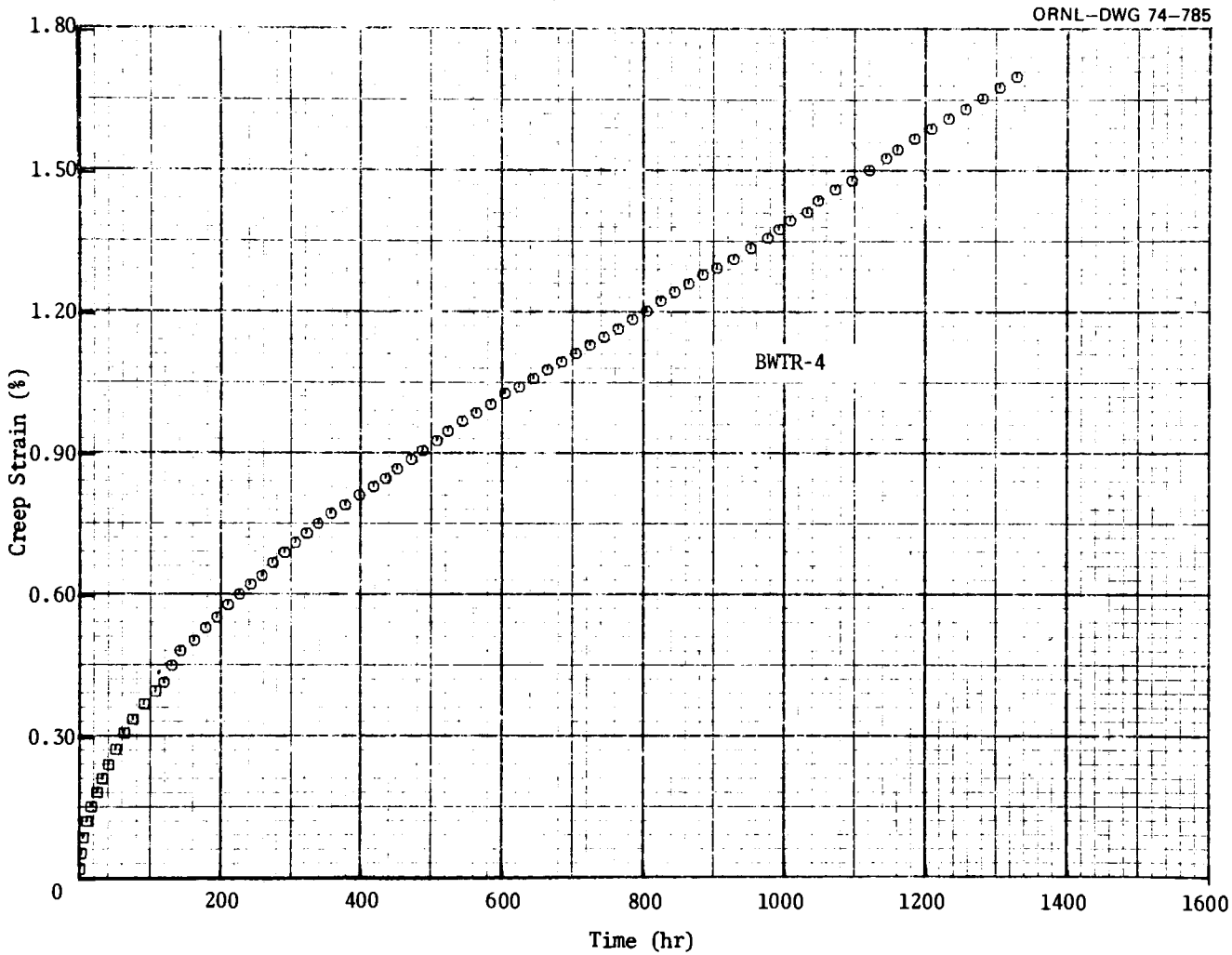

Fig. 5.65. Constant-load biaxial rupture test at 593°C. Tubular specimen with internal pressure and axial tension. Circumferential stress = 10,925 psi; axial stress = 21,850 psi; 1.50 in. outside diameter; 0.075-in. wall thickness. Type 304 stainless steel (heat 9T2796) 1.927-in. rod..

machine after a delay of 700 hr; the malfunction occurred after 121 hr under load.

As described in the previous progress report, a threaded rupture machine specimen (test BWR-14) is being tested with four DCDT's over the 2-in. gage length and a single DCDT and dial gage over the full load train. The purpose of the test is to determine if significant deformation occurs outside the gage length in the threaded-type specimen or if the bending is greater than that occurring in the 3-in. creep machine specimen. Figure 5.66 shows the strain-time results from the five DCDT's. It can be concluded that neither effect is of significance for this particular test. In Fig. 5.67, the results of this test are compared with two previous tests at identical test conditions, 20 ksi and 593°C (1100°F). In that figure, a 2-in. threaded rupture machine specimen was used in test BWR-5 (same as in test BWR-14), while a 3-in. button head creep machine specimen was used in test BWC-5B. The creep rate of test BWR-14 more closely approximates that of test BWR-5. Much of the difference in strains for tests BWR-14 and BWR-5 can be attributed to the unexplained step in strain occurring in test BWR-5 at approximately 30 hr, as shown in Fig. 5.68. This step was recorded with both a DCDT and a dial gage (reading at same location) and thus did occur somewhere within the load train. Included in Fig. 5.68 are results for test BWLF-5 (while initially at 20 ksi), which used a 3-in. button head creep machine specimen.

Test BWC-10 (20 ksi), initiated since the last reporting period, uses a 3-in. button head creep machine specimen with two opposed DCDT's over the full 3-in. gage length and two opposed DCDT's over the center 2 in. of the specimen gage length. In addition, a dial gage measures the full load train deflection. The objective of the test is to determine if the strain becomes significantly localized prior to tertiary creep. Figure 5.69 shows the strain-time results to date, which, at this early time, do not reveal any significant difference. Figure 5.70 compares these data with the other tests at the same stress and temperature. This test closely approximates the two previous tests which were with the threaded-type rupture machine specimens.

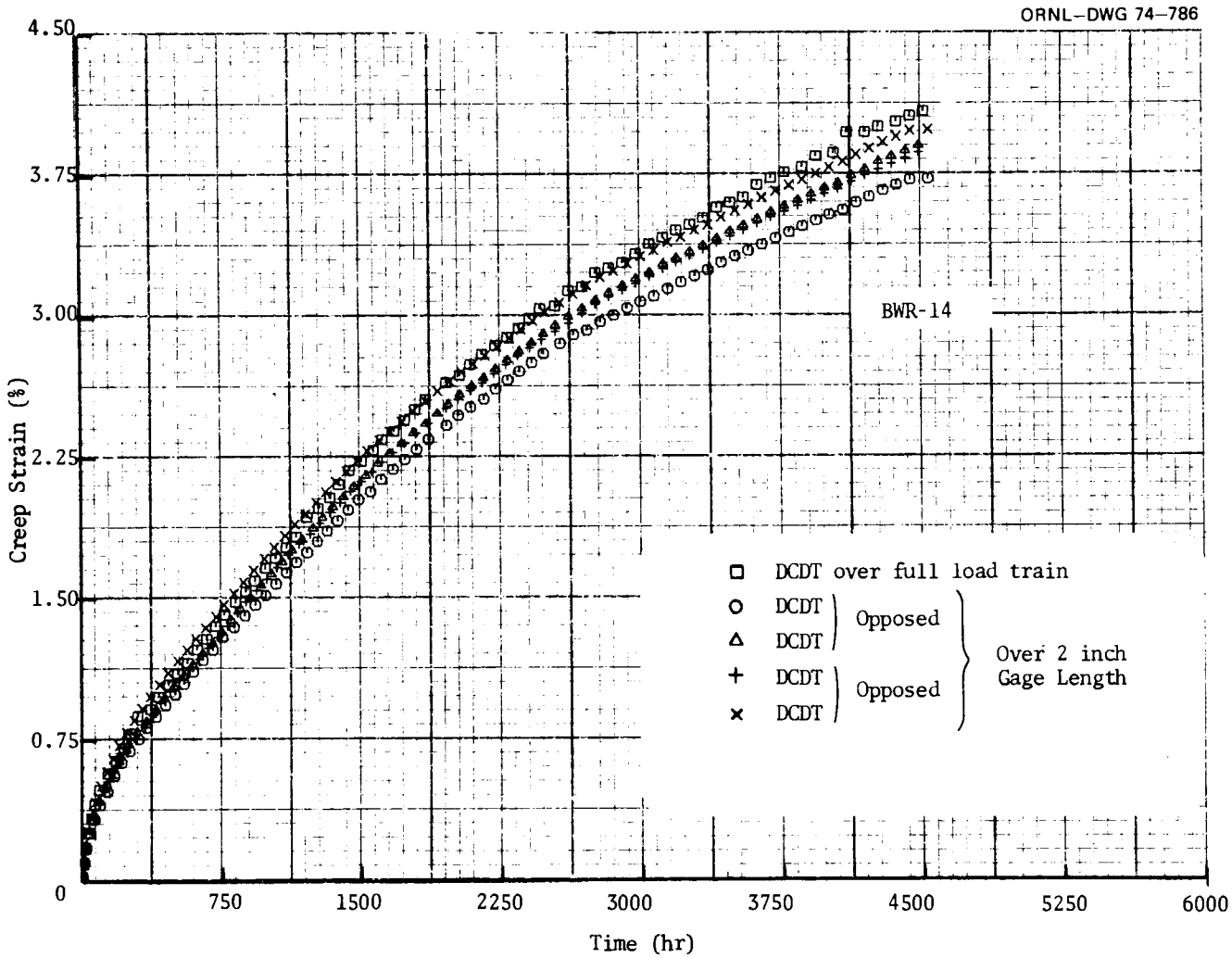

Fig. 5.66. Constant-load uniaxial test to evaluate strain outside of gage length and bending in a threaded rupture machine specimen loaded at 20 ksi and 593°C. Type 304 stainless steel (heat 9T2796) 5/8-in. rod.

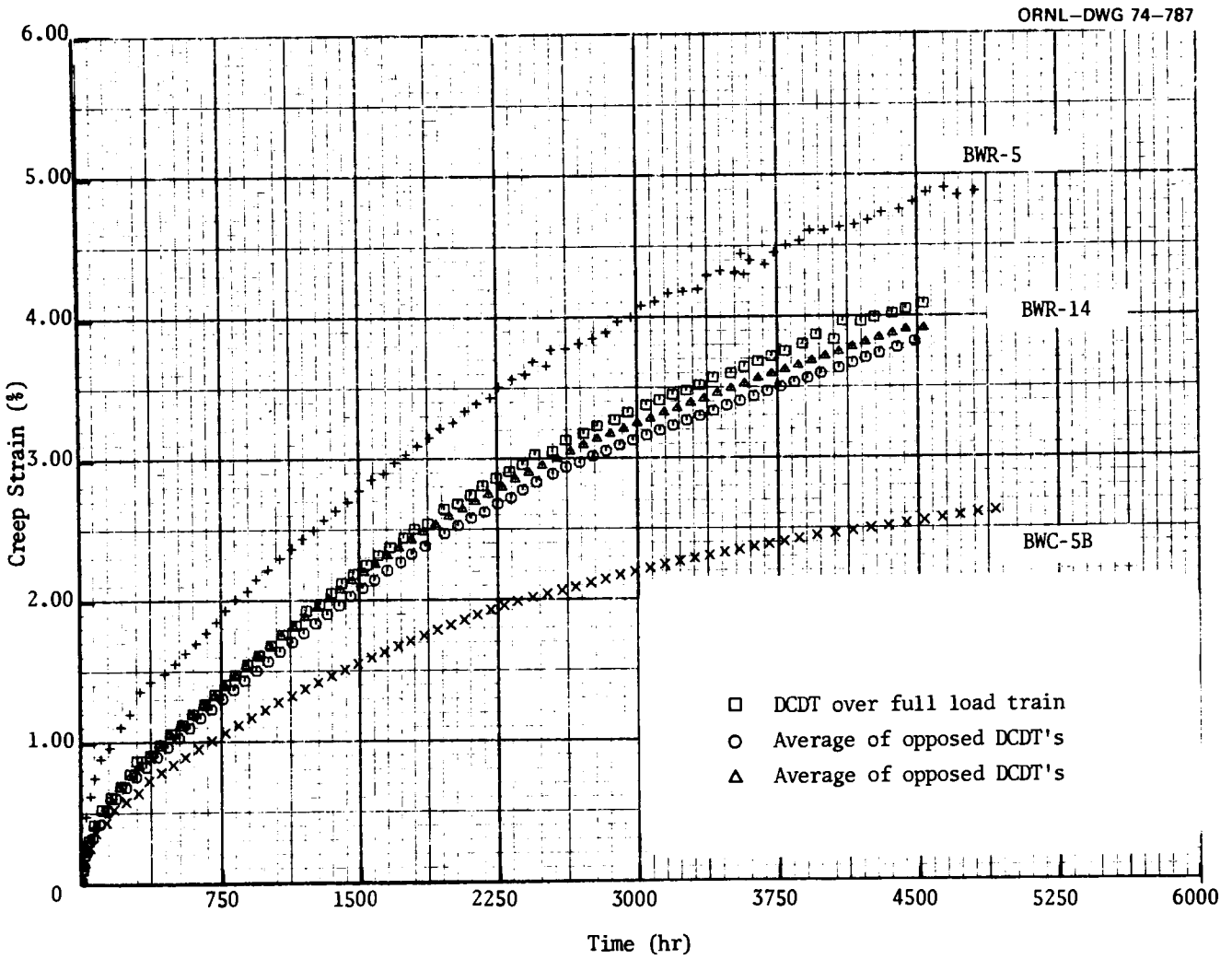

Fig. 5.67. Comparison of constant-load uniaxial tests at 20 ksi and 593°C. Type 304 stainless steel (heat 9T2796) 5/8-in. rod.

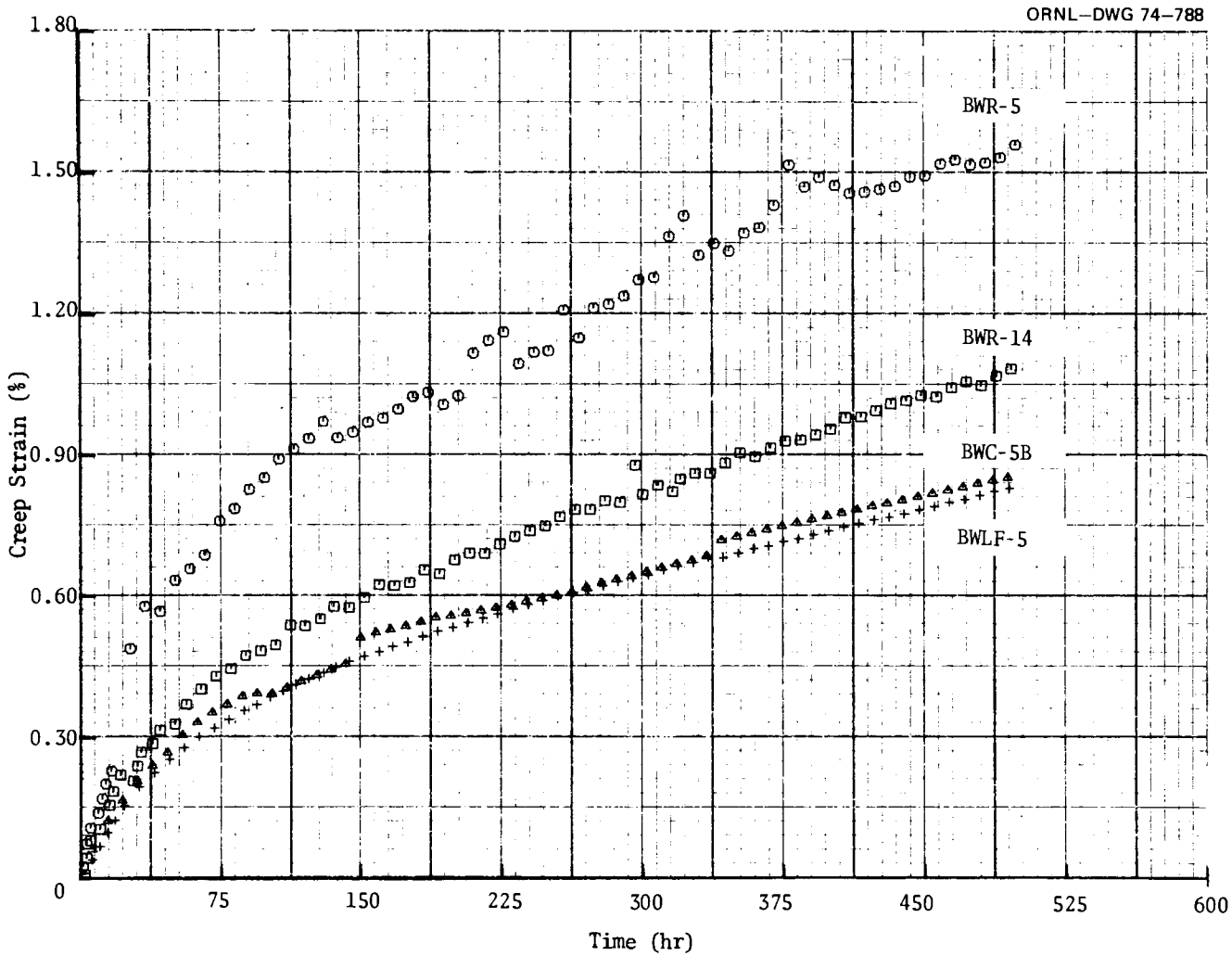

Fig. 5.68. Comparison of uniaxial tests initially at 20 ksi and 593°C. Type 304 stainless steel (heat 9T2796) 5/8-in. rod.

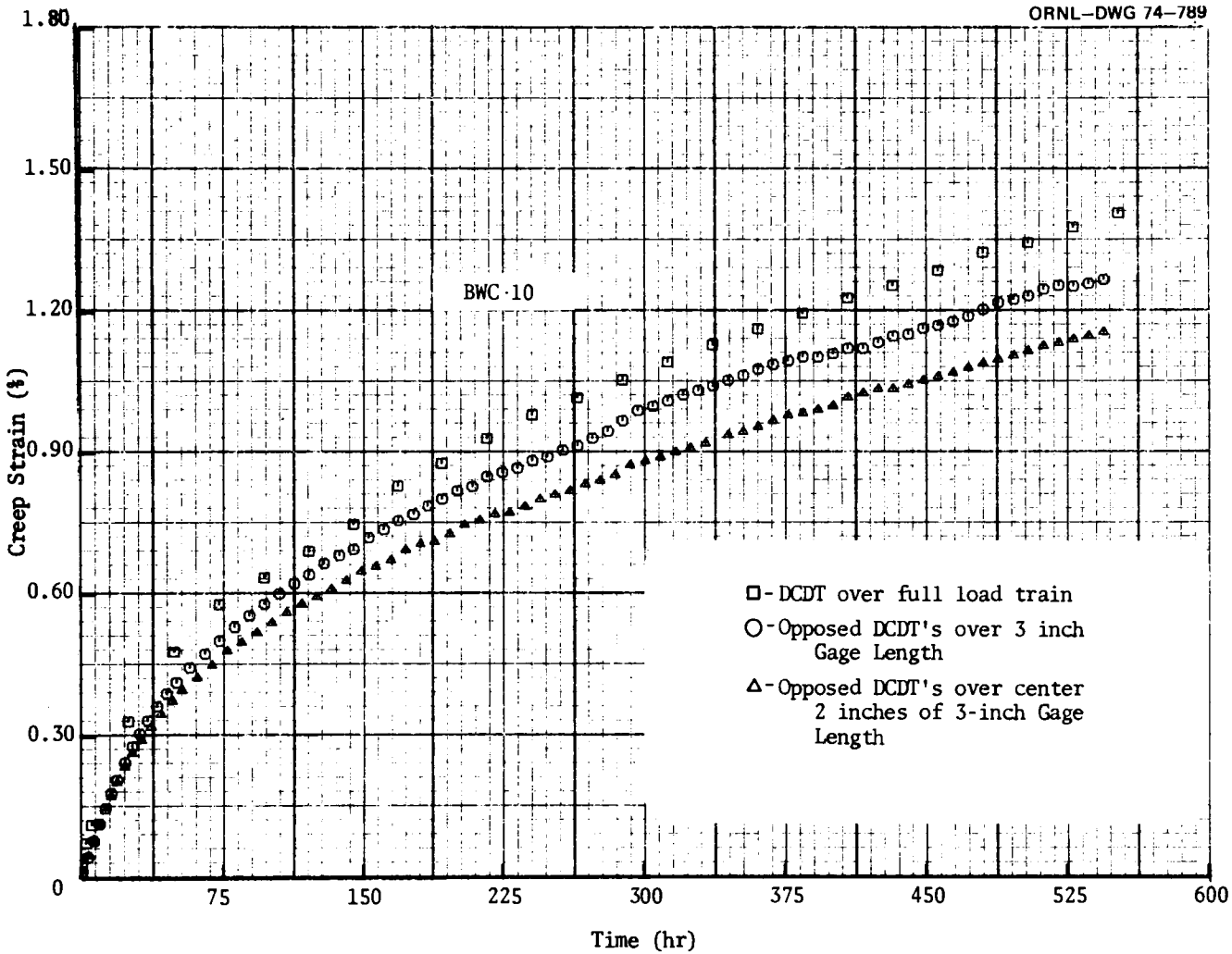

Fig. 5.69. Constant-load uniaxial test to evaluate localization of strain in 3-in. button head creep machine specimen loaded at 20 ksi and 593°C. Type 304 stainless steel (heat 9T2796) 5/8-in. rod.

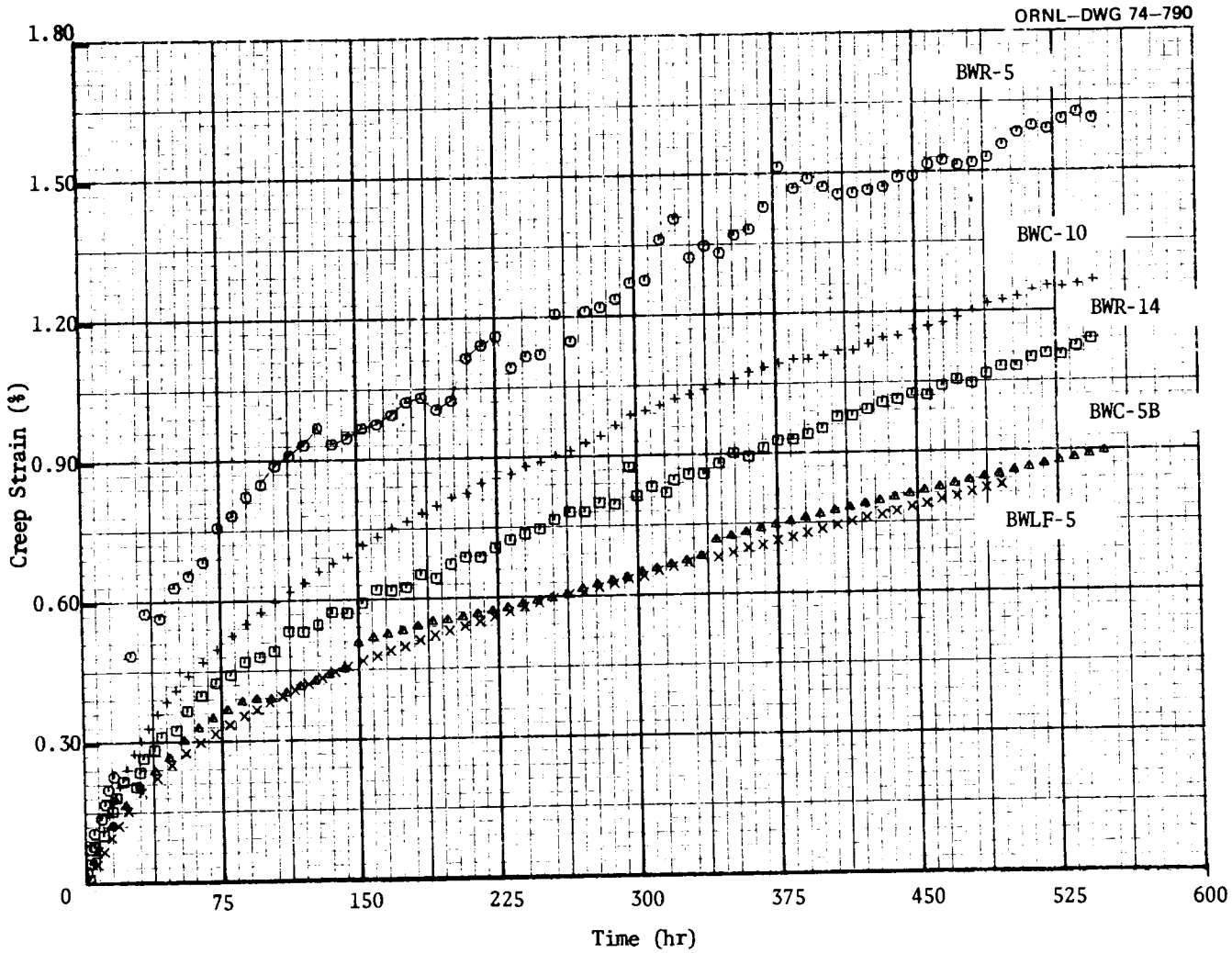

Fig. 5.70. Comparison of all uniaxial tests initially at 20 ksi and 593°C. Type 304 stainless steel (heat 9T2796) 5/8-in. rod.

5.7 REFERENCES

1. H. E. McCoy, *Fuels and Materials Development Program Quart. Progr. Rep. Mar. 31, 1973*, ORNL-TM-4250, pp. 89–92.
2. H. E. McCoy, *Fuels and Materials Development Program Quart. Progr. Rep. Sept. 30, 1973*, ORNL-TM-4405, pp. 55–64.
3. H. E. McCoy, *Fuels and Materials Development Program Quart. Progr. Rep. June 30, 1973*, ORNL-TM-4355, pp. 105–11.
4. H. E. McCoy, *Fuels and Materials Development Program Quart. Progr. Rep. Sept. 30, 1973*, ORNL-TM-4405, pp. 82–6.
5. H. E. McCoy, *Fuels and Materials Development Program Quart. Progr. Rep. June 30, 1973*, ORNL-TM-4355, pp. 116–18.
6. C. E. Pugh et al., *Currently Recommended Constitutive Equations for Inelastic Design Analysis of FFTF Components*, ORNL-TM-3602, pp. 15–27.
7. J. H. Holloman, "Tensile Deformation," *Trans. AIME* 162: 268 (1945).
8. P. Ludwik, *Elemente der Technologischen Mechanik*, Springer, Berlin, 1970.
9. D. C. Ludwigson, "Modified Stress-Strain Relation for FCC Metals and Alloys," *Met. Trans.* 2: 2825 (1971).
10. R. E. Reed-Hill, W. R. Cribb, and S. N. Monteiro, "Concerning the Analysis of Tensile Stress-Strain Data Log d/d_p vs Log Diagrams," *Met. Trans.* 4: 2665–67 (1973).
11. E. Voce, "The Relationship Between Stress and Strain for Homogeneous Deformation," *J. Inst. Metals* 74: 537 (1948).
12. L. D. Blackburn, "Isochronous Stress-Strain Curves for Austenitic Stainless Steels," pp. 15–48 in *The Generation of Isochronous Stress-Strain Curves*, ed. by A. O. Schaefer, American Society of Mechanical Engineers, New York, 1972.
13. H. E. McCoy, *Fuels and Materials Development Program Quart. Progr. Rep. Sept. 30, 1973*, ORNL-TM-4405, pp. 113–16.
14. G. V. Smith, E. J. Dulis, and E. G. Houston, "Creep and Rupture of Several Chromium-Nickel Austenitic Stainless Steels," *ASM (Am. Soc. Metals) Trans.* 42: 935–80 (1950).
15. G. V. Smith, private communication, December 1973.

16. W. F. Simmons and J. A. Van Echo, "The Elevated-Temperature Properties of Stainless Steels," ASTM DS5-S1, 1965.

17. W. F. Simmons and H. C. Cross, "Report on the Elevated Temperature Properties of Stainless Steels," ASTM STP No. 124, 1952.

18. C. F. Etienne, W. Dortland, H. B. Zeedijk, "On the Capability of Austenitic Steel to Withstand Cyclic Deformation During Service at Elevated Temperatures," *Inst. Mech. Engrs. Conf. Pub.* 13: 225.1 (1973).

19. O. R. Carpenter and R. D. Wylie, "16-8-2 Cr-Ni-Mo for Welding Electrode," *Metal Progr.* 70(5): 65–73 (1956).

20. R. H. Caughey and W. G. Benz, Jr., "Material Selection and Fabrication, Main Steam Piping for Eddystone No. 1, 1200°F and 5000 psi Service," *Trans. ASME, J. Eng. Power, Ser. A* 82(1): 293–313 (1960).

21. R. T. King and J. O. Stiegler, "The Effect of Residual Elements on the Ductility of Type 308 Stainless Steel Weld Metal," paper presented at the 1973 Annual Winter Meeting of ASME, Detroit, Michigan, and accepted for inclusion in a special publication.

22. C. V. Dodd, private communication, April 1973.

23. *ASME Boiler and Pressure Vessel Code, Section III, Nuclear Power Plant Components,* The American Society of Mechanical Engineers, New York, 1972.

24. *Interpretations of ASME Boiler and Pressure Vessel Code, Case 1331-8,* The American Society of Mechanical Engineers, New York, 1973.

25. L. D. Blackburn, "Isochronous Stress-Strain Curves for Austenitic Stainless Steels," p. 15 in *Generation of Isochronous Stress-Strain Curves,* ed. by A. O. Schaefer, American Society of Mechanical Engineers, New York, 1972.

26. K. C. Thomas and E. B. Weglein, "The Strengthening of an Austenitic Steel by Phosphorus," *ASM Trans. Quart.* 56: 566 (September 1963).

27. F. C. Hull, "The Effect of Composition on the Stress-Rupture Properties of Fully Austenitic Stainless Steel Welds," 71-PVP-64, paper presented at Pressure Vessels and Piping Conference, San Francisco, May 10–12, 1971.

28. H. R. Voorhees and J. W. Freeman, pp. 126–27 in *The Elevated-Temperature Properties of Weld-Deposited Metal and Weldments, Spec. Tech. Publ.* 226, American Society for Testing and Materials, Philadelphia, 1958.

29. W. Leyda, Babcock & Wilcox Corp., private communication, September 1973.

30. F. C. Monkman and N. J. Grant, "An Empirical Relationship Between Rupture Life and Minimum Creep Rate in Creep Rupture Tests," pp. 593–605 in *American Society for Testing and Materials, Proceedings,* Vol. 56, 1956.

31. R. T. King and G. M. Goodwin, *Fuels and Materials Development Program Quart. Progr. Rep. Sept. 30, 1972,* ORNL-TM-4055, pp. 5.14–5.17.

32. R. T. King and E. Bolling, *Fuels and Materials Development Program Quart. Progr. Rep. Mar. 31, 1972,* ORNL-TM-3797, pp. 225–27.

33. R. T. King and J. O. Stiegler, "Effect of Composition on Fracture Characteristics and Creep Ductility of Type 308 Stainless Steel Weld Metal," paper presented at the 1973 Annual Winter Meeting of ASME, Detroit, Michigan, November 1973, to be published.

34. R. L. Klueh, *Effect of Carbon on the Mechanical Properties of 2 1/4 Cr-1 Mo Steel,* ORNL-4922 (November 1973).

35. C. Li and R. P. Wei, "Calibrating the Electrical Potential Method for Studying Slow Crack Growth," *Mater. Res. Stds.* 6: 392–94 (1966).

36. D. M. Gilbey, *Measurement of the Length of a Central or Edge Crack in a Sheet of Metal by an Electrical Resistance Method,* Royal Aircraft Establishment Technical Report 66402 (December 1966).

37. P. L. Rittenhouse, *Fuels and Materials Development Program Quart. Progr. Rep. June 30, 1973,* ORNL-TM-4355, pp. 59–68.

38. P. L. Rittenhouse, *Fuels and Materials Development Program Quart. Progr. Rep. Sept. 30, 1973,* ORNL-4405, pp. 38–48.

39. R. L. Klueh and D. A. Canonico, *Fuels and Materials Development Program Quart. Progr. Rep. Sept. 30, 1973,* ORNL-TM-4405, pp. 32–7.

40. H. E. McCoy and R. D. Waddell, Jr., "Base-Line Mechanical Property Testing of Reference Heat of Type 304 Stainless Steel," *Fuels and Materials Development Program Quart. Progr. Rep. Mar. 31, 1973,* ORNL-TM-4250, pp. 89–102.

41. R. W. Swindeman, "Stress-Strain Testing," *High-Temperature Structural Design Methods for LMFBR Components Quart. Progr. Rep. June 30, 1973,* ORNL-4356, pp. 6–10.

6. WESTINGHOUSE ADVANCED REACTORS DIVISION

E. C. Bishop

6.1 INTRODUCTION

The program being performed at Westinghouse Advanced Reactors Division is entitled "Validation of High Temperature Design Methods and Criteria," (189a No. 04165). Two of the tasks in this program are "Basic Specimen Testing" and "Tubular Specimen Testing." The objective of these tasks is to design and test specimens of increasing complexity to determine the inelastic behavior and strain tolerances of Types 304 and 316 stainless steel under complex stress distributions. This report covers the work performed during the period from September 1, 1973 to November 30, 1973.

6.2 BASIC SPECIMEN TESTING - N. J. Ettenson, M. Manjoine (Westinghouse Reseach Laboratories)

A variety of specimen designs have been selected for this task, as shown in Table 6.1. Data obtained to date are presented in Table 6.2.

6.2.1 Uniaxially Loaded Specimen Models with Uniform Gage Section (304 SS, Heat 9T2796)

6.2.1.1 Test Piece Description

Types A, B, and G test piece designs, as shown in Table 6.1, are used for this part of the test program.

6.2.1.2 Current Results

Tests have been completed on plane stress models Type A and B (see Table 6.1 for model descriptions). The results are summarized in Table 6.2. Additional analysis of the strain distribution will be compared with the finite element strain predictions.

A completed test of the plane strain model, Type G2, has a lower effective stress because the transverse stresses increase as the plastic deformations occur. After 6715 hours (approximately twice the time for rupture of Type B), the stress was raised from 21 to 25 ksi (Table 6.2 and

Table 6.1 Specimen Types

Specimens from Base Material

A. Plane Stress Specimen
1/3 x 2/3 x 3 in. (8.5 x 17 x 76.2 mm) gage section

B. Plate Specimen
1/3 x 10/3 x 3 in. (8.5 x 85 x 76.2 mm) gage section

C. Plate Specimen with Central Hole of 1/3 in.(8.5 mm) Diameter
1/3 x 10/3 x 3 in. (8.5 x 85 x 76.2 mm) plate section

D. Round Circumferentially Notched Specimen
Major Diameter = 0.96 in. (24.4 mm), Minor Diameter = 0.64 in. (16.2 mm)
Root Radius = 0.018 in. (0.46 mm)
Two nearly identical notches in specimen.

G. Plane Strain Specimen
1/3 x 10/3 x 1 in. (8.5 x 85 x 26 mm) gage section
Ends constrained in transverse direction.

H. Biaxially Loaded Notched Plates
Wedge-opening-loaded Plates with 1/3 in. (8.5 mm) Diameter Notch.

Specimens with Welds

BTW - B-type plate specimen with transverse weld at mid-length of gage section

BAW - B-type plate specimen with axial weld at center of gage section

CTW - C-type specimen with hole through transverse weld

CAW - C-type specimen with hole through axial weld

DTW - D-type specimen with notch root in transverse weld

DZTW - D-type specimen with notch root at weld fusion line or heat affected zone (HAZ)

GTW - G-type specimen with transverse weld at mid-gage length

GAW - G-type specimen with axial weld at center of gage section

Table 6.2 Summary of Creep Data, Type 304 Stainless Steel at 1100°F (593°C)

Test No. (Gage Section)	Loading Data: Stress (ksi)	Stress (MPa)	Plastic Strain (%)	Creep Data: Creep Rate (%/hr)	Increment: Strain (%)	Increment: Time (hr)	Accumulated: Strain (%)	Accumulated: Time (hr)	Permanent Strain (%)
A1	21.0	144.8	4.66	2.2×10^{-3}	1.10	303	1.10	303[a]	5.76
(1/3 x 2/3 x 3 in.)				2.2×10^{-3}	0.89	403	1.99	706[a]	6.65
(8.5 x 17 x 76.2 mm)							3.47	1250[b]	8.13
							3.65	1270[c]	8.31
							7.34	1826	12.00[d]
A2	10.0	68.95	0.215	8.5×10^{-5}	0.228	2180	0.228	2180[a]	0.443
(1/3 x 2/3 x 3 in.)				6.2×10^{-5}	0.028	405	0.256	2585[e]	0.471
(8.5 x 17 x 76.2 mm)	11.0	75.84	0	8.6×10^{-5}	0.124	1349	0.380	3934[e]	0.595
	12.5	85.68	0	2.0×10^{-4}	0.213	1002	0.593	4936[e]	0.808
	15.0	103.4	0.014	2.5×10^{-4}	0.811	1848	1.404[a]	6784[e]	1.619
	21.0	144.8	0.646	4.5×10^{-3}	28.75	4266	30.15	11050[h]	31.0
B1	21.0	144.8	5.34	1.4×10^{-3}	1.76	666	1.76	666[a]	7.10
(1/3 x 10/3 x 3 in.)				8.8×10^{-4}	1.03	1005	2.79	1671[a]	—
(8.5 x 85 x 76.2 mm)				1.7×10^{-3}	—	—	—	3000[c]	—
					1.72	1587	4.51	3258[a]	9.85[g]
								3525[h]	
B2	10.0	68.95	0.273[i]	8.6×10^{-3}	0.31	1644	0.31	1644[a]	0.58
(1/3 x 10/3 x 3 in.)	j			9.0×10^{-3}	0.17	1462	0.45	3106[e]	0.72
(8.5 x 85 x 76.2 mm)	11.0	75.84	0	1.1×10^{-4}	0.16	1804	0.61	4910[e]	0.88
	12.5	85.68	0	2.0×10^{-4}	0.33	1364	0.94	6274[e]	1.21
	15.0	103.4	0.051	4.7×10^{-4}	1.0	1302[a]	1.93	7576[e]	1.98
	21.0	144.8	1.88	8.6×10^{-3}	16.33	1623	18.26	9139[h]	20.19
C1	23.3[k]	160.5	8[n]	—	1.7[n]	100[c]	—	—	—
(1/3 x 10/3 x 3 in.)							22.9[n]	138[d]	
(8.5 x 85 x 76.2 mm)									
CENTRAL HOLE									
1/3 in. (8.5 mm) Dia.									
C2	10.0[k]	68.95	0.14[n]		0.62[n]	2808[a]	0.62[n]	2808[e]	
(1/3 x 10/3 x 3 in.)	11.0[k]	75.84	0		0.4[f]	1120[f]	1.0[n]	3928[f]	
(8.5 x 85 x 76.2 mm)	12.5	35.68	0		0.5[n]	1360[a]	1.5[n]	5398[e]	
CENTRAL HOLE	15.0	103.4	0.28[n]		0.82[n]	1148	2.32[n]	6546	
1/3 in. (8.5 mm) Dia.	18.0	124.1	0.06[n]		3.31[n]	1630[a]	5.63[n]	8176[g]	
			0		0.89[n]	791[a]	6.52[n]	8967	
			0		small	944[a]	6.52[nt]	9911	
						f			

*HT 9T2796, annealed 2000F(1094C)

[a]Interrupted for photographic measurement

[b]Transition at 0.2% OFFSET

[c]Transition at double minimum rate

[d]Rupture, R

[e]Stress raised (step-loaded test)

[f]Test in progress

[g]Crack initiated

[h]Test terminated, crack tearing

[i]Strain gage average, bending noted

[j]Specimen rotated 180° to investigate bending

[k]Net Section Stress, Gross Section stress = 0.9 N.S.S.

[l]Data & fracture bending analyzed

[m]Average strain at central hole

[n]Average overall strain

[p]Test in preparation

[q]Specimen to be sectioned to determine damage at 78% of estimated rupture life

[r]Deflection of notch, inches (25.4 mm)

[t]True strain = ln(Ao/A)

[u]Test interrupted, 1/2 of specimen continued

Table 6.2 Continued

Test No. (Gage Section)	Loading Data: Stress (ksi)	Loading Data: Stress (MPa)	Loading Data: Plastic Strain (%)	Creep Data: Creep Rate (%/hr)	Creep Data: Increment Strain (%)	Creep Data: Increment Time (hr)	Creep Data: Accumulated Strain (%)	Creep Data: Accumulated Time (hr)	Permanent Strain (%)
C3	21.0[k]	144.8	4.4[n]		1.5[n]	325[c]			
(same as above)							4.1[n]	397[h]	8.5[n]
Notched Round									
D = 0.96 in. (24.4 mm),									
d = 0.64 in. (16.2 mm),									
R = 0.019 in. (0.46 mm)									
D1-1	30.0	206.8	2.6[t]		0.3[t]	137	0.3[t]	137	2.9[t]
					0.2[t]	102	0.5[t]	239[g]	3.1[t]
D1-2	30.0		2.2[t]		0.26[t]	137	0.26[t]	137	2.46[t]
					0.22[t]	113	0.48[t]	250[c]	2.68[t]
							10.92[t]	305[d]	13.12[t]
D2-1	25.0	172.4	0.009[r]				0.006[r]	1371	0.015[r]
								1371[g]	2.17[t]
D2-2	25.0		0.009[r]				0.006[r]	1240[c]	
								1371[d]	5.3[t]
D3	21.0	144.8	0.002[r]					5499[h]	
D4	10.0	68.95	0			406		406[e]	
	11.0	75.84	0			477		883[e]	
	12.5	85.68	0			434		1317[e]	
	15.0	103.4	0			404		1721[e]	
	21.0	144.8	0.001[r]		0.004[r]	433		2154[e]	
	25.0	172.4	0.003[r]		0.033[r]	581[g]		3735[u]	
D4-2	25.0	172.4				2904[h]		5058	
D5-1	23.0	158.6				1681[g]		1681	
D5-2						150		1831[d]	
Plane Strain									
(1/3 x 10/3 x 1 in.)									
(8.5 x 85 x 25 mm)									
G2	21.0	144.8	0.43	3.9×10^{-4}	1.34	1195[a]	1.34	1195	1.77
			0	1×10^{-4}	0.83	5520[a]	2.17	6715[e]	2.60
	25.0	172.4	0.01	2.3×10^{-3}	1.8	700			
					2.5	1150[c]	4.67	7865	
					4.43	1433[a]	6.6	8148	
						1837[d]		8552	

[*] HT 9T2796, annealed 2000F(1094C)

[a] Interrupted for photographic measurement

[b] Transition at 0.2% OFFSET

[c] Transition at double minimum rate

[d] Rupture, R

[e] Stress raised (step-loaded test)

[f] Test in progress

[g] Crack initiated

[h] Test terminated, crack tearing

[i] Strain gage average, bending noted

[j] Specimen rotated 180° to investigate bending

[k] Net Section Stress, Gross Section stress = 0.9 N.S.S.

[l] Data & fracture bending analyzed

[m] Average strain at central hole

[n] Average overall strain

[p] Test in preparation

[q] Specimen to be sectioned to determine damage at 78% of estimated rupture life

[r] Deflection of notch, inches (25.4 mm)

[t] True strain = ln(Ao/A)

[u] Test interrupted, 1/2 of specimen continued

Figure 6.1). Failure occurred in 1837 hours which is about three times longer than for the plane stress case. Fractures started at the fillets where there are stress and strain concentrations. However, as the average stress increases, central cracks form in the fillet and grow in size. The specimen at fracture, Figure 6.2a, illustrates the distortion of the surface grid, and Figure 6.2b shows the surface fracture.

6.2.2 Uniaxially Loaded Specimen Models with Non-Uniform Gage Section

6.2.2.1 Test Piece Description

Types C, D, and E test piece designs, as shown in Table 6.1, are used for this part of the test program.

6.2.2.2 Current Results

Tests at two stress levels have been completed on the Type C specimens. The rupture curve, Figure 6.1, shows that the life of Type 304 stainless steel material under a biaxial stress condition is reduced to about 1/8 of the plane stress case Type B specimen.

A third test, C2, is in progress. After step loading to 10, 11, 12.5, and 15 ksi, the load was increased to 18 ksi (Table 6.2). A crack, that started at the central hole, Figure 6.3, was measured for growth at the indicated time intervals.

The notched bar, Type D, having triaxial stresses, exhibited a notch rupture strengthening, Figure 6.1. Four tests (D1, D2, D3, and D5) have been completed at different stress levels (Table 6.2). After 1681 hours, specimen D5, with the minimum amount of strengthening, was dissected to determine the extent of cracking. One of the double notches was sectioned, and the crack patterns are shown in Figure 6.4 a and b. Figure 6.4b shows both the many sub-surface cracks at the grain boundaries and the cracks on the surface.

An analysis of the step load test, D4, is in progress.

6.2.3 Specimens with Welds (304SS, Heat 9T2796)

Tests of welded specimens were initiated. The first weld test BAW-1 (Table 6.1 for model description) was loaded axially to a stress of 25 ksi.

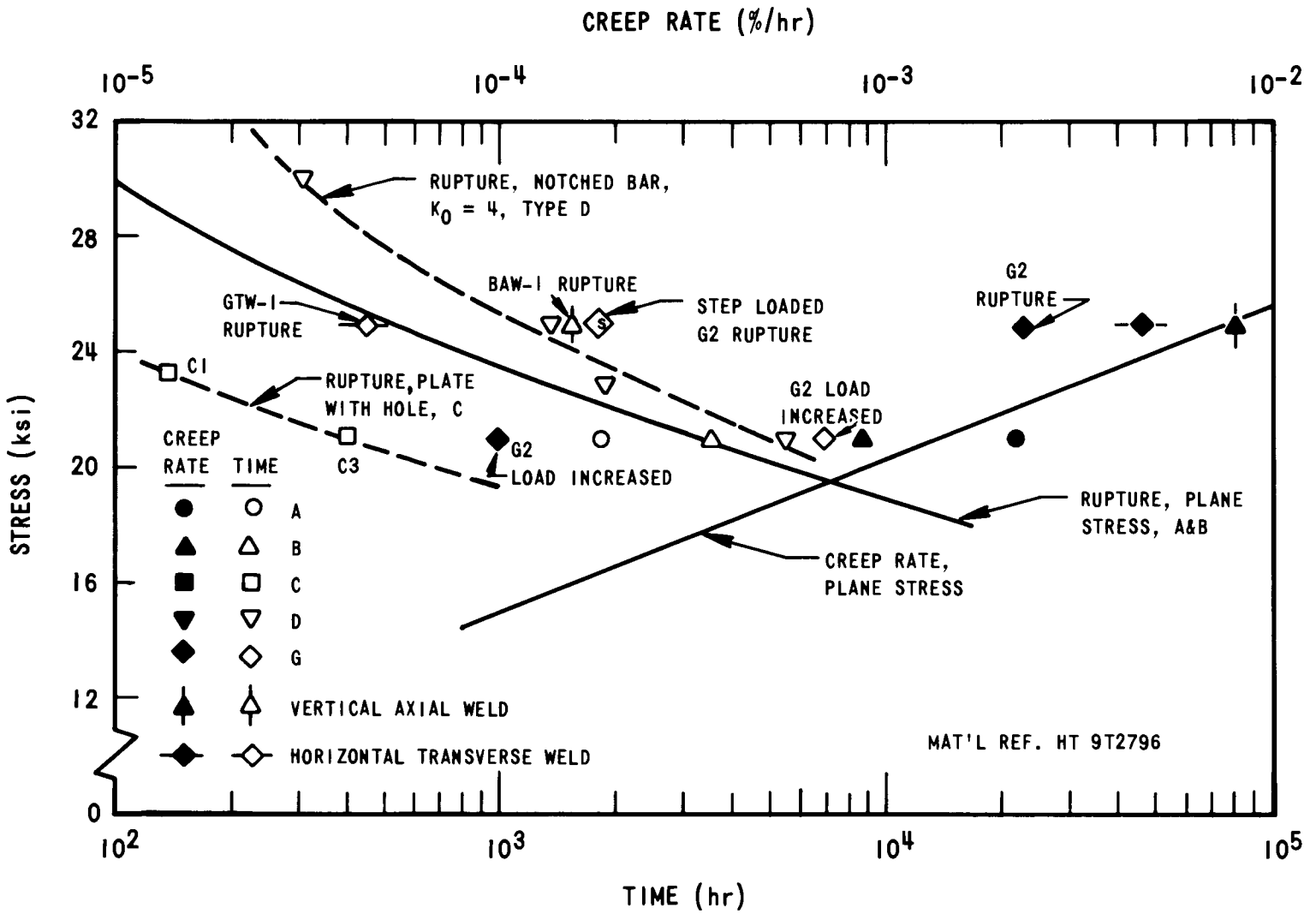

Figure 6.1 Creep Rupture Data for Type 304 Stainless Steel Models (Temperature = 1100°F)

a.

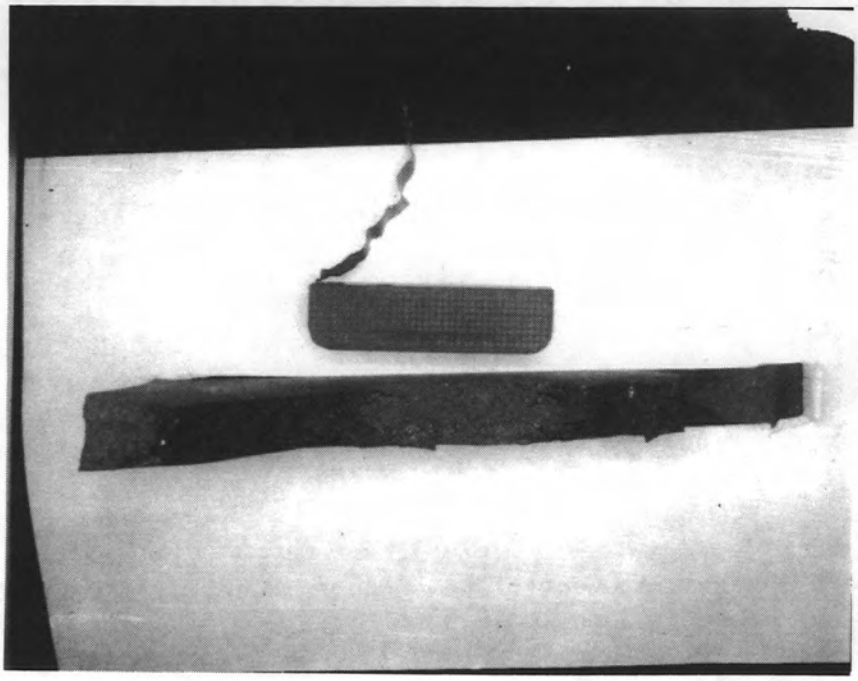

b. FRACTURE SURFACE

Figure 6.2 Fracture of Model G2 after 6715 Hours at 21 KSI and 1837 Hours at 25 KSI

6259-2

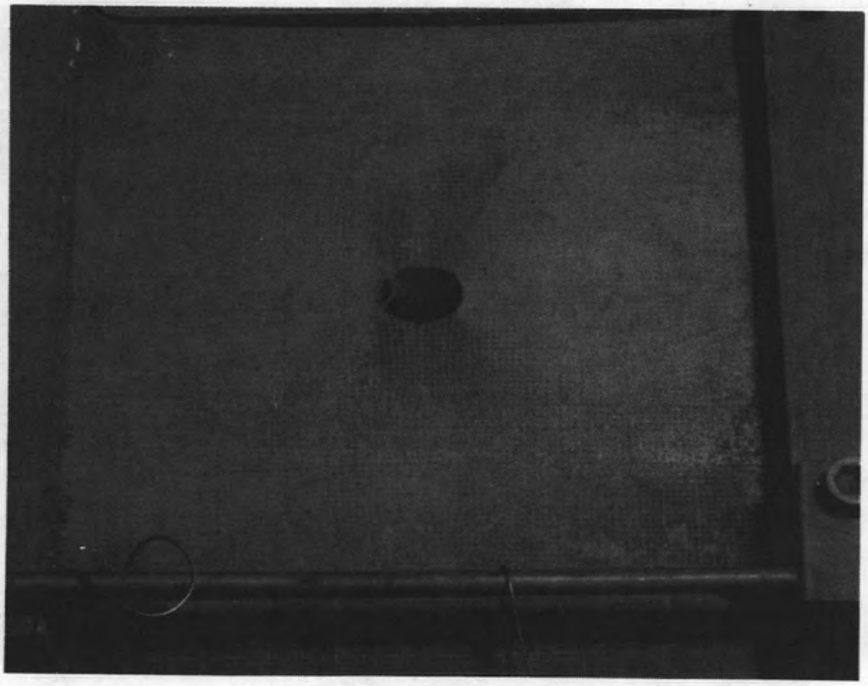

MEASUREMENT OF CRACK ALSO MADE AT 8176 AND 8967 HOURS

Figure 6.3 Crack at Centerline of Hole (Model C2 after 9911 Hours, Step Loaded to 18 KSI)

6259-3

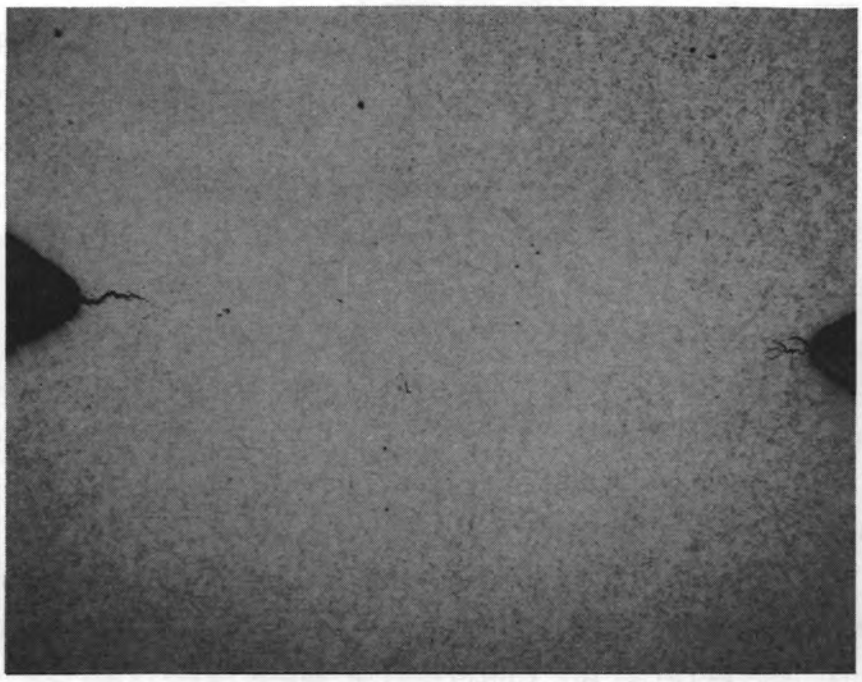

a. 6X

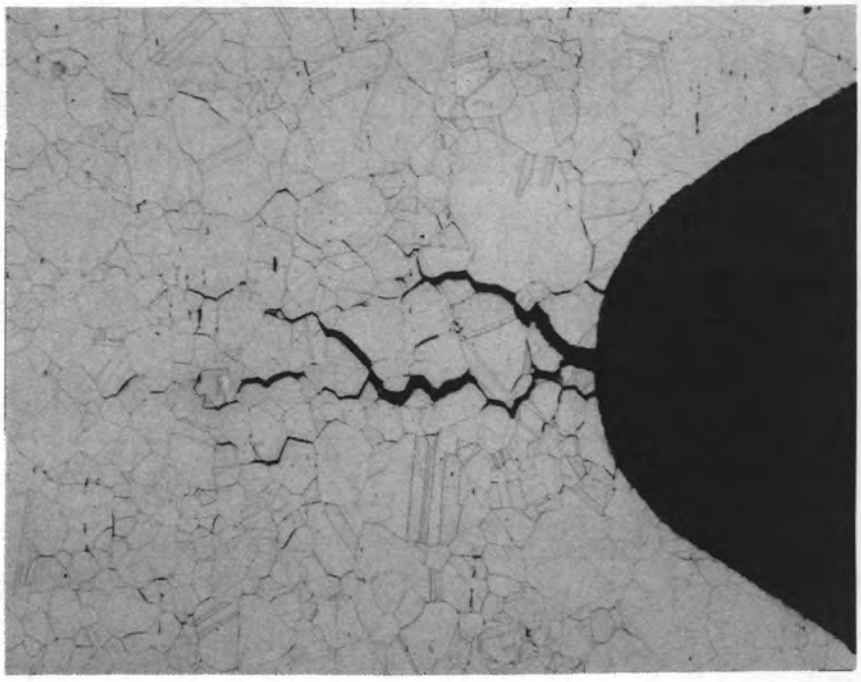

b. 50X

Figure 6.4 Fracture of Notched Bar, D5, after 1681 Hours at 23 KSI

6259-4

For this type of loading where the weld zone, heated affected zones (HAZ), and base metal zones are in parallel, the load taken by each zone depends on the relative creep strengths.

An analysis of the ductilities, as measured from the growth of cracks in each zone, indicated that the minimum ductility occurred in the HAZ. The surface crack pattern shown in Figure 6.5a was initiated in the principal stress direction at 477 hours which was about one-third the time of final rupture. In the Type BAW model, the strain is a maximum at mid-gauge length and diminishes toward the heads as plane strains are developed. Cracks started in the principal stress direction on both HAZ's along the gauge length. The rate of crack propagation was higher in the base metal than on either side of the weld. Eventually, a ductile shear failure shown in Figure 6.5b occurred across the remaining sections of the weld and base metal. The rupture time was about three times longer than for the base metal and about 70 percent of the time for an all weld metal specimen as reported by ORNL.[1]

The second weld test, Model GTW-1, was loaded to 25 ksi and the results indicated a strengthening of the base metal. (Table 6.2 and Figure 6.1). Shortly after mid-life, failure of GTW-1 started in the principal stress direction along one of the HAZ's, Figures 6.6 a and b, and progressed across the face and through the thickness. The rupture life was about one-third of that for the axial weld condition. The strains across the surface will be measured to determine the distributions in the weld zones and base metal.

6.3 TUBULAR SPECIMEN TESTING - K. C. Thomas, P. C. S. Wu

6.3.1 Test Piece Description

The tubular test pieces used in this program are 304 SS, Heat 9T2796, 1.8" O.D. and 1.6" I.D. and 8.7" length. However, thinner wall (1.8" O.D. and 1.7" I.D.) test pieces are being considered for use in future tests to reduce the stress variation through the wall thickness during multiaxial testing.

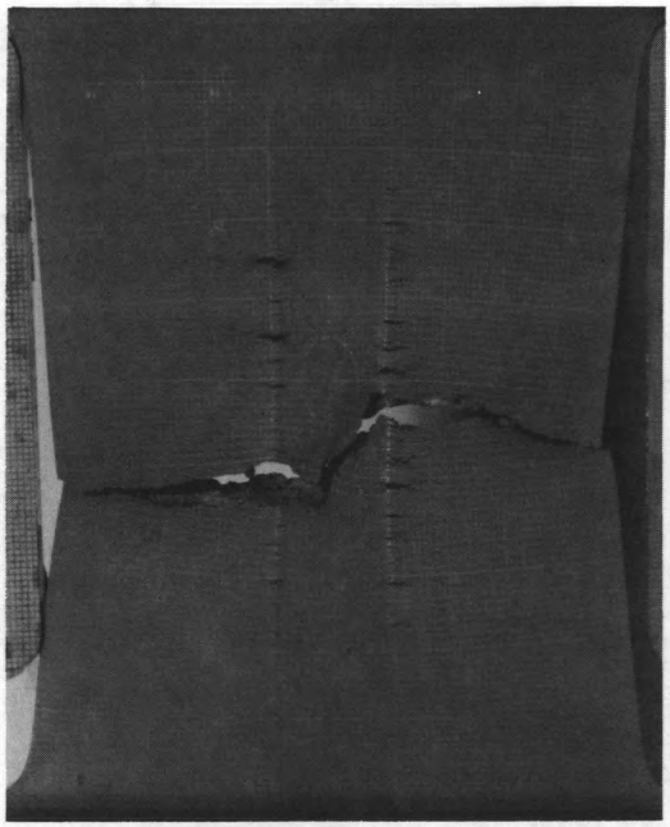

a.

b. FRACTURE SURFACE

Figure 6.5 Fracture of Axial Weld Model, BAW-1, after 1532 Hours at 25 KSI

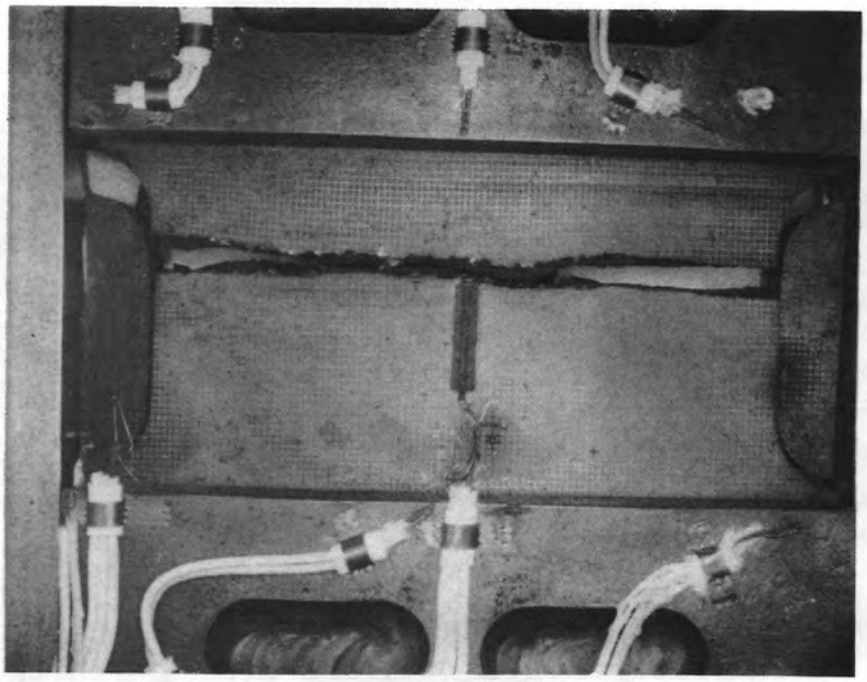

a.

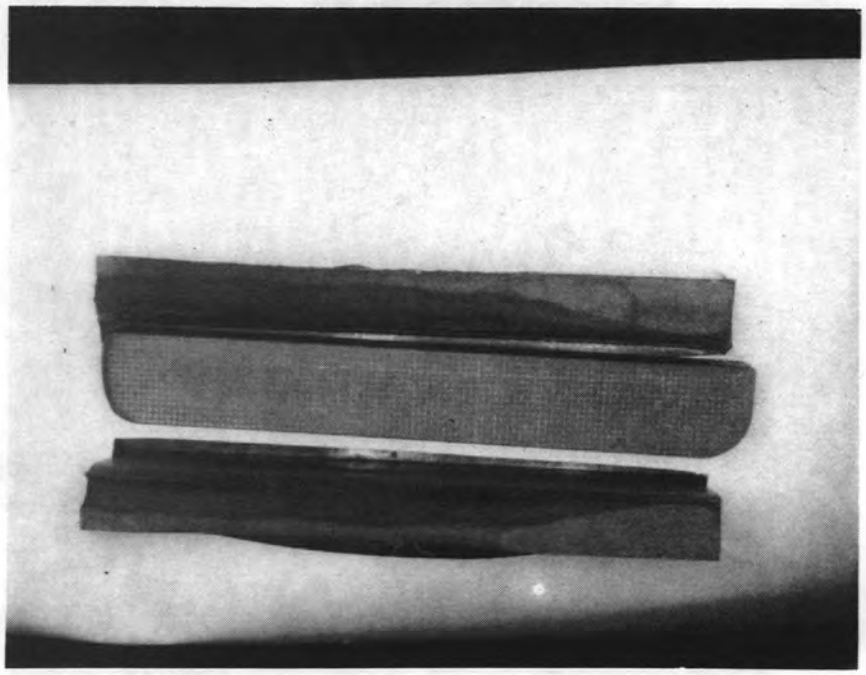

b. FRACTURE SURFACE

Figure 6.6 Fracture of Transverse Weld, Model GTW-1, after 448 Hours at 25 KSI

6.3.2 Uniaxial Creep Testing (304SS, Heat 9T2796 ORNL Reference Heat)

The original test matrix has been completed, however, additional uniaxial creep tests are being considered to provide strain-time relationships at stress levels of 5,000 and 15,000 psi to facilitate data analysis.

6.3.3 Multiaxial Creep Testing (304SS, Heat 9T2796 ORNL Reference Heat)

The test plan for multiaxial creep tests is shown in Table 6.3. Currently, two multiaxial creep tests, no. 4A and no. 5, have been completed. Test no. 10 and no. 11 were initiated during this report period. The results obtained for the multiaxial creep tests are summarized in Table 6.4. Test No. 7 was terminated shortly after it was initiated due to a system malfunction. This test will be repeated following the completion of test no. 10. In addition, test no. 6 and test no. 8 will also be initiated during the next report period.

6.4 RERERENCES

1. Oak Ridge National Laboratory, *Creep Properties of a Type 308 Stainless Steel Pressure Vessel Weld with Controlled Residual Elements,* ORNL-TM-4131, (May 1973).

Table 6.3 Test Plan-Multiaxial Tubular Specimen Testing[a]

Test Number	Nominal Effective Stress (psi)	Nominal Stress Ratio $(\sigma/\sigma)_{\theta z}$	Test Duration (hr)	Status	Remarks
4	10,000	2.0	2,000		Terminated due to malfunction of strain measuring system
4A	10,000	2.0	2,000	b	Repeat test No. 4
5	15,000	2.0	2,000	b	Tested at 1115°F
6	20,000	2.0	2,000	c	
7	10,000	1.5	2,000		Terminated due to malfunction of strain measuring system
7A	10,000	1.5	2,000	c	Repeat test No. 7
8	15,000	1.5	2,000	c	
9	20,000	1.5	2,000	c	
10	10,000	1.0	2,000	d	
11	15,000	1.0	2,000	d	
12	20,000	1.0	2,000	c	
13A	10,000	1.5	500	c	
13B	15,000	1.5	500	c	
13C	20,000	1.5	500	c	
13D	20,000	1.0	500	c	
14A	15,000	2.0	500	c	
14B	15,000	1.5	500	c	
14C	15,000	1.0	500	c	
15A	10,000	2.0	500	c	
15B	15,000	1.5	500	c	
15C	20,000	1.0	500	c	

(a) All test specimens are annealed at 2000°F for 30 minutes and tested at nominal temperature of 1100°F except Test No. 5 which was tested at 1115°F

(b) Test completed

(c) Test to be initiated

(d) Test in progress

Table 6.4 Test Results-Multiaxial Creep Test

Test No.	Nominal Test Temp. (°F)	Test Time (hrs)	Axial Load (lbs)	Nominal Internal Pressure (psi)	Nominal Effective Stress (psi)	Principal Stress Ratio (δ/δ) θ z	Average Loading Strain (%)		Average Creep Strain (%)			
							Axial	Hoop	Radial	Hoop	Axial	Effective
4A	1100	1965.7	323	1209.5	10,000	2.0	0.01048	0.02174	-0.1274	0.12466	0.00245	0.14536
5	1115	1998	484	1814.3	15,000	2.0	0.09208	0.08499	-0.57795	0.054670	0.03125	0.64996
7[a]	1100		1211	1180	10,000	1.5						
10	1100	338	2670	1049.4	10,000	1.0	0.04363	0.01994	-0.04112	0.01994	0.02118	0.04111
11	1100	197	4005	1574	15,000	1.0	0.03288	0.07339	-0.24753	0.10402	0.14351	0.24854

(a) Test terminated due to instability of the strain measuring systems.

7. UNIVERSITY OF CINCINNATI

J. Moteff

7.1 INTRODUCTION

The research program of the Department of Materials Science and Metallurgical Engineering of the University of Cincinnati includes: (a) the evaluation of the time-, temperature-, and stress-dependent properties of the austenitic stainless steels 316 and 304 and of Incoloy 800 and (b) the degree of correlation of these properties with the detailed substructure as observed with a 200 kV transmission electron microscope and with the surface features as observed with a scanning electron microscope. Special consideration has been given to operating conditions typical of LMFBR applications, including the knowledge that the radiation environment can influence the substructure of these metals leading to significant changes in the mechanical property behavior. Related substructure studies on other metals (nickel) and alloys (Hastelloy X) are also being considered primarily to demonstrate mechanistic plastic deformation behavior.

7.2 EXPERIMENTAL PROGRAM — (J. MOTEFF AND V. K. SIKKA)

The work in progress will be presented according to material category. A general description of the types of experiments considered and in a few cases some typical preliminary results will be given for (a) AISI 316 stainless steel, (b) AISI 304 stainless steel and (c) high nickel content alloys Incoloy 800 and Hastelloy X.

7.2.1. AISI 316 Stainless Steel

Experimental programs on 316 stainless steel are continuing in the following areas:

- Effect of stress changes on creep behavior
- Substructure development through elevated temperature creep, tensile and fatigue deformations.
- Recovery behavior of cold-worked sheet and rod material

7.2.1.1 Effect of Stress Changes on Creep Behavior — (V. K. Sikka, C. C. Yu* and H. Nahm)

Detailed experiments are being performed in which specimens are creep tested at one stress level to a given strain and then the stress level is either increased or decreased and the creep deformation recorded until a steady state is nearly achieved. The purpose of these tests are

* Presently at the University of Rochester.

to (a) determine the influence of a change in stress on the creep behavior and to (b) evaluate the substructure responsible for the observed changes in the creep behavior. Several specimens are required for testing under duplicate conditions so that they may be sectioned for TEM studies at different stages of the creep curve.

It is well known that one of the important substructural changes may be characterized by dislocation cells and/or subgrains which are developed in metals and alloys during high temperature deformation at constant stress. The question arises as to whether or not the dislocation cells and/or subgrains play an important role during creep in determining the creep resistance. It would seem intuitively reasonable to suppose that it should since the creep rate, $\dot{\varepsilon}$, is continuously decreasing during primary creep as the dislocation substructure is developing. It has been shown by various investigators that the size of the dislocation cells or subgrains developed during steady-state creep is a strong function of stress and it does not change in size during steady-state creep. Furthermore, the dislocation cell and subgrain size is not a sensitive function of temperature. The creep stress determines the dislocation cell and subgrain size, λ, as shown to be related by:

$$\lambda = k(\sigma/E)^{-n} \qquad (1)$$

where σ/E = the modulus compensated stress and

k = a constant.

The exponent n takes a value of 1 for the case of subgrains and a value of 2 for dislocation cells.

The steady state creep rate ($\dot{\varepsilon}_s$) is a function of stress (σ), temperature (T) and the material structure (st) and in general, is given by the equation:

$$\dot{\varepsilon}_s = f(\sigma,T,st) \quad \exp(-\Delta H_c/kT) \qquad (2)$$

where ΔH_c = the activation energy for creep.

The more specific form of equation (2) is given by:

$$\dot{\varepsilon}_s = A(\sinh \alpha \sigma)^n \exp(-\Delta H_c/kT) \qquad (3)$$

The equation (3) for the cases of low and high stresses respectively can be simplified into:

$$\text{Low Stress} \rightarrow \dot{\varepsilon}_s = A_1\sigma^n \exp(-\Delta H_c/kT) \qquad (4)$$

$$\text{High Stress} \rightarrow \dot{\varepsilon}_s = A_2 e^{\beta\sigma} \exp(-\Delta H_c/kT) \qquad (5)$$

The stress dependence of creep rate at a constant temperature reduces to a linear relationship (σ^1) at a low stress and very high temperature, a power relationship ($\sigma^{5\pm2}$) at intermediate stress levels and an exponential relationship ($e^{\beta\sigma}$) at very high stresses.

The applied stress during creep may be separated into several components as given by:

$$\sigma_a = \sigma_e + \sigma_i \tag{6}$$

where σ_e = the effective stress (flow stress) responsible for dislocation generation and movement and

σ_i = the internal stress which is modified by the substructure development during time on test.

Thus, it is possible that the stress dependence of the steady state creep rate would be more meaningful if an effective rather than the applied stress were used in the analysis. An example of such an effect of the internal stress on strain rate dependence can be cited from the work of Davis et. al.[1] These investigators showed that the steady-state creep rate, $\dot{\varepsilon}_s$, for copper, zinc and iron can be expressed as:

$$\dot{\varepsilon}_s \ \alpha \ \sigma_a^n \tag{7}$$

where n is 4.8 for copper and zinc but 8.3 for iron.

After taking the internal or frictional stress into account, the stress-dependence of the creep rates for copper, zinc and iron could be described by:

$$\dot{\varepsilon}_s \ \alpha \ (\sigma_a - \sigma_i)^4 \tag{8}$$

The above discussion suggests that the steady-state creep rate can be greatly reduced by increasing the internal or frictional stress for a given applied stress. The frictional stress during creep results from a combination of the following processes:

i) Activation of dislocation sources (Frank-Read)

ii) Overcoming the Peierls Stresses

iii) Dislocation interaction - with obstacles such as forest dislocations, precipitates and dislocation boundaries.

iv) Dragging of jogs by dislocations.

v) Dislocation atmosphere

Thus, if a metal can be crept at a high stress to the steady-state range where a given dislocation cell or subgrain size is developed, the stress can be changed to a lower or higher value than the initial value and instantaneous creep rate evaluated. In such an experiment (stress change experiment) the frictional stress should result from the dislocation cell and/or subgrain boundaries and the creep rate should show a new stress dependence. The purpose of this work is to present the results of such stress change experiments on 316 stainless steel and to show the changes in substructure developed in the final stress level.

Creep data and its analysis for stress change experiments on 316 and 304 stainless steel are quite similar and so have been discussed together in this section.

Stress change creep tests have been performed on both 316 and 304 stainless steel specimens. A total of ten creep tests have been run for 316 stainless steel (PNL Heat Number 65808) at a constant temperature of 1350°F (732°C). Stress

levels were changed during six out of ten creep tests. The stress change (increased or decreased) ranged from 26 to 78 percent of the initial applied stress. The stress change was carried out during the steady-state creep and tests were stopped at a certain strain level or at fracture. Creep data of 316 stainless steel samples are summarized in Table 7.1 and creep curves are plotted in Figures 7.1 through 7.3.

A total of thirteen creep tests have been performed on 304 stainless steel (Heat Number 55697). Tests were performed at three different temperatures, 593, 649, and 704°C. Stress levels were changed during creep tests at 593°C (40 - 30 ksi) and creep tests at 704°C (21.0 - 15.4 ksi). The creep tests were stopped at various strain levels and at rupture for substructural studies. The creep data for 304 stainless steel along with preliminary analysis for the 316 and 304 test results will be presented in the next quarterly contribution.

7.2.1.2 Creep, Tensile and Fatigue Deformation Substructure — (V. K. Sikka, H. Nahm)

The cell or subgrain intercept, λ, for tensile, creep and fatigue has been correlated with the modulus compensated stress, τ/Gb. τ represents the shear stress and its values are obtained by dividing the true stress by two. G is the shear modulus and its values are used corresponding to the respective test temperatures. The true stress represents,

TABLE 7.1

CREEP DATA ON AISI 316 STAINLESS STEEL[a]

Test[b] Number	Specimen Number	Applied Stress σ_a, ksi	Applied Stress σ_a, kg mm^{-2}	Initial Strain On Loading ε_o, %	Strain Prior to Stress Change ε_i, %	Strain at Rupture ε_R, %	Steady State Creep Rate $\dot{\varepsilon}_s$, sec^{-1}	Rupture Life t_R, hrs.
1	S-13	19.0	13.36	2.3	-	53.6	1.11×10^{-6}	49.5
2	S-14	14.0	9.85	1.5	-	49.0	1.67×10^{-7}	300.5
3	S-18	19.0	13.36	0.7[d]	-	3.0[e]	1.50×10^{-6}	3.5[e]
4	S-17[c]	19.0	13.36	1.2[d]	2.1	-	1.31×10^{-6}	-
		14.0	9.85	-	-	3.3[e]	-	4.0[e]
5	S-16[c]	19.0	13.36	2.2	2.1	-	1.33×10^{-6}	-
		14.0	9.85	-	-	4.3[e]	1.83×10^{-7}	6.0[e]
6	S-15[c]	19.0	13.36	2.4	2.6	-	1.22×10^{-6}	-
		14.0	9.85	-	-	52.0	1.90×10^{-7}	307.3[e]
7	S-18	-	-	Unstressed (Shoulder Region) for Substructure Controls			-	-
8	S-19	25.0	17.59	2.3	-	50.0	1.44×10^{-5}	5.2
9	S-20[c]	25.0	17.59	2.5	7.1	41.2	8.25×10^{-6}	288.6
		14.0	9.85	-	-	-	1.28×10^{-7}	-
10	S-21[c]	14.0	9.85	0.73	4.6	54.7	2.36×10^{-7}	55.6
		25.0	17.59	-	-	-	1.75×10^{-5}	-
11	S-22[c]	25.0	17.59	1.63	8.2	12.0[e]	1.41×10^{-5}	46.5[e]
		14.0	9.85	-	-	-	1.76×10^{-7}	-

(a) Heat No. PNL 65808.
(b) All creep test were run at a test temperature of 1350°F (732°C).
(c) Represents the initial and final stresses used in a stress change creep test.
(d) Load procedure slightly different from that used in ther other tests.
(e) Strain level and time at the termination of the test.

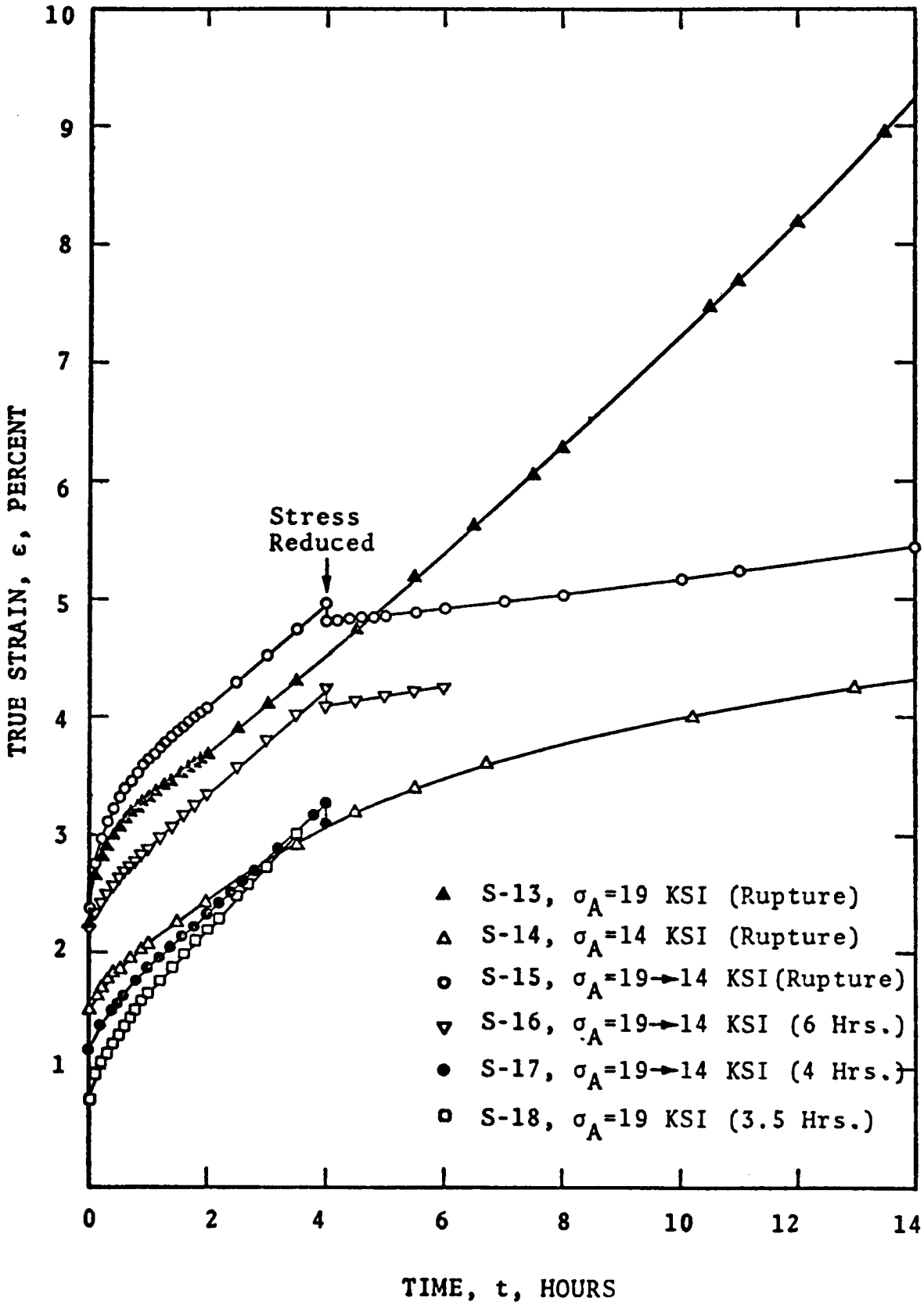

Figure 7.1. Strain-Time Curves for the First 14 Hours of 316 Stainless Steel Creep Tested at 1350°F (732°C).

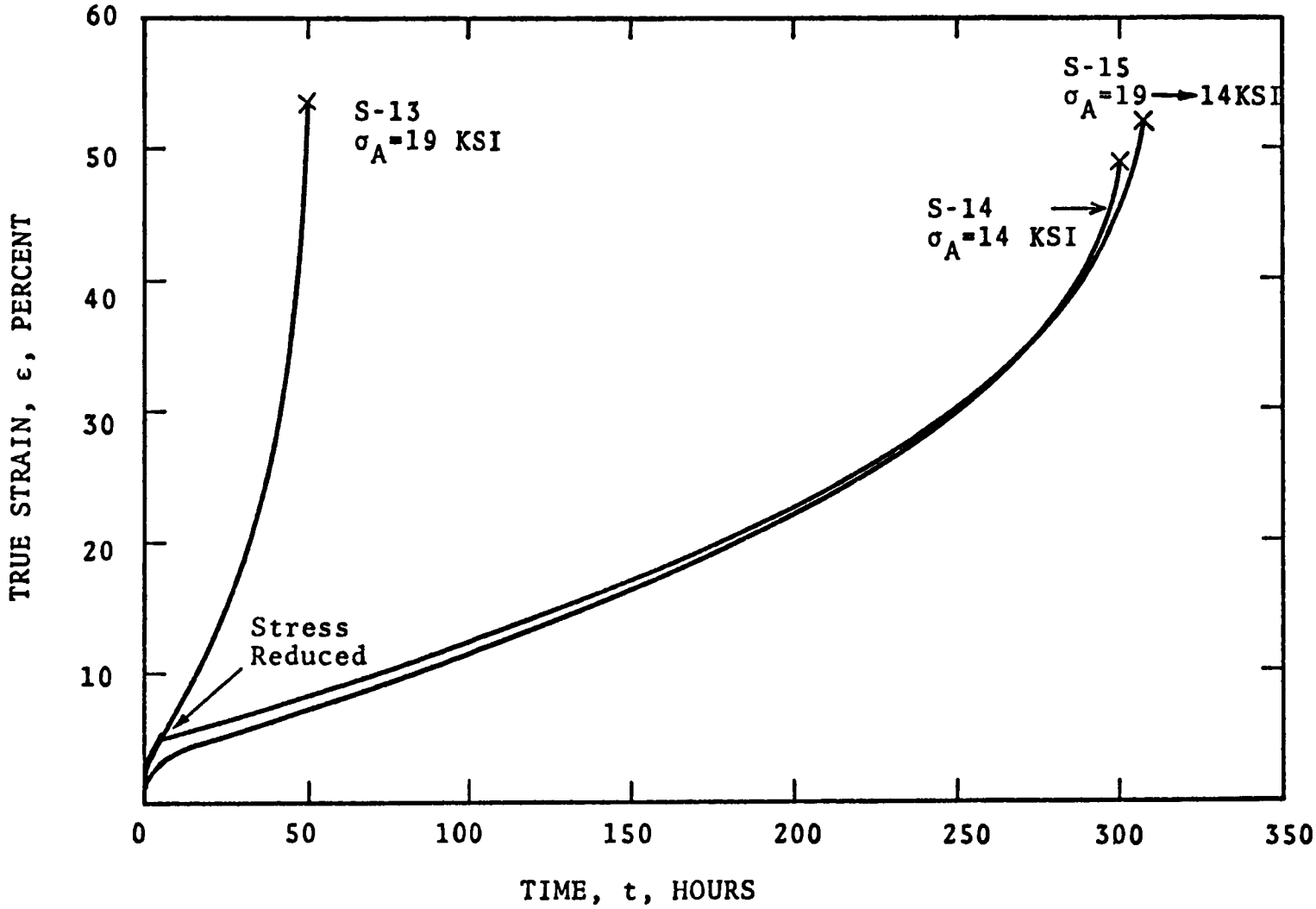

Figure 7.2. Strain-Time Curves for 316 Stainless Steel Tested Under Constant Load at 1350°F (732°C).

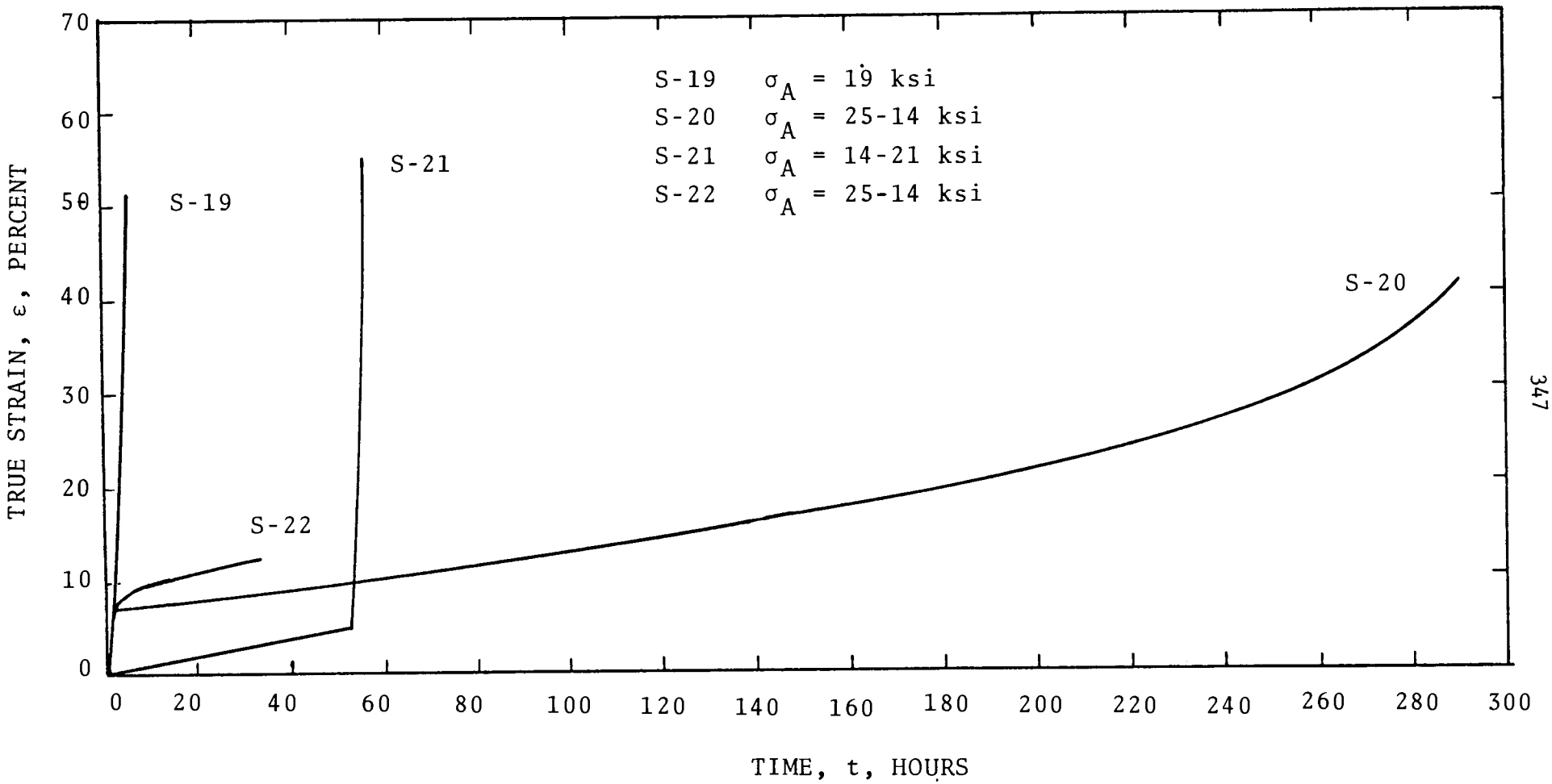

Figure 7.3. Strain-Time Curves for 316 Stainless Steel Tested Under Constant Load at 732°C (1350°F).

the maximum true stress for tensile test, the true applied stress for creep, and the saturation stress for fatigue. A value of 2.54 Å is used for b, the Burgers vector.

The cell or subgrain intercept, λ, as a function of τ/Gb, for tensile and creep tests is plotted in Figure 7.4. for 316 stainless steel. The creep data from Challenger and Moteff[2] and tensile data from Michel, Moteff and Lovell[3] and Challenger and Moteff[4] have also been included in Figure 7.4. The cell and subgrain intercept versus modulus compensated stress for both tensile and creep results for 316 stainless steel can be fitted into the following two expressions:

$$\lambda = 12\ (\tau/Gb)^{-1} \text{ for subgrains} \qquad (9)$$

$$\lambda = 175\ (\tau/Gb)^{-2} \text{ for cells} \qquad (10)$$

The transition from equation (9) to (10) for 316 stainless steel occurs at a modulus compensated stress value of 16. Such an observation can be compared with the data reported on iron-based materials by Young and Sherby[5], where the transition value was reported at $\tau/Gb=10$. Furthermore equation (9) for 316 stainless steel can be compared with the results on copper reported by Staker and Holt[6].

$$\lambda = 10.5\ (\tau/Gb)^{-1} \text{ for copper} \qquad (11)$$

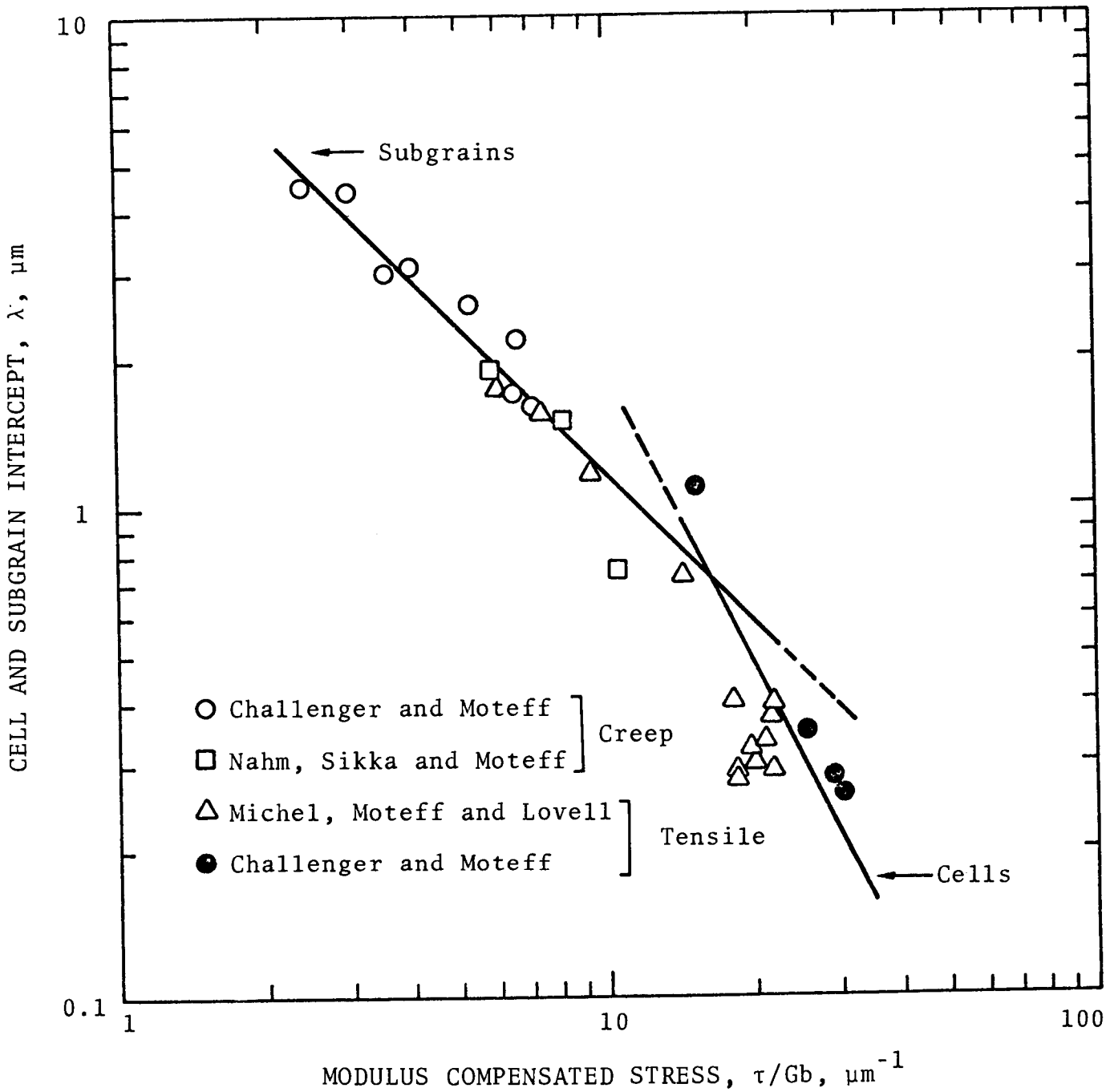

Figure 7.4. Dislocation Cell or Subgrain Intercept, λ, as a Function of Modulus Compensated Stress, τ/Gb, for Tensile and Creep Deformation of 316 Stainless Steel.

Staker and Holt[6] observed only one slope for copper of the λ versus τ/Gb plot, because the τ/Gb values in their test range were less than required for the transition to occur.

7.2.1.3 Recovery and Recrystallization Behavior of Cold Worked Rod and Sheet — (V. K. Sikka and T. Kenfield)

Test samples were prepared from two material sources,

I) Annealed 316 stainless steel bar (0.625 inch round times 12 inches long) obtained from the PNL Reference Heat 65808 and,

II) Pre-rolled, 20 percent cold worked 316 stainless steel sheet specimen (0.020 inch thick) from Heat 65808.

Material II was left in its original condition. Four sets of samples were then prepared from Material I to include the following conditions:

Annealed Control

20 Percent Cold Worked

35 Percent Cold Worked

50 Percent Cold Worked

All cold work was performed at room temperature and the amount of cold work was determined by measuring the thickness changes during rolling. Cold worked material was cut into samples for hot-hardness, room temperature hardness, metallography and the transmission electron microscopy. The test temperatures selected for hot hardness measurements

were in the order of: Room temperature, 100, 200, 250, 300, 350, 400, 500, 550, 600, 700, 800 and 900°C.

The room temperature hardness measurements were made after one hour anneals at the temperatures of: Room temperature, 200, 250, 300, 350, 400, 500, 550, 600, 700, 800, 900 and 1050°C. The isothermal anneals were performed at 710°C for times of 1, 10, 100 and 1000 hours. Hardness measurements were performed at room temperature using a 500 gram load.

The test results and preliminary interpretation of the recovery characteristics of several heats of 316 stainless steel and other austenitic stainless steels will be presented in future progress reports.

7.2.2 AISI 304 Stainless Steel

In addition to the stress change in creep experiments which were discussed in a previous section, work in progress on the 304 stainless steels include:

- Correlation of hot-hardness with the elevated temperature tensile properties
- Creep, tensile and fatigue deformation substructure
- Grain boundary sliding in elevated temperature deformation
- Substructure and hardness characteristics in the region of a fatigue crack tip.

Only information on the first three ideas will be presented in the present contribution.

7.2.2.1 Hot-Hardness Correlation with the Tensile Strength at Temperatures Up to 1250°C – (J. Moteff and R. Bhargava)

Hot hardness measurements[7] were made on AISI 304L stainless steel purchased commercially as 0.076 cm (0.030 inch) thick annealed sheet with a vendor certified chemical analysis. These tests were performed to temperatures of 1250°C and the results compared to hot tensile data obtained from specimens fabricated from the same heat of material.

Figure 7.5 shows a plot of the ultimate tensile strength of 304L stainless steel at various temperatures as a function of the hot-microhardness values determined at the same temperature. At test temperatures greater than 800°C the ultimate tensile strength and hardness seems to follow a simple relation given by,

$$\sigma_u = H/C \qquad (12)$$

where c = 3.1 ± 0.2 is the value of the constant proposed by Moteff and Sieber[8]. This value of C is in reasonable agreement with Tabor's[9] room temperature test values of 2.9 for steels and 3.0 for copper. Cahoon et al.[10] showed values of 3.0 ± 0.1 for steel, brass and aluminum specimens. In the temperature range of RT to 800°C the equation

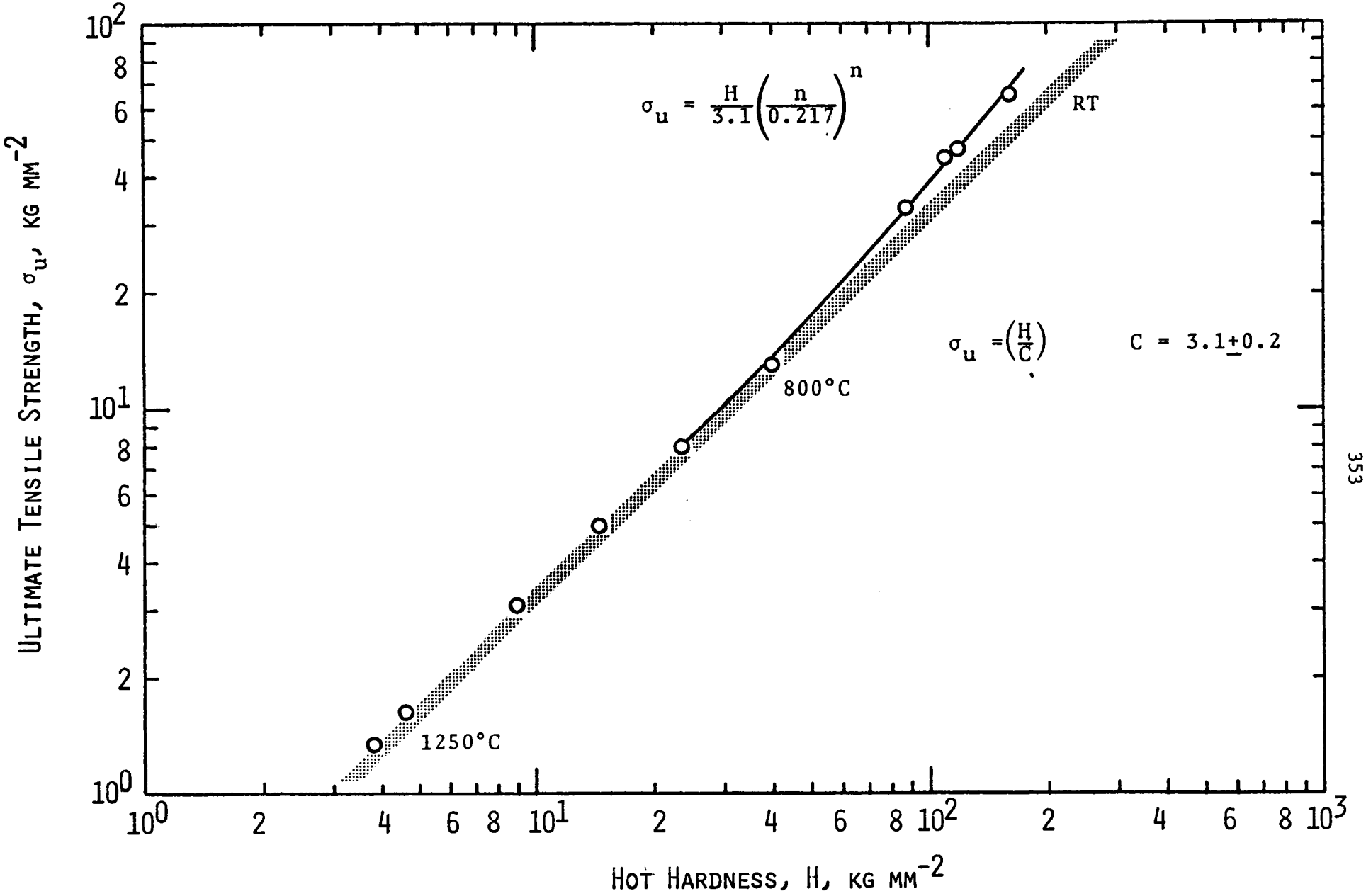

Figure 7.5. Plot of the Ultimate Tensile Strength, σ_u, as a Function of Hot Hardness, H.

$$\sigma_u = \frac{H}{3.1} \left(\frac{n}{0.217}\right)^n \qquad (13)$$

excellently describes the variation of the ultimate tensile strength with hardness.

A prediction of the ultimate tensile strengths based on hardness measurements and strain hardening exponent values obtained from either the Meyers coefficient or the substructure observations has also been made. Figure 7.6 shows a comparison of the calculated ultimate strength levels with that obtained through experimental tensile tests. With the exception of the 1000°C test data, where the discrepancy between the calculated and the experimental ultimate strength values was about 12%, the agreement was well within 5% for all the other temperatures investigated.

7.2.2.2 Creep, Tensile and Fatigue Deformation Substructure — (V. K. Sikka, H. Nahm and R. Bhargava)

The cell and subgrain intercept, λ, as a function of τ/Gb, for tensile, creep and fatigue tests is plotted in Figure 7.7 for 304 stainless steel. The creep data from Cuddy[11], tensile data from Moteff, Bhargava and McCullough[7] and fatigue data from Challenger and Moteff[4] have also been included in Figure 7.7. The cell and subgrain intercept shows a large scatter for 304 stainless steel (See Figure 7) and thus, a tentative line (thin line) has been drawn and fitted to the following equation:

$$\lambda = 9.8(\tau/Gb)^{-1} \qquad (14)$$

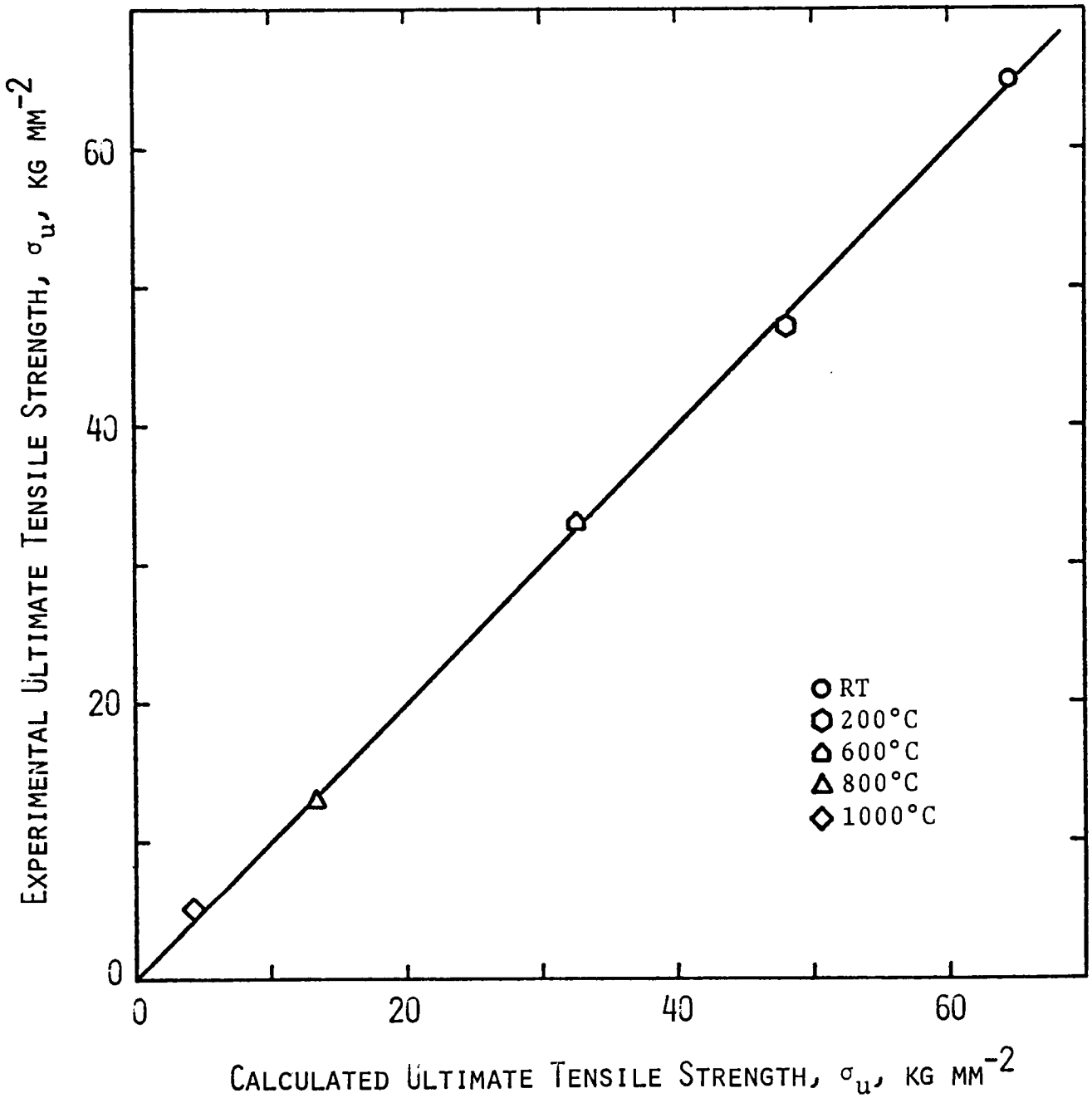

Figure 7.6. Comparison of the Calculated and Experimental Ultimate Tensile Strength.

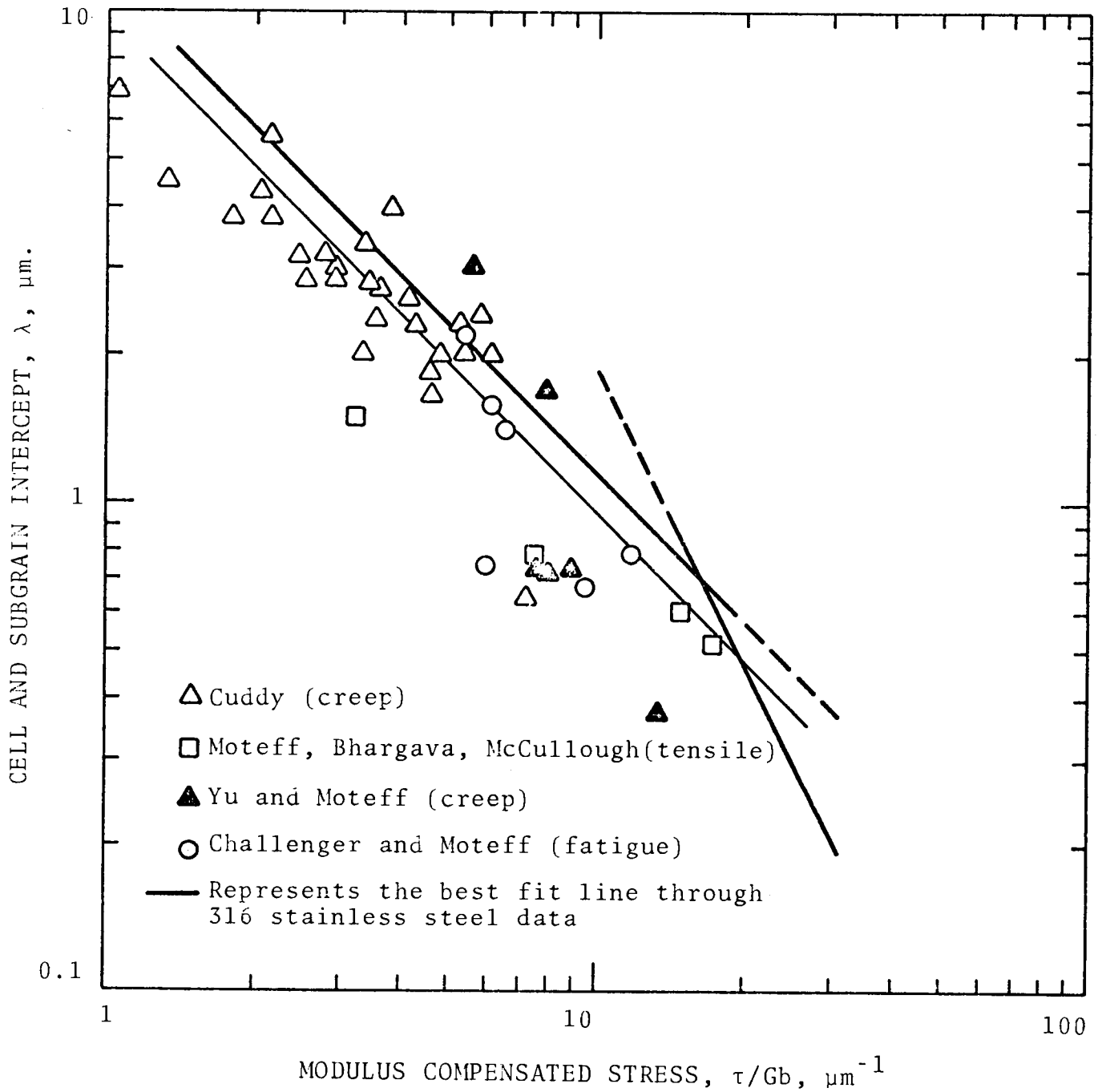

Figure 7.7. Dislocation Cell or Subgrain Intercept, λ, as a Function of Modulus Compensated Stress, τ/Gb, for Tensile and Creep Deformation of 304 Stainless Steel.

The thick line in Figure 7.7 represents results presented previously on 316 stainless steel and has been drawn for the comparison purposes.

The cell and subgrain intercept, λ, as a function of τ/Gb, for fatigue is plotted in Figure 7.8 for both 304 and 316 stainless steels. The fatigue data for 304 stainless steel is obtained from Challenger and Moteff[4] and for 316 stainless steel from Challenger and Moteff[4,12]. It is interesting to note that the data for both 304 and 316 stainless steels in Figure 8 can be fitted to a single equation of the type:

$$\lambda = 7.6(\tau/Gb)^{-2} \tag{15}$$

and no transition occurs in the slope unlike that observed for the results on tensile and creep tests.

Work is in progress to determine the proper correlation between the substructure developed during tensile, creep and fatigue deformation modes.

7.2.2.3 Grain Boundary Sliding in 304 Stainless Steel — (H. Nahm)

The work is underway at the University of Cincinnati to study the grain boundary sliding in the high temperature plastic deformation of AISI 304 stainless steel (ORNL, 9T2796). The specimens were tested in the tension and creep mode at 650°C. The ratio between the grain boundary strain, ε_{gb}, to total strain, ε_t, is plotted as

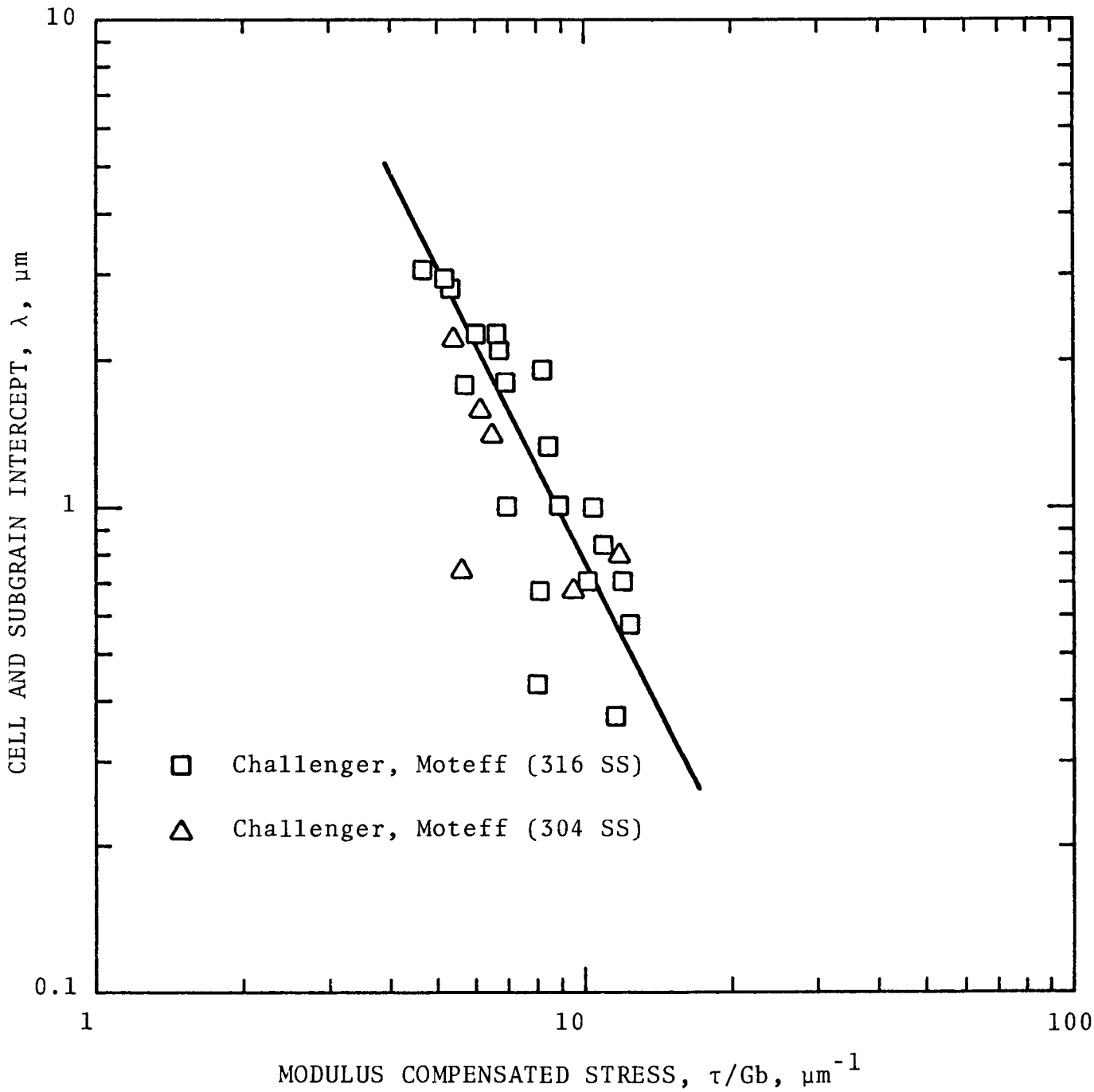

Figure 7.8. Dislocation Cell or Subgrain Intercept, λ, as a Function of Modulus Compensated Stress, τ/Gb, for Fatigue Deformation of 304 and 316 Stainless Steel.

a function of the stress in Figure 7.9. These ratios were obtained by the grain shape analysis of the grains with the intercept distance of 150 to 200 μm.

Data from Garofalo et al.[13] and Langneborg et al.[14] are also included in Figure 7.9. An important observation for most of the austenitic stainless steels is that the grain boundary sliding, ε_{gb} becomes more significant when the stress is decreased. It is in general consistent with the microcracking behavior in the sense that the microcracking increases with the increase in grain boundary sliding[15].

7.2.3 High Nickel Content Alloys

Although most of the work performed on this class of alloys is centered around Incoloy 800, some creep studies have been performed on Hastelloy-X and substructure studies on Hastelloy-X and Ni-270 so that a better interpretation can be made on the general relationship between the substructure and the mechanical properties of nickel base alloys. This information will also be used for comparison with the austenitic stainless steel alloys 304 and 316.

7.2.3.1 Tensile and Fatigue Deformation Substructure for Incoloy 800 — (V. K. Sikka and H. Nahm)

The cell and subgrain intercept, λ, as a function of τ/Gb for short term tensile tests is plotted in Figure 7.10 for Incoloy 800. The data in Figure 7.10 is on Incoloy 800

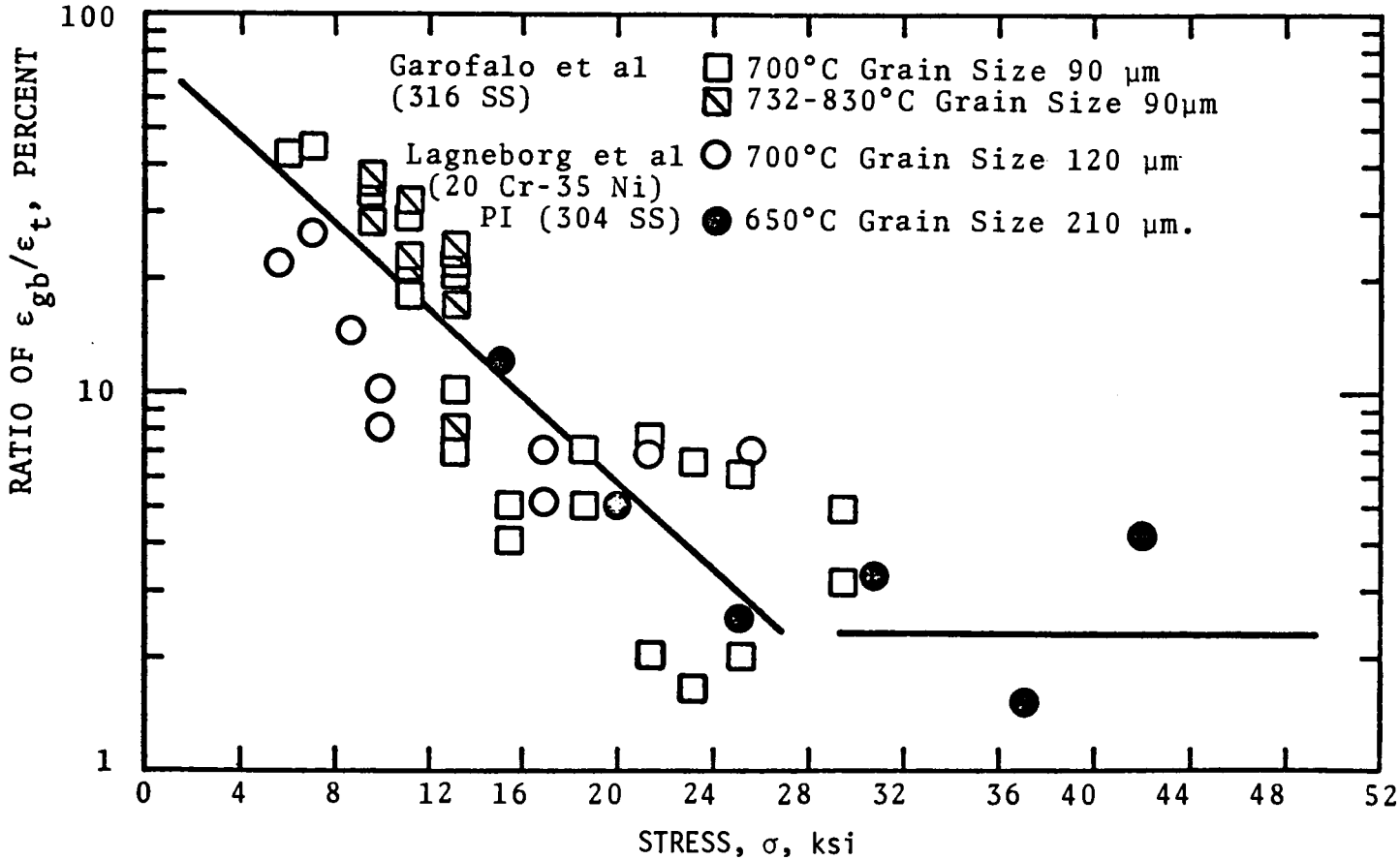

Figure 7.9. Ratio of the Grain Boundary to Total Strain ($\varepsilon_{gb}/\varepsilon_t$) versus stress.

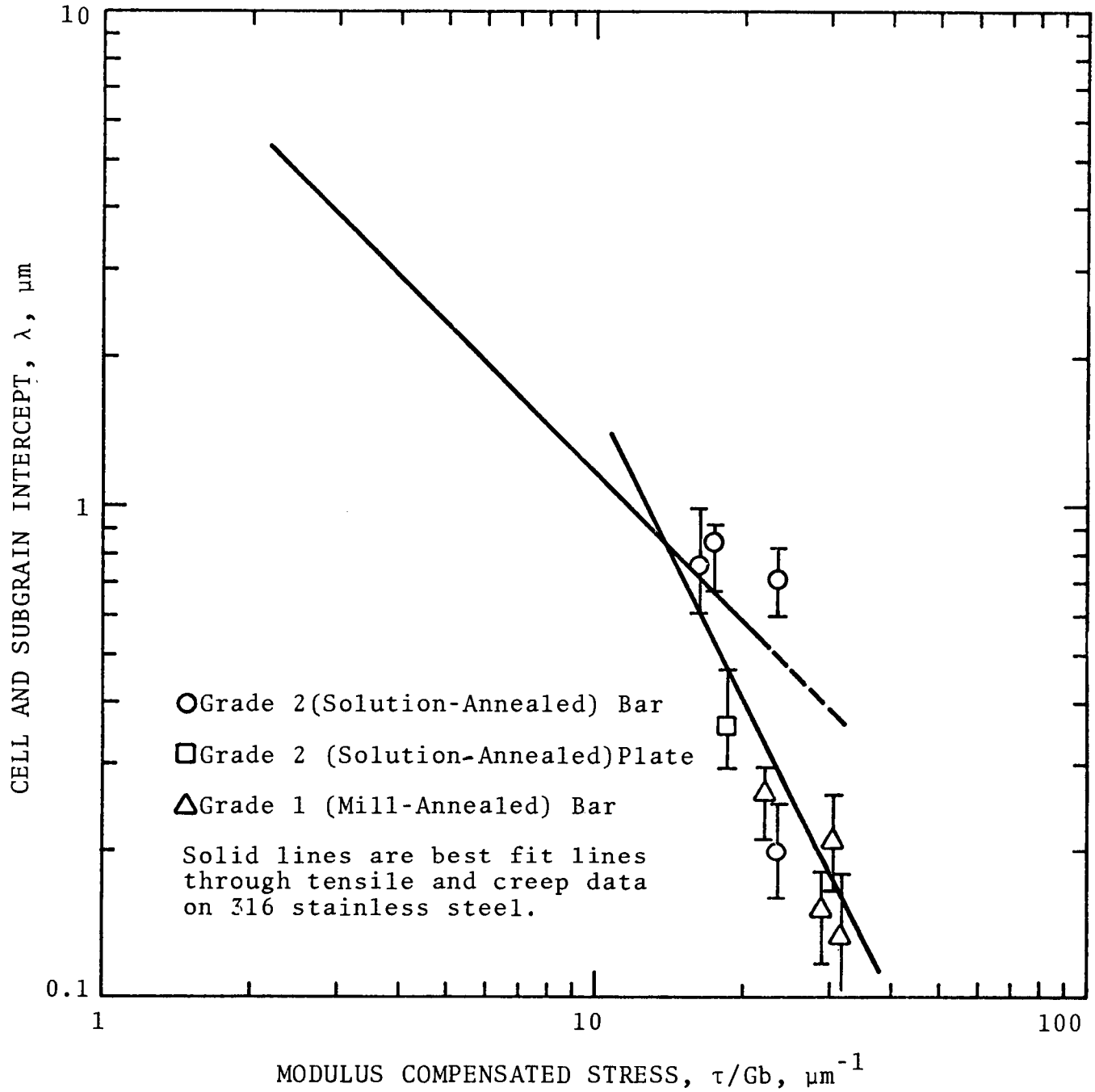

Figure 7.10. Dislocation Cell or Subgrain Intercept, λ, as a Function of Modulus Compensated Stress, τ/Gb, for Tensile Deformation of Incoloy 800.

Grade 1 (Mill-Annealed) Bar Stock, Grade 2 (Solution-Annealed) Plate Stock, and Grade 2 (Solution-Annealed) Bar Stock. The data on Incoloy 800 is only for τ/Gb values greater than ten and has been fitted by a line, which coincides with that reported in equation (10) for 316 stainless steel. The best fit line for λ versus τ/Gb data for 316 stainless steel for τ/Gb values in the range from 1 - 10 has also been plotted in Figure 7.10. The important point to note is that the substructure dimensions are not dependent on the Incoloy-800 grade or the pre-treatment. The three data points, marked by open circles, showed subgrain formation and thus fit on 316 stainless line represented by equation (9). The tensile and creep results on 316, 304 stainless steels and Incoloy 800 show that the substructure developed for the same value of (τ/Gb) the similar for all three materials.

The cell and subgrain intercept, λ, as a function of τ/Gb for fatigue tests is plotted in Figure 7.11. The thick line drawn through the data points is the same as drawn in Figure 7.8 for fatigue data on 304 and 316 stainless steels. The fatigue data on Incoloy 800 in Figure 7.11, when compared with the tensile data in Figure 7.10, shows that the fatigue line is shifted to the left on the tensile line and is similar to the observations for 304 and 316 stainless steels. Furthermore, a review of the tensile, creep and fatigue substructure results for 304, 316 and Incoloy 800 suggest

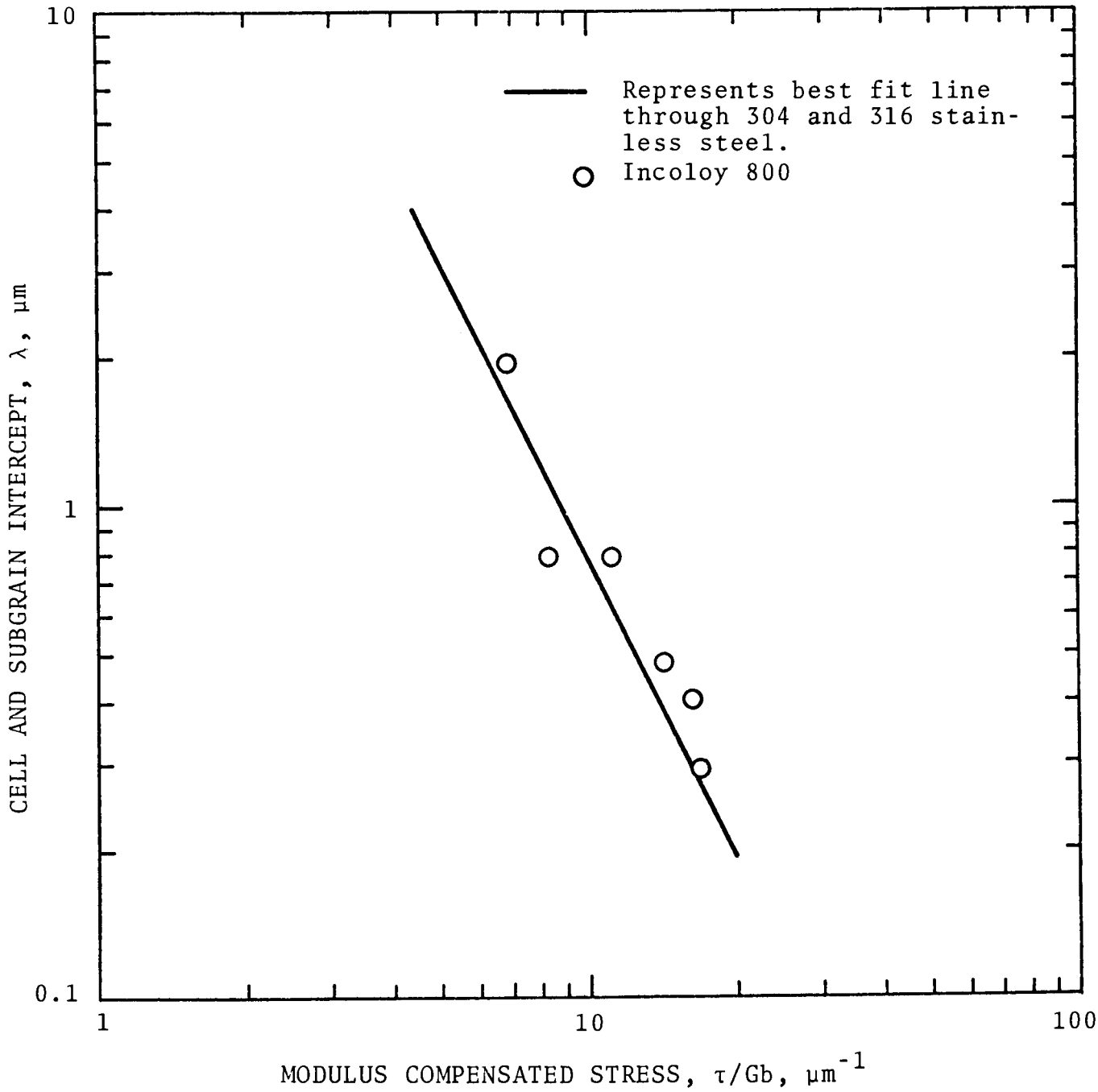

Figure 7.11. Dislocation Cell or Subgrain Intercept, λ, as a Function of Modulus Compensated Stress, τ/Gb, for Fatigue Deformation of Incoloy 800.

the following points.

- Tensile and creep results can be fitted to the same equations for 304, 316 and Incoloy 800.
- The tensile and creep results show a transition in the λ versus τ/Gb lines at a τ/Gb value in the range of 10 - 20.
- The fatigue results on 304, 316 stainless steels and Incoloy 800 are consistent.
- The substructure developed during fatigue corresponds to that developed at high applied stress during creep and tensile.

7.3 REFERENCES

1. P. W. Davies, G. Nelmes, K. R. Williams and B. Wilshire, Metal Science Journal 7, 87 (1973).

2. K. D. Challenger and J. Moteff, Met. Trans. 4, 749 (1973).

3. D. J. Michel, J. Moteff and A. J. Lovell, Acta Met. 21, 1269 (1973).

4. K. D. Challenger and J. Moteff, Scripta Met. 6, 155 (1973).

5. C. M. Young and O. D. Sherby, JISI 211, 640 (1973).

6. M. R. Staker and D. L. Holt, Acta Met. 20, 569 (1972).

7. J. Moteff, R. Bhargava and W. L. McCullough, Submitted to Met. Trans. (1974).

8. J. Moteff and P. R. Sieber, Met. Trans. 4, 749 (1973).

9. D. Tabor, J. Inst. Metals 79, 1 (1951).

10. J. R. Cahoon, W. H. Broughton and A. R. Kutzak, Met. Trans. 2, 1979 (1971).

11. L. J. Cuddy, Met. Trans. 1, 395 (1970).

12. K. D. Challenger and J. Moteff, Met. Trans. 3, 1676 (1972).

13. F. Garofalo, C. Richmond, W. F. Domis and V. Von Gemmingen, Joint International Conference on Creep, p. 1 (1963), London (Inst. Mech. Eng.).

14. R. Lagneborg, R. Attermo, J. Mater. Sci. 4, 195 (1969).

15. H. Nahm, D. J. Michel and J. Moteff, J. Mater. Sci. 8, 104 (1973).

INDEX

Test	Material	Page
Allowable Stresses		
	type 16-8-2 weld metal . . .	244
Chemical Analysis Data		
	ASTM type A508-2 forging . .	172
	type 316 SS	157—159
	type 316H SS	130
	type 16-8-2 weld	232,233
	2 1/4 Cr-1 Mo steel	257
Creep Test Data		
Base-Line Data		
	type 304 SS	177—183,198—204,323—325
	type 316 SS	344—347
	type 16-8-2 weld metal . . .	239—242,249—253
	2 1/4 Cr-1 Mo steel	260—262
Correlations		
	type 304 SS	205, 213—217
	20% cold-worked 316 SS . . .	56—70
	2 1/4 Cr-1 Mo steel	268—271
	type 16-8-2 weldments	246—248,263—265
Creep Plasticity Interaction		
	type 304 SS	216—219
Effect of Irradiation		
	type 316 SS GTA weldments . .	151—154
Elastic Analysis for Slit Tube		
	type 316 SS	87—103
Notch Strengthening		
	type 304 SS	325—329
Multiaxial		
	type 304 SS	330—335
Strain Limits		
	type 316 SS	222,224

Test	Material	Page
Extensometer Evaluation		
	type 304 SS	33–55
Fatigue Test Data		
Cyclic Fatigue Test Data		
	type 304/308 SS welds	2–5
Correlations		
	Incoloy 800	363
Effect of Hold Time		
	type 304 SS	5
Effect of Strain Range		
	type 304/308 SS welds	3,4
Crack Growth Rate Data		
Correlations		
	type 316 SS	163–165
	type 304 SS (J-integral)	166–170
	type 308 SS weld metal (J-integral)	166–170
Effect of Heat Treatment		
	type 304 SS	22–29
Effect of Stress Intensity Factor		
	type 316 SS	158–185
	type 304 SS	22–29
	type 308 SS weld metal	22–29
Effect of Test Temperature		
	type 316 SS	158–165
	type 304 SS (J-integral)	168–170
	type 308 SS weld metal (J-integral)	168–170
Elastic Constants		
	type 304 SS	187–194
	2 1/4 Cr-1 Mo steel	262,265–266
Hardness		
	type 16-8-2 welds	243
Correlations		
	type 304L SS	352–353

Test	Material	Page
Impact Test Data		
Correlations		
	ASTM type A508-2 forging (NDT,C_vE)	171–174
Effect of Heat Treatment		
	Inconel 718	5–8
Effect of Test Temperature		
	ASTM type A508-2 forging	171–174
Stress-Rupture Data		
	20% cold-worked type 316 SS	56–67,74–86
	type 316 SS GTA weld	141–146
	type 16-8-2 weld metal	246–248
	type 308 SS SMA weld metal	253–255
	type 304 SS	326
Subcritical Crack Growth		
	2 1/4 Cr-1 Mo steel	262,267
Tensile Test Data		
	ASTM type A508-2 forging	172
	type 316 SS	157–159
Base-Line Data		
	ASTM type A508-2 forging	72
	2 1/4 Cr-1 Mo steel	257–260
	type 304 SS	15–21,184–186,199–200, 356
	type 316 SS	349
	type 16-8-2 weld metal	235–237
Correlations		
	type 304 SS	185,210–213
Effect of Aging		
	type 304 SS	204,209,211
Effect of Heat Treatment		
	Inconel 718	9–12
	2 1/4 Cr-1 Mo steel	259

Test	Material	Page
Tensile Test Data		
Effect of Strain Rate		
	type 16-8-2 weld metal . . .	235–236
	type 304 SS	15–21,183–188
	20% cold-worked type 316 SS .	112–127,132, 138–139
Effect of Test Temperature		
	type 304 SS	15–21,184, 186–187,200
	type 16-8-2 weld metal . . .	235,236
	2 1/4 Cr-1 Mo steel	258
Thermal Transient Failure Tests		
	20% cold-worked type 316 SS .	70–72

ORNL-4948
UC-79b, -h, -k
(Liquid Metal Fast
Breeder Reactors)

INTERNAL DISTRIBUTION

(3) Central Research Library
ORNL — Y-12 Technical Library
Document Reference Section
(10) Laboratory Records Department
Laboratory Records, ORNL RC
ORNL Patent Office
G. M. Adamson, Jr.
R. J. Beaver
M. Bender
R. G. Berggren
C. R. Brinkman
D. A. Canonico
J. Corum
F. L. Culler
J. E. Cunningham
J. H. DeVan
R. G. Donnelly
G. Fee
M. H. Fontana
W. R. Gall
B. L. Greenstreet
W. O. Harms
(5) M. R. Hill
D. O. Hobson
F. J. Homan
P. R. Kasten
R. T. King
R. L. Klueh
K. C. Liu
(20) A. L. Lotts
R. E. MacPherson
W. R. Martin
W. J. McAfee
H. E. McCoy
H. C. McCurdy
W. T. McDuffee
C. J. McHargue
P. Patriarca
S. Peterson
H. Postma
C. E. Pugh
P. L. Rittenhouse
A. C. Schaffhauser
J. L. Scott
Myrtleen Sheldon
G. M. Slaughter
W. J. Stelzman
J. O. Stiegler
R. W. Swindeman
D. B. Trauger
W. E. Unger
T. N. Washburn
J. R. Weir, Jr.
G. D. Whitman
J. W. Woods
R. G. Wymer
T. Yahr

Subcontractors and Consultants

Atomic International, P.O. Box 309, Canoga Park, CA 91304

R. I. Jetter
A. Little
J. Shively

Babcock & Wilcox Company, P.O. Box 835, Alliance, OH 44601

W. E. Leyda
C. C. Schultz
D. B. Van Fossen

Battelle Memorial Institute, 505 King Avenue, Columbus, OH 43201

C. E. Jaske
E. C. Rodabaugh
G. H. Workman

Brown University, Providence, RI 02912

W. N. Findley

The Catholic University of America, Washington, DC 20017

A. J. Durelli

Combustion Engineering, Inc., 911 West Main Streeet, Chattanooga, TN 37401

T. Cullen
T. Ward

Cornell University, Department of Material Science and Engineering, Ithaca, NY 14850

G. V. Smith

E. P. Esztergar, 7993 Prospect Place, La Jolla, CA 92037

Foster Wheeler Corporation, Nuclear Department, 110 South Orange Avenue, Livingston, NJ 07039

W. R. Apblett, Jr.
R. Barratt

Franklin Institute Research Laboratories, The Benjamin Franklin Parkway, Philadelphia, PA 19103

Zenons Zudans

General Electric Company, 175 Curtner Ave., San Jose, CA 95125

Y. R. Rashid

Gulf General Atomic, P.O. Box 1608, San Diego, CA 92138

M. Jakub
D. I. Roberts

O'Donnell & Associates, Inc., 5100 Centre Avenue, Pittsburgh, PA 15232

W. J. O'Donnell

Pennsylvania State University, University Park, PA 16802

S. Y. Zamrik

Teledyne Materials Research Company, 303 Bear Hill Road, Waltham, MA 02154

W. E. Cooper
J. L. McLean

University of Alabama, College of Engineering, P.O. Box 1968, University, AL 35486

E. Carden

University of California, Lawrence Radiation Laboratory, Inorganic Materials Research Division, Berkeley, CA 94720

Leo Brewer

University of California, Revelle College, Department of Physics, P.O. Box 109, La Jolla, CA 92037

Walter Kohn

University of Cincinnati, Materials Science and Metallurgical Engineering Department, Cincinnati, OH 45221

J. Moteff

University of Illinois, Department of Physics, Urbana, IL 61801

W. S. Williams

EXTERNAL DISTRIBUTION

USAEC DIVISION OF REACTOR RESEARCH AND DEVELOPMENT, Washington, DC 20545

(2) Director

USAEC-RRD SENIOR SITE REPRESENTATIVE, Oak Ridge National Laboratory, Oak Ridge, TN 37830

USAEC OAK RIDGE OPERATIONS OFFICE, P.O. Box E, Oak Ridge, TN 37830

Research and Technical Support Division

USAEC TECHNICAL INFORMATION CENTER, Office of Information Services, P.O. Box 62, Oak Ridge, TN 37830

For distribution as shown in TID-4500 Distribution Category, UC-79b (Fuels and Materials Engineering Development); UC-79h (Structural Materials and Design Engineering); UC-79k (Components)